STEREOSPECIFIC PHOTOTRANSFORMATIONS OF ATROPISOMERIC CHROMOPHORES

A Dissertation
Submitted to the Graduate Faculty
of the
North Dakota State University
of Agriculture and Applied Science

By

Elango Kumarasamy

In Partial Fulfillment
for the Degree of
DOCTOR OF PHILOSOPHY

Major Department:
Chemistry and Biochemistry

October 2014

Fargo, North Dakota

North Dakota State University
Graduate School

Title

STEREOSPECIFIC PHOTOTRANSFORMATIONS OF ATROPISOMERIC CHROMOPHORES

By

Elango Kumarasamy

The Supervisory Committee certifies that this ***disquisition*** complies with North Dakota State University's regulations and meets the accepted standards for the degree of

DOCTOR OF PHILOSOPHY

SUPERVISORY COMMITTEE:

Prof. Sivaguru Jayaraman
Chair

Prof. Mukund P Sibi

Prof. Pinjing Zhao

Prof. Dean Webster

Approved:

October-24-2014
Date

Prof. Gregory R. Cook
Department Chair

ABSTRACT

Photochemical transformations are unique strategy in synthesis that enables us to access complex and structurally diverse organic scaffolds. However, the challenges in controlling the excited-state to perform stereoselective reactions left this method under-utilized. This dissertation describes a novel strategy that employs atropisomeric chromophores to perform stereospecific phototransformations. The success of this strategy is well established in thermal chemistry but not comprehensively investigated in photochemical transformations. This research largely relies on rotamer control in the ground state (NEER principle) wherein the axial chirality in the starting material was transferred to point chirality in the products upon excitation.

The chapter 1 describes the principle differences between the asymmetric thermal and asymmetric photochemical reactions. Further, a survey of methodologies developed towards asymmetric phototransformations and their outcomes are described. A brief introduction about the atropisomeric systems in thermal chemistry and the preliminary investigations in phototransformations are also provided.

In chapter 2, enantiospecific *disrotatory* 4π-ring closure of atropisomeric 2-pyridones were investigated. The differential axial chirality designed (sterics and H-bonding units) displayed distinct temperature and solvent dependency on the enantiospecificity of the reaction. Eyring plot was computed to calculate the differential activation enthalpy and entropy for the reaction. Also, the course of phototransformation was followed through single-crystal XRD to decipher the preferred mode of cyclization for a given isomer of 2-pyridones. The high-pressure racemization and photoreaction study revealed that pressure provided stable chiral axis even at elevated temperature resulting in higher enantiomeric excess (*ee*) in the photoproduct.

The chapters 3-5 describe the [2+2]-photocycloaddition of atropisomeric enamide, maleimide and imine derivatives. The design features on these molecules allowed us to perform complementary reactions that are not observed in the literature. These modifications were significant improvement to “axial to point chiral” strategy that improves the versatility of the photoreactions. For example switching of the excited state in enamides, continuous flow visible-

light photocatalysis of maleimides and unusual photocycloaddition of stabilized imines are notable features.

This dissertation encompasses detailed studies on the mechanism, scope and photophysical studies on new atropisomeric chromophores such as 2-pyridones, enamides, maleimides and imine derivatives that provides excellent avenue to access chirally enriched building blocks.

ACKNOWLEDGEMENTS

I would like to take this opportunity to thank each and everyone who happened to cross my path and be of certain influence during my PhD career at NDSU. My sincerest gratitude and appreciation goes to my advisor/mentor Prof. Sivaguru Jayaraman who undertook a great task of mentoring me and be an element of inspiration. He introduced me to the concept of photochemistry that still fascinates and excites me in every aspect. I have learnt so much from him over the years that not only made me a better scientist but also to conduct as a better professional. I sincerely thank him for being a great moral and knowledge support that kept me going through tough and desperate times during my research.

I would like to thank my committee members Prof. Mukund P Sibi, Prof. Pinjing Zhao and Prof. Dean Webster for their support and positive critic of my research. They were always available and were able to accommodate my stringent requests in setting up my committee meetings and seminars. Their expertize provided a different facet to my research that paved way for new ideas and research endeavors.

It takes a team to build a research group. In that regard, I am really fortunate and proud to be a part of Sivagroup. I sincerely appreciate my lab mates (in no particular order) Dr. Barry C Pemberton, Dr. Anoklase Jean-Luc Ayitou, Dr. Josepha Jesuraj, Dr. Saravana Kumar Rajendran, Nandini Vallavoju, Ramya Raghunathan, Akila Iyer, Anthony Clay, Sunil Kandappa, Dr. Retheesh Krishnan and other who happened to have short stint in our lab either as summer or high school students for their patience, encouragement and support during my hard and successful times.

I would like to thank all the research groups at NDSU *viz.,* Sibi group, Zhao group, Cook group, Sun group, Seth Group and Srivatsava Group for lending their support, chemicals and instruments whenever I needed. I greatly acknowledge their time and interest towards my research and engaging in meaningful discussions that were very useful to my research and career.

I would like to thank the faculty members in the Department of Chemistry and Biochemistry for their support and encouragement during my research.

I would like to thank all the supporting staff in the department of Chemistry and Biochemistry who were always amenable and took care of all our administrative requirements/tasks and helped us to concentrate more on our research. I sincerely thank our staff scientists Dr. Angel Ugrinov, Dr. John Bagu and Daniel Wanner for helping us with X-ray crystallography and NMR studies. I appreciate the help from clerical staff Wendy Leach, Linda Stoetzer, Amy Kain, Dionna Martel, Tina Exner, Jeff Scholl and David Tacke.

I sincerely thank NSF-ND EPSCoR for providing me doctoral dissertation fellowship for two years. I also thank them for providing me “Student Travel Grant” to conduct experimental studies at Columbia University, New York. I would like to thank the Department of Chemistry and Biochemistry for recognizing me with “Chemistry Graduate Student Scholarship”.

I would like to thank all our research collaborators who have shared their expertise and provided new insights that helped us better understand and represent our research to the scientific community.

Prof. Nicholas Turro and Dr. Steffen Jockusch at Columbia University, New York, NY for their collaborative work with respect to photophysical aspects detailed in this dissertation and publications elsewhere.

Prof. Yoshihisa Inoue, Dr. Gaku Fukuhara at Osaka University, Osaka, Japan for their collaborative work with photochemical transformation under elevated pressure detailed in Chapter 2 and publications elsewhere.

I would like to thank all my family members who were with me on this long journey. I sincerely express my gratitude for their endless support, love and patience while I was away in pursuit of my dream. I could not have achieved so much but for their encouragement and I can only hope that I will make them proud in every possible way I could.

Finally, a special thanks to my wife Ramya Raghunathan who took the brunt of my despair yet never gave up on me. She has been my strength and confidence when I needed them most and sincerely thank her to be a part of my life.

DEDICATION

To my father

TABLE OF CONTENTS

LIST OF TABLES

LIST OF FIGURES

LIST OF SCHEMES

LIST OF EQUATIONS

LIST OF CHARTS

LIST OF ABBREVIATIONS

Ac .....Acetyl

BINAP ..... 2,2'-bis(diphenylphosphino)-1,1'-binaphthyl

dba ..... Dibenzylideneacetone

Ts ..... *para*-toluenesulfonyl

MsCl .....Methanesulfonyl chloride

Et_3N .....Triethylamine

Boc ..... *tert*-butyloxycarbonyl

brsm .....Based on the recovered starting material

BuLi ..... Butyllithium

HAT .....Hydrogen atom transfer

CDI ..... 1,1'-Carbonyldiimidazole

equiv. ..... Equivalent(s)

ESI..... Electrospray ionization

PkA..... First eluting enantiomer in the HPLC on a chiral stationary phase

PkB..... Second eluting enantiomer in the HPLC on a chiral stationary phase

d.r. ..... Diastereomeric ratio

e.e ..... Enantiomeric excess

e.r. ..... Enantiomeric ratio

rac ..... Racemic

FTIR ..... Fourier transform infrared spectroscopy

GC .....Gas chromatography

h .....Hours

h ..... Planck's constant

HMPA .....Hexamethylphosphoramide

ID ..... ……Inner diameter

k_B ..... ……Boltzmann's constant

LDA ..... ……Lithium diisopropylamide

LiHMDS ..... ……Lithium bis(trimethylsilyl)amide

NaHMDS ..... ……Sodium bis(trimethylsilyl)amide

M ..... ……Molar

mM ..... ……Millimolar

min ..... ……Minutes

N/A ..... ……Not applicable

NMR ..... ……Nuclear magnetic resonance

DEPT ..... ……Distortionless enhancement by polarization transfer

Ph ..... ……Phenyl

PMB ..... ……*para*-methoxybenzyl

ppm ..... ……Parts per million

c ..... ……Concentration

rt ..... ……Room temperature

satd. ..... ……Saturated

Anhyd. ..... ……Anhydrous

o ..... ……Ortho

m ..... ……Meta

p ..... ……Para

t-Bu ..... ……*tert*-butyl

i-Pr ..... ……isopropyl

Me ..... ……Methyl

Et ..... ……Ethyl

tol.....Tolyl

Bu.....Butyl

Bn.....Benzyl

TMS.....Trimethylsilyl

AcOH.....Acetic acid

Hex.....Hexanes

TFA.....Trifluoroacetic acid

DCE.....1,2-dichloroethane

DCM.....Dichloromethane

$CHCl_3$/$CDCl_3$.....Chloroform/deuterated chloroform

EtOAc.....Ethyl acetate

MCH.....Methylcyclohexane

MeCN.....Acetonitrile

MeOH.....Methanol

EtOH.....Ethanol

IPA.....Isopropyl alcohol (2-propanol)

TFE.....Trifluoroethanol

THF.....Tetrahydrofuran

DMSO.....Dimethylsulfoxide

DMF.....N,N-dimethylformamide

Cy.....Cyclohexyl

Cp.....Cyclopentyl

w/w.....Weight by weight (percentage)

v/v.....Volume by volume (percentage)

TLC.....Thin layer chromatography

R*f*.....Retardation factor

HPLC.....High Performance Liquid Chromatography

GC.....Gas chromatography

HRMS.....High Resolution Mass Spectrometry

ESI.....Electrospray Ionization

XRD.....X-ray diffraction

atm.....Atmosphere(s)

UV/VIS.....Ultra-Violet/Visible light

CD.....Circular dichroism

CPL.....Circularly polarized light

HOMO.....Highest Occupied Molecular Orbital

LUMO.....Lowest Unoccupied Molecular Orbital

NEER.....Non-Equilibrating Excited Rotamers

ISC.....Intersystem crossing

S_1 or S_n.....First or n^{th} singlet excited state

E_T.....Triplet energy of the excited state species

SET.....Single electron transfer

S_o.....Ground state (singlet)

T_1 or T_n.....First or n^{th} triplet excited state

CHAPTER 1: INTRODUCTION TO SYNTHETIC ORGANIC PHOTOCHEMISTRY AND STRATEGIES TOWARDS ASYMMETRIC PHOTOTRANSFORMATIONS

1.1. Introduction

The demand for chiral building blocks in the field of pharmaceutical industry and drug discovery has been increasing at an exponential rate. The percentage of single enantiomer drug in the market is also at a steady increase.[1] Administering enantiomerically pure drugs has its advantage in terms of its potency, safety and cost effectiveness. Yet, the volume of structural and topological diversity in the chiral elements makes it extremely challenging to access them in the desired purity and quantity. In this regard, the field of asymmetric synthesis has evolved into a powerful and indispensible tool in organic synthesis that allow us to access optically pure molecules. However, with the newer additions of both synthetic and natural drug molecules that are piling up every year, need for a vast library of methodologies is necessary. While on one side, rapid expansion of library of methodologies are being investigated, on the other side, revising a methodology that are focused on improving the yield and efficiency with a greener protocol are being given equal importance. In this regard, photochemistry is more appealing as it not only allows us to rapidly build complexity in an organic molecule but also allow us to construct multiple stereogenic centers at once, all with environmentally benign processes.

1.2. Synthetic photochemistry

Light has been an integral part in the evolution and sustenance of life on earth whose interaction with earth is older than life itself. It is the source of energy that maintains our livelihood through photosynthesis. Life on earth has mastered the art of harnessing the power of sun to its advantage over millennia. Yet, synthetic organic chemistry is still at its infancy in employing light for the synthesis of molecules. In 1834, Trommsdorff documented the first organic phototransformation when he observed the crystals of α-santonin (**1**) turn yellow and burst (Scheme 1.1).[2-4] Since then, progress in the synthetic organic photochemistry has been firmly

stepping up towards accessing the desired target molecule with high control over stereochemistry. However, the challenges associated in achieving such goals are vast. The reason lies in little understating of the excited state behavior of the molecules and failure of simple extrapolation of the ground state (thermal reactions) behavior to the excited states. Progress in the organic photochemistry accelerated after the development of spectroscopic techniques that assisted in understanding the process of excitation and relaxation pathways of molecules.

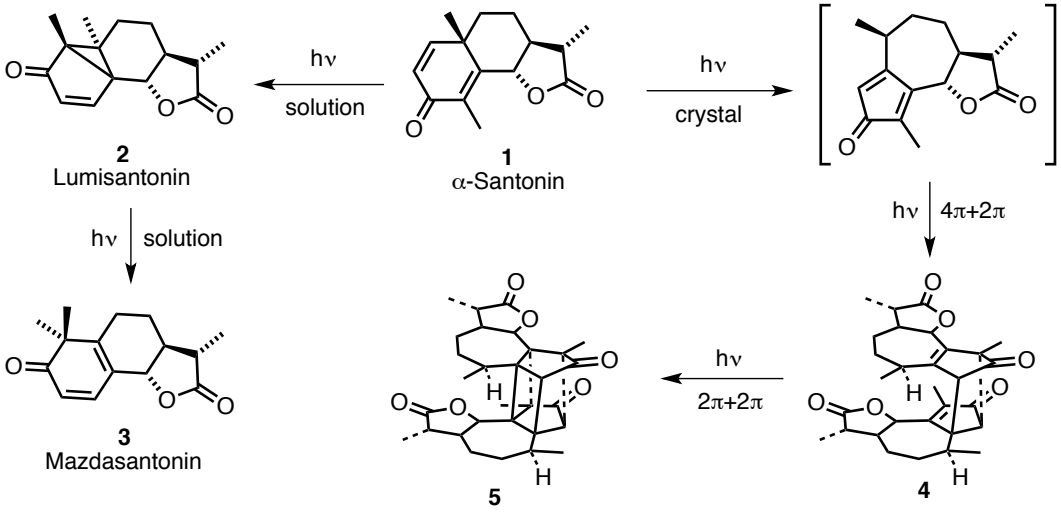

Scheme 1.1: Photoreaction of α-santonin both in solution and in crystal. (Reproduced from reference 4 with permission from American Chemical Society, 2007).

To understand the type of interaction that a chromophore has with light, it is very important to understand the nature of light itself. Light is made up of electromagnetic radiation that spans from low energy infrared (longer wavelength) to high-energy ultraviolet (shorter wavelength) spectrum (figure 1.1).

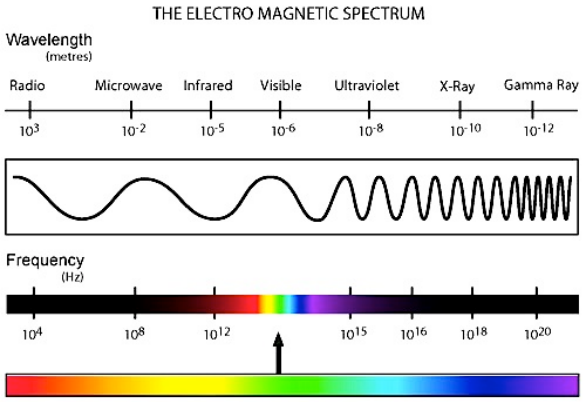

Figure 1.1: Electromagnetic spectrum of light.[5]

When a photon of appropriate (resonance) energy interacts with a chromophore, a process of absorption takes place where the energy of the photon is transferred to the organic molecule promoting it to an electronically excited state. According to Stark-Einstein law, the photon with resonance energy can only bring about single electronic transition. However, this generally accepted rule could have exceptions where more than one photon can be absorbed to cause single electronic transitions as in the case of two-photon absorption events. Now, the excited molecule has multitude of pathways to relax to the ground state either as the same molecule or as a different molecule (products). The resonance energy of a chromophore depends on the type of atom and types of bonds involved in the excitation process. Since the energy is directly related to the frequency of light employed obeying well-known Einstein equation (figure 1.2), it is very important to know the frequency of light employed in arising the desired excitation.

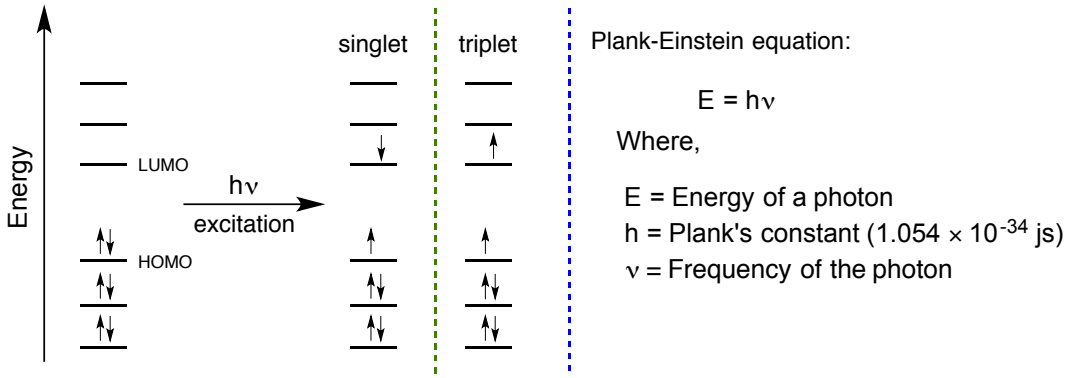

Figure 1.2: Photoexcitation of electron from HOMO to LUMO.

Two principle mechanism by which the excited molecule relax to ground state are radiative and non-radiative processes as described in the simplified Jablonski diagram (figure 1.3). In a non-radiative relaxation process, one electronic state is converted to another by thermal/vibrational relaxation without the emission of light, a process known as internal conversion. Internal conversion can further be divided into two types of processes with respect to whether or not the process accompanied by the change in the multiplicity. If there is no spin change, the transition is termed as “spin allowed transition” where the higher excited singlet states decay to the lowest excited singlet states by thermal relaxation. However, if the transition is accompanied by a spin change it is called “spin forbidden transition” where the singlet excited state is converted to a triplet excited state through a process known as intersystem crossing (*ISC*).

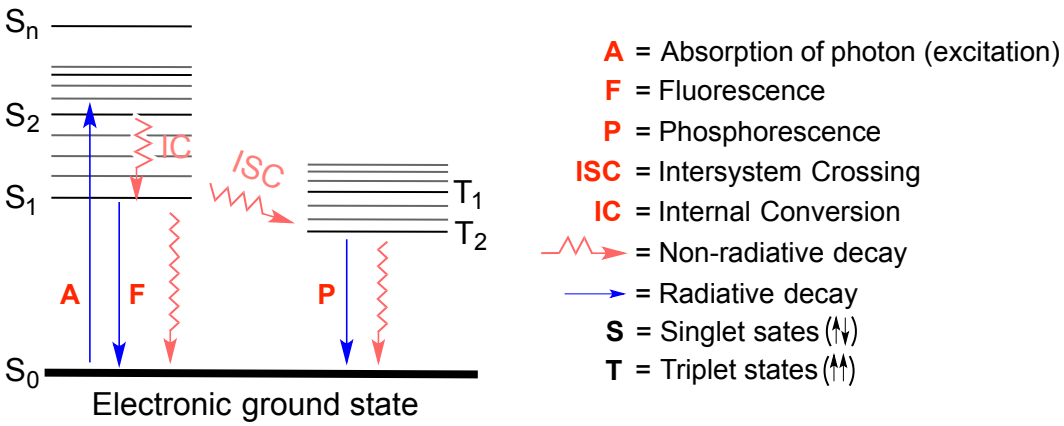

Figure 1.3: Simplified Jablonski diagram.

In a radiative relaxation process, the excited molecule relaxes to ground state by emission of photon (light). In singlet manifold, the excited singlet state (S_n) relaxes to the ground singlet state (S_0) by emission of a photon termed as the fluorescence. In this scenario, there is no overall change in the spin multiplicity. In broader strokes, regardless of which excited state the molecule is promoted in an excitation process, the emission is observed from the lowest excited singlet state known as Kasha’s rule. Exceptions to this rule are observed where molecule emits from their higher excited states ($S_n > 1$). In some cases, the excited singlet state can undergo “spin forbidden” intersystem crossing to the excited triplet state. The radiative emission from the

lowest excited triplet state is called as phosphorescence. Since the process is "spin forbidden" the phosphorescence generally occur at a longer time scales compared to the fluorescence processes.

While a photon has the ability to initiate the above processes not all the excitation leads to the desired products and it's very challenging to control the undesired pathways of relaxation. The efficiency of the given process is defined by its quantum yield (ϕ).

$$\text{Quantum yield } (\Phi) = \frac{\text{Number of molecule undergo desired process}}{\text{Number of photons absorbed}} \qquad \textbf{Equation 1.1}$$

Depending on the type of chromophore involved, the outcome of the reactions can be quite different based on the relative efficiencies of various processes involved after excitation.

1.3. Photochemical apparatus

The history of synthetic photochemistry started to evolve as early as 1800's.[2] Since then, it has slowly developed into a powerful method to construct complex structural organic motifs that are sometimes inaccessible through ground state chemistry.[6,7] Appreciation for the potential of photochemistry has resulted in significant advancement that provides wide array of methods to perform photoreactions. For example, introduction of flow photoreaction has broadened the scope of large-scale reactions in manifold.[8-10]

1.3.1. Choice of irradiation source

The organic chromophores can be excited with wide spectrum of light source ranging from low energy visible region to high energy UV region. Depending on the type of chromophore, the choice of wavelength can be arrived at. The most widely employed irradiation source is mercury arc lamp in combination with immersion well reactors. The mercury arc lamp provides a wide array of spectral distribution that allows us to excite most of the organic chromophores of interest. In general, 3 types of mercury arc lamps are available *viz.,* low, medium and high-pressure arc lamp that differ in their spectral output and intensity. Another important consideration

is the operating temperature of these lamps, which can vary from 50 to 800 ^{o}C. So, these lamps are placed inside a double-jacketed immersion well that is continuously circulated with cold water (suitably connected to flow sensor to cut-off power supply incase water flow drops less than specified level). In some cases, the wide spectral distribution might be disadvantageous that can bring about unwanted side reactions or decomposition.[11] In such instances, a narrow band of light sources are employed as in the case of Rayonet reactors (that comes with varying light sources such as ~254, ~300, ~350 and ~420 nm) or monochromatic laser irradiations.

Yet another important aspect of irradiation is the type of glassware used for the photoreactions. They can also act as a source of filter thus providing desired reaction conditions while employing broadband irradiation source. Most commonly employed glassware includes uranium (> 350 nm), Pyrex (> 300 nm), Vycor (> 240 nm) and Quartz (> 200 nm). Apart from these filter glasses, several specially made filter glasses and filter solutions are available in the literature to accommodate the special needs for a given reaction.[12] The following table 1.1 provides some of the common organic chromophores and their transitions.[13]

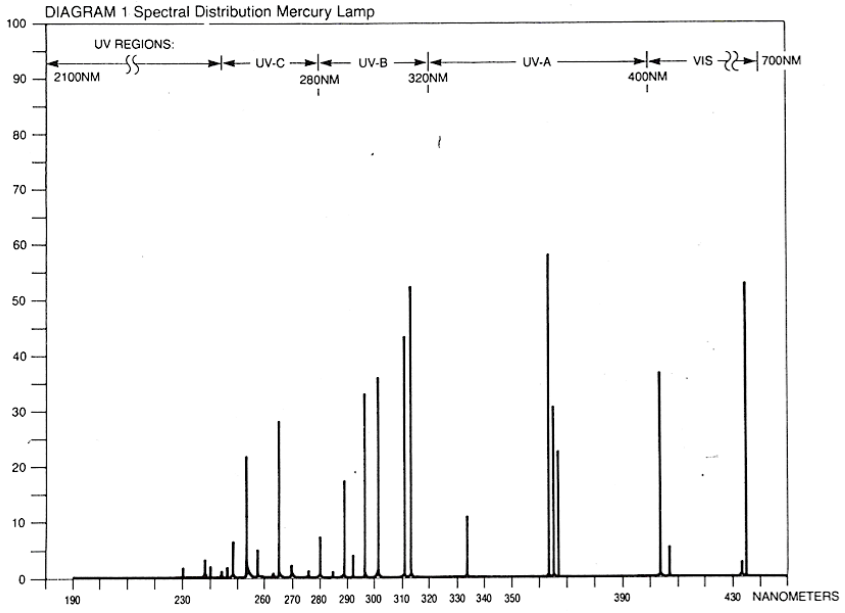

Figure 1.4: Spectral distribution of 450W mercury lamp (courtesy: Hanovia®-UV).

Table 1.1: HOMO-LUMO transition of organic chromophores[a]

Entry	Chromophore	Transition	λ_{max} (nm)	ε_{max} ($mol^{-1}.l.cm^{-1}$)
1	N=O	n-π^*	~ 660	200
2	C=S	n-π^*	~ 520	100
3	N=N	n-π^*	~ 350	100
4	C=C-C=O	n-π^*	~ 350	30
5	C=O	n-π^*	~ 280	20
6	NO2	n-π^*	~ 270	20
7	C≡N	n-π^*	~ 260	150
8	S=O	n-π^*	~ 210	1.5×10^3
9	Benzene ring	π-π^*	~ 260	200
10	Naphthalene	π-π^*	~ 310	200
11	Anthracence	π-π^*	~ 380	1×10^4
12	C=C-C=O	π-π^*	~ 220	2×10^5
13	C=C-C=C	π-π^*	~ 220	2×10^5
14	C=C	π-π^*	~ 180	1×10^5
15	C-C	σ-σ^*	< 180	1×10^5
16	C=H	σ-σ^*	< 180	1×10^3

[a]Data obtained from Burns group meeting hand out, Q. Ong

1.3.2. Choice of solvents

The solvent plays an important role in the organic photochemistry. Several stringent expectations have to be met in order for a solvent to be successfully employed in the photoreactions. Some of the guidelines are listed below,

i) The solvent should dissolve the reactant(s) to form a homogenous solution otherwise transmission of light becomes a concern.

ii) The solvent should be optically transparent in the region where the reactant(s) absorb the light.

iii) The solvent should be photochemically inert thus only serving as a medium for the reaction. It is often noticed that wrong choice of solvents can lead to various side reactions and decomposition.

iv) The solvent should not quench the excited state of the reacting species chemically, thermally or photochemically.

v) Optimal concentration of the solute should be arrived at, as too low or too high concentration might not bring about efficient photoreactions (Beer-Lambert's law).

vi) The solute should be void of any impurities (chemical species or gaseous species such as oxygen) that can affect the light absorption/reaction process.

The following table lists approximate UV cut-off wavelength for some of the common organic solvents.[14,15]

Table 1.2: UV cut-off wavelength of some common organic solvents

Entry	Solvent	UV cut-off	Entry	Solvent	UV cut-off
1	Water	185	10	Chloroform	245
2	Acetonitrile	190	11	Tetrahydrofuran	245
3	*n*-hexanes	195	12	Ethyl acetate	255
4	Ethanol	204	13	Acetic acid	250
5	Methanol	205	14	Carbon tetrachloride	265
6	Cyclohexane	215	15	Dimethylsulfoxide	277
7	Diethyl ether	215	16	Benzene	280
8	1,4-Dioxane	230	17	Toluene	285
9	Methylene chloride	230	18	Acetone	330

1.3.3. Choice of sensitizers

A sensitizer is a chemical species that absorb the light and transfer it to the reactants (either through energy transfer or electron transfer) thus initiating a chemical process. The need for a sensitizer is essential in reactions where the excited state population of the reactant is short lived to undergo desired chemical reaction. Also, sometimes sensitizer act as an optical shield that protects reactant(s)/product(s) from undergoing photodecomposition. Similar to solvents, the sensitizer also has to meet several criteria to be an efficient sensitizer. Some of the criteria are,

i) The sensitizer should absorb the light efficiently and must have sufficient lifetime in the excited state in order to transfer its energy to the reactants.

ii) There should be a spectral overlap between the emission of sensitizer and absorption of reactant (comparable energy levels) for an efficient energy transfer to occur.

iii) The sensitizer should be photostable thus allowing for multiple cycles of energy transfer to occur.

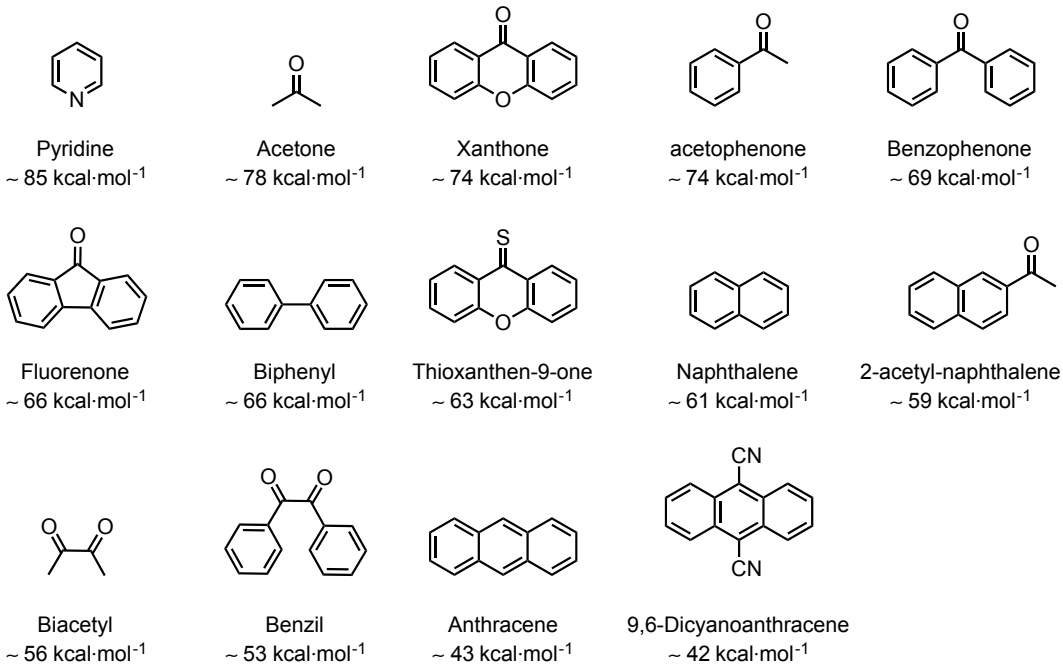

Figure 1.5: List of common triplet sensitizers and their triplet energies.[16]

1.4. Challenges in asymmetric organic phototransformations

Synthetic organic photochemistry has been widely utilized to access some of the highly strained and structurally complex motif with relative ease.[17] Pumping in very high energy into the molecule through absorption in a short time allows us to perform reactions that are impossible by conventional routes.[18] Yet with such a promise, carrying out stereoselective reactions proved to be highly challenging. The reason lies in the inability to control the excited state to a desired pathway. An important requirement to achieve higher stereoselectivity in the photoreactions is preorganization. Pre-organization allows the molecule to be in a reaction-ready state where the energy of the excited chromophore is channeled to a desired pathway. While this strategy seems to be perfect, obtaining necessary preorganization comes with challenges in itself. Over the years, several avenues were looked at in achieving such predisposition that will allow us to perform stereoselective phototransformations. Some of the highly successful strategies in the thermal reaction simply could not be extended to the phototransformations. The fundamental

challenge involved in obtaining higher selectivity in photoreaction is due to inefficient chiral induction process during the short excited-state lifetime of the chromophore.

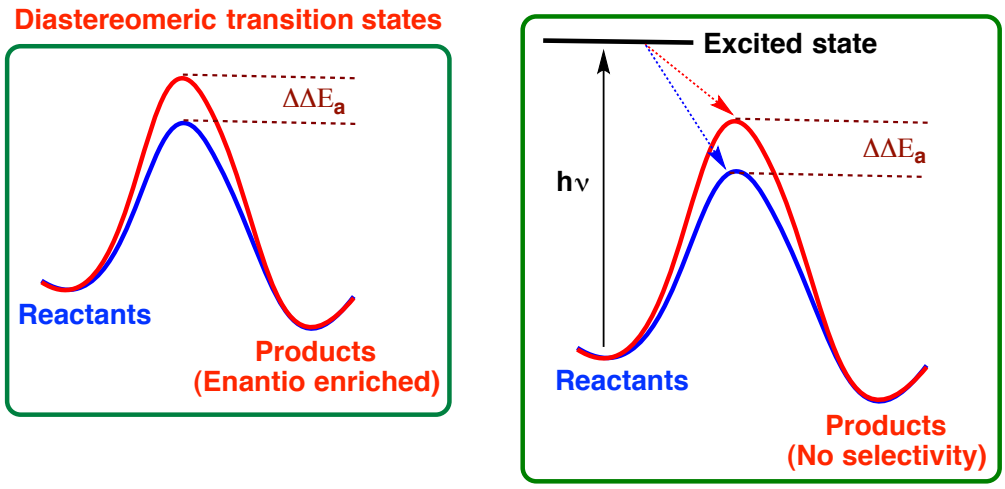

Figure 1.6: Comparison between diastereomeric transition states in thermal (left) and photochemical (right) reactions.

For example, in a thermal reaction, the chiral inductors such as chiral auxiliaries, catalysts--etc interact with prochiral reactants resulting in the desired chiral discrimination. The extent of interaction/stabilization with reactants can affect the outcome of stereoselectivity in the products. For example, a differential activation energy ($\Delta\Delta E_a$) of 2.83 kcal·mol^{-1} at 298 K is sufficient to bring about 99% *ee* for a given enantioselective transformation. Unlike thermal reactions, in a photochemical transformation, such approach proved to be futile. The reason lies in energetics and the reaction coordinates involved in a given reaction. Up on shinning light, the reactants are promoted to the excited state that are highly energetic, short-lived and have very less energy barrier to undergo any transformation that relax them to the ground state. With such a scenario, any means to control the stereoselectivity in the phototransformations proved to be ineffective. Tackling this bottleneck required new approaches that take into the account of inherent reactivity of the excited state molecule and the time limitation to bring about such chiral discrimination. Working towards addressing such an enormous challenge, researchers through painstaking effort, careful observation and design strategy came up with several methodologies to

perform stereoselective phototransformations.[19] The efforts were met with varying degree of success and the following section provides a glimpse of those endeavors.

1.5. Strategies towards asymmetric phototransformations

1.5.1. Chiral light source for asymmetric phototransformations

The earliest known example of asymmetric phototransformation was performed using circularly polarized light (CPL). In 1874, Le Bel envisioned the possibility of employing circularly polarized light to perform stereoselective reactions.[20] In 1894, Van't Hoff reiterated Le Bel's theory and the use of circularly polarized light.[21] Also, the advent of Circular Dichroism (CD) by Cotton in the year 1896 further strengthened the prospect of asymmetric photochemistry. The asymmetric photochemistry with the aid of CPL is often described as "*absolute asymmetric"* as the substrates involved in the reaction do not have net chirality. In principle, the CPL in the asymmetric transformations can be classified into three main categories a) Partial photo-resolution, b) Asymmetric photo-destruction and c) asymmetric synthesis. The photo-resolution using CPL was not experimented until 1929 when Kuhn and coworkers reported the first kinetic photo-resolution of racemic ethyl-α-bromopropionate (**2**) and *N,N*-dimethyl-α-azidopropionamide (**3**) (Scheme 1.2).[22-24]

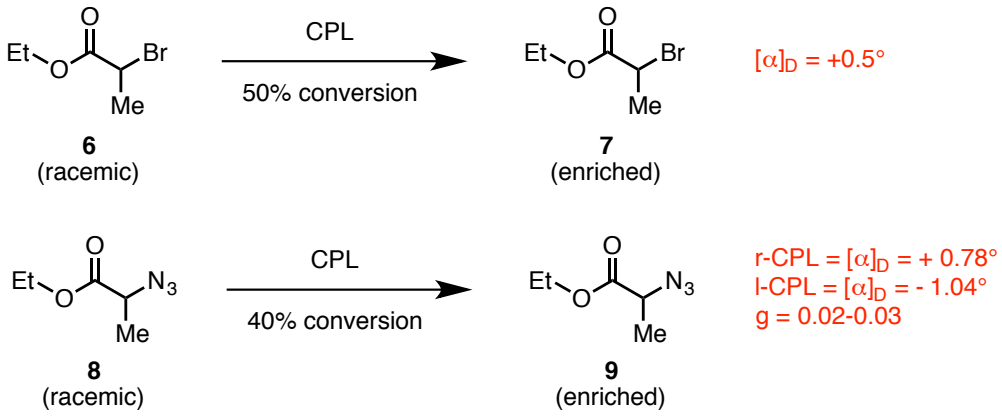

Scheme 1.2: Photo-resolution of ethyl-α-bromopropionate (top) and *N,N*-dimethyl-α-azidopropionamide (bottom) using circularly polarized light.

During the irradiation with CPL, photo-resolution occurred via homolytic cleavage of α-C-Br or α-C-N_3 bond followed by recombination resulting in resolution. The anisotropy factor (g) of the molecule (anisotropy factor is the measure of preferential excitation of one enantiomer over the other towards *l*- and *r*-CPL at a given wavelength) played a crucial role in the determining the optical resolution in a given molecule. Similarly, Rau and coworkers reported the resolution of tertramethyl-tetraaza-spirononadiene (**10**) by asymmetric photo-destruction strategy by using circularly polarized light (Scheme 1.3).[25] From their study, they assumed that the (*S*)-isomer underwent photolysis to a greater extent over the (*R*)-isomer resulting in resolution.

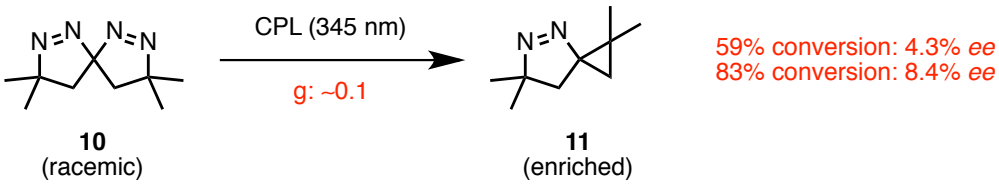

Scheme 1.3: Asymmetric photo-destruction of tertramethyl-tetraaza-spirononadiene **10**.

In principle, the resolution occurs because of the differential reaction rate of one enantiomer over the other that occurs through the differential absorption (molar absorption coefficient) of CPL (right CPL over left CPL) for a given enantiomer. In 1971, Kagan and coworkers demonstrated the absolute asymmetric synthesis of hexahelicenes through the oxidative photocyclization of diarylethylenes (**12**) and (**13**) (Scheme 1.4) in presence of iodine.[26] Control studies revealed the observation are not due to the photo-reduction of hexahelicenes (**14**) that would also result in the net optical activity.

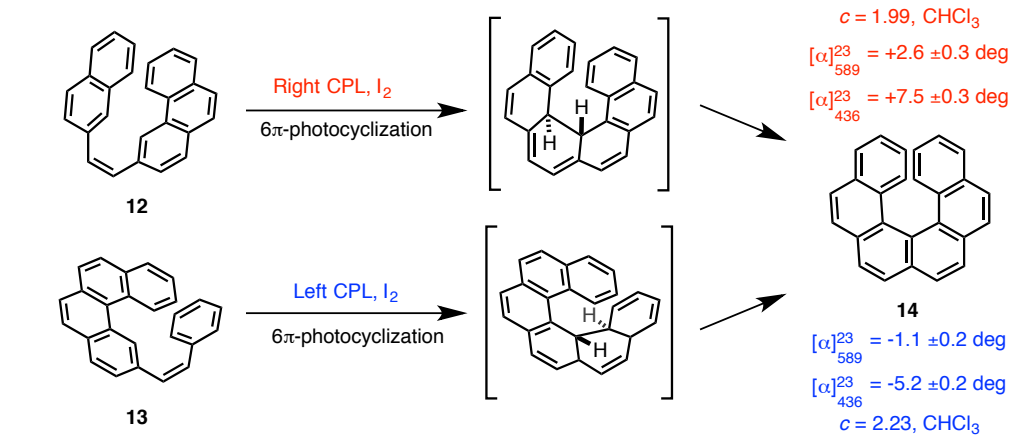

Scheme 1.4: Electrocyclization of diarylethylenes **12**-**13** to helicenes **14** mediated by circularly polarized light.

While most of the research on CPL mediated asymmetric synthesis was focused on prebiotic interest, little emphasis were given to develop a method that will be of synthetic use on a large scale practical application. In 2005, Soai and coworkers demonstrated such a feet by employing CPL on pyrimidyl alcohol (**15**) to result in slight enrichment followed by autocatalytic synthesis leading in very high enantiomeric excess in pyrimidyl alcohol (Scheme 1.5).[27,28]

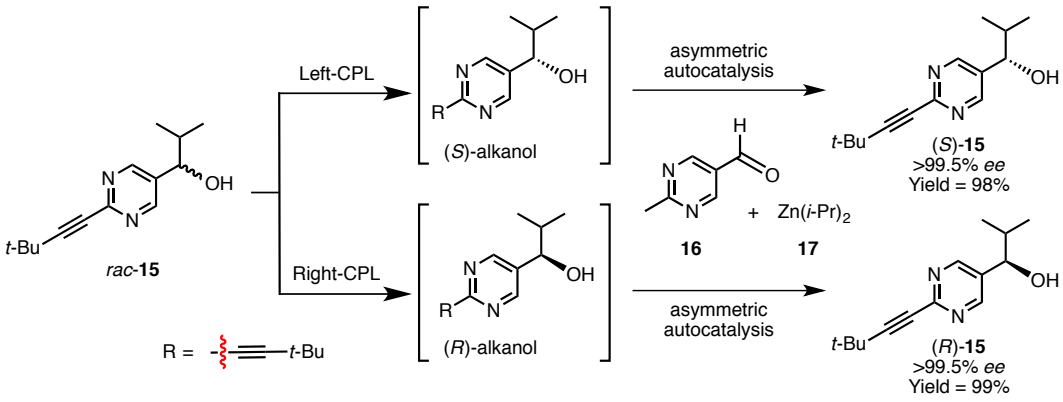

Scheme 1.5: Autocatalytic synthesis of pyrimidyl alkanol **15** mediated by circularly polarized light (Reproduced from reference 27, with permission from American Chemical Society, 1976).

Enantioselective photodecomposition of racemic pyrimidyl alkanol with polarized light (r-CPL or l-CPL) resulted in enantioenriched alkanol, which served as a cryptochiral source that

catalyzed the asymmetric autocatalysis of 2-alkynylpyrimidine carbaldehyde (**16**) and diisopropylzinc (**17**) resulting in highly enantioenriched pyrimidyl alkanol (**15**) (> 99.5% *ee*).

1.5.2. Asymmetric photoreactions in the crystalline state

One of the oldest and successful methodologies employed in asymmetric phototransformation is the solid-state photoreaction. The idea of performing asymmetric phototransformations in crystalline matrix was conceived as early as 1908.[29] However, to perfect the idea that are more practical and applicable required careful understanding and analysis of the crystals and its photo-response.[30] The crystal lattice control the outcome of the reactions and are termed as "Topochemically controlled reactions". The solid-state photoreactions hold huge promise, as even an achiral starting material with suitable crystallization technique would crystallize in chiral space group providing an avenue for "*absolute asymmetric synthesis*". Carrying out asymmetric solid-state photoreactions involve two important aspects *viz.*, i) Generating chiral crystals; ii) Performing topochemically controlled reactions. Out of 230 unique space groups available, only 65 of them are chiral and to carry out asymmetric photoreactions, it is necessary that the molecule crystallize in a chiral space group.[31] Even in the chiral space group, the reactive groups must be placed appropriately (Schmidt distance <4.2 Å) for a successful reaction to take place.[32] Schmidt and coworkers performed extensive studies on the solid-state photoreactions, especially on the [2+2]-photodimerization of cinnamic acid derivatives and put forward some important guidelines for efficient reactions in the solid-state.[33,34]

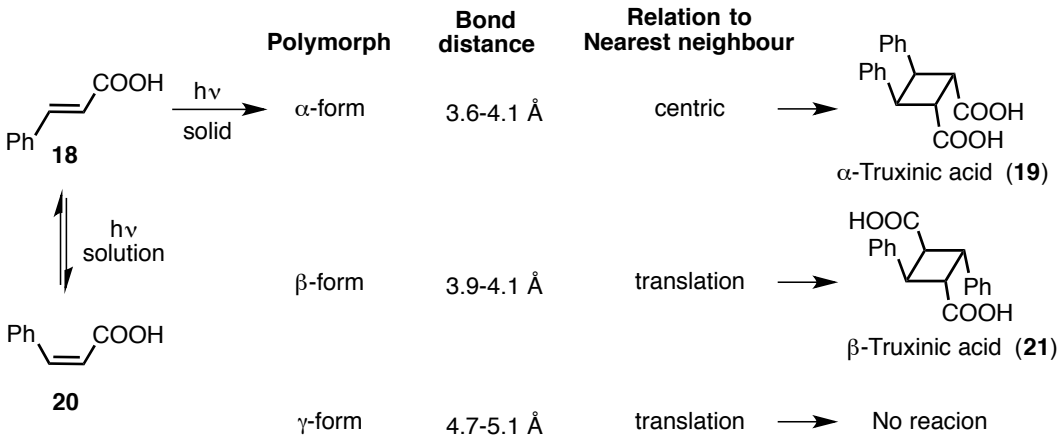

Scheme 1.6: Solid-state photoreaction of cinnamic acid derivatives (Reproduced with permission from reference 35; Copyright American Chemical Society, 1987).

In the case of cinnamic acid derivatives (**18** and **20**), the *cis-trans* isomerization of the double bond predominated in the solution, whereas in the solid-state the preferred dimerization occurred smoothly to produce desired cyclobutane derivatives (Scheme 1.6). However in the solid-state, depending on the polymorph of the crystal employed (α, β and γ) the product outcome differed. In the γ-polymorph, the distance of the double bond was greater than 4.2 Å (4.7-5.1 Å) thus failing to undergo the desired photodimerization. Insights gained from these studies allowed Schmidt and coworkers to extend this methodology to perform bimolecular solid-state photoreactions in a stereoselective fashion. For instance, they have demonstrated lattice-controlled bimolecular photocycloaddition of chiral crystals (Scheme 1.7).[36] The mixture of 2,6-dichlorophenyl-4-phenyl-*trans,trans*-1,3-butadiene (**22**) and its corresponding thienyl analogue (**23**) (~15 %) crystallized in a chiral $P2_12_12_1$ space group that up on irradiation furnished enantioenriched cyclobutane derivatives (**24** and **25**) (*ee* = 70%).[30]

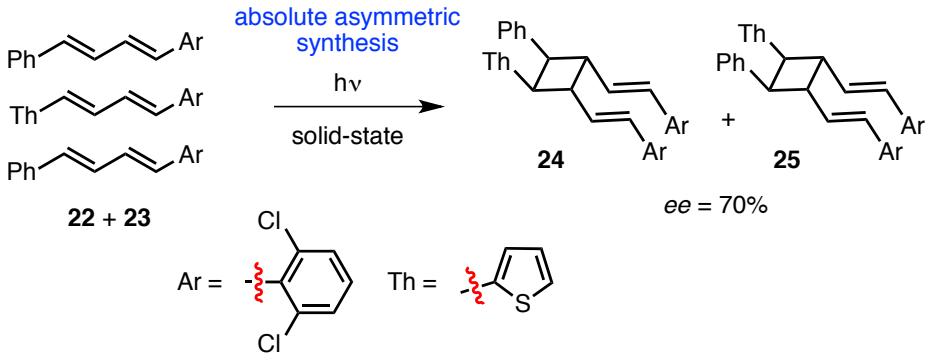

Scheme 1.7: Stereoselective bimolecular solid-state photoreaction 1,3-butadiene derivatives.

The homo-dimerization was avoided by carefully choosing the percentage of thienyl analogue (~15 %) and by selective excitation of longer wavelength absorbing thienyl derivative. Scheffer and coworkers reported the first example of intramolecular absolute asymmetric synthesis through photochemical di-π-methane rearrangement and Norrish-Yang reaction.[37] The dibenzobarralene diester derivative (**26**) crystallized in a chiral space group $P2_12_12_1$ that upon irradiation resulted in the desired dibenzosemibullvalene photoproduct (**27**) with very high *ee* (>99%) as ascertained by ^{1}H-NMR using chiral shift reagent (Scheme 1.8). The temperature during photolysis played a crucial role on the *ee* of the reaction, as higher temperature led to lower *ee*, a reason attributed to the melting of crystal that disrupts the topochemical control.

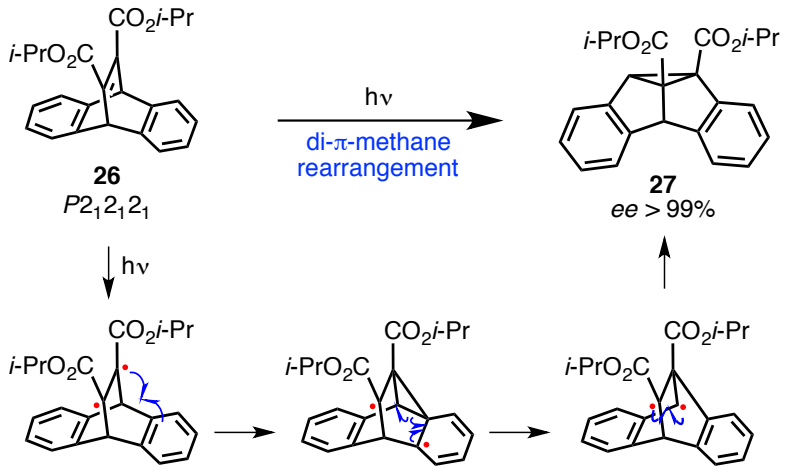

Scheme 1.8: Di-π-methane rearrangement of dibenzobarralene diester derivative **26** in the solid-state.

Similarly, they also employed adamantyl-*p*-chloroacetophenone derivative (**28**) for Norrish-Yang reaction (Scheme 1.9) wherein excitation of the ketone was followed by intramolecular H-abstraction (Norrish type II) from γ-carbon to carbonyl oxygen via a six-membered transition state leading to the formation of corresponding cyclobutanol derivative (**29**) in high *ee* (80%).

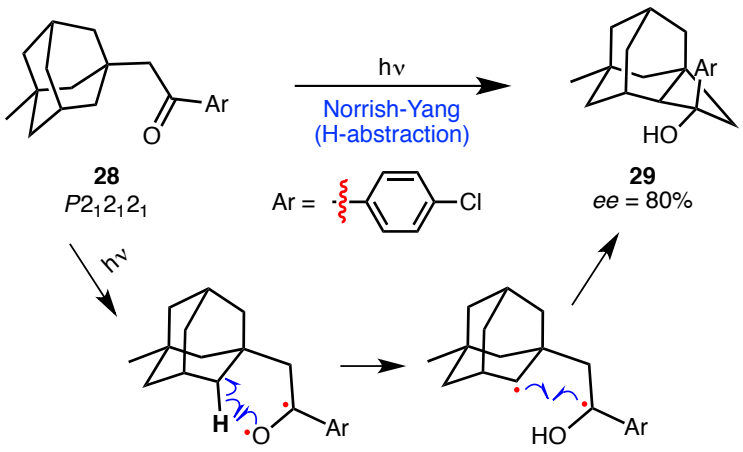

Scheme 1.9: Norrish-Yang reaction of adamantyl-*p*-chloroacetophenone derivative **28**.

In another example of absolute asymmetric synthesis, Sakamoto and coworkers reported [2+2]-photocycloaddition of achiral *N*-(thiobenzoyl)methacrylamide (**30**) in the solid-state to yield thietane photoproduct (**31**) (Scheme 1.10). This topochemically controlled (the distance between the reacting alkene and thiocarbonyl was within the Schmidt's distance) reaction occurred only with modest stereospecificity in the solid-state (40% *ee*). They also showed that by employing seeding technique they were able to access bulk quantities of (+)- or (-)-**30** providing an easy avenue to scale up.

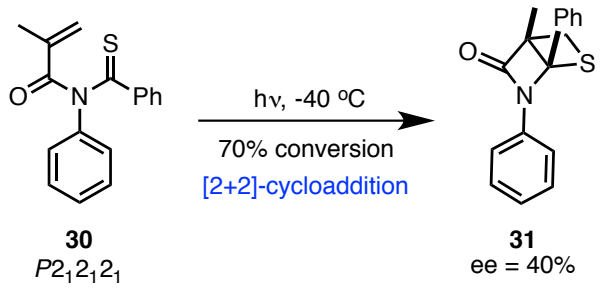

Scheme 1.10: [2+2]-Photocycloaddition of *N*-(thiobenzoyl)methacrylamide derivative **30**.

Similarly, Toda and coworkers reported 6π-electrocyclic ring closure of 3,4-bis(phenylmethylene)-*N*-Me succinimide derivative (**32**) to yield enantioenriched photoproducts (Scheme 1.11).[38]

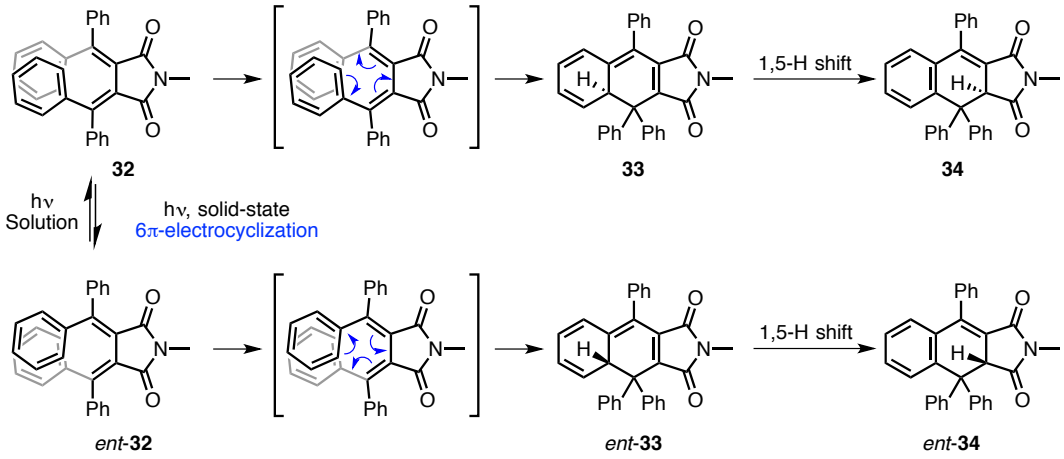

Scheme 1.11: 6π-Electrocyclization of 3,4-bis(phenylmethylene)-*N*-Me succinimide derivative **32**.

However, photoreaction of other derivatives did not yield optically active products. The reason for the failure to yield optically active photoproducts could not be ascertained, as there was not enough crystallographic information about these substrates. While "absolute asymmetric synthesis" was elegant, it largely depended on the ability of the achiral molecule to crystallize in a chiral space group. Unfortunately, most of the achiral molecules do not crystallize in chiral space group and the crystal engineering was still at its infancy to tailor make the desired chiral space group for a given molecule. A modified approach to address this issue was introduced wherein a homochiral auxiliary was either attached or co-crystallized with the achiral molecule. This ensured the resultant mixture crystallized in a non-centrosymmetric fashion thus creating a chiral space group.

The chiral auxiliary can be tethered to an achiral molecule either covalently or ionically. The ionic approach seemed to be more practical and advantageous in terms of easy introduction and removal. Also, the ionic salts have higher melting point, thus proving it to be superior over covalently attached chiral auxiliary in preserving the topochemical control ensuring higher asymmetric induction during photochemical transformation. The chiral auxiliary merely serves as

a tool to access chiral crystal and the asymmetric induction is in principle achieved through the crystal lattice of the molecule. Scheffer and coworker have contributed extensively and demonstrated the wide applicability of this approach to several photochemical transformations in the solid-state.[39] For example, they reported solid-state photoisomerization of *trans,trans*-2,3-diphenyl-1-benzoylcyclopropane derivative (**35**) tethered to ionic chiral auxiliary (Scheme 1.12).

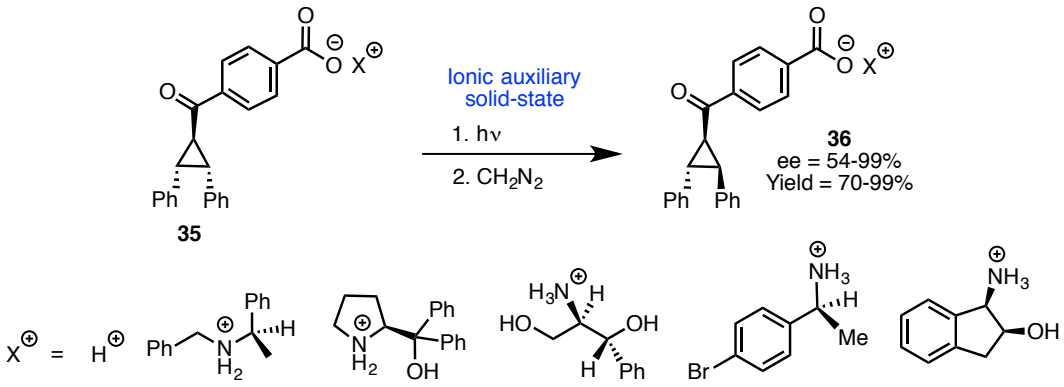

Scheme 1.12: Photoisomerization of ionic auxiliary tethered diphenyl-1-benzoylcyclopropane derivative **35**.

The resulting photoproduct was derivatized to its corresponding methyl ester and analyzed for its *ee.* Out of five chiral auxiliaries examined, three of them resulted in very high *ee* (>90%) while the other two gave rather moderate *ee*'s (54-67%). The possible origin for the observed higher selectivity was attributed to both topochemical and conformational effect. On the other hand, the lack of crystallographic information prevented them from deducing the exact reason for the lower selectivity. Following up their research, the same group elegantly demonstrated a method to access optically active amine through Norrish-Yang cyclization of ionic chiral auxiliary derivatized amino ketone (Scheme 1.13).[40] Irradiation of the aminoketone (**37**) in solution resulted in racemic *cis*- and *trans*-cyclobutanol (**38** and **39**) in 2:1 ratio along with achiral cleavage product (**40**). However, in the ionic auxiliary crystalline state, they reacted in a highly stereoselective fashion to yield cyclobutanol products with *ee* >92%. Also, the minor *trans*-cyclobutanol (**39**) was significantly reduced (ratio >12:1).

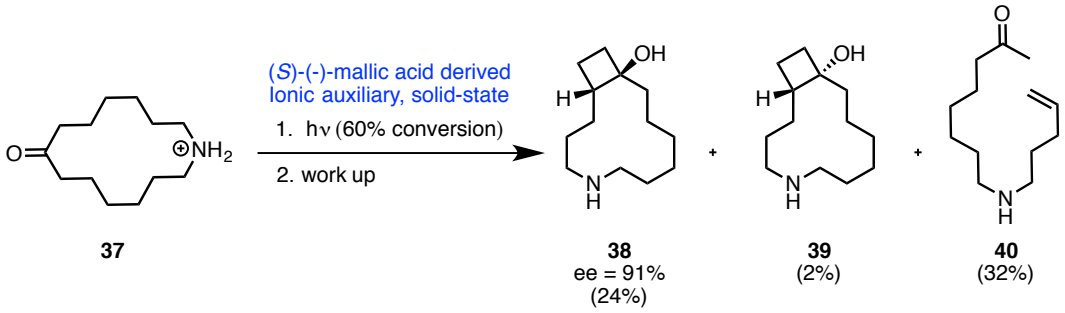

Scheme 1.13: Norrish-Yang reaction of ionic salt of aminoketone derivative **37**.

The high *ee* in the photoproduct (**38**) was attributed to the geometric orientation and restriction of molecular motions in the crystalline lattice that allowed for high topochemical control in the reaction. While this method allows for excellent enantiocontrol in the photoreaction, the formation of cleavage product (**40**) could not be suppressed that seemed to dominate the product(s) yield. A possible reason for this could be the competitive reaction of H-abstraction and cleavage of the 1,4-biradical intermediate.

These ionic chiral auxiliaries provide an excellent avenue for performing highly stereoselective phototransformations. Also, various attributes of these chiral crystals such as the ease of preparation, crystallinity, high melting point due to strong lattice forces, high topochemical control…etc., makes them attractive for asymmetric phototransformations.

1.5.3. Asymmetric photoreactions in nanocrystalline suspensions

One of the elegant approach to pre-organize the chromophores in solution yet retain the success of a solid-state photoreaction is to perform reaction in nanocrystalline suspension. The advantage of this strategy is manifold and the prime one being the scalability of the photoreactions that allow us to perform reactions in multi-gram scales. The conversion in the larger crystals is a concern as they not only crack over extended period of irradiation (losing topochemical control) but also become opaque thus inhibiting the photoreaction of starting material that is inside the crystal matrix. However, the nanocrystals, owing to their smaller size can react to complete conversion and retain their crystallinity allowing one to perform single-

crystal-to-single-crystal transformations. Nakanishi and coworkers demonstrated the first topochemical polymerization of diolefin derivatives *viz*., *p*-phenylenediacrylate (**41**) and 2,5-distyrylpyrazine (**42**) that occurred single-crystal-to-single-crystal.[41]

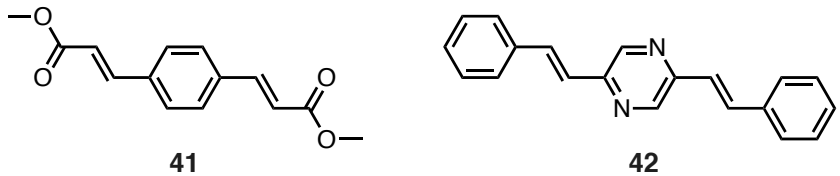

41
p-phenylenediacrylate

42
2,5-distyrylpyrazine

Figure 1.7: *p*-Phenylenediacrylate **41** and 2,5-distyrylpyrazine derivative **42** employed in single-crystal-to-single-crystal phototransformations.

The nanocrystals were prepared by the reprecipitation approach,[42] wherein a saturated solution of diolefin in THF was injected into water while stirring vigorously. The nanocrystals were then subjected to photopolymerization. The other methods that are utilized to prepare nanocrystals involve fast evaporation method[43], sonocrystallization techniques[44]… etc. Garcia-Garibay and coworkers elegantly demonstrated the application of this method by stereocontrolled synthesis of natural product (α)-cuparenone (Scheme 1.14).[45]

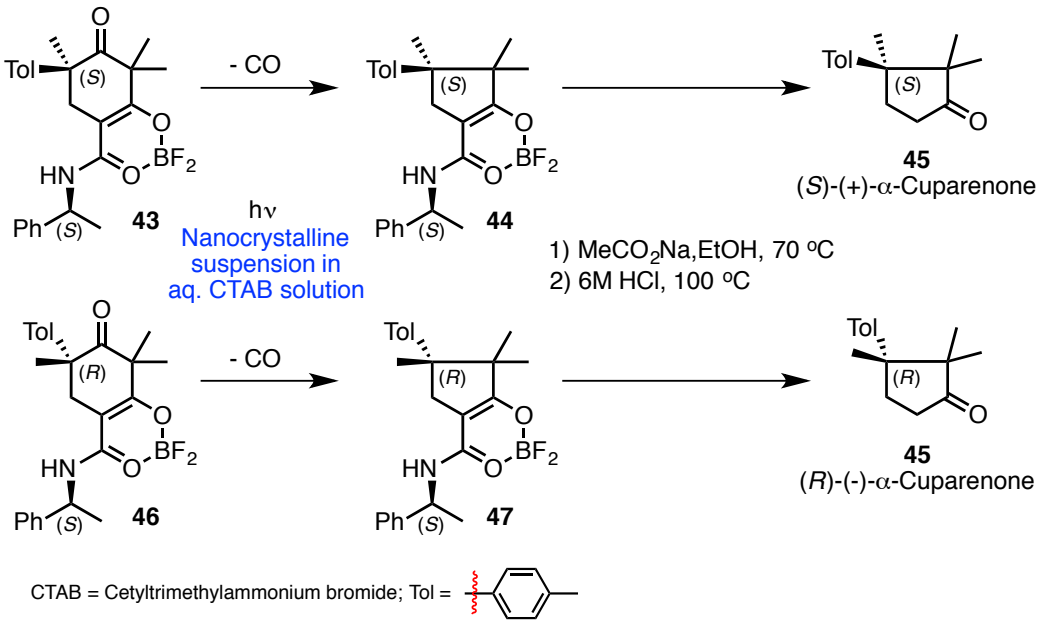

Scheme 1.14: Synthesis of cuparenone **45** natural product through photoreaction in nanocrystalline suspension (reproduced from 45; Copyright: 2007 WILEY-VCH Verlag GmbH & Co. KGaA, Weinheim).

They synthesized both the enantiomer of the natural product by starting with optically pure intermediates that was accessed through resolution of chiral auxiliary tethered β-keto-methylbenzamide derivatives (**43** and **46**). Using this photochemical nanocrystalline solid-solid transformation strategy they were able construct adjacent quaternary chiral center in one step and access both the enantiomers (> 99% *ee*) of the (α)-cuparenone (**45**) in 60% yield over 4 steps, which was a significant improvement over the existing methods to access these natural products.

1.5.4. Asymmetric photoreactions using chiral solvents

Creating asymmetry in the environment of the reacting species, at least in principle can effect asymmetric induction during photochemical transformations. But the type and the extent of interaction that the chiral environment has on the reactants dictate the effectiveness of this approach. Asymmetric induction by chiral solvent was one of the earliest strategies evaluated towards asymmetric phototransformations. Weiss and coworkers examined the *cis-trans* isomerization of 1,2-diphenylcyclopropane (**48**) in the presence of chiral solvents (**50a-c**) and triplet sensitizer acetone or singlet sensitizer naphthalene (Scheme 1.15).[46]

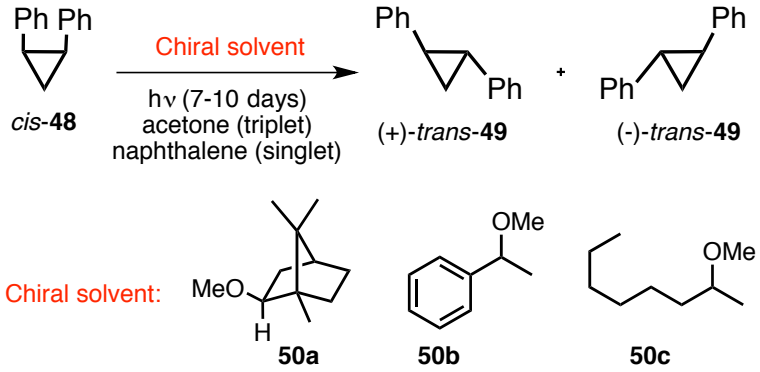

Scheme 1.15: *Cis-trans* isomerization of 1,2-diphenylcyclopropane **48** in chiral solvents.

The analysis of the isolated *trans* sample revealed that the net asymmetric induction in the sample was very poor (2.3% optical purity). The low level of selectivity was attributed to the inability of the chiral solvents to create chiral environment (chiral center of the solvent to be present near the locus of isomerization) or poor interaction. Similarly, Nakazaki and coworkers reported *cis-trans* isomerization of α,β-unsaturated ketone that occurred under direct excitation in presence of L-(+)-tartarate, which resulted in optical purity of 0.5-1.0%.[47] Seebach and coworkers reported asymmetric photopinacolization of ketones in the presence of chiral amino ethers (Scheme 1.16).[48,49] In this reaction, the chiral amine (**52**) acted both as a solvent and a hydrogen donor.

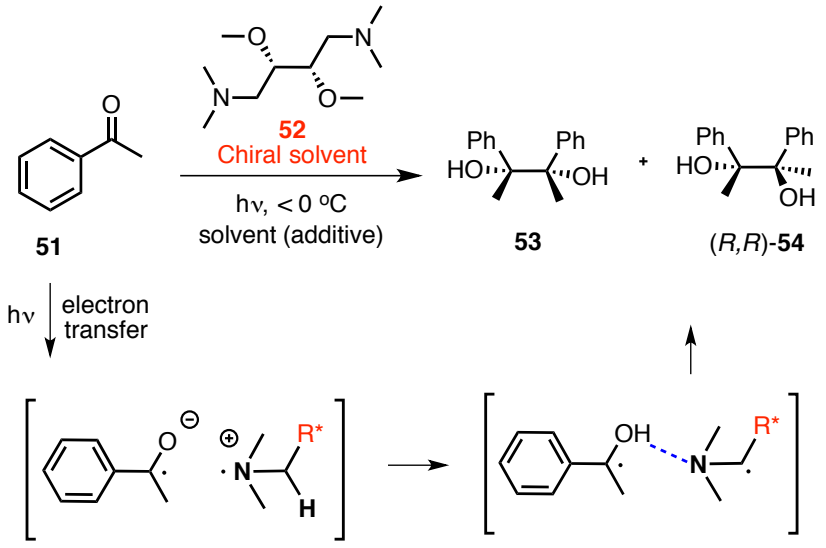

Scheme 1.16: Asymmetric photopinacolization of ketones in presence of chiral amino ethers.

The optical yield obtained for this reaction was significantly higher for this class of chiral inductors. During the reaction, the electron transfer from the amine to the excited ketone resulting in a charge transfer complex. The proton transfer between the charge transfer complex produced a radical pair, which upon combination resulted in the corresponding pinnacol that was biased by the weakly coordinated chiral amine leading to chiral induction. Further, the observation was extended to various carbonyl compounds such as benzaldehyde, propiophenone *etc*., that in presence of additives such as pentane, toluene or methanol resulted in enhanced optical yield (up to 23%). Boyd and coworkers investigated the photochemical synthesis of oxaziridines (**56**) from prochiral nitrones (**55**) in presence of chiral solvents.[50] The reaction proceeded at -78 °C with 1:1 mixture of fluorotrichloromethane and chiral 2,2,2-trifluorophenylethanol to result in enantioenriched oxaziridine product (**56**) (Scheme 1.17). The origin of stereoselectivity was explained based on the chiral complex generated between the nitrone and chiral solvent that was stabilized by hydrogen bond. The temperature and the substituent on the nitrogen greatly affected the outcome of the enantioselectivity in the reaction.

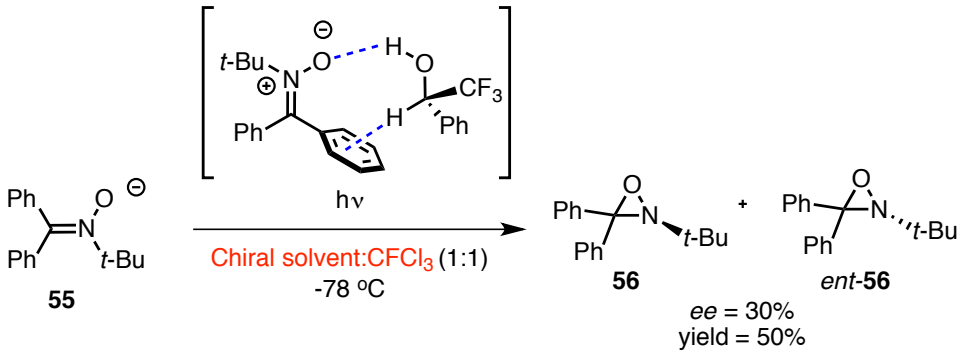

Scheme 1.17: Asymmetric synthesis of oxaziridines from nitrones in presence of chiral solvents.

While the initial investigations shown to be optimistic, further research along these lines proved to be futile. The main reason for its failure laid in the ill defined role played by the chiral solvents such as poor stereodifferentiation as a result of less active role in the reaction and passive chiral environment that could not be defined. Yet another issue associated with this approach is the use of large excess of chiral element to impart chiral induction in the desired reaction that severely limits its use in the large-scale reactions.

1.5.5. Asymmetric phototransformations mediated by chiral sensitizers

The success realized in asymmetric phototransformations through the confinement of chromophores (solid-state photoreactions or supramolecular chemistry) or using chiral light source in solution mainly served as a tool for mechanistic investigations and academic curiosity. Some of the fundamental limitations of these methods such as challenges involved in scaling up of reactions (scalability) posed a huge obstacle in their utility in synthetic chemistry. Photoreactions that happen in solution eliminated this bottleneck by providing an avenue for scalability, but presented with whole new set of challenges in controlling stereoselectivity in phototransformations. Multiple conformations of chromophore that exist in solution and their rapid equilibrium largely affected the process of asymmetric induction. To address this problem, several approaches were looked at such as photoreactions in presence of templates and external chiral source. One of the efficient methods introduced to achieve stereoselectivity was to employ chiral sensitizer. Chiral sensitizers often interacts with substrate that undergoes photochemical

transformation through “excited-state sensitizer-substrate interactions” thus influencing the stereochemical outcome of a reaction.[51] The first report of enantio-differentiating photosensitization was by Hammond and coworkers, who employed a chiral amide to influence the stereochemical isomerization of *trans*-1,2-diphenylcyclopropane (**57**) (Scheme 1.18).[52]

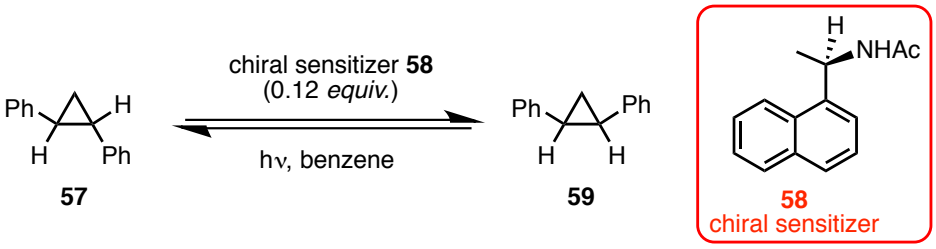

Scheme 1.18: Photoisomerization of *trans*-1,2-diphenylcyclopropane mediated by chiral sensitizer.

A benzene solution of cyclopropane (**57**) was irradiated long enough to result in photostationary state of *cis-trans* isomers (1.03), followed by the specific rotation analysis that revealed a definite asymmetric induction in the isomerization process. They attributed the enantioenrichment to the formation of intimate interaction between chiral donor and acceptor. Following this research, several uni- and bimolecular photoreactions were reported that resulted in excellent selectivity in the photoproduct. For example, Inoue and coworkers reported an elegant approach towards enantioselective isomerization of (*Z*)-cycloheptene to (*E*)-cycloheptene using chiral alkyl pyromellitates (Scheme 1.19).[53] The enantioenriched (*E*)-cycloheptene was trapped *in situ* with dienes at -70 ^{o}C that resulted in the Diels-Alder adduct (**63**) or by oxidation with OsO_4 to afford *trans*-1,2-cycloheptanediol (**62**).

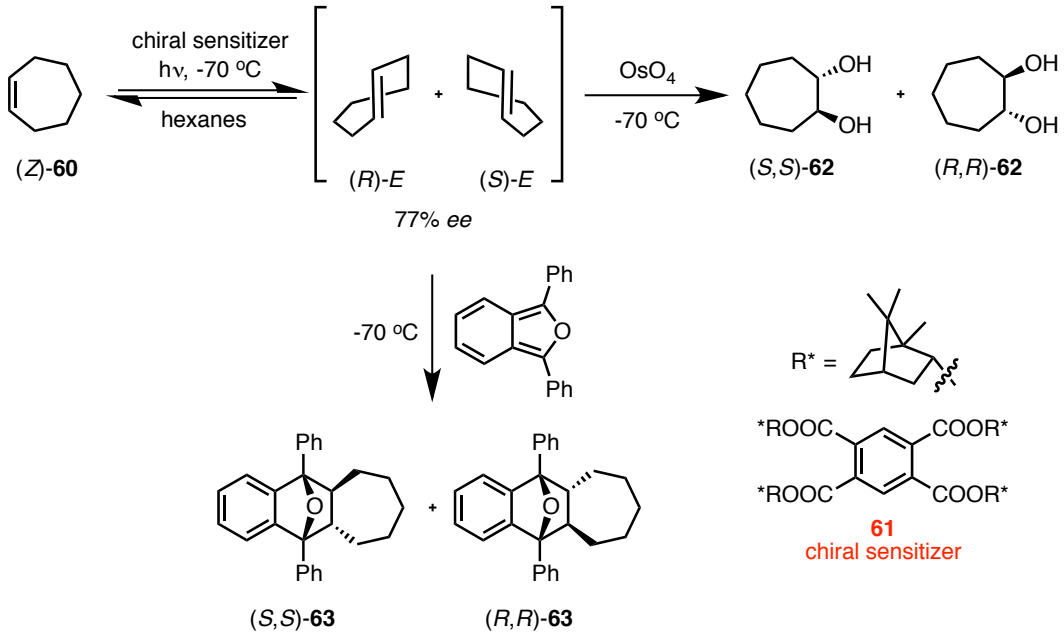

Scheme 1.19: Enantioselective isomerization/ trapping of (*Z*)-cycloheptane.

The thermal [4+2]-cycloaddition was assumed to undergo with stereoretention and the selectivity in the thermal product displayed enantioenrichment in the photoisomerization process. Detailed investigations in related systems revealed that the polar solvents were less efficient for the isomerization reaction leading to poor *ee* in the product. Also, the fluorescence quenching studies bolster the hypothesis that intimate sensitizer-substrate interactions are needed to achieve higher selectivity. Extension of this approach to bimolecular reactions was also investigated, and the studies revealed that the stereoselectivity achieved in the bimolecular reactions are inferior compared to unimolecular reactions. For example, Schuster and coworkers reported enantioselective Diels-Alder reaction between cyclohexadiene (**64**) and styrene derivatives (**65**) sensitized by atropisomeric tetracyanobinapthyl and bis(2,10-dicyanoanthracence) derivatives (Scheme 1.20).[54,55] The reaction proceeded via a ternary complex of singlet excited sensitizer, diene and dienophile (“triplex Diels-Alder”).

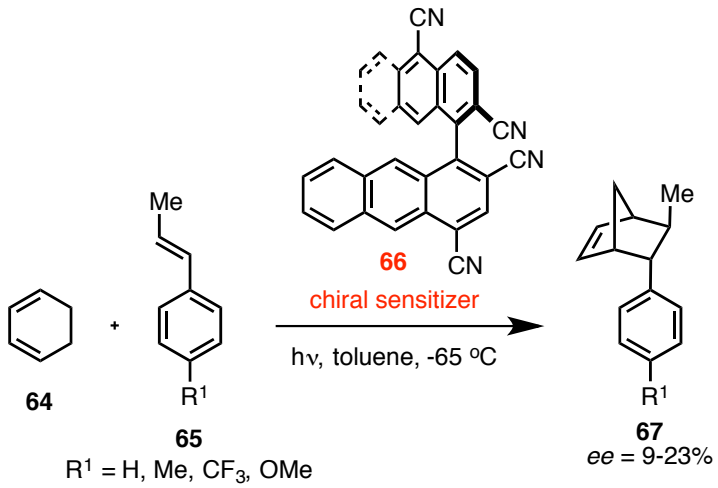

Scheme 1.20: Enantioselective Diels-Alder reactions of styrene derivative mediated by chiral sensitizer.

The photophysical studies revealed the formation of two diastereomeric exciplexes between the sensitizer and styrene that react with the diene. The diastereomeric exciplexes equilibrated even at low temperature (-65 ^{o}C) albeit slowly and the observed *ee* in the product was the result of trapping of the complexes by diene (**64**).

Continued effort in stereodifferentiating sensitization reactions revealed several unique details about the mechanism and limitations of this methodology. The deeper understanding gained through the research provided an avenue to improve the yield and selectivity in the desired reaction. The reactions that are promoted by weak interactions such as exciplex formation between the sensitizer and the substrate are highly sensitive to external environment such as solvent, temperature and concentration. Judicious choice of these parameters will allow us to obtain higher selectivity in the desired photochemical transformations.

1.5.6. Diastereoselective phototransformations using chiral auxiliary

The presence of an optically pure chiral entity in a reaction should impart certain level of asymmetric induction in a given reaction. These diastereoselective reactions were given considerable importance, as several naturally occurring chiral entities were accessible in large quantities. In a situation where the chiral element removed after the reaction (removable chiral

auxiliary), the methodology becomes more useful as it not only provides useful handle to separate the diastereomeric photoproducts by chromatographic techniques, but also allows us to reuse them for further cycle's of reactions, at least in principle. While several attempts were not as fruitful as desired, some of the diastereoselective phototransformations provided excellent chiral induction in the process and led to new directions in asymmetric photochemistry. For example, in 2001, Mariano and coworkers reported highly diastereoselective intramolecular [2+2]-photocycloaddition of chiral auxiliary tethered eniminium salts (Scheme 1.21).[56]

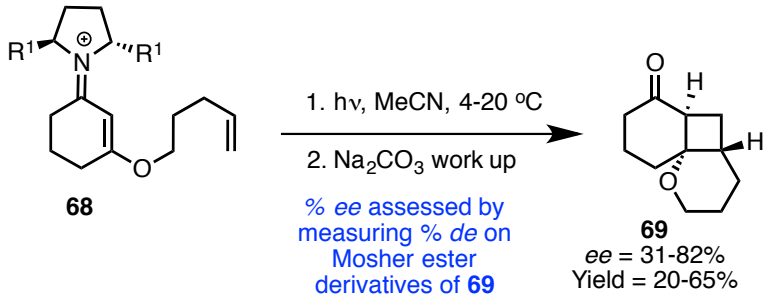

Scheme 1.21: [2+2]-photocycloaddition of chiral eniminium salt **68**.

The C_2-symmetric pyrrolidino-cyclohexeniminium perchlorates (**68**) in acetonitrile underwent facile [2+2]-photocycloaddition, which up on base work up resulted in cyclobutane derivatives (**69**) with good *de*. The observed selectivity was the result of facial shielding provided by the R^1 substituent and the steric bulk of which dictated the outcome of *de* in the photoproduct. Döpp and coworkers reported a highly diastereoselective photo Diels-Alder reaction of 1-acetonapthone (**70**) to a chiral auxiliary derivatized acrylonitrile (**71**) (Scheme 1.22).[57]

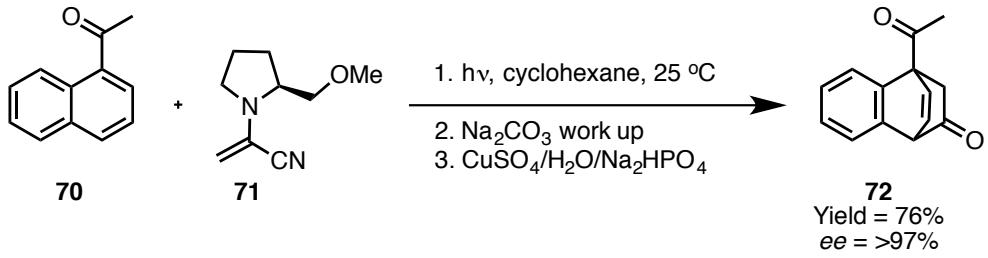

Scheme 1.22: Photo Diels-Alder reactions of chiral ionic salt.

The reaction proceeded smoothly in cyclohexane to furnish the desired Diels-Alder adduct in good yield and selectivity. Further hydrolysis of the adduct resulted in enantioenriched bicyclic systems. Griesbeck and coworkers reported a highly enantio- and diastereoselective synthesis of diazepine (**74**) derivatives through decarboxylative photocyclization (Scheme 1.23).[58]

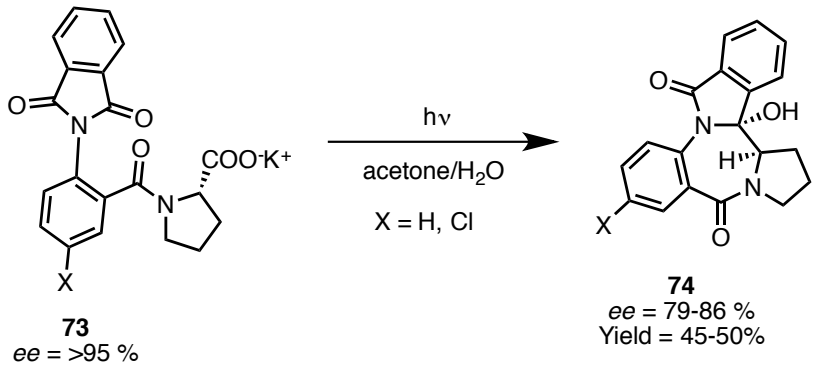

73
ee = >95 %

74
ee = 79-86 %
Yield = 45-50%

Scheme 1.23: Stereoselective synthesis of diazepine derivatives through decarboxylative photocyclization.

The origin of high level of stereoselectivity in the product was explained based on the memory of chirality, wherein the intermediate 1,7-diradical which is formed via decarboxylation retains the chirality via memory effect. The reaction proceeded through a mixture of singlet and triplet biradical intermediate in which the singlet underwent cyclization stereospecifically and the triplet had a leakage in the chiral transfer that was reflected in the enantiomeric excess in the product.

1.5.7. Asymmetric phototransformations mediated by organized assemblies

The photoreaction in confined media is probably an inspiration from nature, where several transformations occur with in confined spaces. The supramolecular cavities serve as a packet that accommodate a guest molecule and sets them in a reaction ready state, which affects the kinetics, selectivity and the outcome of a given reaction. Initial investigations involved the employment of naturally occurring supramolecules such as cyclodextrins or serum albumins. Insights gained from these assemblies led to several synthetic scaffolds such as modified cyclodextrins, zeolites, cucurbiturils, calixarenes, and micelles etc., which were more promising and efficient in promoting asymmetric phototransformations. Ramamurthy and coworkers reported highly enantio-differentiating 4π-photocyclization of tropolone derivatives (**75**) in presence of chirally modified zeolites (Scheme 1.24).[59-61] Several approaches such as zeolites coadsorbed with chiral inductor, chiral auxiliary tethered prochiral substrate, and combination of both were attempted to evaluate the outcome of the stereoselectivity of the photoreaction.

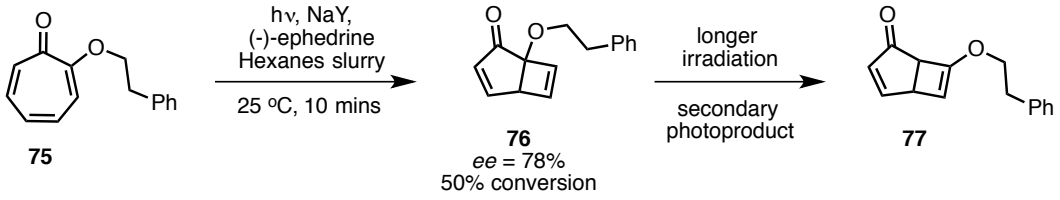

75

76
ee = 78%
50% conversion

77

Scheme 1.24: [2+2]-Photocycloaddition of tropolone ethers.

Irradiation of a slurry of tropolone ether adsorbed NaY in hexanes along with chiral inductor (-)-ephedrine resulted in bicyclo[3.2.0] photoproduct (**76**) in 78% *ee*. However, longer irradiation resulted in the formation of secondary photoproduct (**77**) along with reduction in the enantiomeric excess (*ee* = 68% for 45 mins irradiation). Moisture in the zeolite critically affected the selectivity in the photoproduct, thus posing stringent limitation on the reaction conditions. The origin of selectivity was explained based on “three-point interaction” where the tropolone ether and the ephedrine are held together by H-bonding interaction that are in turn held on the surface of zeolite through cation-π interaction. Also, the cation present in zeolite played significant role in bringing about the selectivity. Similarly, Inoue and coworkers reported enantioselective

photoreaction of photodimerization of 1-anthracence carboxylates (AC, **78**) mediated by γ-cyclodextrin (Scheme 1.25).[62]

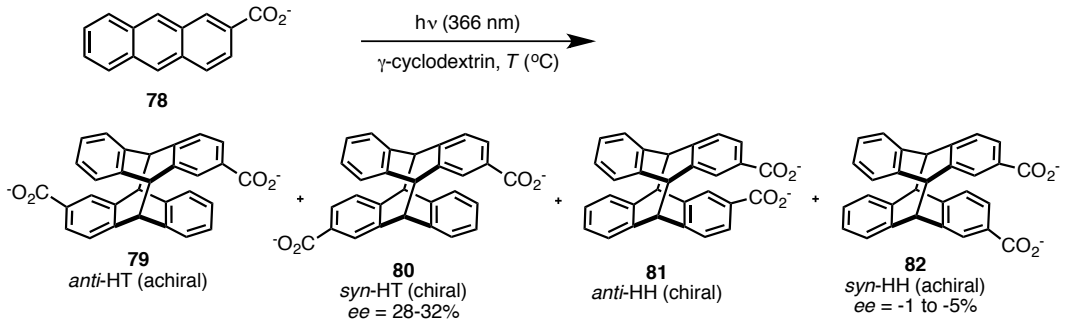

Scheme 1.25: Photodimerization of anthracence carboxylates **78** mediated by supramolecular host.

The γ-cyclodextrins and AC formed 1:2 inclusion complex in the ground state, which upon irradiation resulted in photodimerization. The distribution of photoproducts reflected the ratio of different structural host-guest complexes formed in the ground state. The enantioselectivity in the chiral photoproducts depended on the temperature. For example, the *ee* at 25 and 0 ^{o}C was 32% and 41% respectively. It was one of the highest selectivity obtained for the photodimerization reaction. Sivaguru and coworkers reported photodimerization of 6-methylcoumarin (**83**) in the presence of catalytic amount of cucurbit[8]uril (Scheme 1.26).[63,64] Photodimerization in the absence of cucurbit[8]uril (CB[8]) was ineffective only resulting in 10% conversion in 1 h with mixture of *syn* and *anti* photoadducts. On the other hand, in the presence of 10 mol% CB-[8], the reaction proceeded efficiently with high *syn* selectivity (*syn* HH:HT = 70:30).

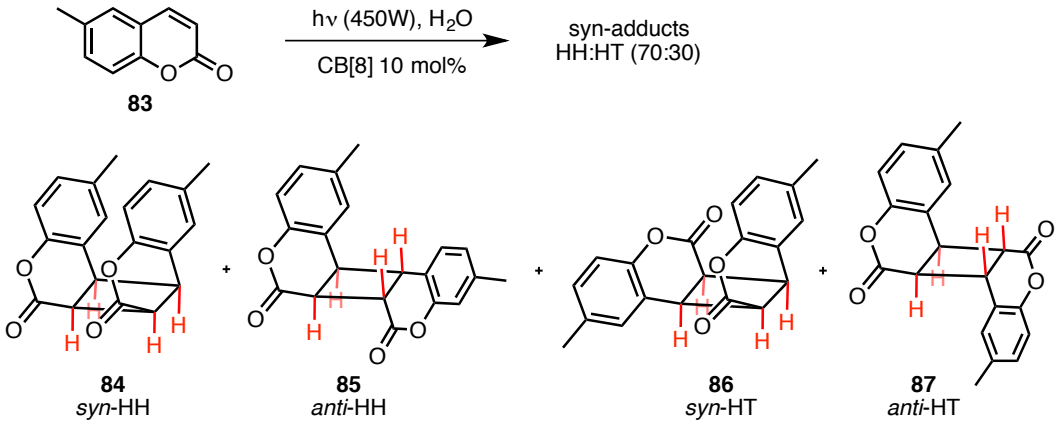

Scheme 1.26: Photodimerization of 6-methyl coumarin **83** mediated by cucurbit-[8]-uril.

Photophysical and kinetic study revealed that the catalyzed reaction was at least 9 times faster than the uncatalyzed reaction. The amount of CB[8] played a critical role in the dimerization reaction. The best efficiency was achieved at 70 mol% beyond which the efficiency dropped down which was attributed to the formation of aggregation of host and formation of 1:1 host-guest complex. They also carried out detailed mechanistic study and proposed catalytic cycle in which the formation of 1:1 complex determined to be the rate-limiting step.

1.5.8. Asymmetric phototransformations mediated by chiral templates

The organized assembly generated by chiral scaffolds (hosts) and prochiral substrates (guests) through non-covalent interactions provides necessary chiral bias for the chiral induction process to take place. However, the outcome of the product's selectivity depends on factors such as how efficient the host can bind to the prochiral guest (which is determined by association constant *Ka*), turn over (to avoid background racemic reaction) and its ability in facial discrimination. Apart from this, the stoichiometry of the chiral host required for the reaction largely depend on the association constant and the product inhibition. While early investigations on template mediated photochemistry were restricted to naturally occurring chiral scaffolds, important insights gained from these studies led to the tailor made chiral scaffolds that promoted stereoselective photoreactions of prochiral photochromophores or reactants. Bach and coworkers

introduced and demonstrated wide utility of Kemp triacid hydrogen bonding template that proved to be superior over existing templates and had wide scope in promoting enantioselective photoreactions. For example, they reported highly enantioselective intramolecular [2+2]-photocycloaddition of 2-quinolone derivatives (**88**) to yield enantioenriched complex cyclobutane scaffolds (Scheme 1.27).[65]

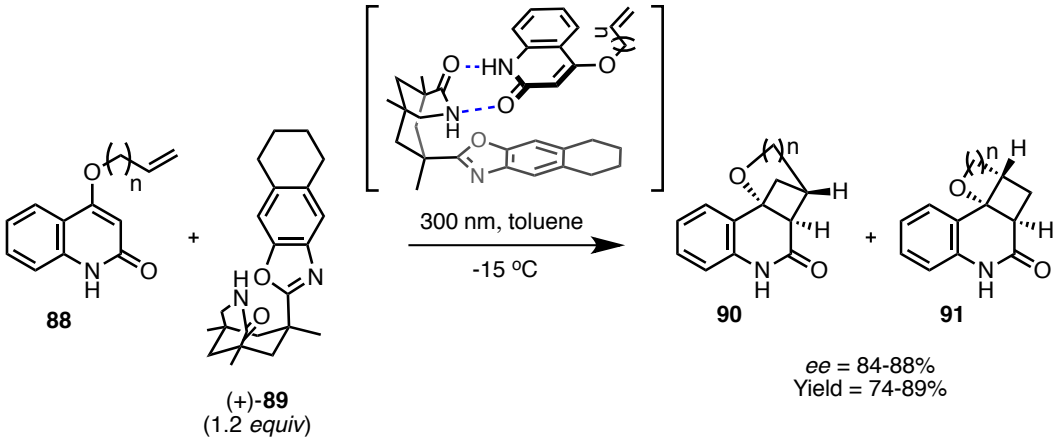

Scheme 1.27: Enantioselective intramolecular [2+2]-photocycloaddition of 2-quinolone derivatives **88** mediated by chiral lactam **89**.

The rigid template backbone provided efficient facial discrimination up on binding (Ka = ~580 M^{-1} determined from binding studies carried out on **89** and 2-quinolinone) to the 2-quinolinone leading to enantioselectivity in the photoreaction. They also showed that up on using the optical antipode of the chiral lactam ((-)-**89**), they could switch the enantiomer in the photoproduct thus allowing them to access both the stereoisomers of the photoproducts. By simple modification of the template backbone that is instilled with the sensitizer ((+)-**93**), they were able to perform sensitized enantioselective photoreactions efficiently (Scheme 1.28).[66]

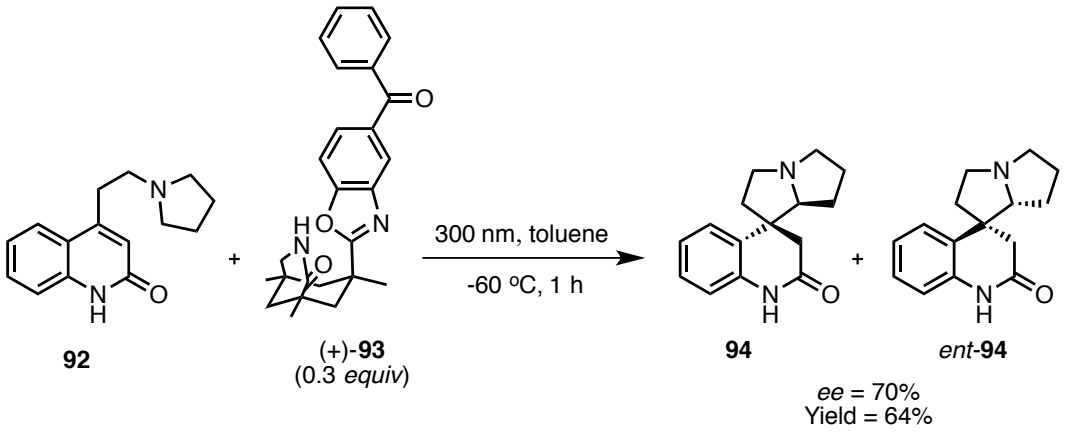

Scheme 1.28: Enantioselective synthesis of pyrrolizidine **94** through photo-induced electron transfer.

The reaction was initiated by photo-induced electron transfer (PET) between the excited benzophenone (part of the template) and amine (which is a part of the reactant) followed by the conjugate addition of the radical to the quinolinone resulting in enantioenriched spirocyclic pyrrolizidine derivatives (**94**). Once again, the origin of enantioselectivity was explained based on the chiral environment provided by the template when the prochiral starting material was bound. As the sensitizer is part of the chiral template, it provided them an opportunity to employ sub-stoichiometric amount of the chiral template. However, the reduction in the enantioselectivity was attributed to the racemic background reaction, which occurred to a significant extent even in the presence of 30 mol% of the template. Nevertheless, benzophenone tethered lactam which played multiple role such as H-bonding chiral template, sensitizer, facial discriminator was an elegant approach towards enantioselective photocatalysis.

In sensitized photoreaction, the excited sensitized transfers its energy to the ground state substrate thus initiating the photoreaction. For this process to occur efficiently (for that matter to occur at all) the sensitizer should have higher or comparable energy states that of the substrate. This puts restriction on the choice of sensitizer that one can employ in the photoreactions. Recent efforts to address this issue resulted in novel chiral scaffolds for the enantioselective photoreactions. For example, Sivaguru, Sibi and coworkers introduced novel binaphthyl thiourea

organocatalyst that was proved to be superior in promoting highly enantioselective [2+2]-photocycloaddition of coumarin derivatives (Scheme 1.29).[67]

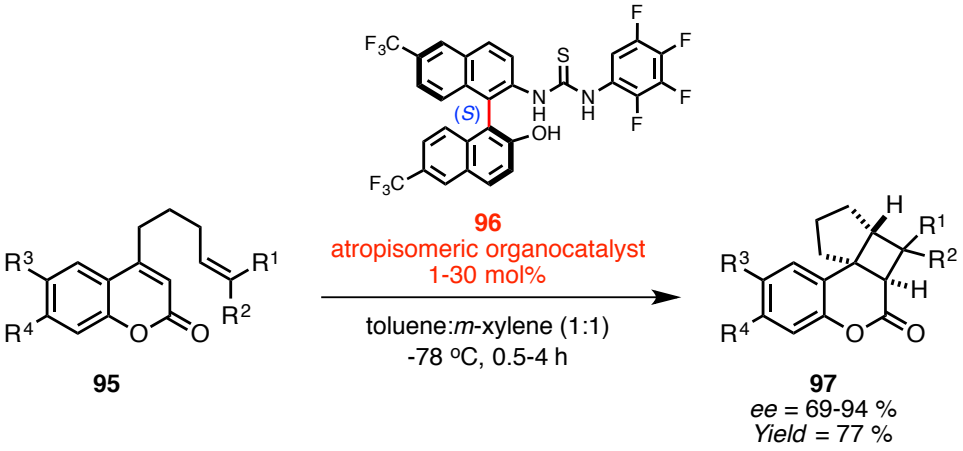

Scheme 1.29: Enantioselective intramolecular [2+2]-photocycloaddition of coumarin mediated by atropisomeric thiourea.

Detailed photophysical analysis revealed that the organocatalyst has lower triplet energy than the prochiral coumarin substrate (**95**), thus an uphill energy transfer was not feasible. However, the substrate bound catalyst resulted in the formation of exciplex (static and dynamic excited state complex) thus allowing facile energy transfer. They also invoked a dual catalytic cycle depending on the amount of organocatalyst present in the reaction (catalyst loading).

These findings not only showed a steep increase in the potential of asymmetric phototransformations but also the practicality aspect of the methodologies introduced in recent literature. Also, these impressive improvements will further pave way for new ideas and approaches that will make the asymmetric phototransformation in solution more viable in the synthetic community.

1.6. Impact of axial chirality in asymmetric transformations

A special class of stereoisomers that lack stereogenic center, yet exist as a pair of enantiomers are called atropisomers (figure 1.8). The chirality arises due to the restricted rotation around a single bond that is dictated by several factors and the important one being the sterics around the chiral axis. This phenomenon in compounds was first observed and reported by Christie and Kenner in 1922 in 6,6'-dinitrobiphenyl-2,2'-dicarboxylic acid (**98**).[68] Since then, several new atropisomeric scaffolds have been identified and designed for various applications in the field of chemistry.[69,70] The important application of atropisomers is in the field of organometallic chemistry as a chiral ligand to the metal center.[71] For example, suitably substituted biphenyl (**99**) and binaphthyl (**100**) are widely used as a coordinating ligand to metal center that binds to the substrate and promote asymmetric transformation.

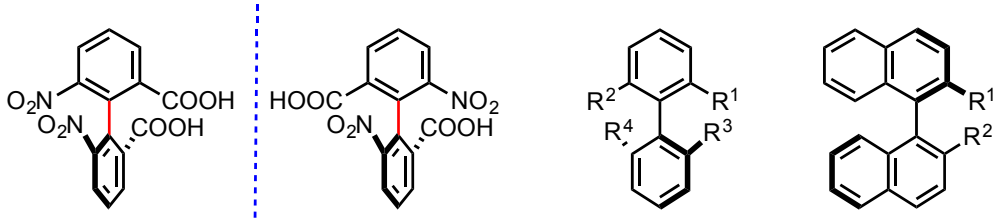

98
6,6'-Dinitrobiphenyl-2,2'-dicarboxylic acid

Figure 1.8: Atropisomeric scaffolds. left: (*P*) and (*M*)-isomers of 6,6'-Dinitrobiphenyl-2,2'-dicarboxylic acid **98**; middle: biphenyl **99** and right: binaphthyl **100**.

While early investigations were mainly focused on the kinetic analysis of these twisted molecules such as racemization barrier, mechanism of racemization, later in the mid 90's, first application of these molecules in the "atropselective"[72] reactions were demonstrated by Curran and Clayden. Their findings kindled new interest in atropisomeric molecules as potential chiral auxiliaries, catalysts and reagents to perform stereospecific transformations. Also, the presence of axial chirality imparts new reactivity/selectivity on compounds that are thus far not observed in achiral or point chiral molecules.

1.6.1. Atropisomeric transformations in thermal chemistry

In 1991, Fuji and coworkers reported the stereospecific alkylation of a ketone (**101**) in which the alkylated product (**102**) retained the stereochemistry of the starting material (Scheme 1.30).[73] The asymmetric induction observed in the product was attributed to the transient axial chirality generated in the achiral enolate intermediate. Presence of the axial chirality was proved by trapping the enolate as an enol ether that showed optical activity.

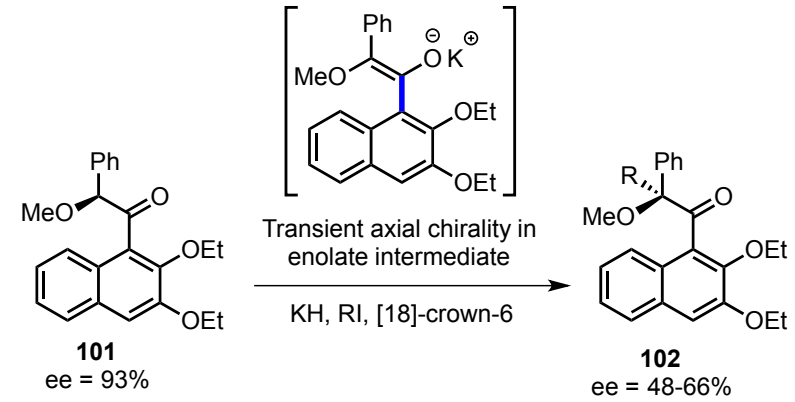

Scheme 1.30: Enantiospecific alkylation of ketone derivative **101**.

This report was followed by Curran's work that served as the first report of stereospecific thermal transformations of atropisomeric compounds. In 1994, Curran and coworkers reported stereospecific transformations of atropisomeric maleimides and acrylanilides with very high atropselectivity.[74] For example, atropisomeric acrylanilide (**103**) underwent facile cycloaddition with benzonitrile oxide to give isoxazoline derivatives (**104** and **105**) with excellent diastereoselectivity (*dr* = 97:3) (Scheme 1.31).

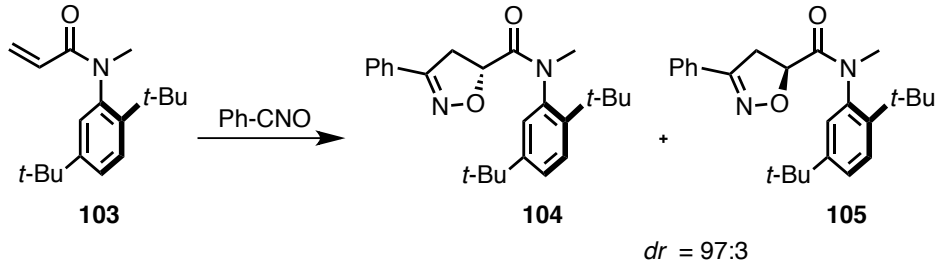

Scheme 1.31: Atropselective photocycloaddition of acrylanilides with benzonitrile oxide (Reproduced with permission from reference 74; Copyright 1994 American Chemical Society).

These atropisomers were stable at room temperature but underwent racemization at elevated temperature due to the labile chiral axis. They also reported radical cyclization of axially chiral acrylanilides (**106**) in which the axial chirality in the starting material was transferred to the point chirality in the product with very high fidelity (Scheme 1.32).[75]

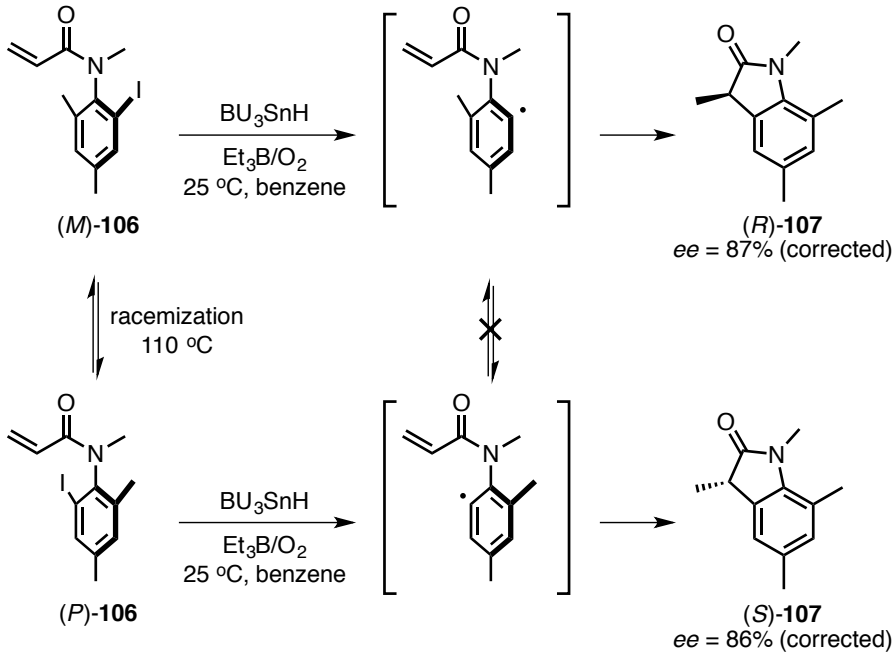

Scheme 1.32: Atropselective radical cyclization of *o*-iodo acrylanilide derivatives (Reproduced with permission from reference 75. Copyright 1999 American Chemical Society).

The acrylanilides had fairly high-energy barrier to racemization (ΔG = 30.8 kcal·mol^{-1}) that prevented them from undergoing racemization at ambient temperature. However, the radical

intermediate generated did not have such high racemization barrier due to the loss of iodide group. Fortunately, in these molecules, the radical cyclization occurred at a much higher rate constant than the racemization leading to excellent chirality transfer in the newly formed stereocenter in the oxindole derivatives (**107**). During the same period, Clayden and coworkers were extensively involved in the evaluation of atropisomeric amides (**108**) as a potential avenue to perform stereospecific transformations.[76] For example, in 1996, they reported stereospecific reduction of ketones in atropisomeric amides (Scheme 1.33).[77]

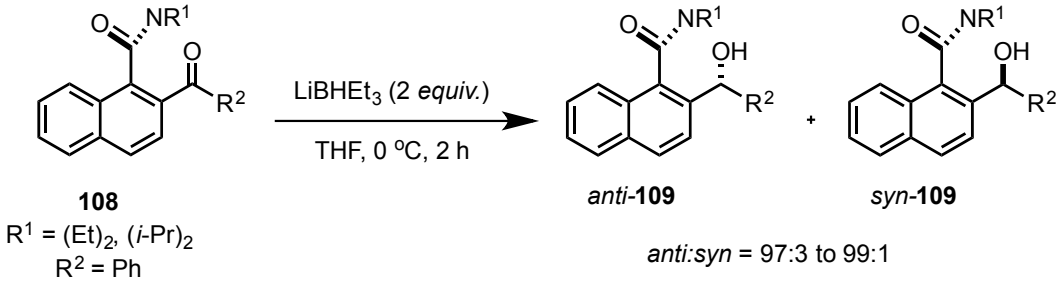

108
R^1 = $(Et)_2$, $(i\text{-}Pr)_2$
R^2 = Ph

anti-**109**

syn-**109**

anti:syn = 97:3 to 99:1

Scheme 1.33: Diastereoselective reduction of atropisomeric amide derivative **108**.

The observed selectivity in the product was rationalized based on the ability of the atropisomer to bias/direct the incoming nucleophile. The nucleophile approached the ketone from the less hindered face away from the amide unit. Enhanced selectivity was observed if bulky nucleophile such as $LiBHEt_3$ was employed. They also expanded the utility of these atropisomeric amides in effecting stereospecific electrophilic addition reactions.[78]

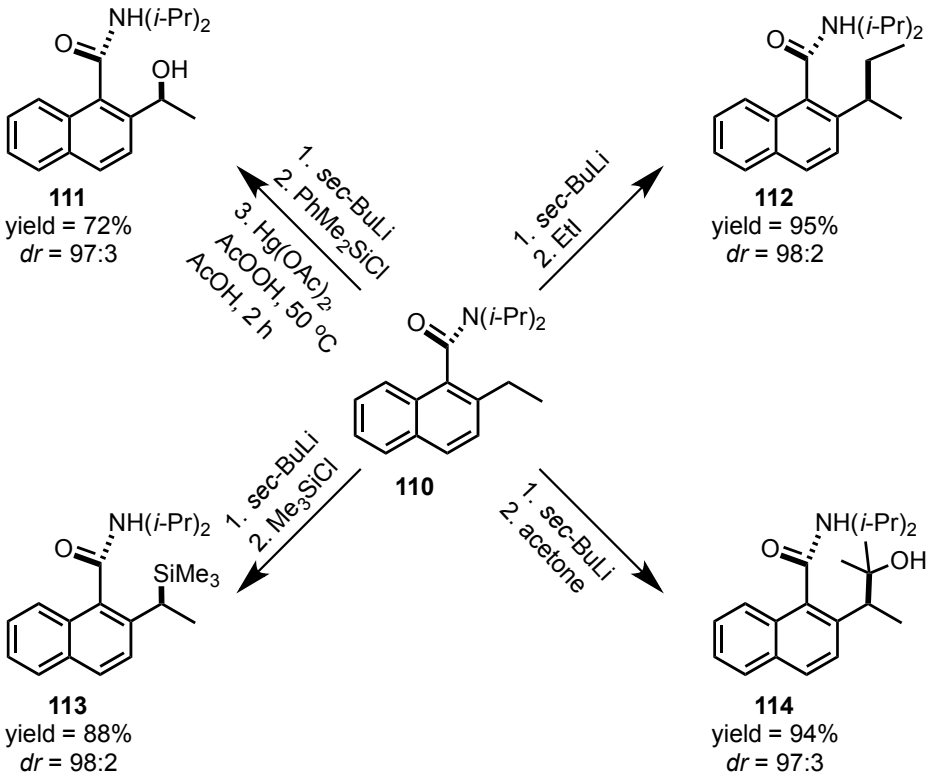

Scheme 1.34: Diastereoselective reactions of ortho lithiated atropisomeric amide derivative **110**.

The laterally lithiated atropisomeric amides adds to several electrophiles to furnish products with excellent diastereoselectivity (Scheme 1.34). Configuration of the major product was assigned as *syn* with respect to the amide carbonyl group and further confirmed by X-ray crystal structure in some cases. Once again, the origin of stereoselectivity was attributed to the stable axial chirality in the atropisomeric amide.

1.6.2. Asymmetric photochemistry of frozen chirality

While the thermal chemistry of atropisomeric compounds was moving at a faster phase, the photochemical counterpart was somewhat still at its infancy. One of the major reasons for its dormancy lied in the concern over the ability of axial chirality to dictate stereoselectivity in the short lived excited state of atropisomeric chromophores. Bach and coworkers who investigated the stereoselectivity in the Paternò-Büchi reaction of excited benzaldehyde with atropisomeric enamides where the atropisomers reacted from the ground state made one of earliest report on photochemical transformations involving atropisomeric chromophores.[79] Further work along this line to evaluate atropisomeric systems for stereospecific photochemical transformations were not pursued with diligence. During this time, Sakamoto and coworkers reported the photochemistry of molecules with "Frozen chirality" that were generated by chiral crystallization of achiral materials.[31] For example, in 2005, they reported the photocycloaddition of molecularly chiral napthamides (**115**) with 9-cyanoanthracene (**116**) in solution (Scheme 1.35).[80]

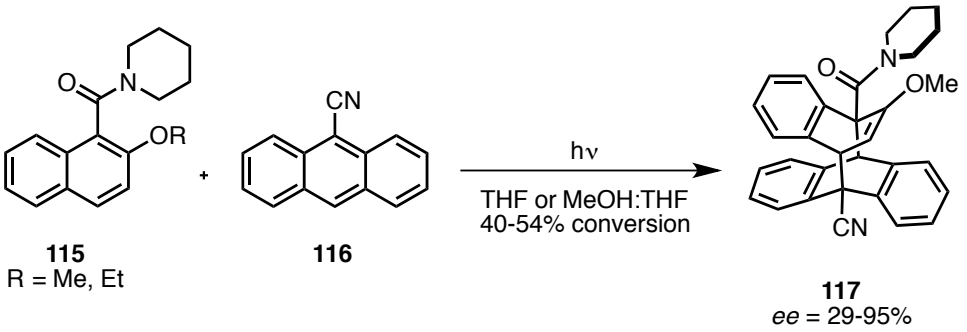

115
R = Me, Et

116

117
ee = 29-95%

Scheme 1.35: Photocycloaddition of molecularly chiral naphthamides with 9-cyanoanthracence.

These molecularly chiral crystals when dissolved in solvent retained their chirality at low temperature ($\tau_{1/2}$ at 20 ^{o}C was ~60 min) long enough to react with 9-cyanoanthracence to result in chiral photoadduct. Similarly, they also reported highly stereoselective [2+2]-photocycloaddition of coumarincarboxamides (**118**) with various alkenes (Scheme 1.36).[81]

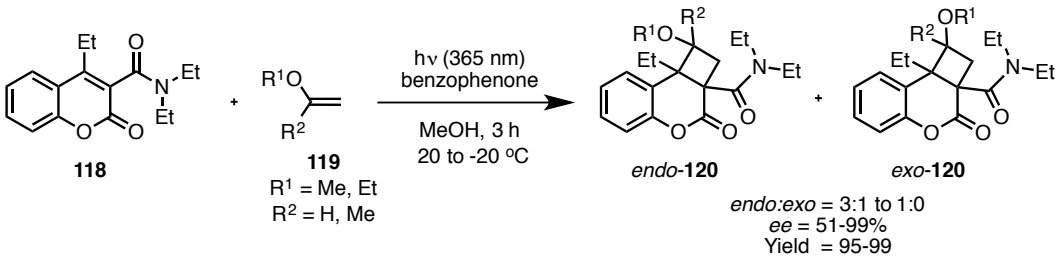

Scheme 1.36: Intermolecular [2+2]-photocycloaddition of molecularly chiral coumarincarboxamides with alkenes.

The methanolic solution of chirally crystallized coumarincarboxamides composed of single enantiomer reacted with alkenes to result in the product albeit with lower *ee*. The reason attributed for lower *ee* was longer reaction time that led to racemization and photoracemization that occurred from the singlet-excited state. The problem was overcome by benzophenone-sensitized (triplet pathway) reaction that resulted in excellent enantiomeric excess in the photoadduct (*ee* = 98%).

While the photochemistry of "Frozen chirality" was promising, the method suffered from the ability of the molecule to crystallize in a chiral space group and the reaction conditions such as reaction time, solvent choice that greatly affected the outcome of the reactivity/selectivity in the desired photochemical transformations.

1.6.3. Ground state conformational control of photoreactivity (NEER principle)

The photochemistry of simple conjugated alkenes that exist as multiple rotamers in the ground state and its control over the photochemical reactivity serves as a perfect platform to extend the well-established concepts to non-biaryl atropisomers providing an excellent avenue for the stereospecific phototransformations.[82-84] The ground state rotamer control of photoreactivity was first introduced by Havinga and Schlatmann, termed as "**N**on-**E**quilibration of **E**xcited **R**otamers" and states that

"Species formed up on π-π* excitation of the various transoid and cisoid ground-state rotamers of a triene or a polyene in general will not equilibrate during the short excited-state lifetime because of the increased bond order of the ground state C-C single bonds"[84]

This statement elucidates that the product distribution will reflect upon the ground-state composition of various conformational equilibrium of rotamers in the starting material. One of the interesting examples of existence of NEER principle was demonstrated in the low temperature irradiation of previtamin D (Scheme 1.37).[82]

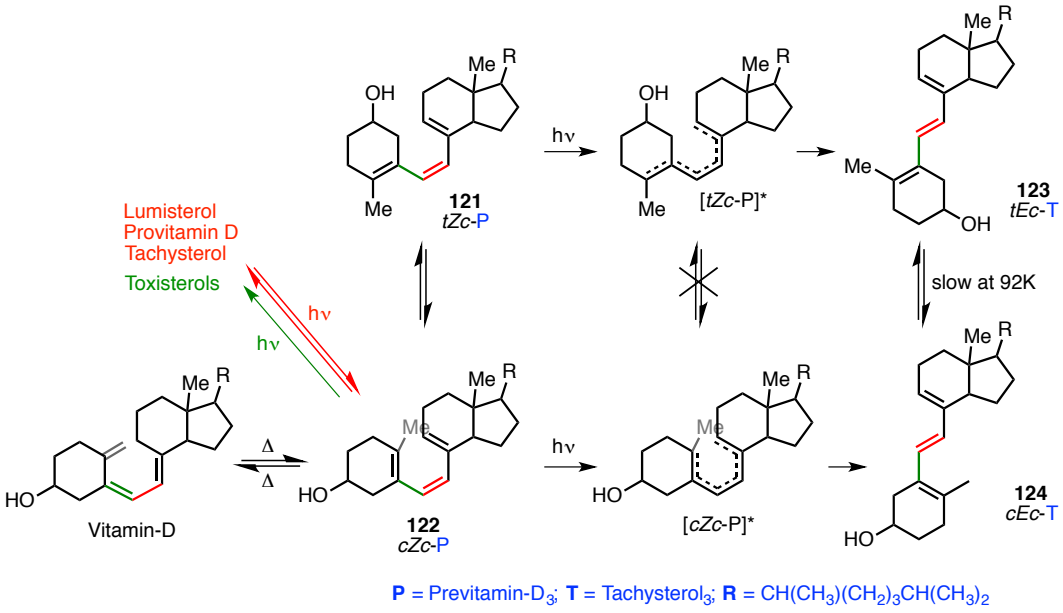

Scheme 1.37: Photochemical *cis-trans* isomerization of previtamin-D (P) and tachysterol$_3$ (T) and NEER principle. (Reproduced from reference 82, with permission from Wiley-VCH Verlag GmbH & Co. KGaA).

Previtamin-D exist in solution as a mixture of *E:Z* rotamers (t*Z*c-P-**121** and c*Z*c-P-**122**) that upon irradiation goes to an excited state. The excited mixture relaxes to the ground state (via rotation around the double bond marked red) to form mixture of tachysterol$_3$ t*E*c-T-**123** and c*E*c-T-**124** and other products. The c*E*c-T-**124** rotamer was a highly unstable molecule (due to steric interaction between methyl group and hydrogens of the double bond) that rapidly converted to t*E*c-T-**123** at room temperature. However, the c*E*c-T rotamer was stable at low temperature as observed from irradiation at 92K in methylcyclohexane/isopentane mixture. This study clearly

showed that the rotamers do not interconvert during the excited state even though the resulting ground state product was highly unstable due to sterics.

The NEER principle serves as the counterpart of Curtin-Hammett principle for ground state reactions. However, the NEER principle hold good as long as the rate of photoreaction is higher at least by a factor 10 than the rate of rotameric interconversion. So at room temperature, the NEER principle operates as long as the barrier to interconversion is greater than 8 kcal·mol^{-1}.

The NEER principle was mainly put forward for the observations in singlet excited state. However, further study on various molecules proved that the NEER principle does operate in triplet state as well. So, this principle can be conveniently extended to the stereospecific photoreactions of non-biaryl atropisomeric systems (figure 1.9). The individual isomers of the atropisomers A or B that have sufficient energy barrier to rotation towards racemization in the ground state when irradiated goes to the excited state A* or B*.

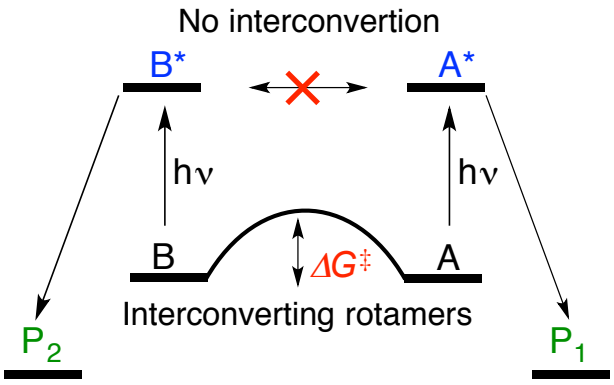

Figure 1.9: NEER principle in non-biaryl atropisomeric systems leading to efficient chirality transfer.

The excited rotamers do not undergo interconversion in the excited state following the NEER principle leading to stereospecific photoproducts that is dictated by the geometry of the starting material (A to P1 and B to P2). If the photoreaction is carried out on optically pure atropisomers, in principle, complete “axial to point chirality” can be achieved. This led us to initiate a research program where our group mainly focused on applying this strategy to stereospecific phototransformations and to achieve highly enantioenriched photoproducts.

1.6.4. Asymmetric photochemistry of non-biaryl atropisomers

In 2009, Sivaguru and coworkers initiated comprehensive analysis on the photochemistry of stable non-biaryl atropisomers in solution. For example, they reported highly enantiospecific 6π-photocyclization of acrylanilides (**125**) in solution resulting in *cis* and *trans* photoproducts (Scheme 1.38).[85,86]

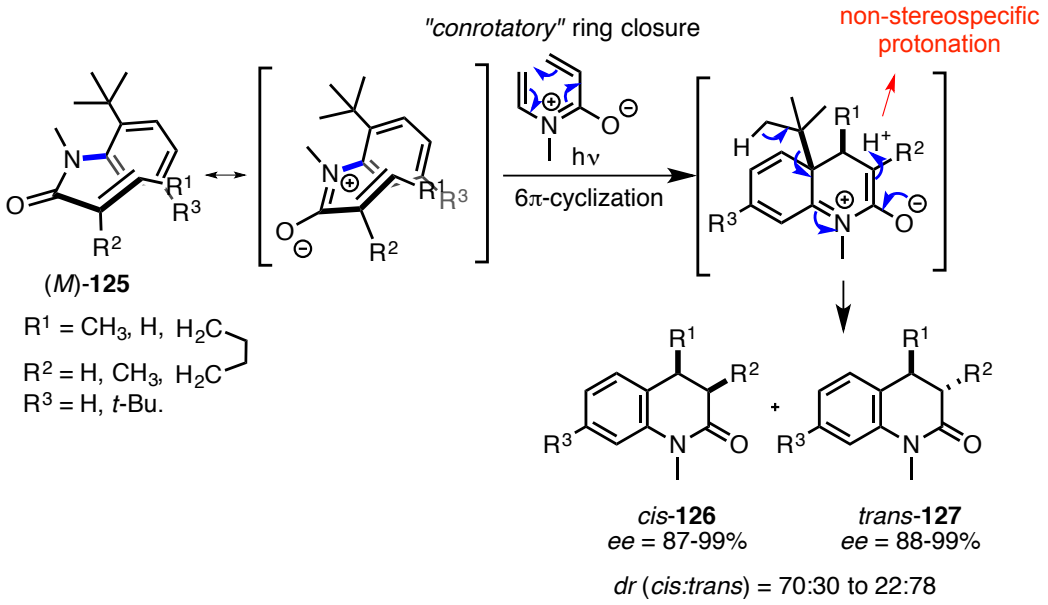

Scheme 1.38: Enantiospecific 6π-ring closure of atropisomeric acrylanilides.

The "*conrotatory*" cyclization occurred on the carbon bearing *t*-Bu group thus eliminating the isoprene unit and relieving the unnecessary strain in the molecule. The enantio- and diastereomeric excess in the photoproducts however depended on the substitution on the alkene and the mechanism of photocyclization. For instance, under direct irradiation (singlet pathway), the presence of β-substitution (R^1) is indispensible to achieve selectivity. In a singlet pathway, the initial *conrotatory* cyclization underwent stereospecifically resulting in planar enolate with defined R^1 chirality. The protonation of the enolate occurred non-stereospecifically resulting in *cis* and *trans* photoproduct (**126** and **127**). On the other hand, in a sensitized irradiation (triplet pathway), the cyclization and the subsequent hydrogen abstraction occurred stereospecifically via radical pathway resulting in highly enantioenriched photoproducts.[87] They also employed other means

such as photoreaction in the solid state where the conformation was rigidly controlled by the crystalline matrix[88] and in the presence of alkali metal ions[89] that promoted radical pathway by spin-orbit coupling to achieve higher selectivity in the α-substituted acrylanilides. In the same year, they also reported stereospecific Norrish-Yang cyclization (hydrogen abstraction) of atropisomeric α-oxoamides (**128**) (Scheme 1.39).[90] The reaction proceeds via the excitation of carbonyl chromophore, which abstracted a hydrogen from suitably positioned *N*-methyl substituent resulting in benzylic 1,4-diradical.

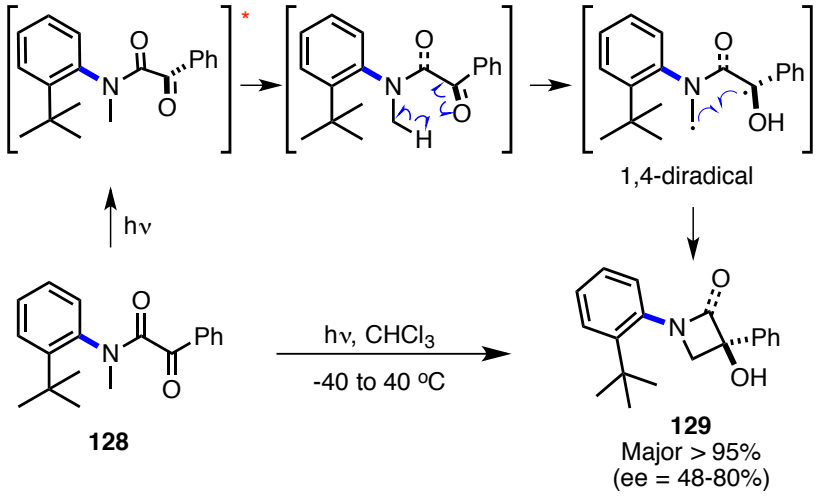

Scheme 1.39: Enantiospecific Norrish-Yang reaction of atropisomeric α-oxoamides **128**.

The benzylic radical then underwent cyclization leading to products such as β-lactam, oxazolidin-4-oneand open chained amide. The ratio of the product distribution depended on the reaction conditions.[91] In the reported condition, the major product was the β-lactam (**129**) that forms through radical recombination. One interesting observation was that the temperature dependence of enantiospecificity. At lower temperature, rotation of 1,4-diradical was inhibited thus resulting in enantioenriched photoproduct (*ee* = 80%).

1.7. Summary and outlook

The approaches and the outcome of the efforts provide an excellent understanding of the advantages and disadvantages of a particular method in achieving stereoselectivity in the desired photochemical transformations. Based on the literature precedence, the success of atropisomeric scaffolds in performing stereoselective thermal transformations and preliminary investigation atropisomeric chromophores in photochemical transformations allowed us to envision a comprehensive evaluation of atropisomeric systems in asymmetric phototransformations. The forthcoming chapters or the theme of this thesis elaborately describes the investigations carried out and the consequence of those works on non-biaryl atropisomeric chromophores in various asymmetric photochemical transformations.

1.8. References

(1) Caner, H.; Groner, E.; Levy, L.; Agranat, I. Trends in the development of chiral drugs. *Drug Discovery Today* **2004**, *9*, 105-110.

(2) Trommsdorff, H. *Ann. Chem. Pharm.* **1834**, *11*, 190-208.

(3) Roth, H. D. The Beginnings of Organic Photochemistry. *Angew. Chem. Int. Ed.* **1989**, *28*, 1193-1207.

(4) Natarajan, A.; Tsai, C. K.; Khan, S. I.; McCarren, P.; Houk, K. N.; Garcia-Garibay, M. A. The Photoarrangement of α-Santonin is a Single-Crystal-to-Single-Crystal Reaction: A Long Kept Secret in Solid-State Organic Chemistry Revealed. *J. Am. Chem. Soc.* **2007**, *129*, 9846-9847.

(5) http://zebu.uoregon.edu/~imamura/122/lecture-2/em.html.

(6) *Handbook of Synthetic Photochemistry*; WILEY-VCH Verlag GmbH & Co. KGaA: Weinheim, 2010.

(7) Knowles, J. P.; Elliott, L. D.; Booker-Milburn, K. I. Flow photochemistry: Old light through new windows. *Beilstein J. Org. Chem.* **2012**, *8*, 2025-2052.

(8) Oelgemöller, M.; Shvydkiv, O. Recent Advances in Microflow Photochemistry. *Molecules*

2011, *16*, 7522-7550.

(9) Hook, B. D. A.; Dohle, W.; Hirst, P. R.; Pickworth, M.; Berry, M. B.; Booker-Milburn, K. I. A Practical Flow Reactor for Continuous Organic Photochemistry. *J. Org. Chem.* **2005**, *70*, 7558-7564.

(10) Lévesque, F.; Seeberger, P. H. Continuous-Flow Synthesis of the Anti-Malaria Drug Artemisinin. *Angew. Chem. Int. Ed.* **2012**, *51*, 1706-1709.

(11) Turro, N. J.; Ramamurthy, V.; Cherry, W.; Farneth, W. The effect of wavelength on organic photoreactions in solution. Reactions from upper excited states. *Chem. Rev.* **1978**, *78*, 125-145.

(12) Stegemeyer, H. Photoluminescence of Solutions. Von C. A. Parker. Elsevier Publishing Co., Amsterdam-London-New York 1968. 1. Aufl., XVI, 544 S., 188 Abb., 53 Tab., geb. Dfl. 85,–. *Angew. Chem.* **1969**, *81*, 1007-1008.

(13) Ong, Q. Organic photochemistry: Fundamentals and Applications. *"Burns group" literature review*.

(14) Reichardt, C.; Welton, T. Solvent Effects on the Absorption Spectra of Organic Compounds. In *Solvents and Solvent Effects in Organic Chemistry*; Wiley-VCH Verlag GmbH & Co. KGaA, 2010; pp 359-424.

(15) *Handbook of Photochemistry, Third Edition*; Taylor & Francis Group, LLC, 2006.

(16) Monati, M.; Credi, A.; Prodi, L.; Gandolfi, M. T.: *Hand book of photochemistry*; 3 ed.; CRC press, 2006.

(17) Penkett, C. S.; Woolford, J. A.; Day, I. J.; Coles, M. P. The Double [3 + 2] Photocycloaddition Reaction. *J. Am. Chem. Soc.* **2009**, *132*, 4-5.

(18) Bach, T.; Hehn, J. P. Photochemical Reactions as Key Steps in Natural Product Synthesis. *Angew. Chem. Int. Ed.* **2011**, *50*, 1000-1045.

(19) In *Chiral Photochemistry*; Inoue, Y., Ramamurthy, V., Eds.; Marcel Dekker: New York, 2004; Vol. 11.

(20) Le Bel, J. A. Sur les relations qui existent entre les formulas atomiques de corps organiques et le pouvior rotatiore de leurs dissolutions. *Bull. Soc. Chim. Fr.* **1874**, *22*, 337-347.

(21) Van't Hoff, J. H.: *Die Lagerung der Atom and Raume*; 2 ed., 1894.

(22) Kuhn, W.; Braun, E. Photochemische Erzeugung optisch aktiver Stoffe. *Die Naturwissenschaften* **1929**, *17*, 227-228.

(23) Kuhn, W.; Knopf, E. Photochemische Erzeugung optisch aktiver Stoffe. *Naturwissenschaften* **1930**, *18*, 183.

(24) Ayitou, A. J.-L.: stereospecific photochemical transformations involving axially chiral acrylanilides and α-oxoamides. North Dakota State Universtiy, 2013.

(25) Blume, R.; Rau, H.; Schuster, O. Molar ellipticity of the pure enantiomer by partial photoresolution. Photoreaction of 4,4,4',4'-tetramethyl-2,2,3',3'-tetraazaspiro[4.4]nona-2,2'-diene. *J. Am. Chem. Soc.* **1976**, *98*, 6583-6586.

(26) Kagan, H.; Moradpour, A.; Nicoud, J. F.; Balavoine, G.; Tsoucaris, G. Photochemistry with circularly polarized light. Synthesis of optically active hexahelicene. *J. Am. Chem. Soc.* **1971**, *93*, 2353-2354.

(27) Kawasaki, T.; Sato, M.; Ishiguro, S.; Saito, T.; Morishita, Y.; Sato, I.; Nishino, H.; Inoue, Y.; Soai, K. Enantioselective Synthesis of Near Enantiopure Compound by Asymmetric Autocatalysis Triggered by Asymmetric Photolysis with Circularly Polarized Light. *J. Am. Chem. Soc.* **2005**, *127*, 3274-3275.

(28) Sato, I.; Sugie, R.; Matsueda, Y.; Furumura, Y.; Soai, K. Asymmetric Synthesis Utilizing Circularly Polarized Light Mediated by the Photoequilibrium of Chiral Olefins in Conjunction with Asymmetric Autocatalysis. *Angew. Chem. Int. Ed.* **2004**, *43*, 4490-4492.

(29) Ostromisslensky, I. Untersuchungen im Gebiete der Spiegelbildisomerie. *Berichte der deutschen chemischen Gesellschaft* **1908**, *41*, 3035-3046.

(30) Green, B. S.; Lahav, M.; Rabinovich, D. Asymmetric synthesis via reactions in chiral crystals. *Acc. Chem. Res.* **1979**, *12*, 191-197.

(31) Sakamoto, M. Absolute Asymmetric Synthesis from Achiral Molecules in the Chiral Crystalline Environment. *Chem. Eur. J.* **1997**, *3*, 684-689.

(32) Schmidt, G. M. J. Photodimerization in the solid state. *Pure Appl. Chem* **1971**, *27*, 647-678.

(33) Cohen, M. D.; Schmidt, G. M. J. 383. Topochemistry. Part I. A survey. *J. Chem. Soc.* **1964**, 1996-2000.

(34) Schmidt, G. M. J. 385. Topochemistry. Part III. The crystal chemistry of some trans-cinnamic acids. *J. Chem. Soc.* **1964**, 2014-2021.

(35) Ramamurthy, V.; Venkatesan, K. Photochemical reactions of organic crystals. *Chem. Rev.* **1987**, *87*, 433-481.

(36) Elgavi, A.; Green, B. S.; Schmidt, G. M. J. Reactions in chiral crystals. Optically active heterophotodimer formation from chiral single crystals. *J. Am. Chem. Soc.* **1973**, *95*, 2058-2059.

(37) Evans, S. V.; Garcia-Garibay, M.; Omkaram, N.; Scheffer, J. R.; Trotter, J.; Wireko, F. Use of chiral single crystals to convert achiral reactants to chiral products in high optical yield: application to the di-.pi.-methane and Norrish type II photorearrangements. *J. Am. Chem. Soc.* **1986**, *108*, 5648-5650.

(38) Toda, F.; Tanaka, K. A new simple chiral helicene 3,4-bis(diphenyl-methylene)-N-methylsuccimide in its chiral crystal. A generation of chirality. *Supramol. Chem.* **1994**, *3*, 87-88.

(39) Gamlin, J. N.; Jones, R.; Leibovitch, M.; Patrick, B.; Scheffer, J. R.; Trotter, J. The Ionic Auxiliary Concept in Solid State Organic Photochemistry. *Acc. Chem. Res.* **1996**, *29*, 203-209.

(40) Cheung, E.; Netherton, M. R.; Scheffer, J. R.; Trotter, J. In the Footsteps of Pasteur: Asymmetric Induction in the Solid-State Photochemistry of Ammonium Carboxylate Salts. *J. Am. Chem. Soc.* **1999**, *121*, 2919-2920.

(41) Takahashi, S.; Miura, H.; Kasai, H.; Okada, S.; Oikawa, H.; Nakanishi, H. Single-Crystal-to-Single-Crystal Transformation of Diolefin Derivatives in Nanocrystals. *J. Am. Chem. Soc.* **2002**, *124*, 10944-10945.

(42) Kasai, H.; Nalwa, H. S.; Oikawa, H.; Okada, S.; Matsuda, H.; Minami, N.; Kakuta, A.; Ono, K.; Mukoh, A.; Nakanishi, H. A Novel Preparation Method of Organic Microcrystals. *Jpn. J. Appl. Phys.* **1992**, *31*, L1132-L1134.

(43) Veerman, M.; Resendiz, M. J. E.; Garcia-Garibay, M. A. Large-Scale Photochemical Reactions of Nanocrystalline Suspensions: A Promising Green Chemistry Method. *Org. Lett.* **2006**, *8*, 2615-2617.

(44) Bučar, D.-K.; MacGillivray, L. R. Preparation and Reactivity of Nanocrystalline Cocrystals Formed via Sonocrystallization. *J. Am. Chem. Soc.* **2006**, *129*, 32-33.

(45) Natarajan, A.; Ng, D.; Yang, Z.; Garcia-Garibay, M. A. Parallel Syntheses of (+)- and (−)-α-Cuparenone by Radical Combination in Crystalline Solids. *Angew. Chem. Int. Ed.* **2007**, *46*, 6485-6487.

(46) Faljoni, A.; Zinner, K.; Weiss, R. G. An attempt to influences the decay modes 1, 2-diphenylcyclopropane excited states with optically active solvents. *Tetrahedron Lett.* **1974**, *15*, 1127-1130.

(47) Nakazaki, M.; Yamamoto, K.; Maeda, M. Asymmetric synthesis of optically active trans doubly bridged ethylene. (-)-(R)-D2-Bicyclo[8.8.0]octadec-1(10)-ene. *J. Org. Chem.* **1980**, *45*, 3229-3232.

(48) Seebach, D.; Daum, H. Asymmetric induction of photopinacolization in a chiral amino ether. *J. Am. Chem. Soc.* **1971**, *93*, 2795-2796.

(49) Seebach, D.; Oei, H.-A.; Daum, H. Asymmetrische Synthese bei Photo-, Elektro- und Alkalimetall-Pinakolisierungen von Benzaldehyd und Phenonen im chiralen Medium DDB. *Chem. Ber.* **1977**, *110*, 2316-2333.

(50) Boyd, D. R.; Neill, D. C. Asymmetric synthesis at a pyramidal nitrogen centre in a chiral medium. *J. Chem. Soc., Chem. Commun.* **1977**, 51-52.

(51) Inoue, Y. Enantiodifferentiating photosensitized reactions. In *Chiral Photochemistry*; Inoue, Y., Ramamurthy, V., Eds.; Marcel Dekker: New York, 2004; Vol. 11; pp 129-177.

(52) Hammond, G. S.; Cole, R. S. Asymmetric Induction during Energy Transfer1. *J. Am. Chem. Soc.* **1965**, *87*, 3256-3257.

(53) Hoffmann, R.; Inoue, Y. Trapped Optically Active (E)-Cycloheptene Generated by Enantiodifferentiating Z−E Photoisomerization of Cycloheptene Sensitized by Chiral Aromatic Esters. *J. Am. Chem. Soc.* **1999**, *121*, 10702-10710.

(54) Kim, J. I.; Schuster, G. B. Enantioselective catalysis of the triplex Diels-Alder reaction: a study of scope and mechanism. *J. Am. Chem. Soc.* **1992**, *114*, 9309-9317.

(55) Kim, J. I.; Schuster, G. B. Enantioselective catalysis of the triplex Diels-Alder reaction:

addition of trans-.beta.-methylstyrene to 1,3-cyclohexadiene photosensitized with (-)-1,1'-bis(2,4-dicyanonaphthalene). *J. Am. Chem. Soc.* **1990**, *112*, 9635-9637.

(56) Chen, C.; Chang, V.; Cai, X.; Duesler, E.; Mariano, P. S. A General Strategy for Absolute Stereochemical Control in Enone−Olefin [2 + 2] Photocycloaddition Reactions. *J. Am. Chem. Soc.* **2001**, *123*, 6433-6434.

(57) Döpp, D.; Pies, M. High asymmetic induction in a photo-Diels-Alder addition. *J. Chem. Soc., Chem. Commun.* **1987**, 1734-1735.

(58) Griesbeck, A. G.; Kramer, W.; Lex, J. Diastereo- and Enantioselective Synthesis of Pyrrolo[1,4]benzodiazepines through Decarboxylative Photocyclization. *Angew. Chem. Int. Ed.* **2001**, *40*, 577-579.

(59) Sivasubramanian, K.; Kaanumalle, L. S.; Uppili, S.; Ramamurthy, V. Value of zeolites in asymmetric induction during photocyclization of pyridones, cyclohexadienones and naphthalenones. *Org. Biomol. Chem.* **2007**, *5*, 1569-1576.

(60) Joy, A.; Scheffer, J. R.; Ramamurthy, V. Chirally Modified Zeolites as Reaction Media: Photochemistry of an Achiral Tropolone Ether. *Org. Lett.* **1999**, *2*, 119-121.

(61) Joy, A.; Ramamurthy, V. Chiral Photochemistry within Zeolites. *Chem. Eur. J.* **2000**, *6*, 1287-1293.

(62) Nakamura, A.; Inoue, Y. Supramolecular Catalysis of the Enantiodifferentiating [4 + 4] Photocyclodimerization of 2-Anthracenecarboxylate by γ-Cyclodextrin. *J. Am. Chem. Soc.* **2002**, *125*, 966-972.

(63) Pemberton, B. C.; Kumarasamy, E.; Jockusch, S.; Srivastava, D. K.; Sivaguru, J. Photophysical aspects of 6-methylcoumarin–cucurbit[8]uril host–guest complexes. *Can. J. Chem.* **2011**, *89*, 310-316.

(64) Pemberton, B. C.; Barooah, N.; Srivatsava, D. K.; Sivaguru, J. Supramolecular photocatalysis by confinement-photodimerization of coumarins within cucurbit[8]urils. *Chem. Commun.* **2010**, *46*, 225-227.

(65) Bach, T.; Bergmann, H.; Harms, K. Enantioselective Intramolecular [2+2]-Photocycloaddition Reactions in Solution. *Angew. Chem. Int. Ed.* **2000**, *39*, 2302-2304.

(66) Bauer, A.; Westkamper, F.; Grimme, S.; Bach, T. Catalytic enantioselective reactions driven by photoinduced electron transfer. *Nature* **2005**, *436*, 1139-1140.

(67) Vallavoju, N.; Selvakumar, S.; Jockusch, S.; Sibi, M. P.; Sivaguru, J. Enantioselective Organo-Photocatalysis Mediated by Atropisomeric Thiourea Derivatives. *Angew. Chem. Int. Ed.* **2014**, 53, 5604-5608.

(68) Christie, G. H.; Kenner, J. The molecular configurations of polynuclear aromatic compounds. *J. Chem. Soc., Transactions* **1922**, *121*, 614-620.

(69) Bringmann, G.; Gulder, T.; Gulder, T. A. M.; Breuning, M. Atroposelective Total Synthesis of Axially Chiral Biaryl Natural Products. *Chem. Rev.* **2010**, *111*, 563-639.

(70) Clayden, J. Non-Biaryl Atropisomers: New Classes of Chiral Reagents, Auxiliaries and Ligands? In *Organic Synthesis Highlights IV*; Wiley-VCH Verlag GmbH, 2000; pp 48-52.

(71) McCarthy, M.; Guiry, P. J. Axially chiral bidentate ligands in asymmetric catalysis. *Tetrahedron* **2001**, *57*, 3809-3844.

(72) *Prof. Dennis Curran coined the term "atropselective reaction" that involve axially chiral molecules*

(73) Kawabata, T.; Yahiro, K.; Fuji, K. Memory of chirality: enantioselective alkylation reactions at an asymmetric carbon adjacent to a carbonyl group. *J. Am. Chem. Soc.* **1991**, *113*, 9694-9696.

(74) Curran, D. P.; Qi, H.; Geib, S. J.; DeMello, N. C. Atroposelective Thermal Reactions of Axially Twisted Amides and Imides. *J. Am. Chem. Soc.* **1994**, *116*, 3131-3132.

(75) Curran, D. P.; Liu, W.; Chen, C. H.-T. Transfer of Chirality in Radical Cyclizations. Cyclization of o-Haloacrylanilides to Oxindoles with Transfer of Axial Chirality to a Newly Formed Stereocenter. *J. Am. Chem. Soc.* **1999**, *121*, 11012-11013.

(76) Clayden, J. Stereocontrol with Rotationally Restricted Amides. *Synlett* **1998**, 810-816.

(77) Clayden, J.; Westlund, N.; Wilson, F. X. Asymmetric induction using atropisomers: Diastereoselective additions to 2-acyl-1-naphthamides. *Tetrahedron Lett.* **1996**, *37*, 5577-5580.

(78) Clayden, J.; Pink, J. H. Atroposelectivity in the Reactions of Laterally Lithiated Tertiary Amides. *Tetrahedron Lett.* **1997**, *38*, 2561-2564.

(79) Bach, T.; Schröder, J.; Harms, K. Diastereoselective photocycloaddition of an axial chiral enamide. *Tetrahedron Lett.* **1999**, *40*, 9003-9004.

(80) Sakamoto, M.; Unosawa, A.; Kobaru, S.; Saito, A.; Mino, T.; Fujita, T. Asymmetric Photocycloaddition in Solution of a Chiral Crystallized Naphthamide. *Angew. Chem. Int. Ed.* **2005**, *44*, 5523-5526.

(81) Sakamoto, M.; Kato, M.; Aida, Y.; Fujita, K.; Mino, T.; Fujita, T. Photosensitized 2 + 2 Cycloaddition Reaction Using Homochirality Generated by Spontaneous Crystallization. *J. Am. Chem. Soc.* **2008**, *130*, 1132-1133.

(82) Maessen, P. A.; Jacobs, H. J. C.; Cornelisse, J.; Havinga, E. Photochemistry of Previtamin D3 at 92 K; Formation of an Unstable Tachysterol3 Rotamer. *Angew. Chem. Int. Ed.* **1983**, *22*, 718-719.

(83) Havinga, E.; Schlatmann, J. L. M. A. Remarks on the specificities of the photochemical and thermal transformations in the vitamin D field. *Tetrahedron* **1961**, *16*, 146-152.

(84) Jacobs, H. J. C. Photochemistry of conjugated trienes: Vitamin D revisited. *Pure Appl. Chem*, *67*, 63-70.

(85) Ayitou, A. J.-L.; Sivaguru, J. Light-Induced Transfer of Molecular Chirality in Solution: Enantiospecific Photocyclization of Molecularly Chiral Acrylanilides. *J. Am. Chem. Soc.* **2009**, *131*, 5036-5037.

(86) Ayitou, A.; Pemberton, B. C.; Kumarasamy, E.; Vallavoju, N.; Sivaguru, J. Fun with Photons: Selective Light Induced Reactions in Solution and in Water Soluble Nano-containers. *Chimia* **2011**, *65*, 202-209.

(87) Ayitou, A. J.-L.; Sivaguru, J. Reactive spin state dependent enantiospecific photocyclization of axially chiral [α]-substituted acrylanilides. *Chem. Commun.* **2011**, *47*, 2568-2570.

(88) Ayitou, A. J.-L.; Vallavoju, N.; Ugrinov, A.; Sivaguru, J. Enantiospecific 6π-photocyclization of atropisomeric α-substituted acrylanilides in the solid-state: role of crystalline confinement on enantiospecificity. *Photochem. Photobiol. Sci.* **2011**, *10*, 1380-1383.

(89) Ayitou, A. J.-L.; Clay, A.; Kumarasamy, E.; Jockusch, S.; Sivaguru, J. Enantiospecific

photochemical 6π-ring closure of α-substituted atropisomeric acrylanilides - role of alkali metal ions. *Photochem. Photobiol. Sci.* **2014**, *13*, 141-144.

(90) Ayitou, A. J.-L.; Jesuraj, J. L.; Barooah, N.; Ugrinov, A.; Sivaguru, J. Enantiospecific Photochemical Norrish/Yang Type II Reaction of Nonbiaryl Atropchiral α-Oxoamides in Solution: Axial to Point Chirality Transfer. *J. Am. Chem. Soc.* **2009**, *131*, 11314-11315.

(91) Jesuraj, J. L.; Sivaguru, J. Photochemical type II reaction of atropchiral benzoylformamides to point chiral oxazolidin-4-ones. Axial chiral memory leading to enantiomeric resolution of photoproducts. *Chem. Commun.* **2010**, *46*, 4791-4793.

CHAPTER 2: ENANTIOSPECIFIC 4π-RING CLOSURE OF ATROPISOMERIC 2-PYRIDONES IN SOLUTION

2.1. Introduction

Pyridin-2-ones and their corresponding heterocyclic analogues are important components in many active pharmaceuticals and drug candidates. In this regard, the chemistry of pyridones was well investigated. The unsubstituted pyridin-2-ones and its corresponding constitutional isomer pyridin-4-ones can exist as tautomer between a keto and an enol form (lactam vs lactim form) that is affected by the polarity of the solvent; nonpolar solvents favoring enol form and polar solvents favoring keto form (Figure 2.1).

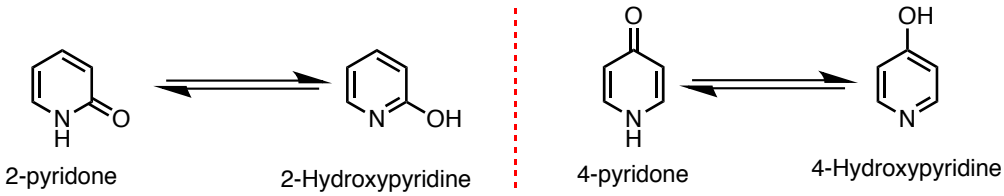

Figure 2.1: Tautomerization in 2-pyridones and 4-pyridones.

The photochemistry of 2-pyriondes was first reported by Paudler and coworkers while investigating photodimerization of α,β-unsaturated lactams.[1,2] Through absorption and dipole moment analysis they proposed that the product obtained was a head-tail cyclobutane resulting from [2+2]-dimerization reaction (Scheme 2.1). However further investigations using various other analytical methods such as NMR spectroscopy, infrared spectroscopy and X-ray crystallography it was confirmed that the product formed was a [4+4]-adduct instead of the [2+2]-adduct.[3,4]

The material in this chapter was co-authored by Elango Kumarasamy (EK), Dr. Josepha L. Jesuraj (JJ), Joseph N. Omlid (JO), Dr. Angel Ugrinov (AU), Dr. Anoklase J.-L. Ayitou (AJA), Dr. Gaku Fukuhara (GF), Dr. Yoshihisa Inoue (YI) and Dr. J. Sivaguru (JS). EK in consultation with JS synthesized all compounds and carried out experiments with the help of JJ and JO. AU recorded XRD data and solved the structures reported in this chapter. AJA and GF carried out pressure experiments on compounds mentioned in this chapter and elsewhere. EK and JS came up with mechanistic rationale of the reaction and the conclusion provided in this section. YI shared his insights in explaining the behavior of atropisomeric compounds under high pressure.

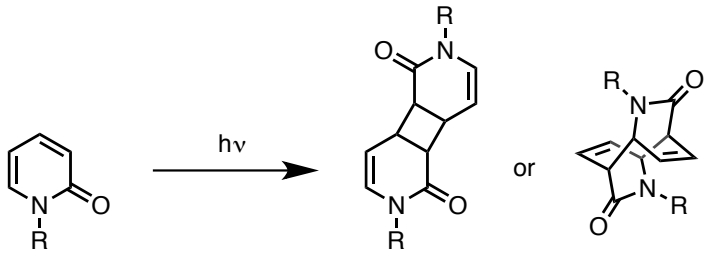

Scheme 2.1: Intermolecular photoreactions of 2-pyridones.

Corey and coworkers reported the first synthetically useful version of intramolecular reactions of 2-pyridones and pyrones in ethereal solution that resulted in cyclobutene derivatives (Scheme 2.2).[5] These scaffolds appeared to be promising in terms of accessing the derivatives of cyclobutadiene which otherwise proved difficult to be synthesized by thermal means.

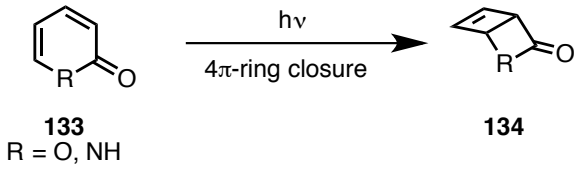

Scheme 2.2: Intramolecular 4π-ring closure of 2-pyridones (R = NH) and pyrones (R = O).

At this point, the photoreactions were called as internal photoaddition reactions. However, further research along this line and understanding of pericyclic reactions led to a set of empirical rules about reactions that occur through concerted transition state preserving the orbital symmetries.[6,7] These set of rules were put forwarded by Woodward and Hoffman called as “Woodward-Hoffman rules” and for their contribution Hoffman was awarded Noble prize in chemistry in 1981 (R. B. Woodward died 2 years before the Nobel prize was announced). Under dilute conditions, UV irradiation of 2-pyridone led to 4π-*disrotatory* ring closure furnishing β-lactam photoproducts with 2 new chiral centers (Scheme 2.3). However, in concentrated solution dimerization was the major reaction pathway leading to complex scaffolds with multiple stereocenters.

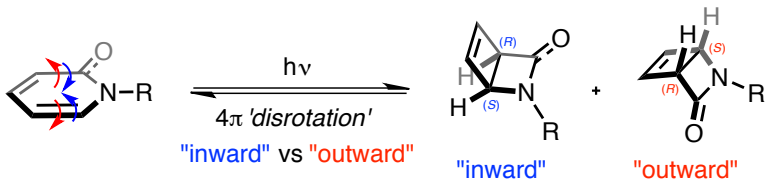

Scheme 2.3: *Disrotatory* modes in intramolecular 4π-ring closure of 2-pyridones.

The 4π-ring closure occurs through the "*disrotatory*" mode as shown in Scheme 2.3. However, the "*disrotation*" can occur in two ways i.e., inward or outward leading to enantiomeric photoproducts. In the absence of any chiral bias, two modes of cyclization occur at equal probability resulting in racemic β-lactam photoproducts. Due to the synthetic potential of 2-pyridones and wide presence of β-lactam in many drug molecules and antibiotics, the need for an enantioselective synthesis was more pressing than ever. Working towards this challenge, several interesting methodologies were developed that met with varying degree of success. Toda *et al.* reported solid-state irradiation of 1:1 inclusion complexes of 2-pyridones (**136**) and optically active host (**135**) that resulted in highly enantioenriched β-lactam derivatives (**137**).[8]

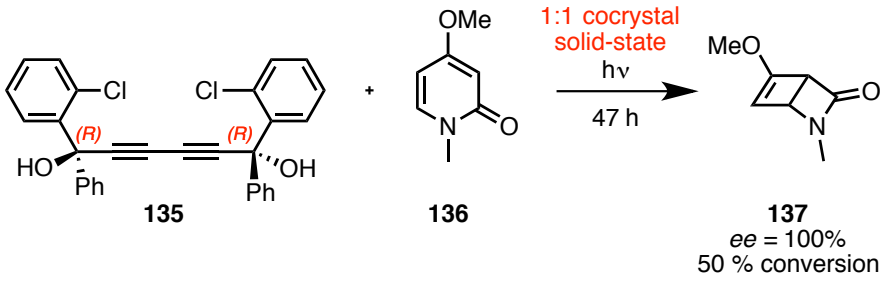

Scheme 2.4: Solid-state 4π-ring closure of 1:1 inclusion complex of 2-pyridones.

While the selectivity in the reaction was very high, the reaction times were much longer and the general applicability of this approach largely depended on the ability of the mixture to form chiral crystals. Similarly, Tanaka and coworkers reported irradiation of inclusion complexes of 2-pyridones and optically active host as a slurry in water (with hexadecyltrimethylammonium bromide as surfactant) which resulted in excellent yield and enantiomeric excess.[9] Bach and coworkers reported the first enantioselective photoreactions of 2-pyridones (**138**) in solution in the presence of Kemp triacid derived chiral host (**139**) resulting in modest enantiomeric excess (20-23%) and yield (Scheme 2.5).[10]

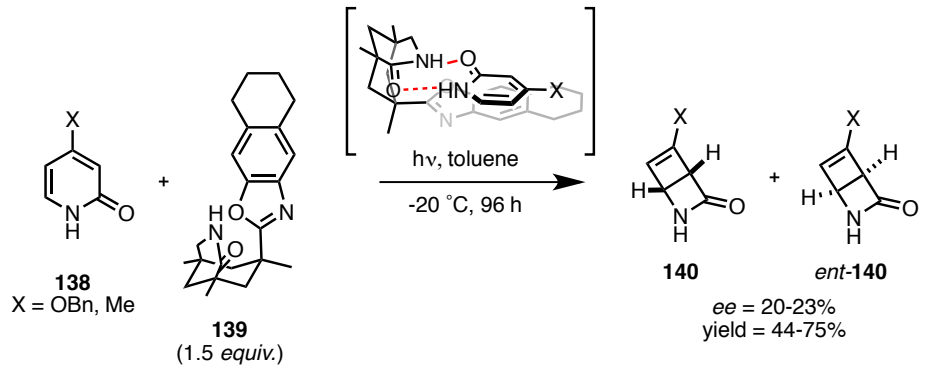

Scheme 2.5: Enantioselective 4π-ring closure of 2-pyridones in solution.

One of the reasons attributed for lower enantioselectivity was poor binding affinity of the 2-pyridones to the chiral template (**139**) resulting in significant background reaction and the catalyst was unable to differentiate the diastereomeric transition state (inward vs. outward) effectively thus resulting only in marginal selectivity. In 2007, Ramamurthy and coworkers reported an elegant approach to achieve higher enantioselectivity in the photoreaction of *N*-alkyl-2-pyridones (**141** and **144**) within zeolites (Scheme 2.6).[11] They employed two strategies to provide asymmetric induction in the reaction *viz.,* chiral inductor and chiral auxiliary approach. In chiral inductor approach, despite using excess of chiral element (10 fold excess), the observed *ee* in the photoproduct was only moderate at best and hugely influenced by the type of zeolite, type of cation, nature of reaction site… etc.

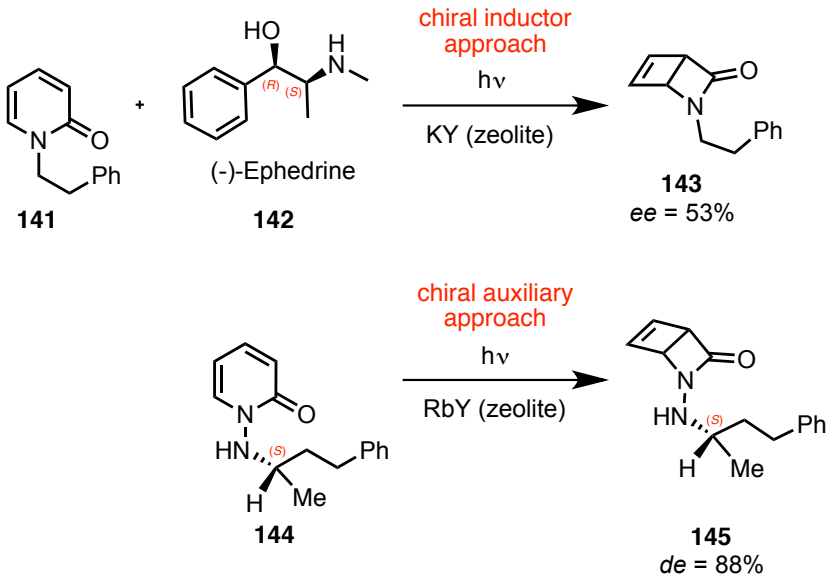

Scheme 2.6: Stereoselective 4π-ring closure of 2-pyridones based on chiral inductor and chiral auxiliary approach.

Computational analysis showed that the "cation-dipolar interaction" to be the primary interaction. In the best scenario, the cation and the substrate interaction provided a rigid complex to which the chiral inductor interacted further favoring one mode of cyclization over the other resulting in enantioenriched β-lactam product. This effect was pronounced in the case of chiral auxiliary where the chiral element is attached to the substrate resulting in higher enantioselectivity in the product.

Based on literature reports, it was evident that each methodology has its own advantages and shortcomings and there was still a need for a method that would furnish β-lactam products in high yield and selectivity. With the promise of atropisomeric systems in the 6π-photocyclization of acrylanilides,[12] we were prompted to evaluate axial-point chiral transfer strategy in 4π-ring closure reaction of 2-pyridones. As a step towards this study, we synthesized atropisomeric 2-pyridones based on the literature reports, which are detailed in the experimental section. The following chart 2.1 lists all of the compounds synthesized towards for our investigations.

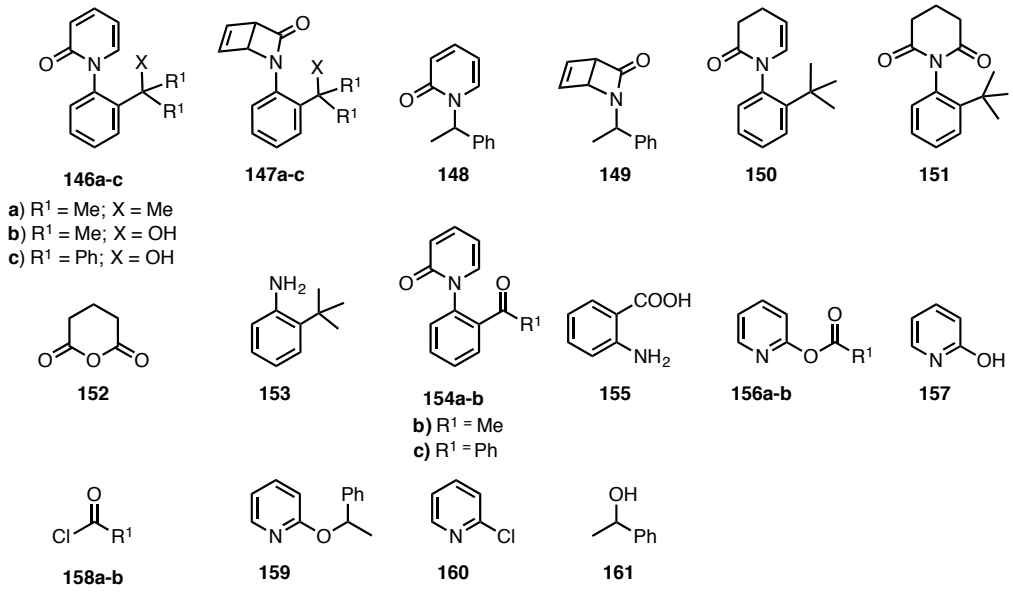

Chart 2.1: Structures of atropisomeric 2-pyridones, their photoproducts and compounds used for their synthesis.

2.2. Evaluation of diastereoselectivity in 4π-ring closure of point chiral auxiliary tethered 2-pyridones.

To understand the influence of chiral auxiliary and its ability to bring about chiral induction in 4π-ring closure of 2-pyridone in solution, we synthesized chiral auxiliary tethered 2-pyridones (**148**) and evaluated its photoreactions (Scheme 2.7). The optically pure 2-pyridone obtained from HPLC separations was subjected to broadband irradiation conditions at various temperatures (25 and -25 °C). The analysis of the results revealed that the diastereoselectivity of the newly formed chiral center was rather low with the best result being diastereomeric excess (*de*) of 10% (entry 9-10).

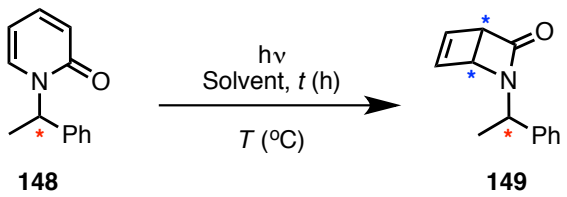

Scheme 2.7: 4π-Ring closure of point chiral auxiliary 2-pyridones **148**.

Table 2.1: Diastereoselective 4π-ring closure of point chiral 2-pyridone **148**

Entry	*T* (°C)	*t* (h)	Solvent	Compd	**149** (% *de*)
1	25	5	MeOH	(+)-**148**	5
2				(-)-**148**	5
3	25	5	MeCN	(+)-**148**	7
4				(-)-**148**	9
5	25	5	Toluene	(+)-**148**	-6
6				(-)-**148**	-5
7	-25	15	MeOH	(+)-**148**	6
8				(-)-**148**	8
9	-25	15	MeCN	(+)-**148**	10
10				(-)-**148**	10
11	-25	15	Toluene	(+)-**148**	-9
12				(-)-**148**	-9

The irradiation was carried out using 450W medium pressure mercury lamp with Pyrex cutoff under constant flow of N_2. The results carry an error of ±3.

The results clearly indicated the inability of the chiral auxiliary to induce desired level of stereoselectivity in the 4π-ring closure reaction even though it's placed right close to the reaction center. Even at low temperature (-25 °C) the influence of chiral auxiliary in bringing about the facial discrimination seemed to be minimal.

2.3. Enantiospecific 4π-ring closure of atropisomeric 2-pyridones

Considering the inefficiency of point chiral auxiliary in inducing desired level of facial selectivity in solution, we envisioned the use of atropisomeric systems as an avenue to bring about stereoselectivity in the 4π-ring closure of 2-pyridones. We reasoned that the steric bias imparted by the axial chirality would prevail even during the excited state and might efficiently discriminate the diastereotopic transition states. We designed three distinct atropisomeric 2-pyridones, **146a-c** in which the sterics that dictates the axial chirality was varied to evaluate its influence on the stereoselectivity in the photoreactions (Figure 2.2). In the first example, we chose to incorporate bulky *tert*-butyl group at the *ortho* position (**146a**) that acted as the steric bias and face-shielding group. In the other two systems (**146b-c**), we incorporated a hydroxyl group to evaluate the influence of H-bonding in stereospecific 4π-ring closure reaction.

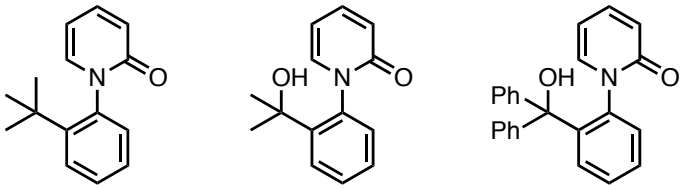

146a **146b** **146c**

Figure 2.2: Atropisomeric 2-pyridones **146a-c** employed for stereospecific 4π-ring closure.

The atropisomeric 2-pyridones were easily synthesized according to procedures reported in the literature.[13,14] The presence of axial chirality was verified through various analytical studies such as HPLC analysis, circular dichroism, optical rotation and single crystal XRD analysis.

2.4. Racemization kinetics of atropisomeric 2-pyridones

2.4.1. Racemization kinetics of atropisomeric 2-pyridones 146a-c

The atropisomeric compounds exist because of the restricted rotation around the chiral axis. If provided sufficient energy, the restricted rotation can be overcome resulting in racemization. However, in stereoselective reactions, the presence of a stable chirality is necessary. This ensures efficient translation of axial to point chirality leading to successful enantio control induction in the resulting photoproducts. So the evaluation of racemization barrier for newly synthesized atropisomeric compounds became critical. Apart from this, the role of H-bonding in stabilizing the axial chirality can be appreciated by a detailed study on the racemization kinetics at various temperatures and solvents. Racemization barrier on optically pure atropisomeric 2-pyridones in a given solvent was evaluated by incubating a solution of optically pure 2-pyridones in oil bath maintained at a constant temperature.

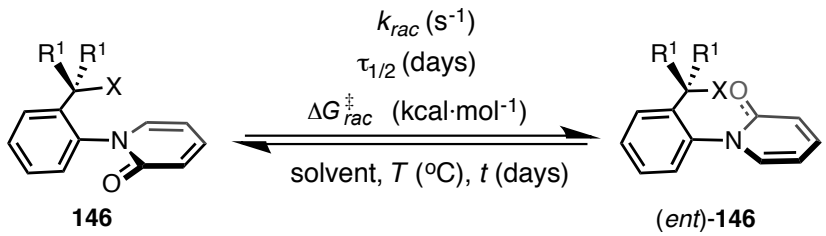

Scheme 2.8: Racemization kinetics of atropisomeric 2-pyridones.

The decrease in the enantiomeric excess (*ee*) over time was monitored using HPLC on a chiral stationary phase. The first order kinetic plot of ln (% *ee*) vs. time gave the rate constant of racemization (k_{rac}). The activation energy barrier, half-life and rate of racemization were calculated from the following equation.[15]

$$k_{rac} = k\left(\frac{k_B T}{h}\right) e^{-\Delta G^{\ddagger}_{rac} / RT} \qquad \textbf{Equation 2.1}$$

$$\Delta G^{\ddagger}_{rac} = -RT \ln\left(\frac{h k_{rac}}{k T k_B}\right) \qquad \textbf{Equation 2.2}$$

The half-life of racemization ($\tau_{1/2rac}$), was calculated using the rate constant of racemization k_{rac} (assuming $1\text{-}P_0 = 0$ at $t = 0$)

$$\ln\left(\frac{\chi_{eq}}{\chi_{eq} - \chi}\right) = \ln\left(\frac{R_0}{2R - R_0}\right) = \ln\left(\frac{R + S}{R - S}\right) = 2k_{enant}\, t \qquad \textbf{Equation 2.3}$$

$$\ln\left(\frac{R_0}{R_0 - \chi}\right) = k_{rac}\, t \qquad \textbf{Equation 2.4}$$

Where,

$k_{rac} = 2k_{enant}$; R_0 is the initial concentration of the (*R*)-enantiomer;

$\chi = R_0 - R$, S (concentration of the racemate at time *t*); and

k_{rac} is the rate constant for racemization

Note: $R_0 = R + S$

At 50% *ee*, the equation becomes:

$$\tau_{1/2rac} = \frac{\ln 2}{2k_{enant}} \quad or \quad \frac{\ln 2}{k_{rac}} \qquad \textbf{Equation 2.5}$$

The following calculation given in table 2.2 is an example (**146a**, CH_3CN, 65 °C) of processing the data obtained from HPLC analysis and fitting the values in the equations to calculate the rate, half-life and energy barrier for racemization. Similar analysis can be performed on other substrates for given conditions (various temperature and solvents) to ascertain the kinetic parameters.

Table 2.2: Calculation of energy barrier for 2-pyridone **146a** in MeCN at 65 °C

Time (h)	% *ee*	ln(% *ee*)	time (days)
0	98	4.59	0.0
10	96	4.56	0.4
24	94	4.54	1.0
48	90	4.50	2.0
72	88	4.48	3.0
96	87	4.47	4.0
120	84	4.43	5.0
144	82	4.41	6.0
216	74	4.30	9.0

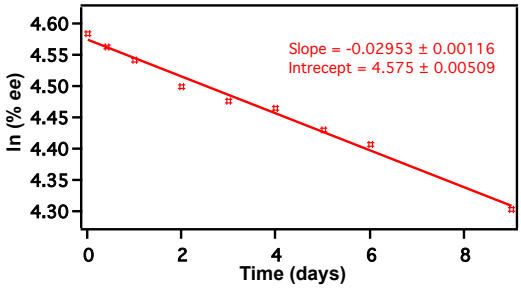

Slope (k_{rac}) = 0.0295 days^{-1} **or** 1.71×10^{-7} s^{-1}

$$\Delta G^{\ddagger}_{rac} = -RT \ln\left(\frac{h k_{rac}}{k T k_B}\right)$$

$$= -8.314 \text{ j·mol}^{-1}\text{·K}^{-1} \times 338\text{K} \ln\left(\frac{6.63 \times 10^{-34} \text{ j·s} \times 1.71 \times 10^{-7} \text{ s}^{-1}}{1 \times 338 \text{ K} \times 1.38 \times 10^{-34} \text{ j·K}^{-1}}\right)$$

$$= 124975.1 \text{ j·mol}^{-1}$$

$$\Delta G^{\ddagger}_{rac} = 29.9 \text{ kcal·mol}^{-1}$$

The racemization kinetics was carried out on atropisomeric 2-pyridones at various temperature and solvent which are listed in the table 2.3

Table 2.3: Rate constant (k_{rac}), half-life ($\tau_{1/2}$) and energy-barrier ($\Delta G^{\ddagger}_{rac}$) for racemization in atropisomeric 2-pyridones **146**

Ent.	T (°C)	Parameters	Compd	H_2O	CH_3OH	CH_3CN	Toluene
1	65	$\tau_{1/2}$ (days)	**146a**	-[a]	23.5	5.3	1.45
2			**146b**	2.5	2.8 (h)[b]	1.1 (h)[b]	0.6 (h)[b]
3			**146c**	-[a]	0.27 (h)[b]	0.47 (h)[b]	0.50 (h)[b]
4		$\Delta G^{\ddagger}_{rac}$ (kcal·mol^{-1})	**146a**	-[a]	29.9	28.9	25.5
5			**146b**	28.4	26.3	25.7	22.8
6			**146c**	-[a]	24.7	25.1	25.2
7		k_{rac} (s^{-1})	**146a**	-[a]	3.4×10^{-7}	1.5×10^{-6}	5.5×10^{-6}
8			**146b**	3.2×10^{-6}	6.8×10^{-5}	1.7×10^{-4}	3.1×10^{-4}
9			**146c**	-[a]	7.05×10^{-4}	4.03×10^{-4}	3.8×10^{-4}
10	45	$\tau_{1/2}$ (days)	**146a**	-[a]	-[c]	77.8	22.7
11			**146b**	27.7	21.8 (h)[b]	10.6 (h)[b]	3.4 (h)[b]
12			**146c**	-[a]	1.3 (h)[b]	2.1 (h)[b]	1.8 (h)[b]
13		$\Delta G^{\ddagger}_{rac}$ (kcal·mol^{-1})	**146a**	-[a]	-[c]	28.8	28.0
14			**146b**	28.2	26.0	25.6	24.8
15			**146c**	-[a]	24.2	24.5	24.4
16		k_{rac} (s^{-1})	**146a**	-[a]	-[c]	1.03×10^{-7}	3.5×10^{-7}
17			**146b**	2.9×10^{-7}	8.8×10^{-6}	1.8×10^{-5}	5.6×10^{-5}
18			**146c**	-[a]	14×10^{-5}	9.5×10^{-5}	11×10^{-5}
19	25	$\tau_{1/2}$ (days)	**146a**	-[a]	-[c]	-[c]	120
20			**146b**	-[c]	4.0	4.6	1.8
21			**146c**	-[a]	15 (h)[b]	46 (h)[b]	46 (h)[b]
22		$\Delta G^{\ddagger}_{rac}$ (kcal·mol^{-1})	**146a**	-[a]	-[c]	-[c]	27.2
23			**146b**	-[c]	25.2	25.3	24.8
24			**146c**	-[a]	24.1	24.8	24.8
25		k_{rac} (s^{-1})	**146a**	-[a]	-[c]	-[c]	6.7×10^{-8}
26			**146b**	-[c]	2.0×10^{-6}	1.7×10^{-6}	4.4×10^{-6}
27			**146c**	-[a]	12×10^{-6}	4.2×10^{-6}	4.1×10^{-6}

Reported values carry an error of ±5%.[a] The compound **146a** and **146c** was not soluble in water, hence data not provided. [b]The half-life of racemization given in hours. [c]The compound did not racemize even after 60 days, hence data not provided.

The analysis of the racemization values in table 2.3 clearly indicated the distinctive behavior of atropisomeric 2-pyridones. For example, 2-pyridone **146a** having *o-tert*-butyl group (pure sterics) had higher racemization barrier at a given temperature compared to **146b-c** that had smaller sterics (Table 2.3; compare entry 1-3). The racemization value followed the order **146a**>**146b**>**146c** for a given temperature and solvent. Also, the type of solvent employed for the racemization kinetics had a huge impact on the racemization values (Table 2.3; compare entry 1). The polar protic solvent (e.g., MeOH) was able to stabilize the axial chirality much better than a non-polar aprotic solvent (e.g., toluene). These effects were pronounced for **146b**, where the hydroxyl group efficiently formed an intra and inter molecular H-bonding with the solvent (Figure 2.3). In short, more/stronger the H-bonds, higher are the stabilization in terms of racemization barrier.

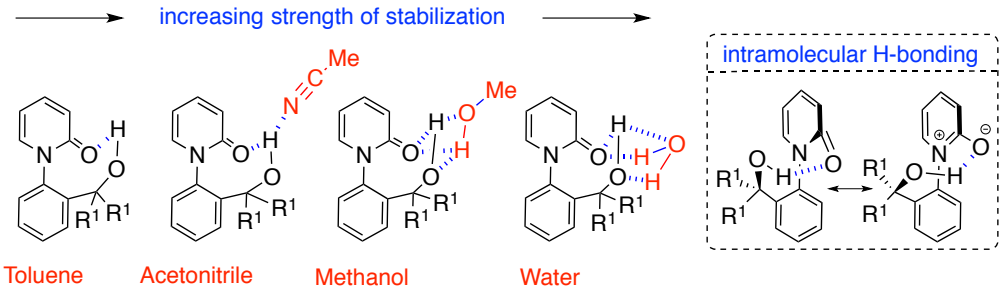

Figure 2.3: Intra- and intermolecular H-bonding stabilization in atropisomeric 2-pyridones.

However, the racemization values of **146c** did not follow the trend detailed above. The non-polar aprotic solvent seemed to stabilize the axial chirality more than the polar protic solvent. This might be due to the hydrophobic nature of the phenyl group that inhibited the H-bonding interaction from the solvent thus decreasing the racemization barrier.

All the results from the racemization kinetics pointed out that the newly synthesized atropisomeric 2-pyridones possess significantly higher racemization barrier at ambient conditions and can be employed for the enantiospecific photochemical transformations without losing the absolute configuration of the individual isomer.

2.4.2. Effect of pressure on racemization kinetics on 2-pyridone 146c

Pressure, volume and temperature are triad of parameters that are highly interrelated. Changing one parameter invariably affects the other, which provides an excellent avenue to probe dynamic chemical processes. It is well known that the atropisomeric compounds are susceptible to racemization at elevated temperature, which prevents us from taking advantage of their chemistry that requires higher temperature. To circumvent this problem, we envisioned exploring the effect of pressure in racemization process and stereospecific phototransformations. By keeping one of these three parameters constant (P, V, T), the relation between the other two can be probed.

The racemization kinetics of atropisomeric 2-pyridone **146c** was carried out at various temperature and pressure. For a qualitative understanding of the influence of pressure on racemization, it is essential to calculate the activation volume ($\Delta V^{\ddagger}_{rac}$) for the racemization process (Eq 2.6 and 2.7).[16] The activation volume was obtained from the difference between the partial molar volume of the transition state and the sum of the partial volumes of the reactant(s) at a given temperature and pressure, which was obtained at the equilibrium between the applied force and internal pressure.

$$\Delta V^{\ddagger}_{rac} = -RT\,(\partial \ln k_{rac} / \partial P)_T \qquad \textbf{Equation 2.6}$$

$$(\ln k_{rac})_T = -(\Delta V^{\ddagger}_{rac} / RT)P + C \qquad \textbf{Equation 2.7}$$

$$\ln[[P]_0 / ([P]_0 - \chi)] = \ln[([P] + [M]) / ([P]-[M])] = k_{rac}\,t \qquad \textbf{Equation 2.8}$$

$$\tau_{1/2} = \ln 2 / k_{rac} \qquad \textbf{Equation 2.9}$$

$$(\ln k_{rac} / T) = \Delta S^{\ddagger}_{rac} / R - (\Delta H^{\ddagger}_{rac} / RT + \ln (k_B / h) \qquad \textbf{Equation 2.10}$$

As temperature and pressure affects the rate constant of racemization; at a given temperature T (in Kelvin), the effect of pressure P (in MPa) on the racemization rate constant k_{rac} is given by equations 2.6-2.10,[17,18] where, $\tau_{1/2}$ is the half-life of racemization, R is the gas

constant (8.314 cm^3 $MPa \cdot K^{-1} \cdot mol^{-1}$), C is a constant, $[P]_0$ is the initial concentration of the *P* isomer, $\chi = [P_0\text{-}([P],[M])]$, ($[P]$,$[M]$) represents the concentration of racemate at time *t*, k_B is the Boltzmann constant, and *h* is Planck's constant. The racemization is a macroscopic phenomenon compared to enantiomerization which is a microscopic phenomenon, the relation between both is given by $k_{rac} = 2 \cdot k_{enant}$, where k_{enant} is the rate constant for enantiomerization.[15]

Racemization studies were carried out using CD spectroscopy in spectrometric-grade solvents in a custom-built high-pressure vessel (refer to experimental section for details). Two distinct set of experiments were performed *viz.*, a) racemization at constant pressure and variable temperature; b) racemization at constant temperature and variable pressure

2.4.3. Racemization kinetics on 2-pyridone 146c at normal pressure (0.1 MPa)

The first set of experiments (Table 2.4, Figure 2.4) was performed under isobaric conditions (0.1 MPa) while varying the temperature. The change in the ellipticity of the CD signal during the course of the study was used to determine the racemization rate constant (k_{rac}), activation free energy ($\Delta G^{\ddagger}_{rac}$), activation enthalpy ($\Delta H^{\ddagger}_{rac}$), and activation entropy ($\Delta S^{\ddagger}_{rac}$) for racemization. Analysis of table 2.4 and figure 2.4 showed that the 2-pyridone **146c** displayed a decrease in half-life upon increasing the temperature. For example, the half-life of **146c** in methylcyclohexanes (MCH) at 323 and 343 K was 2.1 h and 13 min respectively. Similarly, the half-life depended on the type of solvent employed, where a non-polar solvent seemed to stabilize the axial chirality effectively than a polar solvent. For example, half-life of **146c** at 343 K in MCH and ethanol was 13 and 7.7 min respectively.

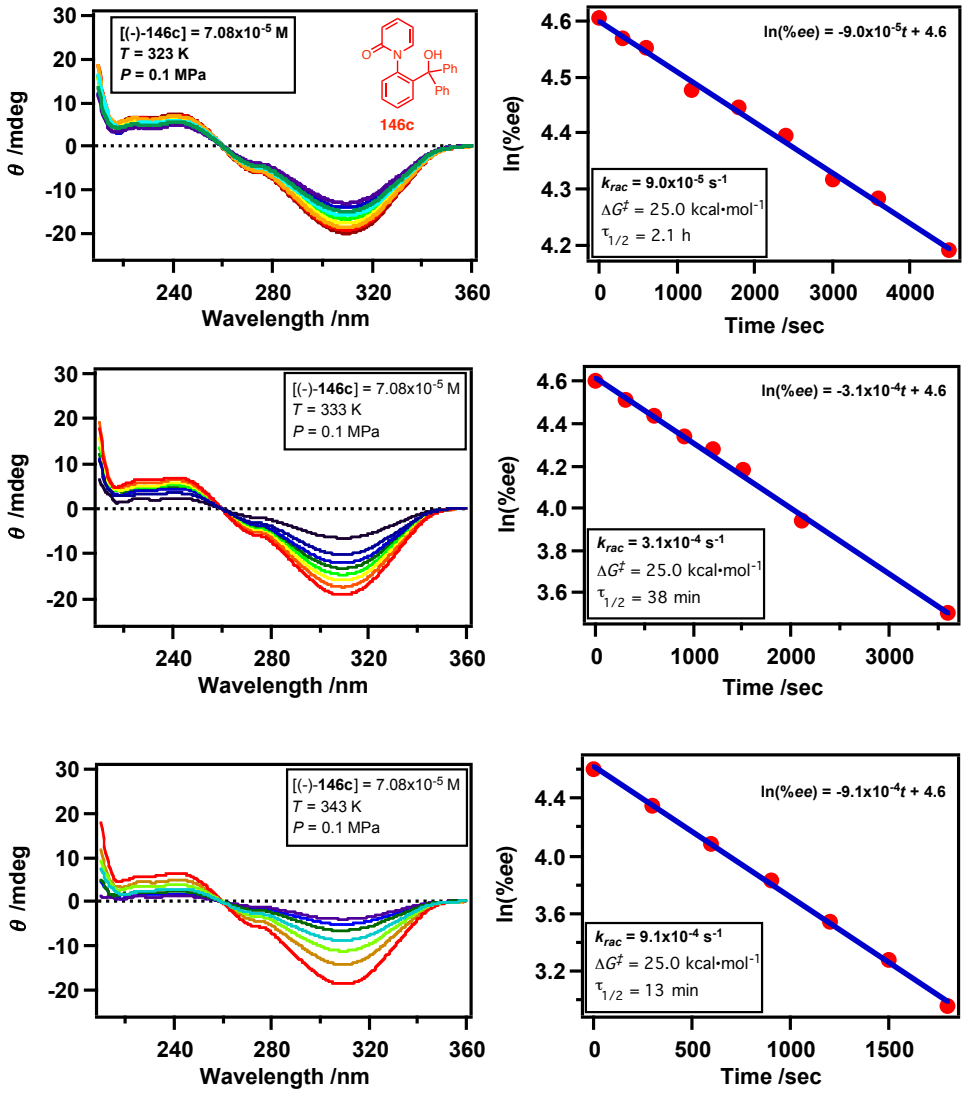

Figure 2.4: Racemization kinetics of optically pure compound (-)-**146c** monitored by CD spectroscopy at 0.1 MPa in MeCN. (Reproduced from reference 19; Copyright: 2013 WILEY-VCH Verlag GmbH & Co©).

Table 2.4: Rate constant (k_{rac}), energy barrier ($\Delta G^{\ddagger}_{rac}$) and half-life of racemization ($\tau_{1/2}$) for optically pure atropisomers **146c** at different temperatures and at pressure of 0.1 MPa.[a]

Entry	Solvent[b]	T (*K*)	k_{rac} (s^{-1})[c]	$\Delta G^{\ddagger}_{rac}$ (kcal·mol^{-1})	$\tau_{1/2}$[c]
1	MeCN	323	9.0×10^{-5}	25.0	2.1 h
2		333	3.1×10^{-4}	25.0	38 min
3		343	9.1×10^{-4}	25.0	13 min
4	EtOH	323	3.5×10^{-4}	24.1	33 min
5		333	1.0×10^{-3}	24.2	12 min
6		343	1.5×10^{-3}	24.6	7.7 min

[a] Analysis of the racemization kinetics was performed inside a built high-pressure cell with diamond windows and monitored by CD spectroscopy. All of these values carry an error of 10 %. [b] 7.36×10^{-5} M in EtOH and 9.03×10^{-5} in MeCN. [c] k_{rac} and $\tau_{1/2}$ were obtained from Equations (2.8) and (2.9), respectively.

The activation enthalpy ($\Delta H^{\ddagger}_{rac}$), and activation entropy ($\Delta S^{\ddagger}_{rac}$) calculated from the Eyring plot (Figure 2.5 and Eq. 2.10) showed that the sign of $\Delta S^{\ddagger}_{rac}$ is negative (-2.55 J·mol^{-1}·K^{-1}) suggesting that the racemization is entropically unfavorable as it involved steric encounters during racemization process, on the other hand a positive value was obtained for $\Delta H^{\ddagger}_{rac}$ (103 kJ·mol^{-1}).

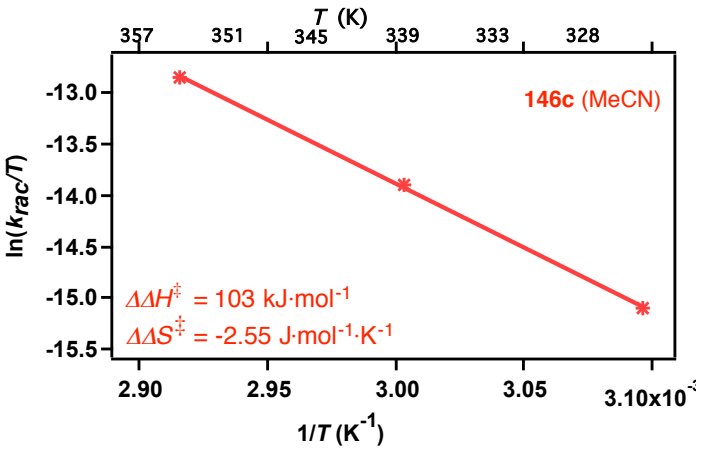

Figure 2.5: Eyring plots for the racemization of 2-pyridone **146c** at 0.1 MPa (MeCN).

2.4.4. Racemization kinetics on 2-pyridone 146c at elevated pressure (12 MPa)

In the second set of experiments (Figure 2.6 and 2.7), the temperature was kept constant and the pressure was varied to determine the activation volume ($\Delta V^{\ddagger}_{rac}$) for the racemization. A comparison is provided in the figure 2.6 that clearly showed the influence of pressure on racemization. For example, the half-life of racemization ($\tau_{1/2}$) at 0.1 MPa and 12 MPa was 0.2 and 2.9 h respectively. To comprehend the influence of pressure on racemization, it is essential to understand the activation volume ($\Delta V^{\ddagger}_{rac}$) involved in the racemization process at various pressures. From equation 2.6 and 2.7, for a given temperature, a rate acceleration will be observed for processes that has negative differential activation volume as observed in case of certain cycloaddition reactions where the transition state partial molar volume is diminished[20-22] compared to a process that has a positive differential activation volume in which case the rate deceleration will be observed.

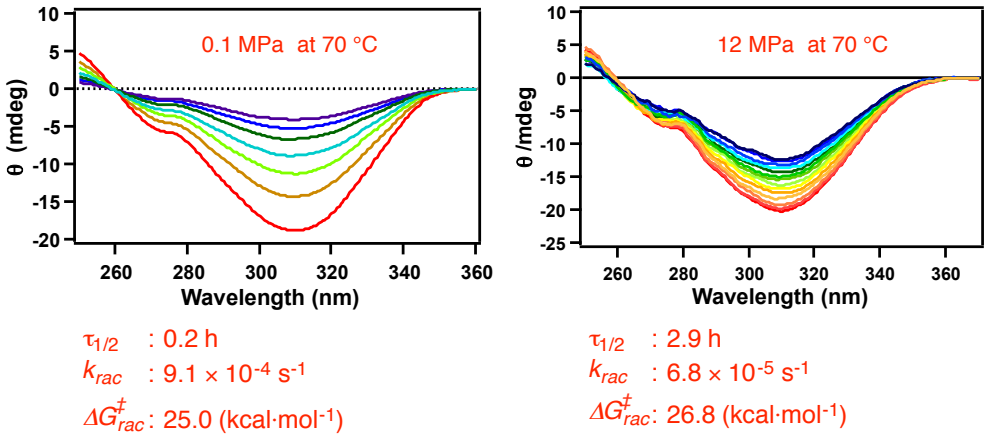

Figure 2.6: Comparison of racemization kinetics of 2-pyridone **146c** in MeCN at 0.1 (left) and 12 MPa (right).

In the non-biaryl atropisomeric 2-pyridone **146c**, the activation volume was positive suggesting that the partial molar volume is increased in the transition state. Thus, the high pressure decelerates the racemization process resulting in higher racemization barrier. Also, the activation volume ($\Delta V^{\ddagger}_{rac}$) in 2-pyridone was considerably larger (651 $cm^3 \cdot mol^{-1}$) that made the pressure to have higher influence on the racemization (moderate increase in pressure slowed

down racemization effectively). In other word, at high pressure, the solvent cluster surrounding the atropisomeric 2-pyridones will be tightly packed inhibiting the racemization process considerably.

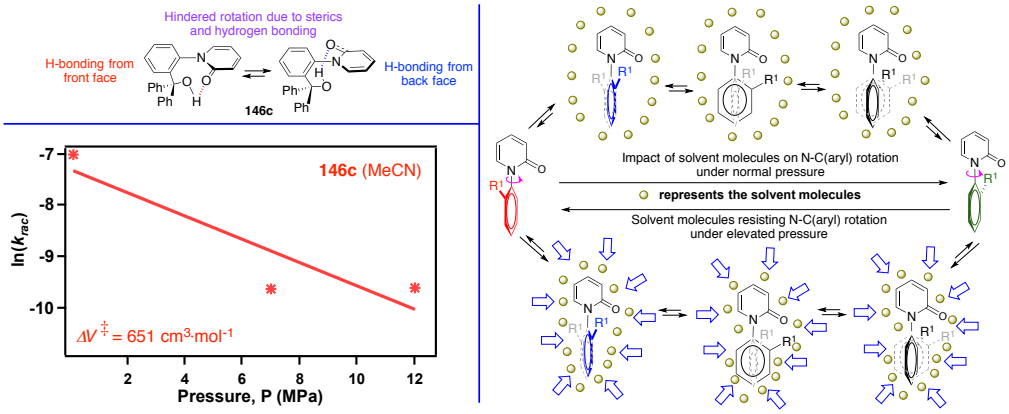

Figure 2.7: Left: Plot of the pressure dependence of racemization to determine the activation volume for 2-pyridone **146c** at 343 K; Right: Effect of pressure and role of solvents and non-bonding interactions on racemization.

2.5. Enantiospecific photoreactions of atropisomeric 2-pyridones

2.5.1. Enantiospecific photoreactions in various solvents

The enantiospecific photoreactions of atropisomeric 2-pyridones were carried out on optically pure *P/M* isomers in various solvents ranging from polar protic to nonpolar aprotic and at various temperatures (Scheme 2.9). The idea was to understand/evaluate the influence of axial chirality, intra/intermolecular H-bonding and temperature during enantiospecific 4π-ring closure of 2-pyridones.

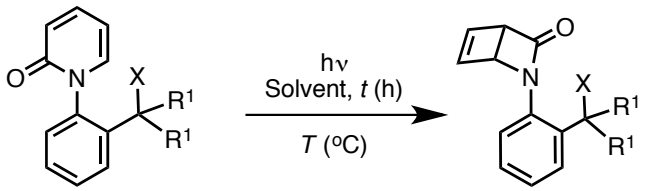

146a-c
a) R^1 = Me; X = Me
b) R^1 = Me; X = OH
c) R^1 = Ph; X = OH

147a-c

Scheme 2.9: Enantiospecific phototransformation of atropisomeric 2-pyridones **146a-c**.

The results in table 2.5 clearly indicated that the solvent and temperature played a crucial role in the enantiomeric excess (*ee*) in the β-lactam photoproduct. The extent of influence depended on the type of atropisomeric 2-pyridone evaluated. For example, the *ee* for the *tert*-butyl substituted 2-pyridone **146a**, was only marginally affected up on changing solvent, with polar protic solvents favoring higher *ee* values (compare values in entry 1, Table 2.5). Similarly, the *ee* of the reaction was only minimally altered upon varying the temperature (compare entries 1 and 5, Table 2.5).

However, the solvent and temperature had significant impact on the *ee* for the 2-pyridones **146b-c** that had the ability to form intra/intermolecular H-bonding. For instance in **146b**, the *ee* was higher in polar protic solvent such as H_2O compared to nonpolar aprotic solvent such as toluene (compare entry 9, Table 2.5). Similarly, lowering the temperature resulted in higher *ee* values in the photoproducts (compare entries 7-11, Table 2.5).

Table 2.5: Enantiospecific 4π-ring closure of atropisomeric 2-pyridones **146a-c**: Enantiomeric excess for **147a-c** in various solvents and temperatures[a]

Entry	*T* (°C)	*t* (h)	Enantiomeric excess in **147** (% *ee*)							
			Toluene		MeCN		MeOH		H_2O	
			(*P*)-**146a**	(*M*)-**146a**	(*P*)-**146a**	(*M*)-**146a**	(*P*)-**146a**	(*M*)-**146a**	(*P*)-**146a**	(*M*)-**146a**
1	65	2	72 (*S,R*)	72 (*R,S*)	84 (*S,R*)	84 (*R,S*)	86 (*S,R*)	86 (*R,S*)	-[b]	-[b]
2	45	3	76 (*S,R*)	76 (*R,S*)	82 (*S,R*)	82 (*R,S*)	88 (*S,R*)	88 (*R,S*)	-[b]	-[b]
3	25[c,d]	5	70 (*S,R*)	70 (*R,S*)	86 (*S,R*)	86 (*R,S*)	84 (*S,R*)	84 (*R,S*)	-[b]	-[b]
4	5	10	72 (*S,R*)	72 (*R,S*)	88 (*S,R*)	88 (*R,S*)	82 (*S,R*)	82 (*R,S*)	-[b]	-[b]
5	-25	15	72 (*S,R*)	72 (*R,S*)	82 (*S,R*)	82 (*R,S*)	86 (*S,R*)	86 (*R,S*)	-[b]	-[b]
6[f]	25	18	67 % conversion		74 % conversion		76 % conversion		-	
			(+)-**146b**	(-)-**146b**	(+)-**146b**	(-)-**146b**	(+)-**146b**	(-)-**146b**	(+)-**146b**	(-)-**146b**
7	65	2	21 (B)	22 (A)	51 (B)	51 (A)	62 (B)	61 (A)	93 (B)	93 (A)
8	45	3	60 (B)	61 (A)	84 (B)	83 (A)	85 (B)	87 (A)	94 (B)	94 (A)
9	25	5	64 (B)	65 (A)	76 (B)	77 (A)	87 (B)	88 (A)	93 (B)	93 (A)
10	5	10	82 (B)	83 (A)	82 (B)	84 (A)	88 (B)	89 (A)	95 (B)	95 (A)
11	-25	15	82 (B)	84 (A)	89 (B)	88 (A)	93 (B)	93 (A)	-[e]	-[e]
12[f]	25	18	75 % conversion		87 % conversion		97 % conversion		98 % conversion	
			(-)-**146c**	(+)-**146c**	(-)-**146c**	(+)-**146c**	(-)-**146c**	(+)-**146c**	(-)-**146c**	(+)-**146c**
13	65	20[g]	69 (B)	69 (A)	70 (B)	70 (A)	86 (B)	86 (A)	-[b]	-[b]
14	45	25[g]	88 (B)	88 (A)	90 (B)	90 (A)	90 (B)	90 (A)	-[b]	-[b]
15	25	35[g]	94 (B)	94 (A)	94 (B)	94 (A)	97 (B)	97 (A)	-[b]	-[b]
16	5	2	63 (B)	63 (A)	75 (B)	76 (A)	79 (B)	79 (A)	-[b]	-[b]
17[f]	25	-[h]	36 % conversion (5 h)		44 % conversion (7 h)		60 % conversion (10 h)		-	

[a] Irradiations were performed using 450W medium pressure mercury lamp under constant flow of N_2. (+) and (-) represents the signs of optical rotation of **146** in MeOH. For **146a**, (*S,R*) and (*R,S*) represent the (*1S,4R*) and (*1R,4S*) configurations, respectively. For **146b** and **146c**, A and B refer to the elution order for a given pair of enantiomers. [b]Not soluble in water. [c]Similar *ee* were observed at Pyrex and 340 nm cutoff filters. [d]The *ee* values at 25 °C in toluene were 82% (2 h), 76% (4 h), 70% (5 h), and 68% (6 h). [e]Below the freezing point of the solvent. [f]The conversion and mass balance were calculated based on ^{1}H NMR using triphenylmethane as the internal standard. [g]The irradiation time given in minutes. For **146c**, to keep the conversions below 10%, irradiation times were shortened as follows, for MeOH 5 mins (65 °C), 11 min (45 °C), and 12 min (25 °C). Similarly for toluene and MeCN irradiation times were limited to 35 mins (25 °C). [h]The irradiation times are given in parenthesis.

2.5.2. Effect of pressure on enantiospecific 4π-ring closure of 2-pyridones 146a-c

The photoreactions of optically pure 2-pyridone **146c** was investigated in MeCN at 70 °C under various pressures (0.1-100 MPa, Table 2.6). At ambient pressure (0.1 MPa) and at high temperature, the *ee* of the photoproduct was rather low (*ee* = 4%). Upon slightly increasing the pressure to 20 MPa, a clear increase in the *ee* value was observed that upon further increasing the pressure to 100 MPa resulted in an *ee* of 27%. Higher pressure enabled efficient transfer of axial chirality from the starting material to point chirality in the photoproduct. Further increase in the pressure resulted in precipitation/crystallization of the 2-pyridone **146c** leading to a cloudy solution inhibiting the photochemical reaction.

Table 2.6: Enantiospecific 4π-ring closure of 2-pyridone **146c** under various pressures in MeCN at 70 °C.[a]

Entry	Compound	*t* (h)	(%) *ee* in photoproduct		
			0.1 MPa	20 MPa	100 MPa
1	(-)-**146c**	1	4 (B)	18 (B)	27 (B)

[a] The samples were placed inside a pressure cell that was equipped with sapphire windows. Irradiation was performed by using an optical fiber that contained a light source from an Xe lamp. The values are an average of two runs and carry an error of ±20%, owing to experimental limitations of handling the samples at elevated pressure and temperature in the cell.[b] (+) and (-) denote the sign of the optical rotation of the reactant.[c] A and B refer to the elution order of the enantiomers during HPLC analysis on a chiral stationary phase.

To appreciate the effect of pressure on the enantiospecificity of the reaction; it is critical to understand the influence of pressure and the solvent molecules on the substrate. Under ambient pressure, the substrate was surrounded by weak solvent cluster that was governed by weak interactions such as van der Waals forces and H-bonding interactions. Upon increasing the pressure, the solvent molecules are forced to close in that freeze the molecular conformation of the substrate. As racemization involved the rotation of N-C_{aryl} bond, it has to overcome the pressure provided by the surrounding solvent molecules, which in turn was highly influenced by the applied pressure. Also, the reorganization of solvent molecules around the chiral axis during N-C_{aryl} bond rotation was highly impacted by the applied pressure. Thus, these changes contribute to the change in the activation volume ($\Delta V^{\ddagger}_{rac}$) values. Larger the value of $\Delta V^{\ddagger}_{rac}$, higher

will be the influence of pressure on racemization. The observed *ee* in the photoproduct can be expressed as a function of differential activation volume ($\Delta\Delta V^{\ddagger}_{S\text{-}R}$) as shown in the equation

$$(\ln k_S/k_R) = -(\Delta\Delta V^{\ddagger}_{S\text{-}R}/RT)P + C \qquad \textbf{Equation 2.11}$$

It is important to note that the $\Delta V^{\ddagger}_{rac}$ and $\Delta\Delta V^{\ddagger}_{S\text{-}R}$ are quite different in the sense that, $\Delta V^{\ddagger}_{rac}$ is the change in volume accompanied during the racemization of atropisomers; on the other hand $\Delta\Delta V^{\ddagger}_{S\text{-}R}$ is the difference in the diastereomeric transition state volume during the course of photochemical transformations.

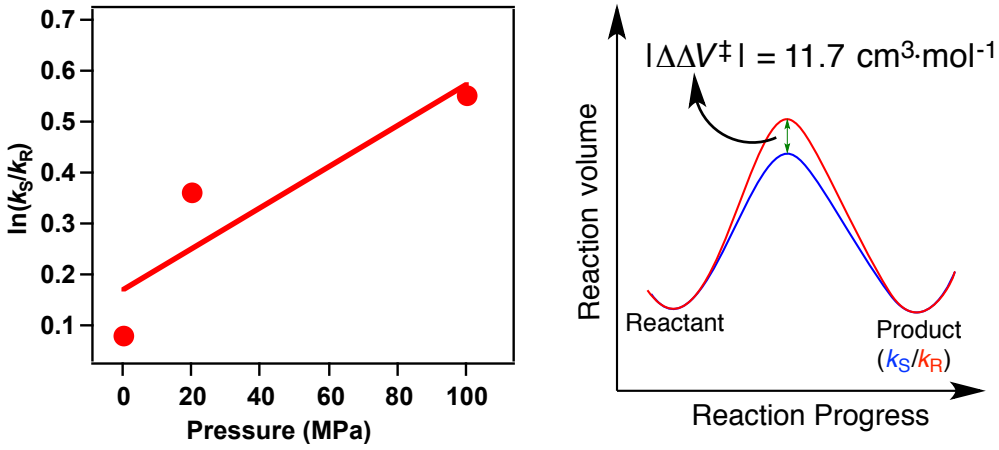

Figure 2.8: Left: Plot of the pressure dependence of the relative rate constant at 343 K to determine the differential activation volume ($\Delta\Delta V^{\ddagger}$) during the 4π-ring closure of 2-pyridone **146c** in MeCN. Right: The absolute value of $\Delta\Delta V^{\ddagger}$ is provided because the sign will depend on which enantiomer in the photoproduct is enhanced during the photochemical transformation. k_S and k_R represent the rate of formation of the individual enantiomeric photoproducts. (Reproduced from reference19, Copyright: 2013 WILEY-VCH Verlag GmbH & Co©).

Thus the $\Delta\Delta V^{\ddagger}_{S\text{-}R}$ (Figure 2.8, right) represents the rate of formation of k_S over its enantiomer k_R that determines the enantiomeric excess in the photoproduct. The plot of ln *k vs.* pressure (Figure 2.8, left) resulted in a straight line suggesting that the pressure did not alter the operating mechanism.

2.5.3. Reaction kinetics of 4π-ring closure of 2-pyridone 146a monitored by UV-Vis spectroscopy

The course of photochemical transformation of atropisomeric 2-pyridones was followed by UV-Vis spectroscopy. A solution of 2-pyridones (**146a** ~0.16 mM and **146b** ~0.22 mM) in a given solvent was irradiated at 25 ^{o}C using 450 W medium pressure mercury lamp with Pyrex filter. The decrease in the concentration of starting material was monitored by UV-Vis spectroscopy. The slope of ln(concentration) vs. time gave the rate of the reaction (Figure 2.9).

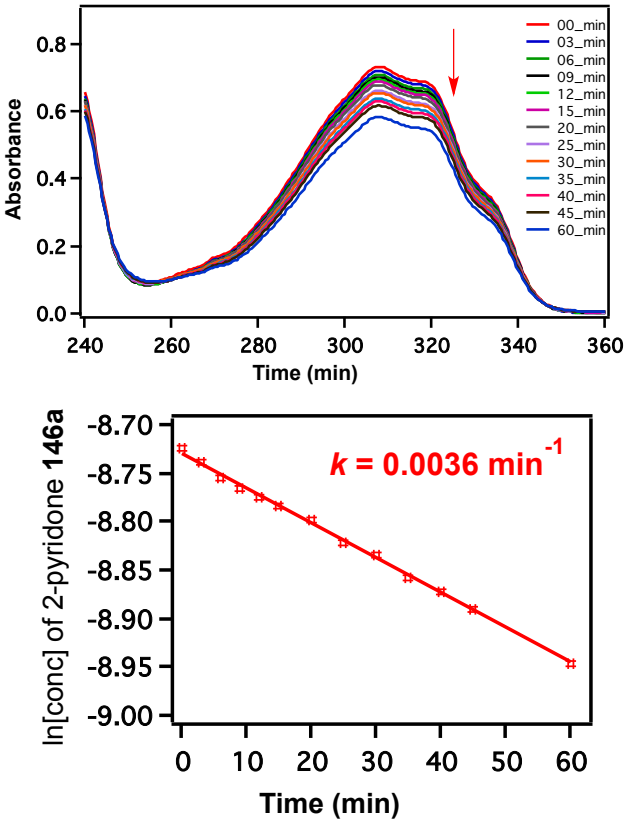

Figure 2.9: Top: Time dependent irradiation of 2-pyridone **146a** in MeCN followed by UV-Vis spectroscopy (*c* ~ 0.16 mM) leading to photoproduct **147a**. Bottom: Plot of ln[*conc.* of **146a**] *vs.* time.

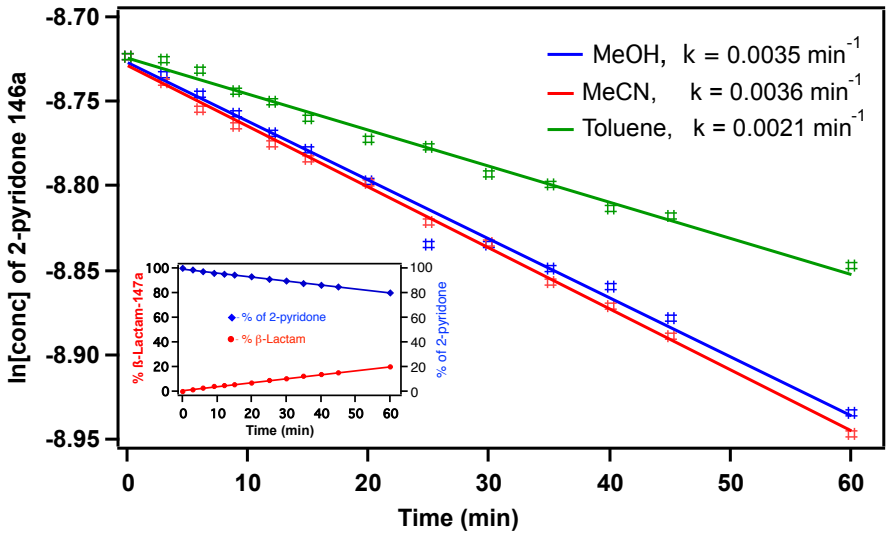

Figure 2.10: Rate of disappearance of 2-pyridone **146a** in different solvents (*c* ~ 0.16 mM). Inset: Time dependent irradiation to monitor the reaction progress. Inset: Formation of β-Lactam – **147a** (Red) and disappearance of the reactant 2-pyridone (**146a** (Blue).

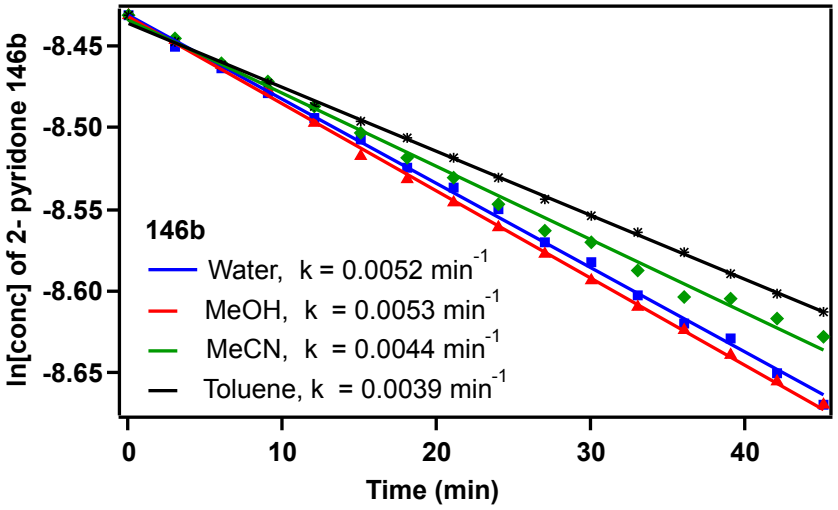

Figure 2.11: Rate of disappearance of 2-pyridone **146b** in different solvents (*c* ~ 0.22 mM).

Comparison of Figure 2.10 and 2.11 clearly indicated that the rate of reaction was faster in polar protic solvents compared to nonpolar aprotic solvents. For example the rate reaction for **146a** in methanol and toluene was 0.0035 min^{-1} and 0.0021 min^{-1} respectively (Figure 2.10). Similar conversions were observed in the case of **146b** as shown in figure 2.11 albeit with smaller slope.

2.5.4. Conversion and mass balance after photoreactions in 2-pyridones

Conversion and mass balance in 2-pyridones **146a-c** (~2.2 mM) were obtained by irradiating a racemic mixture in respective solvents (methanol, acetonitrile, toluene, and water (only for **146b**)). The solution in a Pyrex tube was irradiated using 450 W medium-pressure mercury lamp with 295 nm filter for 18 h at room temperature under constant flow of nitrogen. After the irradiation, a stock solution of internal standard in chloroform (triphenylmethane) was added to the reaction mixture. The solvent from the mixture was completely evaporated under reduced pressure. The residue was dissolved in 1 mL of deuterated chloroform and ^{1}H-NMR was recorded. From the integral value of respective peaks, the % conversion and mass balance was calculated using the formula given below.

$$mol_a = mol_i \; X \left(\frac{\text{Integral of analyte}}{\text{Integral of Int. Std}} \right) X \frac{N_a}{N_i} \qquad \textbf{Equation 2.12}$$

Where, N_a and N_i are the number of nuclei giving rise to the relevant analyte and internal standard signals respectively. Similarly mol_a and mol_i are the molarity of analyte and the internal standard in deuterated chloroform respectively.

Table 2.7: Conversion and mass balance in photoreactions of 2-pyridones **146a-c**.

Entry	Solvent	Compound	Conversion (%)	Mass balance (%)
1	Toluene	**146a**	67	88
2		**146b**	75	92
3		**146c**	36	97
4	Acetonitrile	**146a**	74	84
5		**146b**	87[a]	83[a]
6		**146c**	44	92
7	Methanol	**146a**	76	94
8		**146b**	97	89
9		**146c**	60	87
10	Water	**146a**	-[b]	-[b]
11		**146b**	98	91
12		**146c**	-[b]	-[b]

[a] Reaction at a concentration of 2.2 mM resulted in uncharacterized side product. But when concentration was changed to 0.22 mM, only to 4π-ring closure photoproduct was observed. [b] The compound was not soluble in water. Reported values carry an error of ±5%.

2.5.5. Time dependent irradiation of 2-pyridone 146c in various solvents

The enantiospecific photoreaction that determines the *ee* in the photoproduct competes with racemization during the photoreaction. So, the rate of individual processes (photoreaction vs. racemization) determines the resultant *ee* in the product and the recovered starting material (SM). To understand the effect of longer irradiation times in atropisomeric 2-pyridones and the erosion in enantiomeric purity, we carried out time dependent irradiation of **146a** and **146c**. Time dependent irradiation was carried out by irradiating optically pure isomers in various solvents for a given time period in a Pyrex tube using a 450 W medium-pressure mercury lamp under constant flow of N_2. After the reaction, the solvent was removed and the photoproduct and the starting material were isolated by preparative thin layer chromatography and the *ee* in the photoproduct and in the recovered SM was analyzed on a chiral stationary phase using HPLC.

Analysis of table 2.8 clearly indicated that longer irradiation times led to higher conversion albeit taking a toll in the observed *ee* values in the photoproducts. Interestingly, the enantiomeric excess in the SM also diminished during the course of irradiation time. The *ee* values obtained in the recovered SM in the photoreaction and the analysis of *ee* values in the sample kept in dark for the same time period was quite contrasting. For example, in the case of **146a**, *ee* of recovered SM at 6 h of irradiation was 30% (Table 2.8, entry 4), on the other hand, no racemization was observed in the sample kept in dark ($\tau_{1/2}$ = 120 days in toluene at 25 °C).

Additionally, under our irradiation conditions (Pyrex cutoff), no reversible photoreaction was observed that is usually observed in electrocyclic ring closure reactions. So the reduction in the *ee*, both in the SM and in the photoproduct might not be the result of reversible photoreaction (section 2.5.6). One possible explanation for the observed racemization could be the accelerated racemization during the excited/transition state. In the excited state, the optically pure 2-pyridone can either go to the photoproduct or relax to the ground state. The transformation to the photoproduct occurred with high chiral induction as observed from the *ee* values at the early time of the reaction. On the other hand, if the excited state relaxed to the reactant, then that process might not occur specifically thus resulting in the formation of both the isomers of SM with similar probability resulting in reduced *ee* in the reactant.

Table 2.8: Time dependent irradiation of atropisomeric 2-pyridones **146a** and **146c** in various solvents.

Entry	Compd	Solvent	*T* (°C)	*T* (min)	Conv.[b] (%)	Enantiomeric excess (% ee)[a]			
						Photoproduct		Recovered SM[b]	
						(1*S*,4*R*)-**147a**	(1*R*,4*S*)-**147a**	*(P)*-**146a**	*(M)*-**146a**
1	**146a**	Toluene	25	2[c]	-	82	82	72	76
2				4[c]	-	76	74	48	50
3				5[c]	-	70	70	38	42
4				6[c]	-	68	64	30	30
						(-)-**147c**	(+)-**147c**	(-)-**146c**	(+)-**146c**
5	**146c**	MeOH	65	5	5	86 (B)	86 (A)	62	62
6	**146c**			10	9	74 (B)	74 (A)	56	56
7	**146c**			25	13	54 (B)	54 (A)	27	27
8	**146c**			60	50	24 (B)	24 (A)	2	2
9	**146c**	MeCN	65	20	5	70 (B)	70 (A)	44	44
10	**146c**			45	15	56 (B)	56(A)	28	28
11	**146c**	Toluene	65	20	6	69 (B)	69 (A)	46	46
12	**146c**			50	15	48 (B)	48 (A)	14	14
13	**146c**	MeOH	45	11	5	90 (B)	90 (A)	73	73
14	**146c**	MeCN	45	25	6.5	90 (B)	90 (A)	68	68
15	**146c**	Toluene	45	25	7	88 (B)	88 (A)	66	66
16	**146c**	MeOH	25	12	10	97 (B)	97 (A)	90	90
17	**146c**	MeCN	25	35	10	94 (B)	94 (A)	71	71
18	**146c**	Toluene	25	35	8	94 (B)	94 (A)	70	70

[a] Reported values carry an error of ±3%. A and B refers to elution order for a given pair of enantiomers. [b] Conversion; SM- starting material. [c] Time is reported in hour.

2.5.6. Control studies on photo-reversibility of bicyclo-β-lactam 147 to 2-pyridone 146

The electrocyclic ring closure reactions are known to be reversible depending on the wavelength of irradiation. So we carried out control studies on the photoproduct **147a** under different irradiation conditions to scrutinize the photo-reversibility of bicyclo-β-lactam **147** to its corresponding 2-pyridone **146**. Enantiopure photoproduct (*1S,4R*)-**147a** in toluene (4.36 mM) was irradiated using a 450W medium-pressure mercury lamp under a) Pyrex cutoff; b) 340 nm cutoff and c) Quartz cutoff, at room temperature under constant flow of nitrogen for 5 h. After the irradiation, the solvent was evaporated under reduced pressure, and the crude mixture was dissolved in suitable solvent (hexanes/2-propanol mixture) and analyzed on a chiral stationary phase using HPLC.

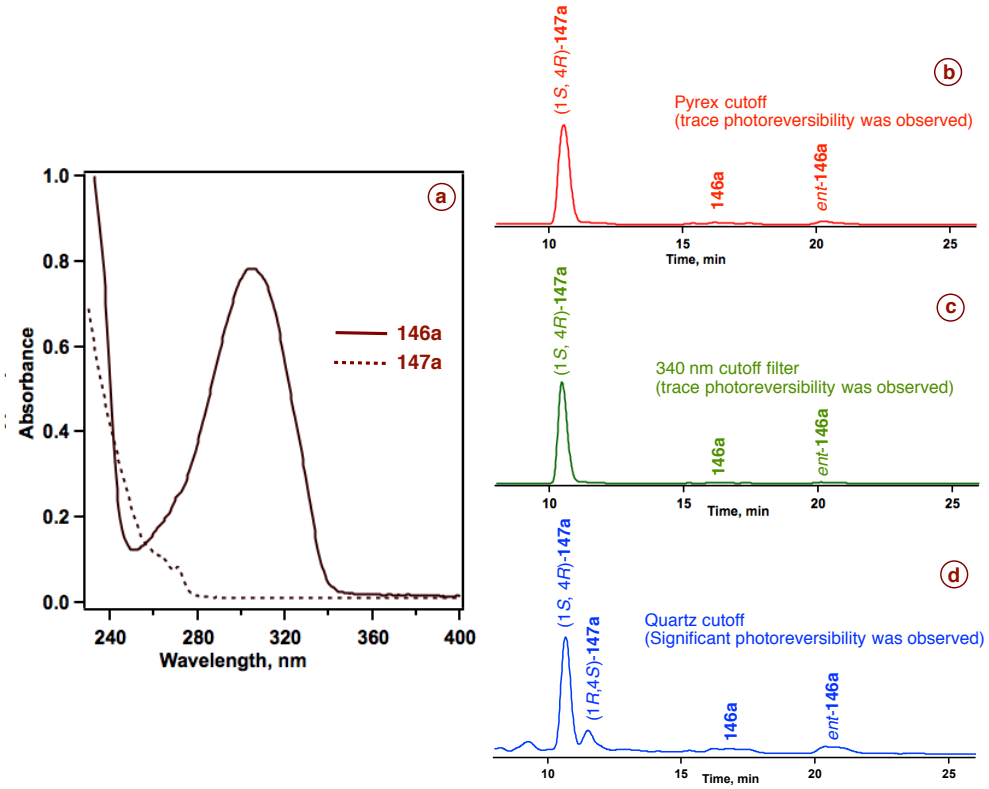

Figure 2.12: (a) UV-Vis spectrum of **146a** and **147a** in methanol (c = ~0.143 mM). (b) Irradiation of (*1S, 4R*)-**147a** in toluene with Pyrex cutoff; (c) with 340 nm cutoff filter and (d) with Quartz cutoff.

a) Irradiation with Pyrex cutoff.

The photo-reversibility under Pyrex cutoff was negligible and the corresponding enantiomer of the photoproduct (*1R, 4S*)-(+)-**147a** as well as the starting material was not observed (Figure 2.12; b).

b) Irradiation with 340nm filter.

The photo-reversibility under 340 nm filter was negligible and the corresponding enantiomer of the photoproduct (*1R, 4S*)-(+)-**147a** as well as the starting material was not observed (Figure 2.12; c).

c) Irradiation with Quartz cutoff.

The photo-reversibility under Quartz cutoff filter was significant. Both the enantiomer of the starting material and the corresponding enantiomer of the photoproduct (*1R, 4S*)-(+)-**147a** were observed (Figure 2.12; d).

This control study clearly showed that the photo-reversibility was highly dependent on the irradiation wavelength. Lower wavelength (Quartz cutoff) irradiation caused significant reversibility in the photoreaction. This can be explained from the UV-vis spectrum of the photoproduct that showed significant absorption (Figure 2.12; a) in the lower wavelength region (<280 nm). As a result the photoproduct is excited at a lower wavelength resulting in the reversibility to form certain percentage of the reactant. On the contrary, the photoproduct does not have absorption profile in the Pyrex cutoff or 340 nm filter cutoff wavelengths where only the reactant is the only absorbing species.

2.6. Eyring plots for calculating differential activation parameters

2.6.1. Eyring plots of atropisomeric 2-pyridones 146a-c

The temperature and solvent dependency of the photoreaction clearly pointed out that the enthalpic and entropic components are operating in the system. To delineate the individual enthalpic and entropic components in the system we resort to the calculation of differential activation parameters ($\Delta\Delta H^{\ddagger}$ and $\Delta\Delta S^{\ddagger}$) using Eyring plots. The following equations were employed to arrive at the Eyring plots.

$$\frac{k_R}{k_S} = \frac{[R]}{[S]}; \quad \text{and } \%\, ee = \frac{[R] - [S]}{[R] + [S]} \times 100; \qquad \textbf{Equation 2.13}$$

this implies:

$$\%\, ee = \frac{\frac{k_R}{k_S}[S] - [S]}{\frac{k_R}{k_S}[S] + [S]} \times 100 \; ; \; \%\, ee = \frac{\frac{k_R}{k_S} - 1}{\frac{k_R}{k_S} + 1} \times 100 \qquad \textbf{Equation 2.14}$$

$$\%\, ee \left(\frac{k_R}{k_S} + 1\right) = \left(\frac{k_R}{k_S} - 1\right) \times 100 \qquad \textbf{Equation 2.15}$$

$$\%\, ee \left(\frac{k_R}{k_S}\right) + \%\, ee = 100 \left(\frac{k_R}{k_S}\right) - 100 \; ; \qquad \textbf{Equation 2.16}$$

this gives $\left(\frac{k_R}{k_S}\right)\left(100 - \%\, ee\right) = \left(100 + \%\, ee\right)$ **Equation 2.17**

Hence,

$$\ln\left(\frac{k_R}{k_S}\right) = \ln \frac{\left(100 + \%\, ee\right)}{\left(100 - \%\, ee\right)} \qquad \textbf{Equation 2.18}$$

Also,

$$\ln\left(\frac{k_R}{k_S}\right) = \ln(k_R) - \ln(k_S) = \frac{-\Delta G_R^{\ddagger}}{RT} - \frac{-\Delta G_S^{\ddagger}}{RT} \qquad \textbf{Equation 2.19}$$

As,

$$\Delta G^{\ddagger} = \Delta H^{\ddagger} - T\Delta S^{\ddagger} \qquad \textbf{Equation 2.20}$$

Hence,

$$\boxed{\ln\left(\frac{k_R}{k_S}\right) = \frac{\Delta\Delta S_{R\text{-}S}^{\ddagger}}{R} - \frac{\Delta\Delta H_{R\text{-}S}^{\ddagger}}{RT}} \qquad \textbf{Equation 2.21}$$

The calculation provided the magnitude and the signs of activation parameters for a given isomer of the atropisomeric 2-pyridones. The values provided crucial information about the enthalpic and entropic components in the system and provided insights into the effect of solvent and temperature on *ee* values in the photoproducts. The following modified Eyring equation was employed to obtain the differential activation parameters for the 4π-ring closure of 2-pyridones.

$$\ln\left(\frac{k_{SR}}{k_{RS}}\right) = \ln\frac{\left(100 + \%\ ee\right)}{\left(100 - \%\ ee\right)} \qquad \textbf{Equation 2.22}$$

$$\Delta G_{SR\text{-}RS}^{\ddagger} = \Delta H_{SR\text{-}RS}^{\ddagger} - T\Delta S_{SR\text{-}RS}^{\ddagger} \qquad \textbf{Equation 2.23}$$

$$\ln\left(\frac{k_{SR}}{k_{RS}}\right) = \frac{\Delta\Delta S_{SR\text{-}RS}^{\ddagger}}{R} - \frac{\Delta\Delta H_{SR\text{-}RS}^{\ddagger}}{RT} \qquad \textbf{Equation 2.24}$$

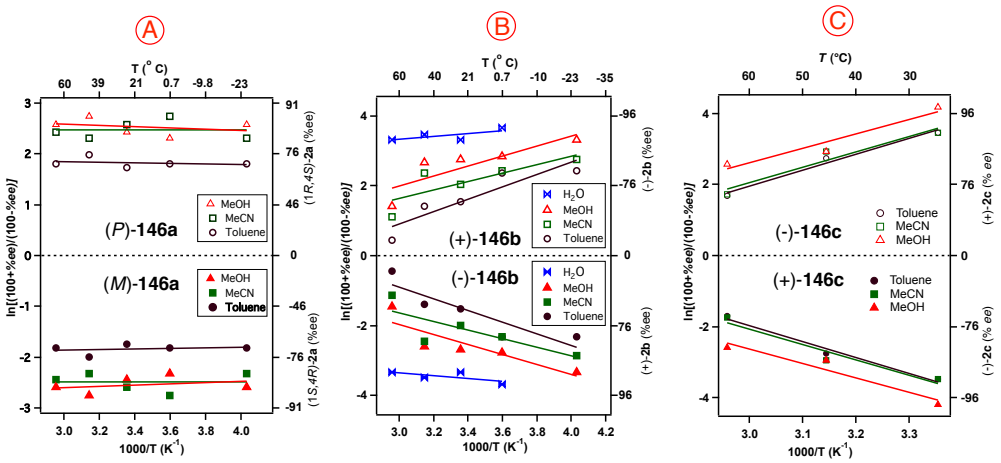

Figure 2.13: Eyring plot for the photoreactivity of atropisomeric 2-pyridones a) **146a** (left), b) **146b** (middle) and c) **146c** (left).

Analysis of Table 2.9 revealed that for **146a**, $\Delta\Delta S^{\ddagger}$ was dominant with a near-zero/minimal contribution from $\Delta\Delta H^{\ddagger}$. This was evident from the near-zero slope of the Eyring plot in all the solvents investigated (Figure 2.13, left). As the contribution from the $\Delta\Delta H^{\ddagger}$ was minimal, the reaction was insensitive to the operating temperature/solvent. This implied that the 4π-ring closure of **146a** was primarily entropically governed. This broader generalization was based on the observed free N-C_{aryl} bond rotation in the photoproduct **147a** compared to the starting material **146a**. The large release in the steric congestion served as the primary driving force (higher $\Delta\Delta S^{\ddagger}$) for the reaction and this manifested itself as the entropic control of the enantiospecificity in **147a**. Also, for (*P*)-**146a**, the positive $\Delta\Delta S^{\ddagger}$ value suggested that (*1S,4R*)-**147a** favored over (*1R,4S*)-**147a**. Similarly, for (*M*)-**146a**, the negative $\Delta\Delta S^{\ddagger}$ value suggested that (*1R,4S*)-**147a** favored over (*1S,4R*)-**147a**.

Table 2.9: Differential activation enthalpic and entropic parameters for enantiospecific 4π-ring closure of atropisomeric 2-pyridones

Entry	Compound	Solvent	$\Delta\Delta H^{\ddagger}$ (kcal·mol^{-1})	$\Delta\Delta S^{\ddagger}$ (cal·K·mol^{-1})
1	(*P*)-**146a**	Toluene	0.123	4.08
2	(*M*)-**146a**		-0.123	-4.08
3	(*P*)-**146a**	Acetonitrile	-0.008	4.91
4	(*M*)-**146a**		0.008	-4.91
5	(*P*)-**146a**	Methanol	0.243	5.87
6	(*M*)-**146a**		-0.243	-5.87
7	(+)-**146b**	Toluene	-3.519	-8.82
8	(-)-**146b**		3.320	8.12
9	(+)-**146b**	Acetonitrile	-2.386	-3.88
10	(-)-**146b**		2.445	4.06
11	(+)-**146b**	Methanol	-2.843	-4.55
12	(-)-**146b**		2.843	4.59
13	(+)-**146b**	Water	-0.847	4.09
14	(-)-**146b**		0.847	-4.09
15	(+)-**146c**	Toluene	8.87	22.7
16	(-)-**146c**		-8.87	-22.7
17	(+)-**146c**	Acetonitrile	8.64	21.8
18	(-)-**146c**		-8.64	-21.8
19	(+)-**146c**	Methanol	8.08	19.0
20	(-)-**146c**		-8.08	-19.0

On the other hand, for **146b**, the differential enthalpic ($\Delta\Delta H^{\ddagger}$) and entropic ($\Delta\Delta S^{\ddagger}$) contributions were highly governed by the type of solvents employed. In a nonpolar solvent (toluene), the relative contribution from enthalpy was substantial compared to a polar solvent (MeOH and H_2O). This was reflected in the larger slope in the Eyring plot upon varying the solvent and temperature (Figure 2.13, middle). For example, nonpolar aprotic solvent such as toluene (where only intramolecular H-bonding is possible) had the largest slope in the graph whose enthalpic contribution was significant. This suggested that the transition state was considerably affected by the intramolecular H-bonding upon photochemical transformations.

Interestingly for **146b**, the signs of $\Delta\Delta H^{\ddagger}$ and $\Delta\Delta S^{\ddagger}$ were different for a given solvent. In MeOH, MeCN, and toluene, $\Delta\Delta H^{\ddagger}$ and $\Delta\Delta S^{\ddagger}$ had the same sign; on the contrary, the $\Delta\Delta H^{\ddagger}$ and $\Delta\Delta S^{\ddagger}$ had opposite signs in water. The *ee* value in the reaction was dictated by the relative contribution form $\Delta\Delta H^{\ddagger}$ and $\Delta\Delta S^{\ddagger}$ as given in $\ln(k_{SR}/k_{RS})$ term (Eq 2.24). Also, $\ln(k_{SR}/k_{RS})$ was affected by the temperature through $\Delta\Delta H^{\ddagger}$/RT term in eq 2.24. For **146b**, the $\Delta\Delta H^{\ddagger}$ and $\Delta\Delta S^{\ddagger}$ values in toluene, MeOH, and MeCN are comparable and had the same sign. So, when the temperature increased, the relative contribution from the $\Delta\Delta H^{\ddagger}$/RT term decreased. This affected the magnitude of the $\ln(k_{SR}/k_{RS})$ term (eq 2.24) thus reflecting in temperature dependence of the *ee* values. The degree of change in the $\ln(k_{SR}/k_{RS})$ term depended on the contribution from $\Delta\Delta H^{\ddagger}$. For example, toluene showed a pronounced change (higher contribution from $\Delta\Delta H^{\ddagger}$) and water shows marginal change (lower contribution from $\Delta\Delta H^{\ddagger}$) in the $\ln(k_{SR}/k_{RS})$ value. However, since $\Delta\Delta H^{\ddagger}$ and $\Delta\Delta S^{\ddagger}$ values carry opposite signs in water, regardless of their relative contributions, the $\ln(k_{SR}/k_{RS})$ term increased but only moderately as $\Delta\Delta H^{\ddagger}$/RT contribution is lower. As a result, for a given isomer of the **146b**, same enantiomer was enhanced but with minimal change in *ee* across the temperature.

For **146c**, a similar trend was followed as observed in the case of **146b** in toluene, MeOH and MeCN (Table 2.9, entries 15-20). Due to the fast racemization of **146c** at higher temperatures, $\Delta\Delta H^{\ddagger}$ and $\Delta\Delta S^{\ddagger}$ values were computed at low conversions (~ 5-10%) to estimate their influence at the initial stages of the reaction. As observed in **146b**, the $\Delta\Delta H^{\ddagger}$ values for **146c** are comparable to the $\Delta\Delta S^{\ddagger}$ values for a given reaction temperature and solvent (toluene, MeOH and MeCN). Since, both $\Delta\Delta H^{\ddagger}$ and $\Delta\Delta S^{\ddagger}$ had the same sign in MeOH, MeCN, and toluene, the change in temperature affected the contribution from the $\Delta\Delta H^{\ddagger}$/RT (higher temperature decreases $\Delta\Delta H^{\ddagger}$/RT) thus changing the magnitude of the $\ln(k_{SR}/k_{RS})$. This is reflected in the temperature dependence of the *ee* values (similar to **146b**).

2.6.2. Enthalpy-Entropy compensation plots atropisomeric 2-pyridones 146a-c

The enthalpy-entropy compensation[23] plot (Figure 2.14) of **146a-c** fitted for different solvents resulted in a strait line passing through the origin (Figure 2.14-top). This suggested that irrespective of the solvent employed, same mechanism was operating in all the substrates investigated.

Similarly, the enthalpy-entropy compensation plot was fitted for the individual substrates (Figure 2.14-bottom). The slope of entropy-enthalpy compensation plot has a unit of temperature (called the isokinetic temperature, β, the temperature at which enantioselectivity become identical irrespective of the solvents employed).[24] The slope was 0.39 in both **146b-c**, while it was 0.025 in the case of **146a** (Figure 2.14-bottom). As the temperature affects the slope values, the smaller slope value in the case of **146a** indicated a higher contribution from entropic factor than enthalpic factor (entropic control) in the stereodifferentiating mechanism.

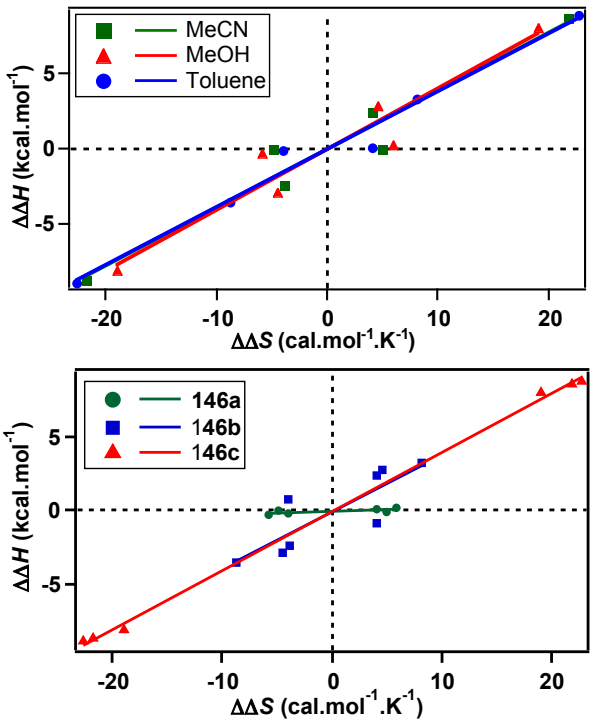

Figure 2.14: Enthalpy-entropy compensation plot fitted with respect to different solvents employed (Top) and fitted for individual substrates **146a-c** (bottom).

2.7. Mechanistic rationale through single crystal XRD analysis

2.7.1. Investigation of mechanistic rationale using single crystal XRD analysis of 146a and 147a

The photoreaction of 2-pyridones occurs via a 4π-*conrotatory* ring closure with equal probability to both inward and outward mode. However, the atropisomeric system was designed to bias one over the other to obtain enantiospecific photoreaction. While the result from table 2.5 clearly suggested enantiomeric excess in the reaction, the preferred mode of ring closure (inward vs outward) for a given isomer of the pyridone was not known. To gain more insights into to the mechanistic rationale, we followed the course of reaction through single crystal XRD. Individual optically pure isomers of 2-pyridone **146a** were crystallized and its absolute configuration was determined using Flack parameters. Similarly, absolute configurations of the photoproducts were also determined. Combining the results obtained from the enantiospecific reactions and absolute configurations of the individual isomers (both starting material and the photoproduct), a clear mechanistic pathway was realized. According to the result, the (*P*)-**146a** preferentially favored the formation of (*1S,4R*)-**147a** photoproduct and the (*M*)-**146a** preferentially favored the formation of (*1R,4S*)-**147a** (Scheme 2.10).

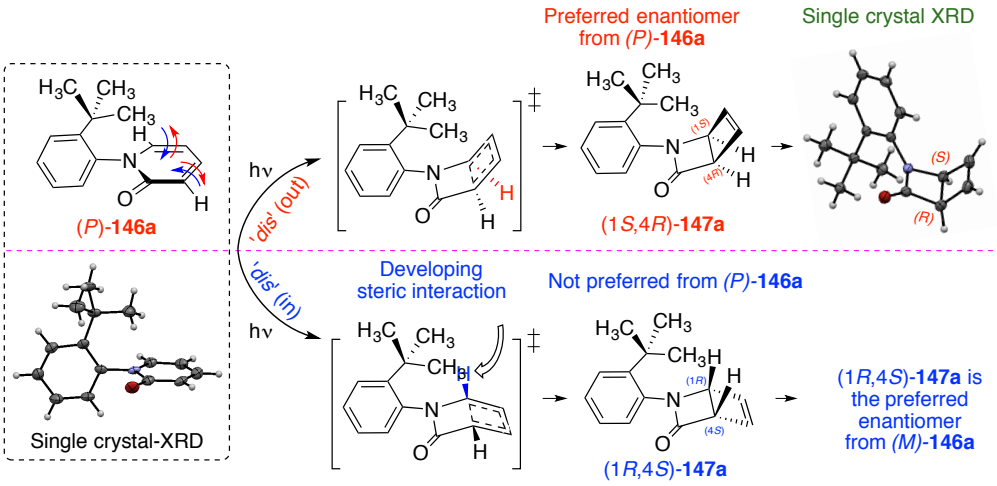

Scheme 2.10: Mechanistic rationale for 4π-ring closure of atropisomeric 2-pyridones **146a**.

Mechanistically, for (*P*)-**146a,** the 4π *dis*-"inward" cyclization was likely hindered by the developing steric interactions between the hydrogens in the pyridone ring and the *o-tert*-butyl group in the transition state, while the 4π *dis*-"out" where the cyclization occurring away from *o-tert*-butyl group was favored, resulting in the observed enantioenriched photoproduct. In terms of enthalpic and entropic factors governing the cyclization, apart from internal steric present in the molecule, external factors such as solvent molecules and temperature played crucial role in determining the enantiospecificity of the reaction. For sterically bulky **146a**, few solvent molecules would be enough to freeze the C−N bond rotation irrespective of the temperature. So, temperature did not have much influence on the enantiospecificity of the reaction. On the other hand, for **146b** and **146c**, apart from smaller sterics and intramolecular H-bonds, intermolecular H-bonds with the solvent (with the amide carbonyl) are necessary to freeze the C−N bond rotation (Scheme 2.11). So the temperature affected the enantiospecificity of the reaction as it determined strength and magnitude of the H-bonds.

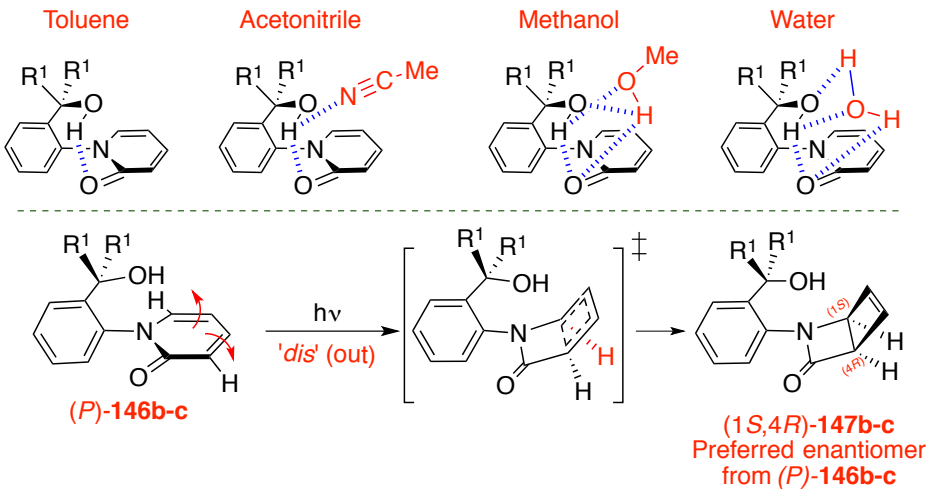

Scheme 2.11: Mechanistic rationale for 4π-ring closure of atropisomeric 2-pyridones **146b-c**.

Qualitatively, the difference in $\Delta\Delta G^{\ddagger}$ [which is related to $\ln(k_{SR}/k_{RS})$] for the preferred mode of cyclization for a given enantiomer of 2-pyridone (*dis*-"in" vs *dis*-"out") depended on both steric impediments and the strength and number of H-bonds, that was dictated by the solvent

clusters above and below the plane of the pyridone ring. According to scheme 2.10, the *dis*-"in" cyclization in (*P*)-**146** isomer would suffer from greater molecular constraints (steric constraints for **146a**; sterics, H-bonding, and solvent clusters for **146b** and **146c**) over the *dis*-"out" cyclization, which was revealed in the $\Delta\Delta G^{\ddagger}$ values. The degree of $\Delta\Delta G^{\ddagger}$ was mainly controlled by the entropic difference in the transition state ($\Delta\Delta S^{\ddagger}$) in **146a** (for *dis*-"in" vs *dis*-"out" mode of cyclization). On the other hand, the degree of $\Delta\Delta G^{\ddagger}$ was controlled by both entropic and enthalpic factors in **146b** and **146c**.

2.8. Variable temperature NMR studies on Photoproduct 147a

The axial chirality in the starting material responsible for the enantiospecificity in the photoreaction was lost in the photoproduct. As established,[25] the reduced C-N-C bond angle in the β-lactam photoproduct allows for the facile bond rotation making it enantiomeric. As temperature plays an essential part in the racemization and energy barrier to rotation, we attempted to record variable temperature NMR studies to ascertain the energy barrier for hindered rotation in N-C_{aryl} bond. Optically pure photoproduct (*1R,4S*)-**147a** was taken in $CHCl_3$ and proton NMR (400 MHz) was recorded at various temperature. Even at -50 °C, We did not notice any diastereotopic peaks due to the restricted rotation around N-C_{aryl} bond. It is clear that the N-C_{aryl} bond rotation was fast in the β-lactam photoproduct due to the reduced C-N-C bond angle.

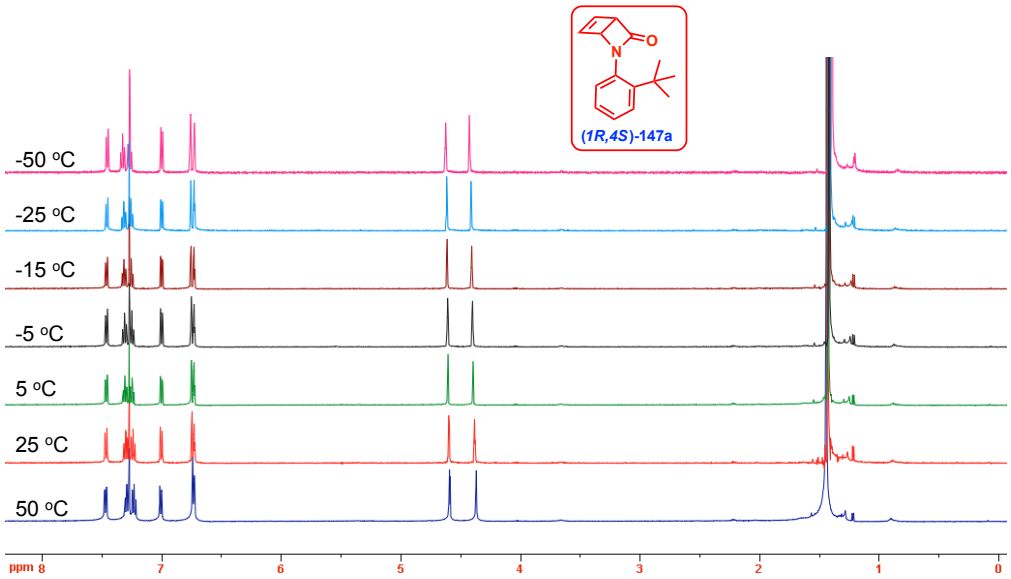

Scheme 2.12: Variable temperature NMR carried out on (*1R,4S*)-**147a** photoproduct.

2.9. Correlating experimental CD spectra, computed CD spectra and X-ray structures.

The experimental CD spectra of individual isomers of **146a** and its photoproducts **147a** were correlated with electronic spectra that were computed using DFT calculations.[26,27] The crystal structures of (*M*)-**146a**, (*P*)-**146a**, (*1S,4R*)-**147a** and (*1R,4S*)-**147a** were optimized using DFT method at B3LYP/6-311++G(2d) level. The optimized structures from the DFT calculations were then subjected for TD-DFT (B3LYP/6-311++G(2d) calculations and the electronic CD spectra of the individual stereoisomers were obtained from the output file using the GaussSum software package v2.2 (sigma values from 0.3 to 0.7 eV). The optimization was performed with "50-50 nstates= 12". The computed CD spectra were compared with the experimental data. The basis set was a good approximation to the basis set limit as evident from good agreement between the experimental and computed spectra with only minor differences between length and velocity rotational strengths. Additionally, we were interested in the qualitative comparison between the spectral shapes for the individual isomers with the experimental CD spectra. During optimization, methanol was used as a solvent in the case of **146a**, while for **147a**, the optimization was done in the gas phase. Although there were observable differences in the wavelength shifts (10-20 nm) between the experimental and computed CD spectra, the sign of ellipticity matched for a given stereoisomer (Figure 2.15 and 2.16).

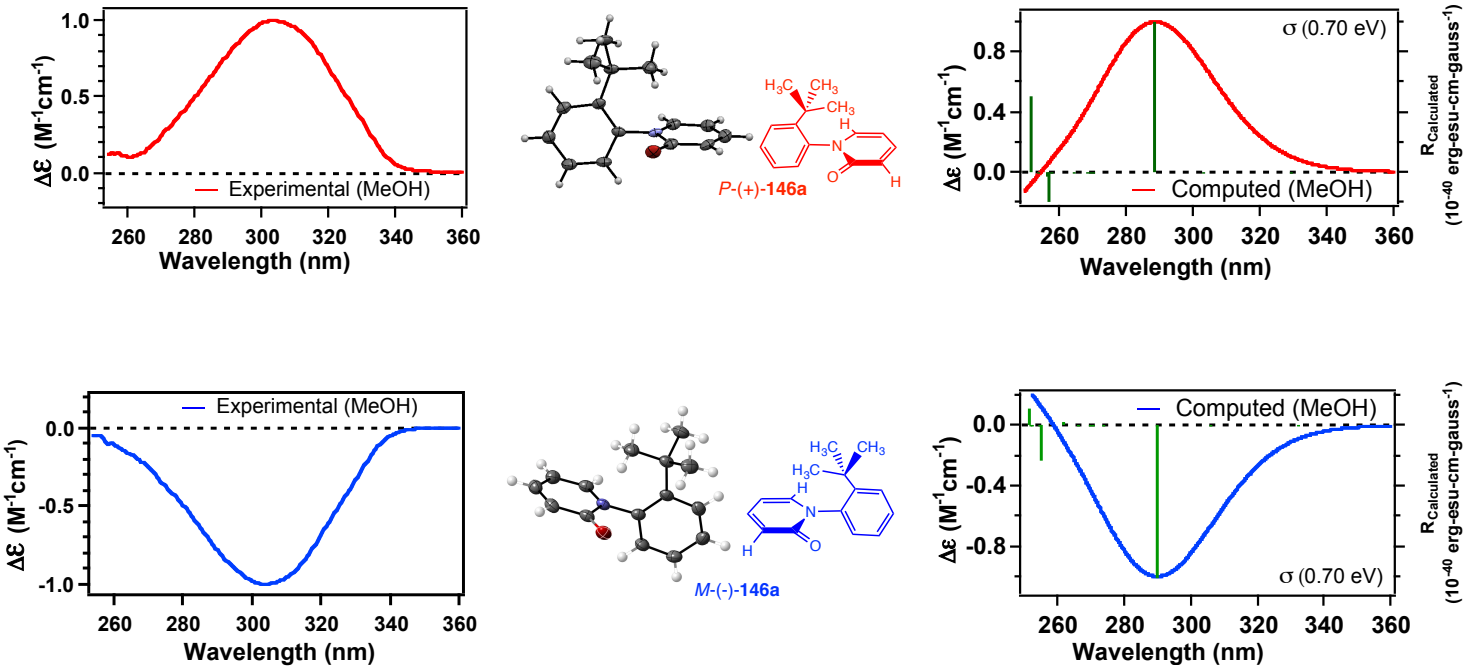

Figure 2.15: Left: Experimental CD spectra of (*P*)-**146a** (top) and (*M*)-**146a** (bottom). Right: Computed CD spectra of (*P*)-**146a** (top) and (*M*)-**146a** (bottom) (Reproduced from *ΔΔ* 28, with permission from American Chemical Society, 2011).

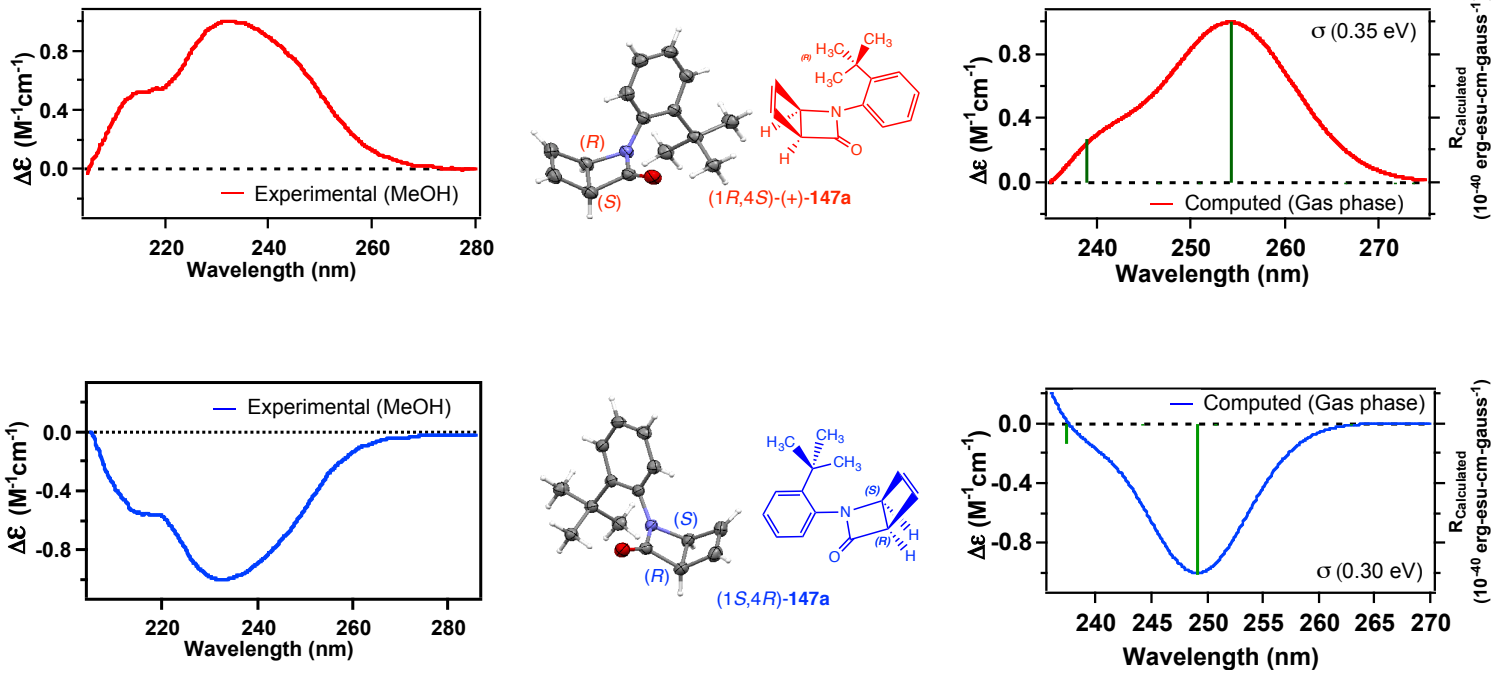

Figure 2.16: Left: Experimental CD spectra of (*1R,4S*)-**147a** (top) and (*1S,4R*)-**147a** (bottom). Right: Computed CD spectra of (*1R,4S*)-**147a** (top) and (*1S,4R*)-**147a** (bottom). (Reproduced from reference 28, with permission from American Chemical Society, 2011).

2.10. X-Ray structural parameters

Structure determination: Single crystal X-ray diffraction data of the compounds **146a**, **146b** and **147a** were collected on a Bruker Apex Duo diffractometer with a Apex 2 CCD area detector at T = 100K. Cu radiation was used. Single crystal X-ray diffraction data sets of compounds **146c** and **147c** were collected on a SIEMENS diffractometer with a 1K CCD area detector (graphite-monochromated Mo Kα radiation) at ambient temperature. All structures were process with Apex 2 v2010.9-1 software package (SAINT v. 7.68A, XSHELL v. 6.3.1). Direct method was used to solve the structures after multi-scan absorption corrections. Details of data collection and refinement are given in the table below.

Table 2.10: X-Ray structural parameters for 2-pyridones **146a-c**

	(*M*)-**146a**	(*P*)-**146a Mono**	(*P*)-**146a Ortho**	**146b**	**146c**
Formula	$C_{15}H_{17}NO$	$C_{15}H_{17}NO$	$C_{15}H_{17}NO$	$C_{14}H_{15}NO_2$	$C_{24}H_{19}NO_2$
FW	227.30	227.30	227.30	229.27	353.40
cryst. Size [mm]	.21x.19x.07	0.16x.12x.08	.22x.12x.07	.21x.17x.08	.60x.12x.08
cryst. system	Monoclinic	Monoclinic	Orthorhombic	Orthorhombic	Monoclinic
Space Group, Z	P2(1), 8	P2(1), 8	P2(1), 8	Pbca, 8	P2(1)/n, 4
a [Å]	15.3180(4)	15.3223(5)	6.8746 (2)	8.5768(4)	17.601(1)
b [Å]	11.4327(3)	11.4272(3)	12.4881 (4)	15.0166(6)	6.388(4)
c [Å]	16.0022(4)	16.0413(5)	30.4034 (9)	18.4260(8)	18.243(1)
α [Å]	90	90	90	90	90
ß [Å]	117.601(1)	117.824(2)	90	90	114.990(8)
γ [Å]	90	90	90	90	90
V [$Å^3$]	2483.48(11)	2483.96(13)	2610.15(14)	2373.16(18)	1859.10(18)
ρ_{calc} [g/cm^3]	1.216	1.216	1.157	1.283	1.263
μ [cm^{-1}]	0.592	0.592	0.563	0.691	0.080
Radiation Type	Cu	Cu	Cu	Cu	Mo
F(000)	976	976	976	976	744
no of measured refl.	30596	28036	25477	17287	13835
no of indep. reflec.	8491	8142	4435	2058	3349
no of refl. (I ≥ 2σ)	8378	7885	4390	2026	2142
Resolution [Å]	0.84	0.84	0.84	0.83	0.83
R1/wR2 (I ≥ 2σ)[a] [%]	4.19 / 11.50	6.87 / 17.15	2.61 / 6.92	3.69 / 9.92	4.68 / 10.82
R1/wR2 (all data) [%]	4.25 / 11.59	7.02 / 17.24	2.64 / 6.95	4.23 / 11.23	9.00 / 13.68
Crystalliz. solvent	CH_2Cl_2	CH_2Cl_2	Hex / CH_2Cl_2	MeOH	Hex / $CHCl_3$

[a] $R1 = \Sigma||F_O| - |F_C|| / \Sigma|F_O|$, $wR2 = [\Sigma w[(F_O)^2 - (F_C)^2]^2 / \Sigma w(F_O^2)^2]^{1/2}$ for $F_O^2 > 2\sigma(F_O^2)$, $w = [\sigma^2(F_O)^2 + (AP)^2 + BP]^{-1}$ where $P = [(F_O)^2 + 2(F_C)^2] / 3$ and A, B coefficients for all compounds are as follow: M-**146a**, A (B) = 0.0447 (2.0145); P-**146a** Mon, A (B) = 0.0264 (6.6473); P-**146a** Orth, A (B) = 0.0383 (0.4633);**146b**, A (B) = 0.0614 (0.6753); **146c**, A (B) = 0.0739 (0.0).

Table 2.11: X-Ray structural parameters for bicyclo β-lactam photoproduct **147**.

	(1*S*,4*R*)-**147a**	(1*R*,4*S*)-**147a**	**147c**
Formula	$C_{15}H_{17}NO$	$C_{15}H_{17}NO$	$C_{24}H_{19}NO_2$
FW	227.30	227.30	353.40
cryst. Size [mm]	.19x.18x.05	.25x.11x.05	.80x.60x.16
cryst. system	Monoclinic	Monoclinic	Monoclinic
Space Group, Z	P2(1), 2	P2(1), 2	P2(1)/c, 4
a [Å]	8.5144(2)	8.5149(10)	8.502(4)
b [Å]	5.8077(2)	5.8102(7)	12.948(6)
c [Å]	13.3132(4)	13.3204(16)	17.246(8)
α [Å]	90	90	90
ß [Å]	108.292(1)	108.261(5)	90.711(5)
γ [Å]	90	90	90
V [$Å^3$]	625.06(3)	625.82(13)	1898.3
ρ_{calc} [g/cm^3]	1.208	1.206	1.237
μ [cm^{-1}]	0.588	0.587	0.078
Radiation Type	Cu	Cu	Mo
F(000)	244	244	744
no of measured refl.	7374	7444	14955
no of indep. reflec.	2087	2084	4301
no of refl. (I ≥ 2σ)	2075	2061	2919
Resolution [Å]	.84	.84	0.76
R1/wR2 (I ≥ 2σ)[a] [%]	2.57 / 6.61	2.77 / 7.11	4.39 / 11.45
R1/wR2 (all data) [%]	2.58 / 6.63	2.79 / 7.14	7.09 / 13.36
Crystalliz. solvent	Hex / IPA	Hex/CH_2Cl_2	Hex / $CHCl_3$

[a] $R1 = \Sigma||F_O| - |F_C|| / \Sigma|F_O|$, $wR2 = [\Sigma w[(F_O)^2 - (F_C)^2]^2 / \Sigma w(F_O^2)^2]^{1/2}$ for $F_O^2 > 2\sigma(F_O^2)$, $w = [\sigma^2(F_O)^2 + (AP)^2 + BP]^{-1}$ where $P = [(F_O)^2 + 2(F_C)^2] / 3$ and A, B coefficients for all compounds are as follow: *1S,4R*_**147a**, 0.0369 (0.1018); *1R,4S*_**147a**, 0.0415 (0.0941); **147c**, A (B) = 0.0578 (0.3379).

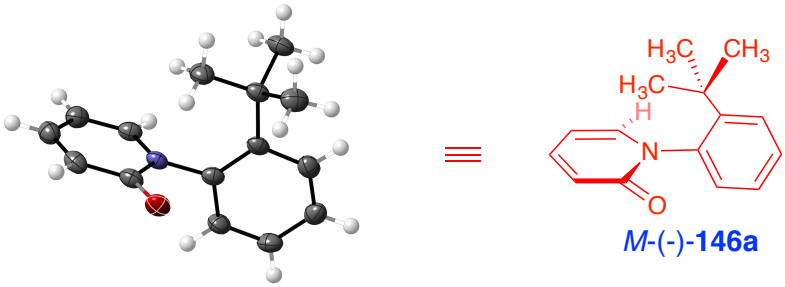

Figure 2.17: X-ray structure of (*M)*-(-)-**146a** (crystallized from dichloromethane).

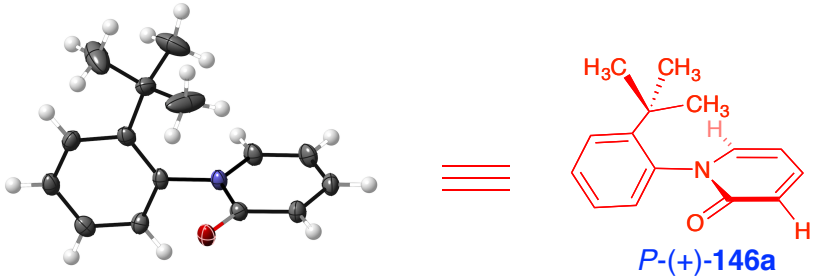

Figure 2.18: X-ray structure of (*P)*-(+)-**146a** (crystallized from dichloromethane).

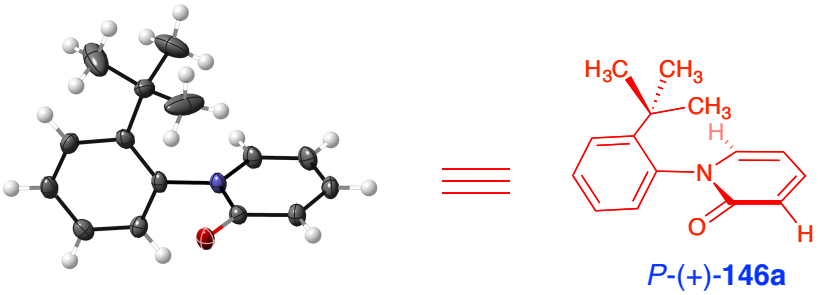

Figure 2.19: X-ray structure of (*P*)-(+)-**146a** (crystallized from hexanes/dichloromethane).

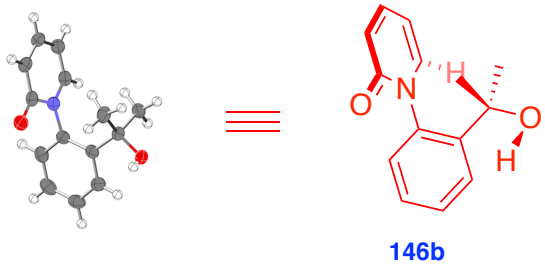

Figure 2.20: X-ray structure of **146b** (crystallized from methanol).

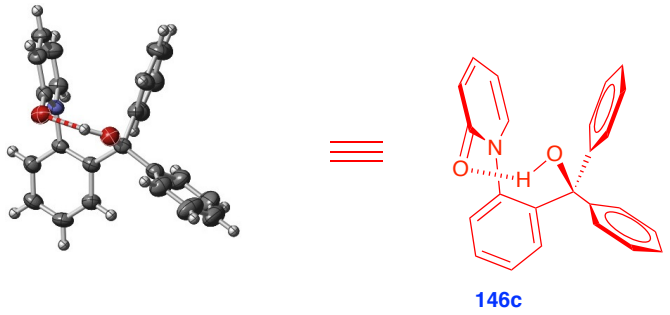

Figure 2.21: X-ray structure of **146c** (crystallized from hexanes/chloroform).

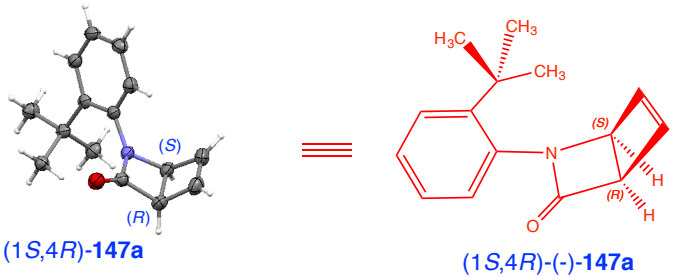

Figure 2.22: X-ray structure of photoproduct (*1S,4R*)-(-)-**147a** (crystallized from Hex./IPA).

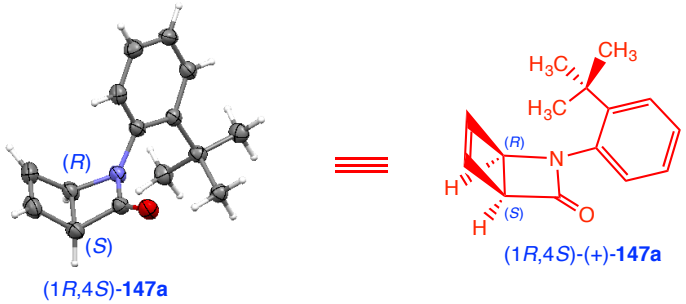

Figure 2.23: X-ray structure of photoproduct (*1R,4S*)-(+)-**147a** (crystallized from Hex./DCM).

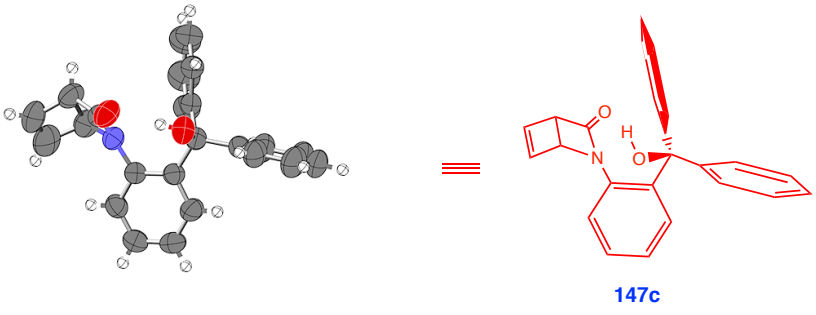

Figure 2.24: X-ray structure of photoproduct **147c** (crystallized from hexanes/chloroform).

2.11. Summary and outlook

The enantiospecific *disrotatory* 4π-ring closure in atropisomeric 2-pyridones proceeded efficiently to furnish enantioenriched β-lactam products. The *ortho* substituents that impart axial chirality to the molecule were modified to understand the influence of sterics and H-bonding in the molecule. The H-bonding substrates displayed distinct temperature and solvent dependency on the racemization and enantiospecificity of the reaction, while the molecule that lacked H-bonding ability (pure sterics) had only marginal dependence on the racemization and enantiospecificity of the reaction. Eyring plot was computed to calculate the differential activation enthalpy and entropy for the reaction. Also, the course of phototransformation was followed through single crystal XRD to decipher the preferred mode of cyclization for a given isomer of atropisomeric 2-pyridones. The high-pressure racemization and photoreaction study revealed that pressure provided stable chiral axis even at elevated temperature resulting in higher enantiomeric excess in the photoproduct.

2.12. Experimental section

2.12.1. General methods

All commercially obtained reagents/solvents were used as received; chemicals were purchased from Alfa Aesar®, Sigma-Aldrich®, Acros®, TCI America®, Mallinckrodt®, and Oakwood® Products, and were used as received without further purification. Unless stated otherwise, reactions were conducted in oven-dried glassware under nitrogen atmosphere. ^{1}H-NMR and ^{13}C-NMR spectra were recorded on Varian 400 MHz (100 MHz for ^{13}C) and on 500 MHz (125 MHz for ^{13}C) spectrometers. Data for ^{1}H NMR are reported as chemical shift (δ ppm) with the corresponding integration values. Coupling constants (*J*) are reported in hertz (Hz). Standard abbreviations indicating multiplicity were used as follows: s (singlet), b (broad), d (doublet), t (triplet), q (quartet), m (multiplet) and virt (virtual). Data for ^{13}C-NMR spectra are reported in terms of chemical shift (δ ppm). Electrospray Ionization Spectra were recorded on a Bruker – Daltronics® BioTof mass spectrometer in positive (ESI^{+}) ion mode. HPLC analyses were performed on Waters® HPLC equipped with 2525 pump. Waters® 2767 sample manager was

used for automated sample injection. All HPLC injections were monitored using a Waters® 2487 dual wavelength absorbance detector at 254 and 270 nm. Analytical and semi-preparative injections were performed on chiral stationary phase using various columns as indicated below.

i) Regis® PIRKLE COVALENT (*R*,*R*) WHELK–01

a) 25 cm x 4.6 mm column for analytical injections.

b) 25 cm x 10 mm column for semi-preparative injections.

ii) CHIRACEL® OD-H

a) 0.46 cm x 25 cm column for analytical injections.

b) 10 mm x 25 cm column for semi-preparative injections.

iii) CHIRALPACK® IC

a) 0.46 cm x 25 cm column for analytical injections.

b) 10 mm x 25 cm column for semi-preparative injections

iv) CHIRALPAK® AD-H

a) 0.46 cm x 15 cm column for analytical injections.

b) 10 mm x 25 cm column for semi-preparative injections.

v) CHIRALPACK® IC

a) 0.46 cm x 25 cm column for analytical injections.

b) 10 mm x 25 cm column for semi-preparative injections

vi) CHIRALPACK® ASH

a) 0.46 cm x 25 cm column for analytical injections.

Masslynx software version 4.1 was used to monitor/analyze the HPLC injections and to process HPLC traces. Igor Pro® Software version 6.0 was used to process the HPLC graphics. UV-Vis spectra were recorded on Shimadzu 2501PC UV-Vis spectrometer using UV quality fluorimeter cells (with range until 190 nm) purchased from Luzchem. Optical activity values were recorded on JASCO® DIP – 370 digital polarimeter. CD spectra were recorded on JASCO® DIP – 710 digital CD spectrometer. When necessary, the compounds were purified by combiflash equipped with dual wavelength UV-Vis absorbance detector (Teledyn ISCO) using hexanes:ethyl acetate as the mobile phase and Redisep® cartridge filled with silica (Teledyne ISCO) as

stationary phase. In some cases, compounds were purified by column chromatography on silica gel (Sorbent Technologies®, silica gel standard grade: porosity 60 Å, particle size: 230 x 400 mesh, surface area: 500 – 600 m^2/g, bulk density: 0.4 g/mL, pH range: 6.5 – 7.5). Unless indicated, the Retardation Factor (R*f*) values were recorded using a 5-50% hexanes:ethyl acetate (or) 5-10% chloroform:methanol as mobile phase and on Sorbent Technologies®, silica Gel TLC plates (200 mm thickness w/UV_{254}).

All computations were performed using Gaussian 03 package.[29] GaussView 3.09 and GaussSum software package v2.2 were used to process, render the structures and spectra.

The plot of CD spectrum was carried out using molar ellipticity vs wavelength (nm) and the molar ellipticity was calculated using the formula,[30]

Molar ellipticity $[\Delta\varepsilon] = [\theta] / 32980cl$

Where,

c = Concentration in mols/lit; *l* = Path length in cm; θ = Ellipticity measured in millidegrees.

2.12.2. High-pressure spectroscopic measurements, apparatus, setup and data collection

Circular Dichroism (CD) experiments at various pressures were performed on a JASCO J-820YH spectropolarimeter. All spectroscopic measurements under high pressure were performed using a custom built high-pressure vessel (Figures 2.25). This high-pressure vessel was fitted with three optical windows made of sapphire or diamond with an effective aperture of 9 mm or 3 mm i.d., respectively. The apparatus was designed and manufactured by Teramecs Co., Kyoto, Japan. The window materials were sapphire for UV-vis and fluorescence spectroscopy and birefringence-free diamond for CD spectroscopy.

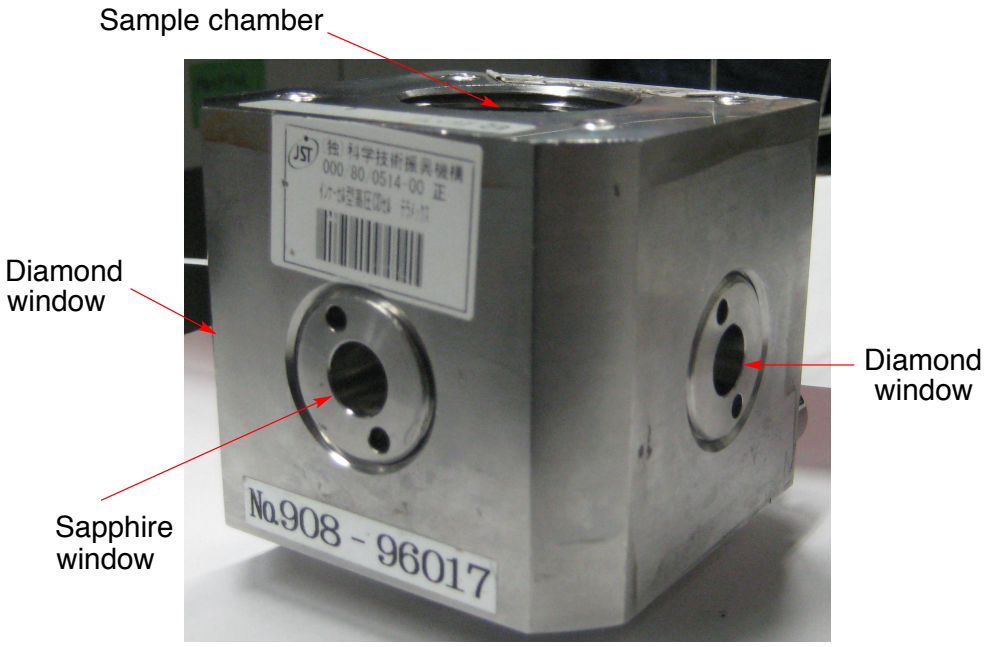

Figure 2.25: Custom designed high-pressure vessel for spectroscopic measurements.

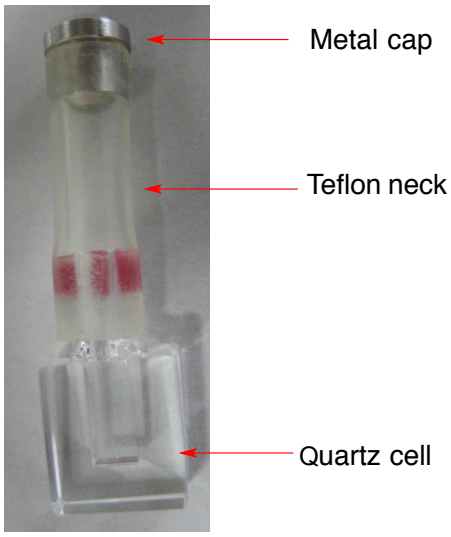

Figure 2.26: Custom designed quartz cell for high-pressure experiments.

A quartz inner cell (Figure 2.26) with an inner dimension 3 mm (W) × 2 mm (D) × 7 mm (H) connected to a short flexible Teflon tube for adjusting the volume change under pressure was filled with a sample solution. The top end of the quartz cell was stoppered, and the whole cell was placed inside the pressure vessel. The vessel was fixed in the sample chamber of the spectrometer (Figure 2.27). The temperature in the sample chamber was maintained using a temperature control unit and the sample was maintained at a set hydrostatic pressure (varying from 0.1 MPa to 25 MPa).

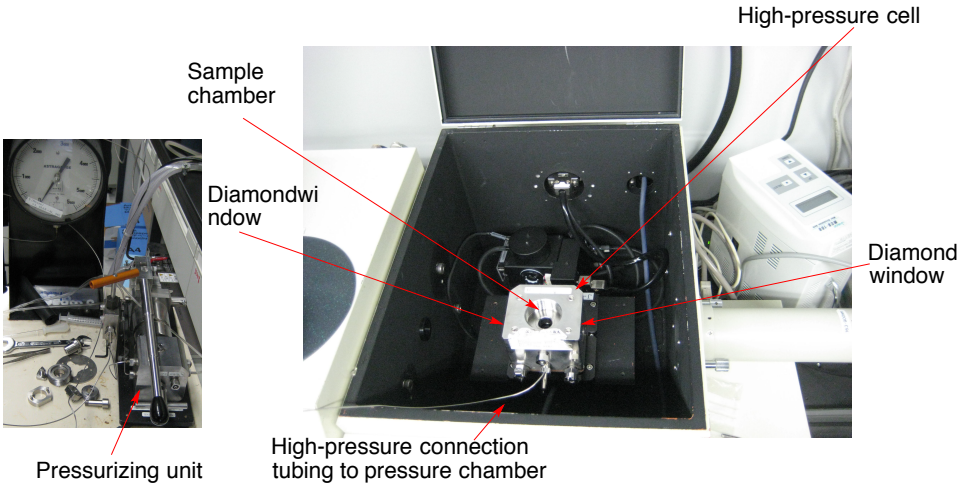

Figure 2.27: High pressure setup in a CD spectrometer.

2.12.3. Procedure for the synthesis of 2-benzyloxypyridine derivative 159

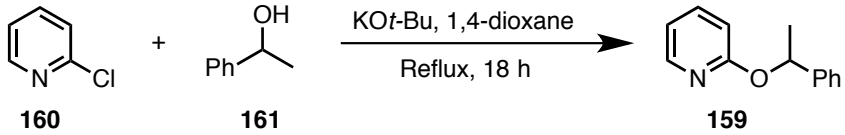

160 **161** **159**

Scheme 2.13: Synthesis of 2-benzyloxypyridine derivative **159**.

The 2-benzyloxypyridine derivative **160** was synthesized according to a procedure reported in the literature.[31] To a solution of 1-phenylethanol **161** (3.24 g, 26.5 mmol) in 1,4-dioxane (40 mL) at room temperature, 2-chloropyridine (2.0 g, 17.7 mmol) and potassium *tert*-butoxide (2.97 g, 26.5 mmol) was added. The resulting mixture was heated to 100 ^{o}C and maintained for 18 h. After the reaction, the mixture was cooled to room temperature and diluted with DI water (15 mL). The aqueous layer was extracted with ethyl acetate (3 × 15 mL). The combined organic layer was washed with brine solution (20 mL), filtered and solvent was evaporated and reduced pressure to yield the crude product. The crude was purified by combiflash using hexanes:ethyl acetate mixture.

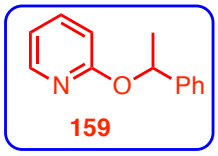

159

R*f* = 0.80 (80% hexanes:20% ethyl acetate). Yield = 76%

^{1}H-NMR (400 MHz, $CDCl_3$, δ ppm): 8.10-8.08 (m, 1H), 7.53-7.49 (m, 1H), 7.45-7.42 (m, 2H), 7.34-7.30 (m, 2H), 7.26-7.22 (m, 1H), 6.80-6.73 (m, 2H), 6.22 (q, *J* = 6.5 Hz, 1H) and 1.63 (d, *J* = 6.5 Hz, 3H).

2.12.4. Procedure for the synthesis of point chiral pyridone derivative 148

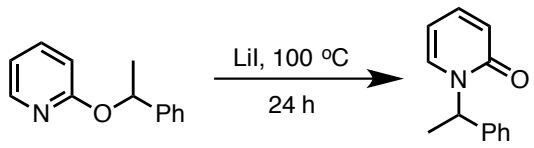

159 **148**

Scheme 2.14: synthesis of point chiral 2-pyridone derivative **148**.

A mixture of 2-benzyloxypyridine derivative **159** (1.3, 6.52 mmol) and LiI (0.44 g, 3.26 mmol) in a sealed vial was heated to 100 °C in an oil bath for 8 h. After the reaction, the mixture was diluted with ethyl acetate (20 mL) and filtered through celite bed. The filtered solution was concentrated to get the crude product. The crude was purified by combiflash using hexanes:ethyl acetate mixture to get the pure product.

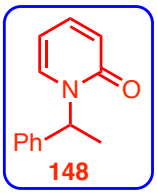

148

R*f* = 0.40 (100% ethyl acetate). Yield = 27%

^{1}*H-NMR* (400 MHz, $CDCl_3$, δ ppm): 7.35-7.21 (m, 6H), 7.07-7.04 (m, 1H), 6.58-6.55 (m, 1H), 6.43 (q, *J* = 7.1 Hz, 1H), 6.08-6.04 (m, 1H) and 1.68 (d, *J* = 7.1 Hz, 3H).

^{13}*C NMR* (100 MHz, $CDCl_3$, δ ppm): 162.6, 140.4, 138.9, 134.5, 129.0, 128.1, 127.6, 120.9,106.5, 52.5 and 19.2.

HPLC analysis conditions:

For analytical conditions,

I). Column : CHIRALPAK-IC
Abs. detector : 254 nm and 270 nm
Mobile phase : Hexanes:2-propanol = 95:5
Flow rate : 1.0 mL/min
Retention times (min) : ~23.77 [(+)-**148**] and ~24.89 [(-)-**148**]

II). Column : CHIRALPAK-ASH
Abs. detector : 254 nm and 270 nm
Mobile phase : Hexanes:2-propanol = 80:20
Flow rate : 0.5 mL/min
Retention times (min) : ~22.30 [(+)-**148**] and ~45.54 [(-)-**148**]

For preparative conditions,

I) Column : CHIRALPAK-IC

Abs. detector : 254 nm and 270 nm

Mobile phase : Hexanes:2-propanol = 85:15

Flow rate : 3 mL/min

Retention times (min) : ~52.56 [(+)-**148**] and ~70.14 [(-)-**148**]

Optical Rotation $[\alpha]_D^{28}$:

HPLC retention time (CHIRALPAK-IC) at ~ 23.77 min, (*c* ~0.036%, MeOH) = +356 deg.

HPLC retention time (CHIRALPAK-IC) at ~ 24.89 min, (*c* ~0.036%, MeOH) = -350 deg.

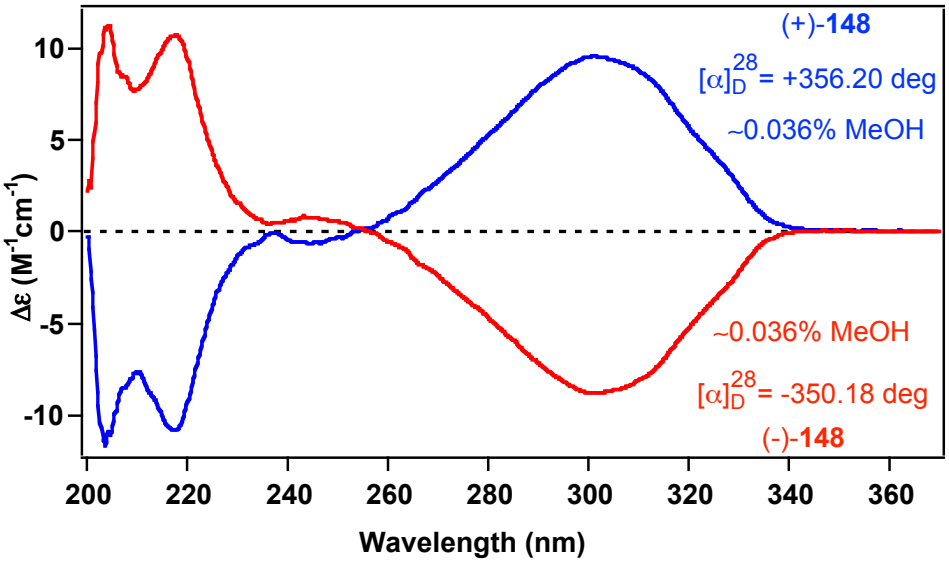

Figure 2.28: CD spectra of point chiral pyridone derivative **148** measured in methanol (*c* = [(+)-**148**] ~0.121 mM and [(-)-**148**]) ~0.111 mM).

2.12.5. Synthesis of piperidine-2,6-dione derivative 151

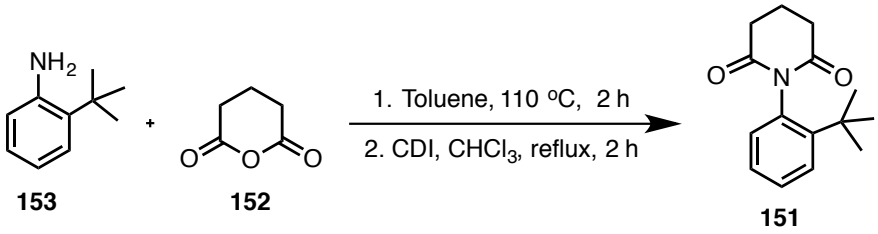

Scheme 2.15: Synthesis of piperidine-2,6-dione derivative **151**.

Piperidine-2,6-dione derivative **151** was synthesized using a procedure reported in the literature.[13] To a solution of 2-*tert*-butylaniline **153** (5 g, 33.5 mmol) in toluene (40 mL), glutaric anhydride **152** (4.6 g, 40.2 mmol) was added. The reaction mixture was refluxed for 1.5 h and cooled to room temperature. The precipitated solid was filtered and washed with pentane to get the crude product as a white solid. The crude was sufficiently pure to proceed to the next stage.

To the crude (8.6 g, 32.5 mmol) in chloroform (175 mL) under N_2 atmosphere, 1, 1'-carbonyldiimidazole (5.8 g, 35.8 mmol) was slowly added. The reaction mixture was refluxed for 12 h. After the reaction, the mixture was cooled to room temperature and washed with DI water (2 x 150 mL), 2N HCl (1 x 150 mL or until the solution is neutral) and brine solution (1 x 150 mL). The organic layer was dried over *anhyd.* Na_2SO_4, filtered and the solvent was evaporated under reduced pressure. The crude product was purified by combiflash using hexanes:ethyl acetate mixture (80:20) to get the title compound **151** as a white solid (isolated yield = 70%).

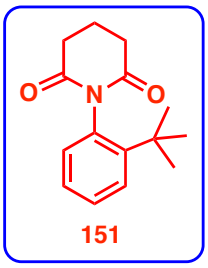

R*f* = 0.4 (80% hexanes:20% ethyl acetate).

^{1}H-NMR (400 MHz, $CDCl_3$, δ ppm): 7.56-7.53 (dd, *J* = 8.0, 1.6 Hz, 1H), 7.34-7.32 (m, 1H), 7.26-7.22 (m, 1H), 6.79-6.77 (dd, *J* = 8.0, 1.6 Hz, 1H), 2.80-2.77 (t, *J* = 6.4 Hz, 4H), 2.11-2.05 (Q, *J* = 6.4 Hz, 2H) and 1.27 (s, 9H).

^{13}C-NMR (100 MHz, $CDCl_3$, δ ppm): 173.3, 146.8, 133.4, 131.4, 131.2, 129.2, 127.4, 36.0, 33.6, 31.7 and 17.2.

2.12.6. Synthesis of 2-*tert*-butyl-dihydro-2-pyridone derivative 150

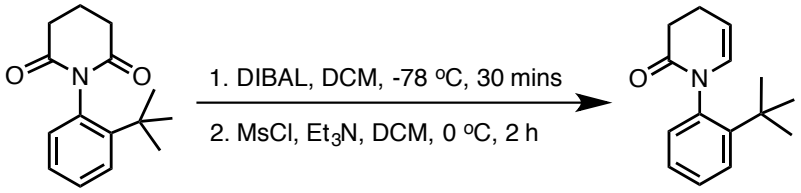

151 **150**

Scheme 2.16: Synthesis of 2-*tert*-butyl-dihydro-2-pyridone derivative **150**.

To a solution of piperidine-2,6-dione **151** (5.6 g, 22.7 mmol) in DCM at -78 ^{o}C under N_2 atmosphere, DIBAL (1M solution in hexanes, 5.8 g, 40.9 mmol) was slowly added over a period of 10 min and stirred for 15 min at -78 ^{o}C. The reaction mixture was quenched with DI water (40 mL) at -78 ^{o}C, followed by the addition of 2N NaOH (12 mL). The reaction mixture was slowly warmed to room temperature and poured into a saturated solution of sodium potassium tartarate (250 mL). The organic layer was separated and the aqueous layer was extracted with DCM (2 x 200 mL). The combined organic layers were dried over *anhyd.* Na_2SO_4, filtered and the solvent was evaporated under reduced pressure to get the crude product that was directly to taken to next step.

To a solution of crude (3.4 g, 13.7 mmol) in DCM (50 mL) at 0 ^{o}C, triethylamine (5.8 mL, 41.0 mmol) was added followed by the addition of methanesulfonyl chloride (1.7 mL, 21.8 mmol) over a period of 10 min. The mixture was stirred for 2 h at 0 ^{o}C and warmed to room temperature. To the reaction mixture DI water (150 mL) was added, stirred and the layers were separated. The organic layer was washed with *satd.* $NaHCO_3$ solution (150 mL) and *satd.* brine solution (150 mL). The organic layer was dried over *anhyd.* Na_2SO_4, filtered and the solvent was evaporated under reduced pressure. The crude product was purified by combiflash using hexanes:ethyl acetate mixture (80:20) to get the product.

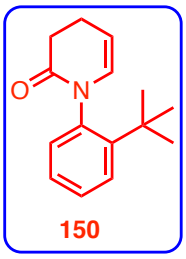

150

R*f* = 0.70 (80% hexanes:20% ethyl acetate), Yield = 70%.

^{1}H-NMR (400 MHz, $CDCl_3$, δ ppm): 7.51-7.49 (dd, *J* = 8.0, 1.6 Hz, 1H), 7.31-7.23 (m, 1H), 7.23-7.21 (m, 1H), 6.98-6.96 (dd, *J* = 7.6, 1.6 Hz, 1H), 6.04-6.02 (td, *J* = 8.0, 1.6 Hz, 1H), 5.22-5.18 (m, 1H), 2.67-2.63 (m, 2H), 2.452.41 (m, 2H) and 1.34 (s, 9H).

^{13}C-NMR (100 MHz, $CDCl_3$, δ ppm): 170.4, 147.7, 139.6, 133.0, 131.1, 128.8, 128.7, 127.7, 105.1, 35.9, 32.2, 31.9 and 20.6.

2.12.7. Synthesis of atropisomeric *tert*-butyl-2-pyridone 146a

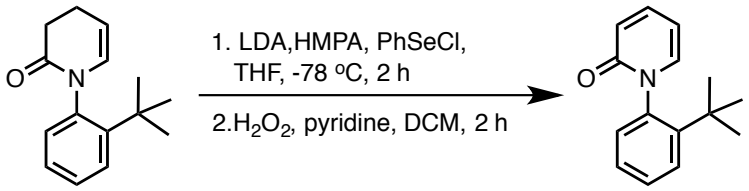

150 **146a**

Scheme 2.17: Synthesis of *tert*-butyl-2-pyridone **146a**.

To a solution of diisopropylamine (3.0 mL, 21.0 mmol) in dry THF (30 mL) at 0 ^{o}C under N_2 atmosphere, *n*-butyl lithium (1.6 M in hexanes, 12.6 mL, 20.1 mmol) was slowly added over a period of 10 min. The reaction mixture was warmed to room temperature and stirred for 30 min. The reaction mixture was cooled to -78 ^{o}C, and a solution of dihydropyridin-2(1*H*)-one **150** (2.2 g, 9.6 mmol) in dry THF (30 mL) was slowly added over a period of 20 min and then the mixture was stirred for 45 min -78 ^{o}C. A mixture of phenylselenyl chloride (1.8 g, 9.6 mmol) and hexamethyl phosphoramide (1.7 g, 9.6 mmol) in dry THF (30 mL) was slowly added to the reaction mixture over a period of 20 min. The reaction mixture was stirred for 45 min at -78 ^{o}C. The reaction mixture was carefully quenched with *satd.* NH_4Cl solution over a period of 20 min. The reaction mixture was warmed to room temperature slowly and the layers were separated. The aqueous layer was extracted with ethyl acetate (2 x 45 mL). The combined organic layers were dried over *anhyd.* Na_2SO_4, filtered and the solvent was evaporated under reduced pressure to get the crude product.

The crude was dissolved in DCM and cooled to 0 ^{o}C. To this solution, pyridine (1.5 mL, 19.1 mmol) was added, followed by the addition of H_2O_2 (30% in water, 2.2 mL, 19.1 mmol). The reaction mixture was warmed to room temperature and stirred for 30 min. To the reaction mixture DI water (10 mL) was added, stirred for 10 min and the layers were separated. The organic layer was dried over *anhyd.* Na_2SO_4, filtered and the solvent was evaporated under reduced pressure. The crude was purified by column chromatography using hexanes:2-propanol mixture (90:10) to get the title compound **146a** as a white to pale yellow solid (isolated yield = 42%).

TLC condition - R*f* = 0.25 (80% hexanes:20% ethyl acetate)

[1]H-NMR (400 MHz, $CDCl_3$, δ ppm): 7.59-7.56 (dd, *J* = 8.0, 1.6 Hz, 1H), 7.39-7.33 (m, 2H), 7.27-7.19 (m, 2H), 6.99-6.96 (dd, *J* = 7.6, 1.6 Hz, 1H), 6.60-6.58 (m, 1H), 6.21-6.17 (m, 1H) and 1.23 (s, 9H).

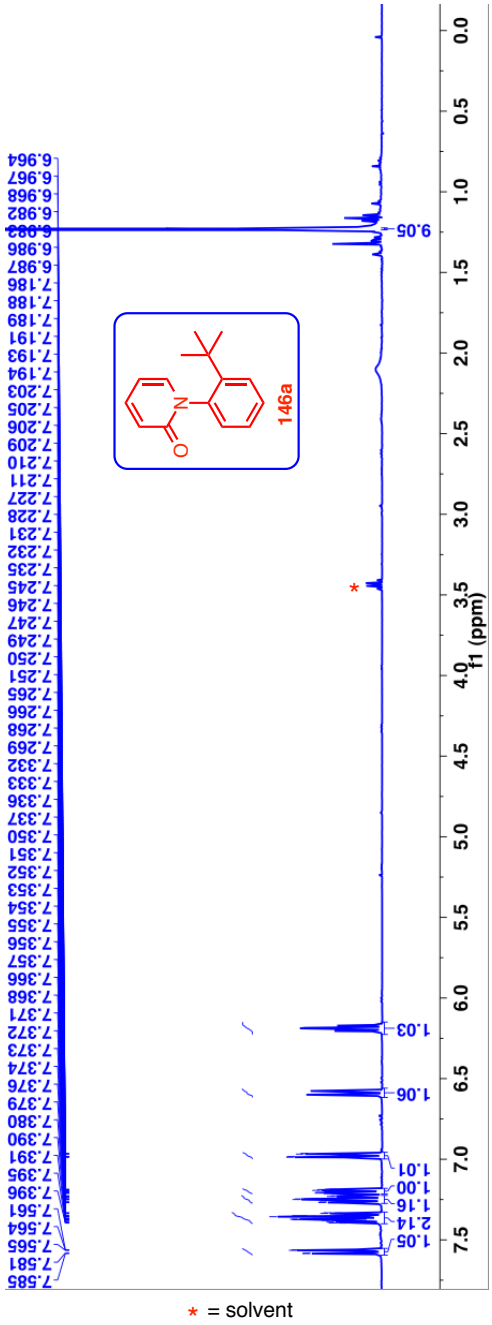

Figure 2.29: [1]H-NMR (400 MHz, $CDCl_3$, δ ppm) of *tert*-butyl-2-pyridone **146a**.

^{13}C-NMR (100 MHz, $CDCl_3$, δ ppm): 163.9, 146.3, 140.4, 139.7, 139.3, 130.4, 129.5, 129.4, 127.6, 122.1, 105.3, 36.1 and 31.9.

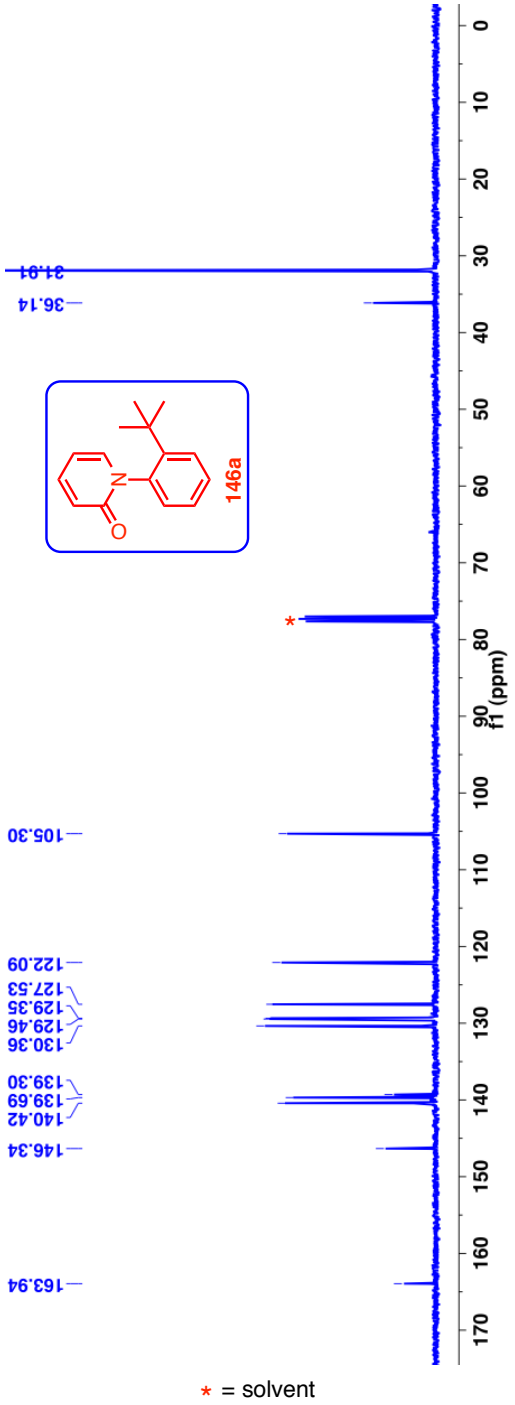

Figure 2.30: ^{13}C-NMR (100 MHz, $CDCl_3$, δ ppm) of *tert*-butyl-2-pyridone **146a**.

HRMS-ESI (m/z) ([M + Na]$^+$):

Calculated : 250.1202

Observed : 250.1201

|Δm| : 0.4 ppm

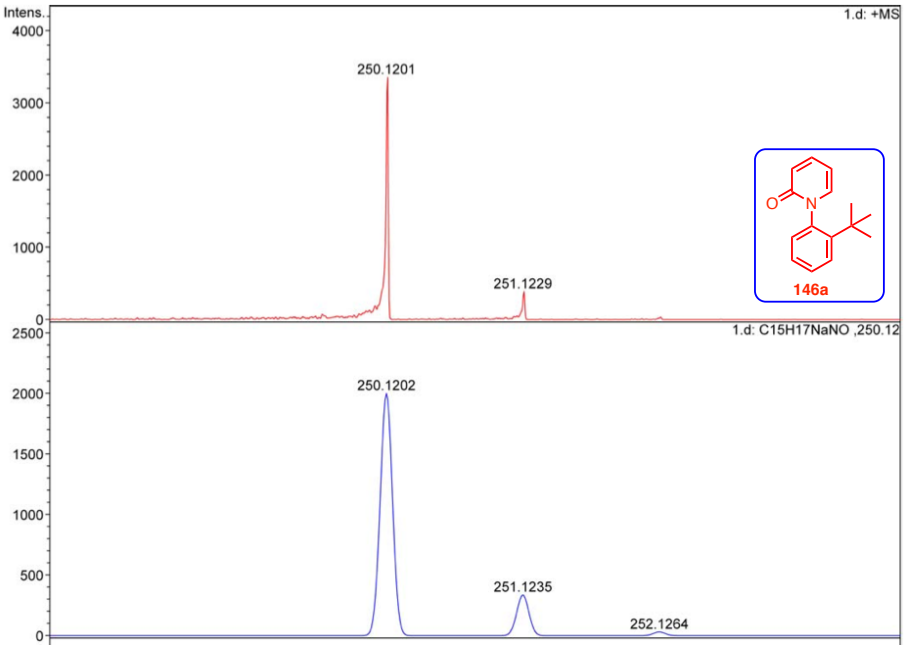

Figure 2.31: HRMS of *tert*-butyl-2-pyridone **146a**.

HPLC analysis conditions:

For analytical conditions,

I). Column : CHIRALPAK–AD-3

Abs. detector : 254 nm and 270 nm

Mobile phase : Hexanes:2-propanol = 95:5

Flow rate : 1.0 mL/min

Retention times (min) : ~8.90 [*P*-(+)-**146a**] and ~9.90 [*M*-(-)-**146a**]

II) Column : RR-WHELK-01 10/100 FEC

Abs. detector : 254 nm and 270 nm

Mobile phase : Hexanes:2-propanol = 95:5

Flow rate : 1 mL/min

Retention times (min) : ~28.49 [*M*-(-)-**146a**] and ~35.88 [*P*-(+)-**146a**]

For preparative conditions

I). Column : RR-WHELK-01 10/100 FEC

Abs. detector : 254 nm and 270 nm

Mobile phase : Hexanes:2-propanol = 95:5

Flow rate : 2.5 mL/min

Retention times (min) : ~51.45 [*M*-(-)-**146a**] and ~103.27 [*P*-(+)-**146a**]

Optical Rotation $[\alpha]_D^{28}$:

HPLC retention time (RR-WHELK-01 10/100 FEC) at ~ 28.49 min, (*c* ~0.034%, MeOH) = -72.2 deg.

HPLC retention time (RR-WHELK-01 10/100 FEC) at ~ 35.88 min, (*c* ~0.034%, MeOH) = +69.4 deg.

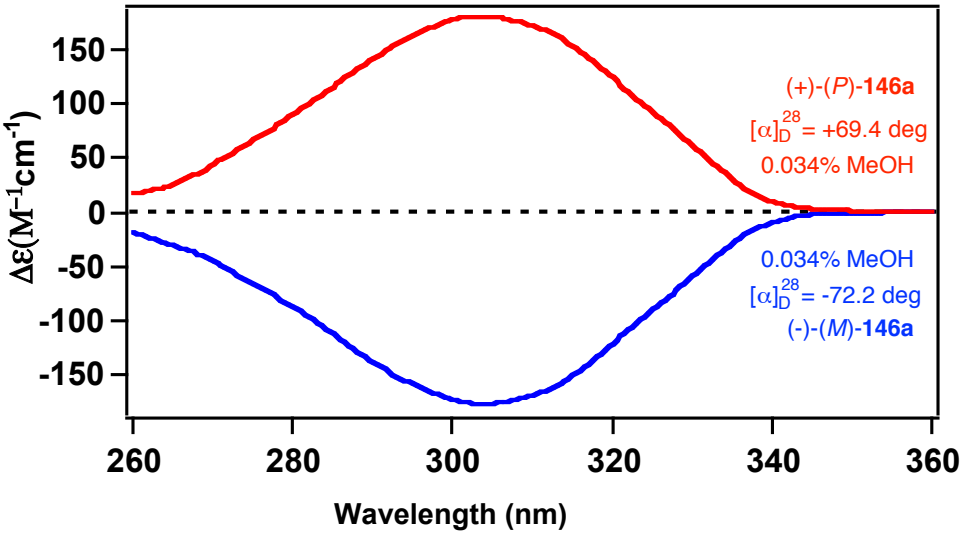

Figure 2.32: CD spectra of *tert*-butyl-pyridone **146a** measured in methanol (*c* ~ 0.26 mM).

2.12.8. Synthesis of 2-pyridyl derivative 156a-b

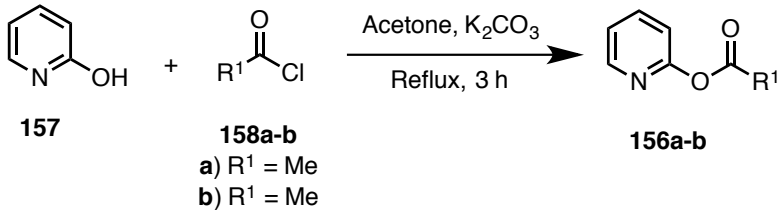

Scheme 2.18: Synthesis of 2-pyridyl derivative **156a-b**.

2-pyridyl derivative **156** was synthesized using a procedure reported in the literature.[14] To stirred slurry of 2-hydroxypyridine **157** (5.0 g, 52.6 mmol) and *anhyd.* potassium carbonate (18.2 g, 131.7 mmol) in dry acetone (100 mL) under N_2 atmosphere, corresponding acid chloride **158** (2.5 *equiv.*) was slowly added over a period of 15 min. The reaction mixture was refluxed for 3 h. The reaction mixture was cooled to room temperature and filtered through celite bed. The solvent was evaporated under reduced pressure to get the crude product. The crude was purified by combiflash using hexanes:ethyl acetate mixtures. (Isolated crude yield: 80-85%).

TLC condition - R*f* = 0.45 (50% hexanes:50% ethyl acetate).

Note: The 2-pyridyl acetate (**156a,** R^1 = Me) decomposes in silica column or when stored. It is better to proceed to the next stage immediately. The solvent removal was carried out at 20-25 ^{o}C to avoid any decomposition.

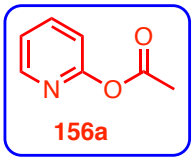

^{1}*H-NMR* (400 MHz, $CDCl_3$, δ ppm): 8.29-8.28 (m, 1H), 7.71-7.67 (m, 1H), 7.13-7.67 (m, 1H), 6.99-6.97 (d, J = 8 Hz, 1H) and 2.22 (s, 3H).

^{13}*C-NMR* (100 MHz, $CDCl_3$, δ ppm): 169.1, 157.9, 148.5, 139.8,122.3, 116.7 and 21.3.

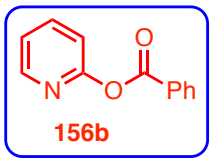

^{1}*H-NMR* (400 MHz, $CDCl_3$, δ ppm): 8.11-8.09 (m, 2H), 7.59-7.51 (m, 2H), 7.47-7.43 (m, 3H), 6.68-6.66 (d, *J* = 9.2 Hz, 1H) and 6.39-6.35 (t, *J* = 6.4 Hz, 1H).

^{13}*C-NMR* (100 MHz, $CDCl_3$, δ ppm): 171.9, 165.7, 142.4, 134.6, 133.4, 130.5, 130.2, 128.6, 120.4 and 108.1.

2.12.9. Synthesis of pyridin-2(1*H*)-one derivative 154a-b

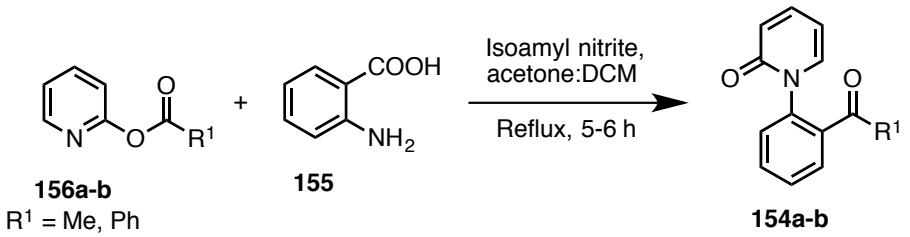

156a-b
R^1 = Me, Ph

155

154a-b

Scheme 2.19: Synthesis of pyridin-2(1*H*)-one derivative **154a-b**.

A solution of 2-pyridyl derivative **156a-b** and isoamyl nitrite (10.6 mL, 78.9 mmol) in dry DCM (55 mL) were refluxed under N_2 atmosphere. A solution of anthranilic acid **155** (10.8 g, 78.9 mmol) in dry acetone (50 mL) was added to the refluxing mixture slowly over a period of 2 h and then refluxed for 5 h. The reaction mixture was cooled to room temperature and the solvent was evaporated under reduced pressure. The crude product was purified by combiflash in hexanes:ethyl acetate mixture (50:50) to afford the title compound **154** as a brown solid. (Isolated yield: 50-55%).

R*f* = 0.15 (50% hexanes:50% ethyl acetate)

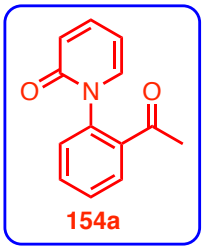

154a

^{1}*H-NMR* (400 MHz, $CDCl_3$, δ ppm): 7.28-7.70 (dd, *J* = 7.6 Hz, 1H), 7.61-7.57 (dt, *J* = 7.6, 1.6 Hz, 1H), 7.52-7.49 (dt, *J* = 7.6, 1.2 Hz, 1H), 7.43-7.39 (m, 1H), 7.31-7.24 (m, 2H), 6.59-6.57 (m, 1H), 6.29-6.26 (dt, *J* = 6.8, 1.6 Hz, 1H) and 2.48 (s, 3H).

^{13}*C-NMR* (100 MHz, $CDCl_3$, δ ppm): 199.4, 162.5, 140.6, 138.4, 138.1, 137.3, 132.6, 129.1, 128.6, 128.2, 121.8, 106.5 and 28.7.

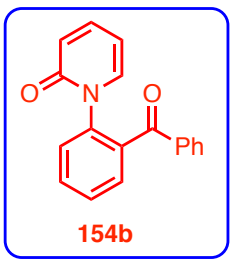

154b

^{1}*H-NMR* (400 MHz, $CDCl_3$, δ ppm): 7.81-7.79 (m, 2H), 7.65-7.61 (m, 1H), 7.53-7.48 (m, 3H), 7.40-7.35 (m, 4H), 7.28-7.24 (m, 1H) 6.41-6.39 (d, *J* = 9.2 Hz, 1H) and 6.20-6.17 (dt, *J* = 8.0, 0.8 Hz, 1H).

^{13}*C-NMR* (100 MHz, $CDCl_3$, δ ppm): 195.2, 162.3, 140.3, 139.4, 138.3, 137.1, 136.7, 133.3, 131.9, 130.5, 129.9, 129.5, 128.43, 128.42, 128.1, 126.7, 121.7 and 106.1.

2.12.10. Synthesis of 2-pyridones 146b and 146c

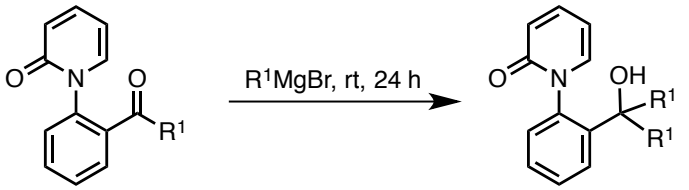

154a-b
a) R^1 = Me
b) R^1 = Ph

146a-b

Scheme 2.20: Synthesis of pyridin-2(1*H*)-one **146b** and **146c**.

To a solution of pyridin-2(1*H*)-one **154** (1.0 g, 4.7 mmol) in dry THF under N_2 atmosphere, corresponding magnesium bromide (3M solution in diethyl ether, 2.0 *equiv.*) was slowly added over a period of 20 min and stirred for 12 h at room temperature. The reaction mixture was cooled to 0 ^oC and quenched with *satd.* NH_4Cl solution slowly over a period of 10 min. The reaction mixture was warmed to room temperature and the layers were separated. The aqueous layer was extracted with DCM (2 x 15 mL). The combined organic layers were dried over *anhyd.* Na_2SO_4, filtered and the solvent was evaporated under reduced pressure. The crude was purified by column chromatography using chloroform:methanol mixture (98:2) to get the title compound **146b-c** as a brown solid (Isolated yield: 50-55%).

R*f* = 0.60 (95% chloroform:5% methanol) for **146b**.

R*f* = 0.54 (50% hexanes:50% ethyl acetate) for **146c**.

[1]H-NMR (400 MHz, $CDCl_3$, δ ppm): 7.56-7.58 (dd, *J* = 8.0, 1.6 Hz, 1H), 7.56-7.58 (m, 2H), 7.27-7.58 (m, 1H), 7.21-7.24 (m, 1H), 6.97-6.98 (d, *J* = 7.6 Hz, 1H), 6.54-6.58 (d, *J* = 9.2 Hz, 1H), 6.19-6.23 (t, 1H), 3.61 (s, 1H), 1.52 (s, 3H) and 1.34 (s, 3H).

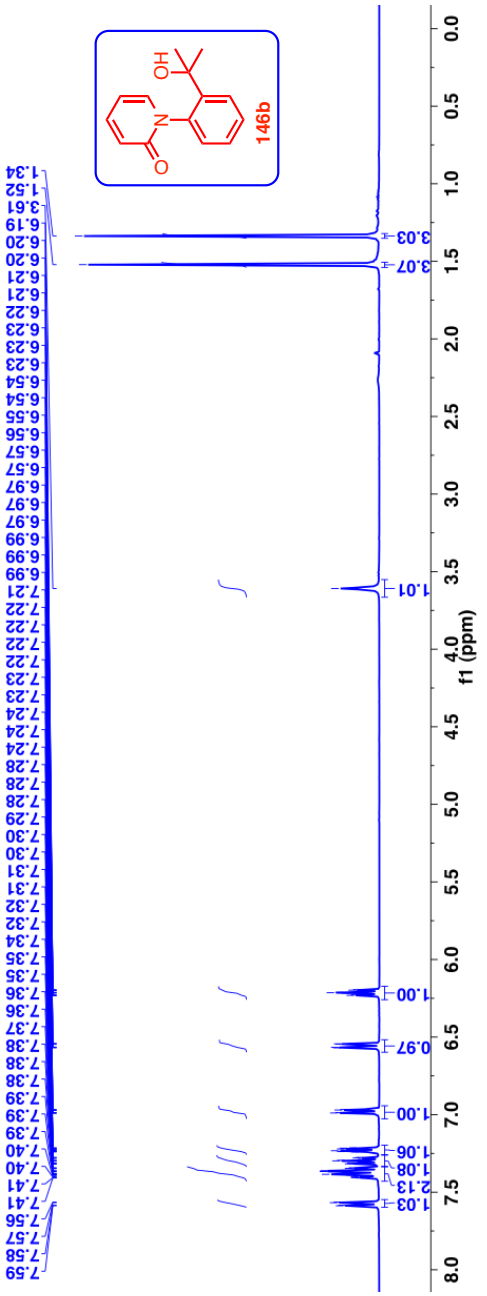

Figure 2.33: [1]H-NMR (400 MHz, $CDCl_3$, δ ppm) of atropisomeric 2-pyridone **146b**.

^{13}C-NMR (100 MHz, $CDCl_3$, δ ppm): 164.5, 144.7, 140.7, 139.2, 138.7, 129.9, 129.7, 128.9, 128.0, 121.7, 106.1, 72.5, 31.9 and 31.5.

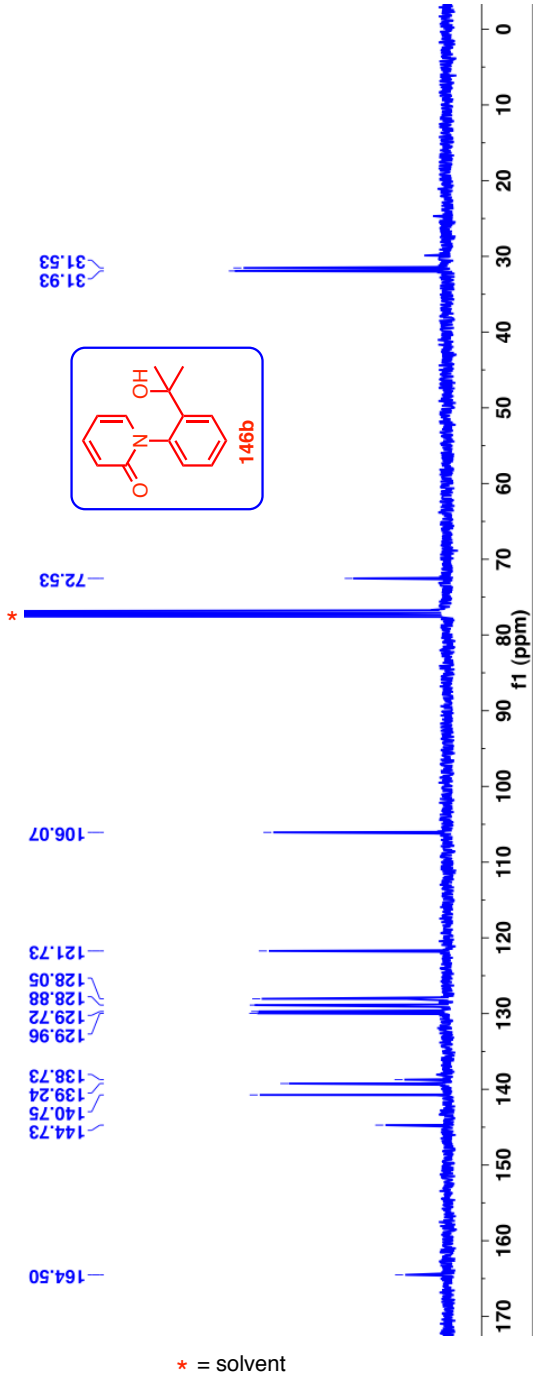

Figure 2.34: ^{13}C-NMR (100 MHz, $CDCl_3$, δ ppm) of atropisomeric 2-pyridone **146b**.

HRMS-ESI (m/z) ([M + Na]$^+$):

Calculated : 252.0995

Observed : 252.1002

|Δm| : 0.8 ppm

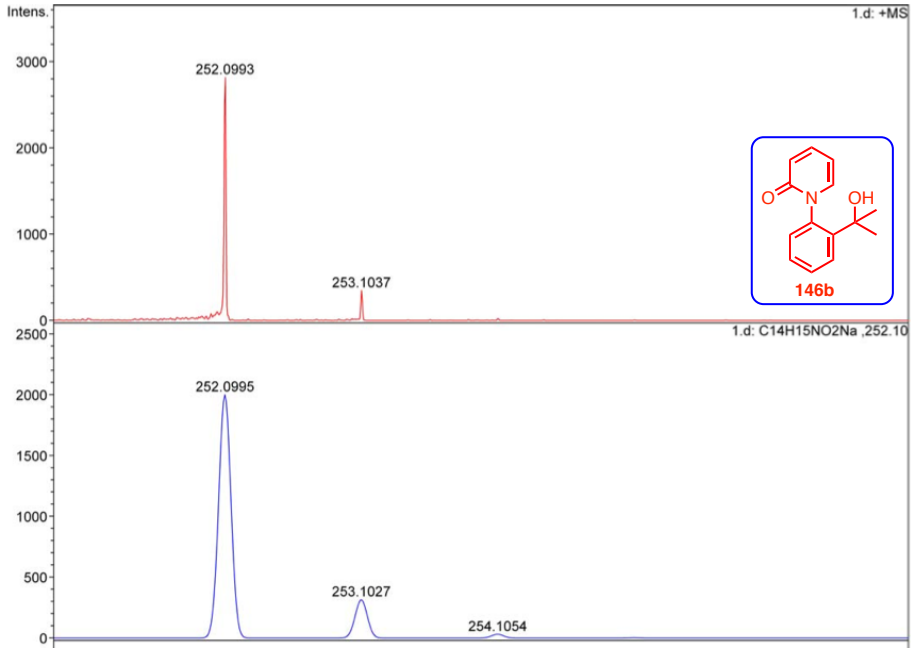

Figure 2.35: HRMS of atropisomeric 2-pyridone **146b**.

HPLC analysis conditions:

For analytical conditions

I). Column : CHIRALPAK–AD-3

Abs. detector : 254 nm and 270 nm

Mobile phase : Hexanes:2-propanol = 95:5

Flow rate : 1 mL/min

Retention times (min) : ~14.30 [(+)-**146b**] and ~14.85 [(-)-**146b**]

II). Column : RR-WHELK-01 10/100 FEC

Abs. detector : 254 nm and 270 nm

Mobile phase : Hexanes:2-propanol = 90:10

Flow rate : 1.5 mL/min

Retention times (min) : ~16.20 [(-)-**146b**] and ~33.30 [(+)-**146b**]

For preparative conditions

I). Column : RR-WHELK-01 10/100 FEC

Abs. detector : 254 nm and 270 nm

Mobile phase : Hexanes:2-propanol = 95:5

Flow rate : 3.0 mL/min

Retention times (min) : ~38.12 [(-)-**146b**] and ~80.00 [(+)-**146b**]

Optical Rotation $[\alpha]_D^{28}$:

HPLC retention time (RR-WHELK-01) at ~16.20 min, (*c* ~0.019%, MeOH) = -116 deg.

HPLC retention time (RR-WHELK-01) at ~33.30 min, (*c* ~0.019%, MeOH) = +116 deg.

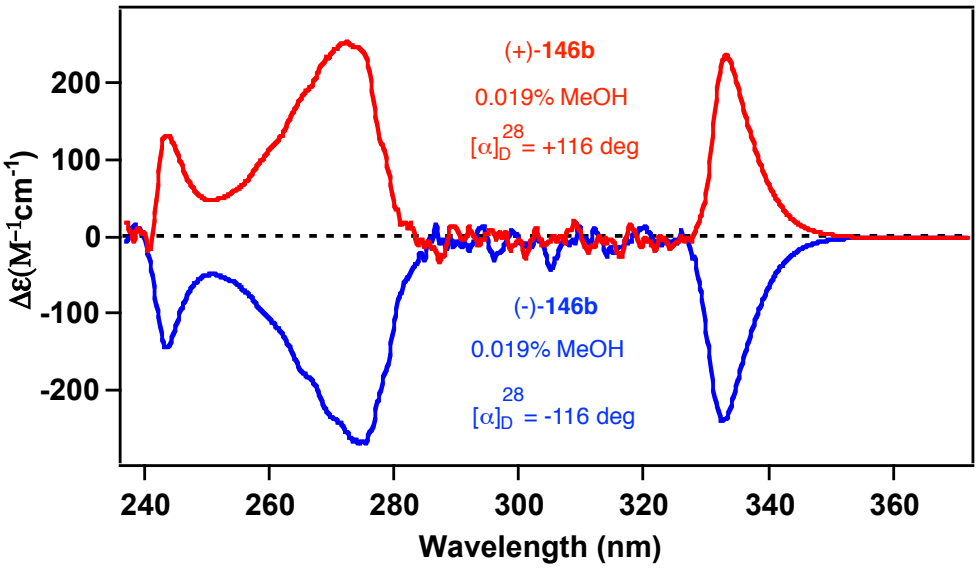

Figure 2.36: CD spectra of atropisomeric 2-pyridone **146b** measured in methanol (*c* ~ 0.14 mM for [(+)-**146b**] and ~ 0.15 mM for [(-)-**146b**]).

[1]H-NMR (400 MHz, $CDCl_3$, δ ppm): 7.53-7.50 (m, 2H), 7.44-7.39 (dt, 1H), 7.35-7.25 (m, 5H), 7.24-7.17 (m, 2H), 7.14-7.01 (m, 5H), 6.55-6.53 (m, 1H), 6.49-6.46 (m, 1H), 6.31 (s, 1H) and 5.7-5.73 (m, 1H).

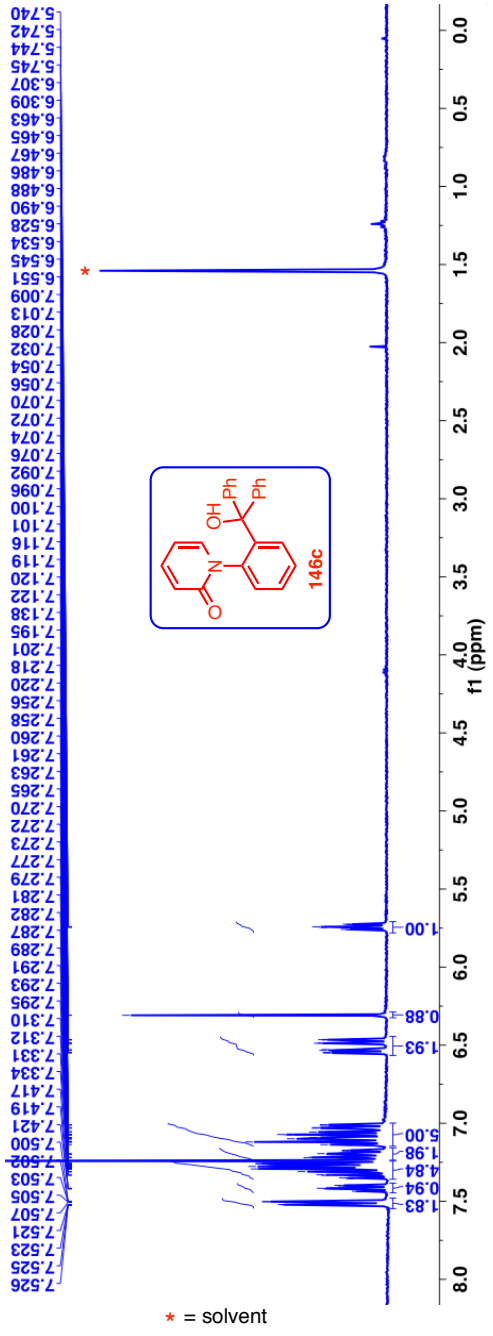

Figure 2.37: [1]H-NMR (400 MHz, $CDCl_3$, δ ppm) of atropisomeric 2-pyridone **146c**.

^{13}C-NMR (100 MHz, $CDCl_3$, δ ppm): 164.9, 146.8, 146.3, 144.5, 140.5, 139.8, 139.1, 131.7, 130.0, 129.8, 129.4, 128.2, 128.0, 127.97, 127.1, 126.8, 126.7, 120.8, 106.4 and 80.2.

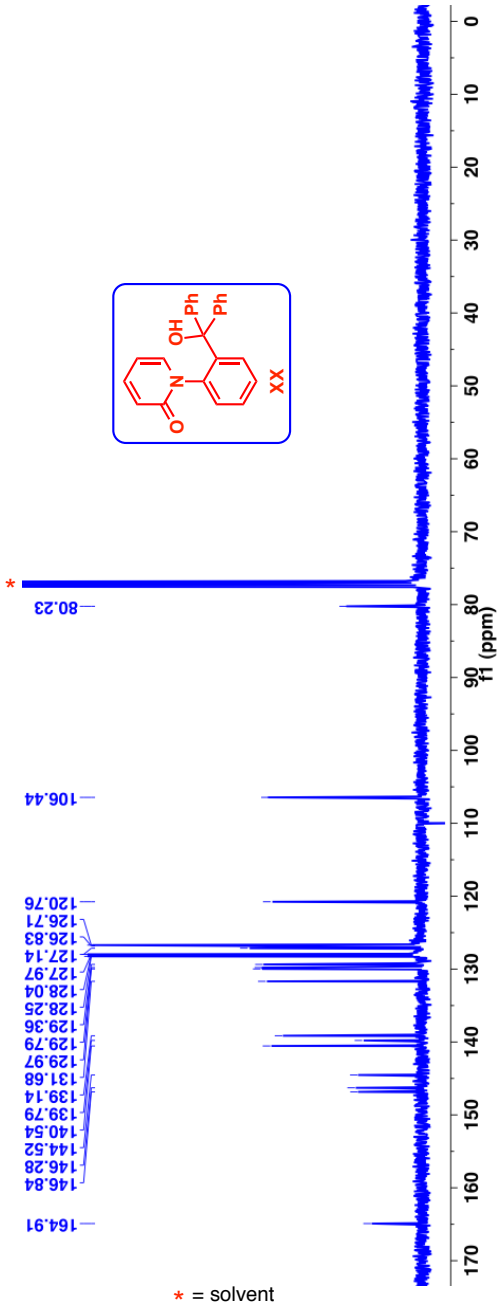

Figure 2.38: ^{13}C-NMR (100 MHz, $CDCl_3$, δ ppm) of atropisomeric 2-pyridone **146c**.

HRMS-ESI (m/z) ([M + Na]$^+$):

Calculated : 376.1308

Observed : 376.1299

|Δm| : 2.4 ppm

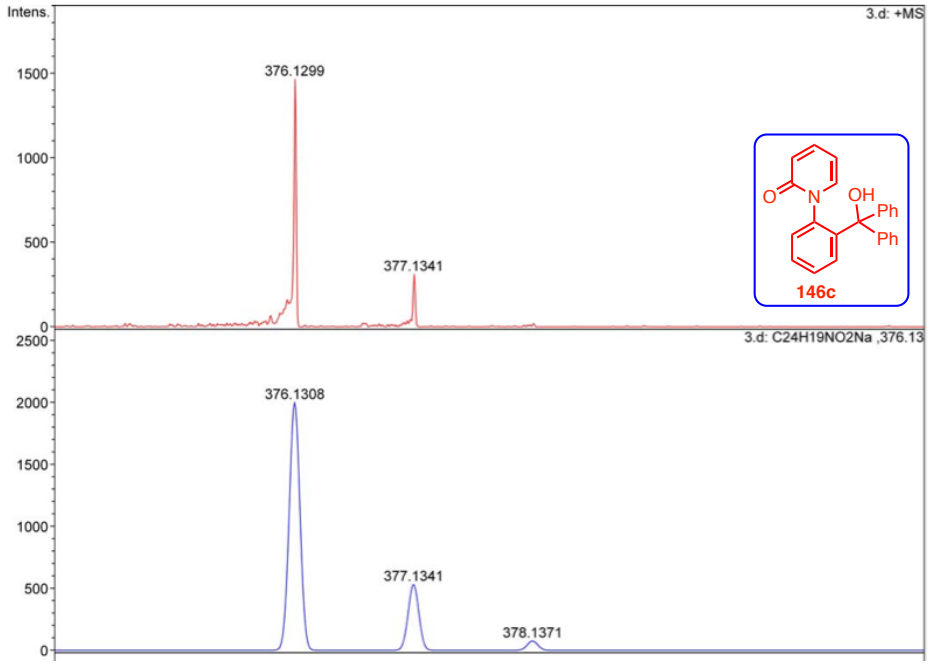

Figure 2.39: HRMS of atropisomeric 2-pyridone **146c**.

HPLC analysis conditions:

For analytical conditions

I). Column : RR-WHELK-01 10/100 FEC

Abs. detector : 254 nm and 270 nm

Mobile phase : Hexanes:2-propanol = 90:10

Flow rate : 1.5 mL/min

Retention times (min) : ~23.93 [(-)-**146c**] and ~38.52 [(+)-**146c**]

For preparative conditions

I). Column : RR-WHELK-01 10/100 FEC

Abs. detector : 254 nm and 270 nm

Mobile phase : Hexanes:2-propanol = 90:10

Flow rate : 4.0 mL/min

Retention times (min) : ~25.23 [(-)-**146c**] and ~44.62 [(+)-**146c**]

Optical Rotation $[\alpha]_D^{28}$:

HPLC retention time (RR-WHELK-01) at ~ 23.93 min, (*c* ~0.100%, $CHCl_3$) = -206 deg.

HPLC retention time (RR-WHELK-01) at ~ 38.52 min, (*c* ~0.100%, $CHCl_3$) = +206 deg.

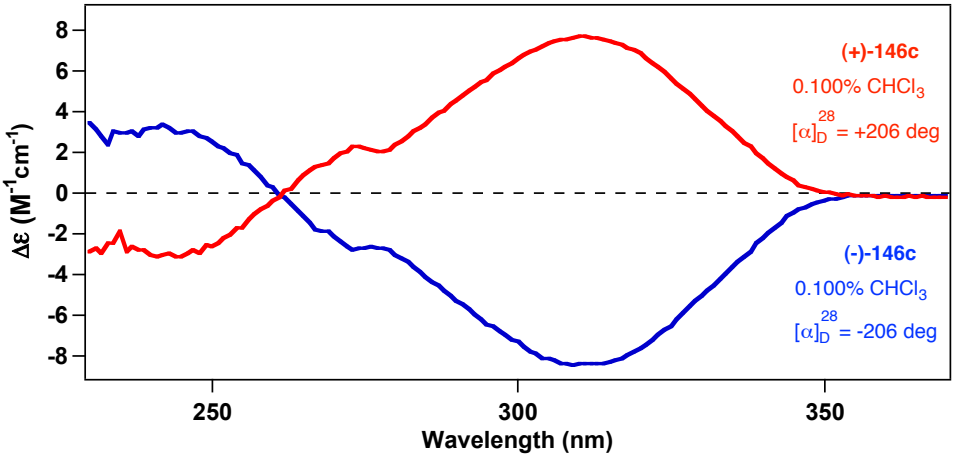

Figure 2.40: CD spectra of atropisomeric 2-pyridone **146c** measured in acetonitrile (*c* ~ 0.141 mM).

2.12.11. Process for photoreaction of 2-pyridones

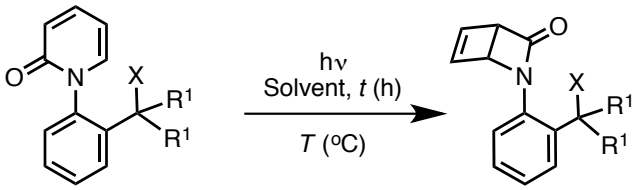

146a-c **147a-c**

a) R^1, X = Me
b) R^1 = Me, X = OH
c) R^1 = Ph, X = OH

Scheme 2.21: General irradiation procedure for 2-pyridone **147a-c**.

Optically pure *P/M* isomer of substituted pyridones **146a-c** (4.36 mM of **146a-b**; 2.83 mM of **146c**) in respective solvents (methanol, acetonitrile, toluene, and water (only for **146b**)) were irradiated for a given time interval in Pyrex tube using a 450 W medium-pressure mercury lamp, at various temperatures and under constant flow of nitrogen. After irradiation, the solvent was evaporated under reduced pressure and the photoproducts were isolated by preparative thin layer chromatography and characterized by NMR spectroscopy, mass spectrometry, single crystal XRD, CD, $[\alpha]_D$ and by HPLC. HPLC analysis of the crude photoproduct on chiral stationary phases gave the optical purity of the photoproducts.

Note: Concentration employed for light induced 4π-ring closure is critical. High concentration leads to [4+4]-photocycloaddition side products.

2.12.12. General procedure for photoreactions under high pressure

The photochemical reactions under elevated pressure was performed as follows: optically pure atropisomeric 2-pyridone was dissolved in dry (1.4 mM) and transferred into a custom designed quartz cell; the cell is then placed in a high-pressure vessel that is equipped with a sapphire window. The irradiations were carried out using an optical fiber carrying a light source from a Xenon lamp with 300±10 nm band-pass filter from Asahi® spectra 302 Max power supply unit.

[1]H-NMR (400 MHz, $CDCl_3$, δ ppm): 7.44-7.42 (m, 1H), 7.28-7.18 (m, 2H), 6.98-6.96 (m, 1H), 6.72-6.68 (m, 2H), 4.57-4.56 (t, *J* = 2.4 Hz, 1H), 4.35-4.34 (m, 1H) and 1.40 (s, 9H).

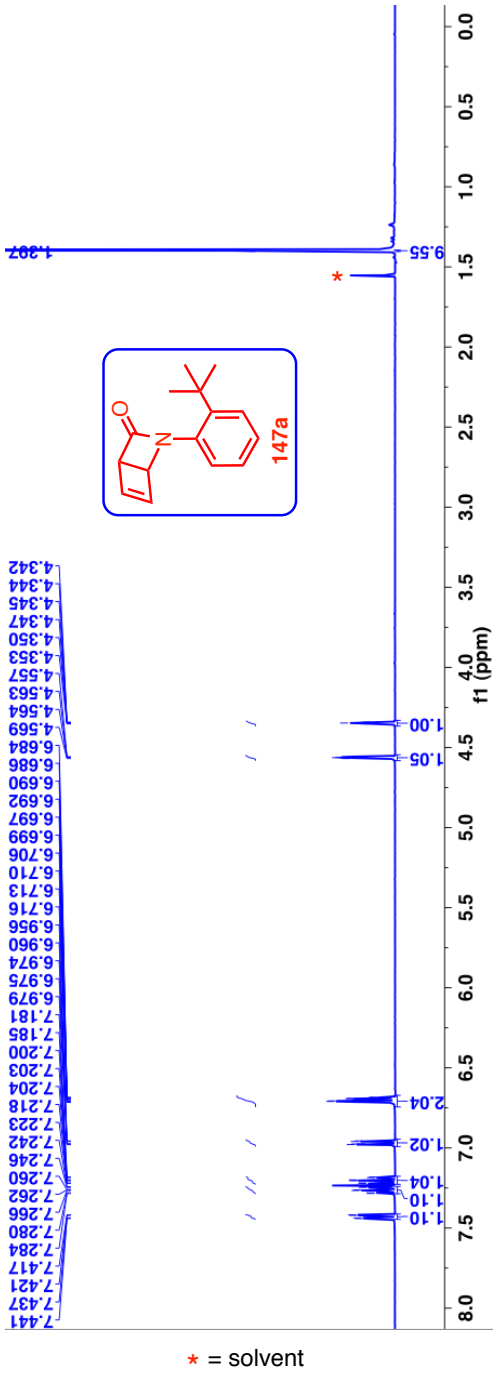

Figure 2.41: [1]H-NMR (400 MHz, $CDCl_3$, δ ppm) of β-lactam photoproduct **147a**.

^{13}C-NMR (100 MHz, $CDCl_3$, δ ppm): 170.6, 149.1, 141.3, 138.9, 137.9, 128.8, 128.7, 127.5, 127.3, 58.7, 58.2, 35.5 and 31.6.

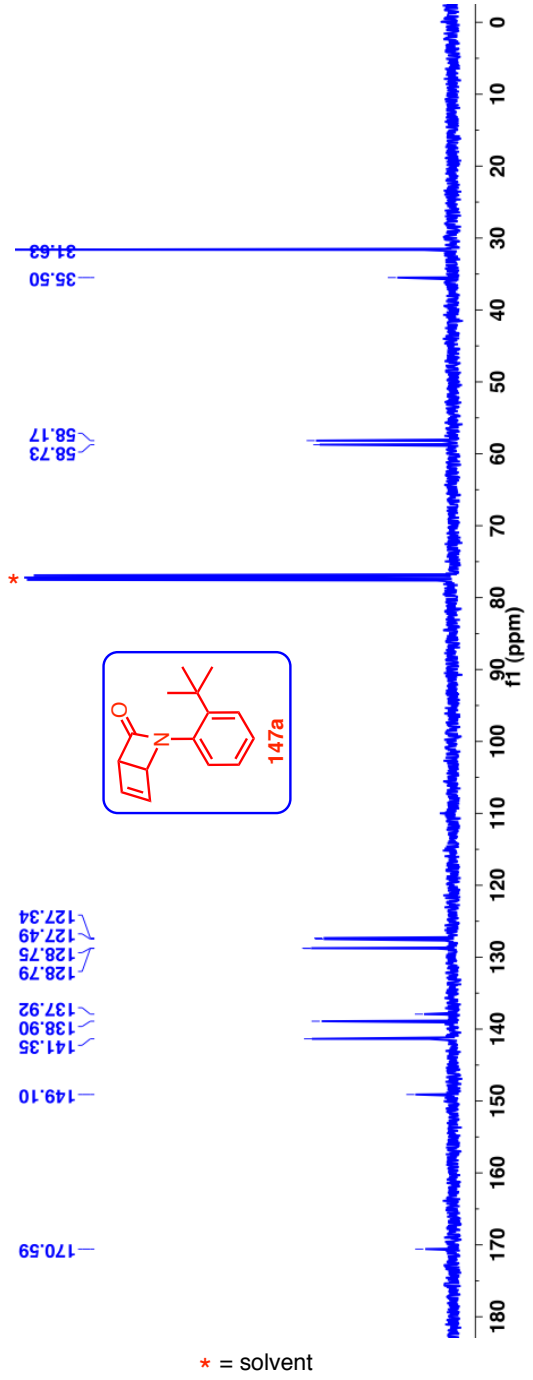

Figure 2.42: ^{13}C-NMR (100 MHz, $CDCl_3$, δ ppm) of β-lactam photoproduct **147a**.

HRMS-ESI (m/z) ([M + Na]$^+$):

Calculated : 250.1202

Observed : 250.1203

|Δm| : 0.4 ppm

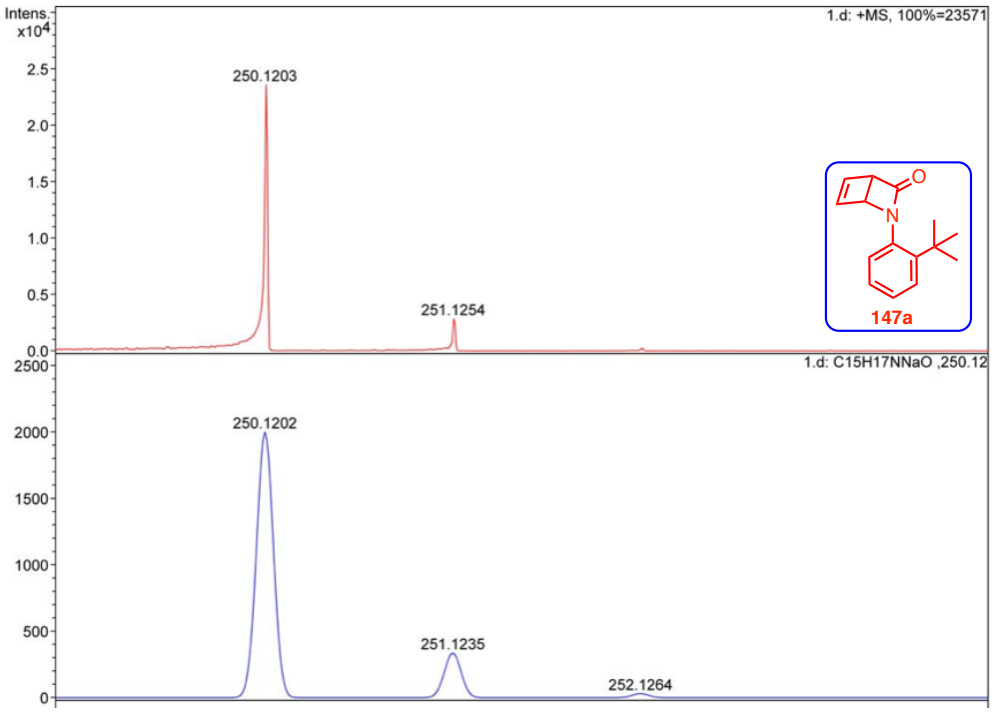

Figure 2.43: HRMS of β-lactam photoproduct **147a**.

HPLC analysis conditions:

For analytical conditions

I). Column : CHIRALPAK-AD-3

Abs. detector : 254 nm and 270 nm

Mobile phase : Hexanes:2-propanol = 95:5

Flow rate : 0.5 mL/min

Retention times (min) : ~10.30 min [(*1S*,*4R*)-(-)-**147a**] and ~11.12 min [(*1R*,*4S*)-(+)-**147a**].

For preparative conditions

I). Column : RR-WHELK-01 10/100 FEC

Abs. detector : 254 nm and 270 nm

Mobile phase : Hexanes:2-propanol = 98:2

Flow rate : 3.0 mL/min

Retention times (min): ~55.32 min [(*1S*,*4R*)-(-)- **147a**] and ~75.12 min [(*1R*,*4S*)-(+)- **147a**]

Optical Rotation $[\alpha]_D^{28}$:

HPLC retention time (CHIRALCEL-AD-3) at ~ 10.30 min, (*c* ~0.024%, MeOH) = -91.6 deg.

HPLC retention time (CHIRALCEL-AD-3) at ~ 11.32 min, (*c* ~0.023%, MeOH) = +95.8 deg.

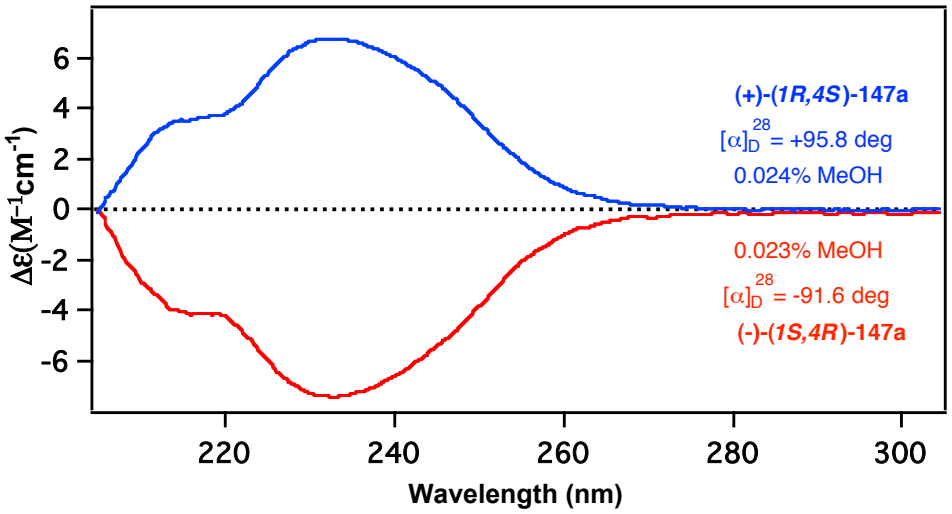

Figure 2.44: CD spectra of β-lactam photoproduct **147a** measured in methanol (*c* ~ 0.16 mM for [(+)-**147a**] and ~ 0.18 mM for [(-)-**147a**] respectively).

[1]H-NMR (400 MHz, $CDCl_3$, δ ppm): 7.54-7.51 (m, 1H), 7.28-7.25 (m, 2H), 7.07-7.04 (m, 1H), 6.70-6.67 (m, 2H), 4.75-4.74 (m, 1H), 4.32-4.31 (m, 1H), 2.83 (broad s, 1H) and 1.64 (s, 6H).

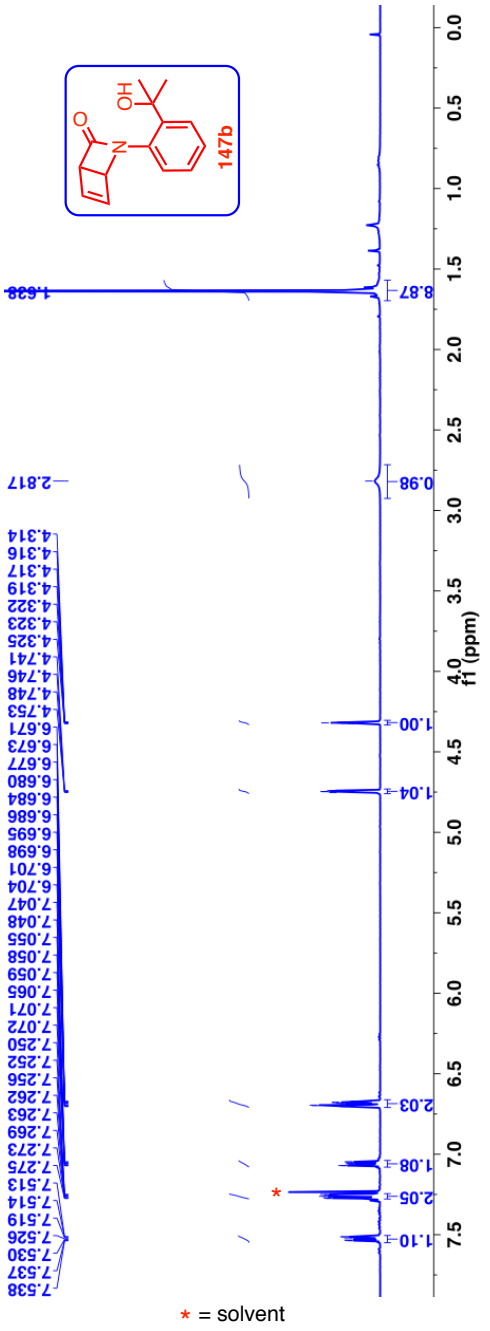

Figure 2.45: [1]H-NMR (400 MHz, $CDCl_3$, δ ppm) of β-lactam photoproduct **147b**.

^{13}C NMR (100 MHz, $CDCl_3$, δ ppm): 170.5, 145.4, 141.6, 139.3, 136.3, 128.5, 128.3, 127.3, 126.8, 72.7, 58.8, 57.7, 31.5 and 31.4.

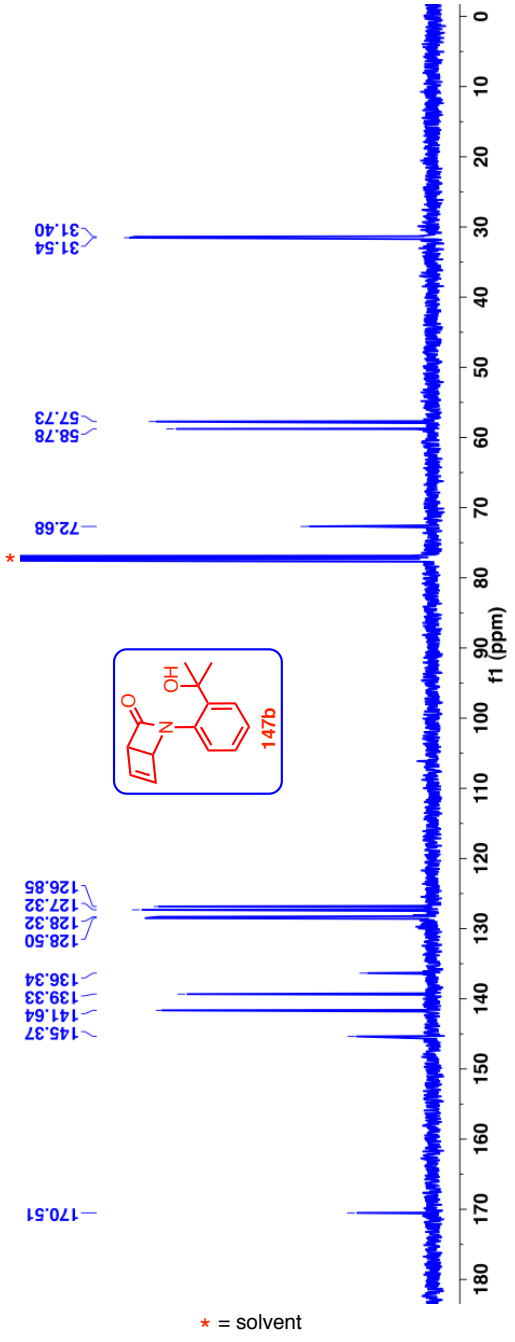

Figure 2.46: ^{13}C-NMR (100 MHz, $CDCl_3$, δ ppm) of β-lactam photoproduct **147b**.

HRMS-ESI (m/z) ([M + Na]$^+$):

Calculated : 252.0995

Observed : 252.0999

|Δm| : 1.6 ppm

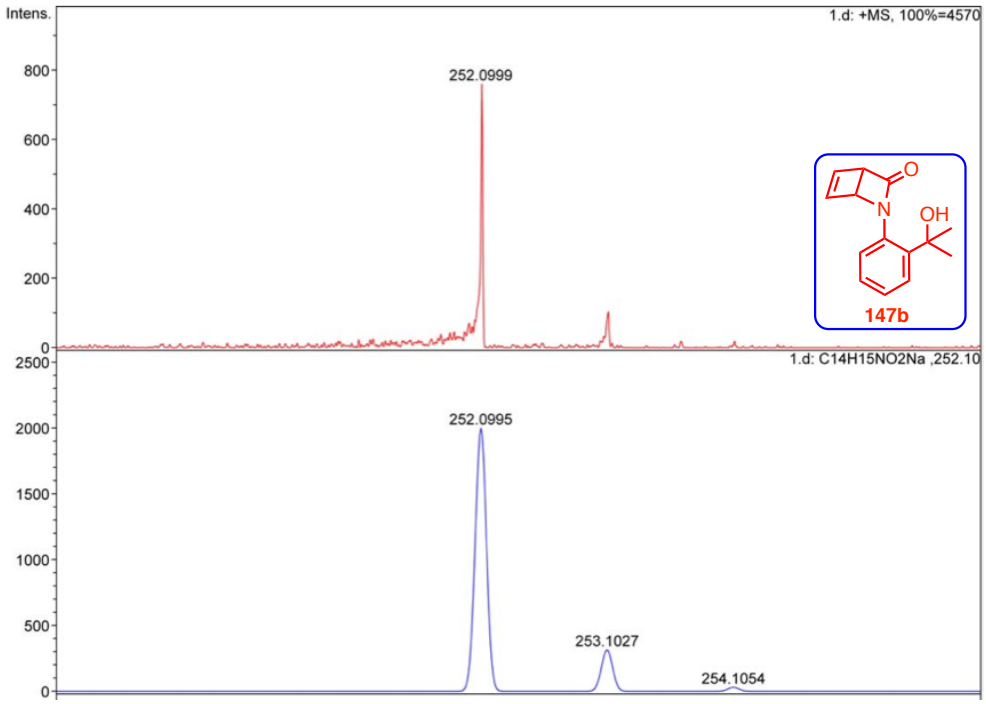

Figure 2.47: HRMS of β-lactam photoproduct **147b**.

HPLC analysis conditions

For analytical conditions

I). Column : CHIRALPAK-AD-3

Abs. detector : 254 nm and 270 nm

Mobile phase : Hexanes:2-propanol = 95:5

Flow rate : 1 mL/min

Retention times (min) : 11.37 min [(+)-**147b**] and 13.59 min [(-)-**147b**]

II). Column : RR-WHELK-01 10/100 FEC

Abs. detector : 254 nm and 270 nm

Mobile phase : Hexanes:2-propanol = 90:10

Flow rate : 1.5 mL/min

Retention times (min): ~11.95 min [(-)-**147b**] and ~17.10 min [(+)-**147b**]

For preparative conditions

I). Column : RR-WHELK-01 10/100 FEC

Abs. detector : 254 nm and 270 nm

Mobile phase : Hexanes:2-propanol = 97:3

Flow rate : 4.0 mL/min

Retention times (min): ~60.52 min [(-)-**147b**] and ~80.37 min [(+)-**147b**]

Optical Rotation $[\alpha]_D^{28}$:

HPLC retention time (RR-WHELK-01) at ~11.95 min, (*c* ~0.024%, MeOH) = -18.8 deg.

HPLC retention time (RR-WHELK-01) at ~17.10 min, (*c* ~0.024%, MeOH) = +18.8 deg.

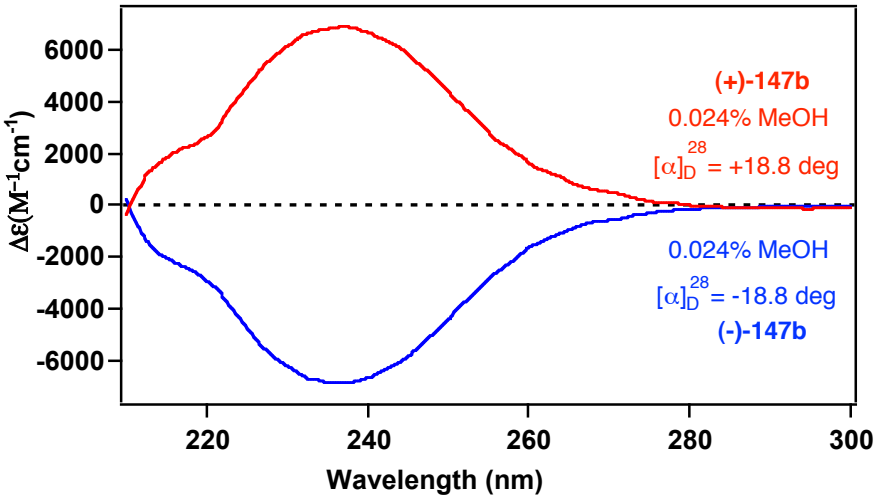

Figure 2.48: CD spectra of β-lactam photoproduct **147b** measured in methanol (*c* ~ 0.080 mM).

[1]H-NMR (400 MHz, $CDCl_3$, δ ppm): 7.49-7.46 (m, 2H), 7.41-7.40 (m, 2H), 7.33-7.28 (m, 5H), 7.25-7.20 (m, 2H), 7.17-7.08 (m, 2H), 6.91-6.88 (dd, 1H), 6.58-6.57 (m, 1H), 6.50-6.49 (m, 1H), 5.85 (s, 1H), 3.67-3.66 (m, 1H) and 3.61-3.62 (t, 1H).

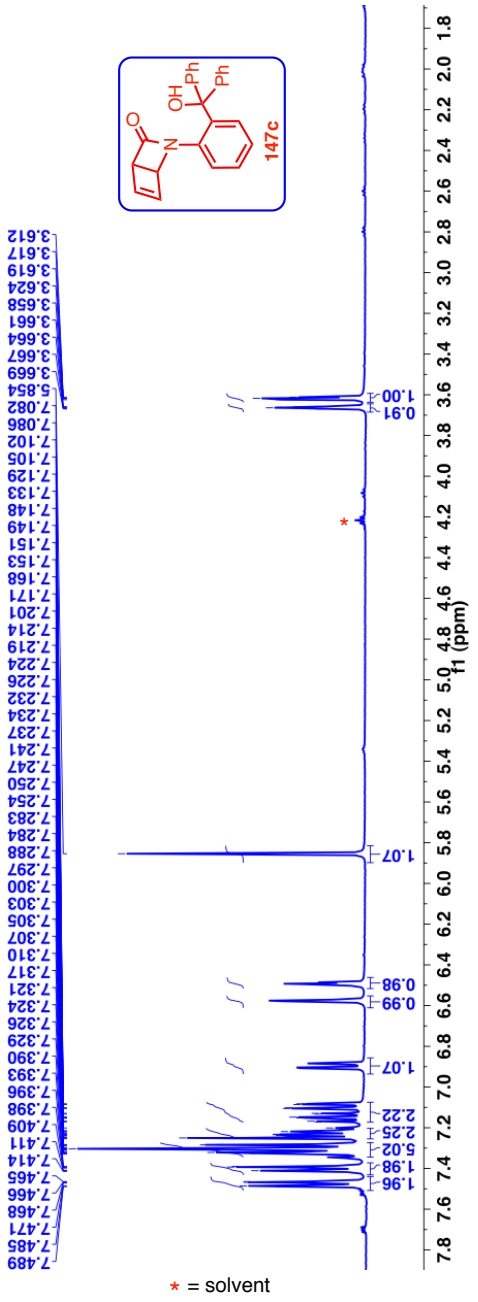

Figure 2.49: [1]H-NMR (400 MHz, $CDCl_3$, δ ppm) of β-lactam photoproduct **147c**.

^{13}C-NMR (100 MHz, $CDCl_3$, δ ppm): 165.6, 147.5, 147.0, 145.2, 141.3, 140.5, 139.9, 132.3, 130.7, 130.5, 130.1, 128.96, 128.8, 128.7, 127.9, 127.6, 127.4, 121.4, 107.2 and 80.96.

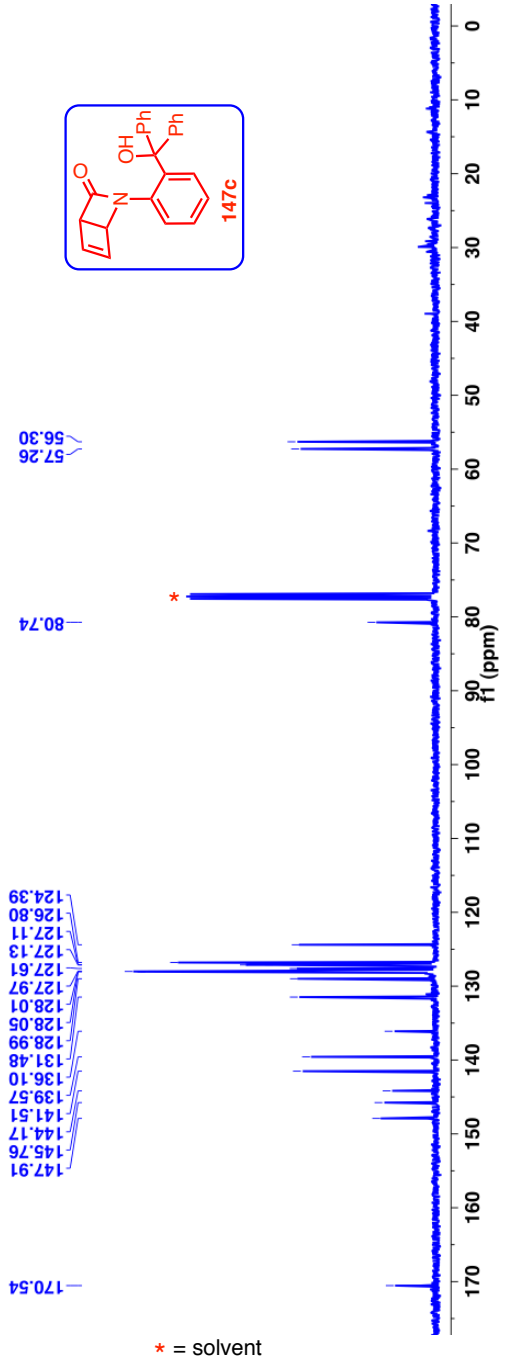

Figure 2.50: ^{13}C-NMR (100 MHz, $CDCl_3$, δ ppm) of β-lactam photoproduct **147c**.

HRMS-ESI (m/z) ([M + Na]$^+$):

Calculated : 376.1308

Observed : 376.1312

|Δm| : 1.1 ppm

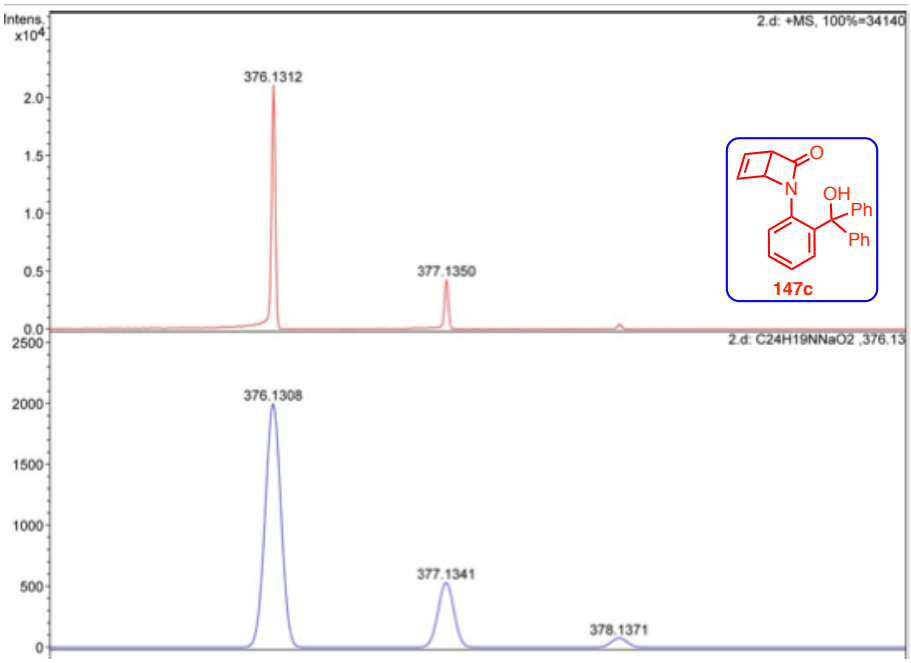

Figure 2.51: HRMS of β-lactam photoproduct **147c**.

HPLC analysis conditions:

For analytical conditions

I). Column : RR-WHELK-01 10/100 FEC

Abs. detector : 254 nm and 270 nm

Mobile phase : Hexanes:2-propanol = 90:10

Flow rate : 1.5 mL/min

Retention times (min) : ~12.48 min [(-)-**147c**] and ~17.92 min [(+)-**147c**]

For preparative conditions

I). Column : RR-WHELK-01 10/100 FEC

Abs. detector : 254 nm and 270 nm

Mobile phase : Hexanes:2-propanol = 90:10

Flow rate : 3.0mL/min

Retention times (min) : ~31.89 min [(-)-**147c**] and ~42.78 min [(+)-**147c**]

Optical Rotation $[\alpha]_D^{28}$:

HPLC retention time (RR-WHELK-01) at ~ 12.48 min, (*c* ~0.032%, MeOH) = -46.6 deg.

HPLC retention time (RR-WHELK-01) at ~ 17.92 min, (*c* ~0.030%, MeOH) = +43.3 deg.

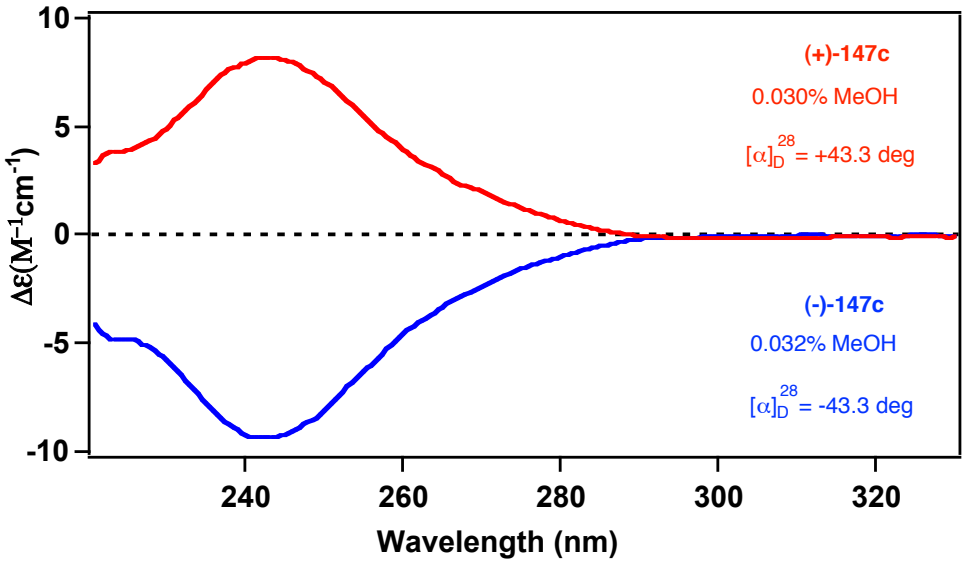

Figure 2.52: CD spectra of β-lactam photoproduct **147c** measured in methanol (*c* ~ 0.15 mM).

2.12.13. HPLC analysis of photoproducts upon irradiation of (*P*)-(+)-146a and (*M*)-(-)-146a.

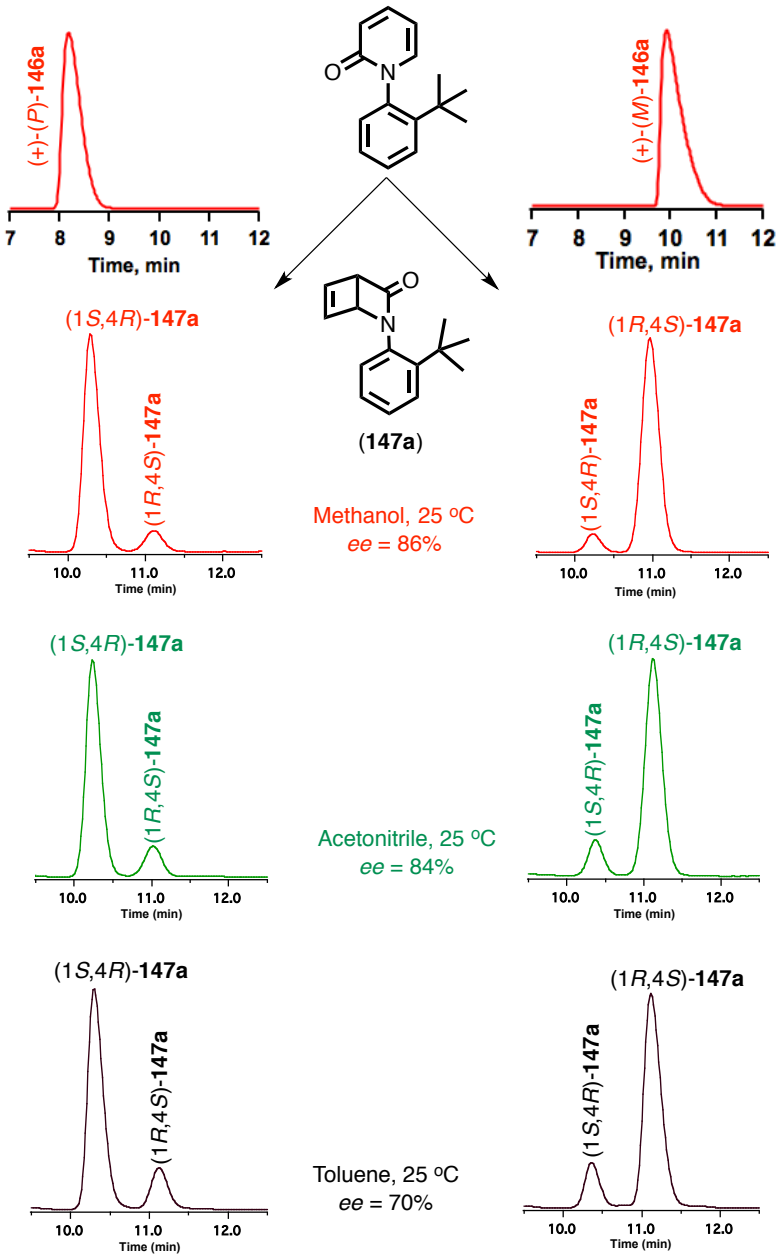

Figure 2.53: HPLC chromatogram of photoproducts upon irradiation of *P*-(+)-**146a** and *M*-(-)-**146a**.

2.12.14. HPLC analysis of photoproducts upon irradiation of (+)-146b and (-)-146b.

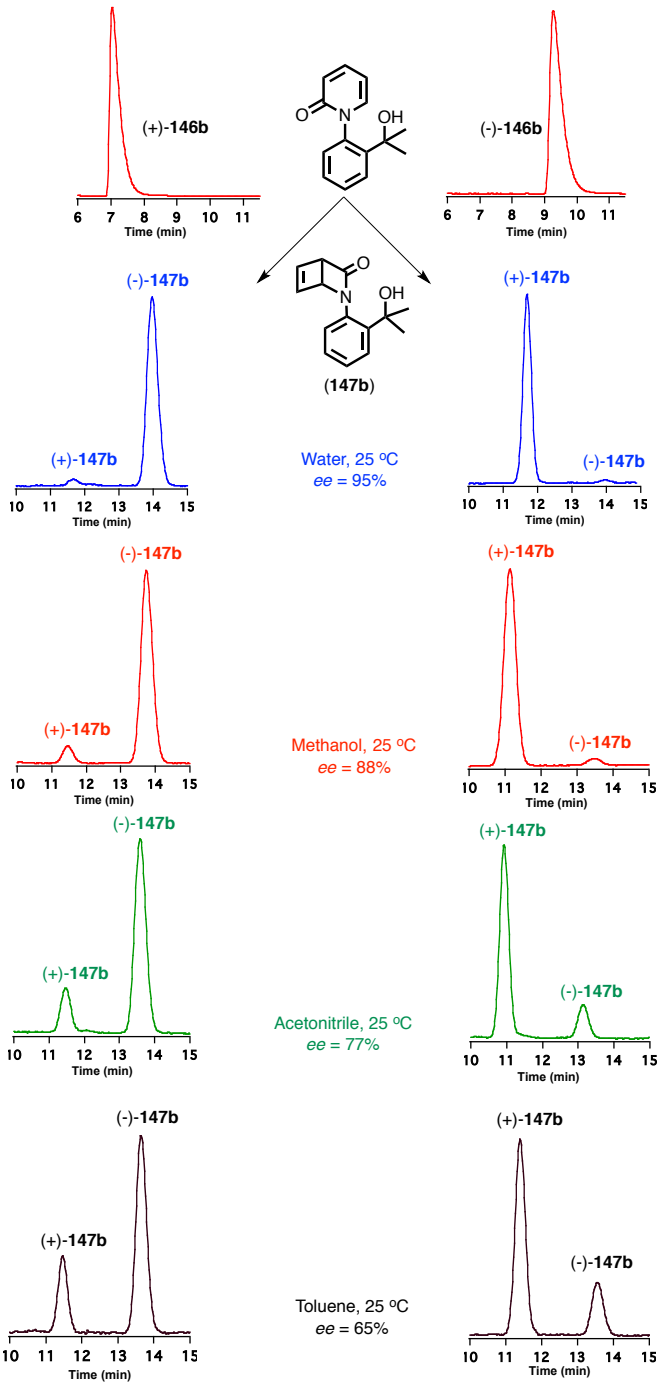

Figure 2.54: HPLC chromatogram of photoproducts upon irradiation of (+)-**146b** and (-)-**146b**.

2.13. References

(1) Taylor, E. C.; Paudler, W. W. Photodimerization of some α,β-unsaturated lactams. *Tetrahedron Lett.* **1960**, *1*, 1-3.

(2) Taylor, E. C.; Kan, R. O.; Paudler, W. W. The Photolysis of 2-Aminopyridines and 2-Pyridones. *J. Am. Chem. Soc.* **1961**, *83*, 4484-4485.

(3) Slomp, G.; MacKellar, F. A.; Paquette, L. A. structure studies by nuclear magnetic resonance spectroscopy. i. the photodimer of n-methyl-2-pyridone. *J. Am. Chem. Soc.* **1961**, *83*, 4472-4473.

(4) Laing, M. *Proc. Chem. Soc.* **1964**, 343.

(5) Corey, E. J.; Streith, J. Internal Photoaddtion Reactions of 2-Pyrone and N-Methyl-2-pyridone: A New Synthetic Approach to Cyclobutadiene. *J. Am. Chem. Soc.* **1964**, *86*, 950-951.

(6) Woodward, R. B.; Hoffmann, R. Stereochemistry of Electrocyclic Reactions. *J. Am. Chem. Soc.* **1965**, *87*, 395-397.

(7) Woodward, R. B.; Hoffmann, R. The Conservation of Orbital Symmetry. *Angew. Chem. Int. Ed.* **1969**, *8*, 781-853.

(8) Toda, F.; Koichi, T. Enantioselective photoconversion of pyridones into β-lactam derivatives in inclusion complexes with optically active host compounds. *Tetrahedron Lett.* **1988**, *29*, 4299-4302.

(9) Tanaka, K.; Fujiwara, T.; Urbanczyk-Lipkowska, Z. Highly Enantioselective Photocyclization of 1-Alkyl-2-pyridones to β-Lactams in Inclusion Crystals with Optically Active Host Compounds. *Org. Lett.* **2002**, *4*, 3255-3257.

(10) Bach, T.; Bergmann, H.; Harms, K. Enantioselective Photochemical Reactions of 2-Pyridones in Solution. *Org. Lett.* **2001**, *3*, 601-603.

(11) Sivasubramanian, K.; Kaanumalle, L. S.; Uppili, S.; Ramamurthy, V. Value of zeolites in asymmetric induction during photocyclization of pyridones, cyclohexadienones and naphthalenones. *Org. Biomol. Chem.* **2007**, *5*, 1569-1576.

(12) Ayitou, A. J.-L.; Sivaguru, J. Light-Induced Transfer of Molecular Chirality in Solution: Enantiospecific Photocyclization of Molecularly Chiral Acrylanilides. *J. Am. Chem. Soc.* **2009**, *131*, 5036-5037.

(13) Bennett, D. J.; Blake, A. J.; Cooke, P. A.; Godfrey, C. R. A.; Pickering, P. L.; Simpkins, N. S.; Walker, M. D.; Wilson, C. Stereoselectivity in reactions of atropisomeric lactams and imides. *Tetrahedron* **2004**, *60*, 4491-4511.

(14) Rayabarapu, D. K.; Majumdar, K. K.; Sambaiah, T.; Cheng, C.-H. Unusual 1,4-Addition of 2-Pyridyl Carboxylates to Benzynes: A Convenient Route to 1-(2-Acylphenyl)-2-pyridones. *J. Org. Chem.* **2001**, *66*, 3646-3649.

(15) Christian, W. *Dynamic Stereochemistry of Chiral Compounds. Principles and Applications*, *RSC publishing: Cambridge, UK., 2008*.

(16) Lawrance, G. A.; Stranks, D. R. Volumes of activation for intramolecular racemization mechanisms. High-pressure racemization of bipyridyl, phenanthroline and oxalato complexes of chromium(III) in solution. *Inorg. Chem.* **1977**, *16*, 929-935.

(17) Inoue, Y.; Matsushima, E.; Wada, T. Pressure and Temperature Control of Product Chirality in Asymmetric Photochemistry. Enantiodifferentiating Photoisomerization of Cyclooctene Sensitized by Chiral Benzenepolycarboxylates. *J. Am. Chem. Soc.* **1998**, *120*, 10687-10696.

(18) Kaneda, M.; Nakamura, A.; Asaoka, S.; Ikeda, H.; Mori, T.; Wada, T.; Inoue, Y. Pressure control of enantiodifferentiating photoisomerization of cyclooctenes sensitized by chiral benzenepolycarboxylates. The origin of discontinuous pressure dependence of the optical yield. *Org. Biomol. Chem.* **2003**, *1*, 4435-4440.

(19) Ayitou, A. J. L.; Fukuhara, G.; Kumarasamy, E.; Inoue, Y.; Sivaguru, J. Enantiospecific Photochemical Transformations under Elevated Pressure. *Chem. Eur. J.* **2013**, *19*, 4327-4334.

(20) Trost, B. M.; Parquette, J. R.; Marquart, A. L. Effect of High Pressure on a Transition-Metal-Catalyzed Cycloaddition. *J. Am. Chem. Soc.* **1995**, *117*, 3284-3285.

(21) Matsumoto, K.; Kim, J. C.; Hayashi, N.; Jenner, G. High pressure mediated three component Strecker synthesis of α-aminonitriles from ketones, aromatic amines and trimethylsilyl cyanide. *Tetrahedron Lett.* **2002**, *43*, 9167-9169.

(22) Kuster, C. J. T.; Scheeren, H. W. High-Pressure Promoted Cycloadditions for Application in Combinatorial Chemistry. In *High Pressure Chemistry*; Wiley-VCH Verlag GmbH, 2007; pp 284-304.

(23) Leffler, J. E. The Enthalpy-Entropy Relationship and its implications for organic chemistry. *J. Org. Chem.* **1955**, *20*, 1202-1231.

(24) Giese, B. The isoselective relationship. *Acc. Chem. Res.* **1984**, *17*, 438-442.

(25) Kitagawa, O.; Fujita, M.; Kohriyama, M.; Hasegawa, H.; Taguchi, T. Stereoselective synthesis of diastereomeric atropisomeric lactam with various ring sizes and their structural characterization. *Tetrahedron Lett.* **2000**, *41*, 8539-8544.

(26) O'Boyle, N. M.; Tenderholt, A. L.; Langner, K. M. Software News and Updates. cclib: A library for package-independent computational chemistry algorithms. *J. Comput. Chem.* **2008**, *29*, 839-845.

(27) Stephens, P. J.; Harada, N. ECD Cotton Effect Approximated by the Gaussian Curve and Other Methods. *Chirality* **2010**, *22*, 229-233.

(28) Kumarasamy, E.; Jesuraj, J. L.; Omlid, J. N.; Ugrinov, A.; Sivaguru, J. Light-Induced Enantiospecific 4π Ring Closure of Axially Chiral 2-Pyridones: Enthalpic and Entropic Effects Promoted by H-Bonding. *J. Am. Chem. Soc.* **2011**, *133*, 17106-17109.

(29) Frisch, M. J.; Trucks, G. W.; Schlegel, H. B.; Scuseria, G. E.; Robb, M. A.; Cheeseman, J. R.; Montgomery, J. A., Jr.; Vreven, T.; Kudin, K. N.; Burant, J. C.; Millam, J. M.; Iyengar, S. S.; Tomasi, J.; Barone, V.; Mennucci, B.; Cossi, M.; Scalmani, G.; Rega, N.; Petersson, G. A.; Nakatsuji, H.; Hada, M.; Ehara, M.; Toyota, K.; Fukuda, R.; Hasegawa, J.; Ishida, M.; Nakajima, T.; Honda, Y.; Kitao, O.; Nakai, H.; Klene, M.; Li, X.; Knox, J. E.; Hratchian, H. P.; Cross, J. B.; Bakken, V.; Adamo, C.; Jaramillo, J.; Gomperts, R.; Stratmann, R. E.; Yazyev, O.; Austin, A. J.; Cammi, R.; Pomelli, C.; Ochterski, J. W.; Ayala, P. Y.; Morokuma, K.; Voth, G. A.; Salvador, P.; Dannenberg, J. J.; Zakrzewski, V. G.; Dapprich, S.; Daniels, A. D.; Strain, M. C.; Farkas, O.;

Malick, D. K.; Rabuck, A. D.; Raghavachari, K.; Foresman, J. B.; Ortiz, J. V.; Cui, Q.; Baboul, A. G.; Clifford, S.; Cioslowski, J.; Stefanov, B. B.; Liu, G.; Liashenko, A.; Piskorz, P.; Komaromi, I.; Martin, R. L.; Fox, D. J.; Keith, T.; Al-Laham, M. A.; Peng, C. Y.; Nanayakkara, A.; Challacombe, M.; Gill, P. M. W.; Johnson, B.; Chen, W.; Wong, M. W.; Gonzalez, C.; Pople, J. A.: Gaussian 03. revision B.03 ed.; Gaussian, Inc.: Wallingford, CT, 2004.

(30) Hembury, G. A.; Borovkov, V. V.; Inoue, Y. Chirality-Sensing Supramolecular Systems. *Chem. Rev.* **2007**, *108*, 1-73.

(31) Lanni, E. L.; Bosscher, M. A.; Ooms, B. D.; Shandro, C. A.; Ellsworth, B. A.; Anderson, C. E. Synthesis of Substituted N-Benzyl Pyridones via an O- to N-Alkyl Migration. *J. Org. Chem.* **2008**, *73*, 6425-6428.

CHAPTER 3: STEREOSPECIFIC INTRAMOLECULAR [2+2]-PHOTOCYCLOADDITION OF ATROPISOMERIC ENAMIDES

3.1. Introduction

The [2+2]-photocycloaddition reaction is one of the hallmarks of photochemical transformations employed in the organic synthesis.[1,2] The diversity of the provides avenues to access several carbocyclic and heterocyclic four membered derivatives with high stereochemical control.[3] For example, [2+2]-photocycloaddition of 2,3-dihydro-4-pyridone was extensively investigated to access several natural products and structurally important motifs as demonstrated by Comins and coworkers in the diastereoselective synthesis of lupin alkaloid plumerinine (**165**) (Scheme 3.1).[4,5] In their stereoselective synthetic protocol, the key strategy involved [2+2]-photocycloaddition of 2,3-dihydro-4-pyridone derivatives.

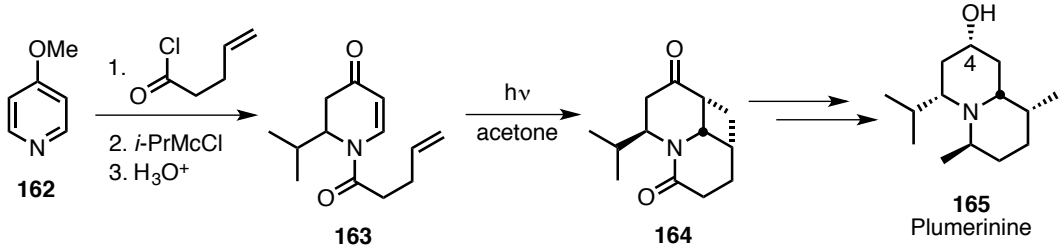

Scheme 3.1: Synthesis of plumerinine alkaloid through [2+2]-photocycloaddition reaction.

In 2013, Bach and coworkers reported the corresponding enantioselective [2+2]-photocycloaddition version of 4-pyridone derivatives (Scheme 3.2).[6] Coordination of chiral Lewis acid (**168**) to the enone derivative (**166**) resulted in the bathochromic shift in UV-vis spectrum and also provided efficient enantiotopic facial discrimination.

The material in this chapter was co-authored by Elango Kumarasamy (EK) Dr. J. Sivaguru (JS). EK in consultation with JS synthesized all compounds and carried out all the experiments provided in this chapter. EK and JS came up with the mechanistic rationale and the conclusion described in this chapter.

Irradiating the complex with monochromatic light at 366 nm enabled them to perform enantioselective [2+2]-photocycloaddition reaction (broad wavelength irradiation leads to lower *ee* in the photoproduct due to racemic background reaction). Utilizing this strategy they demonstrated the enantioselective synthesis of (+)-lupinine and (+)-thermopsine natural products.

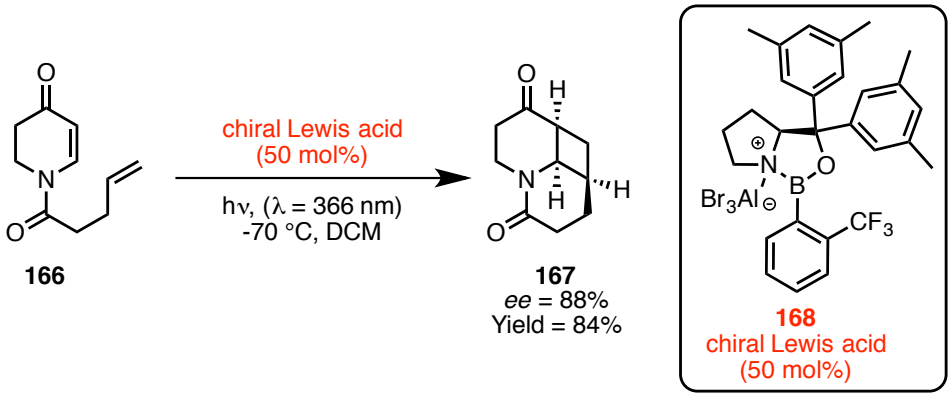

Scheme 3.2: Enantioselective [2+2]-photocycloaddition of 5,6-dihydro-4-pyridones.

In the above-mentioned systems, the enone was in excited state to which the ground state alkene adds resulting in cyclobutane derivatives. Similar to 5,6-dihydro-4-pyridones, the photochemistry of 3,4-dihydro-2-pyridones (structural isomer of 2,3-dihydro-4-pyridones) was well explored.[7] For example, Bach and coworkers reported Paternò-Büchi reactions of dihydro-2-pyridones with benzaldehyde that resulted in oxetane photoproducts (Scheme 3.3).[3,8,9]

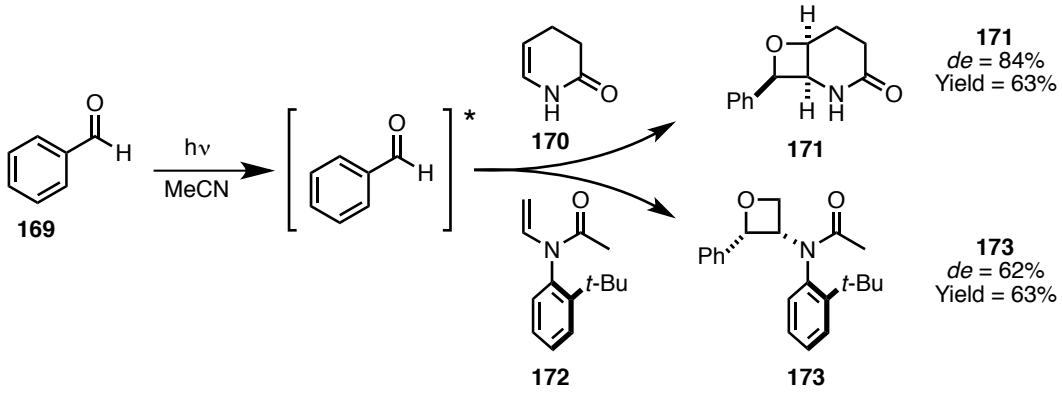

Scheme 3.3: Paternò-Büchi reactions of enamides with carbonyl compounds.

In this diastereoselective reaction, the excited benzaldehyde (**169**) reacted to the ground state cyclic enamide 3,4-dihydro-2-pyridone (**170**) (scheme 3.3, top) and atropisomeric acyclic enamide (**172**) (scheme 3.3, bottom) to furnish desired oxetane photoproducts in good yield. In the later case, the bulky *t*-Bu group provided necessary bias to the incoming carbonyl group resulting in diastereoselective oxetane photoproduct (*de* = 62%). However in these systems, the carbonyl chromophore is in the excited state, which adds to the ground state of the enamides.[10] We envisioned a complementary photoreaction that involved the excited state of enamides (scheme 3.4). The motivation behind this idea was to evaluate the possibility of accessing cyclobutane and oxetane derivatives. Also, this methodology avoids other side reactions involved in the excited state chemistry of carbonyl compounds such as α-cleavage, H-abstraction, disproportionation, pinacol coupling.

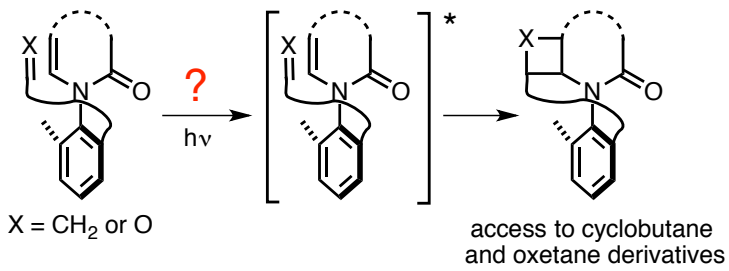

Scheme 3.4: Possibility of intramolecular [2+2]-photocycloaddition in enamides.

Another important modification that we aimed to evaluate in the photochemistry of atropisomeric enamides was to replace the traditional bulky group such as *t*-butyl group that provided axial chirality with less bulkier group such as methyl group. While it is known that the two less bulky groups can create a chiral axis, the strength of such chiral axis was not evaluated thoroughly. We intended to carry out detailed racemization kinetics to gain quantitative understanding of less bulky groups over *t*-butyl group in imparting stable chiral axis. Added advantage of this method is that one of the methyl groups could be modified to hold the ground state alkene partner allowing us to freeze the axial chirality upon photoreaction (permanently locking the axial chirality) eliminating the axial chirality in the photoproduct. Keeping these ideas

in mind, we synthesized the following atropisomeric enamides (chart 3.1) according to the procedures reported in literature.

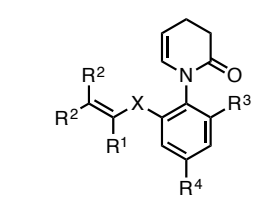

174a-d

a) X = CH_2; R^1,R^2,R^4 = H; R^3 = Me
b) X = CH_2; R^1,R^4 = H; R^2,R^3 = Me
c) X = CH_2; R^1,R^3,R^4 = Me; R^2 = H
d) X = C_2H_4; R^1,R^2,R^4 = H; R^3 = H

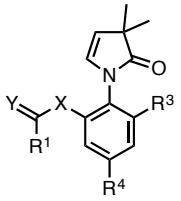

174e-j

e) X,Y = CH_2; R^1,R^4 = H; R^3 = Me
f) X = C_2H_4; Y = CH_2; R^1,R^4 = H; R^3 = Me
g) X = OCH_2; Y = CH_2; R^1,R^4 = H; R^3 = Me
h) X = CH_2; Y = O; R^1,R^3,R^4 = H
i) X = CH_2; Y = O; R^1 = Me; R^3,R^4 = H
j) X = CH_2; Y = O; R^1 = Ph; R^3,R^4 = Me

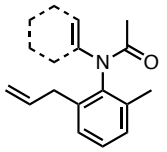

174k-l

k) CH=CH_2
l) Cyclohexenyl

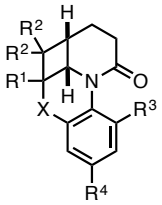

175a-d

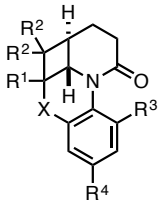

176a-d

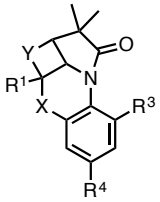

175e-j
Y = CH_2, O

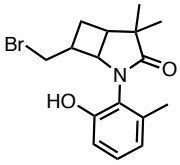

177

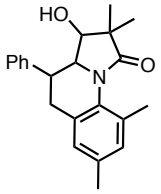

178

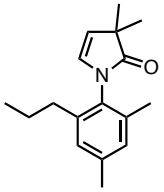

179

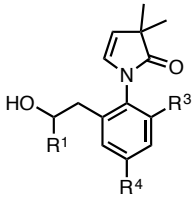

180

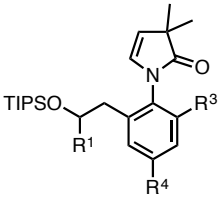

181

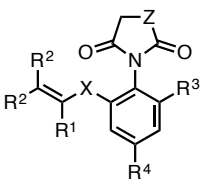

182a-g
Z = CMe_2, C_2H_4

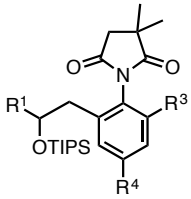

183a-c

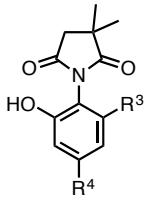

184

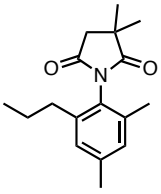

185

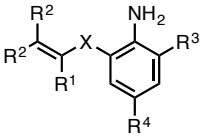

186

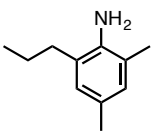

187

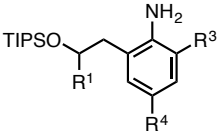

188

Chart 3.1: Structures of atropisomeric enamides, their photoproducts and compounds used for their synthesis.

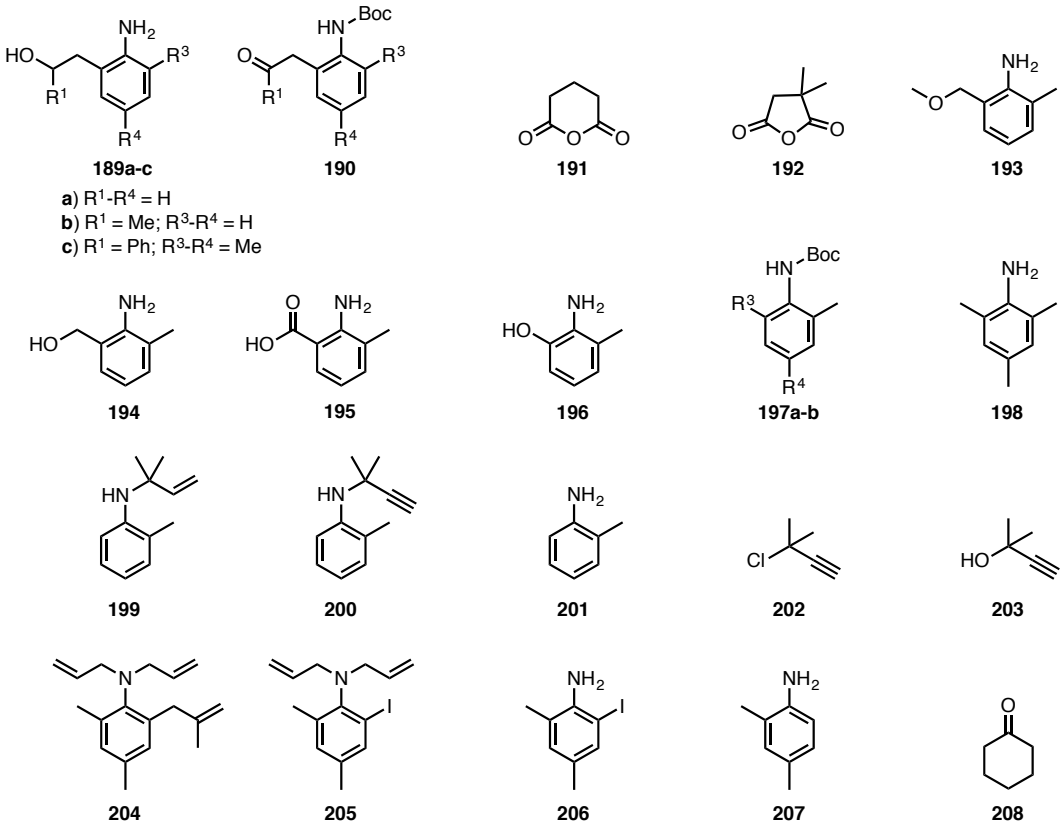

189a-c 190 191 192 193

194 195 196 197a-b 198

199 200 201 202 203

204 205 206 207 208

a) R^1-R^4 = H
b) R^1 = Me; R^3-R^4 = H
c) R^1 = Ph; R^3-R^4 = Me

Chart 3.1: Structures of atropisomeric enamides, their photoproducts and compounds used for their synthesis (continued).

3.2. Racemization kinetics of atropisomeric enamides

The racemization kinetics of atropisomeric enamides was carried out in order to gain insights into the energy barrier to racemization. Following similar protocol described in section 2.4 in chapter 2, racemization kinetics was performed and barriers for racemization were calculated

Table 3.1: Activation energy, rate and half-life for racemization of optically pure non-biaryl atropisomeric enamides **174**.[a]

Entry	Compd	Solvent	T (°C)	$\tau_{1/2rac}$	$\Delta G^{\ddagger}_{rac}$ (kcal·mol^{-1})	k_{rac} (s^{-1})
1	**174a**	IPA	75	9.8 days	30.2	8.2×10^{-7}
2	**174b**	IPA	75	15.0 days	30.5	5.4×10^{-7}
3	**174c**	IPA	75	10.2 days	30.2	7.8×10^{-7}
4	**174e**	IPA	75	4.7 h	27.5	4.1×10^{-5}
5	**174f**	IPA	75	9.6 h	28.0	2.0×10^{-5}
6	**174g**	Hex-IPA	23	44 min	22.2	2.6×10^{-4}
7	**174j**	IPA	75	0.9 h	26.3	2.1×10^{-4}
8	**174l**	IPA	75	17.8 h	28.4	1.1×10^{-5}

[a] Reported values carry an error of ±5%. Hex- hexanes, IPA- 2-propanol.

Analysis of racemization parameters in table 3.1 clearly indicated that the energy barrier for racemization in atropisomeric enamides depended on the type of substitution and ring size apart from the solvent and temperature.

In the six membered enamides **174a-c**, energy barrier for racemization was fairly high. The energy barrier imparted by two methyl substituents was comparable if not higher than the chiral axis provided by single *tert*-butyl group as in the case of *tert*-butyl-2-pyridone (**146a** in chapter 2). For example, the racemization barrier of enamide **174a** was 30.2 kcal·mol^{-1} (IPA, 75 °C), where as for *tert*-butyl-2-pyridone **146a** was 29.9 kcal·mol^{-1} (MeOH, 65 °C). While an absolute comparison cannot be made as the solvent and the temperature of racemization study were slightly different, the result clearly showed that the two smaller bulkier groups flanking the

chiral axis can be as efficient as single bulky steric biasing group in providing a stable chiral axis. Substitution on the alkenyl tether had slight influence resulting in higher racemization barrier (compare entries 1-3, table 3.1).

On the other hand, the energy barrier for the five membered atropisomeric enamides **174e-g** significantly reduced. It is well established that the non-biaryl atropisomeric system with reduced ring size (reduced C-N-C bond angle), have a lower energy barrier for racemization.[11] For example, substrate **174e**, which had similar substituent under similar racemization conditions, had a racemization barrier of 27.5 kcal·mol^{-1} with the half-life of 4.7 h (**174a** had a half-life of 9.8 days at 75 °C). Further, the racemization barrier was highly influenced when the flanking group was altered as in the case of **174g**. For example, when the alkenyl tether was replaced for an oxy alkenyl tether (where the flanking group was methyl and oxygen instead of a methyl and methylene group), the racemization barrier was significantly reduced to 22.2 kcal·mol^{-1} with the half-life of 44 mins at 23 °C.

Acyclic enamides with sufficient steric bulk around the chiral axis presented a high-energy barrier towards racemization. For example, substrate **174l**, had a racemization value of 28.4 kcal·mol^{-1} with the half-life of 17.8 h in IPA at 75 °C. Even though the substrate lacked the rigidity of a cyclic system, the presence of sufficient steric bulk around the chiral axis compensate resulting in higher racemization barrier.

A smaller change in the sterics greatly affected the racemization barrier on atropisomeric enamides. As the racemization barrier critically influences the outcome of stereospecificity in the photoproduct, the substituents and structural analysis provided crucial information about the requirement to design a stable axially chiral enamides for an efficient “axial to point chiral transfer” in the desired [2+2]-photocycloaddition reaction.

3.3. Photophysical studies on non-biaryl atropisomeric enamides

The photophysical studies of non-biaryl atropisomeric enamides **174a-c** were carried out in two spectrometric grade solvents *viz* ethanol (EtOH) and methylcyclohexane (MCH). The standard reference for fluorescence quantum yield was phenol in water (ϕ_r = 0.14) and the fluorescence quantum yield was calculated using the following equation,[12]

$$\phi_S = \phi_r (I_s/I_r)(A_s/A_r)(\eta_s^2/\eta_r^2) \qquad \textbf{Equation 3.1}$$

Where,

ϕ_s is the fluorescence quantum yield of the sample,

ϕ_r is the fluorescence quantum yield for the reference solution (i.e. phenol in water),

I_s is the fluorescence intensity of the sample,

I_r is the fluorescence intensity of the reference solution (phenol in water),

A_s is the absorbance value of the sample,

A_r is the absorbance value of the reference solution (phenol in water),

η_s is the refractive index of the solvent (ethanol = 1.361 and MCH = 1.422) for the sample and

η_r is the refractive index of the solvent (water = 1.333) for the reference (phenol in water).

3.3.1. Emission measurements of atropisomeric enamide 174a.

The following parameters were maintained during Fluorescence acquisition.

Excitation slit-width = 1 nm; Emission slit-width = 2 nm;

Integration time = 0.1 sec; Wavelength increment = 1 nm;

The fluorescence quantum yield (ϕ_f) of **174a** was ~ 0.094 in EtOH and ~ 0.103 in MCH.

The phosphorescence spectra were recorded at 77 K in EtOH and MCH glass. The following parameters were employed during acquisition:

Excitation: 298 nm for EtOH and 299 nm for MCH; emission: 318-576 nm for EtOH and 319-578 nm for MCH; excitation slit-width: 5 nm; emission slit-width: 8 nm; time per flash: 3000

msec for EtOH and 2500 msec for MCH; flash per count: 10; delay time: 100 msec; wavelength increment: 3 nm; sample window: 2500 msec for EtOH and 2000 msec for MCH.

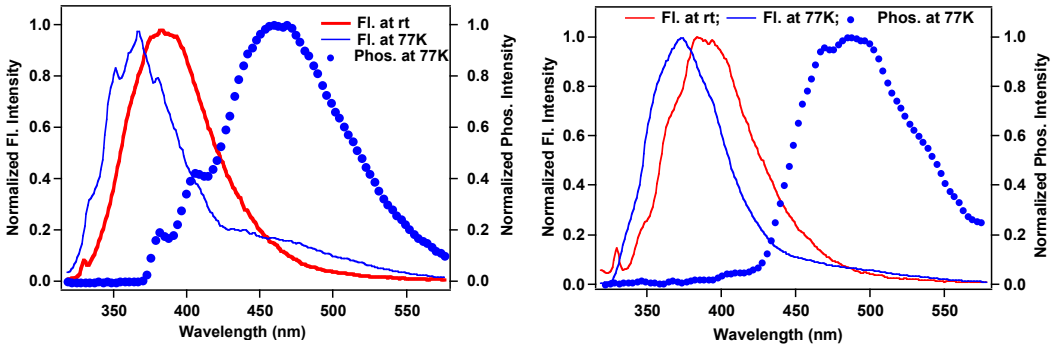

Figure 3.1: Fluorescence at room temperature (—), fluorescence at 77 K (—) and phosphorescence at 77 K (•) for **174a** recorded in EtOH (left) and MCH (right) (*c*~1.03 mM).

The phosphorescence decay profiles were recorded at 77 K in EtOH and MCH using a PhosLamp with a trigger pulse delay of 1%. The sample in EtOH was excited at 298 nm and the emission was monitored at 462 nm. The sample in MCH was excited at 299 nm and the emission was monitored at 491 nm. Following parameters were maintained during acquisition: Excitation slit-width = 5 nm; emission slit-width = 8 nm; time (phosphorescence) range = 2.8 sec; number of sweeps = 200.

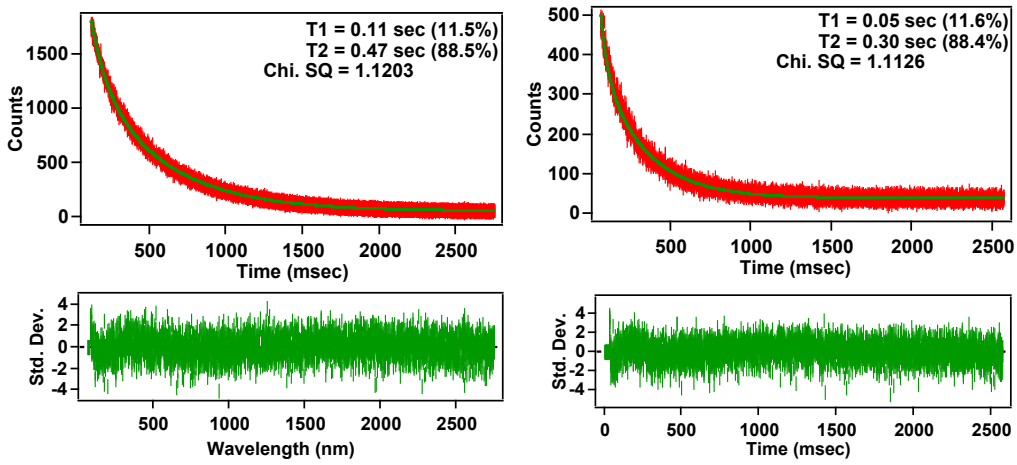

Figure 3.2: Phosphorescence decay profile of **174a** in EtOH (left) and MCH (right) at 77 K (*c* ~ 1.03 mM).

3.3.2. Emission measurements of atropisomeric enamide 174b.

The following parameters were maintained during Fluorescence acquisition.

Excitation slit-width = 1nm; Emission slit-width = 2 nm;

Integration time = 0.1 sec; Wavelength increment = 1 nm;

The fluorescence quantum yield (ϕ_f) of **174b** was ~0.057 in EtOH and ~ 0.067 in MCH.

The phosphorescence spectra were recorded at 77 K in EtOH and MCH glass. The following parameters were employed during acquisition:

Excitation: 297 nm for EtOH and 301 nm for MCH; Emission: 317-574 nm for EtOH and 321-582 nm for MCH; excitation slit-width: 5 nm; emission slit-width: 8 nm; time per flash: 3000 msec for EtOH and 2500 msec for MCH; flash per count: 10; delay time: 100 msec; wavelength increment: 3 nm; sample window: 2500 msec for EtOH and 2000 msec for MCH.

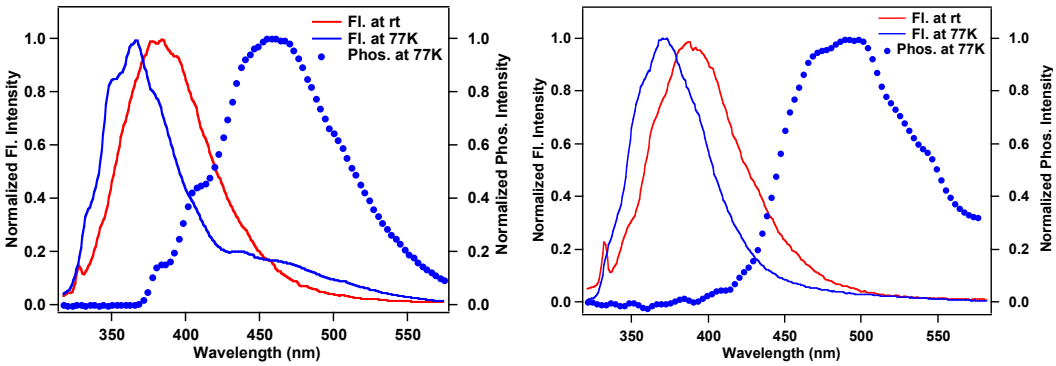

Figure 3.3: Fluorescence at room temperature (—), fluorescence at 77 K (—) and phosphorescence at 77 K (•) for **174b** recorded in EtOH (left) and MCH (right) (*c* ~ 0.91 mM).

The phosphorescence decay profiles were recorded at 77 K in EtOH and MCH using a PhosLamp with a trigger pulse delay of 1%. The sample in EtOH was excited at 297 nm and the emission was monitored at 460 nm. The sample in MCH was excited at 301 nm and the emission was monitored at 488 nm. Following parameters were maintained during acquisition:

Excitation slit-width = 5 nm; emission slit-width = 8 nm; time (phosphorescence) range = 2.8 sec; number of sweeps = 200.

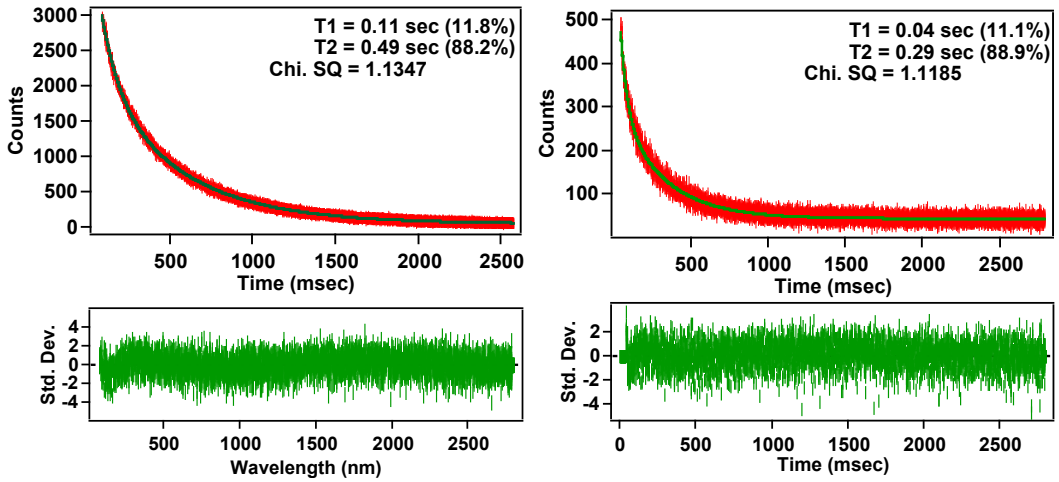

Figure 3.4: Phosphorescence decay profile of **174b** in EtOH (left) and MCH (right) at 77 K (*c* ~ 0.91 mM).

3.3.3. Emission measurements of atropisomeric enamide 174c.

The following parameters were maintained during Fluorescence acquisition.

Excitation slit-width = 1nm; Emission Slit-width = 2 nm;

Integration time = 0.1 sec; Wavelength increment = 1 nm;

The fluorescence quantum yield (ϕ_f) of **174c** was ~0.082 in EtOH and ~0.098 in MCH.

The phosphorescence spectra were recorded at 77 K in EtOH and MCH glass. The following parameters were employed during acquisition:

Excitation: 297 nm for EtOH and 301 nm for MCH; Emission: 317-574 nm for EtOH and 321-582 nm for MCH; excitation slit-width: 5 nm; emission slit-width: 8 nm; time per flash: 3000 msec for EtOH and 2500 msec for MCH; flash per count: 10, delay time: 100 msec; wavelength increment: 3 nm; sample window: 2500 msec for EtOH and 2000 msec for MCH.

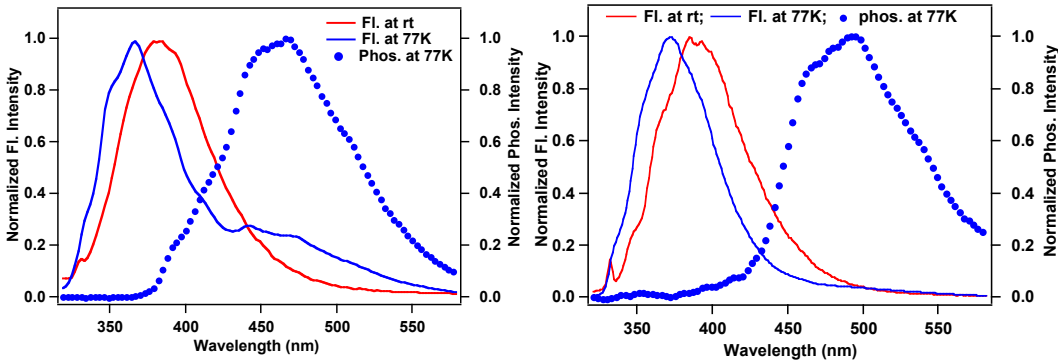

Figure 3.5: Fluorescence at room temperature (—), fluorescence at 77 K (—) and phosphorescence at 77 K (•) for **174c** recorded in EtOH (left) and MCH (right) ($c \sim 0.91$ mM).

The phosphorescence decay profiles were recorded at 77 K in EtOH and MCH using a PhosLamp with a trigger pulse delay of 1%. The sample in EtOH was excited at 297 nm and the emission was monitored at 467 nm. The sample in MCH was excited at 301 nm and the emission was monitored at 492 nm. Following parameters were maintained during acquisition: Excitation slit-width = 5 nm; emission slit-width = 8 nm; time (phosphorescence) range = 2.8 sec; number of sweeps = 200.

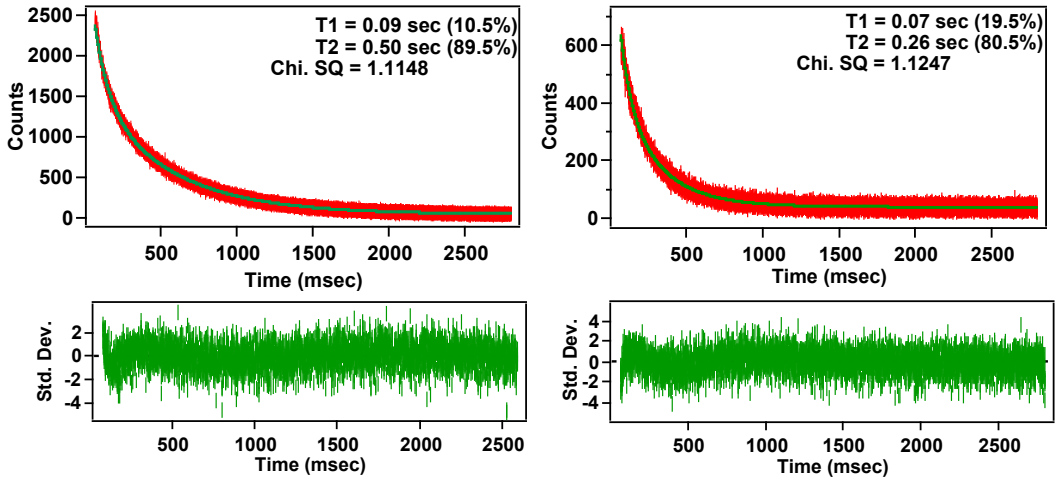

Figure 3.6: Phosphorescence decay profile of **174c** in EtOH (left) and MCH (right) at 77 K ($c \sim 0.91$ mM).

Table 3.2: Fluorescence quantum yield, phosphorescence lifetime and triplet energy of atropisomeric enamide **174a-c** in ethanol and methylcyclohexane.

Entry	Compd	Solvent	Fluorescence quantum yield (ϕ_f)	Phosphorescence lifetime (sec)	Triplet energy (kcal.mol^{-1})
1	**174a**	EtOH	~ 0.094	~ 0.47	~ 73.88
2		MCH	~ 0.103	~ 0.30	~ 72.56
3	**174b**	EtOH	~ 0.057	~ 0.49	~ 74.07
4		MCH	~ 0.067	~ 0.29	~ 73.3
5	**174c**	EtOH	~ 0.082	~ 0.50	~ 75.44
6		MCH	~ 0.098	~ 0.26	~ 73.88

3.4. Stereospecific [2+2]-photocycloaddition of atropisomeric enamides

The atropisomeric enamides were classified based on the ring size and the type of ground state partners (alkenyl vs. carbonyl groups) and were investigated towards the stereospecific photocycloaddition reaction.

3.4.1. Stereospecific [2+2]-photocycloaddition of six membered enamides 174a-d

The first set of investigations were carried out on six membered enamides **174a-d**. The photoreaction of enamides proceeded efficiently under acetone sensitized irradiation conditions resulting in the desired cyclobutane products. The direct irradiation did not result in the product formation, which was verified by irradiating enamides in various solvents (toluene, methanol and acetonitrile). Photophysical analysis of the atropisomeric enamides revealed that the triplet energy was around ~73 kcal·mol^{-1} and enabled us to employ other sensitizers such as xanthone and acetophenone that had similar triplet energies. However, the conversion depended on the type of sensitizer employed. For instance, the conversions in **174a** for 3 h irradiation with xanthone and acetone as sensitizers were comparable (70 and 76% conversions). On the other hand, the conversion for 3 h with acetophenone was rather poor (29% conversion).

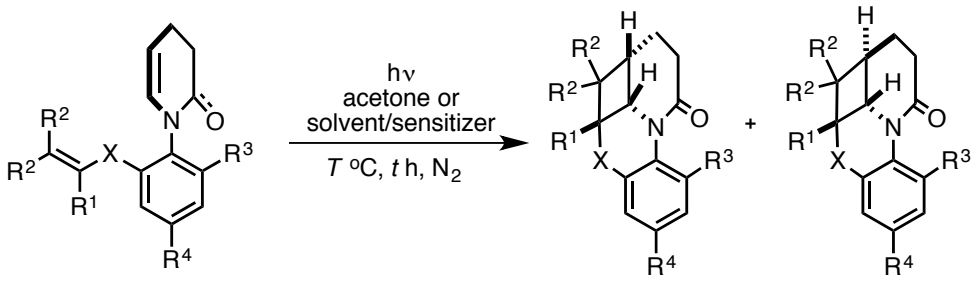

174a-d **175a-d** **176a-d**

a) R^1-R^2,R^4 = H; R^3 = Me; X = CH_2
b) R^1,R^4= H; R^2-R^3 = Me; X = CH_2
c) R^1,R^3-R^4 = Me; R^2 = H; X = CH_2
d) R^1-R^2,R^4 = H; R^3 = Me; X = CH_2-CH_2

Scheme 3.5: Stereospecific [2+2]-photocycloaddition of 6-membered enamides **174a-d**.

Surprisingly, the butenyl tethered atropisomeric enamide **174d**, did not result in the desired reaction both under direct and sensitized irradiation conditions. Even longer irradiation times (6 h) only led to conversion less than 10%. In most cases, the starting material was recovered with significant amount of decomposition in longer irradiated samples. We believe that the butenyl chain length was not suitable for photoreaction, presumably because of the unfavored approach of the alkene towards the excited enamide.

Table 3.3: Stereospecific [2+2]-photocycloaddition of 6-membered enamides **174a-d**[a]

Entry	Substrate	Solv/sens.	*t* (h)	product	Conv. (MB)[b]	[%] ee,[c] *dr* (2:3)[d]
1	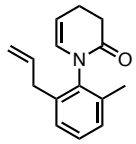	acetone	3	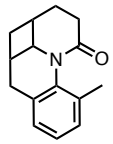	70 (96)	
	(+)-**174a**			(-)-(*R*,*R*,*R*)-**175a**		> 98% *ee* (> 98:2)
	(-)-**174a**			(+)-(*S*,*S*,*S*)-**175a**		> 98% *ee* (> 98:2)
		MeOH/xanthone	3	**175a**	76 (89)	> 98% *ee* (> 98:2)
		MeOH/acetophenone	3	**175a**	29 (92)	> 98% *ee* (> 98:2)
2	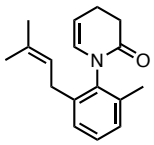	acetone	24	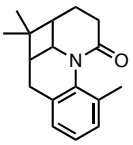	39 (79)	
	(+)-**174b**			(B)-**175b**		> 98% *ee* (2.8:1)
	(-)-**174b**			(A)-**175b**		> 98% *ee* (2.8:1)
		MeOH/xanthone	3	**175b**	21 (82)	> 98% *ee* (4.3:1)
		MeOH/acetophenone	12	**175b**	20 (87)	> 98% *ee* (4.3:1)
3	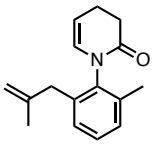	acetone	2.5	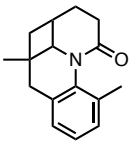	90 (77)	
	(+)-**174c**			(-)-(*R*,*R*,*R*)-**175c**		> 98% *ee* (> 98:2)
	(-)-**174c**			(+)-(*S*,*S*,*S*)-**175c**		> 98% *ee* (> 98:2)
		MeOH/xanthone	2.5	**175c**	92 (84)	> 98% *ee* (> 98:2)
		MeOH/acetophenone	12	**175c**	33 (86)	> 98% *ee* (> 98:2)
4	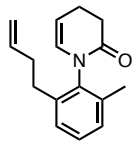	acetone	3	-[e]	-	-
	174d					

[a](+) and (-) represent the sign of optical rotation (MeOH at 25 °C). Reported values are an average of 3 runs with ±3% error. Photoreaction was performed with 30 mol% sensitizer at 25 °C except for **174a-b** which the was done at -30 °C to avoid unwanted side products. For **174a** and **174c** an uncharacterized product was observed with 8-10% yield. A and B refer to the elution order for a given pair of enantiomers in the HPLC. Absolute configuration was determined by single crystal XRD using Flack parameters. [b] The *ee* values were determined by HPLC on a chiral stationary phase, Identical ee values were observed for both photoproducts **175b** and **176b**. [c] The diastereomeric ratio (*dr*) was determined by ^{1}H-NMR spectroscopy. Conversion (% Convn) and mass balance (% MB) were calculated by ^{1}H-NMR spectroscopy with Ph_3CH as an internal standard. [e] No photoproduct was observed.

The photoreaction of allyl tether substituted enamide **174a-c** was monitored thin layer chromatography. After the consumption of starting material, the solvent was evaporated under reduced pressure and the residue was purified by chromatography to get pure photoproducts. Analysis of the photoproducts revealed the presence of two diastereomers **175** and **176**. The relative orientation of the hydrogen atoms in the lactam ring was *cis* in photoproduct **175**. On the other hand, the relative orientation of the hydrogen atoms in the lactam ring was *trans* in the case of photoproduct **176**. The diastereomeric ratio (*dr*) between photoproducts **175** and **176** was calculated from the ^{1}H-NMR analysis of the crude reaction mixture.

Analysis of table 3.3 revealed that the reaction proceeded with excellent control over enantiospecificity resulting in enantioenriched photoproduct (*ee* >98%). However, the *dr* depended on the type of alkenyl tether involved in the reaction. For example, *dr* >98:2 was observed in the photoreaction of **174a** and **174c** whose terminal carbon was unsubstituted. On the other hand, the *dr* of **174b** whose terminal carbon in the alkenyl tether was disubstituted was only 2.8:1 in acetone and 4.3:1 in methanol.

3.4.2. Stereospecificity in the [2+2]-photocycloaddition of 5 membered enamides 174e-g

The photoreaction of the 5-membered enamides proceeded smoothly at room temperature yielding the cyclized photoproduct in good isolated yield. On the contrary to the butenyl tethered six membered enamide **174d** that underwent recovery of the starting material and decomposition, the butenyl tethered enamide **174f** underwent smooth photoreaction to yield the corresponding cyclobutane photoproduct. While the *dr* in the photoproduct was high in all the cases, the enantiomeric excess in the photoproduct depended on the substituents governing the axial chirality. The alkenyl substituted enamides as in the case of atropisomeric enamides **174e-f** (that had methyl and methylene group around the chiral axis), resulted in photoproducts with >96% *ee*. On the other hand, the oxy alkenyl tether as in the case of **174g** (that had oxygen and methylene group around the chiral axis) only resulted in the photoproducts with <20% *ee*.

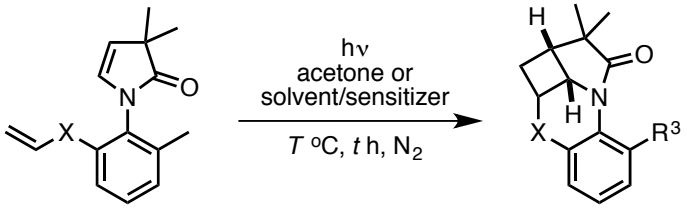

174e-g

175e-g

e) X = CH_2
f) X = CH_2-CH_2
g) X = O

Scheme 3.6: Stereospecific [2+2]-photocycloaddition of 5-membered enamides **174e-g**.

The enantiomeric excess in the photoproducts can be appreciated by analyzing the racemization barrier of the enamides investigated. The enamides **174e-f** had a half-life of 4.7 h at 75 °C that provided stable chiral axis at room temperature for an efficient chirality transfer to occur resulting in >96% *ee* in the photoproduct. On the other hand, the half-life of racemization for enamide **174g** was 44 mins at 23 °C which only presented very small energy barrier towards racemization. So, the racemization competed with photoreaction significantly eroding the optical purity of the starting material. As a consequence, the resultant *ee* of the photoreaction was very low (<20%). This study reiterated the importance of stable axial chirality in effecting very high enantiomeric excess in the photoproduct.

Table 3.4: Stereospecific [2+2]-photocycloaddition of 5-membered enamides **174e-g**[a]

Entry	Substrate	Solv/sens.	*t* (h)	product	Yield [%], [%] *ee*
1	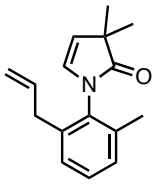	acetone	0.5	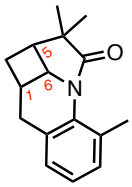	85[b]
	(+)-**174e**			(-)-(1*R*,5*S*,6*R*)-**175e**	> 98% *ee*
	(-)-**174e**			(+)-(1*S*,5*R*,6*S*)-**175e**	> 98% *ee*
		MeCN/xanthone	0.5	**175e**	84 (89)[c]
		MeCN/acetophenone	0.5	**175e**	38 (88)[c]
2	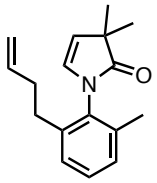	acetone	1.3	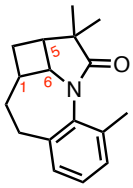	77[b]
	(+)-**174f**			(-)-(1*R*,5*S*,6*R*)-**175f**	> 96% *ee*
	(-)-**174f**			(+)-(1*S*,5*R*,6*S*)-**175f**	> 96% *ee*
		MeCN/xanthone	1.3	**175f**	84 (94)[c]
		MeCN/acetophenone	1.3	**175f**	20 (92)[c]
3	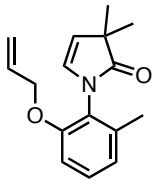	acetone	1.3	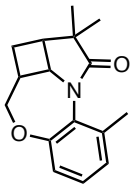	72[b]
	(A)-**174g**			(A)-**175g**	> 20% *ee*
	(B)-**174g**			(B)-**175g**	> 20% *ee*

[a]The conditions, notations and footnotes are similar as listed in the table 3.3. The photoreactions were performed at 25 °C. [b]The yields reported are for the isolated photoproducts. [c]The conversion was calculated from NMR using triphenylmethane as an internal standard, mass balance is given in parenthesis.

3.4.3. [2+2]-Photocycloaddition of enamides with carbonyl partners

The photoreaction of atropisomeric enamides **174h-j** with carbonyl compounds not only provided access to oxetane photoproduct but also provided an excellent opportunity to evaluate the ability of enamides to act both as an excited state and ground state partner (Paternò-Büchi reaction) in the [2+2]-photocycloaddition reactions.

Depending on the type of carbonyl group involved (aldehyde vs ketone), the nature and the location of the excited state in the photoreaction changed between $n\pi^*$ or $\pi\pi^*$. For example, when the carbonyl tether was an aldehyde as in the case of **174h**, the excited state was on the enamides that allowed for sensitized irradiation conditions to result in oxetane photoproduct **175h** (the direct irradiation did not give rise to the desired photoproduct). On the other hand, when the carbonyl partner was methyl ketone as in the case of **174i**, certain percentage of photoproduct formed (~7% conversion) resulted from the excitation of methyl ketone as observed in the direct irradiation conditions (in MeCN). This trend significantly improved up on employing phenyl ketone as the carbonyl partner in **174j** that on direct irradiation resulted in complete conversion in 3 h. In this case, a complete switch in the excited state occurred wherein the enamide acted as a ground state partner to the excited phenyl ketone resulting in oxetane photoproducts (Paternò-Büchi reaction).

Initial screening of photoreaction on the carbonyl derivatives as in the case of **174h-j** was conducted on achiral compounds. We anticipated that the approach could be easily transformed to stereospecific reactions by simply installing bulky group at the *ortho* position of the N-phenyl ring to make them axially chiral. So the phenyl ketone derivative **174j** was synthesized atropisomeric and the enantiospecificity in the reaction was evaluated.

Table 3.5: Stereospecific [2+2]-photocycloaddition of enamides with carbonyl group **174h-j**[a]

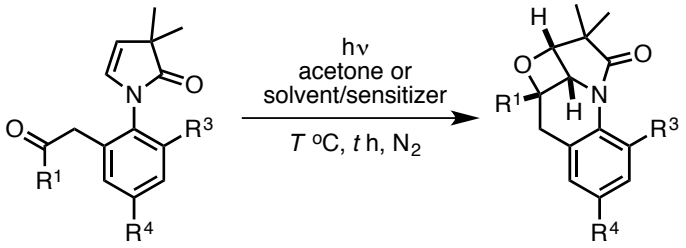

174h-j **175h-j**

Entry	Substrate	Solv/sens.	*t* (h)	product	Yield [%], [%] *ee*
7	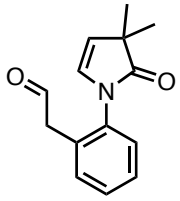	acetone	1	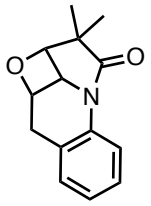	70[b]
	174h			**175j**	
8	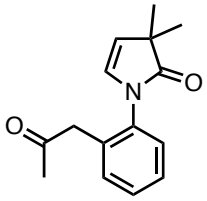	acetone	2.5	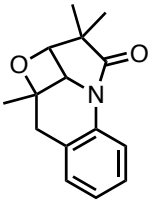	78
		MeCN	2.5		< 7.0
	174i			**175j**	
9	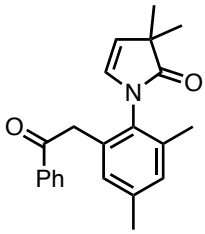	acetone	8	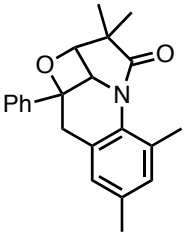	94 (82)[c,d]
		THF	3		75[b]
	(+)-**174j**			(-)-**175j**	89% *ee*
	(-)-**174j**			(+)-**175j**	88% *ee*

[a]The conditions, notations and footnotes are similar as listed in the table 3.2. The photoreactions were performed at 25 °C. [b] The yield reported are for the isolated photoproducts. [c]The conversion was calculated from NMR using triphenylmethane as an internal standard, mass balance is given in parenthesis. [d]The reaction was performed at -30 °C to avoid the formation of uncharacterized impurity.

Photoreaction on individual optically pure isomers resulted in 72% *ee* at room temperature that increased to 88% upon lowering the temperature albeit with longer reaction times. Also, room temperature irradiation resulted in an uncharacterized impurity that seems to increase at higher temperature. So, the reaction temperature was maintained at -30 °C to avoid the formation of the undesired product (further studies to identify the side product will be carried out in the lab).

These studies clearly demonstrated the ability of atropisomeric enamides to act as both excited state and ground state reaction partner to yield cyclobutane and oxetane photoproducts in excellent yield. The enantio- and diastereomeric excess in the product was dictated by the substituent on the alkenyl tether and barrier for C-N_{aryl} restricted bond rotation.

3.4.4. [2+2]-Photocycloaddition of atropisomeric acyclic enamides 174k-l

The [2+2]-photocycloaddition of the acyclic enamides where the excited state is in the enamide was not investigated so far. So, we attempted to evaluate atropisomeric acyclic enamides **174h-i** towards the stereospecific [2+2]-photocycloaddition reaction.

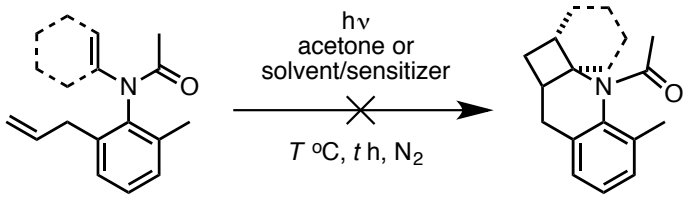

174k-l **175k-l**

Scheme 3.7: Stereospecific [2+2]-photocycloaddition of acyclic enamides **174k-l**.

Both under direct and sensitized irradiation conditions, no photoreaction was observed. Even after prolonged irradiation, only starting material was recovered. This observation was somewhat disappointing as these compounds had fairly high energy-barrier to rotation and its basic chromophore responsible for the photoreaction was kept intact except lacking the rigidity of a cyclic system.

3.5. Mechanistic rationale for [2+2]-photocycloaddition of alkene to enamides 174

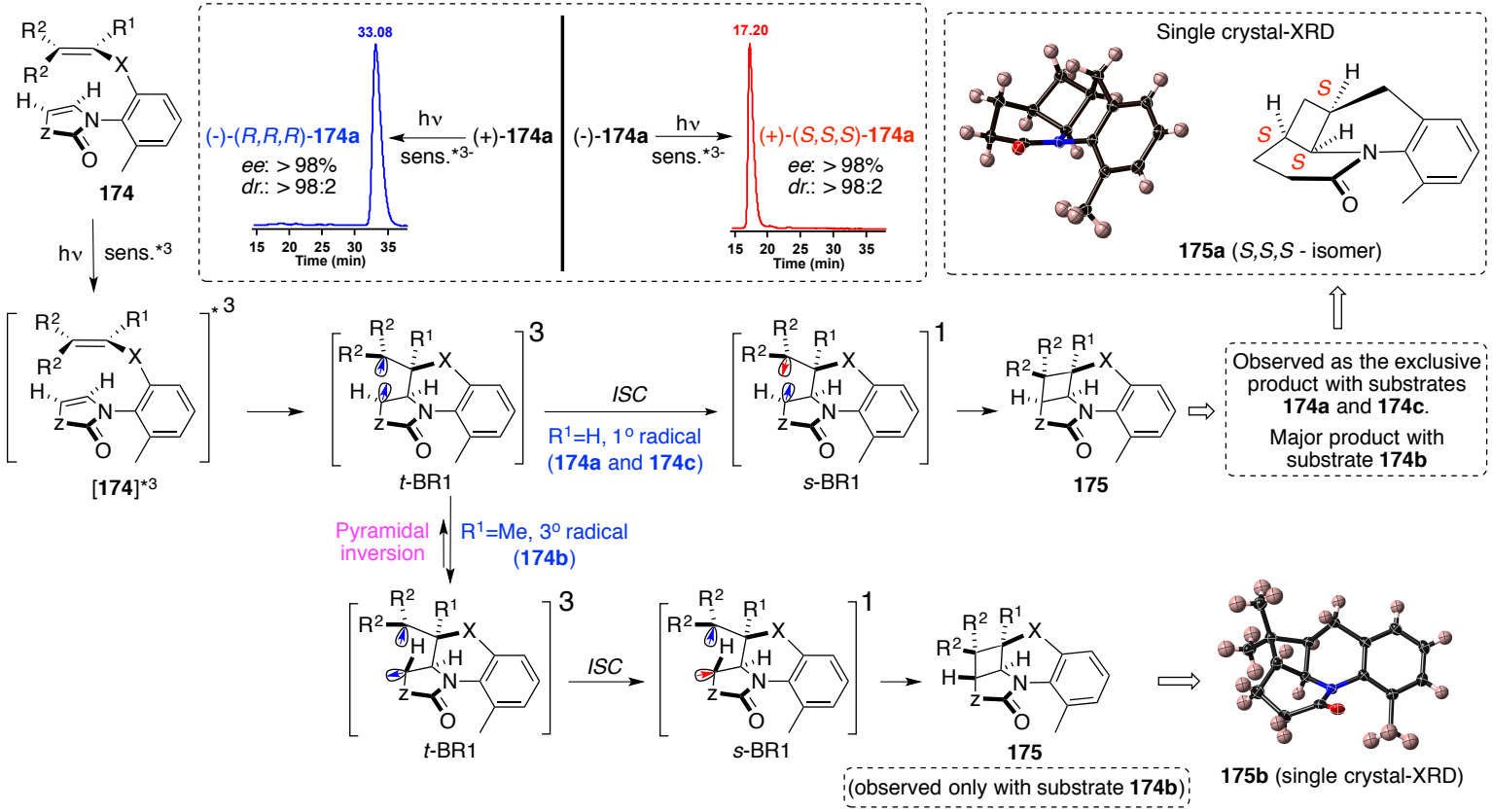

Scheme 3.8: Mechanistic rationale for stereospecific [2+2]-photocycloaddition of atropisomeric enamides **174** to alkenes

The possible mechanistic pathway for the [2+2]-photocycloaddition was hypothesized from the photophysical and photochemical data. We believe that the photoreaction was initiated from the triplet state of the enamide ([**174**]^{*3}) upon sensitization. This speculation was based on the observation that the triplet energy transfer from external sensitizers such as acetone (E_T~ 74 kcal·mol^{-1}), xanthone (E_T~ 74 kcal·mol-1) and acetophenone (E_T~ 73 kcal·mol-1) having similar triplet energies occurred very efficiently and that the direct irradiation (in methanol, acetonitrile, chloroform or toluene) did not yield the desired cyclobutane photoproduct. The possible explanation for the observed *ee* value that occurred with high fidelity and diastereomeric ratio in the photoproduct is given in the scheme 3.7.

We believe that upon sensitization, triplet excited state of the enamide **174** ([**174**]^{*3}) was produced that cyclized to form the triplet 1,4-biradical *t*-BR1. Depending on the type of R^2 substituent, the triplet 1,4-biradical *t*-BR1 can be either primary radical as in the case of **174a** and **174c-g** (where the R^2 = H) or tertiary radical as in the case of **174b** (where the R^2 = Me). In the case of primary radical, the intersystem crossing to singlet 1,4-biradical, *s*-BR1 and subsequent cyclization occurred rapidly resulting in cyclobutane photoproduct **175** with high enantiomeric excess and diastereomeric ratio (*ee* and *dr* >98%). On the other hand, if the radical is tertiary, the intersystem crossing and cyclization occurred slowly causing a minor leakage in the diastereocontrol. The reason was in the stability of the tertiary radical that lived long enough for the pyramidal inversion of the β-carbon of the lactam ring to occur resulting in *t*-BR2. Now the mixture of 1,4-biradicals *viz.*, *t*-BR1 and *t*-BR2 intersystem crosses to singlet 1,4-biradicals *viz.,* *s*-BR1 and *s*-BR2 leading to enantiomeric and diastereomeric photoproducts **175** and **176** respectively. The first cyclization leading to the formation of 1,4-biradicals occurred with very high axial to point chiral transfer leading to excellent control over enantiospecificity in the photoproduct. Thus the strategy provided an avenue to build quaternary chiral center with high enantiomeric purity as in the case of **174c**.

A similar mechanistic pathway can be envisioned for the [2+2]-photocycloaddition of enamides to the carbonyl group. However, depending on the type of carbonyl group, the mechanism can slightly varied. For example, in the case of **174h-j**, a certain percentage of ketone

excited state could be involved where enamide acted as a ground state partner leading to same oxetane photoproducts.

3.6. Cleavage of oxygen tethered and oxetane photoproducts

The oxygen in the alkenyl tether as in the enamide **175g** was strategically placed to enable us to cleave the tether after the photoreaction. This revealed enantioenriched and functionalizable building block for further synthetic transformations. The cleavage was achieved using BBr_3 in DCM at ambient conditions with excellent yield.

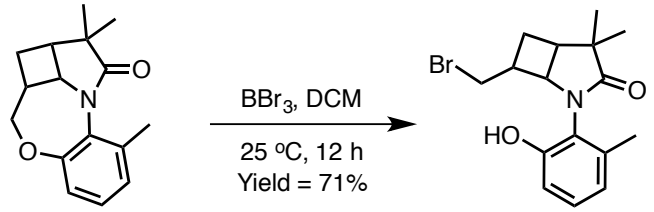

175g **177**

Scheme 3.9: Cleavage of ether linkage of photoproduct **174g** using BBr_3.

Similarly, the cleavage of oxetane ring in the photoproduct **175j** was achieved by hydrogenolysis using $Pd(OH)_2$ in methanol with good isolated yield.

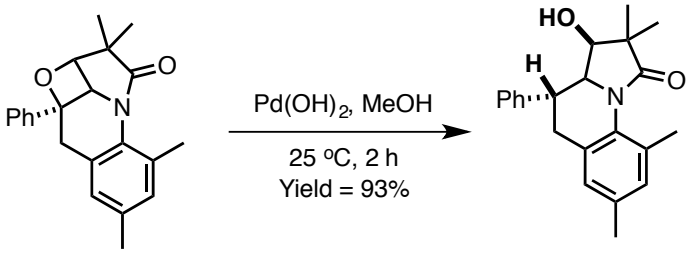

175j **178**

Scheme 3.10: Cleavage of oxetane in the photoproduct **175j** using $Pd(OH)_2$.

3.7. X-ray structural parameters

Structure determination: Single crystal X-ray diffraction data of the compounds **17a**, **175c** and **176b** were collected on a Bruker Apex Duo diffractometer with a Apex 2 CCD area detector at T = 100K. Cu radiation was used. All structures were processed with Apex 2 v2011.4-1 software package (SAINT v. 7.68A, XSHELL v. 6.14). Direct method was used to solve the structures after multi-scan absorption corrections. Details of data collection and refinement are given in the table below.

Table 3.6: Single crystal X-ray diffraction data of the compounds **175a**, **175c** and **176b**

Entry	**175a**-(*S,S,S*)	**175a**-(*R,R,R*)	**175c**-(*R,R,R*)	**175c**-(*S,S,S*)	**176b**
Formula	$C_{15}H_{17}NO$	$C_{15}H_{17}NO$	$C_{17}H_{21}NO$	$C_{17}H_{21}NO$	$C_{17}H_{21}NO$
FW	227.30	227.30	255.35	255.35	255.35
cryst. size_max [mm]	0.37	0.20	0.34	0.37	0.33
cryst. size_mid [mm]	0.14	0.16	0.28	0.35	0.17
cryst. size_min [mm]	0.04	0.04	0.23	0.09	0.03
cryst. system	Hexagonal	Hexagonal	Monoclinic	Monoclinic	Triclinic
Space Group, Z	$P6_1$, 6	$P6_5$, 6	$P2_1$, 2	$P2_1$, 2	P-1, 4
a [Å]	7.3117(2)	7.3171(2)	6.8497(2)	6.8456(2)	9.3999(7)
b [Å]	7.3117(2)	7.3171(2)	13.0702(3)	13.0609(2)	9.6886(6)
c [Å]	37.2526(9)	37.2390(11)	7.9554(2)	7.9584(2)	16.2607(10)
α [Å]	90	90	90	90	100.574(3)
ß [Å]	90	90	105.727(1)	105.815(1)	98.903(3)
γ [Å]	120	120	90	90	103.446(3)
V [Å^3]	1724.74(8)	1726.66(8)	685.56(3)	684.62(3)	1385.48(16)
ρ_{calc} [g/cm^3]	1.313	1.312	1.237	1.239	1.224
μ [cm^{-1}]	0.639	0.638	0.589	0.590	.583
Radiation Type	Cu	Cu	Cu	Cu	Cu
F(000)	732	732	276	276	552
no of measured refl.	14783	13311	8534	7269	34128
no of indep. refl.	1958	1966	2442	2403	4965
no of refl. (I ≥ 2σ)	1949	1930	2426	2376	4361
Resolution [Å]	.84	.84	.84	.84	.84
R1/wR2 (I ≥ 2σ)[a] [%]	2.99/7.73	2.87/7.51	2.83/7.83	2.79/7.32	4.32/10.58
R1/wR2 (all data) [%]	3.01/7.74	2.93/7.56	2.85/7.85	2.81/7.35	4.97/11.01

Table 3.7: Single crystal X-ray diffraction data of the compounds **175e-f**

Entry	**175e**-(*R,S,R*)	**175e**-(*S,R,S*)	**175f**-(*R,R,R*)	**175f**-(*S,S,S*)
Formula	$C_{16}H_{19}NO$	$C_{16}H_{19}NO$	$C_{17}H_{21}NO$	$C_{17}H_{21}NO$
FW	241.32	241.32	255.35	255.35
cryst. size_max [mm]	0.376	0.23	0.196	0.268
cryst. size_mid [mm]	0.145	0.044	0.104	0.19
cryst. size_min [mm]	0.044	0.032	0.022	0.048
cryst. system	Orthorhombic	Orthorhombic	Orthorhombic	Orthorhombic
Space Group, Z	$P2_12_12_1(4)$	$P2_12_12_1(4)$	$P2_12_12_1(4)$	$P2_12_12_1(4)$
a [Å]	9.3935(2)	9.3923(2)	8.5255(2)	8.5245(2)
b [Å]	10.7059(3)	10.7073(2)	12.7647(4)	12.7658(4)
c [Å]	12.8032(3)	12.7975(3)	13.2058(4)	13.206(4)
α [Å]	90.00	90.00	90.00	90.00
ß [Å]	90.00	90.00	90.00	90.00
γ [Å]	90.00	90.00	90.00	90.00
V [Å^3]	1287.57(5)	1287.00(5)	1437.13(7)	1437.11(7)
ρ_{calc} [g/cm^3]	1.245	1.245	1.180	1.180
μ [cm^{-1}]	0.599	0.599	0.562	0.562
Radiation Type	Cu	Cu	Cu	Cu
F(000)	520.0	520.0	552.0	552.0
no of measured refl.	10713	8410	10687	7402
no of indep. refl.	2228	2181	2514	2508
no of refl. (I ≥ 2σ)	2169	2075	2401	2434
Resolution [Å]	0.84	0.84	0.84	0.84
R1/wR2 (I ≥ 2σ)[a] [%]	2.59/6.57	2.84/7.15	2.73/6.84	2.76/6.80
R1/wR2 (all data) [%]	2.68/6.64	3.05/7.29	2.92/6.97	2.87/6.89

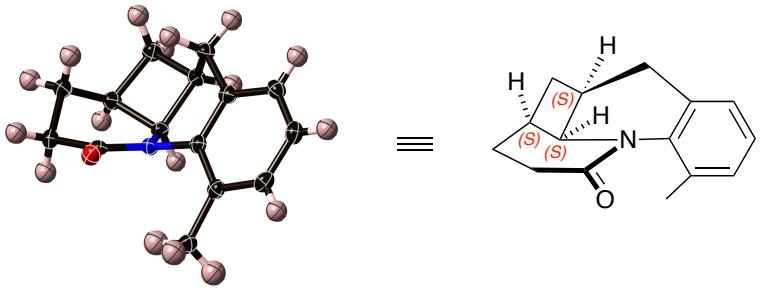

Figure 3.7: X-ray structure of photoproduct (+)-(*S,S,S*)-**175a** (crystallized from hexanes/IPA) .

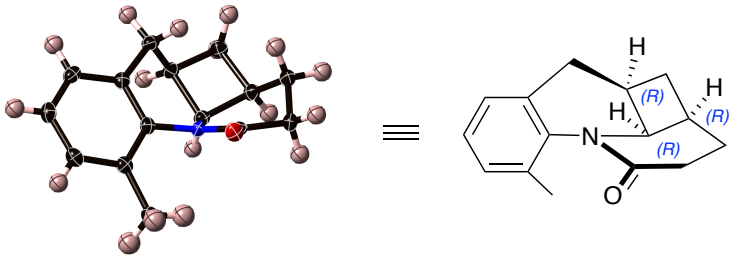

Figure 3.8: X-ray structure of photoproduct (-)-(*R,R,R*)-**175a** (crystallized from hexanes/IPA).

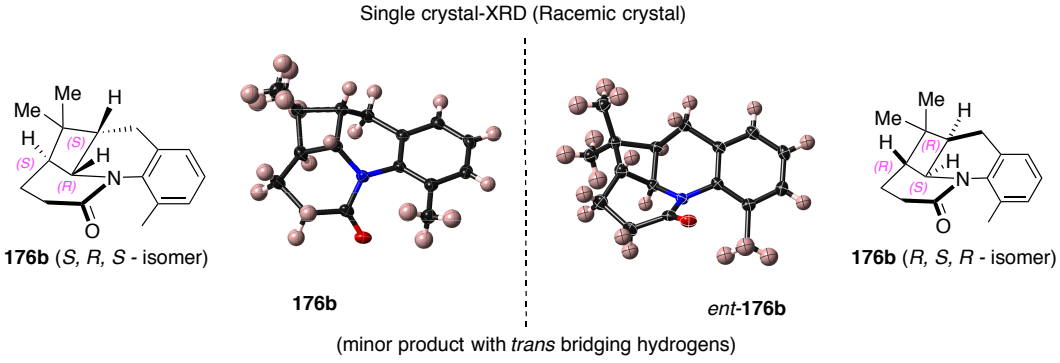

Figure 3.9: X-ray structure of photoproduct **176b** (crystallized from hexanes/$CHCl_3$).

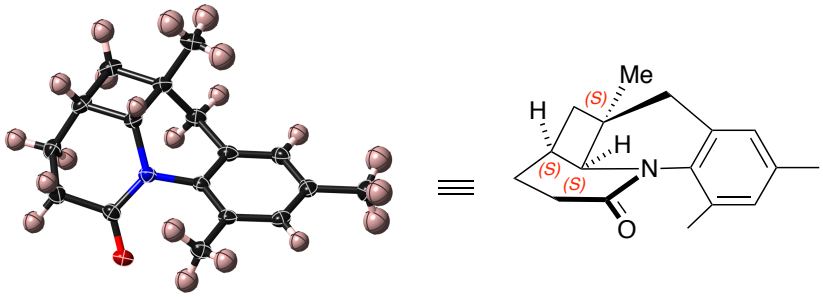

Figure 3.10: X-ray structure of photoproduct (+)-(*S,S,S*)- **175c** (crystallized from hexanes/$CHCl_3$).

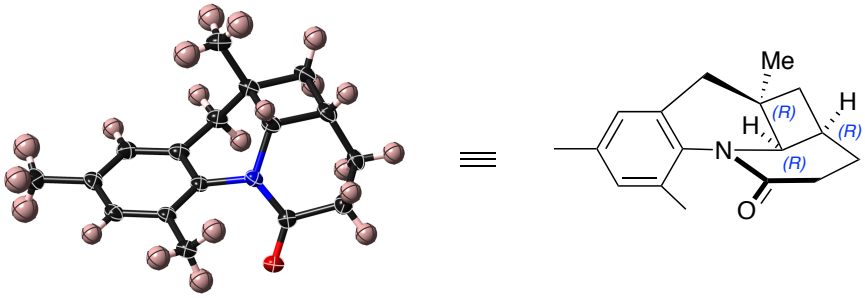

Figure 3.11: X-ray structure of photoproduct (-)-(*R,R,R*)-**175c** (crystallized from hexanes/$CHCl_3$).

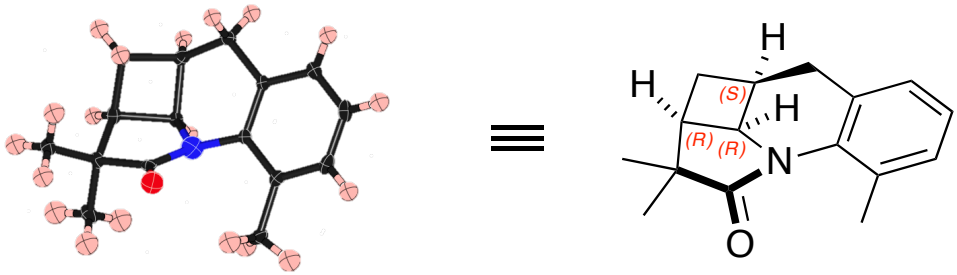

Figure 3.12: X-ray structure of photoproduct (+)-(*S,R,R*)-**175e** (crystallized from hexanes/$CHCl_3$).

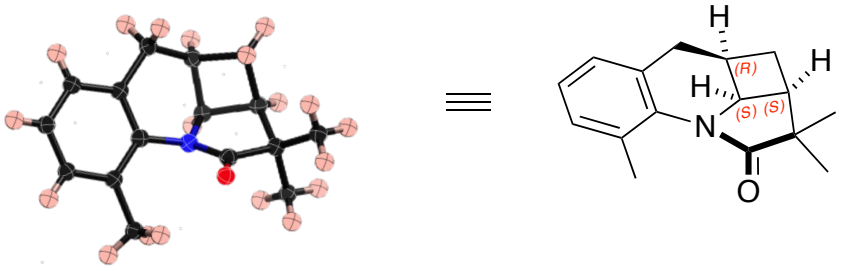

Figure 3.13: X-ray structure of photoproduct (-)-(*R,S,S*)-**175e** (crystallized from hexanes/$CHCl_3$).

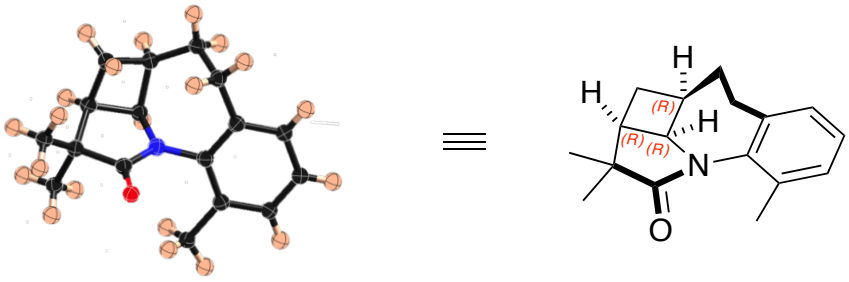

Figure 3.14: X-ray structure of photoproduct (+)-(*R,R,R*)-**175f** (crystallized from hexanes/$CHCl_3$).

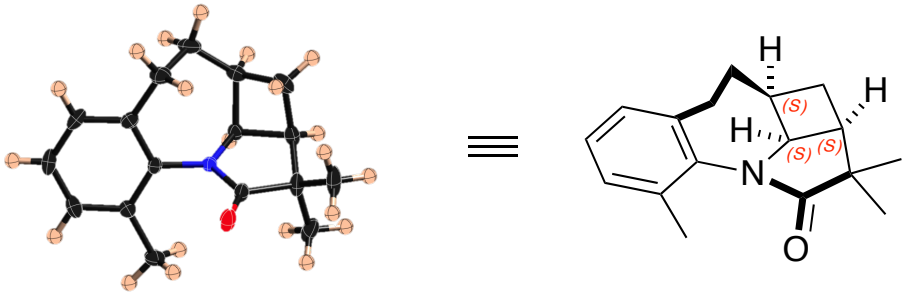

Figure 3.15: X-ray structure of photoproduct (-)-(*S,S,S*)- **175f** (crystallized from hexanes/$CHCl_3$).

3.8. Summary and outlook

The evaluation of intramolecular [2+2]-photocycloaddition of atropisomeric enamides provided an excellent avenue to access both cyclobutane and oxetane photoproducts. The presence of a stable axial chirality ensured efficient chirality (axial to point chiral) transfer resulting in enantiomerically enriched photoproducts. On the other hand, the substituents on the alkenyl tether dictated the diastereomeric excess in the photoproduct, which in turn was controlled by the stability of the radical intermediates generated. The photophysical and photochemical data provided insights about the mechanistic pathway and explained the observed stereoselectivity in the photoproducts. Depending on the type of carbonyl chromophore involved in the reaction, the enamide either acted as an excited state or ground state partner leading to same photoproduct. Further the oxygen-tethered photoproducts was cleaved to reveal more functionalizable enantioenriched synthetic building blocks.

3.9. Experimental section

All commercially obtained reagents/solvents were used as received; chemicals were purchased from Alfa Aesar®, Sigma-Aldrich®, Acros organics®, TCI America®, Mallinckrodt®, and Oakwood® Products, and were used as received without further purification. Unless stated otherwise, reactions were conducted in oven-dried glassware under nitrogen atmosphere. ^{1}H-NMR and ^{13}C-NMR spectra were recorded on Varian 400 MHz (100 MHz for ^{13}C) and on 500 MHz (125 MHz for ^{13}C) spectrometers. Data from the ^{1}H-NMR spectroscopy are reported as chemical shift (δ ppm) with the corresponding integration values. Coupling constants (*J*) are reported in hertz (Hz). Standard abbreviations indicating multiplicity were used as follows: s (singlet), b (broad), d (doublet), t (triplet), q (quartet), m (multiplet) and virt (virtual). Data for ^{13}C NMR spectra are reported in terms of chemical shift (δ ppm). High-resolution mass spectrum data in Electrospray Ionization mode were recorded either on a Bruker – Daltronics® BioTof mass spectrometer in positive (ESI+) ion mode or on a Waters® SYNAPT G2-Si connected to ACQUITY UPLC system. HPLC analyses were performed on Waters® HPLC equipped with 2525 pump. Waters® 2767 sample manager was used for automated sample injection. All HPLC

injections were monitored using a Waters® 2487 dual wavelength absorbance detector at 254 and 270 nm. Analytical and semi-preparative injections were performed on chiral stationary phase using various columns as indicated below.

i) Regis® PIRKLE COVALENT (*R*,*R*) WHELK–01
   a) 25 cm x 4.6 mm column for analytical injections.
   b) 25 cm x 10 mm column for semi-preparative injections.
ii) CHIRACEL® OD-H
   a) 0.46 cm x 25 cm column for analytical injections.
   b) 10 mm x 25 cm column for semi-preparative injections.
iii) CHIRALPACK® IC
   a) 0.46 cm x 25 cm column for analytical injections.
   b) 10 mm x 25 cm column for semi-preparative injections
iv) CHIRALPAK® AD-H
   a) 0.46 cm x 15 cm column for analytical injections.
   b) 10 mm x 25 cm column for semi-preparative injections.
v) CHIRALCEL – OD-3
   a) 0.46 cm x 15 cm column for analytical injections.
vi) CHIRAPAK – AD-3
   a) 0.46 cm x 15 cm column for analytical injections.

Masslynx software version 4.1 was used to monitor/analyze the HPLC injections and to process HPLC traces. Igor Pro® Software version 6.0 was used to process the HPLC graphics. UV-Vis spectra were recorded on Shimadzu 2501PC UV-Vis spectrometer using UV quality fluorimeter cells (with range until 190 nm) purchased from Luzchem. Optical activity values were recorded on JASCO® DIP – 370 digital polarimeter. CD spectra were recorded on JASCO® J-815 with JASCOPTC-423S/15 temperature controller maintained by liquid nitrogen. When necessary, the compounds were purified by combiflash equipped with dual wavelength UV-Vis absorbance detector (Teledyn ISCO) using hexanes:ethyl acetate as the mobile phase and Redisep® cartridge filled with silica (Teledyne ISCO) as stationary phase. In some cases, compounds were purified by column chromatography on silica gel (Sorbent Technologies®, silica gel standard grade: porosity 60 Å, particle size: 230 x 400 mesh, surface area: 500 – 600 m^2/g, bulk density:

0.4 g/mL, pH range: 6.5 – 7.5). Unless indicated, the Retardation Factor (R*f*) values were recorded using a 5-50% hexanes:ethyl acetate as mobile phase and on Sorbent Technologies®, silica Gel TLC plates (200 mm thickness w/UV_{254}).

The plot of CD spectrum was carried out using molar ellipticity vs wavelength (nm) and the molar ellipticity was calculated using the formula,[13]

Molar ellipticity $[\Delta\varepsilon] = [\theta] / 32980cl$

Where,

c = Concentration in mols/lit; *l* = Path length in cm; θ = Ellipticity measured in millidegrees.

Photophysical Methods:

Spectrophotometric solvents (Sigma-Aldrich®) were used when ever necessary unless or otherwise mentioned. UV quality fluorimeter cells (with range until 190 nm) were purchased from Luzchem®. Absorbance measurements were performed using a Shimadzu® UV-2501PC UV-Vis spectrophotometer. Emission spectra were recorded on a Horiba Scientific® Fluorolog 3 spectrometer (FL3-22) equipped with double-grating monochromators, dual lamp housing containing a 450-watt CW xenon lamp and a UV xenon flash lamp (FL-1040), Fluorohub/MCA/MCS electronics and R928 PMT detector. Emission and excitation spectra were corrected in all the cases for source intensity (lamp and grating) and emission spectral response (detector and grating) by standard instrument correction provided in the instrument software. Fluorescence (steady state) and phosphorescence (77 K) emission spectra were processed by FluorEssence® software. Phosphorescence lifetime measurements were performed using DAS6® V6.4 software. The goodness-of-fit was assessed by minimizing the reduced chi squared function and further judged by the symmetrical distribution of the residuals.

3.10. General procedure for the synthesis of substituted aniline derivatives and their precursors

3.10.1. Synthesis of 2-amino benzyl alcohol derivative 194

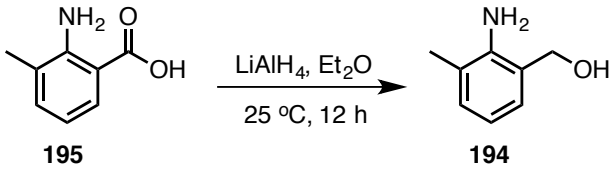

195 **194**

Scheme 3.11: Synthesis of 2-amino benzyl alcohol derivative **194**.

The benzyl alcohol derivative was **194** synthesized according to the literature reported procedure.[14] To a slurry of lithium aluminum hydride (2.5 *equiv.*) in dry THF (50 mL) under N_2 atmosphere at 0 ^{o}C, a solution of 3-methylanthranillic acid **195** (4.0 g, 1.0 *equiv*) in dry THF (50 mL) was added over a period of 15 min without allowing the internal temperature to rise above 5 ^{o}C. The resulting mixture was allowed to warm to room temperature over 12 h. After the completion of the reaction, the mixture was cooled to 0 ^{o}C and quenched with saturated Na_2SO_4 solution (20 mL). To the resulting solid DCM (75 mL) was added, stirred for 15 min, filtered and the filtered solid was washed with DCM (50 mL). The combined organic layer was dried over *anhyd.* Na_2SO_4, filtered and the solvent was removed under reduced pressure to get the crude product. The crude product was directly taken to next step without further purification.

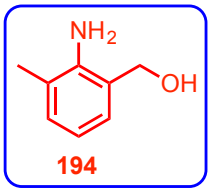

194

R*f* = 0.45 (50% hexanes: 50% ethyl acetate) for **194** (Yield = 90%).

^{1}H-NMR (400 MHz, $CDCl_3$, δ ppm): 7.03-7.01 (m, 1H), 6.92-6.90 (m, 1H), 6.65-6.61 (m, 1H), 4.61 (s, 2H), 3.40 (bs, 3H) and 2.15 (m, 3H).

^{13}C-NMR (100 MHz, $CDCl_3$, δ ppm): 144.3, 130.7, 127.3, 124.4, 122.9, 117.9, 64.7 and 17.5.

3.10.2. Synthesis of 2-methoxymethyl aniline derivative 193

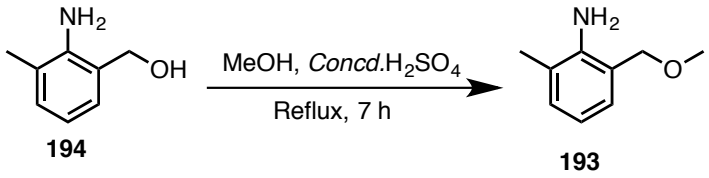

194 **193**

Scheme 3.12: Synthesis of 2-methoxymethyl aniline derivative **193**.

To a solution of amino benzyl alcohol derivative **194** (5.0 g, 1.0 *equiv*) in methanol (40 mL) at 0 ^{o}C, *Concd*. H_2SO_4 (1.1 *equiv.*) was added slowly. The resulting mixture was heated to 50 ^{o}C for 7 h. After the completion of reaction, the mixture was cooled to 10 ^{o}C and neutralized with saturated Na_2CO_3 carefully during which a brisk effervescence was observed. The aqueous layer was extracted with DCM (3 × 40 mL). The combined organic layer was dried over *anhyd.* Na_2SO_4, filtered and the solvent was removed under reduced pressure to get the crude product. The crude product was purified by combiflash using hexanes: ethyl acetate mixture.

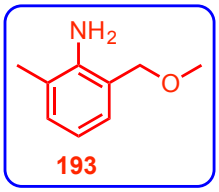

193

R*f* = 0.80 (50% hexanes: 50% ethyl acetate) for **193** (Yield = 77%).

^{1}H-NMR (400 MHz, $CDCl_3$, δ ppm): 7.05-7.03 (m, 1H), 6.96-6.94 (m, 1H), 6.6-6.62 (m, 1H), 4.49 (s, 2H), 4.12 (bs, 2H), 3.33 (s, 3H) and 2.17 (s, 3H).

^{13}C-NMR (100 MHz, $CDCl_3$, δ ppm): 144.6, 130.7, 128.3, 122.5, 121.5, 117.5, 74.1, 57.6,and 17.5.

3.10.3. Synthesis of 2-alkenyl-6-methylaniline 186a-b

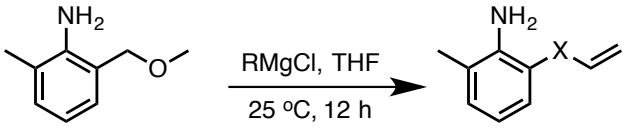

193 **186a-b**

a) X = CH_2
b) X = CH_2-CH_2

Scheme 3.13: Synthesis of 2-alkenyl-6-methylaniline derivative **186a-b**.

To a solution methoxy aniline derivative **193** (5.3 g, 1.0 *equiv*) in dry THF (40 mL) at 0 °C, allyl magnesium halide (2.0 M in THF, 2.2 *equiv*) was added slowly over 15 min. The resulting mixture was allowed to warm to room temperature over 15 h. After the completion of reaction, the mixture was cooled to 0 °C and quenched with *dil.* HCl. The aqueous layer was extracted with DCM (3 × 50 mL). The combined organic layer was dried over *anhyd.* Na_2SO_4, filtered and the solvent was removed under reduced pressure to get the crude product. The crude product was purified by combiflash using hexanes: ethyl acetate mixture.

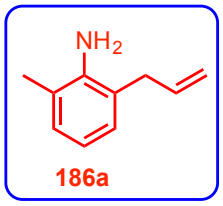

186a

R*f* = 0.70 (90% hexanes: 10% ethyl acetate) for **186a**, (Yield = 60%).

^{1}H-NMR (400 MHz, $CDCl_3$, δ ppm): 7.02-6.96 (m, 2H), 6.73-6.69 (m, 1H), 6.04-5.94 (m, 1H), 5.18-5.13 (m, 2H), 3.65 (bs, 2H), 3.35 (d, *J*= 6 Hz, 2H) and 2.21 (s, 3H).

^{13}C-NMR (100 MHz, $CDCl_3$, δ ppm): 143.2, 136.3, 129.0, 128.2, 123.6, 122.6, 118.4, 116.3, 36.98 and 17.8.

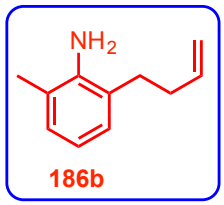

186b

R*f* = 0.60 (90% hexanes: 10% ethyl acetate) for **186b**, (Yield = 75%).

^{1}H-NMR (400 MHz, $CDCl_3$, δ ppm): 6.95-6.93 (m, 2H), 6.68-6.64 (m, 1H), 5.9-5.83 (m, 1H), 5.15-4.97 (m, 2H), 3.77 (bs, 2H), 2.61-2.57 (m, 2H), 2.40-2.35 (m, 2H) and 2.18 (s, 3H).

^{13}C-NMR (100 MHz, $CDCl_3$, δ ppm): 142.4, 138.4, 128.6, 127.4, 125.6, 122.4, 118.3, 115.2, 33.1, 31.2 and 17.98.

3.10.4. Synthesis of 3-chloro-3-methylbut-1-yne 203

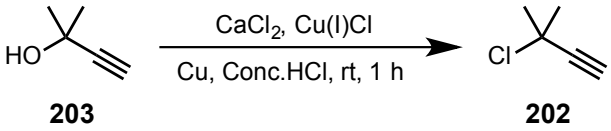

203 **202**

Scheme 3.14: Synthesis of 3-chloro-3-methylbut-1-yne **202**.

The 3-chloro-3-methylbut-1-yne **202** was synthesized according to the literature reported procedure.[15] To a mixture of *anhyd.* calcium chloride (3.3 g, 29.7 mmol) cuprous chloride (2.4 g, 24.2 mmol) copper powder (37.7 mg, 0.6 mmol) and *conc.* hydrochloric acid (25 mL) was added acetylinic alcohol (5 g, 59.4 mmol) at 0 ^{o}C over ten mins. The resulting mixture was stirred for 1 h at 0 ^{o}C. The phases were separated and the organic layer was washed with ice-cold conc. hydrochloric acid (2 X 20 mL). The organic layer was dried over *anhyd*. potassium carbonate (5 g), filtered and the crude product was purified by distillation under reduced pressure to yield 65 % of the pure acetylinic chloride.

Note: As tertiary acetylinic chloride is highly acid and heat sensitive, distillation temperature was kept below 50 ^{o}C and small amount of *anhyd.* K_2CO_3 was kept in the distillation flask to avoid any decomposition or isomerization.

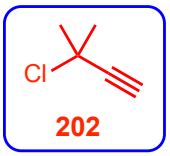

202

^{1}H-NMR (400 MHz, $CDCl_3$, δ ppm): 2.59 (s, 1H) and 1.83 (s, 6H).

^{13}C-NMR (100 MHz, $CDCl_3$, δ ppm): 86.7, 72.0, 57.1, 34.7 and 32.3.

3.10.5. Synthesis of N-acetylinic-aniline derivative 200

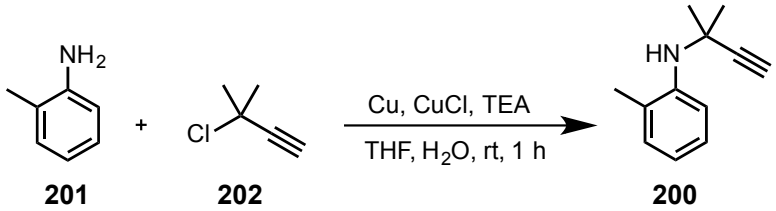

Scheme 3.15: Synthesis of N-acetylinic-aniline derivative **200**.

The N-acetylinic-aniline derivative **200** was synthesized according to the procedure reported in the literature.[16] To a mixture of aniline **201** (3 g, 30 mmol), cuprous chloride (85 mg), copper powder (85 mg), triethylamine (5.4 mL, 39 mmol), water (0.8 mL) and THF (8 mL) at room temperature added acetylinic chloride **202** (4.0 g, 39 mmol) in THF (8mL) slowly over 10 mins. The resulting mixture was stirred at room temperature over 1 h. To the reaction mixture DI water (10 mL) and DCM (20 mL) was added, stirred for 5 mins and the layers were separated. The aqueous layer was extracted with DCM (2 X 20 mL). The combined organic layer was dried over *anhyd.* Na_2SO_4, filtered and concentrated under reduced pressure to get the crude product. The crude product was purified by combiflash using hexanes:ethyl acetate mixture (95:5) to get the pure product.

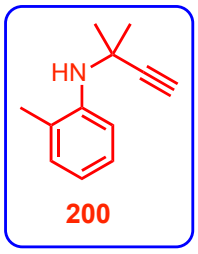

R*f* = 0.50 (95% hexanes:5% ethyl acetate), Yield = 40 %

^{1}H-NMR (400 MHz, $CDCl_3$, δ ppm): 7.33 -7.31 (m, 1H), 7.12-7.08 (m, 2H), 6.75-6.72 (m, 1H), 3.54 (s, 1H), 2.38 (m, 1H), 2.15 (s, 3H) and 1.67 (s, 6H).

^{13}C-NMR (100 MHz, $CDCl_3$, δ ppm): 143.7, 130.5, 126.7, 123.8, 118.3, 114.5, 88.9, 70.7, 47.8, 30.8 and 18.0.

3.10.6. Synthesis of N-allyl-aniline derivative 199

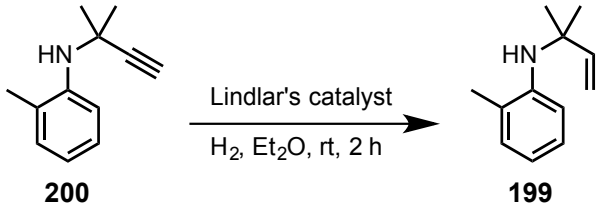

Scheme 3.16: Synthesis of N-allyl-aniline derivative **199**.

In a flame dried flask charged Lindlar's catalyst (5% Pd on $CaCO_3$ poisoned with lead, 95 mg, 5 Wt%) under nitrogen atmosphere. To this added a solution of acetylinic aniline **200** (1.9 g, 11 mmol) in dry diethyl ether (60 mL) through cannula. The nitrogen was evacuated and the flask was filled with H_2. The mixture was stirred at room temperature for 2 h. After the reaction, the solution was filtered through celite bed and the bed was washed with diethyl ether (20 mL). The combined organic layer was concentrated to get the crude product. The crude product was purified by combiflash using hexanes:ethyl acetate mixture (95:5) to get pure product.

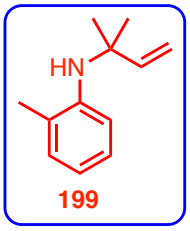

R*f* = 0.60 (95% hexanes:5% ethyl acetate), Yield = 90%

^{1}H-NMR (400 MHz, $CDCl_3$, δ ppm): 7.03-6.99 (m, 2H), 6.83-6.81 (m, 1H), 6.63-6.59 (m, 1H), 6.01-5.99 (m, 1H), 5.21-5.16 (m, 1H), 5.12-5.09 (m, 2H), 3.56 (s, 1H), 2.13 (s, 3H) and 1.42 (s, 6H).

^{13}C-NMR (100 MHz, $CDCl_3$, δ ppm): 146.5, 144.7, 130.4, 126.5, 122.7, 116.9, 113.7, 112.9, 54.6, 28.8 and 18.1.

3.10.7. Synthesis of 2-methyl-6-allyl-aniline derivative 186c

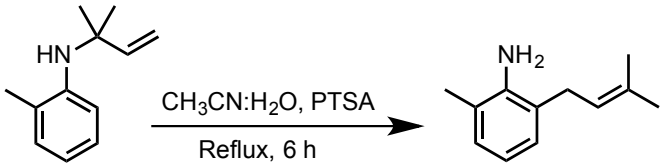

199 **186c**

Scheme 3.17: Synthesis of 2-methyl-6-allyl-aniline derivative **186c**.

A solution of 2-methyl-N-allyl-aniline derivative **199** (1.7 g, 9.7 mmol) and *p*-toluenesulfonic acid monohydrate (185 mg, 0.97 mmol) in 9:1 acetonitrile:water mixture (120 mL) was refluxed for 6 h. After the reaction, the mixture was cooled to room temperature and the solvent was removed under reduced pressure. The residue was taken up in DCM (50 mL) and the organic layer was washed with DI water (50 mL), dried over *anhyd.* Na_2SO_4, filtered and the solvent was removed under reduced pressure to get the crude product. The crude product was purified by combiflash using hexanes:ethyl acetate mixture (90:10) to get the title product as a pale yellow liquid in 65% yield.

TLC condition - R*f* = 0.30 (90% hexanes:10% ethyl acetate)

^{1}H-NMR (400 MHz, $CDCl_3$, δ ppm): 6.94-6.91 (m, 2H), 6.66-6.63 (m, 1H) 5.24-5.21(m, 1H), 3.60 (s, 2H), 3.23-3.21 (d, *J*= 6.8 Hz, 2H), 2.16 (s, 3H) and 1.74 (s, 6H).

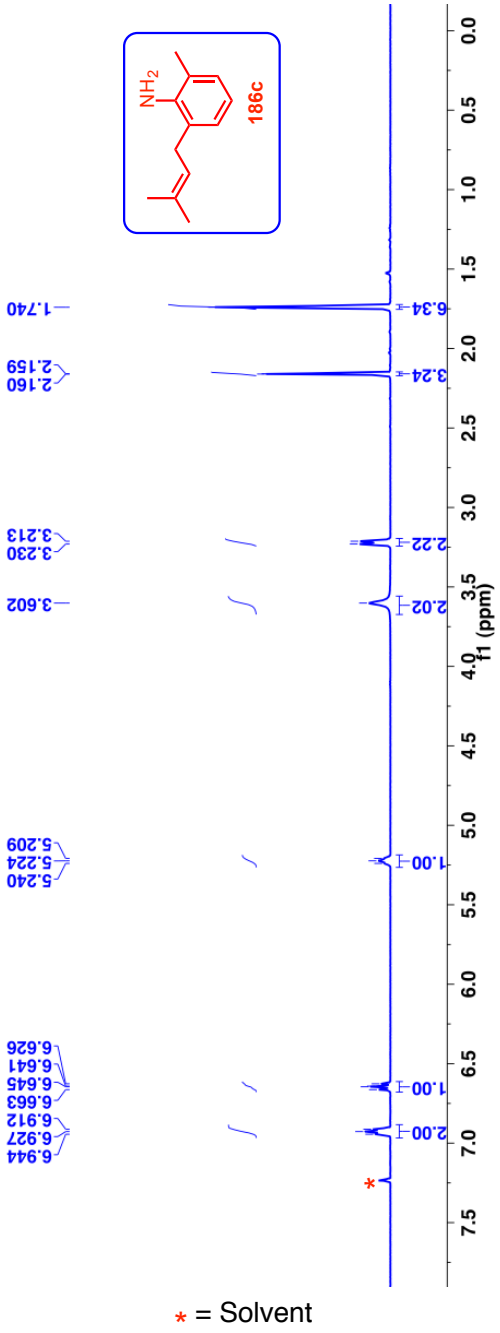

Figure 3.16: ^{1}H-NMR (400 MHz, $CDCl_3$, δ ppm) of 2-methyl-6-allylanine derivative **186c**.

^{13}C-NMR (100 MHz, $CDCl_3$, δ ppm): 143.1, 133.6, 128.7, 127.7, 125.5, 122.38, 122.36, 118.4, 31.4, 26.0, 18.1 and 17.9.

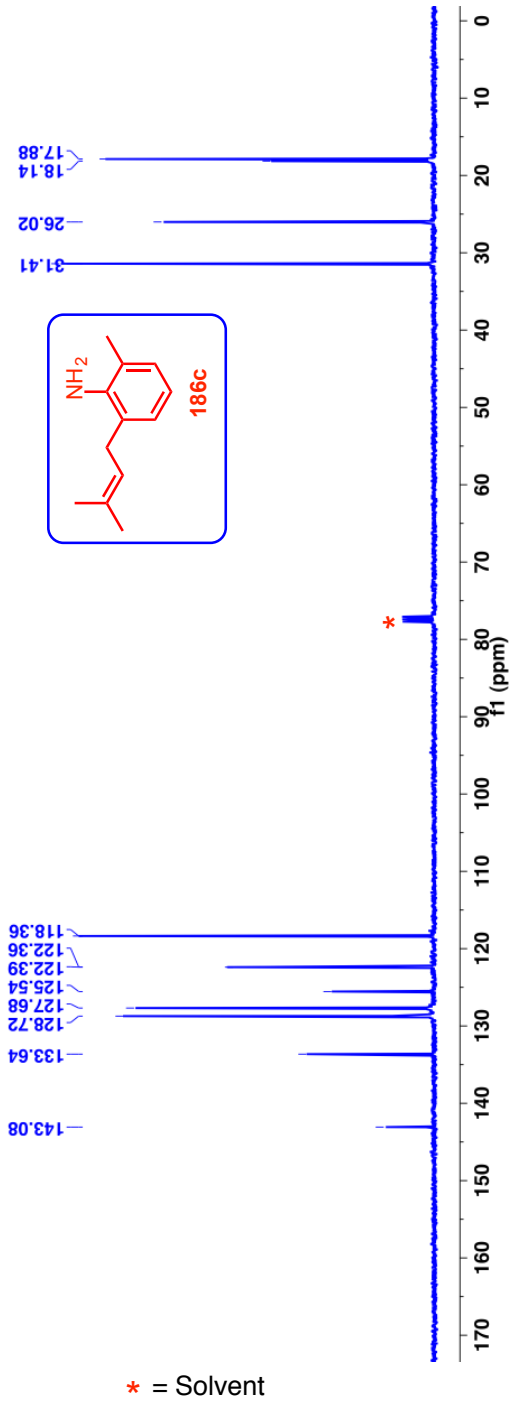

Figure 3.17: ^{13}C-NMR (100 MHz, $CDCl_3$, δ ppm) of 2-methyl-6-allylanine derivative **186c**.

HRMS-ESI (m/z) ([M + H]$^+$):

Calculated : 176.1434

Observed : 176.1436

|Δm| : 1.1 ppm

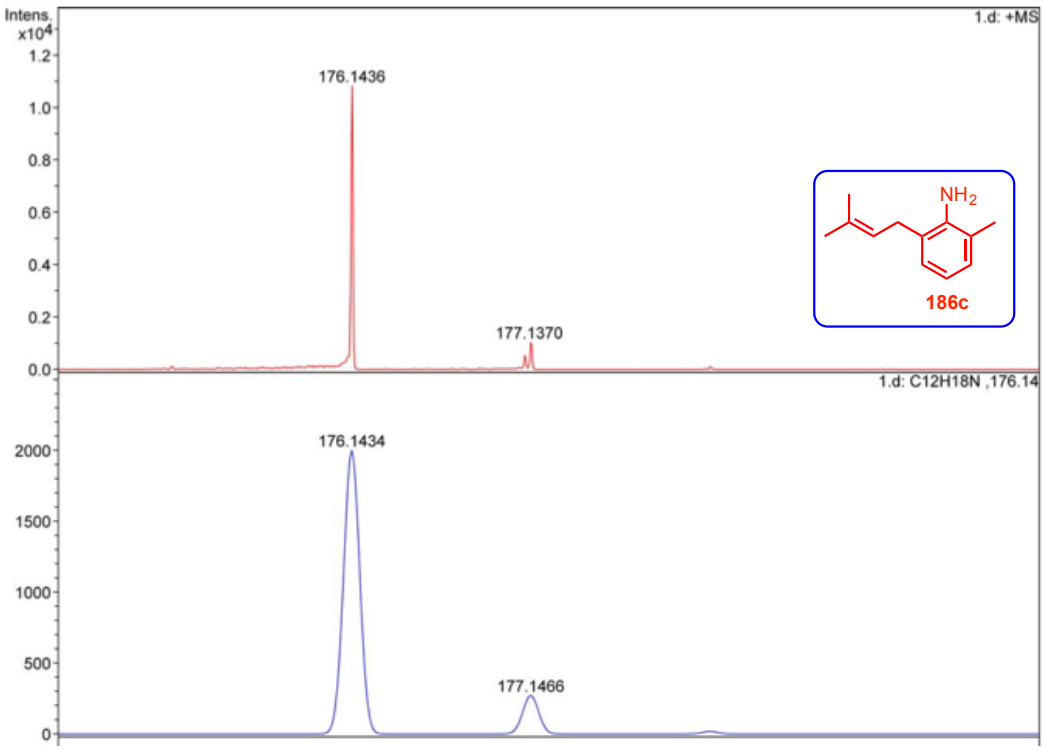

Figure 3.18: HRMS of 2-methyl-6-allylanine derivative **186c**.

3.10.8. Synthesis of 2-iodo-4,6-dimethylaniline 206

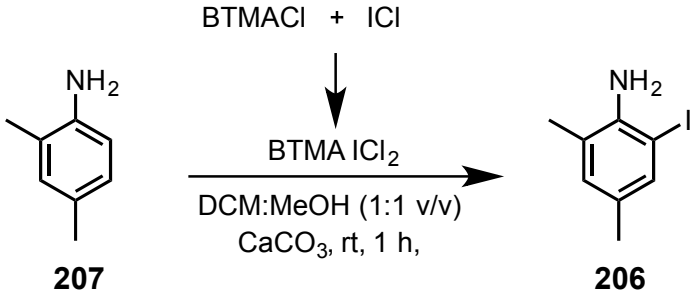

Scheme 3.18: Synthesis of 2-iodo-4,6-dimethylaniline **206**.

Synthesis of iodinating agent benzyltrimethylammonium dichloroiodate (**BTMA ICl_2**):

The compound was synthesized using previously reported procedure.[17] To a solution of iodinemonochloride (3.0 g, 18.6 mmol) in DCM (37 mL) at room temperature added a solution of benzyltrimethylammonium chloride (3.5 g, 18.6 mmol) in de-mineralized water (22 mL) slowly over a period of 10 mins. The resulting mixture was stirred at room temperature for 30 mins. The layers were separated and the organic layer was washed with DM water (10 mL), dried over *anhyd.* Na_2SO_4, filtered and the solvent was removed under reduced pressure to get the crude product as a brownish yellow solid. The crude product was directly used for iodination reaction without further purification (isolated crude product yield: 98%).

Note: The iodine monochloride was purchased as 1M solution in DCM, which was again diluted using required amount of DCM. The crude BTMA ICl_2 can also be recrystallized in DCM: diethyl ether mixture.

To a mixture of aniline **207** (1.0 g, 8.2 mmol) and calcium carbonate (1.4 g) in DCM:methanol (50:50 mixture, 50 mL) at room temperature added a solution of benzyltrimethylammonium dichloroiodate (2.9 g, 8.2 mmol) in DCM (30 mL) slowly over 30 mins. The resulting mixture was stirred at room temperature for 1 h. After the reaction, the mixture was filtered through celite bed under vacuum and the bed was washed with DCM (50 mL). The combined filtrate was concentrated under reduced pressure. The residue was taken up in 5% $NaHSO_3$ aqueous solution (40 mL) and the aqueous layer was extracted with diethyl ether

(3 × 30 mL). The combined organic layer was dried over *anhyd.* Na_2SO_4, filtered and the solvent was removed under reduced pressure to get the crude product. The crude product was purified by combiflash using hexanes:ethyl acetate mixture (95:5) to get the title compound as a brownish solid.

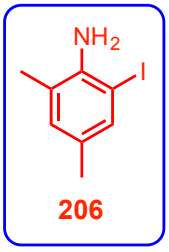

206

R*f* = 0.35 (95% hexanes:5% ethyl acetate), Yield = 67%

^{1}H-NMR (400 MHz, $CDCl_3$, δ ppm): 7.34 (s, 1H) and 6.82 (s, 1H), 3.90 (bs, 2H), 2.18 (s, 3H) and 2.16 (s, 3H).

^{13}C-NMR (100 MHz, $CDCl_3$, δ ppm): 142.5, 137.0, 131.6, 129.5, 122.7, 85.0, 20.0 and 19.1.

3.10.9. Synthesis of N-Diallyl-2-Iodo-4,6-Dimethylaniline 205

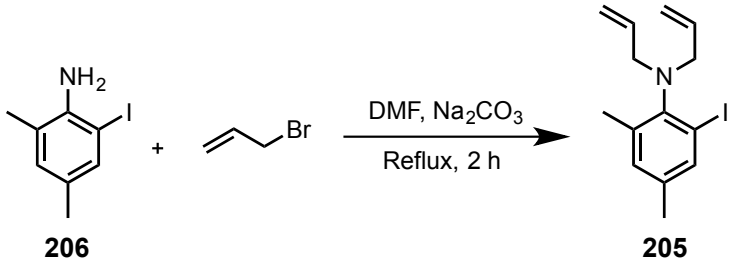

206 **205**

Scheme 3.19: Synthesis of 2-iodo-4,6-dimethylaniline **205**.

The compound was synthesized according to the literature reported procedure.[18] Mixture of aniline (5 g, 20.2 mmol), allyl bromide (4.4 mL, 50.9 mmol) and sodium carbonate (6.4 g, 60.6 mmol) in DMF (150 mL) was heated to 150 ^{o}C in a sealed tube and maintained for 2 h. After the reaction, the mixture was cooled to room temperature and poured into cold de-mineralized water (200 mL). The aqueous layer was extracted with diethyl ether (3 X 50 mL). The combined organic layer was washed with DI water (2 X 50 mL) to remove traces of DMF, dried over *anhyd.* Na_2SO_4, filtered and the solvent was removed under reduced pressure to get the crude product. The crude product was purified by combiflash using hexanes:ethyl acetate mixture (98:2) to get the title compound as a pale yellow oil (isolated yield = 90%).

TLC condition - R*f* = 0.90 (90% hexanes:10% ethyl acetate)

^{1}H-NMR (400 MHz, $CDCl_3$, δ ppm): 7.52 (s, 1H), 6.90 (s, 1H), 5.97-5.87 (m, 2H), 5.14-5.09 (m, 2H), 5.02-4.99 (m, 2H), 3.74-3.60 (m, 4H), 2.27 (s, 3H) and 2.20 (s, 3H).

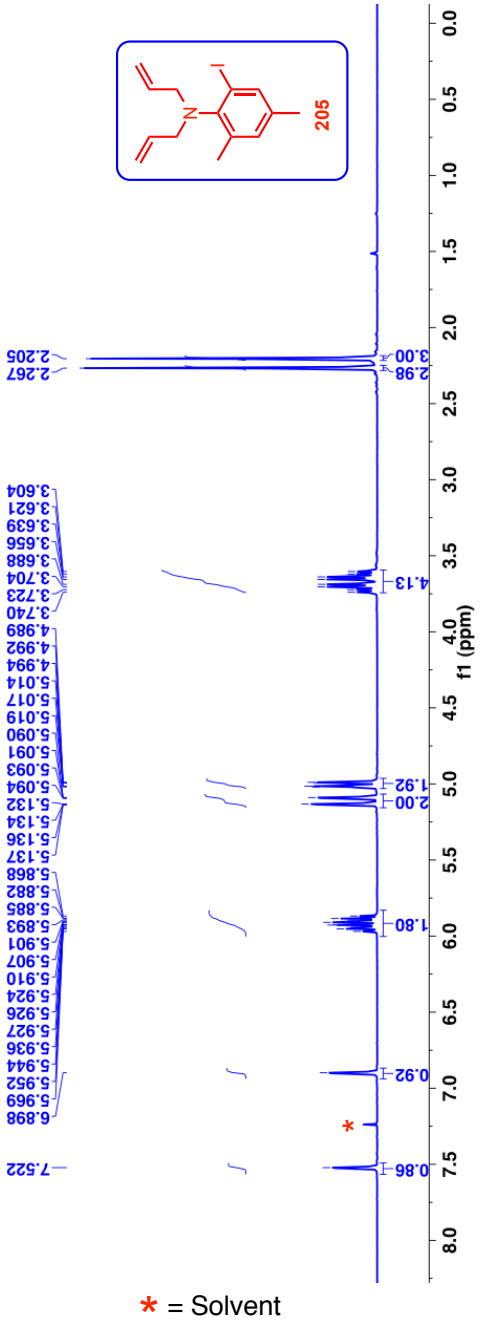

Figure 3.19: ^{1}H-NMR (400 MHz, $CDCl_3$, δ ppm) of N-allyl-2-iodo-4,6-dimethylaniline **205**.

^{13}C-NMR (100 MHz, $CDCl_3$, δ ppm): 147.7, 139.0, 138.1, 137.0, 136.9, 132.4, 116.6, 104.6, 56.2, 20.3 and 20.0.

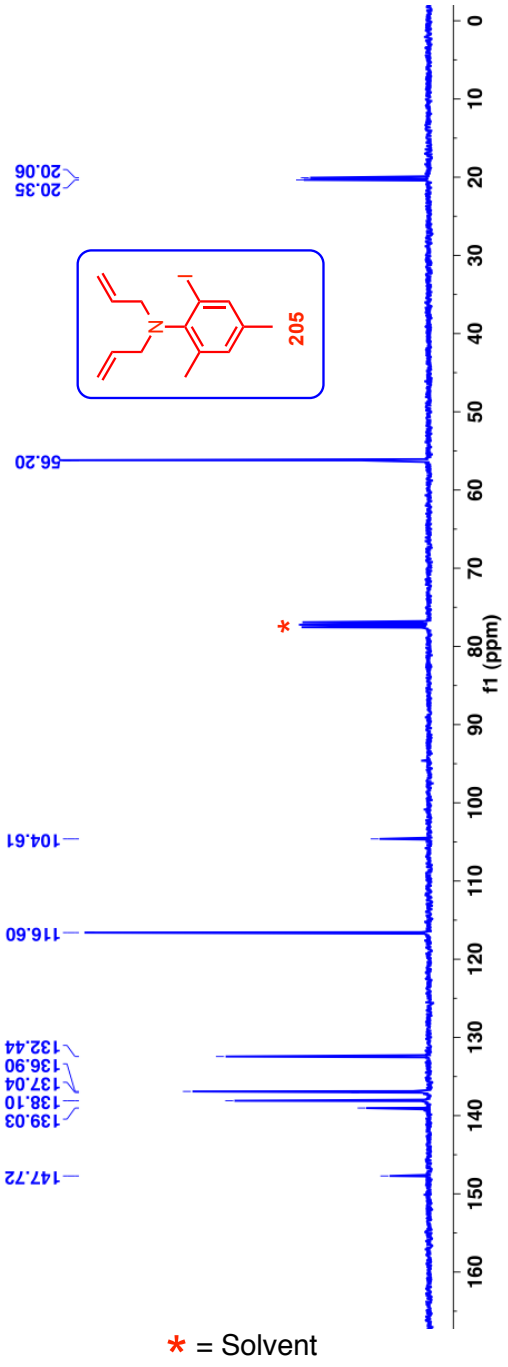

Figure 3.20: ^{13}C-NMR (100 MHz, $CDCl_3$, δ ppm) of N-diallyl-2-iodo-4,6-dimethylaniline **205**.

HRMS-ESI (m/z) ([M + H]$^+$):

Calculated : 328.0557

Observed : 328.0548

|Δm| : 2.7 ppm

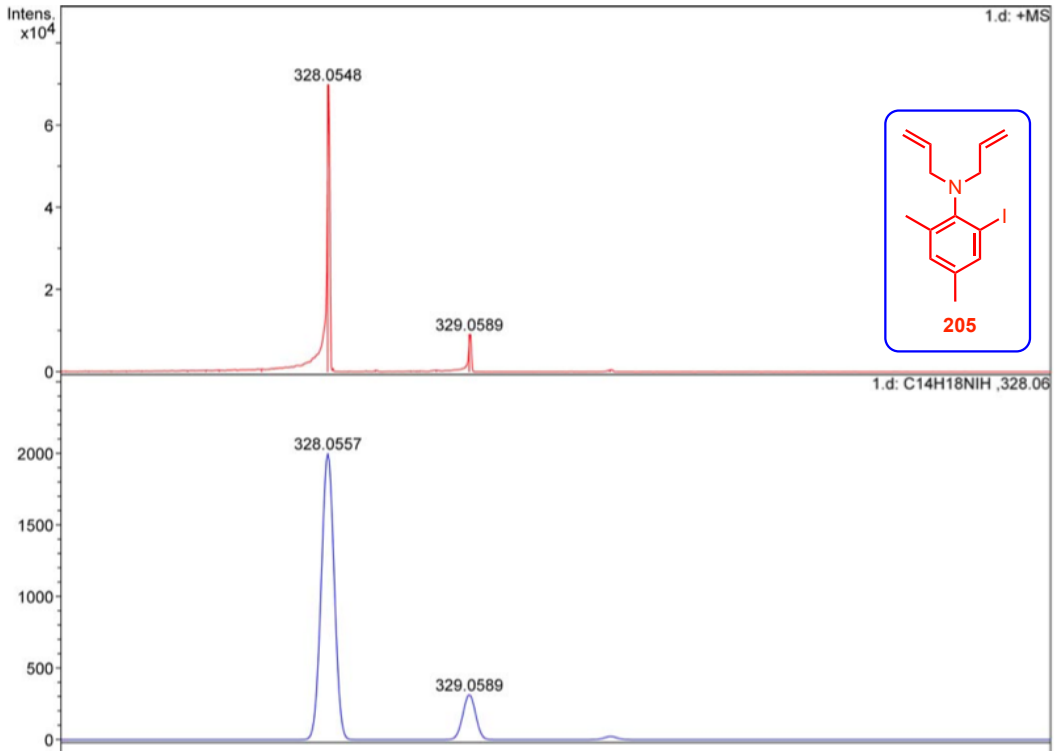

Figure 3.21: HRMS of N-diallyl-2-iodo-4,6-dimethylaniline **205**.

3.10.10. Synthesis of N-Diallyl-2,4-Dimethyl-6-allyl-aniline derivative 204

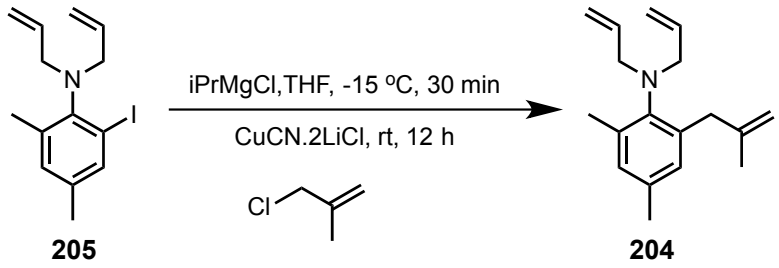

205 **204**

Scheme 3.20: Synthesis of N-Diallyl-2,4-Dimethyl-6-allyl-aniline derivative **204**.

The compound was synthesized according to a procedure reported in the literature.[19] To a solution of N-diallyl-2-iodo aniline derivative **205** (5.9 g, 18.0 mmol) in dry THF (120 mL) at -15 ^{o}C under N_2 atmosphere added iPrMgCl·LiCl (1.3M in THF, 15.2 mL, 19.8 mmol) slowly over 10 mins. The mixture was maintained at -15 ^{o}C for 45 mins after which 3-chloro-2-methylpropene (2.13 mL, 21.6 mmol) and CuCN.2LiCl (0.16 mL, 0.9 mmol) was added. The reaction mixture was slowly allowed to warm to room temperature over 12 h. The reaction mixture was quenched with *Satd.* NH_4Cl solution (50 mL), stirred and the layers were separated. The aqueous layer was extracted with diethyl ether (2 X 75 mL). The combined organic layer was dried over *anhyd.* Na_2SO_4, filtered and the solvent was removed under reduced pressure to get the crude product. The crude product was purified by combiflash using hexanes:ethyl acetate mixture (95:5) to get the title compound as a pale yellow oil (isolated yield = 92%).

TLC condition - R*f* = 0.75 (100% hexanes)

^{1}H-NMR (400 MHz, $CDCl_3$, δ ppm): 6.79 (s, 2H), 5.86-5.76 (m, 2H), 5.09-5.08 (m, 1H), 5.05-5.03 (m, 1H), 4.99-4.96 (m, 2H), 4.82-4.81 (m, 1H), 4.58- 4.578 (m, 1H), 3.64-3.51 (m, 4H), 3.37 (s, 2H), 2.25 (s, 3H), 2.22 (s, 3H) and 1.697 (s, 3H).

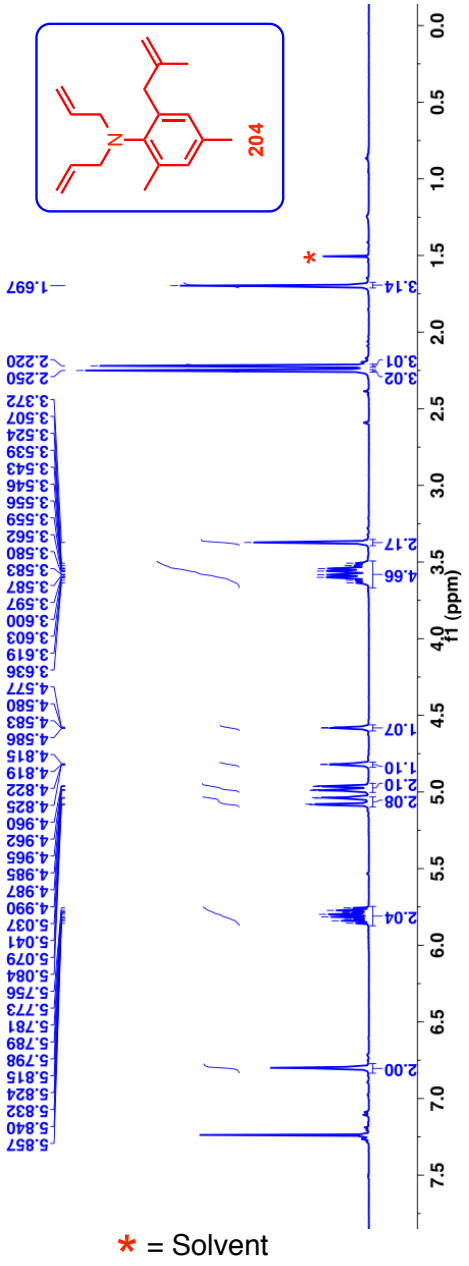

Figure 3.22: ^{1}H-NMR (400 MHz, $CDCl_3$, δ ppm) of N-Diallyl-2,4-Dimethyl-6-allyl-aniline **204**.

^{13}C-NMR (100 MHz, $CDCl_3$, δ ppm): 145.9, 138.96, 137.5, 137.3, 134.7, 130.1, 129.6, 128.6, 116.1, 112.1, 56.8, 40.2, 23.0, 21.0 and 19.9.

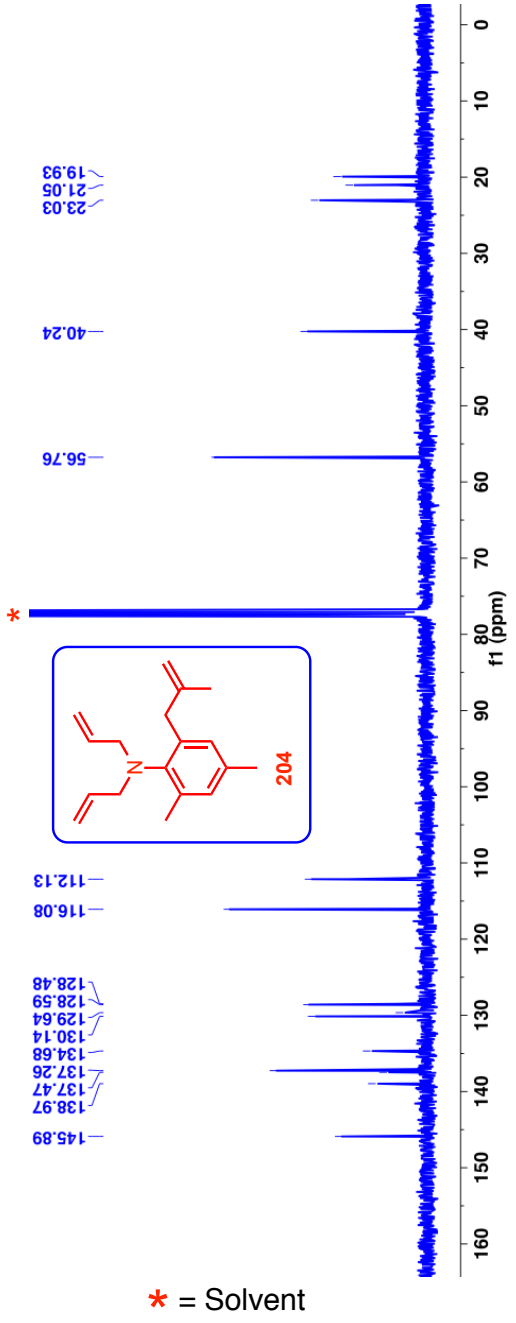

Figure 3.23: ^{13}C-NMR (100 MHz, $CDCl_3$, δ ppm) of N-Diallyl-2,4-Dimethyl-6-allyl-aniline **204**.

HRMS-ESI (m/z) ([M + H]$^+$):

Calculated : 256.2060

Observed : 256.2051

|Δm| : 3.5 ppm

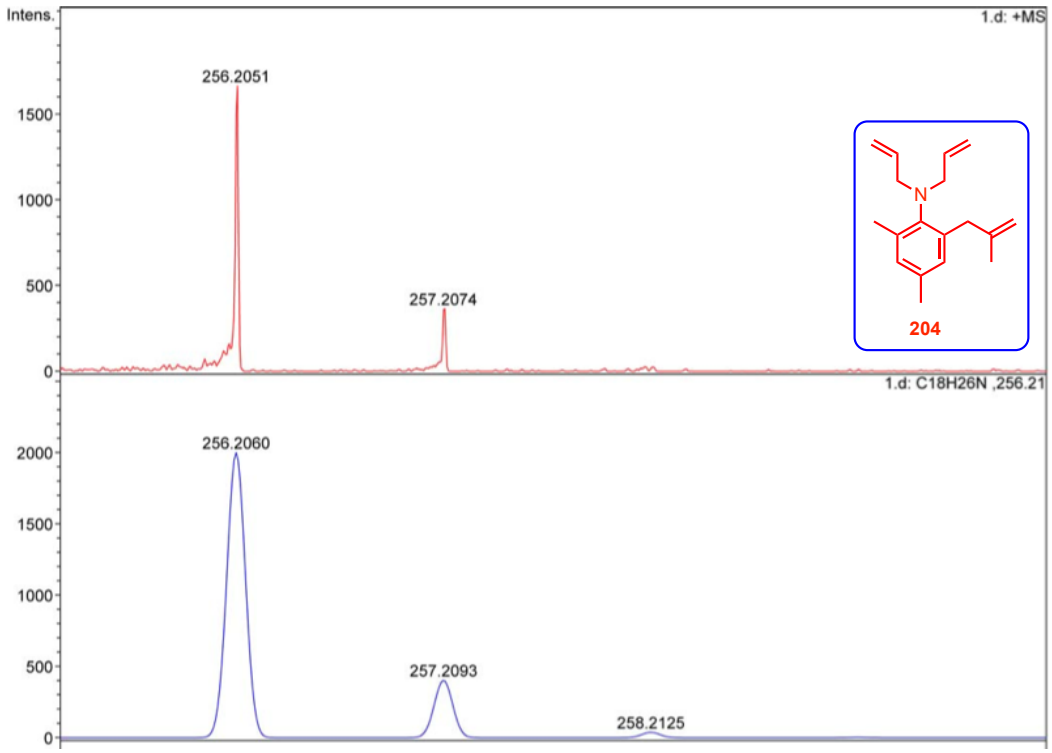

Figure 3.24: HRMS of N-Diallyl-2,4-Dimethyl-6-allyl-aniline **204**.

3.10.11. Synthesis of 2,4-Dimethyl-6-allyl-aniline derivative 186d

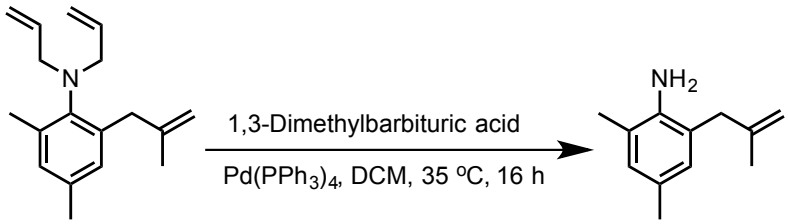

Scheme 3.21: Synthesis of 2,4-Dimethyl-6-allyl-aniline derivative **186d**.

Deallylation of aniline **204** was achieved using a procedure reported in the literature.[20] In a flame dried flask charged $Pd(PPh_3)_4$ (183 mg, 0.16 mmol) and 1,3-dimethylbarbituric acid (12.8 g, 82 mmol). To this mixture added a solution of N-diallyl-6-(2-methylallyl)-aniline derivative **204** (4.2 g, 16.4 mmol) in dry DCM (100 mL) via cannula. The resulting solution was heated to 35 ^{o}C and maintained for 16 h. After the reaction the mixture was cooled to room temperature and the solvent was removed under reduced pressure. The residue was taken in a *Satd*. Na_2CO_3 solution (250 mL) and the aqueous layer was extracted with diethyl ether (3 X 75 mL). The combined organic layer was washed with *Satd*. Na_2CO_3 solution (2 X 50 mL), dried over *anhyd.* Na_2SO_4, filtered and the solvent was removed under reduced pressure to get the crude product. The crude product was purified by combiflash using hexanes:ethyl acetate mixture (95:5) to get the title compound as a pale yellow oil (isolated yield = 92%).

Note: The product accompanied by inseparable di-allylated 1,3-dimethylbarbituric acid byproduct. So the mixture was taken to next step where it gets removed by filtration after the reaction. The relative percentage of the product was determined by ^{1}H-NMR spectroscopy.

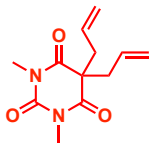

Di-allylated 1,3-dimethyl-barbituric acid

TLC condition - R*f* = 0.35 (100% hexanes)

^{1}H-NMR (400 MHz, $CDCl_3$, δ ppm): 6.78 (s, 1H), 6.72 (s, 1H), 4.85-4.84 (m, 1H), 4.73-4.728 (m, 1H), 3.54 (bs, 2H), 3.24 (s, 2H), 2.20 (s, 3H), 2.13 (s, 3H) and 1.71 (s, 3H).

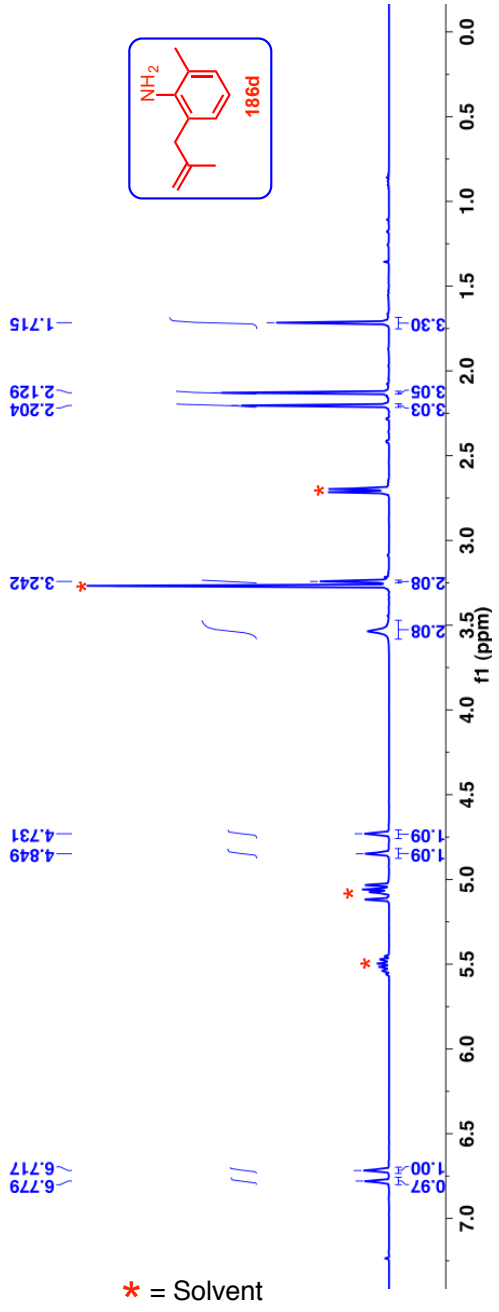

Figure 3.25: ^{1}H-NMR (400 MHz, $CDCl_3$, δ ppm) of 2,4-Dimethyl-6-allyl-aniline derivative **186d**.

^{13}C-NMR (100 MHz, $CDCl_3$, δ ppm): 144.0, 141.0, 129.61, 129.56, 127.2, 123.5, 122.6, 111.7, 41.6, 22.5, 20.6 and 17.7.

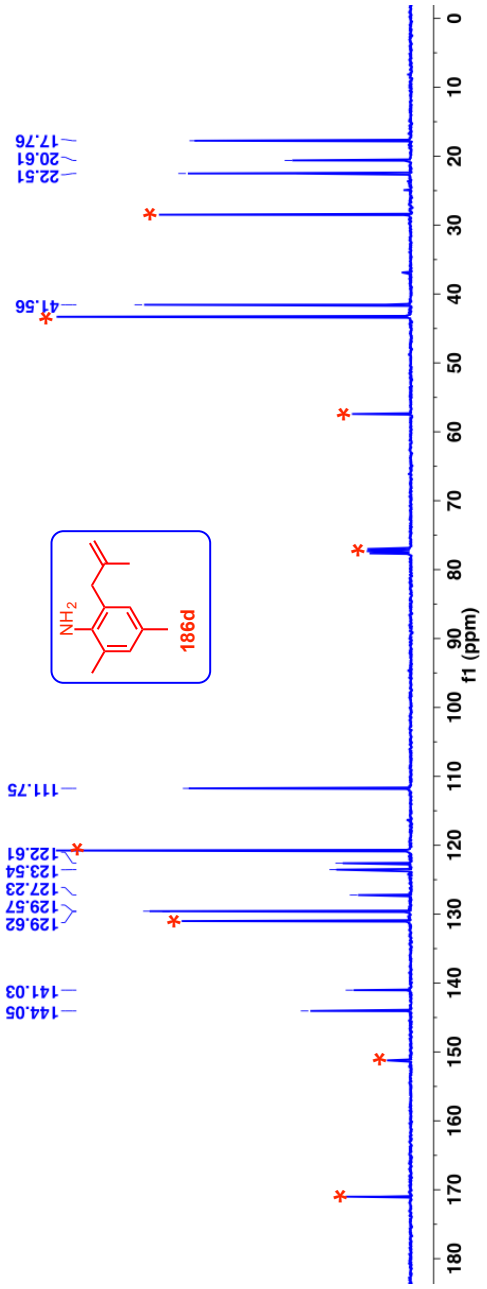

Figure 3.26: ^{13}C-NMR (100 MHz, $CDCl_3$, δ ppm) of 2,4-Dimethyl-6-allyl-aniline derivative **186d**.

HRMS-ESI (m/z) ([M + H]$^+$):

Calculated : 176.1434

Observed : 176.1438

|Δm| : 2.3 ppm

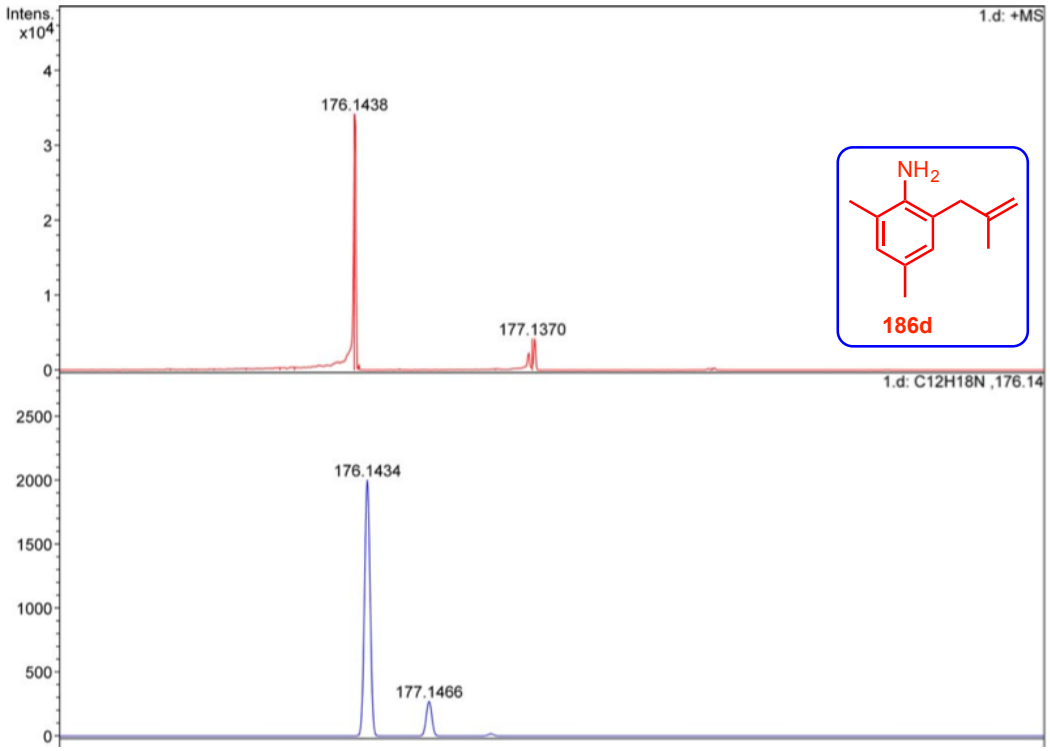

Figure 3.27: HRMS of 2,4-Dimethyl-6-allyl-aniline derivative **186d**.

3.10.12. Synthesis of *tert*-butyl-o-toluylcarbamate derivative 197a-b

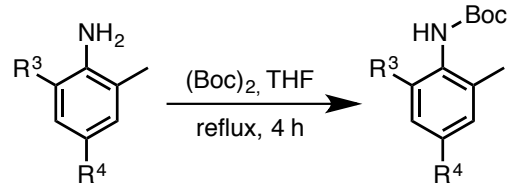

201 (R^3,R^4 = H)
198 (R^3,R^4 = Me)

197a-b

Scheme 3.22: Synthesis of *tert*-butyl-*o*-toluylcarbamate derivative 1**97a-b**.

Boc protected *o*-toluylcarbamate derivative **197a-b** was synthesized according to a procedure reported in the literature.[21] A mixture of aniline (2.0 g, 18.7 mmol) and $(Boc)_2O$ (4.9 g, 22.44 mmol) in a dry THF (20 mL) was refluxed for 4 h. After the reaction, the solution was cooled to room temperature, DI water (50 mL) and ethyl acetate (20 mL) was added, stirred for 10 min and the layers were separated. The aqueous layer was extracted with ethyl acetate (2 × 15 mL). The combined organic layer was washed with brine solution (10 mL), dried over *anhyd.* Na_2SO_4, filtered and the solvent was removed under reduced pressure to get the crude product. The crude product was purified by combiflash using hexanes: ethyl acetate mixture.

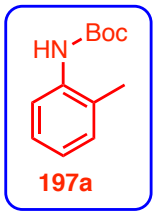

197a

R*f* = 0.60 (80% hexanes: 20% ethyl acetate) for 1**97a,** (Yield = 89%).

^{1}H-NMR (400 MHz, $CDCl_3$, δ ppm): 7.79-7.77 (m, 1H), 7.19-7.10 (m, 2H), 7.01-6.96 (m, 1H), 6.43 (bs, 1H), 2.21 (s, 3H) and 1.54 (s, 9H).

^{13}C-NMR (100 MHz, $CDCl_3$, δ ppm): 153.4, 136.6, 130.5, 127.9, 126.9, 123.98, 121.5, 80.4, 28.6 and 17.9.

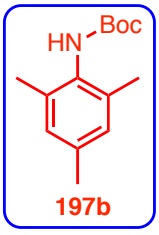

197b

R*f* = 0.50 (80% hexanes: 20% ethyl acetate) for **197b,** (Yield = 87%).

^{1}H-NMR (400 MHz, CD_3OD, δ ppm): 6.83 (s, 2H), 2.21 (s, 3H), 2.16 (s, 6H) and 1.48 (s, 9H)

^{13}C-NMR (100 MHz, CD_3OD, δ ppm): 159.7, 140.2, 139.8, 135.8, 132.4, 83.1, 31.6, 23.8 and 21.1.

3.10.13. Synthesis of 2-aminophenyl-propanol derivative 189b

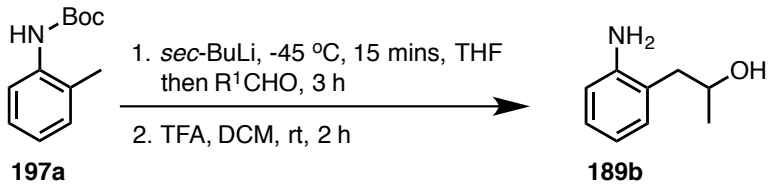

197a **189b**

Scheme 3.23: Synthesis of 2-aminophenyl-propanol derivative **189b**.

The lithiation protocol was followed as the procedure reported in the literature.[22] To a solution of Boc protected aniline derivative **197a** (2.40 g, 11.6 mmol) in dry THF (25 mL) at -45 ^{o}C, *sec*-BuLi (1.4M in cyclohexanes, 29.0 mmol) was added over a period of 15 min. The solution was stirred for 15 min followed by the addition of acetaldehyde (2.28 mL, 40.6 mmol). The mixture was allowed to warm to room temperature over a period of 30 min and further stirred for 2 h. After the reaction, the solution was cooled to 0 ^{o}C, quenched with saturated NH_4Cl solution extracted with ethyl acetate (2 x 20 mL). The combined organic layer was washed with brine solution (20 mL), dried over *anhyd.* Na_2SO_4, filtered and the solvent was removed under reduced pressure to get the crude product. The crude product was directly taken to next step without purification.

The crude product was dissolved in DCM (50 mL) and cooled to 0 ^{o}C followed by the addition of trifluoroacetic acid (11 mL). The mixture was warmed to room temperature and stirred for further 2 h. After the reaction, DI water (30 mL) was added to the mixture, stirred and the layers were separated. The organic layer was washed with 3M HCl (2 x 15 mL). The combined aqueous layer was washed with DCM (2 x 15 mL) and cooled to 0 ^{o}C. The pH of the solution was adjusted to 12 by the slow addition of solid NaOH pellets, extracted with diethyl ether (3 x 20 mL). The combined organic layer was washed with water (20 mL), brine solution (20 mL), dried over Na_2SO_4, filtered and concentrated to get the crude. The crude was purified by combiflash to get the pure product.

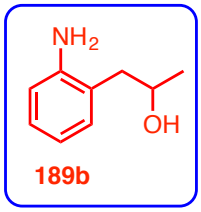

189b

R*f* = 0.35 (50% hexanes: 50% ethyl acetate) for **189b,** (Yield = 63%).

^{1}H-NMR (400 MHz, $CDCl_3$, δ ppm): 7.06-6.98 (m, 2H), 6.76-6.72 (m, 1H), 6.66-6.63 (m, 1H), 4.02 (h, *J* = 6.2 Hz, 1H), 3.51-3.49 (m, 3H), 2.64-2.62 (m, 2H) and 1.21 (d, *J* = 6.2 Hz, 3H).

^{13}C-NMR (100 MHz, $CDCl_3$, δ ppm): 145.4, 131.5, 127.8, 124.6, 119.3, 116.7, 68.9, 41.4 and 23.5.

3.10.14. Synthesis of 2,4-Dimethyl-6-propylaniline 187

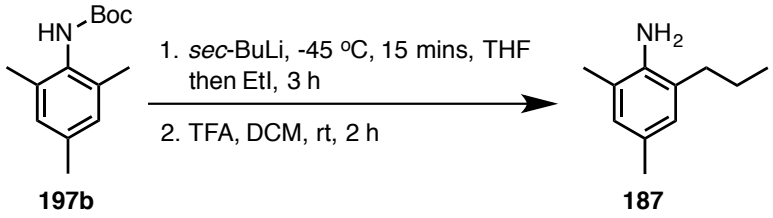

197b **187**

Scheme 3.24: Synthesis of 2,4-Dimethyl-6-propylaniline **187**.

To a solution of Boc protected aniline derivative **197b** (5.0 g, 21.3 mmol) in dry THF (25 mL) at -45 ^{o}C, *sec*-BuLi (1.4M in cyclohexanes, 53.1 mmol) was added. The solution was stirred for 15 min followed by the addition of ethyl iodide (5.2 mL, 63.75 mmol). The mixture was allowed to warm to room temperature over a period of 30 min and further stirred for 2 h. After the reaction, the solution was cooled to 0 ^{o}C, quenched with saturated NH_4Cl solution extracted with ethyl acetate (2 x 20 mL). The combined organic layer was washed with brine solution (20 mL), dried over *anhyd.* Na_2SO_4, filtered and the solvent was removed under reduced pressure to get the crude product. The crude product was directly taken to next step without purification.

The crude product was dissolved in DCM (200 mL) and cooled to 0 ^{o}C followed by the addition of trifluoroacetic acid (50 mL). The mixture was warmed to room temperature and stirred for further 2 h. After the reaction, the reaction mixture was cooled to 0 ^{o}C, added DI water (75 mL), adjusted the pH to 12 by adding solid NaOH pellets without allowing the internal temperature to rise above 10 ^{o}C, extracted with DCM (2 x 30 mL). The combined organic layer was washed with water (20 mL), brine solution (20 mL), dried over Na_2SO_4, filtered and concentrated to get the crude product. To the crude product, diethyl ether (75 mL) was added, stirred for 15 min and filtered through celite bed and the solid was washed with diethyl ether (20 mL). The combined filtrate was concentrated and purified by combiflash to get the pure product.

R*f* = 0.70 (80% hexanes: 20% ethyl acetate) for **187,** (Yield = 40%).

^{1}H-NMR (400 MHz, $CDCl_3$, δ ppm): 6.82 (s, 2H), 5.65 (bs, 2H), 2.53 (t, *J*=7.6 Hz, 2H), 2.28 (s, 3H), 2.23 (s, 3H), 1.67 (h, *J* = 7.4 Hz, 2H) and 1.02 (t, *J* = 7.2 Hz, 3H).

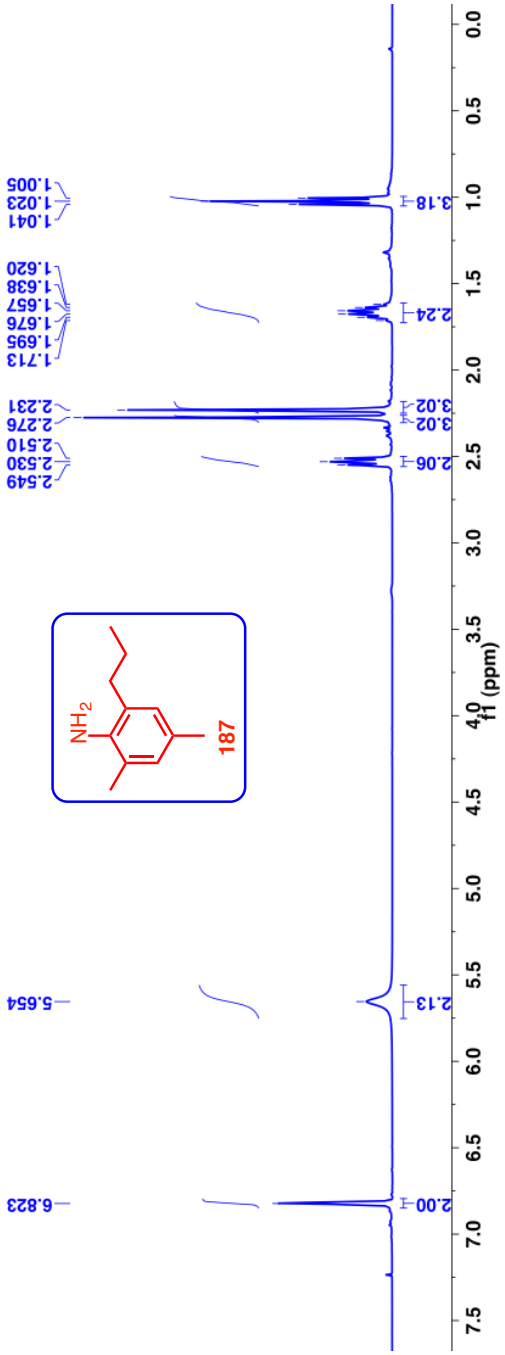

Figure 3.28: ^{1}H-NMR (400 MHz, $CDCl_3$, δ ppm) of 2,4-Dimethyl-6-ethyl-aniline derivative **187**.

^{13}C-NMR (100 MHz, $CDCl_3$, δ ppm): 136.5, 129.9, 129.4, 128.7, 128.4, 124.7, 33.7, 22.6, 20.8, 17.9 and 14.3.

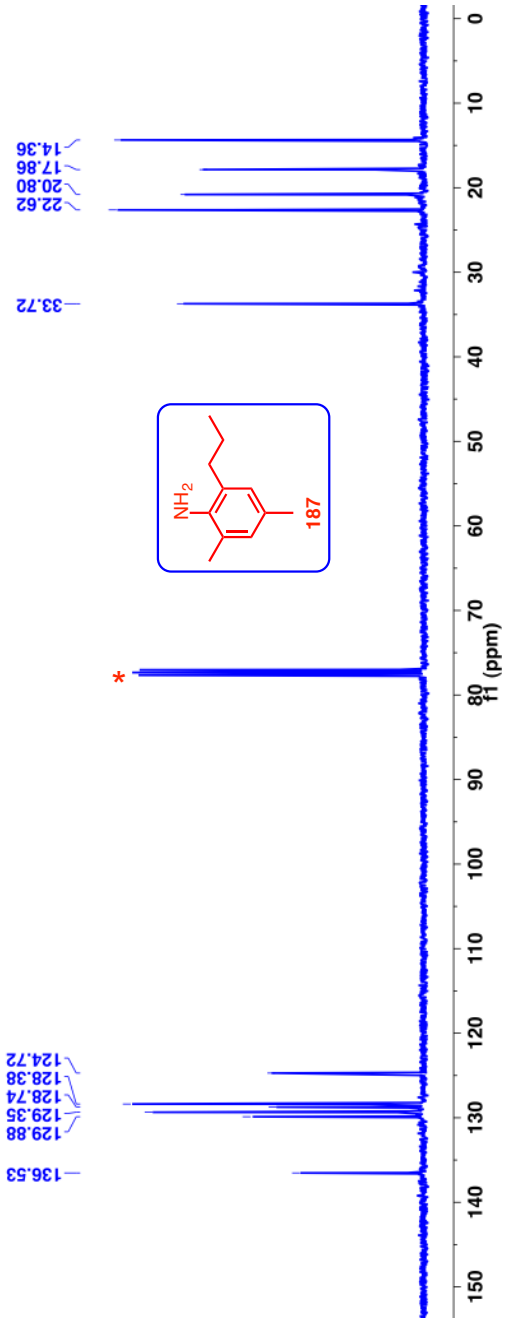

* = solvent

Figure 3.29: ^{13}C-NMR (100 MHz, $CDCl_3$, δ ppm) of 2,4-Dimethyl-6-ethyl-aniline derivative **187**.

HRMS-ESI (m/z) ([M + Na]$^+$):

Calculated : 164.1434

Observed : 164.1438

|Δm| : 2.4 ppm

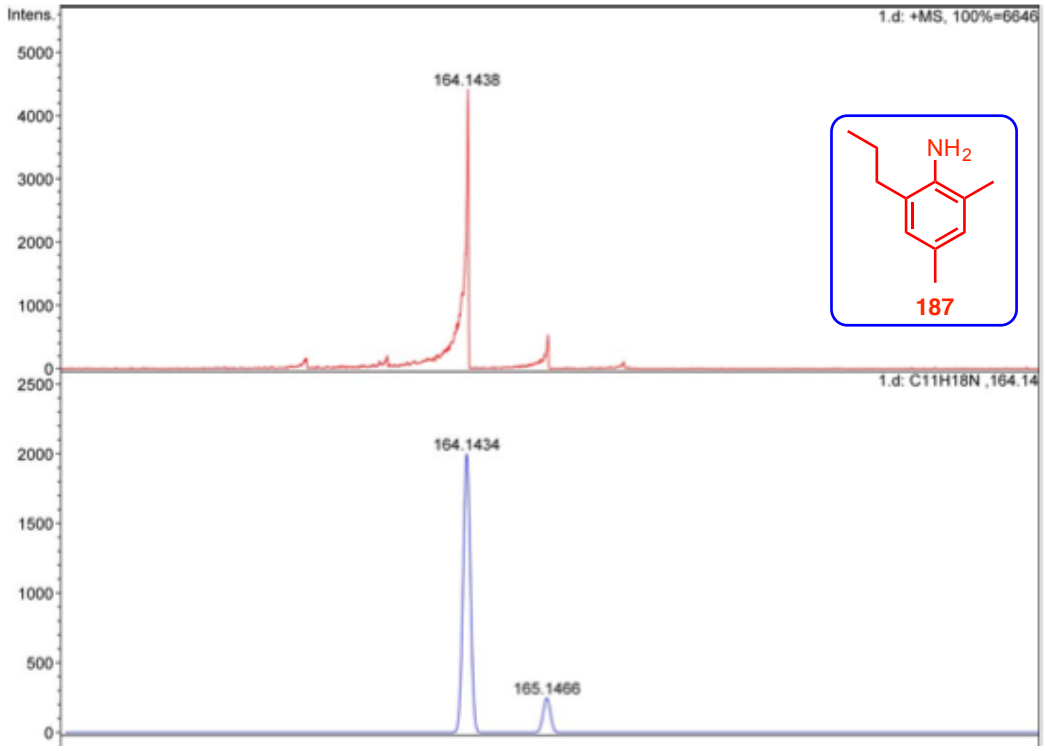

Figure 3.30: HRMS of 2,4-Dimethyl-6-ethyl-aniline derivative **187**.

3.10.15. Synthesis of (2,4-Dimethyl-6-(2-oxo-2-phenyl)-Boc derivative 190

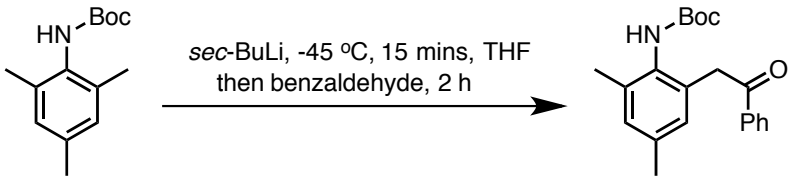

197b **190**

Scheme 3.25: Synthesis of (2,4-dimethyl-6-(2-oxo-2-phenylethyl)-Boc derivative **190**.

To a solution of Boc protected aniline derivative **197b** (2.0 g, 8.50 mmol) in dry THF (25 mL) at -45 °C, *sec*-BuLi (1.4M in cyclohexanes, 21.2 mmol) was added. The solution was stirred for 15 min followed by the addition of benzaldehyde (2.6 mL, 25.5 mmol) and the mixture was allowed to warm to room temperature over a period of 30 min and further stirred for 2 h. After the reaction, the solution was cooled to 0 °C, quenched with saturated NH_4Cl solution extracted with ethyl acetate (2 x 20 mL). The combined organic layer was washed with brine solution (20 mL), dried over *anhyd.* Na_2SO_4, filtered and the solvent was removed under reduced pressure to get the crude product. The crude product was purified by combiflash using hexanes:ethylacetate mixtures.

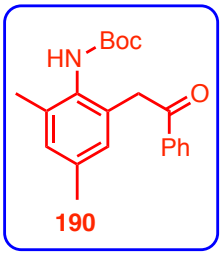

R*f* = 0.50 (50% hexanes: 50% ethyl acetate) for **9c,** (Yield = 62%).

^{1}H-NMR (400 MHz, $CDCl_3$, δ ppm): 8.03-8.01 (m, 2H), 7.58-7.54 (m, 1H), 7.47-7.43 (m, 2H), 6.96 (s, 1H), 6.84 (s, 1H), 6.43 (bs, 1H), 4.25 (s, 2H), 2.25 (s, 3H), 2.24 (s, 3H) and 1.43 (s, 9H).

^{13}C-NMR (100 MHz, $CDCl_3$, δ ppm): 198.7, 154.3, 137.0, 136.8, 136.7, 133.5, 132.8, 132.4, 130.8, 129.2, 128.9, 128.7, 79.9, 42.5, 28.5, 21.2 and 18.6.

3.10.16. Synthesis of (2,4-Dimethyl-6-(2-oxo-2-phenyl)-Boc derivative 189c

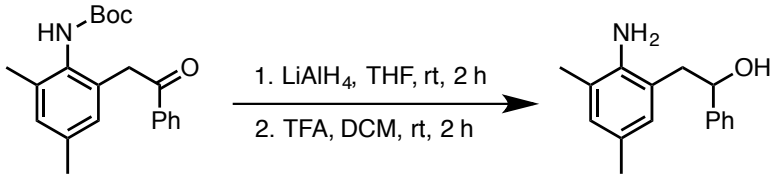

190 **189c**

Scheme 3.26: Synthesis of 4,6-dimethylphenyl-(2-(2-hydroxy-2-phenylethyl)-)-Boc.

To a slurry of $LiAlH_4$ (0.11 g, 2.95 mmol) in dry THF (15 mL) at 0 ^oC slowly added a solution of (2,4-dimethyl-6-(2-oxo-2-phenylethyl)-Boc derivative **190** (1.0 g, 2.95 mmol) over a period of 10 min. After the addition, the mixture was allowed to warm to room temperature and further stirred for 2 h. After the reaction, the solution was cooled to 0 ^oC, quenched with saturated NH_4Cl solution extracted with ethyl acetate (2 x 20 mL). The combined organic layer was washed with brine solution (20 mL), dried over *anhyd.* Na_2SO_4, filtered and the solvent was removed under reduced pressure to get the crude product. The crude product was directly taken to next step.

The crude product was dissolved in DCM (20 mL) and cooled to 0 ^oC followed by the addition of trifluoroacetic acid (11 mL). The mixture was allowed to warm to room temperature and further stirred for 2 h. After the reaction, DI water (20 mL) was added to the mixture, stirred and the layers were separated. The organic layer was washed with 3M HCl (2 x 10 mL). The combined aqueous layer was washed with DCM (2 x 10 mL) and cooled to 0 ^oC. The pH of the solution was adjusted to 12 by the slow addition of solid NaOH pellets, extracted with diethyl ether (3 x 15 mL). The combined organic layer was washed with DI water (20 mL), brine solution (20 mL), dried over Na_2SO_4, filtered and concentrated to get the crude. The crude was purified by combiflash to get the pure product.

R*f* = 0.45 (50% hexanes: 50% ethyl acetate) for **189c,** (Yield = 53%).

^{1}H-NMR (400 MHz, $CDCl_3$, δ ppm): 8.32 (bs, 3H), 7.21-7.14 (m, 5H), 6.81 (s, 1H), 6.55 (s, 1H), 4.78 (d, *J* = 7.8 Hz, 1H), 3.03-2.97 (m, 1H), 2.86-2.82 (m, 1H) and 2.18 (s, 6H).

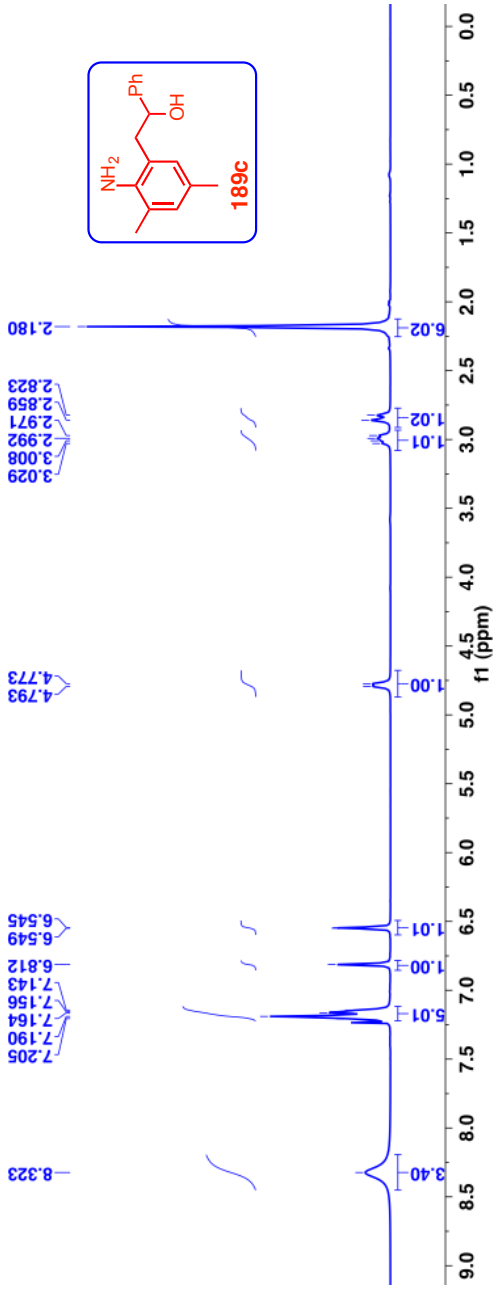

Figure 3.31: ^{1}H-NMR (400 MHz, $CDCl_3$, δ ppm) of 1-phenylethanol-aniline derivative **189c**.

^{13}C-NMR (100 MHz, $CDCl_3$, δ ppm): 142.98, 137.6, 132.0, 131.4, 130.95, 130.8, 128.5, 127.9, 127.7, 125.8, 75.95, 41.7, 20.8 and 17.3.

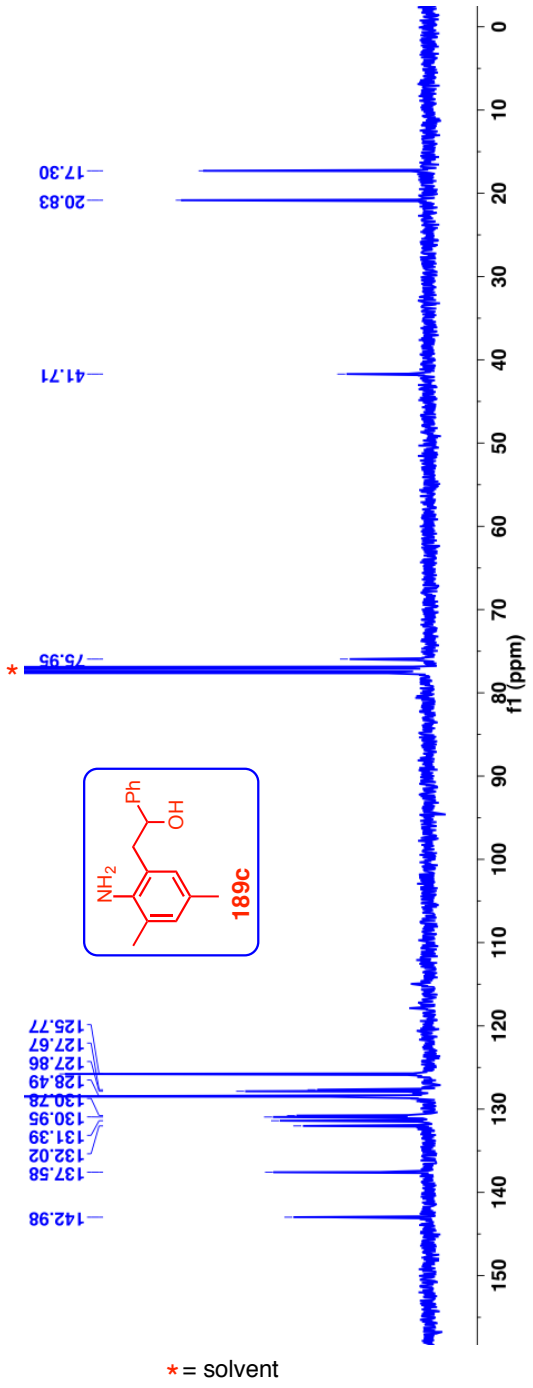

Figure 3.32: ^{13}C-NMR (100 MHz, $CDCl_3$, δ ppm) of 1-phenylethanol-aniline derivative **189c**.

HRMS-ESI (m/z) ([M + H]$^+$-H_2O):

Calculated : 224.1434

Observed : 224.1437

|Δm| : 1.3 ppm

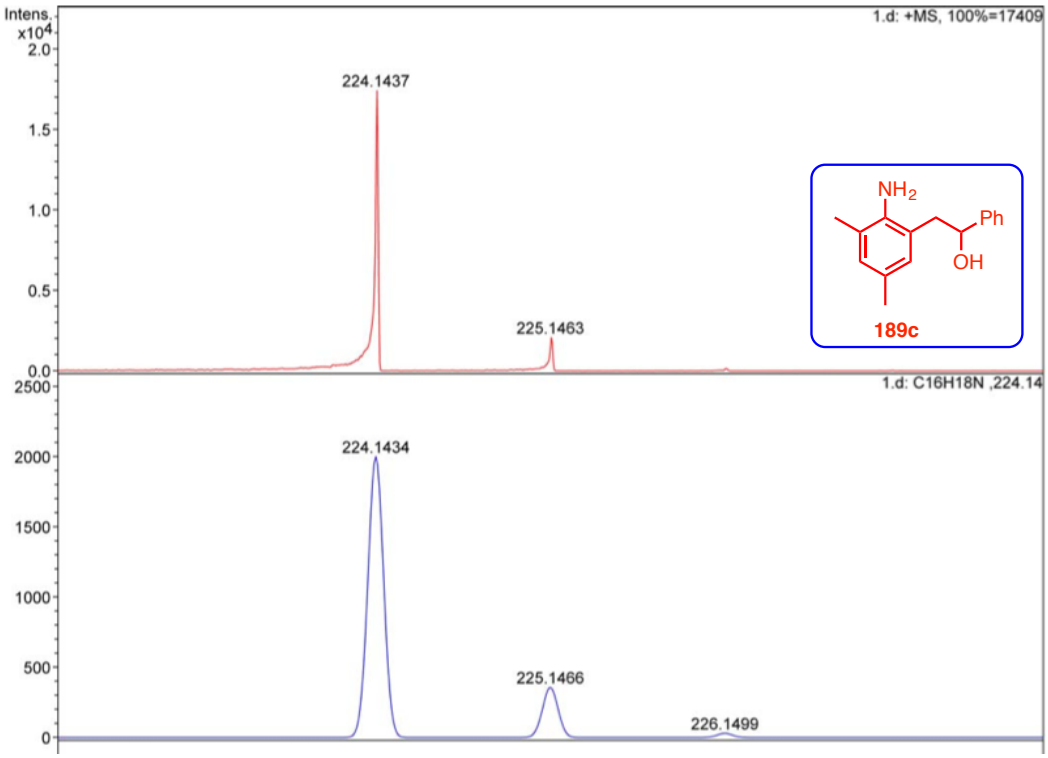

Figure 3.33: HRMS of 1-phenylethanol-aniline derivative **189c**.

3.10.17. Synthesis of (2,4-Dimethyl-6-(2-oxo-2-phenyl)-Boc derivative 188a-c

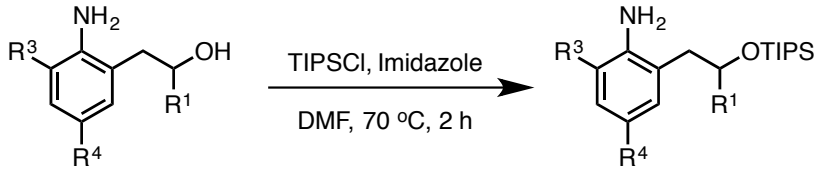

189a-c **188a-c**

a) R^1-R^4 = H
b) R^1=Me; R^3-R^4=H
c) R^1=Ph; R^3-R^4=Me

Scheme 3.27: Synthesis of TIPS protected alcohol derivatives **188a-c**.

The TIPS protected imide was synthesized following procedure reported in the literature.[23] To a solution of corresponding aniline **189a-c** (1.0 g, 1.0 *equiv.*) and imidazole (2.4 *equiv.*) in dry DMF (10 mL) at room temperature, triisopropylsilyl chloride (TIPSCl, 1.2 *equiv.*) was added. The resulting mixture was heated to 70 ^{o}C and maintained until complete consumption of starting material. After the reaction, the mixture was cooled to room temperature, added DI water (40 mL), extracted with Diethyl ether (3 × 15 mL). The combined organic layer was washed with DI water (15 mL), brine solution (15 mL), dried over *anhyd.* Na_2SO_4, filtered and the solvent was removed under reduced pressure to get the crude product. The crude product was purified by combiflash using hexanes: ethyl acetate mixture.

R*f* = 0.85 (80% hexanes: 20% ethyl acetate) for **188a,** (Yield = 80%).

^{1}H-NMR (400 MHz, CD_3OD, δ ppm): 6.98-6.92 (m, 2H), 6.72-6.70 (m, 1H), 6.66-6.62 (m, 1H), 3.92 (t, *J* = 6.0 Hz, 2H), 2.75 (t, *J* = 6.0 Hz, 2H) and 1.05-0.997 (m, 21H).

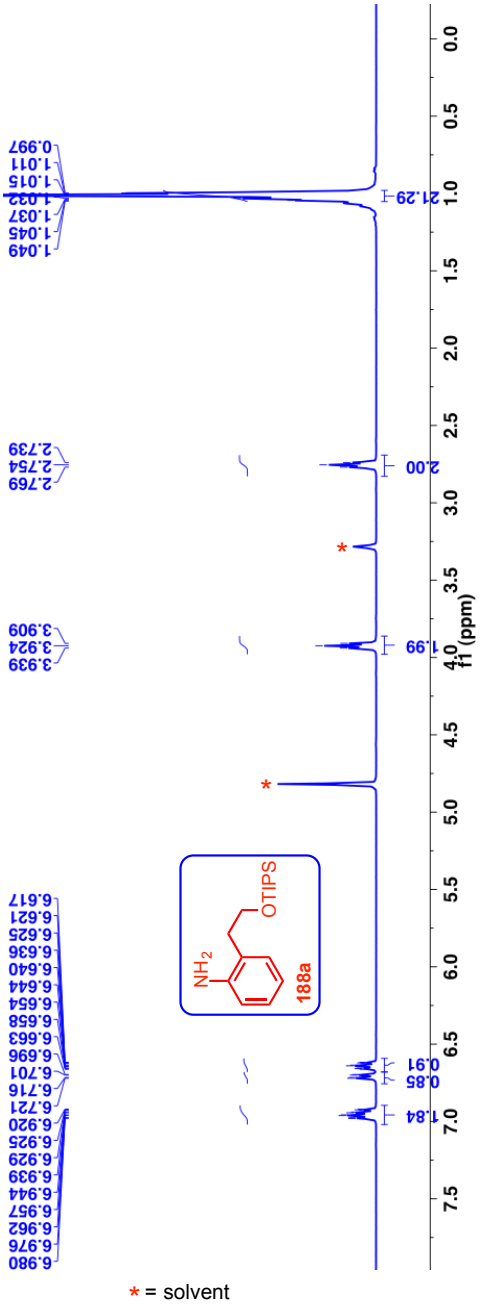

Figure 3.34: ^{1}H-NMR (400 MHz, CD_3OD, δ ppm) of silyloxy-ethyl-aniline derivative **188a**.

^{13}C-NMR (100 MHz, CD_3OD, δ ppm): 149.6, 134.3, 130.95, 129.6, 122.7, 120.1, 68.6, 38.8, 21.2 and 15.9.

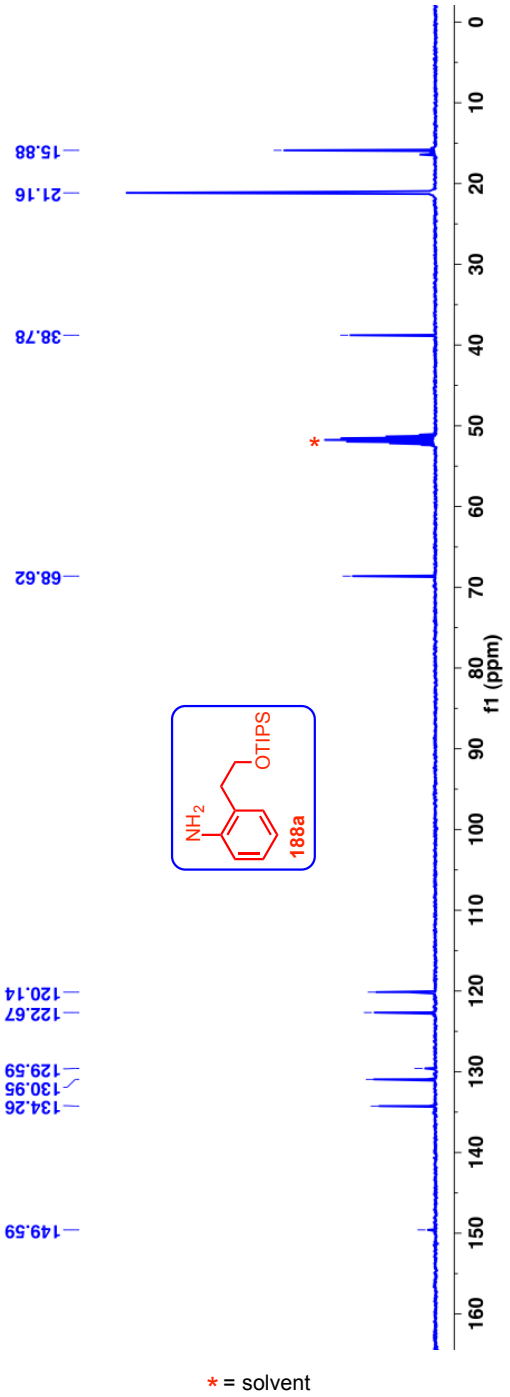

Figure 3.35: ^{13}C-NMR (100 MHz, CD_3OD, δ ppm) of silyloxy-ethyl-aniline derivative **188a**.

HRMS-ESI (m/z) ([M + H]$^+$):

Calculated : 294.2248

Observed : 294.2255

|Δm| : 2.4 ppm

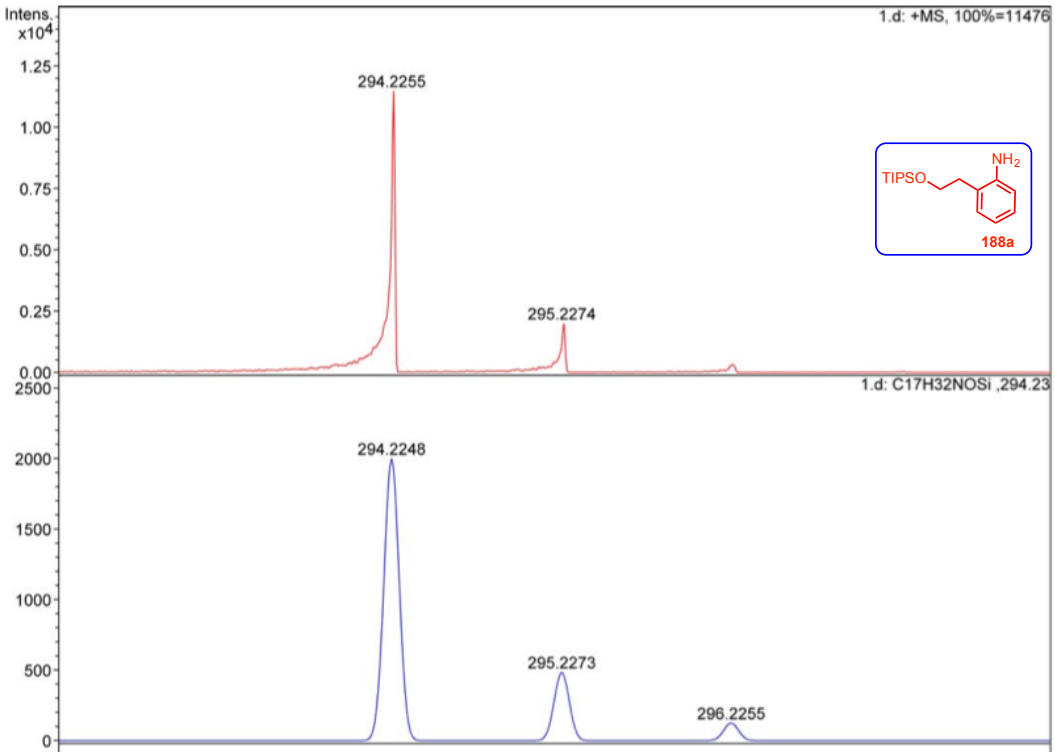

Figure 3.36: HRMS of silyloxy-ethyl-aniline derivative **188a**.

R*f* = 0.70 (80% hexanes: 20% ethyl acetate) for **188b,** (Yield = 89%).

^{1}H-NMR (400 MHz, $CDCl_3$, δ ppm): 7.03-6.97 (m, 2H), 6.71-6.63 (m, 2H), 4.31-4.24 (m, 1H), 3.94 (bs, 2H), 2.80-2.67 (m, 2H), 1.19 (d, *J* = 6.0 Hz, 3H) and 1.04-1.02 (m, 21H).

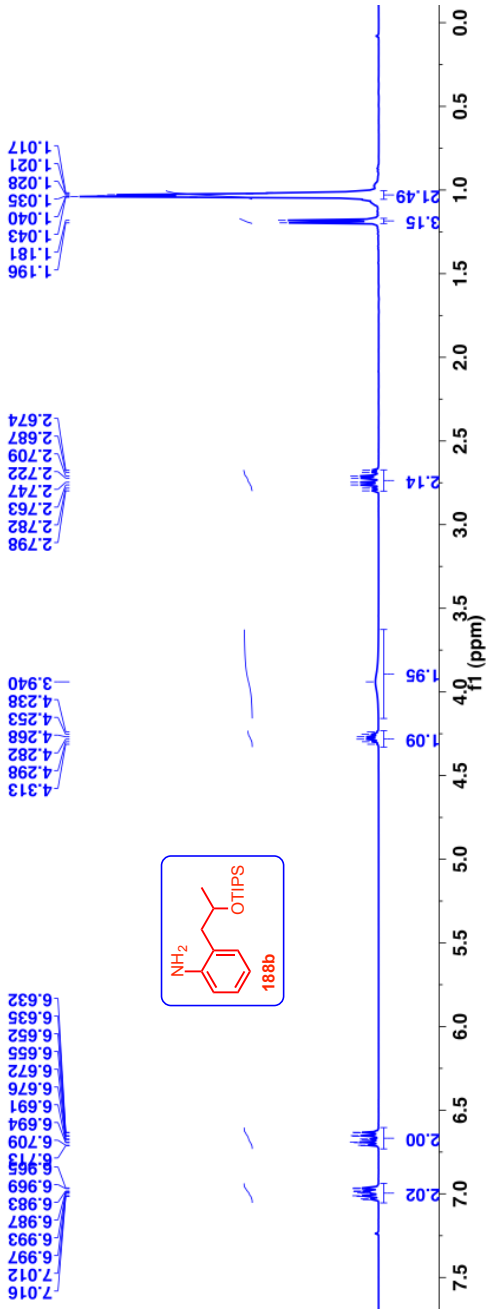

Figure 3.37: ^{1}H-NMR (400 MHz, $CDCl_3$, δ ppm) of silyloxy-2-propyl-aniline derivative **188b**.

^{13}C-NMR (100 MHz, $CDCl_3$, δ ppm): 145.9, 131.7, 127.5, 124.5, 118.7, 116.1, 70.0, 42.3, 23.9, 18.3, 18.2 and 12.8.

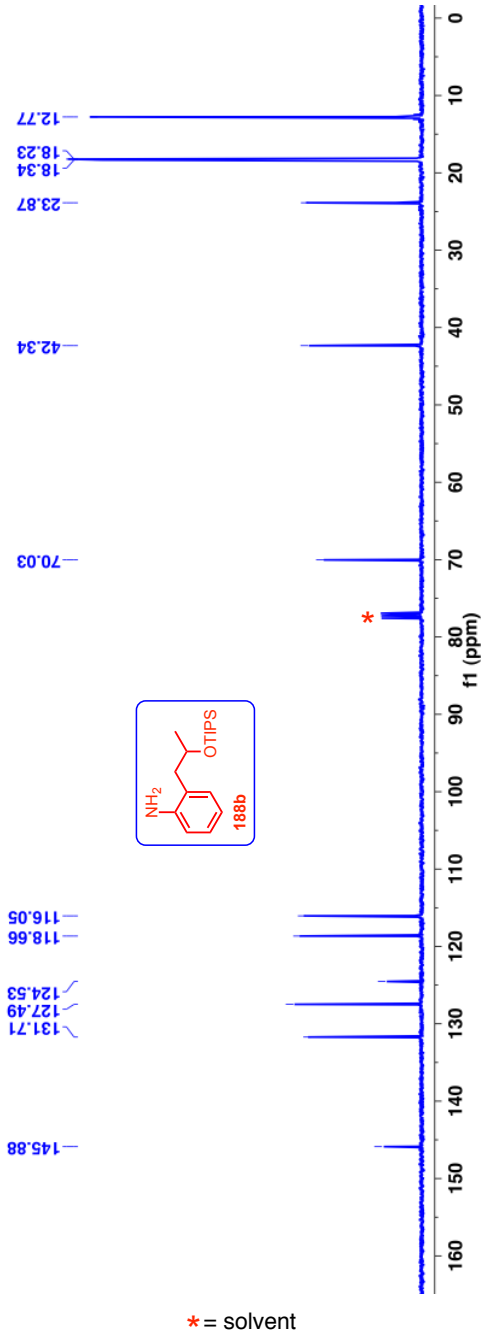

Figure 3.38: ^{13}C-NMR (100 MHz, $CDCl_3$, δ ppm) of silyloxy-2-propyl-aniline derivative **188b**.

HRMS-ESI (m/z) ([M + H]$^+$):

Calculated : 308.2410

Observed : 308.2417

|Δm| : 2.3 ppm

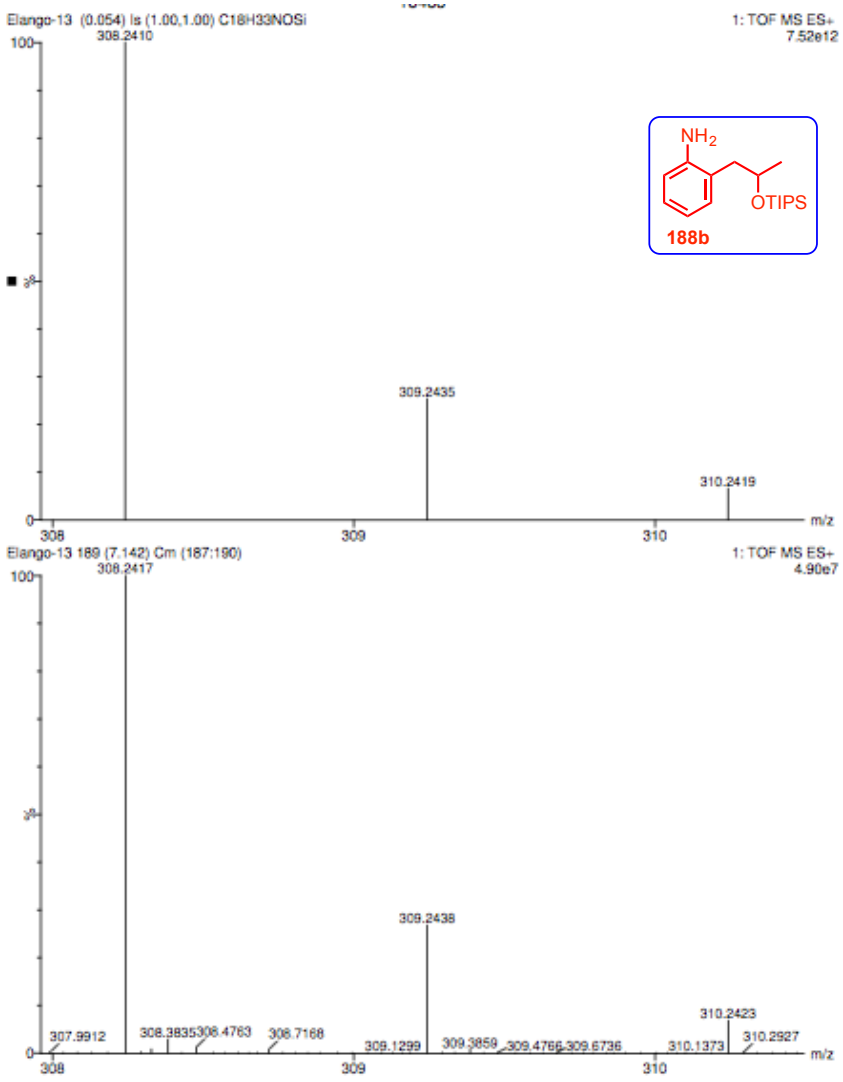

Figure 3.39: HRMS of silyloxy-2-propyl-aniline derivative **188b**.

R*f* = 0.85 (80% hexanes: 20% ethyl acetate) for **188c,** (Yield = 53%).

^{1}H-NMR (400 MHz, $CDCl_3$, δ ppm): 7.297-7.23 (m, 5H), 6.75 (s, 1H), 6.65 (s, 1H), 5.03-5.00 (m, 1H), 3.49 (bs, 2H), 3.04 (dd, *J* = 13.9, 7.5 Hz, 1H), 2.80 (dd, *J* = 14.0, 4.9 Hz, 1H), 2.18 (s, 3H), 2.11 (s, 3H), 0.96 (s, 12H) and 0.89-0.88 (m, 9H).

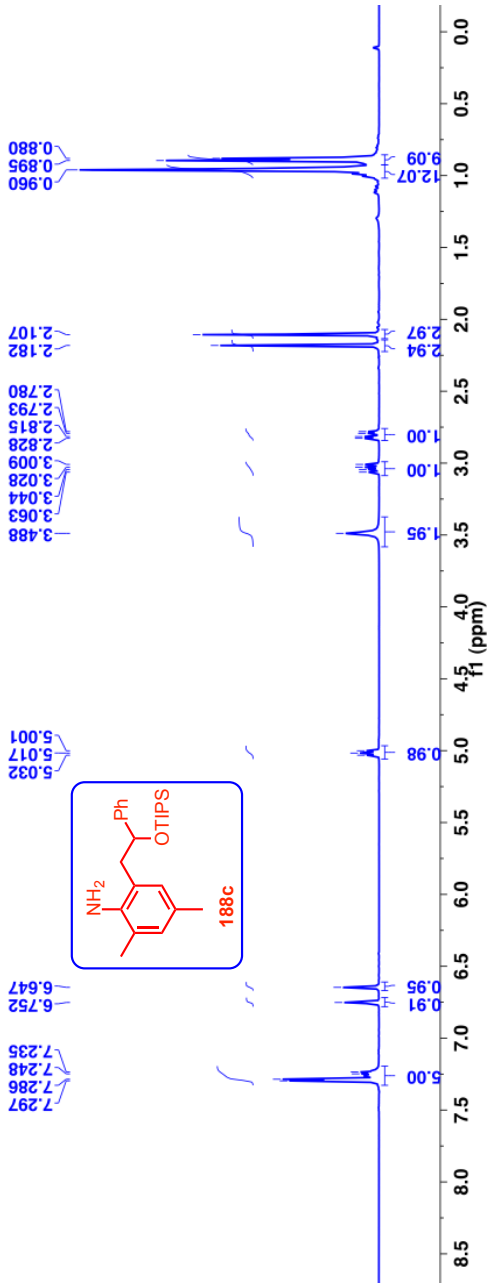

Figure 3.40: ^{1}H-NMR (400 MHz, $CDCl_3$, δ ppm) of silyloxy-2-phenylethyl-aniline derivative **188c**.

^{13}C-NMR (100 MHz, $CDCl_3$, δ ppm): 145.6, 141.5, 130.3, 129.5, 128.2, 127.4, 127.2, 126.2, 123.7, 122.6, 77.2, 20.6, 18.1, 18.04, 18.0 and 12.6.

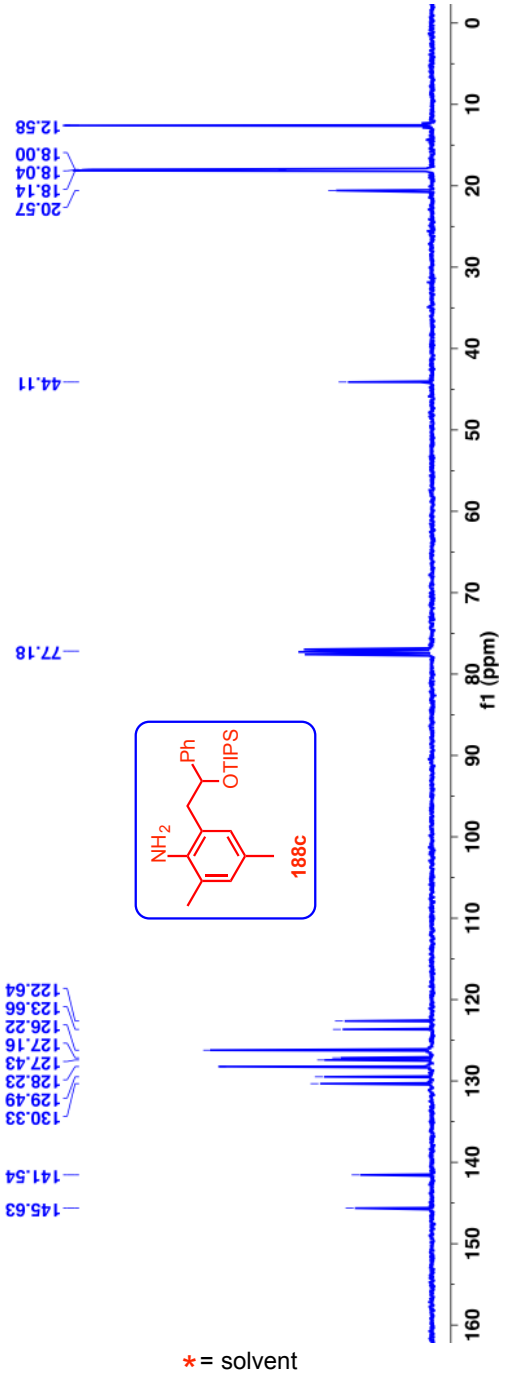

Figure 3.41: ^{13}C-NMR (100 MHz, $CDCl_3$, δ ppm) of silyloxy-2-phenylethyl-aniline derivative **188c**.

HRMS-ESI (m/z) ([M + Na]$^+$):

Calculated : 420.2693

Observed : 420.2703

|Δm| : 2.4 ppm

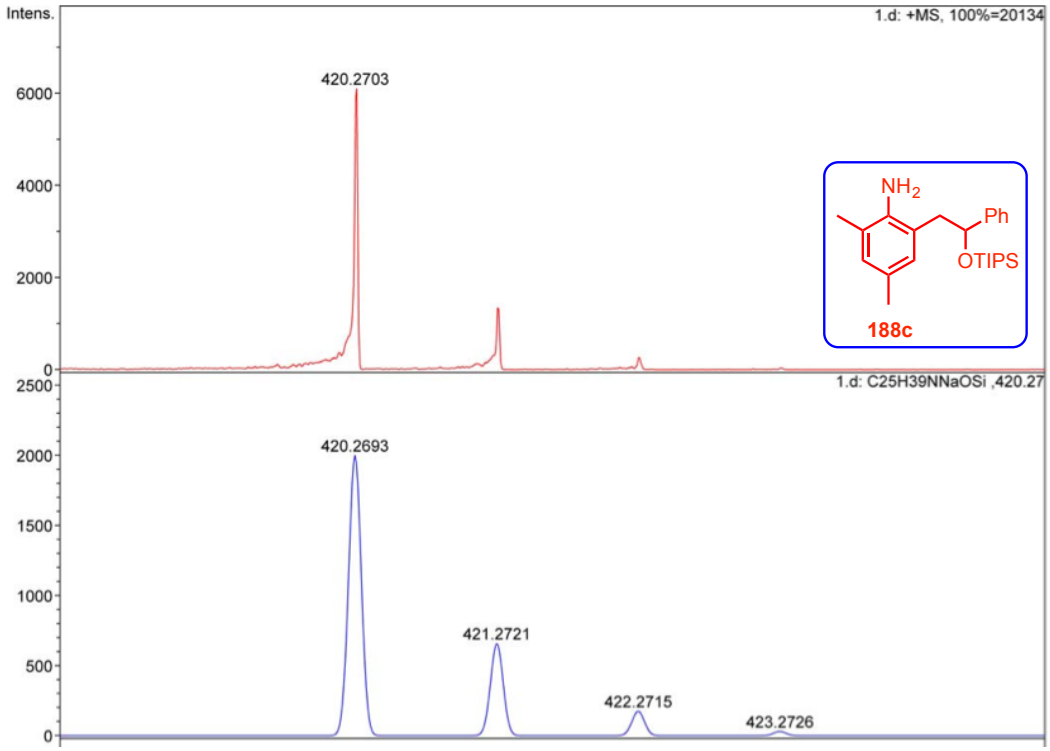

Figure 3.42: HRMS of silyloxy-2-phenylethyl-aniline derivative **188c**.

3.11. General procedure for synthesis of atropisomeric enamides and their precursors

3.11.1. Synthesis of six membered piperidine-2,6-dione derivatives 182a-d

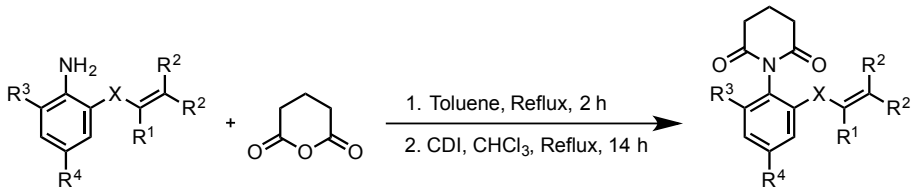

186a-d **191** **182a-d**

a) R^1-R^4 = H; X = CH_2
b) R^1,R^3-R^4 = H; R^2 = Me; X = CH_2
c) R^1 = Me, R^2-R^4 = H; X = CH_2
d) R^1-R^4 = H; X = CH_2-CH_2

Scheme 3.28: Synthesis of piperidine-2,6-dione derivatives **182a-d**.

The Piperidine-2,6-dione derivatives **182a-d** (7.6 mmol) were synthesized according to the literature reported procedure.[24] To a solution of corresponding aniline derivative **7** (10 mmol) in toluene (20 mL) at 25 ^oC, glutaric anhydride **191** (9.1 mmol) was added. The resulting mixture was refluxed for 2 h. The reaction mixture was cooled to room temperature and the residue was diluted with n-pentane (50 mL). The precipitated solid was filtered and washed with n-pentane (20 mL) and dried under vacuum. The crude product was directly taken to next step without further purification.

To the crude product from above reaction dissolved in chloroform under N_2 atmosphere 1,1'-carbonyldiimidazole (12 mmol) was added. To resulting solution was refluxed for 14 h. After the reaction, the solution was cooled to room temperature and DI water was added. The mixture was stirred and the layers were separated. The organic layer was washed with DI Water (2 X 100 mL), cold aqueous 2N HCl (2 X 75 mL or until the imidazole byproduct is removed) and brine solution (1 X 100 mL). The organic layer was dried over *anhyd.* Na_2SO_4, filtered and the solvent was evaporated under reduced pressure to get the crude product. The crude product was purified by combiflash using hexanes:ethyl acetate mixture (80:20) to get the title product.

Note: During the addition of 1,1'-carbonyldiimidazole evolution of CO_2 gas was observed.

R*f* = 0.60 (50% hexanes:50% ethyl acetate) for **182a**, Yield = 76%

^{1}H-NMR (400 MHz, $CDCl_3$, δ ppm): 7.25-7.12 (m, 1H), 7.15-7.11 (m, 2H), 5.84-5.74 (m, 1H), 5.06-5.03 (m, 1H), 5.01-5.00 (m, 1H), 3.14-3.12 (m, 2H), 2.81-2.77 (m, 4H), 2.12-2.05 (m, 2H) and 2.04 (S, 3H).

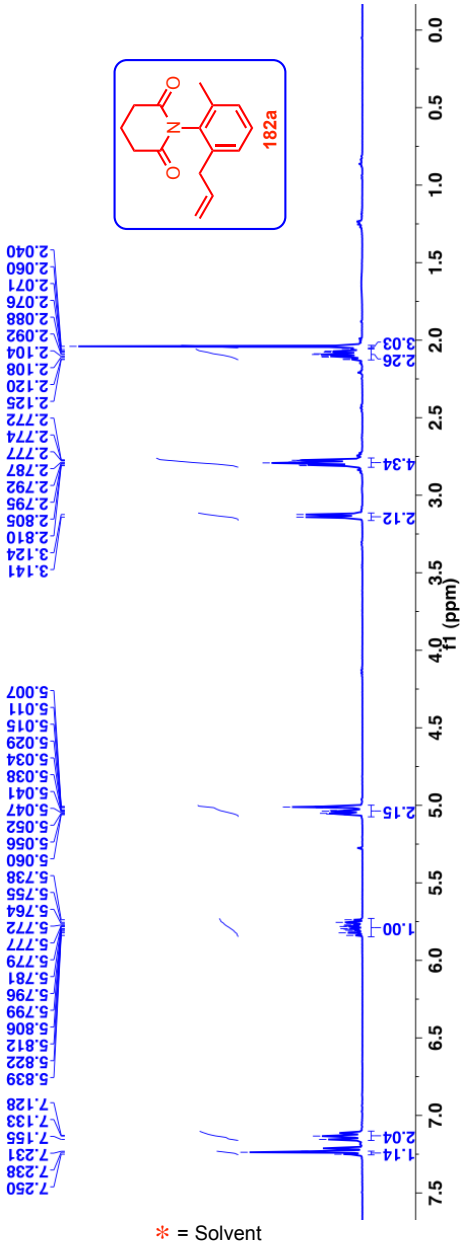

Figure 3.43: ^{1}H-NMR (400 MHz, $CDCl_3$, δ ppm) of 2-allyl-6-methyl-glutarimide derivative **182a**.

^{13}C-NMR (100 MHz, $CDCl_3$, δ ppm): 172.1, 137.3, 136.6, 135.7, 133.5, 129.2, 129.1, 128.1, 116.3, 36.6, 33.3, 17.8 and 17.5.

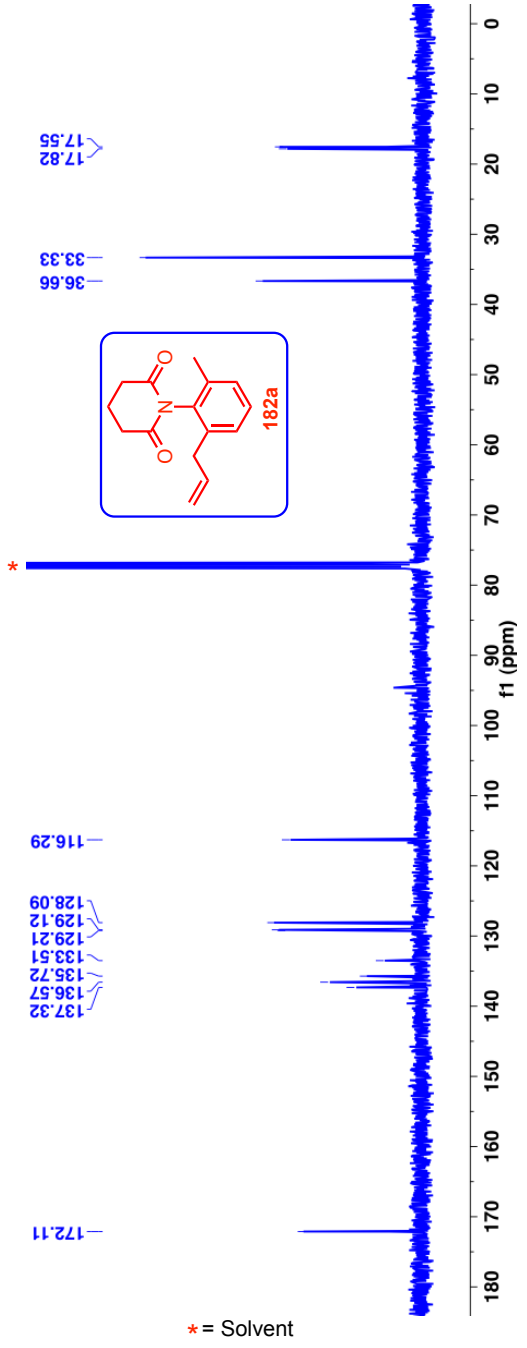

Figure 3.44: ^{13}C-NMR (100 MHz, $CDCl_3$, δ ppm) of 2-allyl-6-methyl-glutarimide derivative **182a**.

HRMS-ESI (m/z) ([M + Na]$^+$):

Calculated : 266.1151

Observed : 266.1153

|Δm| : 0.7 ppm

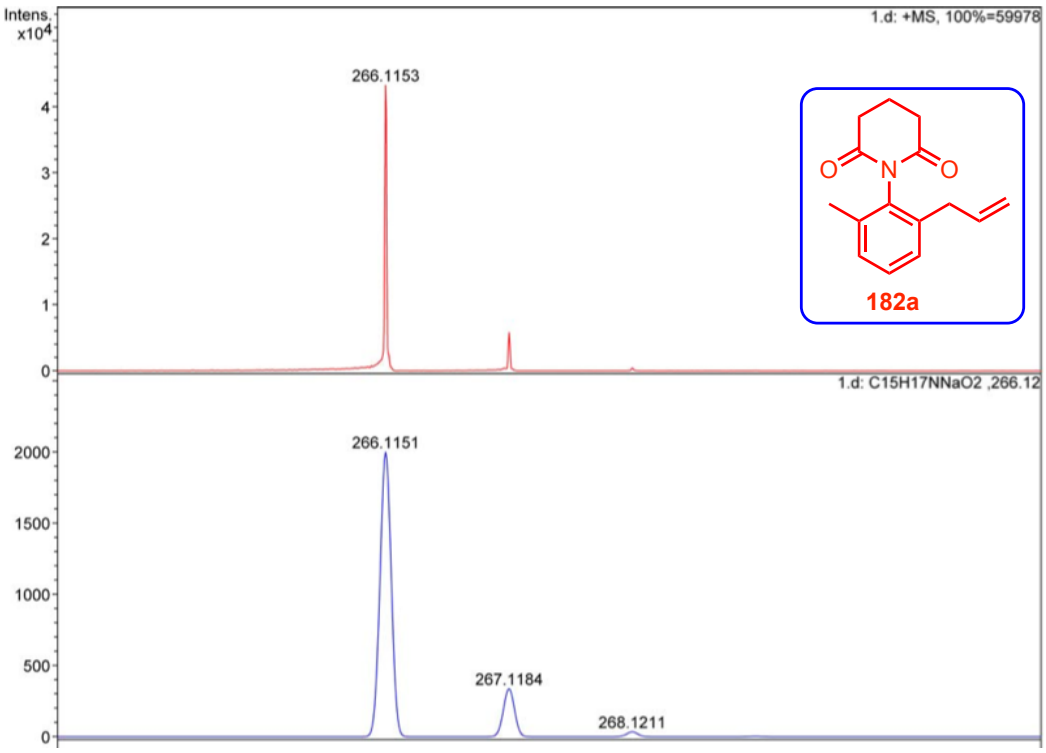

Figure 3.45: HRMS of 2-allyl-6-methyl-glutarimide derivative **182a**.

R*f* = 0.60 (50% hexanes:50% ethyl acetate) for **182b**.

^{1}H-NMR (400 MHz, $CDCl_3$, δ ppm): 7.23-7.19 (m, 1H), 7.12-7.08 (m, 2H), 5.15-5.11 (m, 1H), 3.06-3.04 (d, *J*= 6.8 Hz, 2H), 2.8-2.76 (m, 4H), 2.10-2.05 (m, 2H), 2.03 (s, 3H), 1.69 (s, 3H) and 1.61 (s, 3H).

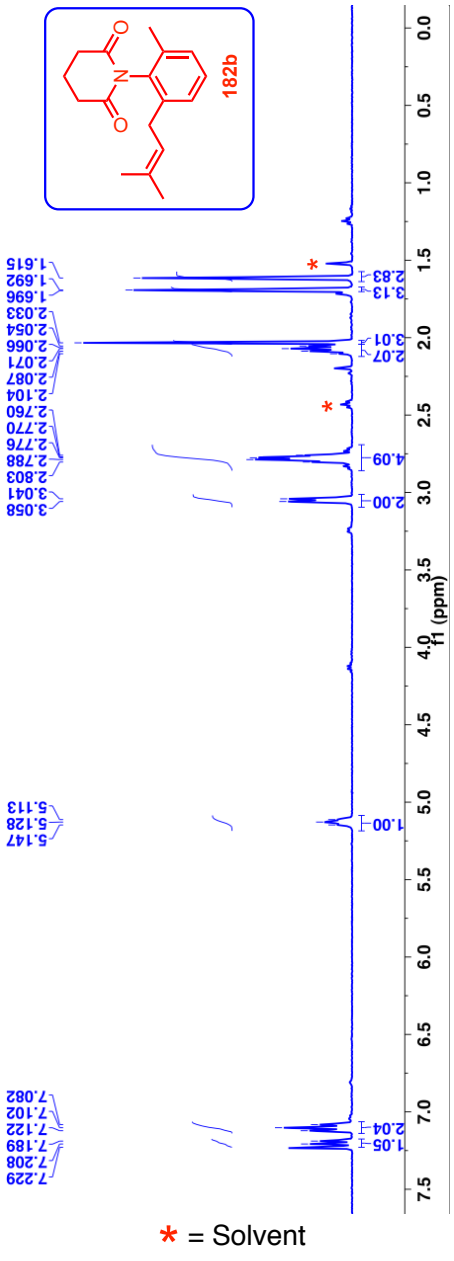

Figure 3.46: ^{1}H-NMR (400 MHz, $CDCl_3$, δ ppm) of 2-dimethylallyl-glutarimide derivative **182b**.

^{13}C-NMR (100 MHz, $CDCl_3$, δ ppm): 172.1, 138.7, 135.5, 133.3, 133.1, 129.0, 128.8, 127.7, 122.2, 33.3, 30.5, 25.8, 18.1, 17.8 and 17.6.

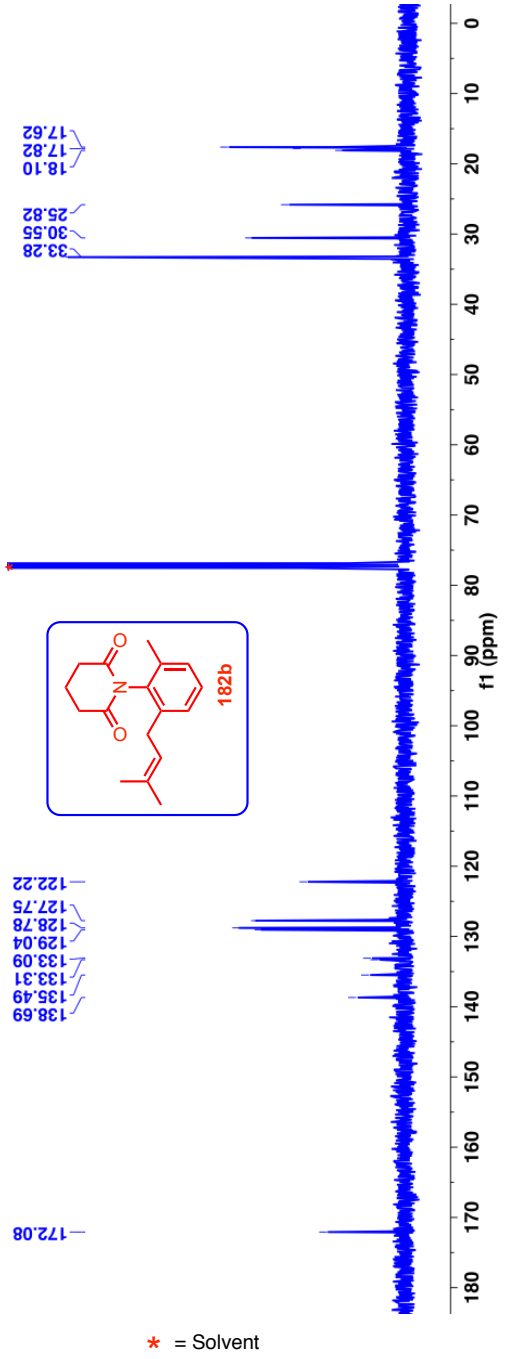

Figure 3.47: ^{13}C-NMR (100 MHz, $CDCl_3$, δ ppm) of 2-dimethylallyl-glutarimide derivative **182b**.

HRMS-ESI (m/z) ([M + Na]$^+$):

Calculated : 294.1465

Observed : 294.1464

|Δm| : 0.3 ppm

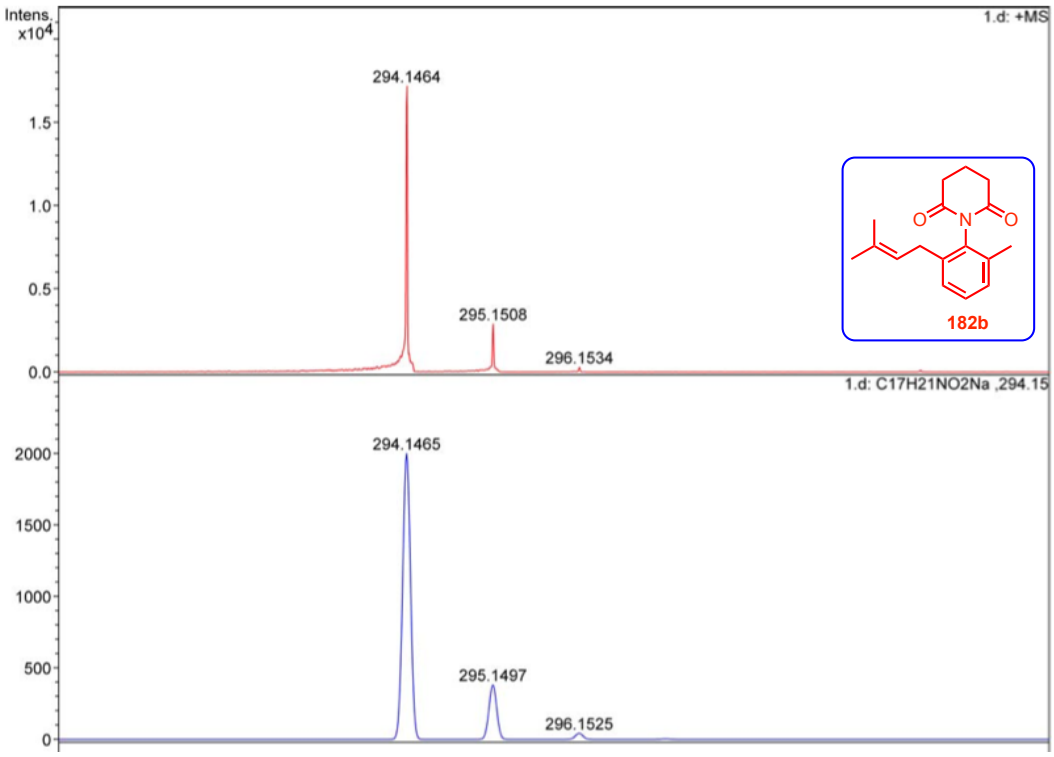

Figure 3.48: HRMS of 2-dimethylallyl-glutarimide derivative **182b**.

R*f* = 0.70 (50% hexanes:50% ethyl acetate) for **182c**.

^{1}H-NMR (400 MHz, $CDCl_3$, δ ppm): 6.97 (s, 1H), 6.92 (s, 1H), 4.78-4.77 (m, 1H), 4.69-4.68 (m, 1H), 3.07 (s, 2H), 2.78-2.75 (m, 4H), 2.29 (s, 3H), 2.10-2.03 (m, 2H), 1.99 (s, 3H) and 1.55 (s, 3H).

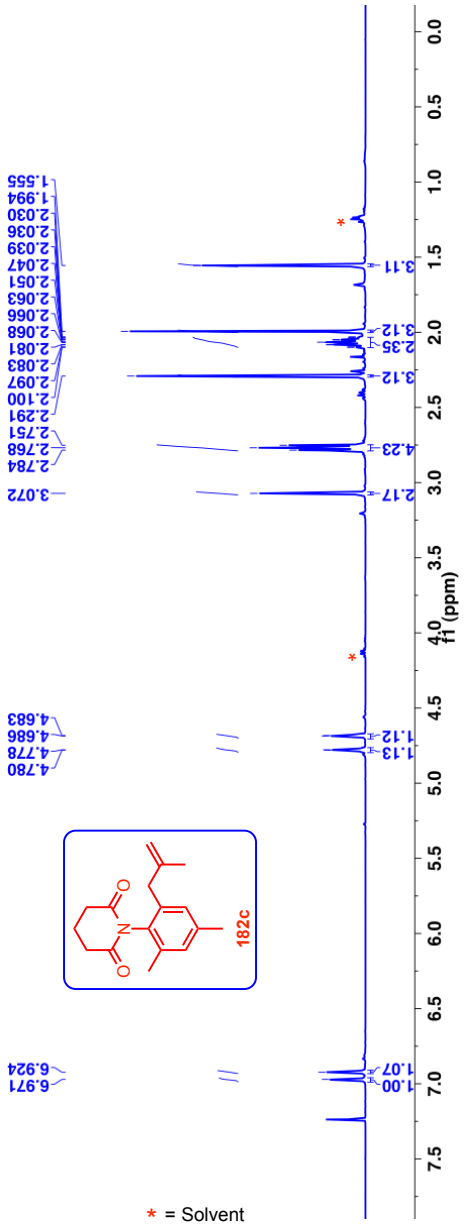

Figure 3.49: ^{1}H-NMR (400 MHz, $CDCl_3$, δ ppm) of 2-methylallyl-glutarimide derivative **182c**.

^{13}C-NMR (100 MHz, $CDCl_3$, δ ppm): 172.1, 144.4, 138.6, 136.4, 135.3, 131.3, 130.1, 129.5, 112.4, 41.3, 33.2, 22.0, 21.3, 17.7 and 17.6.

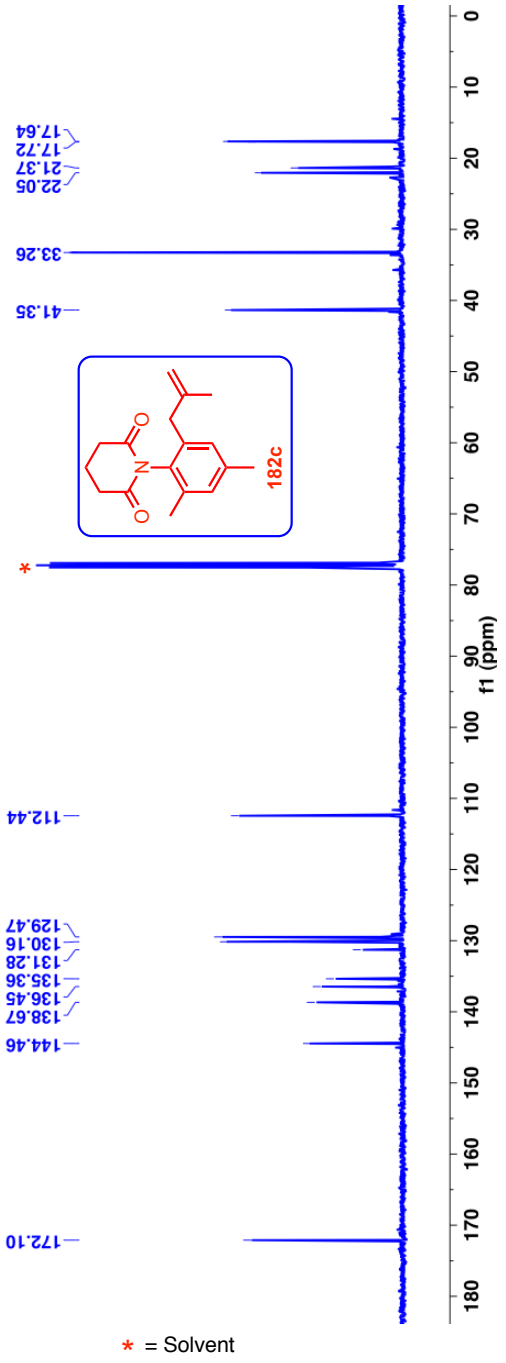

Figure 3.50: ^{13}C-NMR (100 MHz, $CDCl_3$, δ ppm) of 2-methylallyl-glutarimide derivative **182c**.

HRMS-ESI (m/z) ([M + Na]$^+$):

Calculated : 294.1465

Observed : 294.1464

|Δm| : 0.3 ppm

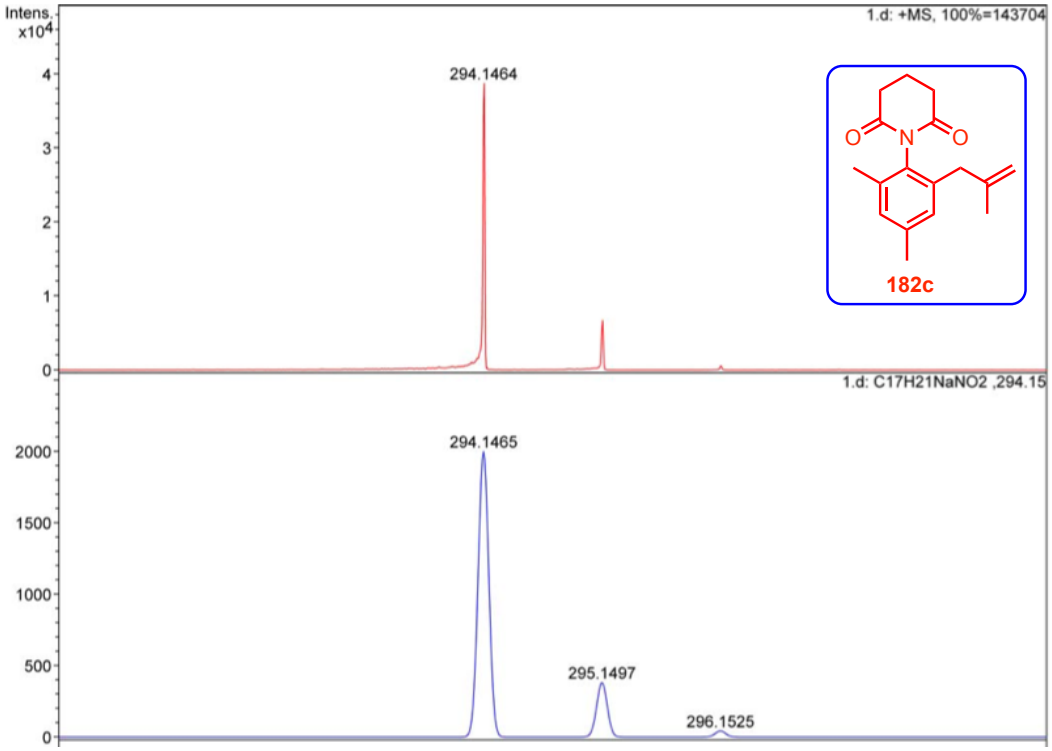

Figure 3.51: HRMS of 6-methylallyl-glutarimide derivative **182c**.

R*f* = 0.30 (80% hexanes:20% ethyl acetate) for **182d**

^{1}H-NMR (400 MHz, $CDCl_3$, δ ppm): 7.26-7.22 (m, 1H), 7.16-7.13 (m, 2H), 5.86-5.76 (m, 1H), 5.03-4.94 (m, 2H), 2.80 (t, *J* = 6.5 Hz, 2H), 2.43-2.39 (m, 2H), 2.27-2.22 (m, 2H), 2.11-2.06 (m, 2H) and 2.05 (s, 3H).

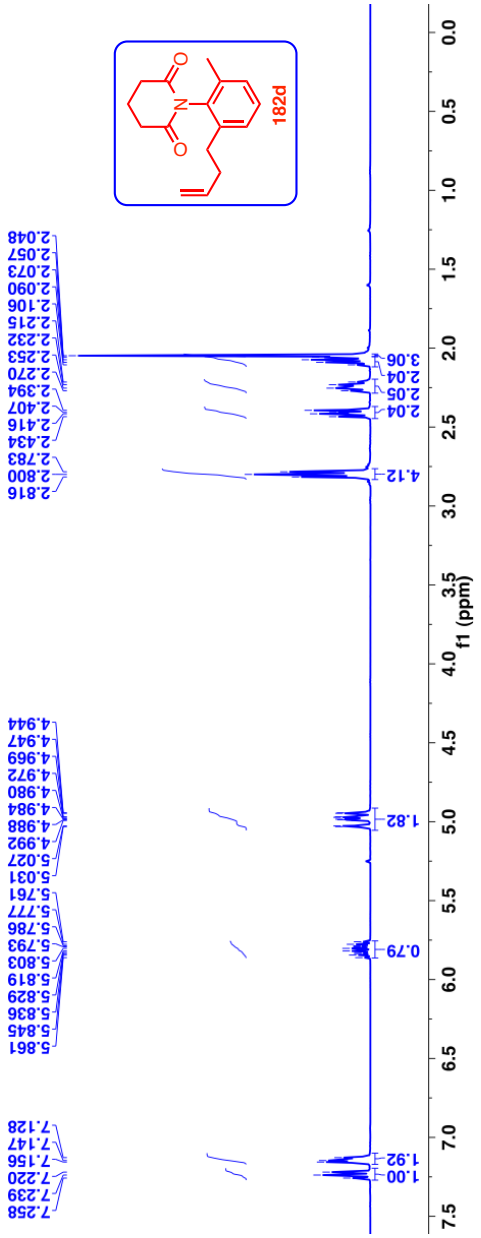

Figure 3.52: ^{1}H-NMR (400 MHz, $CDCl_3$, δ ppm) of 2-butenyl-glutarimide derivative **182d**.

^{13}C-NMR (100 MHz, $CDCl_3$, δ ppm): 172.3, 138.8, 138.2, 135.5, 133.3, 129.0, 128.8, 127.5, 115.1, 33.97, 33.3, 30.98, 17.9 and 17.7.

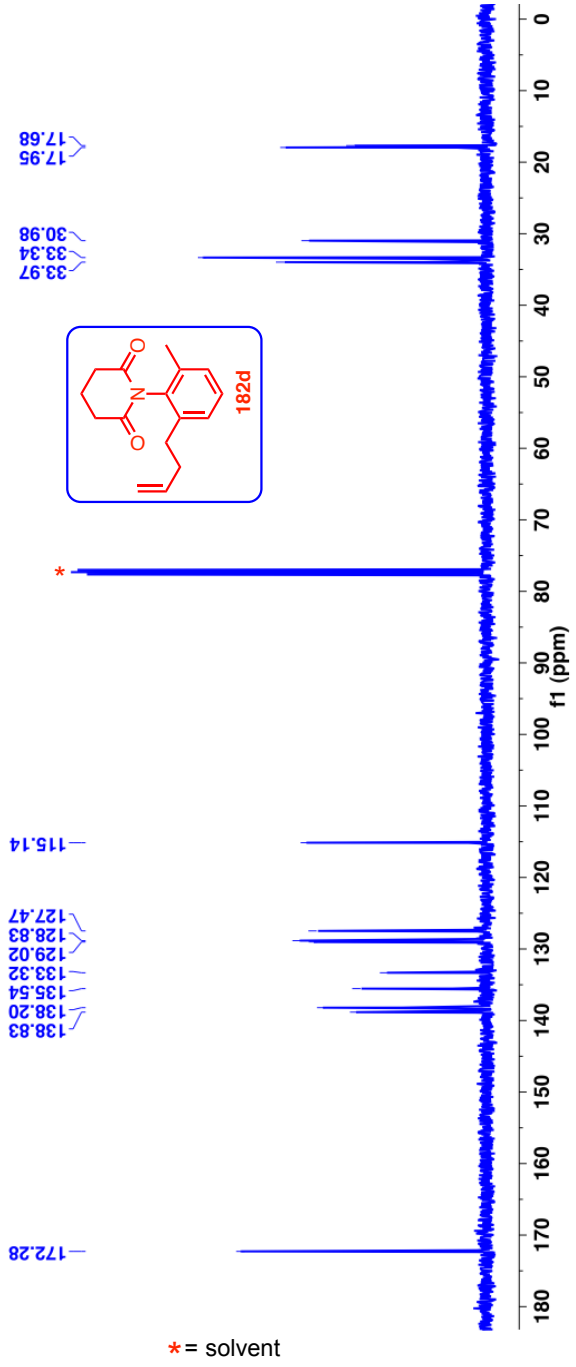

Figure 3.53: ^{13}C-NMR (100 MHz, $CDCl_3$, δ ppm) of 2-butenyl-glutarimide derivative **182d**.

HRMS-ESI (m/z) ([M + Na]$^+$):

Calculated : 280.1308

Observed : 280.1312

|Δm| : 1.4 ppm

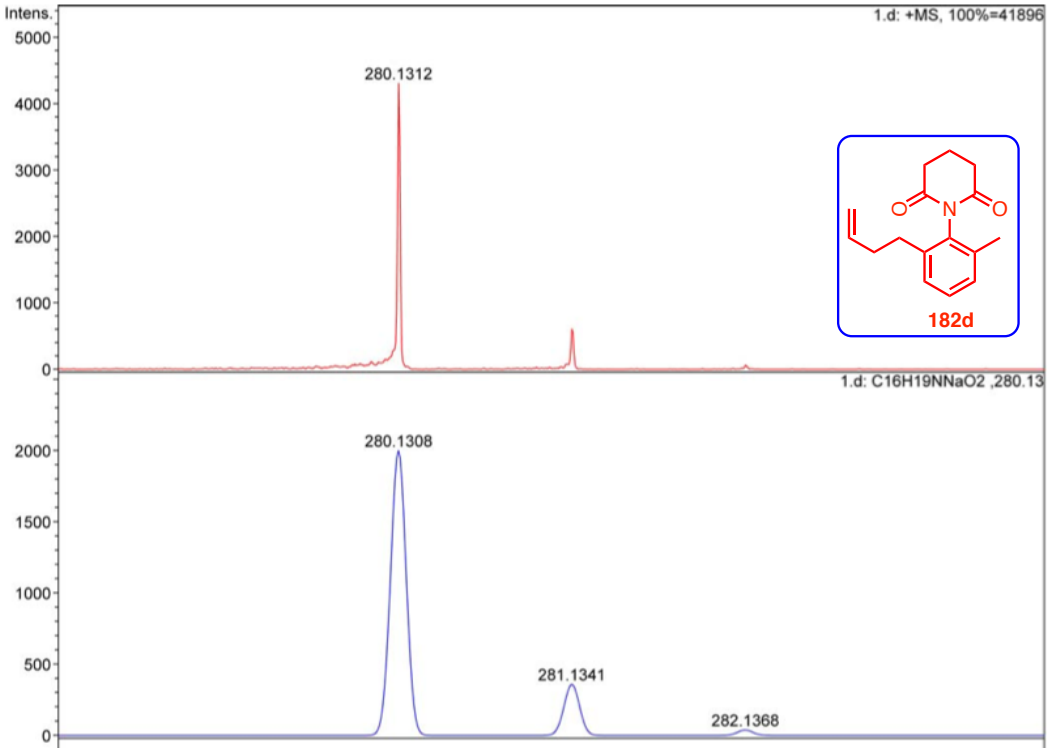

Figure 3.54: HRMS of 6-butenyl-glutarimide derivative **182d**.

3.11.2. Synthesis pyrrolidine-2,5-dione derivatives 182-185

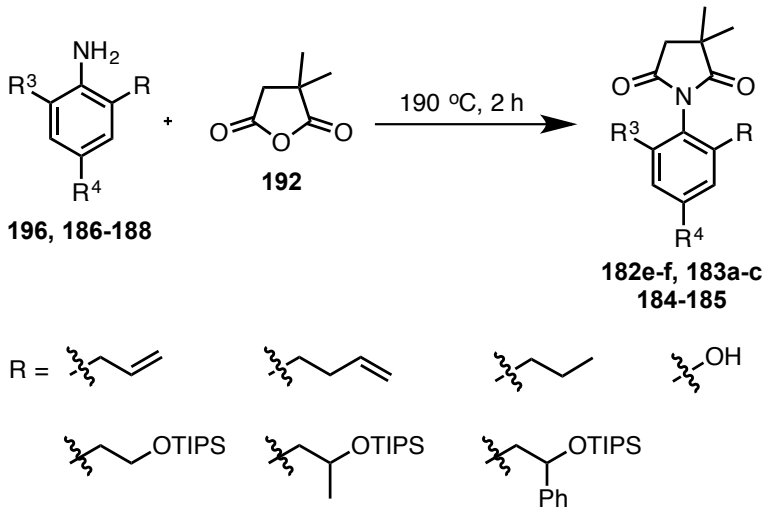

Scheme 3.29: Synthesis of pyrrolidine-2,5-dione derivatives **182-185**.

A mixture of aniline **196, 186-188** (1.0 g, 6.79 mmol) and 2,2-dimethylsuccinicanhydride **192** (1.1 *equiv*, 7.45 mmol) in a round bottom flask was heated to 190 ^{o}C and maintained for 2 h. After the reaction, the mixture was cooled to room temperature and the residue was purified by combiflash using hexanes and ethyl acetate mixtures (90:10).

R*f* = 0.85 (80% hexanes:20% ethyl acetate) for **182e** (Yield = 80%).

^{1}H-NMR (400 MHz, $CDCl_3$, δ ppm): 7.27-7.23 (m, 1H), 7.16-7.12 (m, 2H), 5.84-5.74 (m, 1H), 5.03-4.97 (m, 2H), 3.18 (d, *J*=6.8 Hz, 2H), 2.71 (s, 2H), 2.08 (s, 3H), 1.421 (s, 3H) and 1.416 (s, 3H).

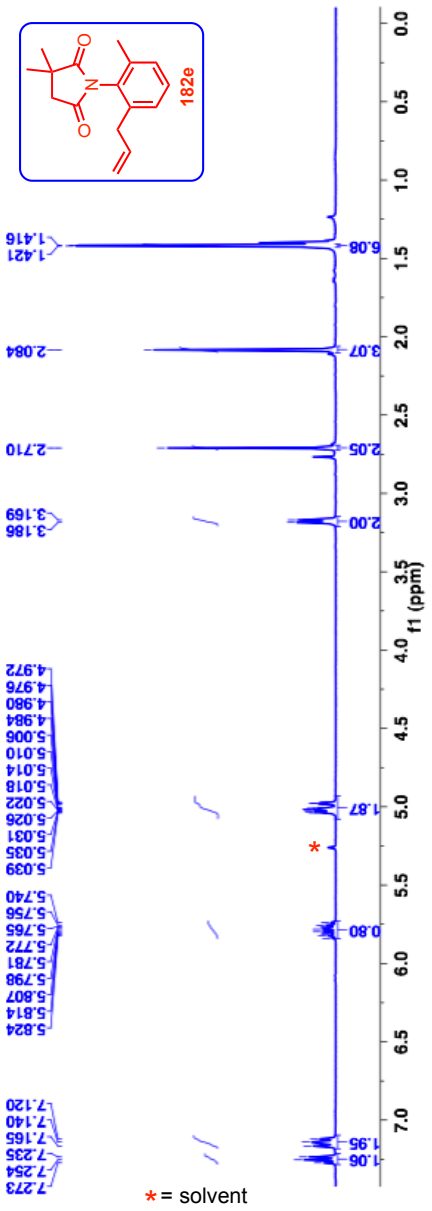

Figure 3.55: ^{1}H-NMR (400 MHz, $CDCl_3$, δ ppm) of 6-methyl-2-allyl-succinimide derivative **182e**.

^{13}C-NMR (100 MHz, $CDCl_3$, δ ppm): 182.2, 175.03, 137.97, 137.2, 136.2, 136.1, 130.3, 129.8, 129.4, 128.3, 116.6, 44.2, 40.8, 36.5, 26.4, 25.6, and 17.9.

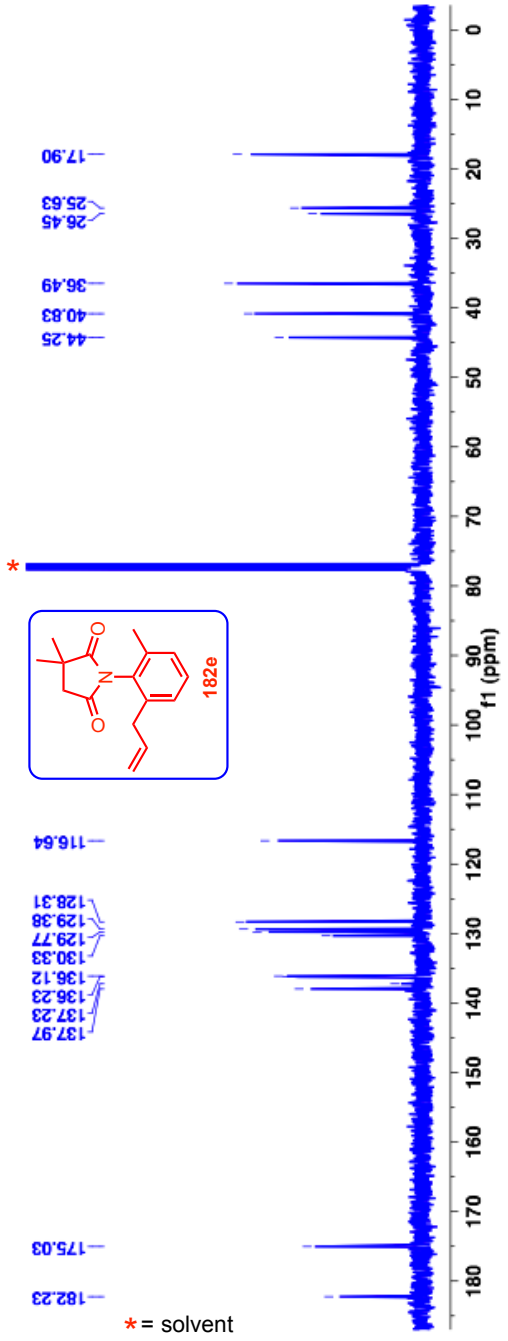

Figure 3.56: ^{13}C-NMR (100 MHz, $CDCl_3$, δ ppm) of 6-methyl-2-allyl-succinimide derivative **182e**.

HRMS-ESI (m/z) ([M + Na]$^+$):

Calculated : 280.1308

Observed : 280.1310

|Δm| : 0.7 ppm

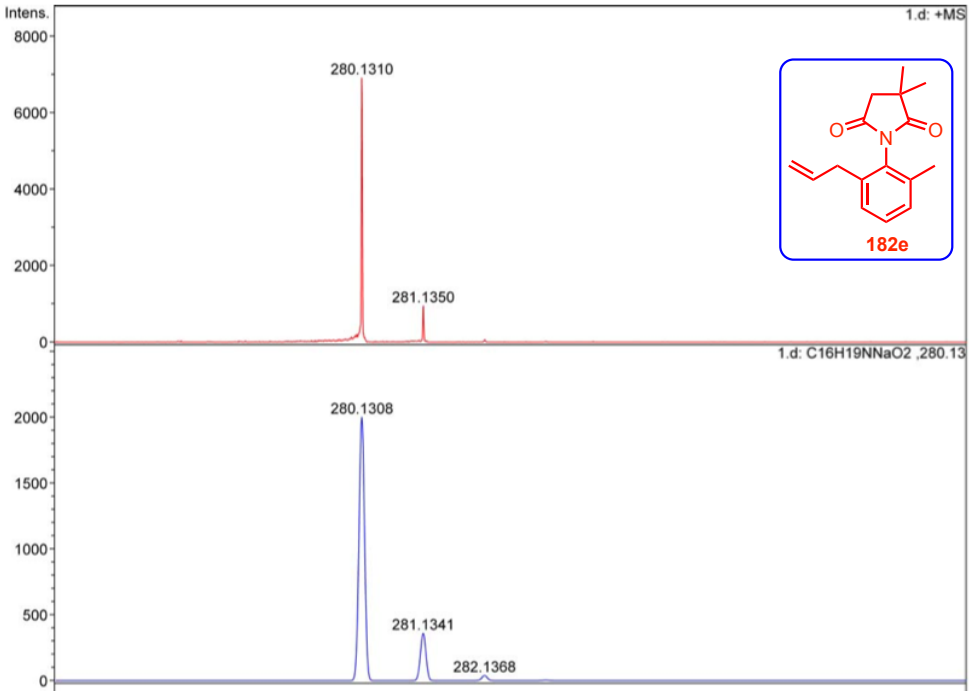

Figure 3.57: HRMS of 6-methyl-2-allyl-succinimide derivative **182e**.

R*f* = 0.85 (80% hexanes:20% ethyl acetate) for **182f** (Yield = 83%).

^{1}H-NMR (400 MHz, $CDCl_3$, δ ppm): 7.27-7.24 (m, 1H), 7.15-7.13 (m, 2H), 5.83-5.73 (m, 1H), 5.01-4.93 (m, 2H), 2.74 (s, 2H), 2.47-2.43 (m, 2H), 2.23-2.19 (m, 2H), 2.08 (m, 3H), 1.437 (s, 3H) and 1.43 (s, 3H).

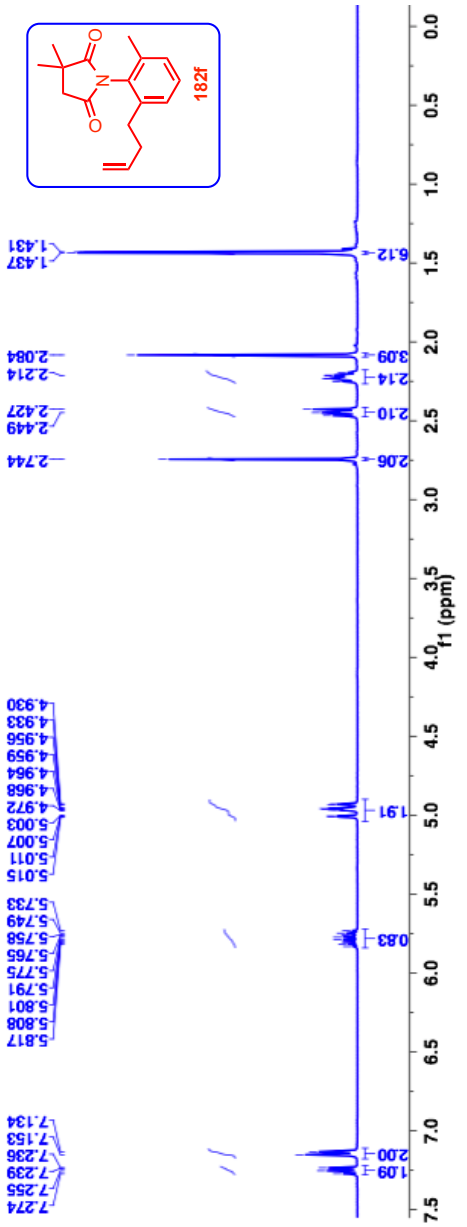

Figure 3.58: ^{1}H-NMR (400 MHz, $CDCl_3$, δ ppm) of 6-butenyl-succinimide derivative **182f**.

^{13}C-NMR (100 MHz, $CDCl_3$, δ ppm): 182.52, 175.2, 139.7, 137.9, 136.1, 130.1, 129.7, 129.0, 127.8, 115.2, 44.3, 40.8, 34.4, 31.2, 26.2, 25.95 and 17.95.

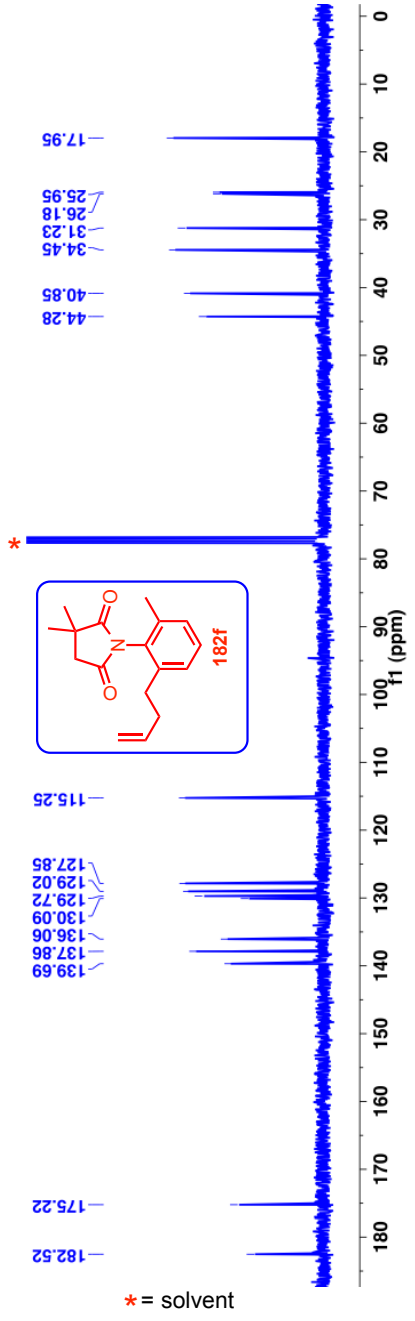

Figure 3.59: ^{13}C-NMR (100 MHz, $CDCl_3$, δ ppm) of 6-butenyl-succinimide derivative **182f**.

HRMS-ESI (m/z) ([M + Na]$^+$):

Calculated : 294.1465

Observed : 294.1463

|Δm| : 0.7 ppm

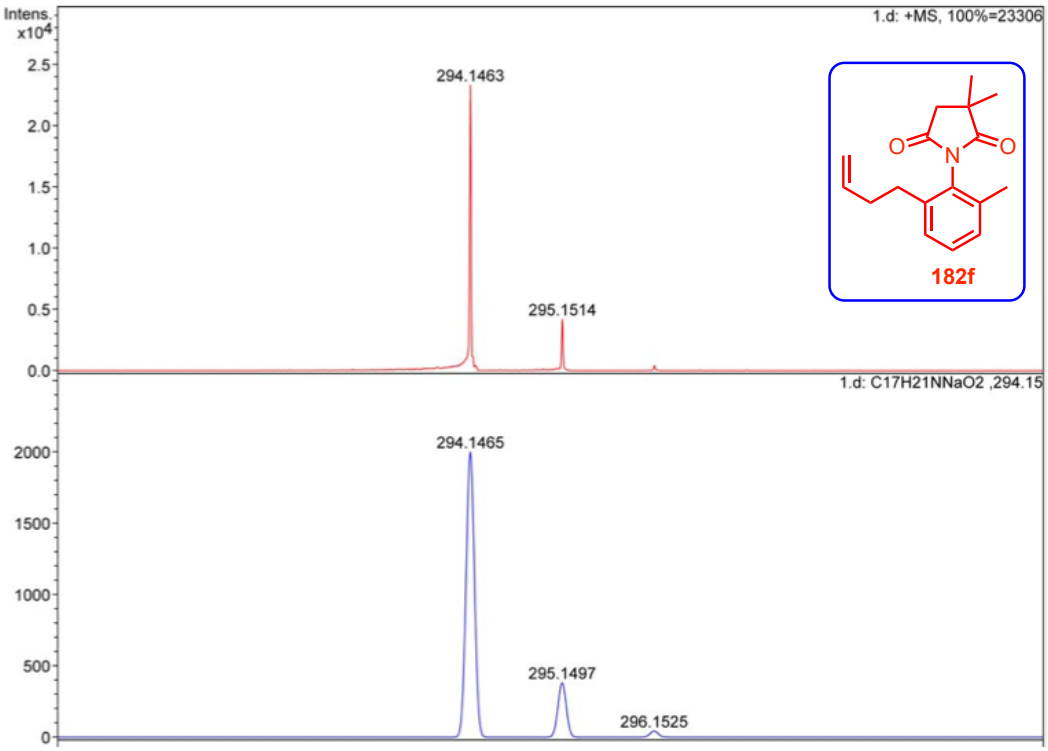

Figure 3.60: HRMS of 6-butenyl-succinimide derivative **182f**.

R*f* = 0.85 (80% hexanes:20% ethyl acetate) for **184** (Yield = 74%).

^{1}H-NMR (400 MHz, $CDCl_3$, δ ppm): 7.25 (bs, 1H), 7.01-6.97 (m, 1H), 6.74-6.71 (m, 1H), 6.54-6.52 (m, 1H), 2.61 (s, 2H), 2.03 (s, 3H), 1.35 (s, 3H) and 1.28 (s, 3H).

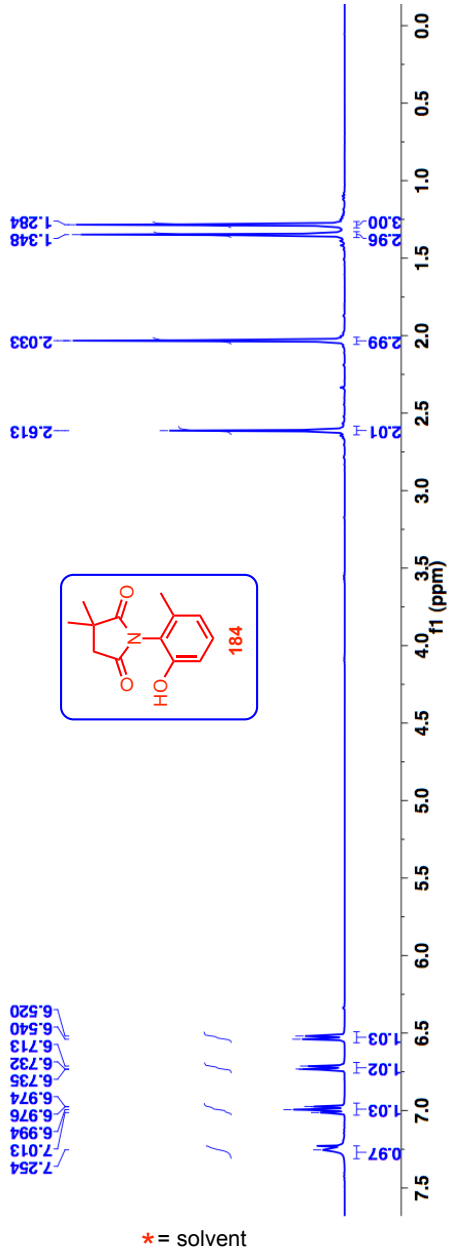

Figure 3.61: ^{1}H-NMR (400 MHz, $CDCl_3$, δ ppm) of 6-hydroxy-succinimide derivative **184**.

^{13}C-NMR (100 MHz, $CDCl_3$, δ ppm): 183.4, 176.5, 152.5, 137.3, 130.4, 122.1, 118.6, 114.4, 43.9, 40.96, 26.2, 25.3 and 17.6.

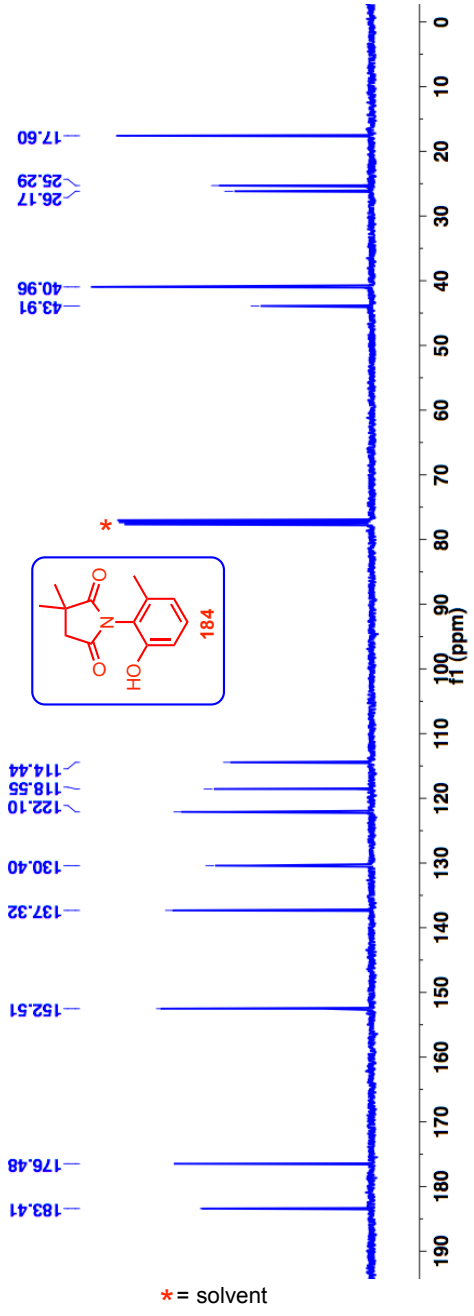

Figure 3.62: ^{13}C-NMR (100 MHz, $CDCl_3$, δ ppm) of 6-hydroxy-succinimide derivative **184**.

HRMS-ESI (m/z) ([M + Na]$^+$):

Calculated : 256.0944

Observed : 256.0949

|Δm| : 1.9 ppm

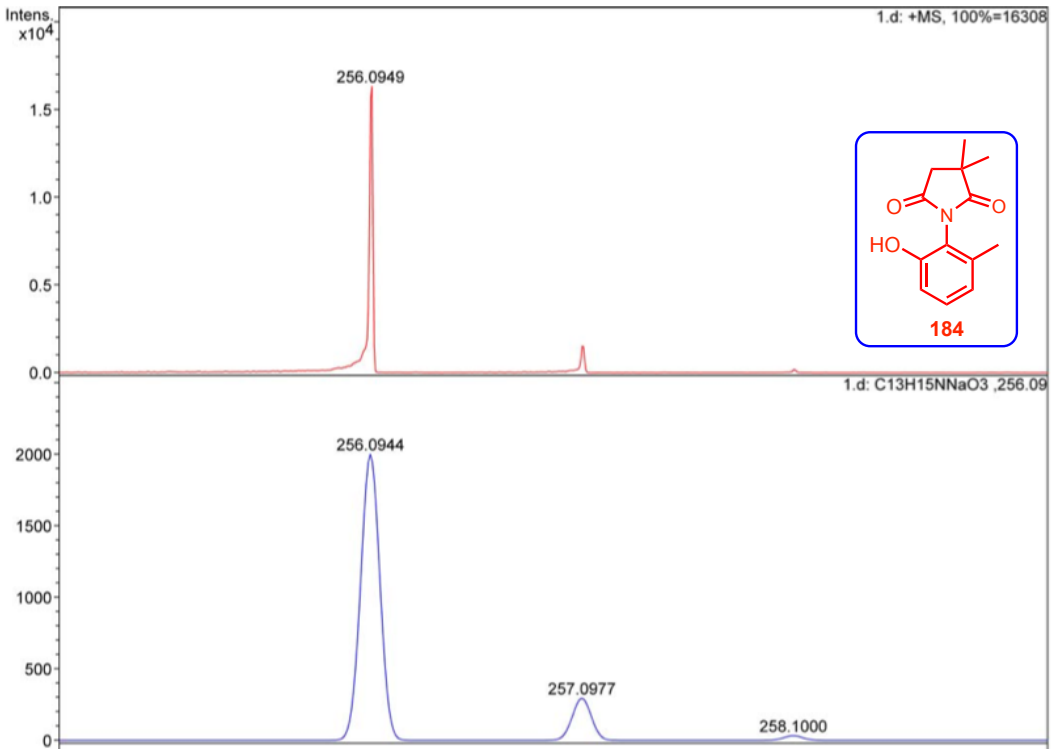

Figure 3.63: HRMS of 6-hydroxy-succinimide derivative **184**.

R*f* = 0.85 (80% hexanes:20% ethyl acetate) for **183a** (Yield = 84%).

^{1}H-NMR (400 MHz, $CDCl_3$, δ ppm): 7.41-7.24 (m, 3H), 7.04-7.02 (m, 1H), 3.78-3.75 (t, *J*= 7.6 Hz), 2.72 (s, 2H), 2.68-2.62 (m, 2H), 1.43 (s, 3H), 1.41 (s, 3H) and 1.08-0.97 (m, 21H).

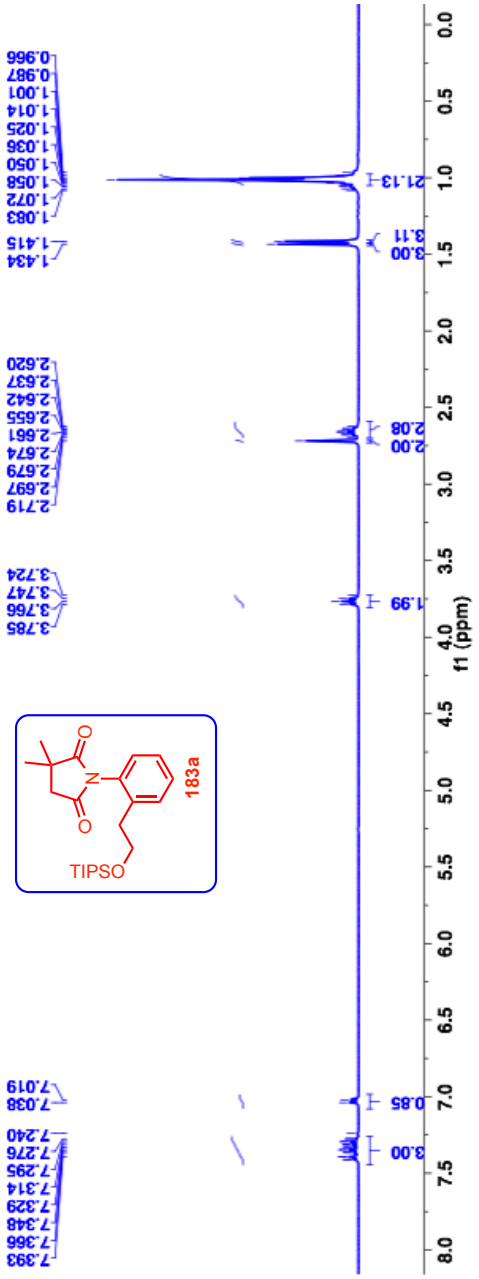

Figure 3.64: ^{1}H-NMR (400 MHz, $CDCl_3$, δ ppm) of 6-silyloxyethyl-succinimide derivative **183a**.

^{13}C-NMR (100 MHz, $CDCl_3$, δ ppm): 182.7, 175.3, 136.9, 131.3, 129.6, 128.6, 127.7, 63.6, 44.2, 40.8, 35.3, 26.2, 25.6, 18.2 and 12.1.

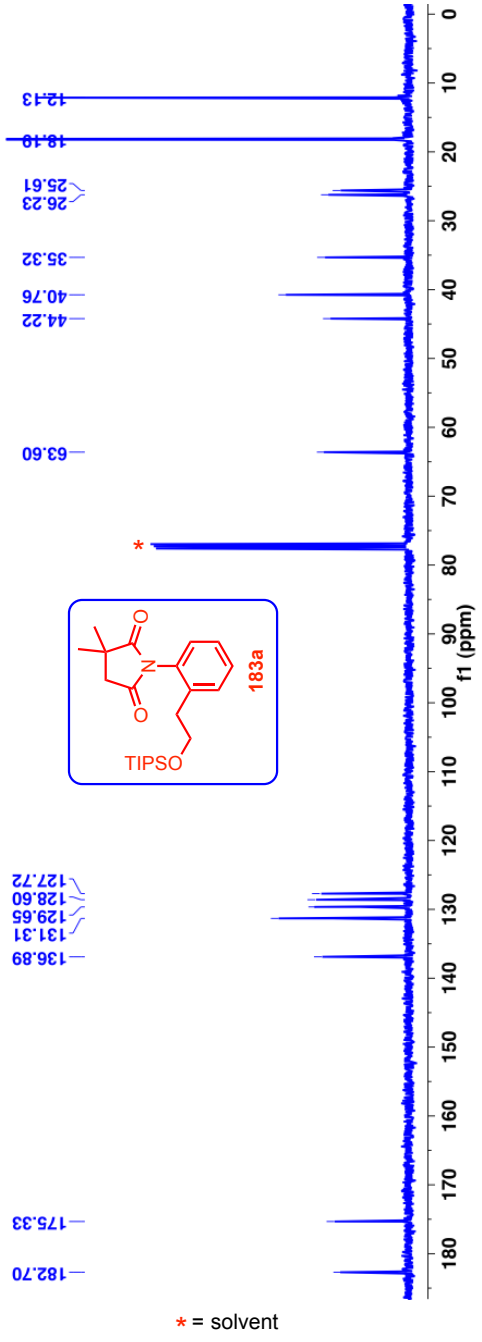

Figure 3.65: ^{13}C-NMR (100 MHz, $CDCl_3$, δ ppm) of 6-silyloxyethyl-succinimide derivative **183a**.

HRMS-ESI (m/z) ([M + Na]$^+$):

Calculated : 426.2435

Observed : 426.2428

|Δm| : 1.6 ppm

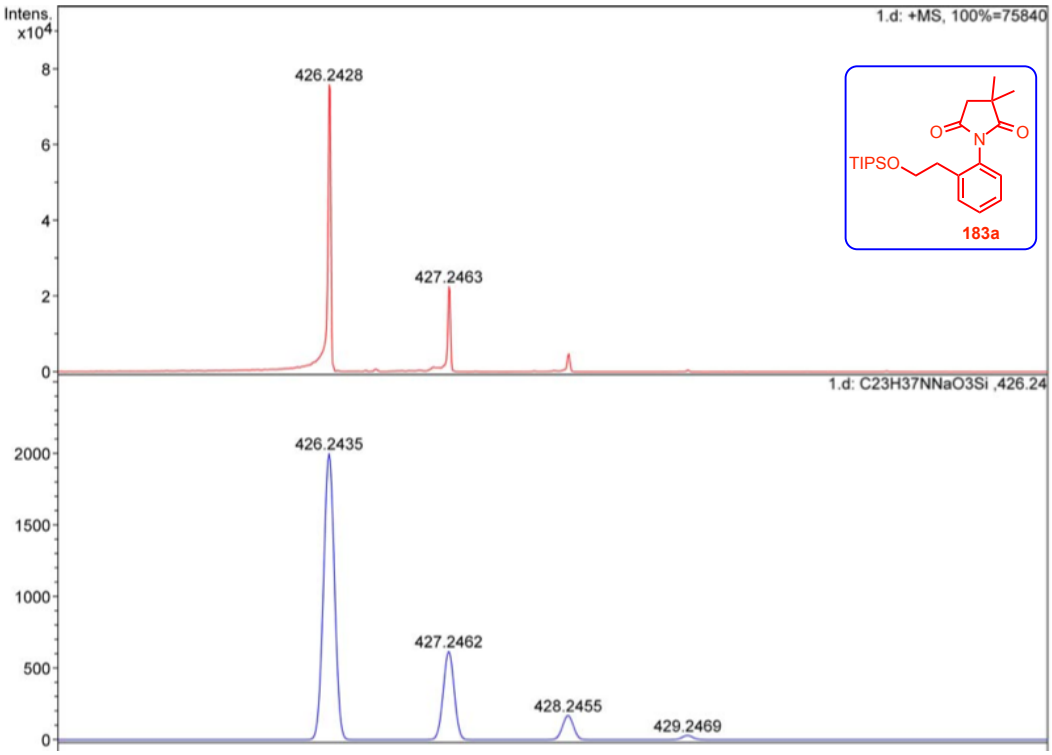

Figure 3.66: HRMS of 6-silyloxyethyl-succinimide derivative **183a**.

R*f* = 0.80 (50% hexanes:50% ethyl acetate) for **183b** (Yield = 90%).

^{1}H-NMR (400 MHz, $CDCl_3$, δ ppm): 7.39-7.25 (m, 3H), 7.01-6.99 (m, 1H), 4.1, 3-4.03 (m, 1H), 2.77-2.70 (m, 3H), 2.46-2.39 (m, 1H), 1.42 (d, J = 4.3 Hz, 3H), 1.40 (d, J = 2.6 Hz, 3H) and 1.00 (m, 24H).

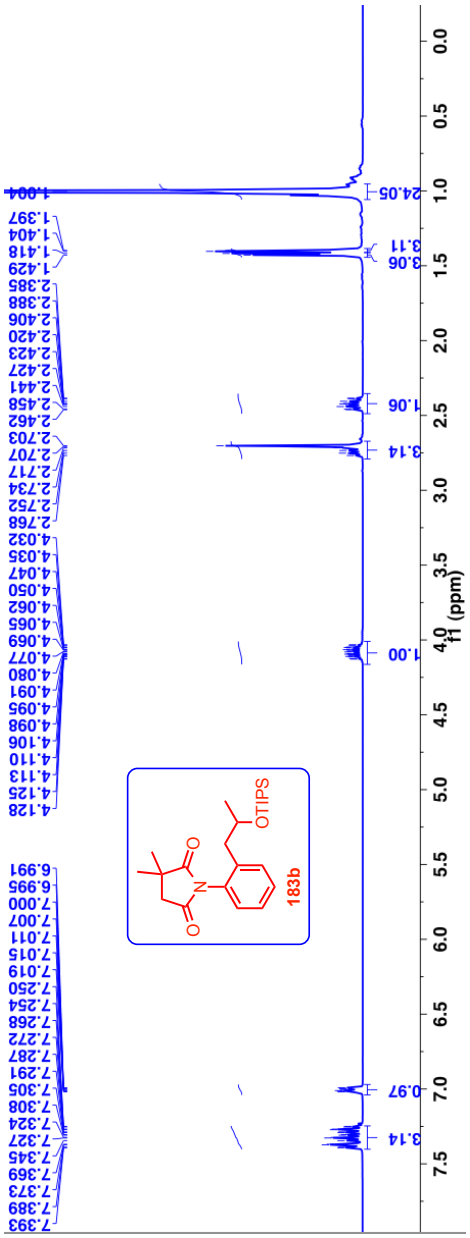

Figure 3.67: ^{1}H-NMR (400 MHz, $CDCl_3$, δ ppm) of 6-silyloxypropyl-succinimide derivative **183b**.

^{13}C-NMR (100 MHz, $CDCl_3$, δ ppm): 182.6, 182.5, 175.2, 175.1, 137.3, 137.2, 131.8, 131.5, 131.46, 129.5, 129.4, 128.6, 128.5, 127.6, 127.5, 69.3, 69.1, 44.2, 44.17, 41.9, 41.7, 40.7, 40.66, 26.2, 26.08, 25.8, 25.7, 23.9, 23.8, 18.3, 18.26, 12.7 and 12.66.

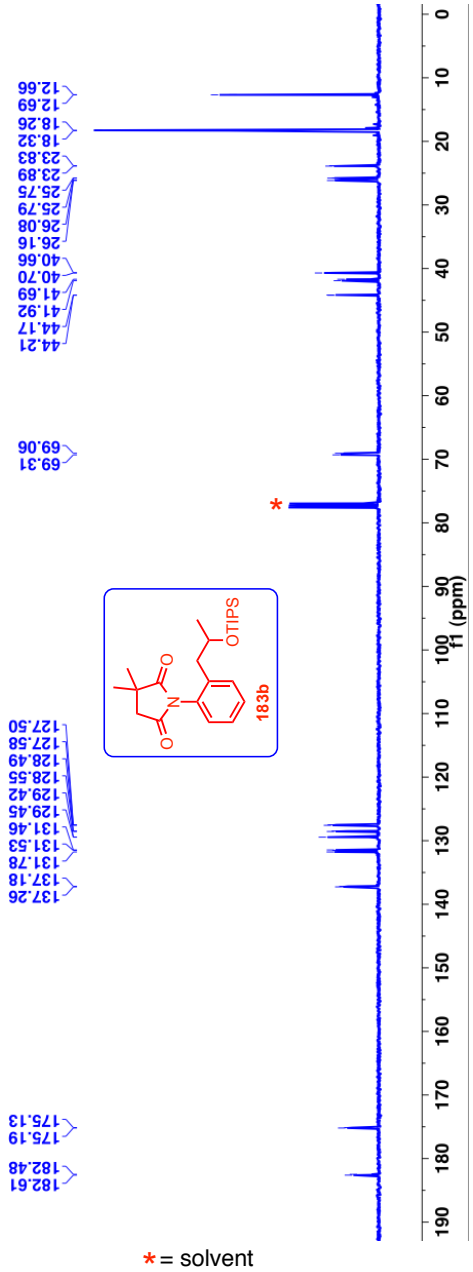

Figure 3.68: ^{13}C-NMR (100 MHz, $CDCl_3$, δ ppm) of 6-silyloxypropyl-succinimide derivative **183b**.

HRMS-ESI (m/z) ([M + Na]$^+$):

Calculated : 440.2591

Observed : 440.2584

|Δm| : 1.6 ppm

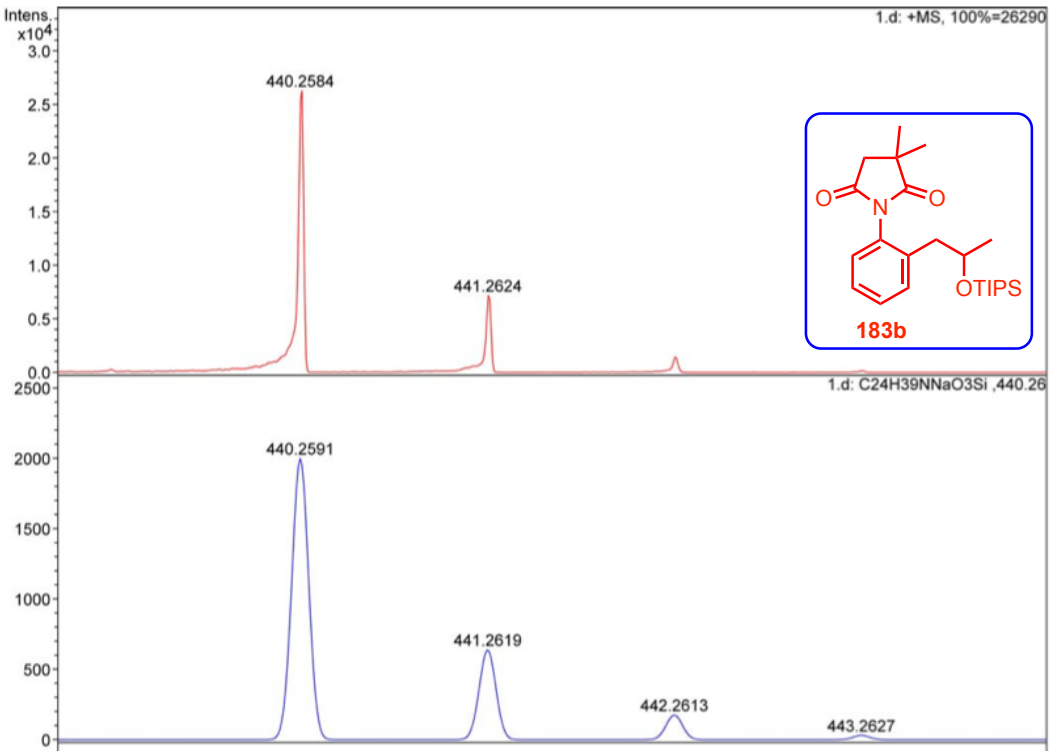

Figure 3.69: HRMS of 6-silyloxypropyl-succinimide derivative **183b**.

R*f* = 0.65 (80% hexanes:20% ethyl acetate) for **183c** (Yield = 62%).

^{1}H-NMR (400 MHz, $CDCl_3$, δ ppm): 7.24-7.08 (m, 11H), 6.94 (s, 1H), 6.90 (s, 1H), 6.88 (s, 1H), 5.95 (d, *J* = 4.8 Hz, 1H), 5.50 (d, *J* = 4.8 Hz, 1H), 5.32 (dd, *J* = 9.4, 4.8 Hz, 2H), 4.94 (t, *J* = 5.8 Hz, 1H), 4.79 (t, *J* = 6.8 Hz, 1H), 2.97 (dd, *J* = 13.6, 7.0 Hz, 1H), 2.74 (d, *J* = 5.8 Hz, 2H), 2.66 (dd, *J* = 13.4, 6.9 Hz, 1H), 2.27 (s, 3H), 2.26 (s, 3H), 2.04 (s, 3H), 1.99 (s, 3H), 1.27 (s, 6H), 1.23 (s, 3H), 1.22 (s, 3H), 0.91-0.86 (m, 32H) and 0.80-0.79 (m, 10H).

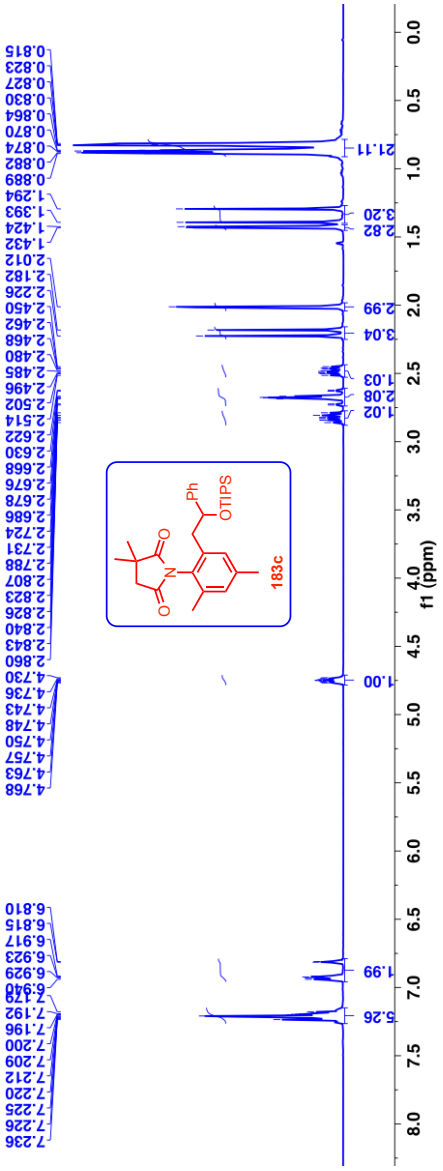

Figure 3.70: ^{1}H-NMR (400 MHz, $CDCl_3$, δ ppm) of 6-silyloxyphenethyl-succinimide **183c**.

^{13}C-NMR (100 MHz, $CDCl_3$, δ ppm): 182.1, 181.9, 145.96, 145.4, 137.9, 137.5, 137.0, 136.99, 136.1, 132.3, 132.1, 132.0, 131.7, 130.8, 130.5, 129.9, 129.8, 128.1, 128.0, 127.3, 127.2, 126.5, 126.4, 117.2, 117.15, 76.7, 75.9, 46.1, 45.97, 43.73, 42.7, 24.1, 23.9, 23.7, 23.4, 18.2, 18.13, 18.10, 18.04, 17.9, 12.5 and 12.5.

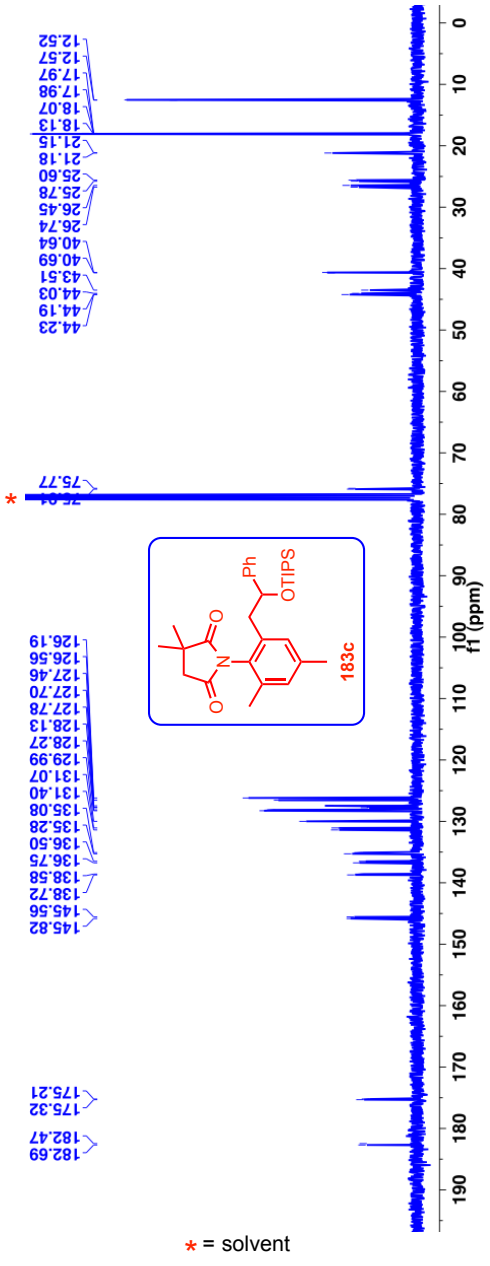

Figure 3.71: ^{13}C-NMR (100 MHz, $CDCl_3$, δ ppm) of 6-silyloxyphenethyl-succinimide **183c**.

HRMS-ESI (m/z) ([M + Na]$^+$):

Calculated : 530.3061

Observed : 530.3056

|Δm| : 0.9 ppm

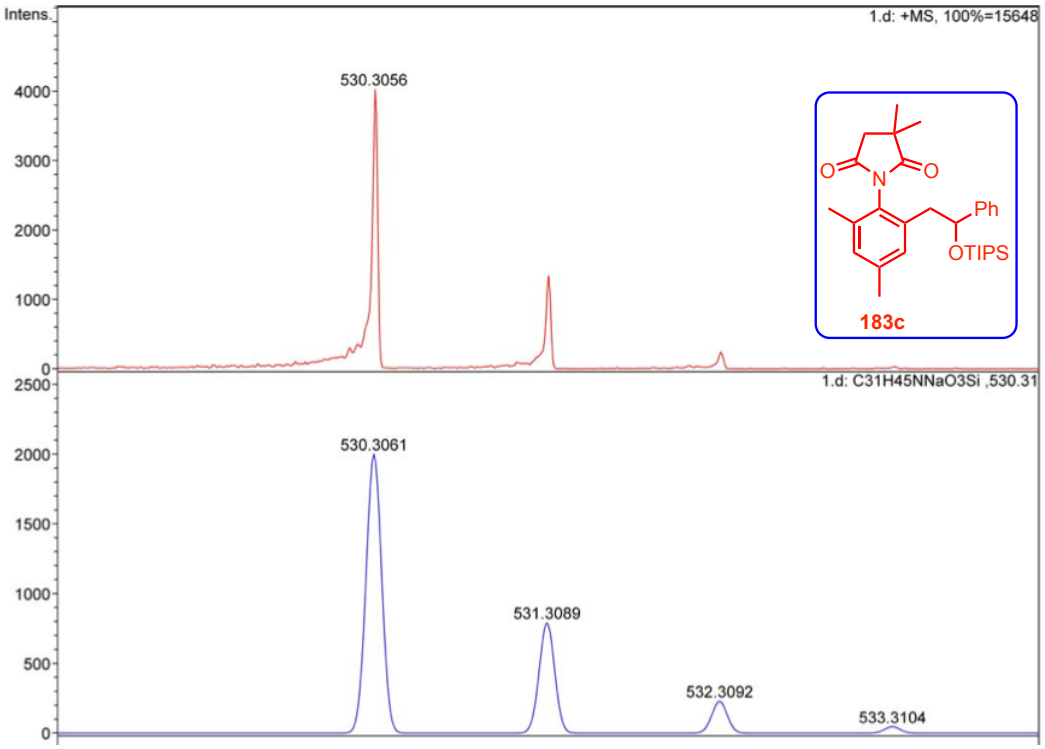

Figure 3.72: HRMS of 6-silyloxyphenethyl-succinimide **183c**.

R*f* = 0.85 (80% hexanes:20% ethyl acetate) for **185** (Yield = 60%).

^{1}H-NMR (400 MHz, $CDCl_3$, δ ppm): 6.95 (s, 2H), 2.78 (s, 2H), 2.28 (d, *J* = 8.4 Hz, 5H), 2.04 (s, 3H), 1.54-1.45 (m, 2H), 1.42 (s, 3H), 1.41 (s, 3H) and 0.89 (t, *J* = 7.3 Hz, 3H).

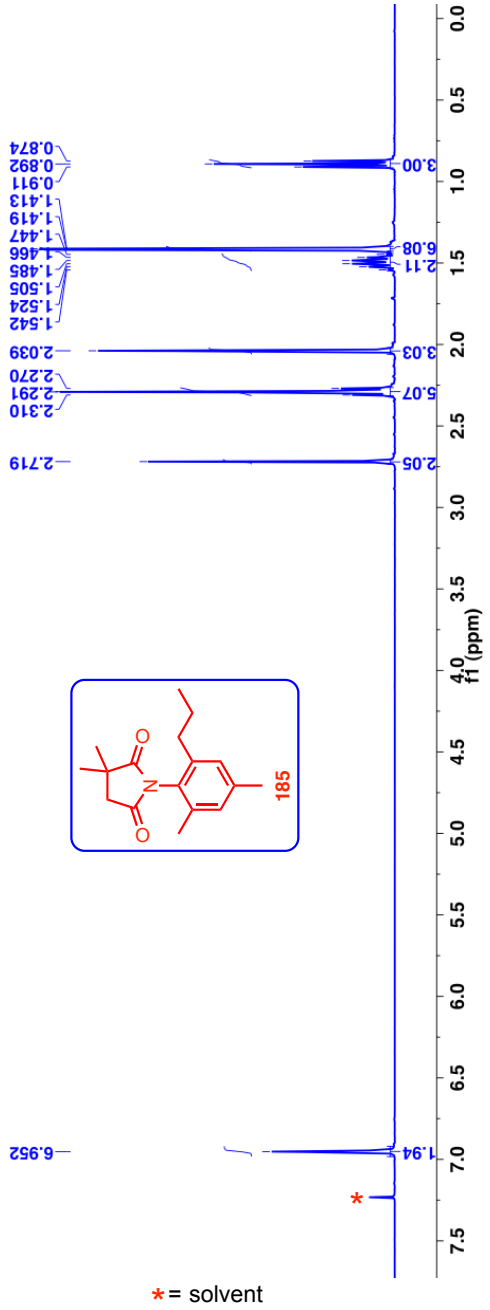

Figure 3.73: ^{1}H-NMR (400 MHz, $CDCl_3$, δ ppm) of 6-ethyl-succinimide derivative **185**.

^{13}C-NMR (100 MHz, $CDCl_3$, δ ppm): 182.6, 175.4, 140.0, 139.4, 135.6, 129.7, 128.7, 127.4, 44.2, 40.8, 34.0, 26.2, 25.9, 23.7, 21.4, 17.8 and 14.4

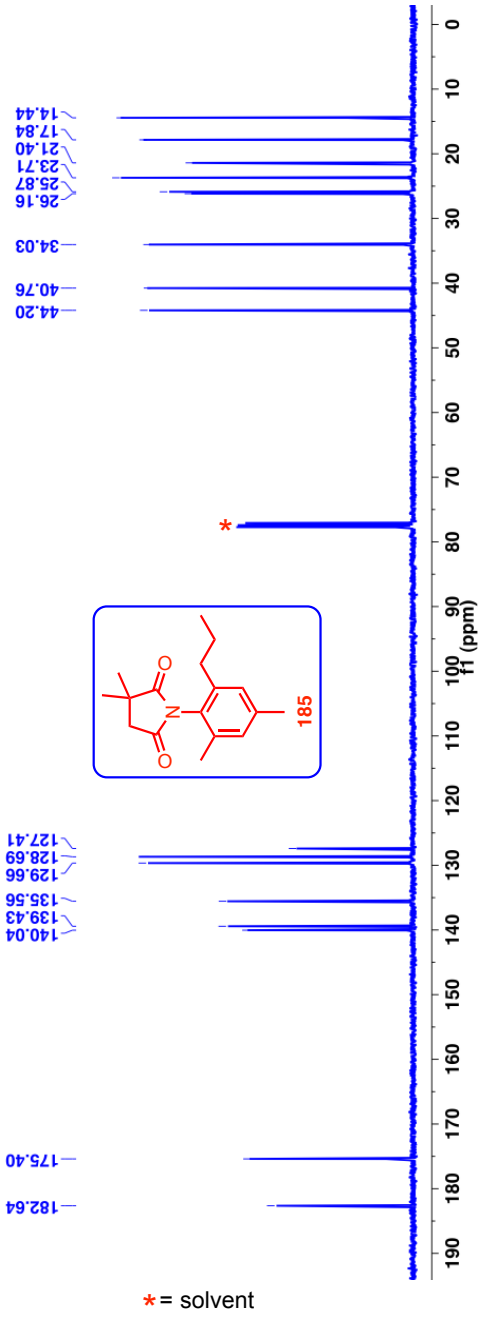

Figure 3.74: ^{13}C-NMR (100 MHz, $CDCl_3$, δ ppm) of 6-ethyl-succinimide derivative **185**.

HRMS-ESI (m/z) ([M + Na]$^+$):

Calculated : 296.1621

Observed : 296.1624

|Δm| : 1.0 ppm

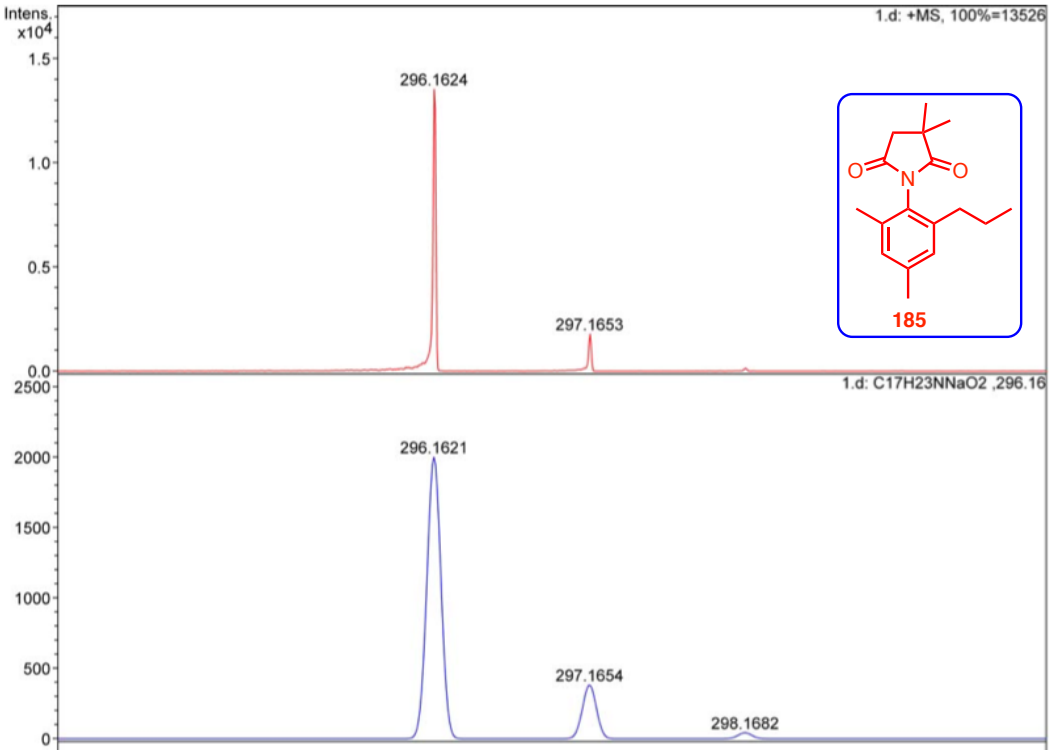

Figure 3.75: HRMS of 6-ethyl-succinimide derivative **185**.

3.11.3. Synthesis of 2-methyl-6-allyloxy-pyrrolidine-2,5-dione derivative 182g

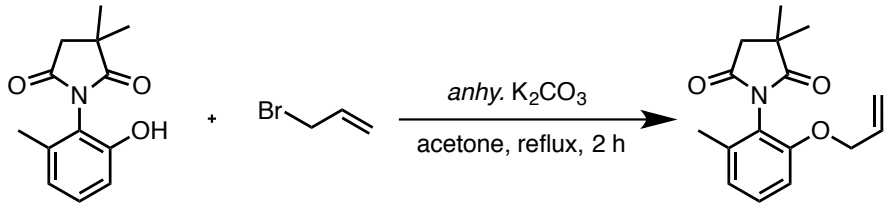

184 **182g**

Scheme 3.30: Synthesis of 2-methyl-6-allyloxy-pyrrolidine-2,5-dione derivative **182g.**

To a solution imide derivative **184** (1.0 g, 4.29 mmol) and *anhyd.* potassium carbonate (1.78 g, 12.87 mmol) in dry acetone (15 mL) at room temperature under N_2 atmosphere allyl bromide (0.94 mL, 10.75 mmol) was added. The resulting mixture was refluxed for 2 h. After the reaction, the mixture was cooled to room temperature and the solid was filtered and the solid was washed with acetone (10 mL). The combined organic layer was concentrated under reduced pressure to get the crude product. The crude product was purified by combiflash using hexanes: ethyl acetate mixture.

R*f* = 0.70 (50% hexanes:50% ethyl acetate) for **182g** (Yield = 82%).

^{1}H-NMR (400 MHz, $CDCl_3$, δ ppm): 7.22-7.18 (m, 1H), 6.86-6.84 (m, 1H), 6.77-6.75 (m, 1H), 5.93-5.83 (m, 1H), 5.29-5.24 (m, 1H), 5.18-5.15 (m, 1H), 4.44 (dt, *J* = 5.3, 1.6 Hz, 2H), 2.68 (s, 2H), 2.09 (s, 3H), 1.39 (s, 3H) and 1.38 (s, 3H).

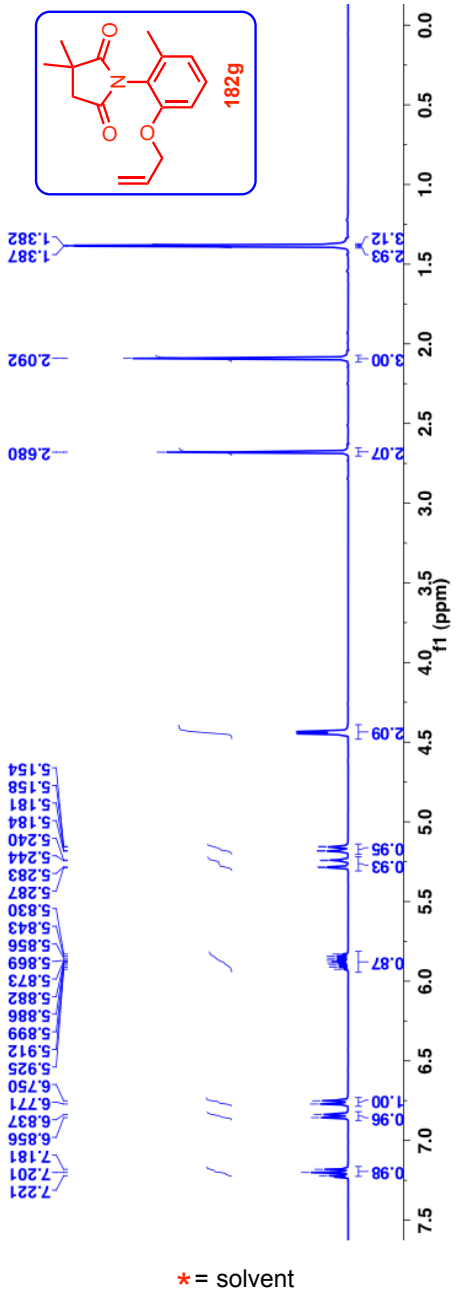

Figure 3.76: ^{1}H-NMR (400 MHz, $CDCl_3$, δ ppm) of 6-allyloxy-succinimide derivative **182g**.

^{13}C-NMR (100 MHz, $CDCl_3$, δ ppm): 182.3, 175.0, 154.1, 137.8, 132.9, 130.2, 122.9, 120.6, 117.8, 110.8, 69.4, 44.2, 40.9, 26.1, 25.8 and 17.6.

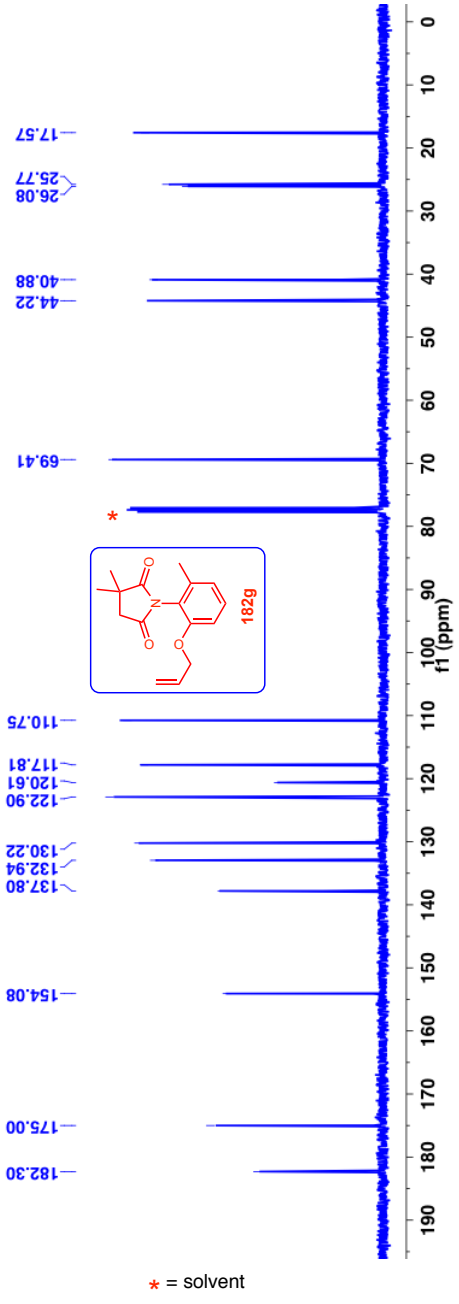

Figure 3.77: ^{13}C-NMR (100 MHz, $CDCl_3$, δ ppm) of 6-allyloxy-succinimide derivative **182g**.

HRMS-ESI (m/z) ([M + Na]$^+$):

Calculated : 296.1257

Observed : 296.1246

|Δm| : 3.7 ppm

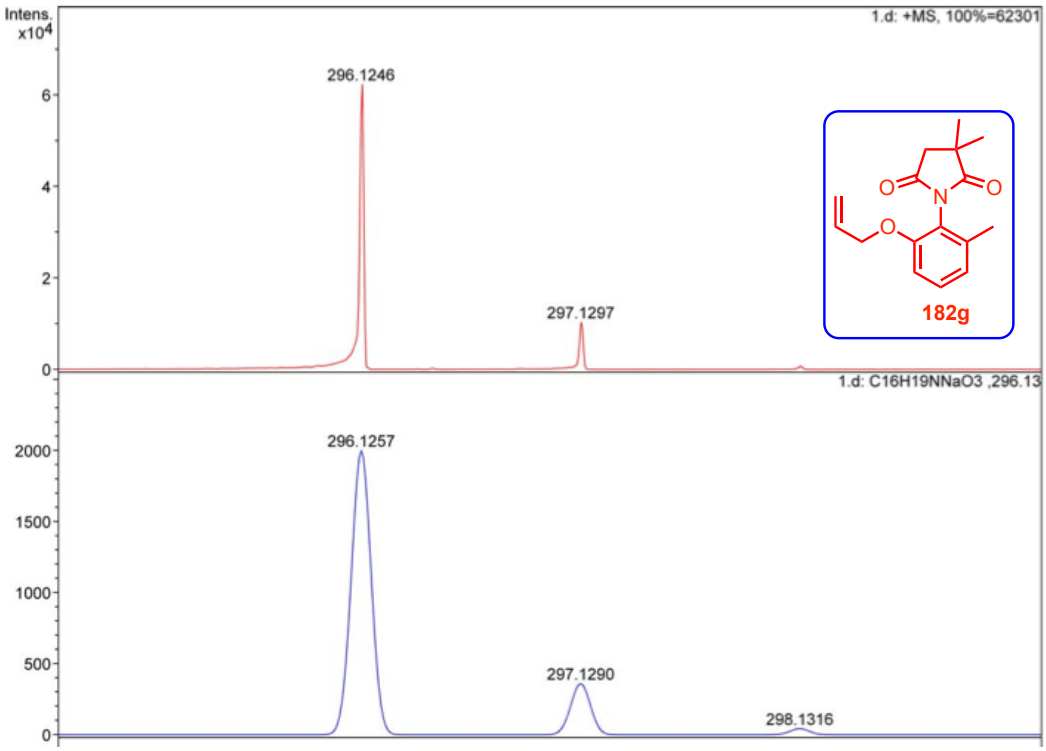

Figure 3.78: HRMS of 6-allyloxy-succinimide derivative **182g**.

3.11.4. Synthesis of atropisomeric enamide derivatives 174a-g

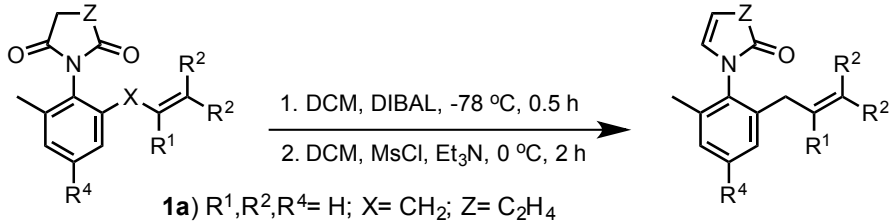

182a-g

1a) R^1,R^2,R^4= H; X= CH_2; Z= C_2H_4
1b) R^1,R^4 = H; R^2= CH_3; X= CH_2; Z= C_2H_4
1c) R^1,R^4= CH_3; R^2= H; X= CH_2; Z= C_2H_4
1d) R^1,R^2,R^4= H; X,Z= C_2H_4
1e) R^1,R^2,R^4= H; X= CH_2; Z = CMe_2
1f) R^1,R^2,R^4= H; X= C_2H_4; Z = CMe_2
1g) R^1,R^2,R^4= H; X= OCH_2; Z = CMe_2

174a-g

Scheme 3.31: Synthesis of atropisomeric enamide derivatives **174a-g**.

To a solution of corresponding piperidine-2,6-dione derivative **182a-g** (7.6 mmol) in DCM (25 mL) under N_2 atmosphere at -78 ^oC was added DIBAL (25% Wt/Wt in hexanes, 13.7 mmol). The mixture was stirred at -78 ^oC for 30 mins. The reaction mixture was quenched with DI water (10 mL) followed by the addition of *aq.* 2N NaOH solution (10 mL). The reaction mixture was slowly warmed to room temperature and the mixture was poured into saturated solution of Rochelle's salt (sodium potassium tartarate, 200 mL). The aqueous layer was extracted with DCM (3 X 75 mL). The combined organic layer was dried over *anhyd.* Na_2SO_4, filtered and the solvent was evaporated under reduced pressure to get the crude product. The crude product was directly taken to next step without further purification.

To the crude product from above reaction dissolved in DCM (75 mL) at 0 ^oC under N_2 atmosphere was added methanesulfonyl chloride (12.16 mmol) and triethylamine (22.8 mmol). The resulting solution was stirred at 0 ^oC for 2 h. After the reaction, DI water (50 mL) was added and the mixture was stirred for 10 mins and the layers were separated. The aqueous layer was extracted with of DCM (2 X 20 mL). The combined organic layer was dried over *anhyd.* Na_2SO_4, filtered and the solvent was evaporated under reduced pressure to get the crude product. The crude product was purified by combiflash using hexanes:ethyl acetate mixture (80:20) to get the title product **1** in 65% yield over two steps.

Note: The samples turn dark brown over time, so they were stored in amber vials in freezer.

R*f* = 0.40 (50% hexanes:50% ethyl acetate) for **174a**.

^{1}H-NMR (400 MHz, $CDCl_3$, δ ppm): 7.23-7.09 (m, 3H), 5.91-5.81 (m, 2H), 5.26-5.22 (m, 1H), 5.05-5.01 (m, 2H), 3.26-3.24 (m, 2H), 2.68-2.64 (t, *J* = 8 *Hz*, 2H), 2.47-2.43 (m, 2H) and 2.16 (s, 3H).

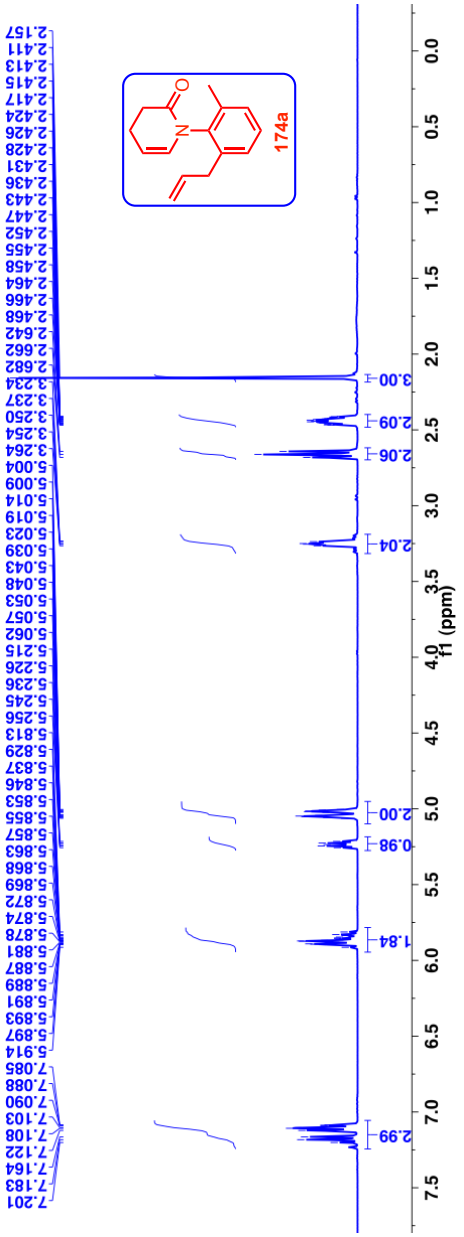

Figure 3.79: ^{1}H-NMR (400 MHz, $CDCl_3$, δ ppm) of 6-allyl-dihydropyridone derivative **174a**.

^{13}C NMR (100 MHz, $CDCl_3$, δ ppm): 168.95, 138.3, 138.0, 136.6, 136.4, 130.9, 129.2, 128.6, 127.98, 116.4, 106.4, 36.1, 31.9, 20.7 and 17.9.

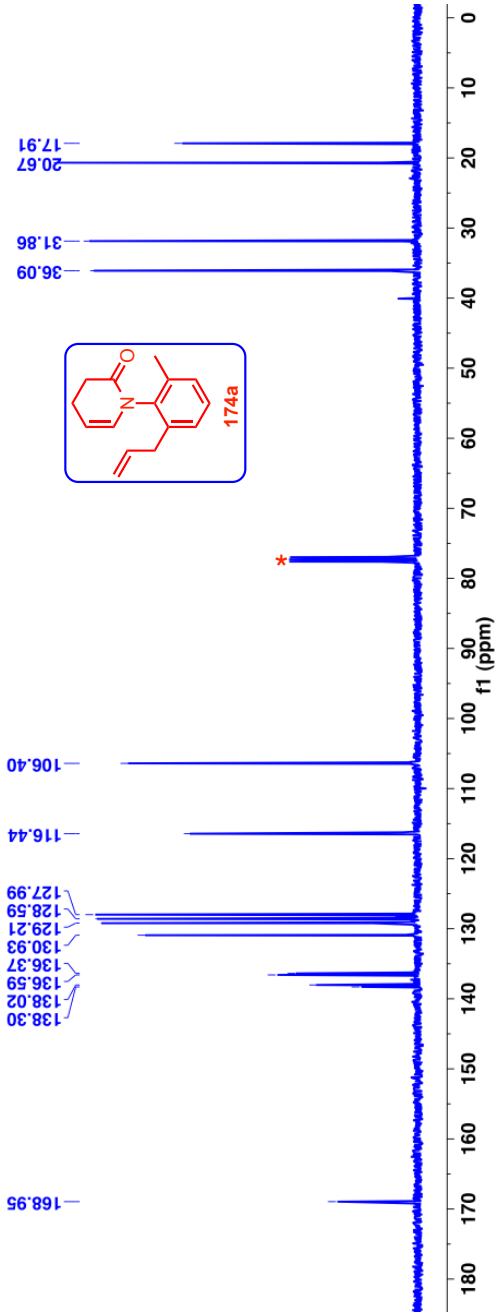

Figure 3.80: ^{13}C-NMR (100 MHz, $CDCl_3$, δ ppm) of 6-allyl-dihydropyridone derivative **174a**.

HRMS-ESI (m/z) ([M + Na]$^+$): Calculated: 250.1202; Observed: 250.1208; |Δm|: 2.4 ppm

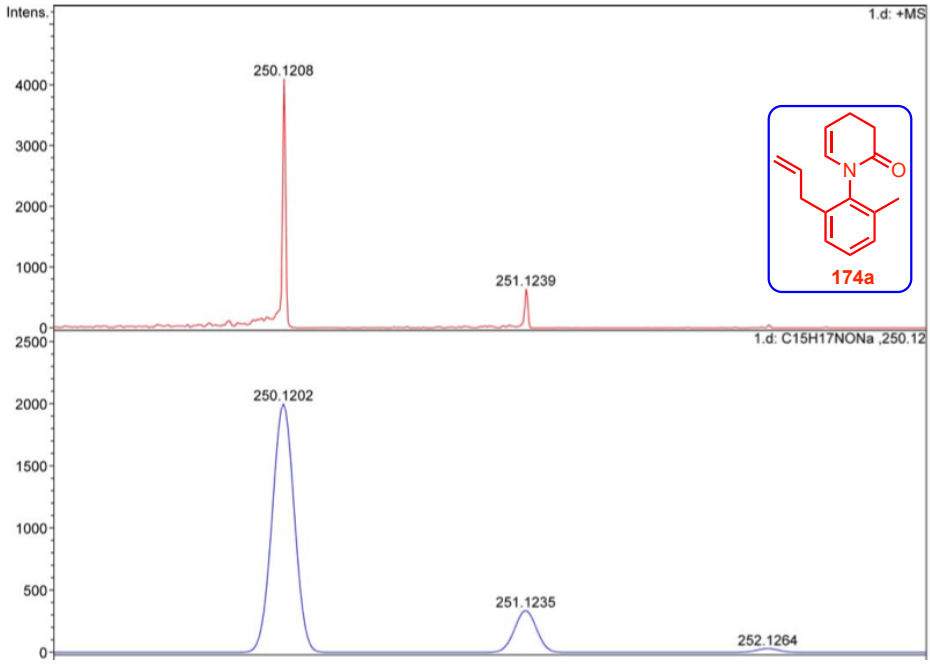

Figure 3.81: HRMS of 6-allyl-dihydropyridone derivative **174a**.

HPLC analysis conditions:

For analytical conditions,

I). Column : RR-WHELK-01 10/100 FEC; Abs. detector wavelength : 254 nm and 270 nm; Mobile phase: Hexanes:2-propanol = 95:5; Flow rate: 1.0 mL/min; Retention times (min): ~ 28.92 [(+)-**174a** and ~ 32.13 [(-)-**174a**]

II). Column: CHIRALPAK-IC; Abs. detector wavelength: 254 nm and 270 nm; Mobile phase: Hexanes:2-propanol = 90:10; Flow rate: 1.0 mL/min; Retention times (min): ~ 16.24 [(-)-**174a**] and ~ 19.64 [(+)-**174a**

For preparative conditions,

I). Column: CHIRALPAK-IC; Abs. detector wavelength: 254 nm and 270 nm; Mobile phase: Hexanes:2-propanol = 95:5; Flow rate: 3.0 mL/min; Retention times (min): ~ 32.72 [(-)-**174a** and ~ 40.62 [(+)-**174a**]

Optical rotation $[\alpha]_D^{26}$:

HPLC retention time (RR-WHELK-01) at ~ 28.92 min, (*c* ~0.725%, MeOH) = +34.37 deg

HPLC retention time (RR-WHELK-01) at ~ 32.13 min, (*c* ~0.725%, MeOH) = -32.27 deg.

R*f* = 0.40 (50% hexanes:50% ethyl acetate) for **174b**.

^{1}H-NMR (400 MHz, $CDCl_3$, δ ppm): 7.18-7.15 (m, 1H), 7.09-7.07 (m, 2H), 5.90-5.88 (m, 1H), 5.25-5.17 (m, 2H), 3.19-3.17 (d, *J* = 7.2 Hz, 2H), 2.69-2.65 (m, 2H), 2.46-2.42 (m, 2H), 2.15 (s, 3H), 1.69 (m, 3H) and 1.64 (m, 3H).

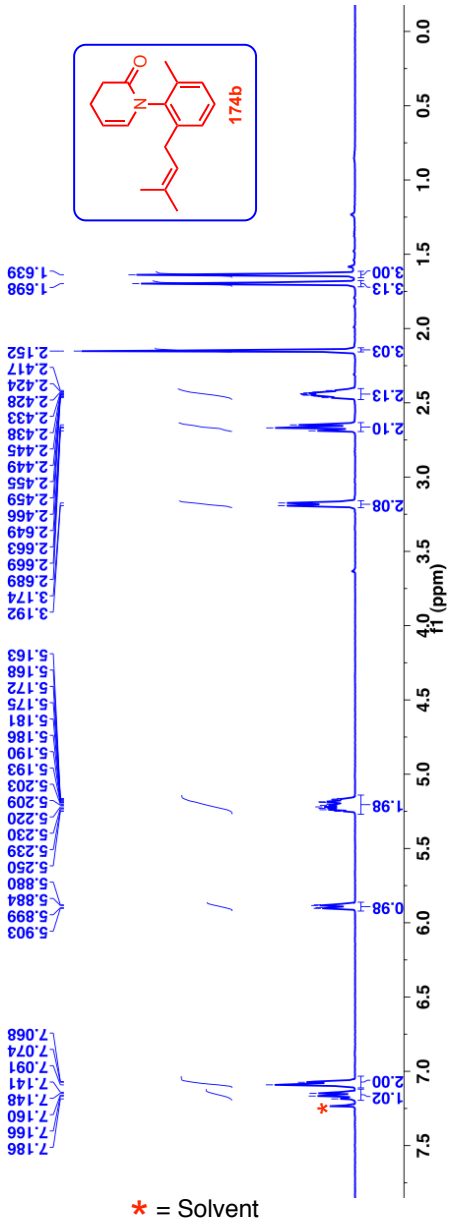

Figure 3.82: ^{1}H-NMR (400 MHz, $CDCl_3$, δ ppm) of 6-dimethylallyl-dihydropyridone **174b**.

^{13}C-NMR (100 MHz, $CDCl_3$, δ ppm): 168.9, 139.5, 138.2, 136.2, 133.1, 130.9, 128.8, 128.5, 127.7, 122.4, 106.2, 31.8, 30.2, 25.9, 20.7, 18.1 and 17.9.

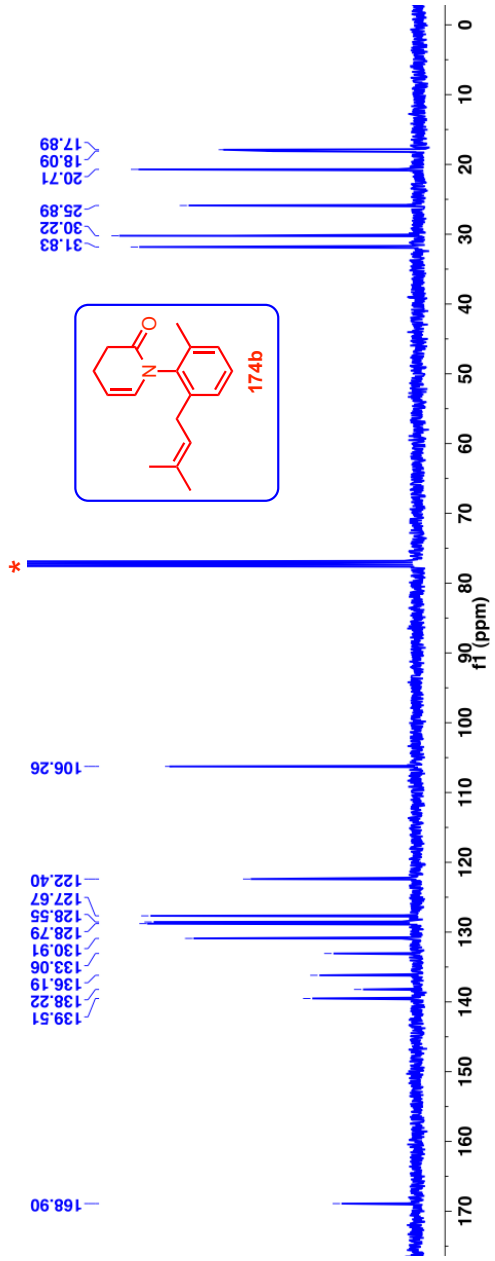

Figure 3.83: ^{13}C-NMR (100 MHz, $CDCl_3$, δ ppm) of 6-dimethylallyl-dihydropyridone **174b**.

HRMS-ESI (m/z) ([M + Na]$^+$):

Calculated : 278.1515

Observed : 278.1516

|Δm| : 0.4 ppm

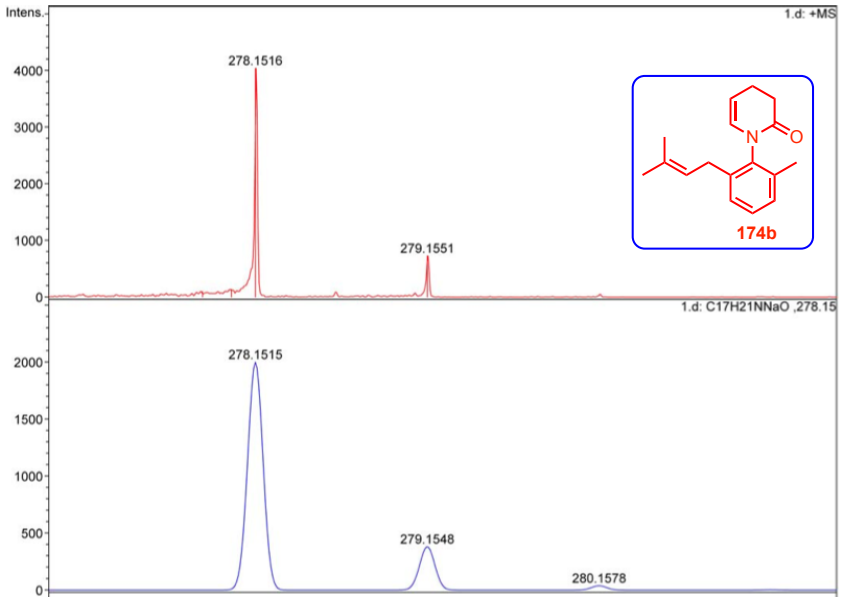

Figure 3.84: HRMS of 6-dimethylallyl-dihydropyridone **174b**.

HPLC analysis conditions:

For analytical conditions,

I). Column : CHIRALPAK-IC

Abs. detector wavelength : 254 nm and 270 nm

Mobile phase : Hexanes:2-propanol = 90:10

Flow rate : 1.5 mL/min

Retention times (min) : ~ 8.94 [(-)-**174b** and ~ 10.89 [(+)-**174b**]

For preparative conditions,

I). Column : CHIRALPAK-IC

Abs. detector wavelength : 254 nm and 270 nm

Mobile phase : Hexanes:2-propanol = 95:5

Flow rate : 3.0 mL/min

Retention times (min) : ~ 28.39 [(-)-**174b** and ~ 35.92 [(+)-**174b**]

Optical rotation $[\alpha]_D^{26}$:

HPLC Rt (CHIRALPACK® IC) at ~8.94 min, (*c* ~0.369%, MeOH) = -70.90 deg.

HPLC Rt (CHIRALPACK® IC) at ~ 10.89 min, (*c* ~0.369%, MeOH) = +70.63 deg.

R*f* = 0.50 (50% hexanes:50% ethyl acetate) for **174c**.

^{1}H-NMR (400 MHz, $CDCl_3$, δ ppm): 6.94 (s, 1H), 6.90 (s, 1H), 5.88-5.85 (td, *J* =7.6, 1.6 Hz, 1H), 5.22-5.18 (m, 1H), 4.80-4.797 (m, 1H), 4.64-4.636 (m, 1H), 3.21-3.11 (m, 2H) 2.67-2.63 (m, 2H), 2.45-2.395 (m, 2H), 2.27 (s, 3H), 2.11 (s, 3H) and1.63 (s, 3H).

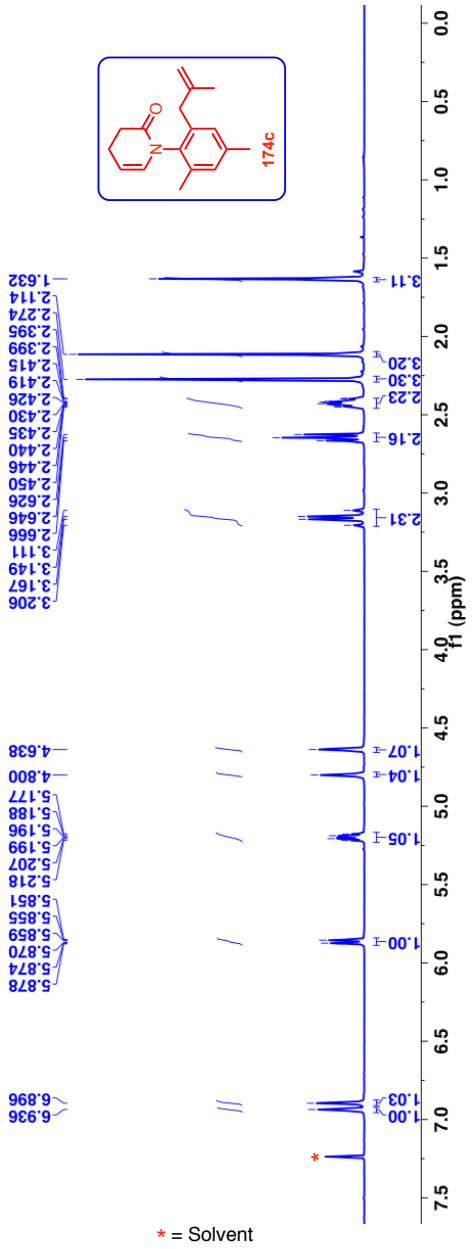

Figure 3.85: ^{1}H-NMR (400 MHz, $CDCl_3$, δ ppm) of 6-methylallyl-dihydropyridone derivative **174c**.

^{13}C-NMR (100 MHz, $CDCl_3$, δ ppm): 168.98, 144.2, 138.1, 137.1, 136.1, 135.9, 131.1, 130.0, 129.0, 112.6, 105.99, 40.1, 31.9, 22.6, 21.3, 20.7 and 17.8.

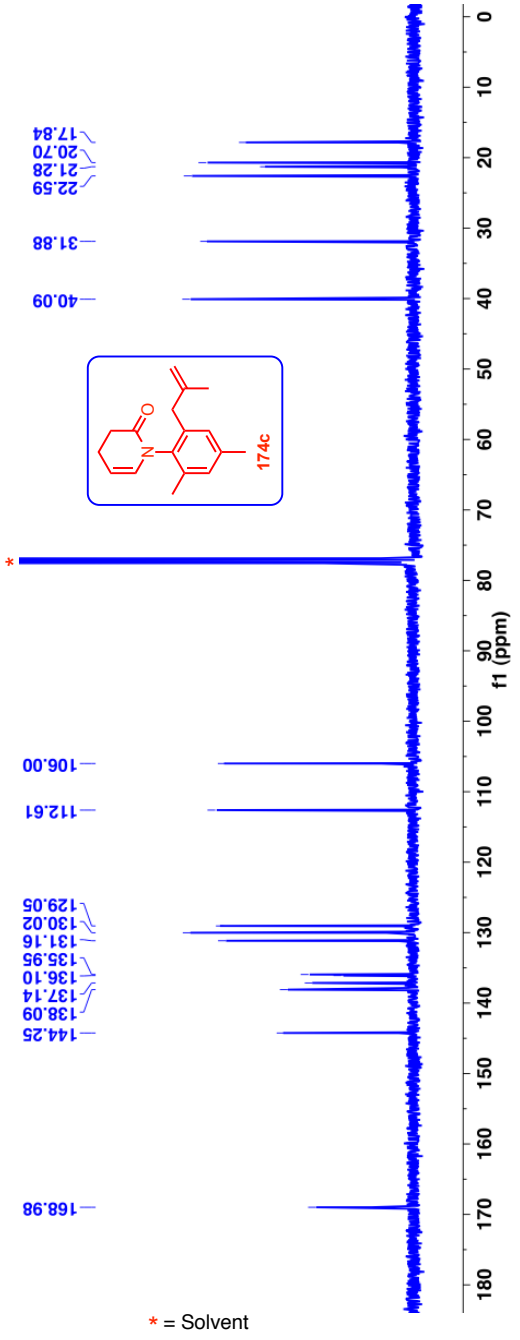

Figure 3.86: ^{13}C-NMR (100 MHz, $CDCl_3$, δ ppm) of 6-methylallyl-dihydropyridone derivative **174c**.

HRMS-ESI (m/z) ([M + Na]$^+$):

Calculated : 278.1515

Observed : 278.1517

|Δm| : 0.7 ppm

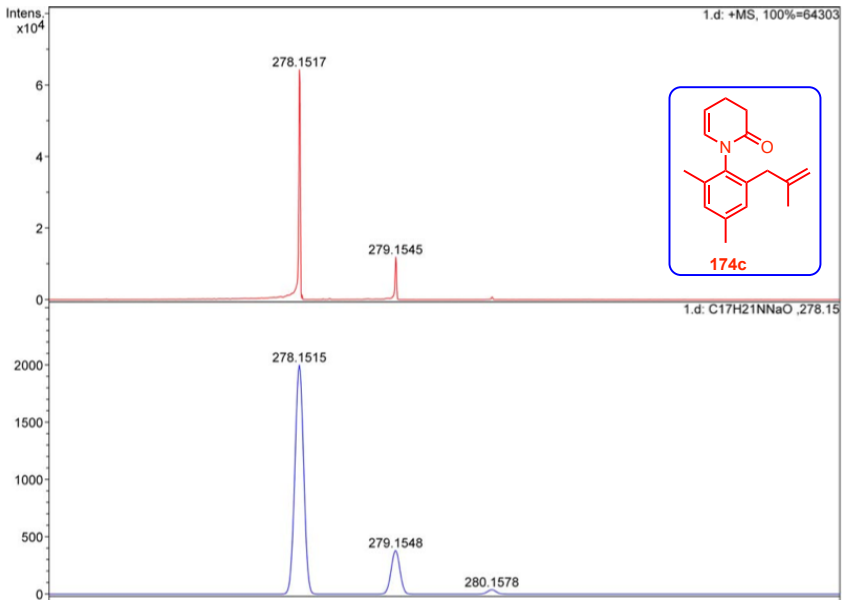

Figure 3.87: HRMS of 6-methylallyl-dihydropyridone derivative **174c**.

HPLC analysis conditions:

For analytical conditions,

I). Column : CHIRALPACK® IC

Abs. detector wavelength : 254 nm and 270 nm

Mobile phase : Hexanes:2-propanol = 90:10

Flow rate : 1.0 mL/min

Retention times (min) : ~ 15.55 [(-)-**174c** and ~ 17.83 [(+)-**174c**]

For preparative conditions,

I). Column : CHIRALPAK-IC

Abs. detector wavelength : 254 nm and 270 nm

Mobile phase : Hexanes:2-propanol = 95:5

Flow rate : 3.0 mL/min

Retention times (min) : ~ 33.97 [(-)-**174c** and ~ 40.57 [(+)-**174c**]

Optical rotation $[\alpha]_D^{26}$:

HPLC Rt (CHIRALPACK® IC) at ~ 15.55 min, (*c* ~0.700%, MeOH) = -48.07 deg.

HPLC Rt (CHIRALPACK® IC) at ~ 17.83 min, (*c* ~0.700%, MeOH) = +48.80 deg.

R*f* = 0.35 (80% hexanes:20% ethyl acetate) for **174d** (Yield = 70%).

^{1}H-NMR (400 MHz, $CDCl_3$, δ ppm): 7.20-7.16 (m, 1H), 7.12-7.09 (m, 2H), 5.91 (dt, *J* = 7.6, 1.6 Hz, 1H), 5.87-5.77 (m, 1H), 5.28-5.24 (m, 1H), 5.04-4.93 (m, 1H), 2.69-2.66 (m, 2H), 2.62-2.49 (m, 2H), 2.48-2.43 (m, 2H), 2.32-2.26 (m, 2H) and 2.16 (s, 3H).

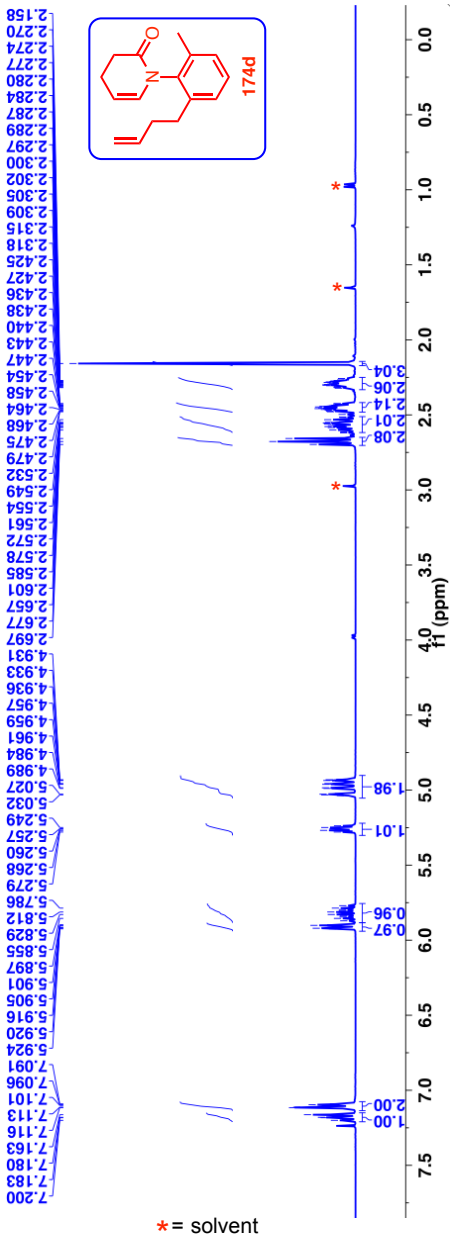

Figure 3.88: ^{1}H-NMR (400 MHz, $CDCl_3$, δ ppm) of 6-butenyl-dihydropyridone derivative **174d**.

^{13}C-NMR (100 MHz, $CDCl_3$, δ ppm): 169.1, 139.7, 138.3, 136.3, 131.1, 128.9, 128.5, 127.7, 115.1, 106.5, 34.4, 31.9, 31.1, 20.7 and 17.9.

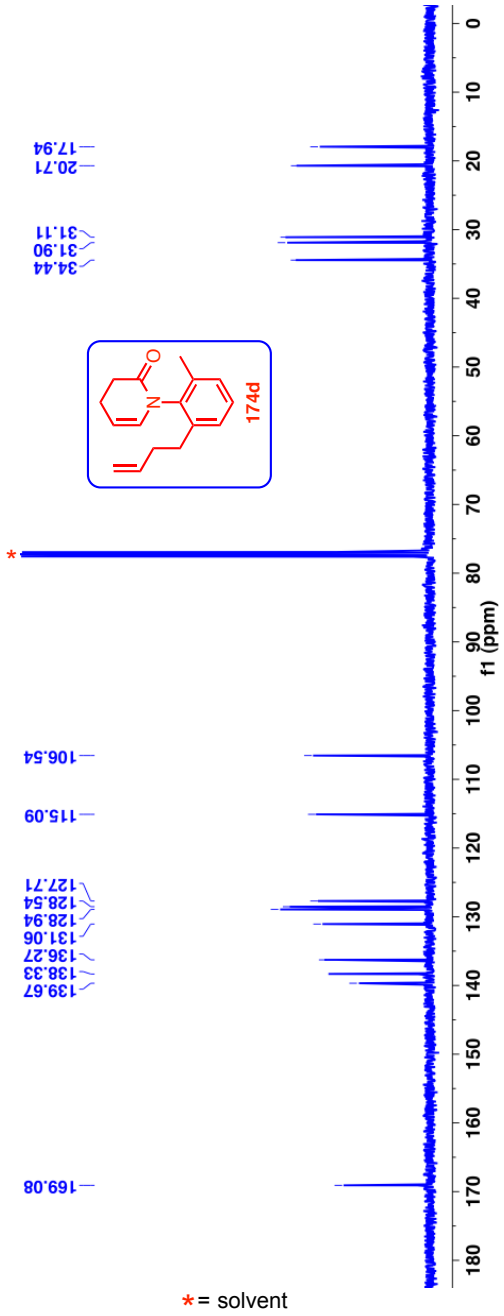

Figure 3.89: ^{13}C-NMR (100 MHz, $CDCl_3$, δ ppm) of 6-butenyl-dihydropyridone derivative **174d**.

HRMS-ESI (m/z) ([M + Na]$^+$):

Calculated : 264.1359

Observed : 264.1365

|Δm| : 2.3 ppm

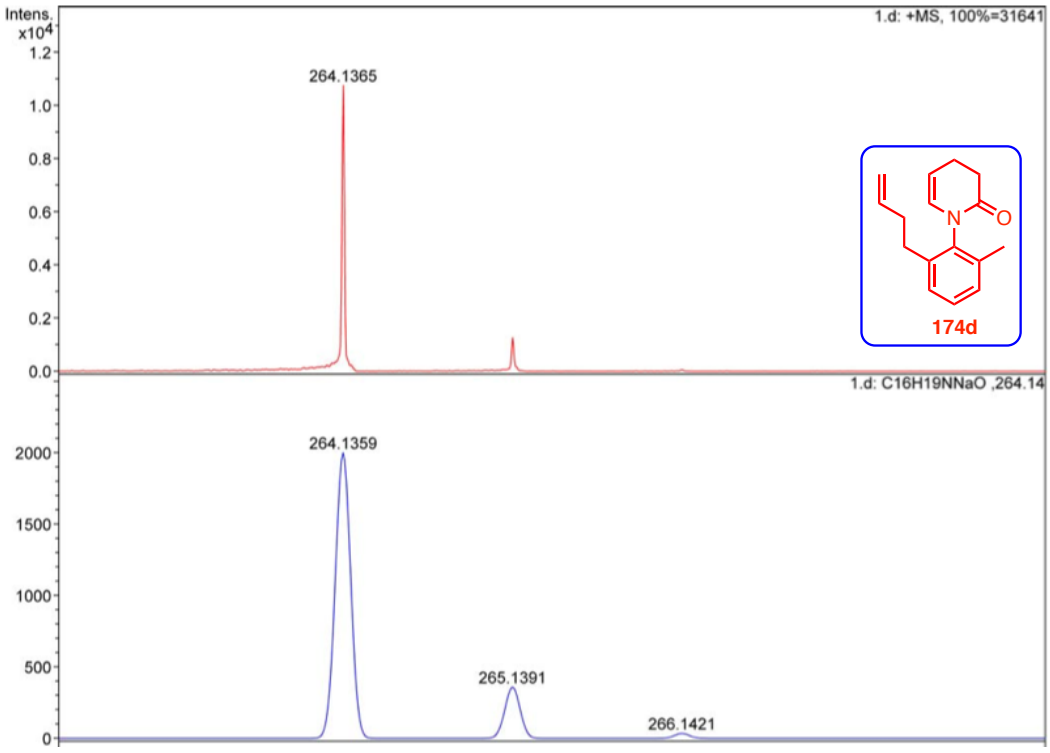

Figure 3.90: HRMS of 6-butenyl-dihydropyridone derivative **174d**.

R*f* = 0.40 (80% hexanes:20% ethyl acetate) for **174e** (Yield = 75%).

^{1}H-NMR (400 MHz, $CDCl_3$, δ ppm): 7.21-7.18 (m, 1H), 7.12-7.09 (m, 2H), 6.29 (d, *J*= 4.8 Hz, 1H), 5.90-5.80 (m, 1H), 5.47 (d, *J*= 4.8 Hz, 1H), 5.03-4.94 (m, 2H), 3.25-3.23 (m, 2H), 2.14 (s, 3H) 1.30 (s, 3H) and 1.29 (s, 3H).

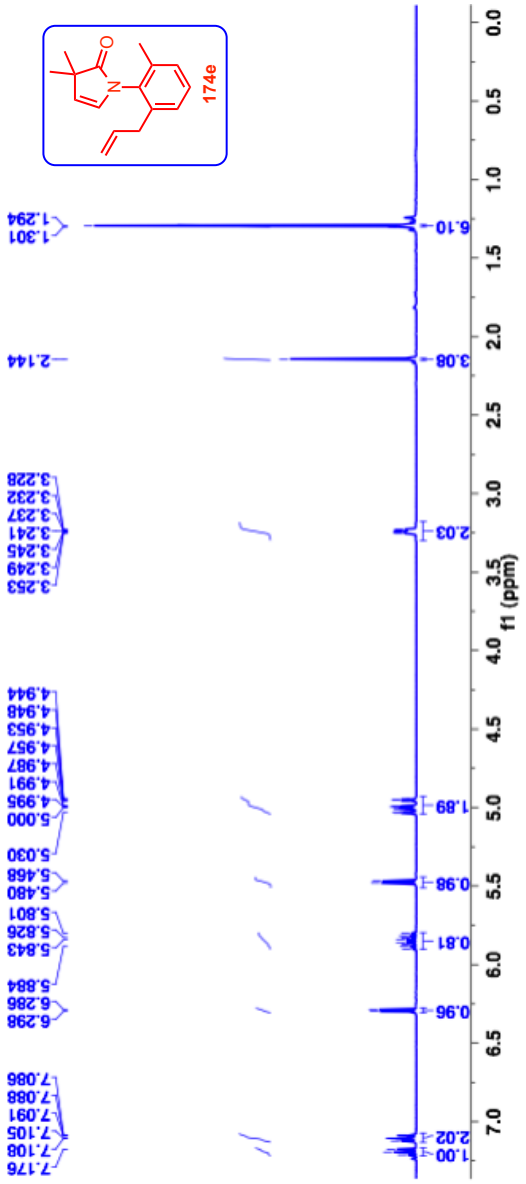

Figure 3.91: ^{1}H-NMR (400 MHz, $CDCl_3$, δ ppm) of 6-allyl-pyrrolone derivative **174e**.

^{13}C-NMR (100 MHz, $CDCl_3$, δ ppm): 181.62, 138.6, 136.97, 136.6, 134.4, 131.5, 129.1, 128.7, 127.97, 117.8, 116.5, 46.2, 36.1, 23.9, 23.6 and 18.1.

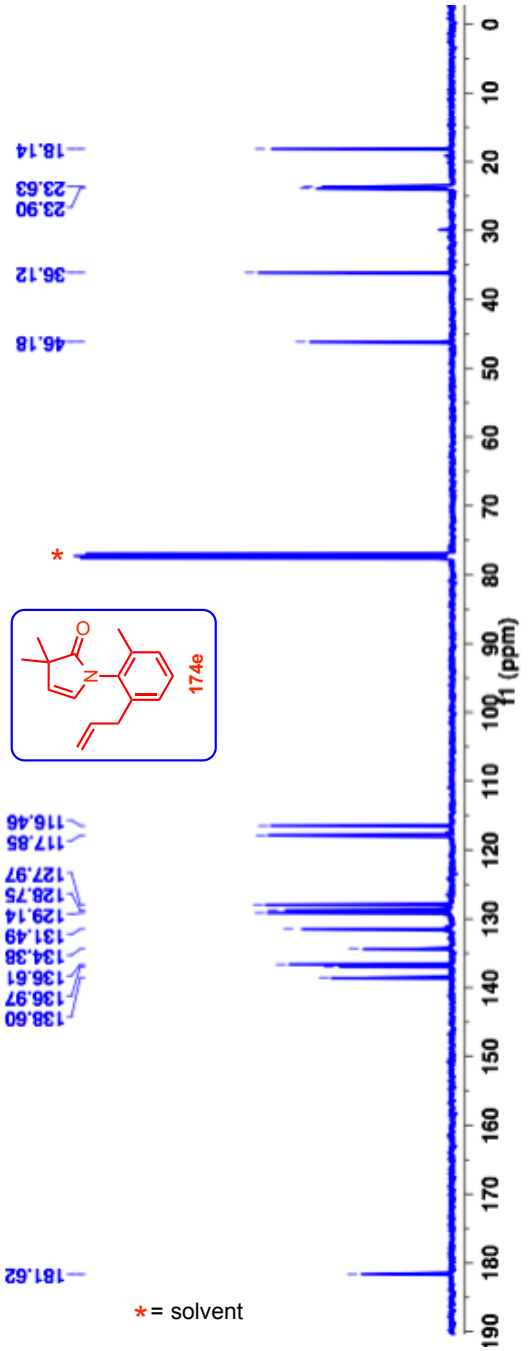

Figure 3.92: ^{13}C-NMR (100 MHz, $CDCl_3$, δ ppm) of 6-allyl-pyrrolone derivative **174e**.

HRMS-ESI (m/z) ([M + Na]$^+$):

Calculated : 264.1359

Observed : 264.1358

|Δm| : 0.4 ppm

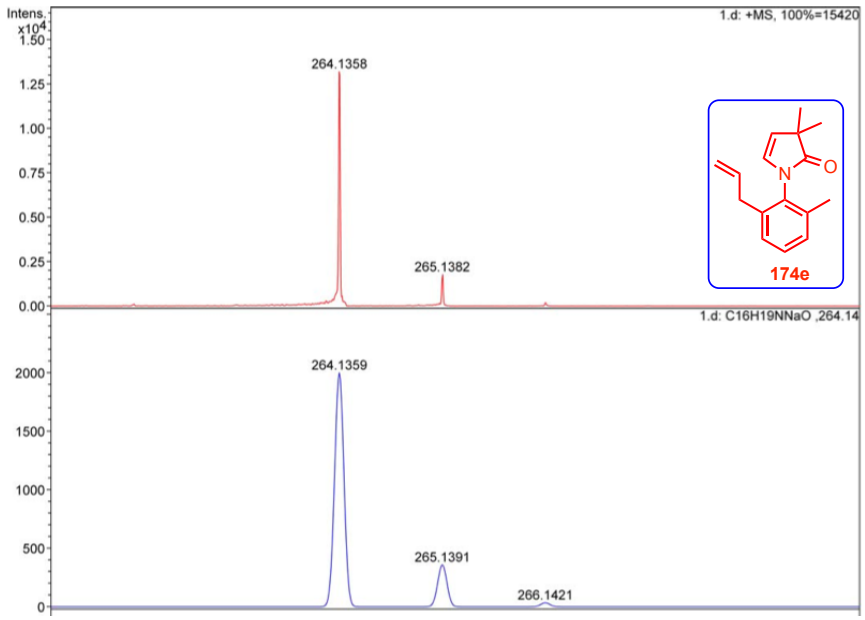

Figure 3.93: HRMS of 6-allyl-pyrrolone derivative **174e**.

HPLC analysis conditions:

For analytical conditions,

I). Column : CHIRALPAK-IC

Abs. detector wavelength : 254 nm and 270 nm

Mobile phase : Hexanes:2-propanol = 95:5

Flow rate : 1.0 mL/min

Retention times (min) : ~ 12.05 [(-)-**174e**] and ~ 14.52 [(+)-**174e**

For preparative conditions,

I). Column : CHIRALPAK-IC

Abs. detector wavelength : 254 nm and 270 nm

Mobile phase : Hexanes:2-propanol = 98:2

Flow rate : 3.0 mL/min

Retention times (min) : ~ 27.55 [(-)-**174e** and ~ 34.63 [(+)-**174e**]

Optical rotation $[\alpha]_D^{26}$:

HPLC retention time (CHIRALPAK-IC) at ~ 12.05 min, (*c* ~ 0.12 %, MeOH) = -18.18 deg.

HPLC retention time (CHIRALPAK-IC) at ~ 14.52 min, (*c* ~ 0.12 %, MeOH) = +18.55 deg.

R*f* = 0.40 (80% hexanes:20% ethyl acetate) for **174f** (Yield = 72%).

^{1}H-NMR (400 MHz, $CDCl_3$, δ ppm): 7.21-7.17 (m, 1H), 7.11-7.09 (m, 2H), 6.31 (d, *J*= 4 Hz, 1H), 5.83-5.73 (m, 1H), 5.497 (d, *J*= 4.8 Hz, 1H), 5.00-4.91 (m, 2H), 2.61-2.48 (m, 2H), 2.30-2.18 (m, 2H), 2.14 (s, 3H), 1.297 (s, 3H) and 1.29 (s, 3H).

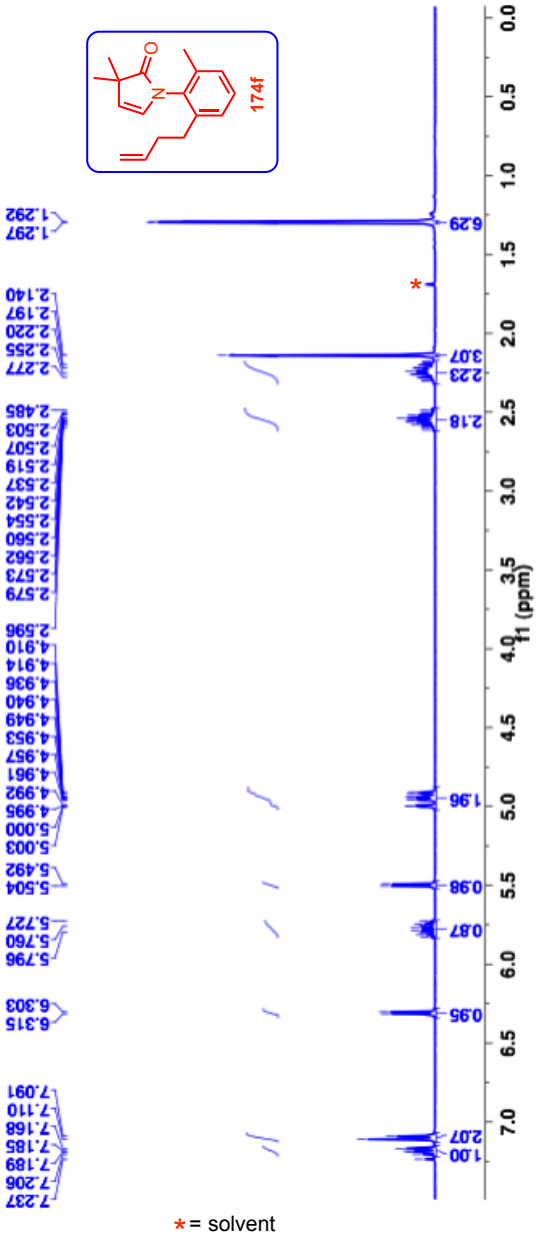

Figure 3.94: ^{1}H-NMR (400 MHz, $CDCl_3$, δ ppm) of 6-butenyl-pyrrolone derivative **174f**.

^{13}C-NMR (100 MHz, $CDCl_3$, δ ppm): 181.7, 140.5, 138.1, 136.97, 134.4, 131.5, 128.9, 128.7, 127.8, 118.1, 115.1, 46.2, 34.8, 31.4, 23.8, 23.7 and 18.1.

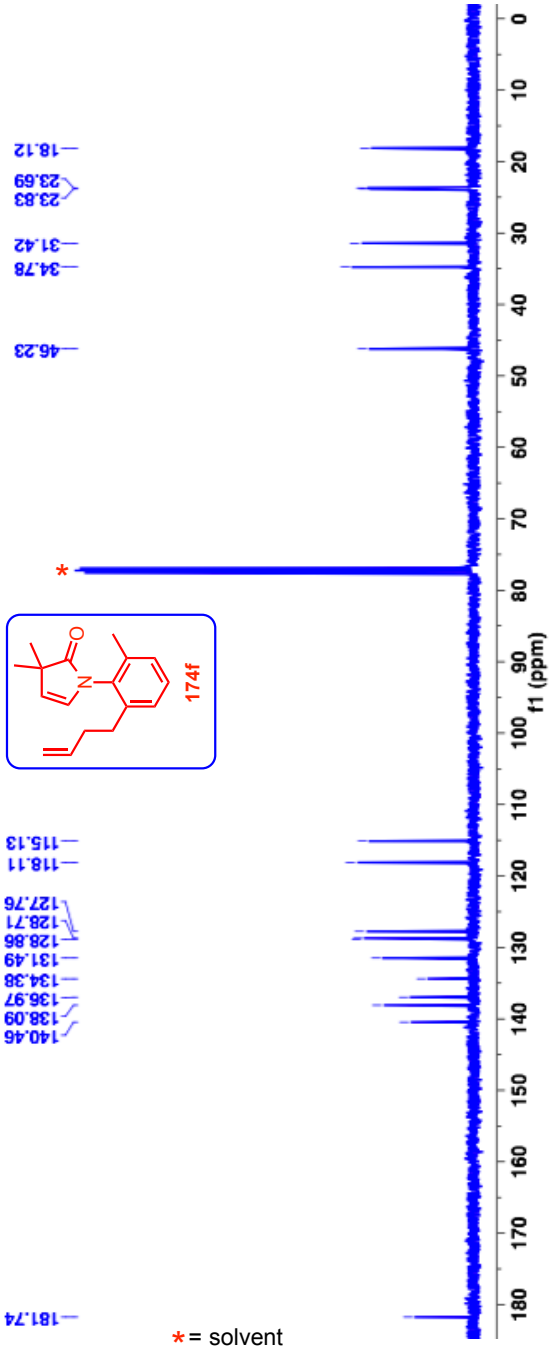

Figure 3.95: ^{13}C-NMR (100 MHz, $CDCl_3$, δ ppm) of 6-butenyl-pyrrolone derivative **174f**.

HRMS-ESI *(m/z)* ([M + Na]$^+$): Calculated: 278.1515; Observed: 278.1504; |Δm|: 3.9 ppm

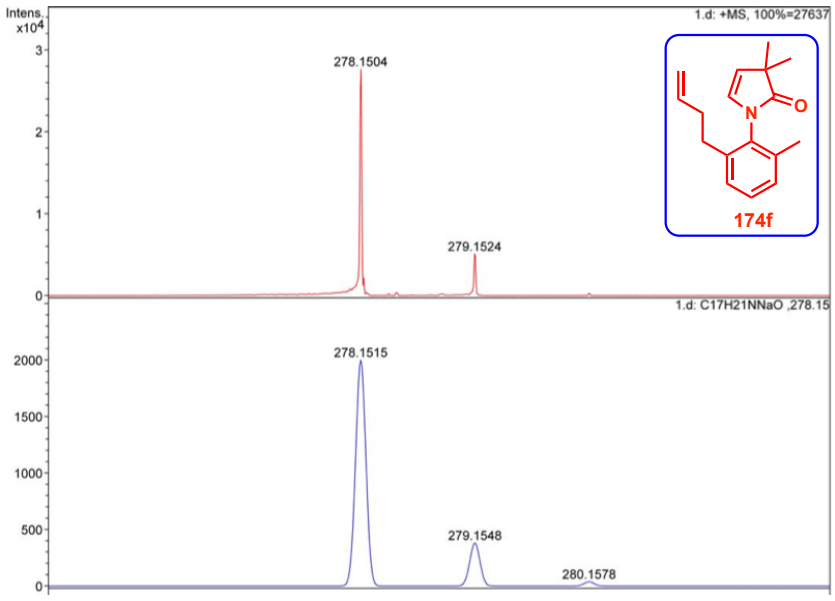

Figure 3.96: HRMS of 6-butenyl-pyrrolone derivative **174f**.

HPLC analysis conditions:

For analytical conditions,

I). Column : CHIRALPAK-IC

Abs. detector wavelength : 254 nm and 270 nm

Mobile phase : Hexanes:2-propanol = 90:10

Flow rate : 1.0 mL/min

Retention times (min) : ~ 10.78 [(-)-**174f**] and ~ 12.57 [(+)-**174f**]

For preparative conditions,

I). Column : CHIRALPAK-IC

Abs. detector wavelength : 254 nm and 270 nm

Mobile phase : Hexanes:2-propanol = 95:5

Flow rate : 3.0 mL/min

Retention times (min) : ~ 21.58 [(-)-**174f** and ~ 25.58 [(+)-**174f**]

Optical rotation $[\alpha]_D^{24}$:

HPLC Rts (CHIRALPAK-IC) at ~ 10.78 min, (*c* ~ 0.83 %, MeOH) = -24.26 deg.

HPLC Rts (CHIRALPAK-IC) at ~ 12.57 min, (*c* ~ 0.83 %, MeOH) = +24.54 deg.

R*f* = 0.45 (80% hexanes:20% ethyl acetate) for **174g** (Yield = 63%).

^{1}H-NMR (400 MHz, $CDCl_3$, δ ppm): 7.16-7.12 (m, 1H), 6.84-6.82 (m, 1H), 6.76-6.74 (m, 1H), 6.35 (d, *J* = 4.8 Hz, 1H), 5.97-5.87 (m, 1H), 5.41 (d, *J* = 4.8 Hz, 1H), 5.34 (dq, *J* = 17.2, 1.8 Hz, 1H), 5.17 (dq, *J* = 10.8, 1.6 Hz, 1H), 4.45 (dt, *J* = 4.8, 1.6 Hz, 2H), 2.16 (s, 3H), 1.28 (s, 3H) and 1.27 (s, 3H).

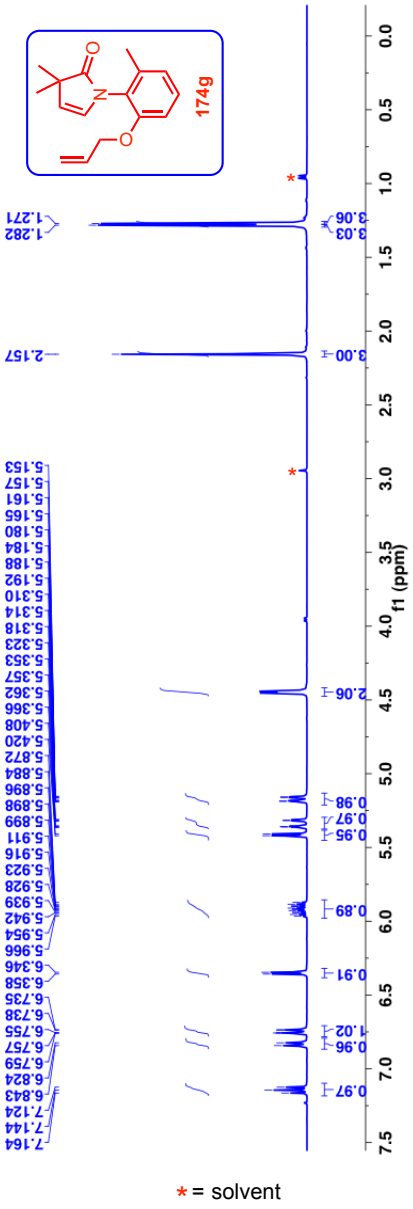

Figure 3.97: ^{1}H-NMR (400 MHz, $CDCl_3$, δ ppm) of 6-allyloxy-pyrrolone derivative **174g**.

^{13}C-NMR (100 MHz, $CDCl_3$, δ ppm): 181.8, 154.9, 138.2, 133.1, 132.1, 128.9, 124.96, 122.98, 117.0, 116.96, 110.8, 69.3, 46.0, 24.0, 23.7 and 17.9.

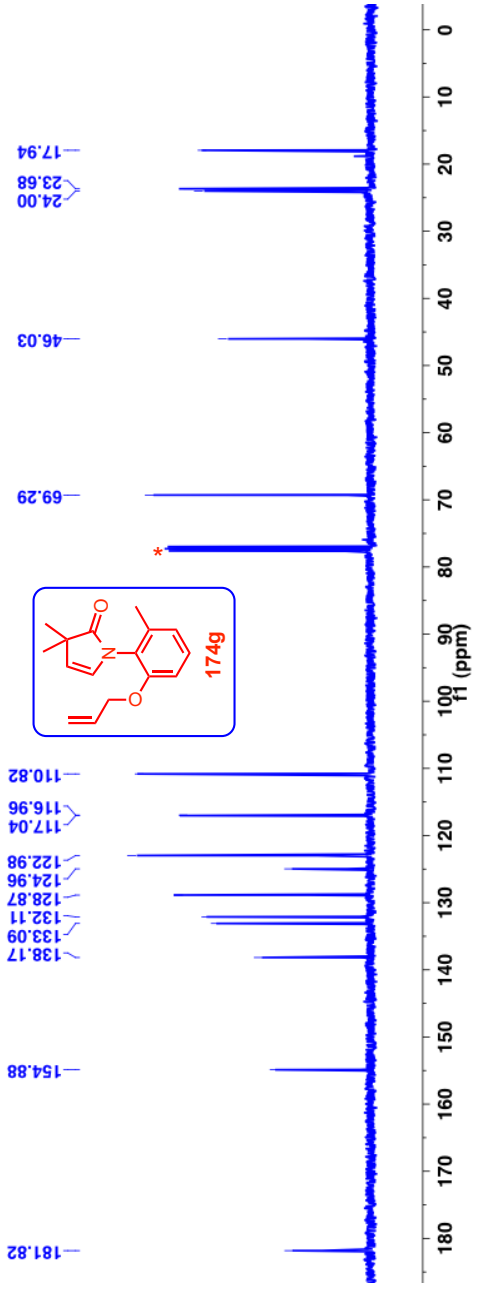

Figure 3.98: ^{13}C-NMR (100 MHz, $CDCl_3$, δ ppm) of 6-allyloxy-pyrrolone derivative **174g**.

HRMS-ESI (m/z) ([M + Na]$^+$):

Calculated : 280.1308

Observed : 280.1296

|Δm| : 4.3 ppm

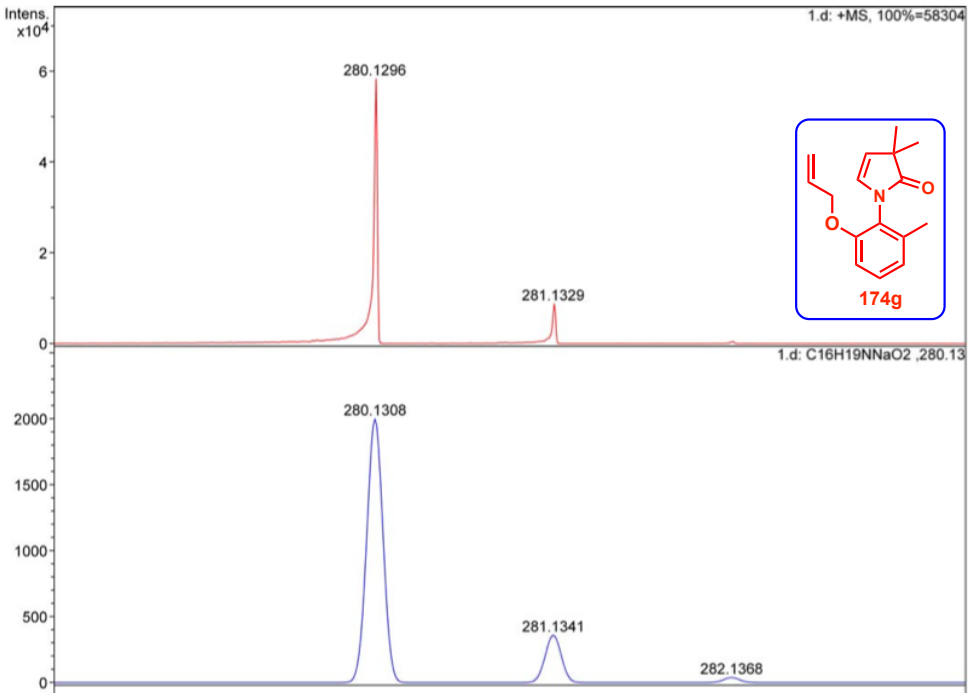

Figure 3.99: HRMS of 6-allyloxy-pyrrolone derivative **174g**.

HPLC analysis conditions:

For analytical conditions,

I). Column : CHIRALPAK-ADH

Abs. detector wavelength : 254 nm and 270 nm

Mobile phase : Hexanes:2-propanol = 95:5

Flow rate : 1.0 mL/min

Retention times (min) : ~ 6.80 [(PkA)-**174g**] and ~ 10.55 [(PkB)-**174g**

For preparative conditions,

I). Column : CHIRALPAK-ADH

Abs. detector wavelength : 254 nm and 270 nm

Mobile phase : Hexanes:2-propanol = 95:5

Flow rate : 3.0 mL/min

Retention times (min) : ~ 9.87 [(PkA)-**174g** and ~ 15.69 [(PkB)-**174g**]

(PkA and PkB refers to the order of elution of the isomers in HPLC on a chiral stationary phase)

R*f* = 0.85 (80% hexanes:20% ethyl acetate) for **181a** (Yield = 84%).

^{1}H-NMR (400 MHz, $CDCl_3$, δ ppm): 7.37-7.34 (m, 1H), 7.28-7.21 (m, 2H), 7.14-7.12 (m, 1H), 6.48 (d, *J* = 4.8 Hz, 1H), 5.45 (d, *J* = 4.8 Hz, 1H), 3.82 (t, *J* = 6.9 Hz, 1H), 2.77 (t, *J* = 6.9 Hz, 1H), 1.29 (s, 6H) and 1.05-0.94 (m, 21H).

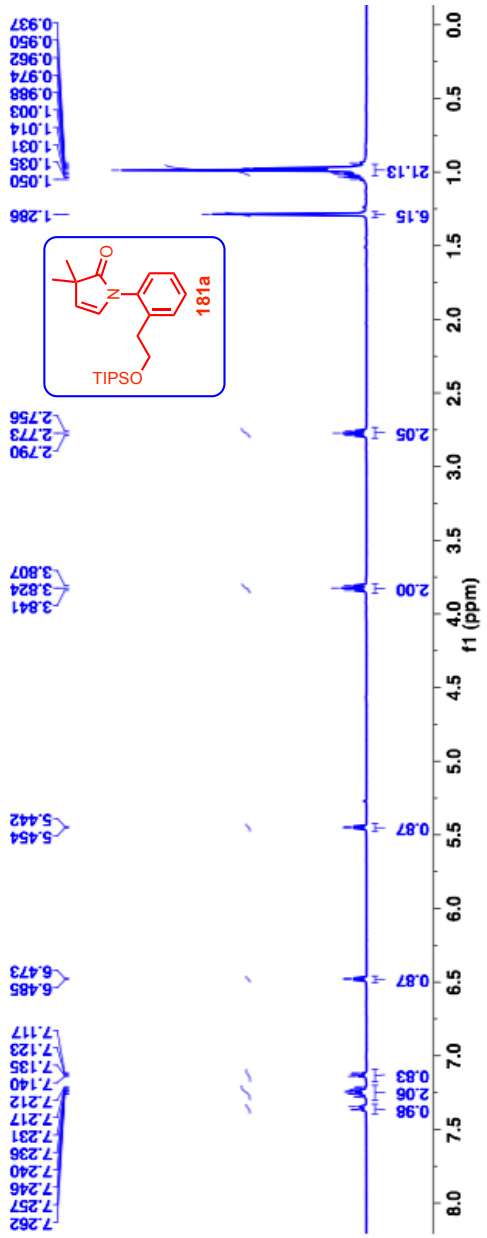

Figure 3.100: ^{1}H-NMR (400 MHz, $CDCl_3$, δ ppm) of 6-silyloxyethyl-pyrrolone derivative **181a**.

^{13}C-NMR (100 MHz, $CDCl_3$, δ ppm): 181.99, 136.9, 135.98, 132.0, 131.3, 128.3, 127.5, 127.4, 117.7, 63.7, 46.3, 35.2, 23.7, 18.2 and 12.1.

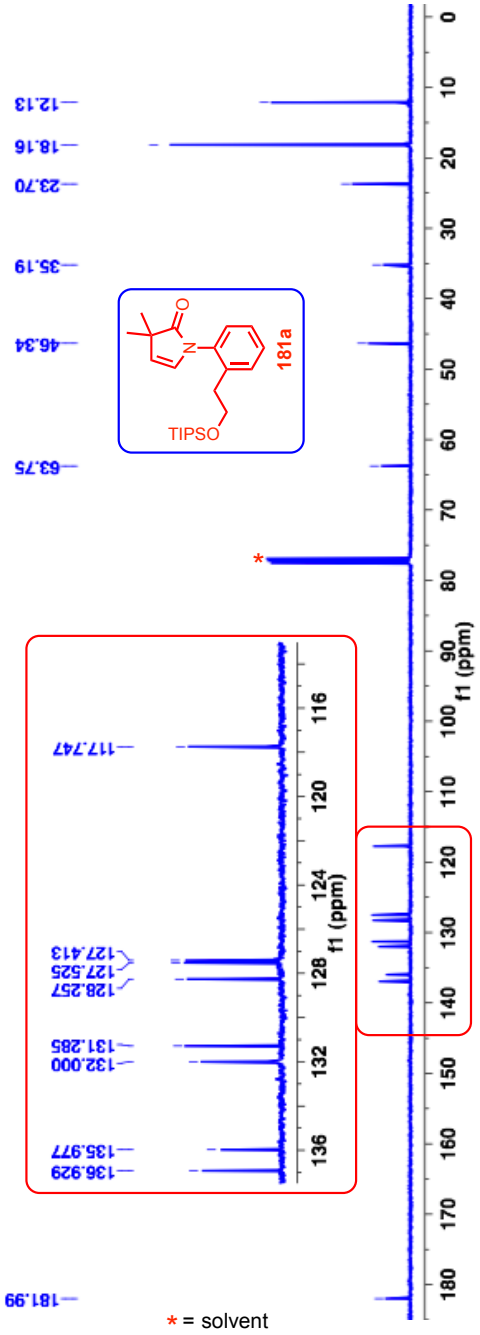

Figure 3.101: ^{13}C-NMR (100 MHz, $CDCl_3$, δ ppm) of 6-silyloxyethyl-pyrrolone derivative **181a**.

HRMS-ESI (m/z) ([M + Na]$^+$):

Calculated : 410.2488

Observed : 410.2480

|Δm| : 1.9 ppm

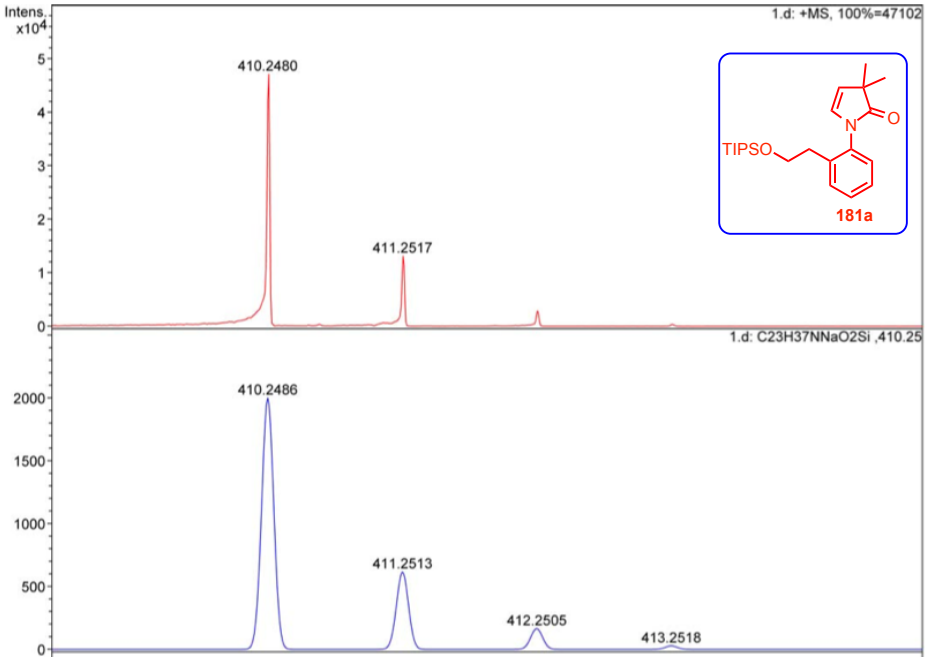

Figure 3.102: HRMS of 6-silyloxyethyl-pyrrolone derivative **181a**.

^{1}H-NMR (400 MHz, $CDCl_3$, δ ppm): 7.34-7.32 (m, 1H), 7.25-7.198 (m, 2H), 7.12-7.09 (m, 1H), 6.80 (d, *J*= 4.8Hz, 1H), 5.44 (d, *J*= 4.8Hz, 1H), 4.10 (h, J = 6.2 Hz, 1H), 2.77-2.62 (m, 2H), 1.28 (s, 3H), 1.276 (s, 3H), 1.06 (d, J = 6.0 Hz, 3H) and 0.96 (m, 21H).

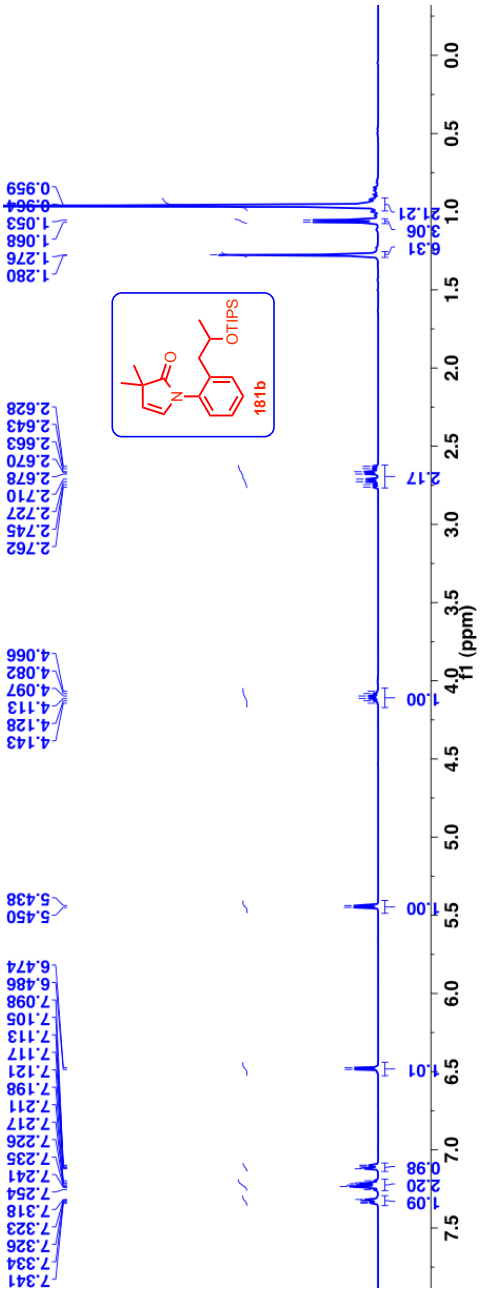

Figure 3.103: ^{1}H-NMR (400 MHz, $CDCl_3$, δ ppm) of 6-silyloxypropyl-pyrrolone derivative **181b**.

^{13}C-NMR (100 MHz, $CDCl_3$, δ ppm): 181.8, 136.97, 136.1, 132.1, 131.8, 128.1, 127.4, 127.3, 117.7, 69.5, 46.3, 41.8, 24.2, 23.8, 23.7, 12.3, 18.2 and 12.7.

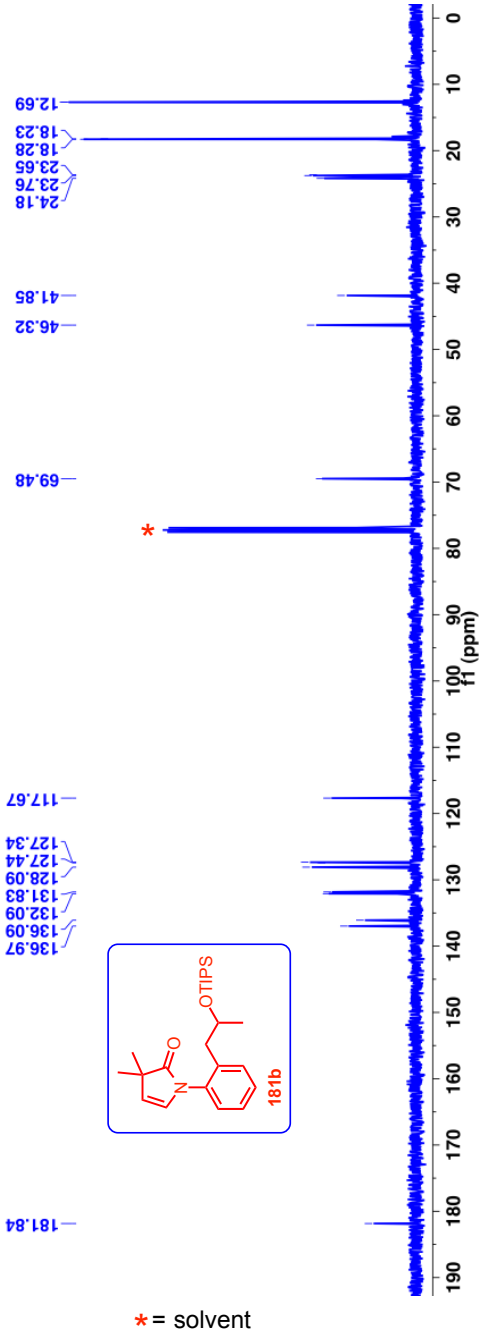

Figure 3.104: ^{13}C-NMR (100 MHz, $CDCl_3$, δ ppm) of 6-silyloxypropyl-pyrrolone derivative **181b**.

HRMS-ESI (m/z) ([M + Na]$^+$):

Calculated : 424.2642

Observed : 424.2649

|Δm| : 1.7 ppm

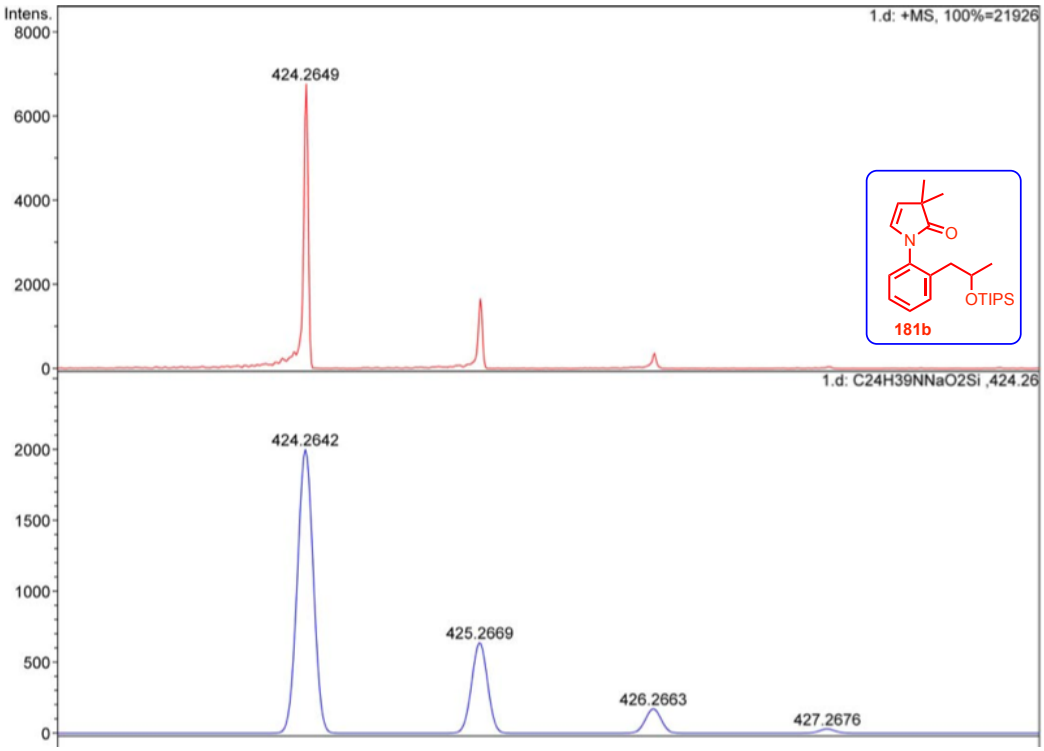

Figure 3.105: HRMS of 6-silyloxypropyl-pyrrolone derivative **181b**.

(The compound exists as a diastereomers due to both axial and point chirality); R*f* = 0.85, 0.80 (80% hexanes:20% ethyl acetate) for **181c** (Yield = 60%).

^{1}H-NMR (400 MHz, $CDCl_3$, δ ppm): 7.24-7.08 (m, 11H), 6.94 (s, 1H), 6.90 (s, 1H), 6.88 (s, 1H), 5.95 (d, *J* = 4.8 Hz, 1H), 5.50 (d, *J* = 4.8 Hz, 1H), 5.32 (dd, *J* = 9.4, 4.8 Hz, 2H), 4.94 (t, *J* = 5.8 Hz, 1H), 4.79 (t, *J* = 6.8 Hz, 1H), 2.97 (dd, *J* = 13.6, 7.0 Hz, 1H), 2.74 (d, *J* = 5.8 Hz, 2H), 2.66 (dd, *J* = 13.4, 6.9 Hz, 1H), 2.27 (s, 3H), 2.26 (s, 3H), 2.04 (s, 3H), 1.99 (s, 3H), 1.27 (s, 6H), 1.23 (s, 3H), 1.22 (s, 3H), 0.91-0.86 (m, 32H) and 0.80-0.79 (m, 10H).

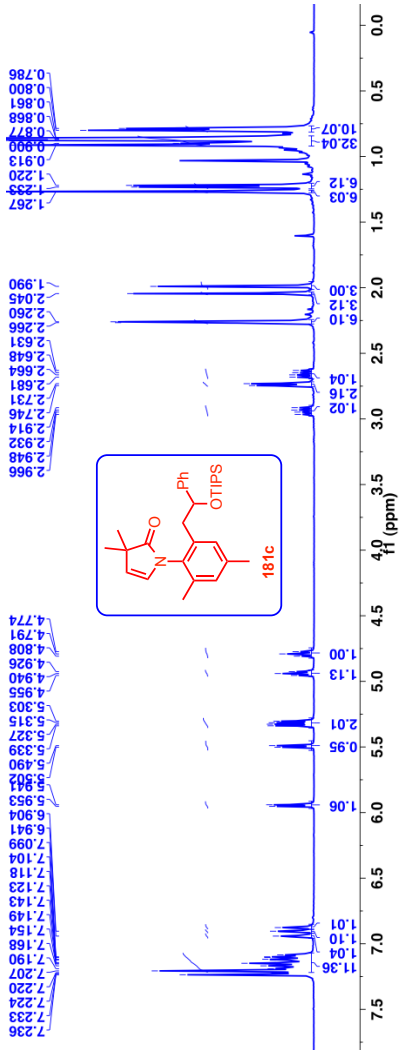

Figure 3.106: ^{1}H-NMR (400 MHz, $CDCl_3$, δ ppm) of 6-silyloxyphenethyl pyrrolone **181c**.

^{13}C-NMR (100 MHz, $CDCl_3$, δ ppm): 182.1, 181.9, 145.96, 145.4, 137.9, 137.5, 137.0, 136.99, 136.1, 132.3, 132.1, 132.0, 131.7, 130.8, 130.5, 129.9, 129.8, 128.1, 128.0, 127.3, 127.2, 126.5, 126.4, 117.2, 117.15, 76.7, 75.9, 46.1, 45.97, 43.73, 42.7, 24.1, 23.9, 23.7, 23.4, 18.2, 18.13, 18.10, 18.04, 17.9, 12.5 and 12.5.

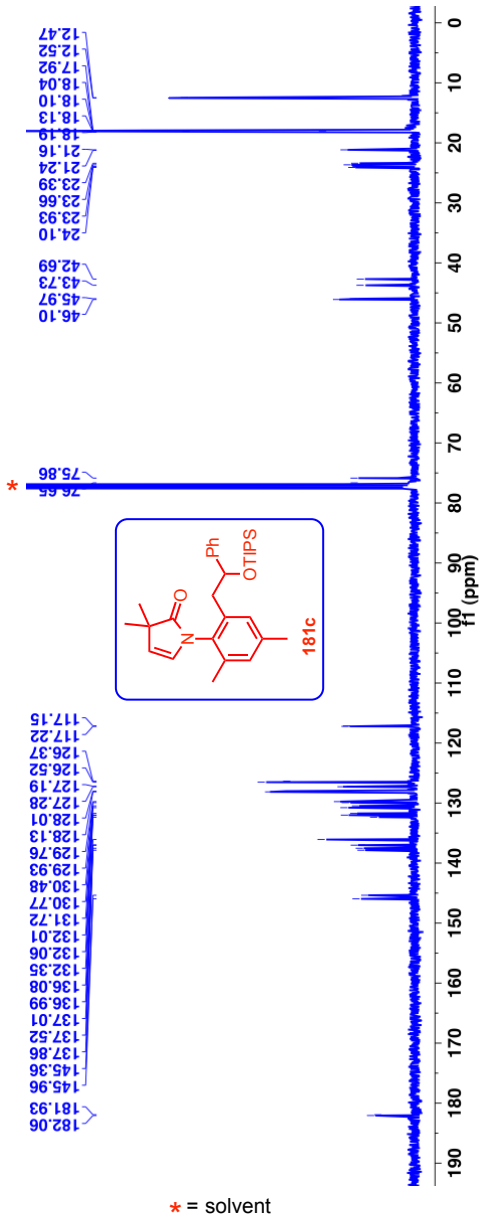

Figure 3.107: ^{13}C-NMR (100 MHz, $CDCl_3$, δ ppm) of 6-silyloxyphenethyl-pyrrolone **181c**.

HRMS-ESI (m/z) ([M + Na]$^+$):

Calculated : 514.3112

Observed : 514.3101

|Δm| : 2.1 ppm

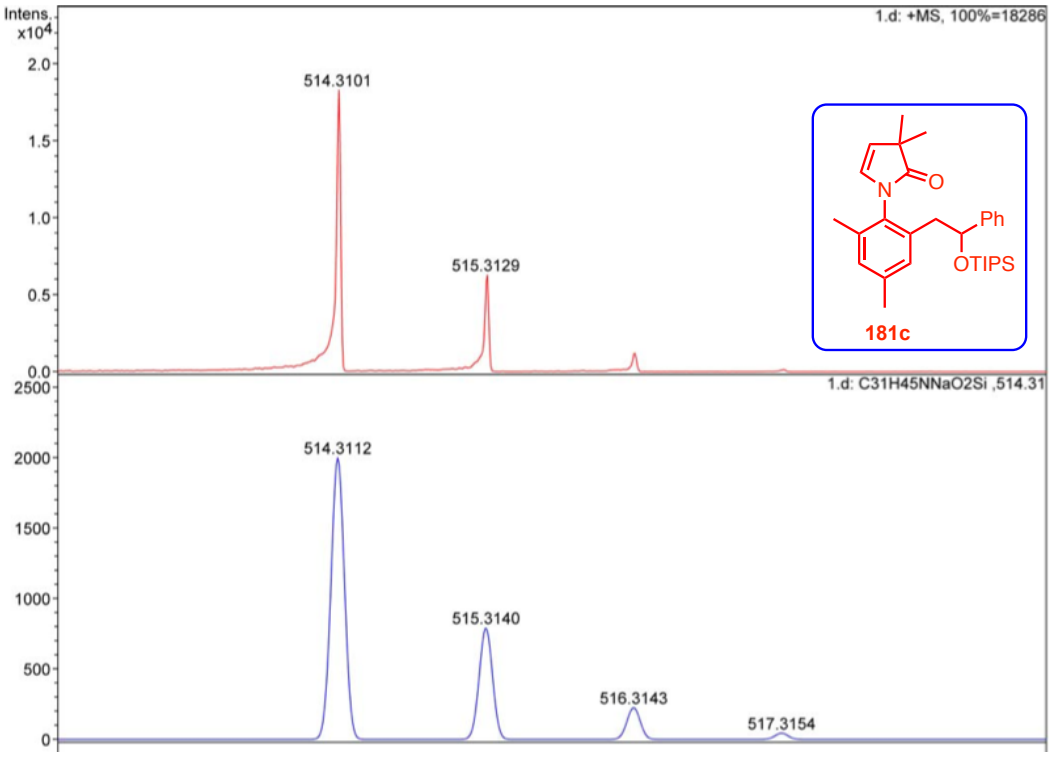

Figure 3.108: HRMS of 6-silyloxyphenethyl-pyrrolone **181c**.

R*f* = 0.75 (80% hexanes:20% ethyl acetate) for **179** (Yield = 66%).

^{1}H-NMR (400 MHz, $CDCl_3$, δ ppm): 6.91 (s, 2H), 6.29 (d, *J* = 4.8 Hz, 1H), 5.48 (d, *J* = 4.8 Hz, 1H), 2.43-2.35 (m, 2H), 2.28 (s, 3H), 2.10 (s, 3H), 1.56-1.44 (m, 2H), 1.295 (s, 6H) and 0.89 (t, *J* = 7.3 Hz, 3H).

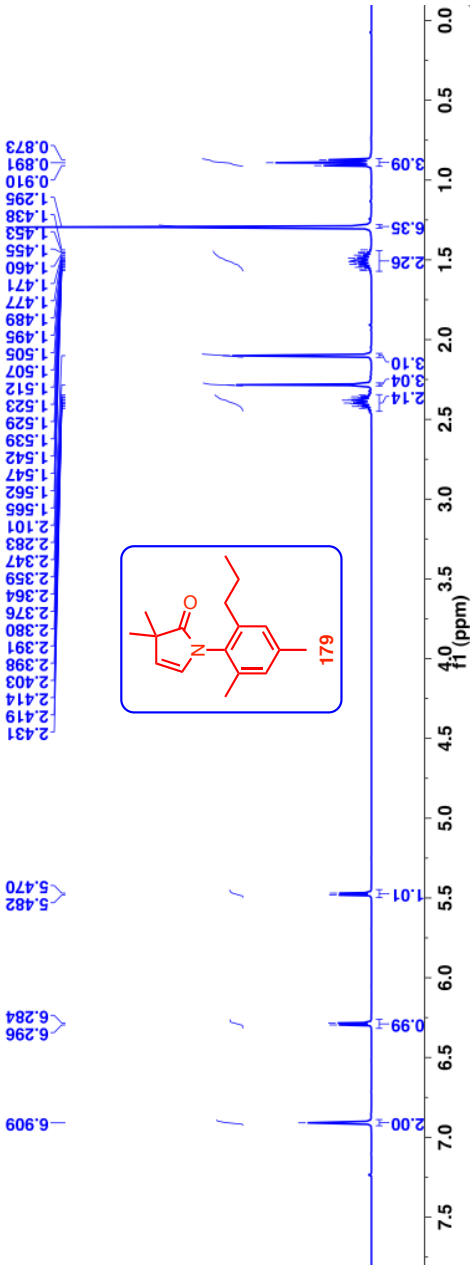

Figure 3.109: ^{1}H-NMR (400 MHz, $CDCl_3$, δ ppm) of 6-ethyl-pyrrolone derivative **179**.

^{13}C-NMR (100 MHz, $CDCl_3$, δ ppm): 181.8, 140.9, 138.3, 136.5, 131.8, 131.8, 129.4, 128.5, 117.8, 46.2, 34.2, 24.1, 23.9, 23.7, 21.3, 18.0 and 14.5.

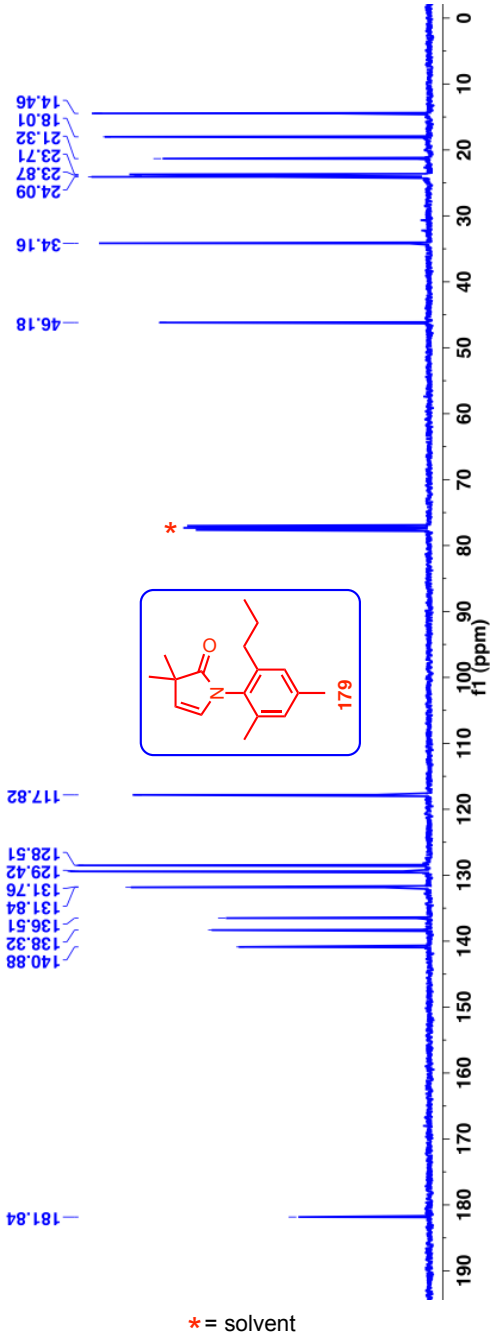

Figure 3.110: ^{13}C-NMR (100 MHz, $CDCl_3$, δ ppm) of 6-ethyl-pyrrolone derivative **179**.

HRMS-ESI (m/z) ([M + Na]$^+$):

Calculated : 280.1672

Observed : 280.1673

|Δm| : 3.6 ppm

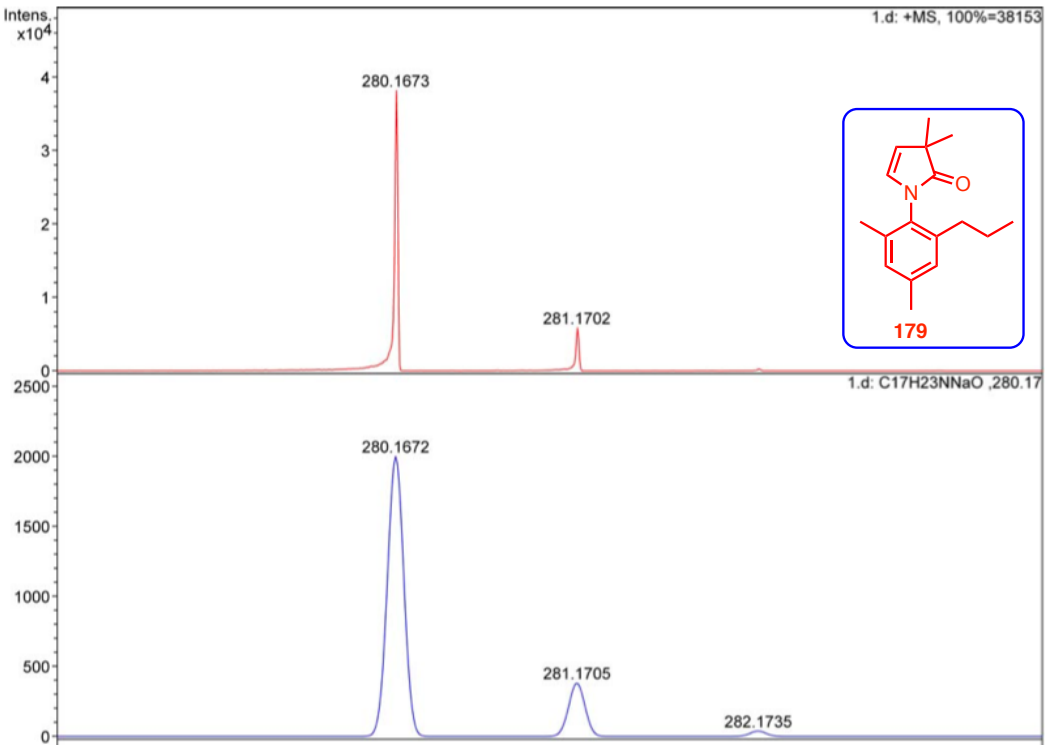

Figure 3.111: HRMS of 6-ethyl-pyrrolone derivative **179**.

3.11.5. Synthesis of silyloxyethyl-pyrrol-2-one derivative 180a-c

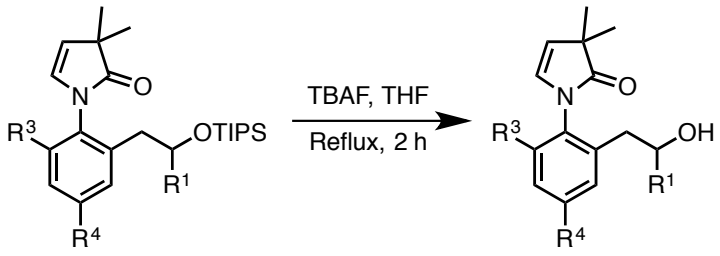

181a-c **180a-c**

h) R^1,R^4= H; R^3= CH_3
i) R^1,R^3= H; R^4= H;
j) R^1= Ph; R^3,R^4= H

Scheme 3.32: Synthesis of 2-hydroxyphenyl-pyrrol-2-one derivative **180a-c**.

To a solution of silyloxyethyl derivative **181a-c** (2.0 g, 1.0 *equiv.*) in THF (20 mL) under at room temperature, TBAF (1M in THF, 1.1 *equiv.*) was added. The resulting solution was heated to reflux and maintained until complete consumption of starting material. After the reaction, the mixture was cooled to room temperature and diluted with DI water (30 mL) and extracted with ethyl acetate (2 × 20 mL). The combined organic layer was dried over *anhyd.* Na_2SO_4, filtered and the solvent was evaporated under reduced pressure to get the crude product. The crude product was purified by combiflash using a hexanes:ethyl acetate mixture (50:50) to get the title product.

R*f* = 0.30 (50% hexanes:50% ethyl acetate) for **180a** (Yield = 66%).

^{1}H-NMR (400 MHz, $CDCl_3$, δ ppm): 7.33-7.22 (m, 3H), 7.12-7.09 (m, 1H), 6.44 (d, *J*= 4.8 Hz, 1H), 5.47 (d, *J*= 4.8 Hz, 1H), 3.74 (s, 1H), 2.73 (t, *J*= 6.4 Hz, 2H), 2.63 (bs, 1H) and 1.27 (s, 6H).

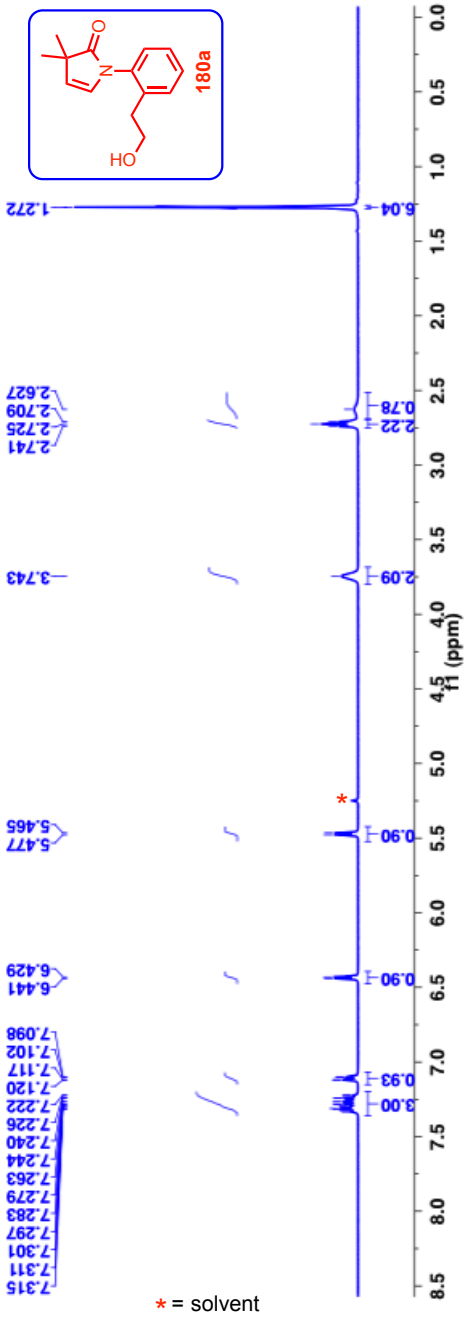

Figure 3.112: ^{1}H-NMR (400 MHz, $CDCl_3$, δ ppm) of 6-hydroxyethyl-pyrrolone derivative **180a**.

^{13}C-NMR (100 MHz, $CDCl_3$, δ ppm): 182.6, 136.7, 136.0, 131.7, 130.8, 128.7, 127.7, 127.6, 118.4, 62.5, 46.6, 34.5 and 23.6.

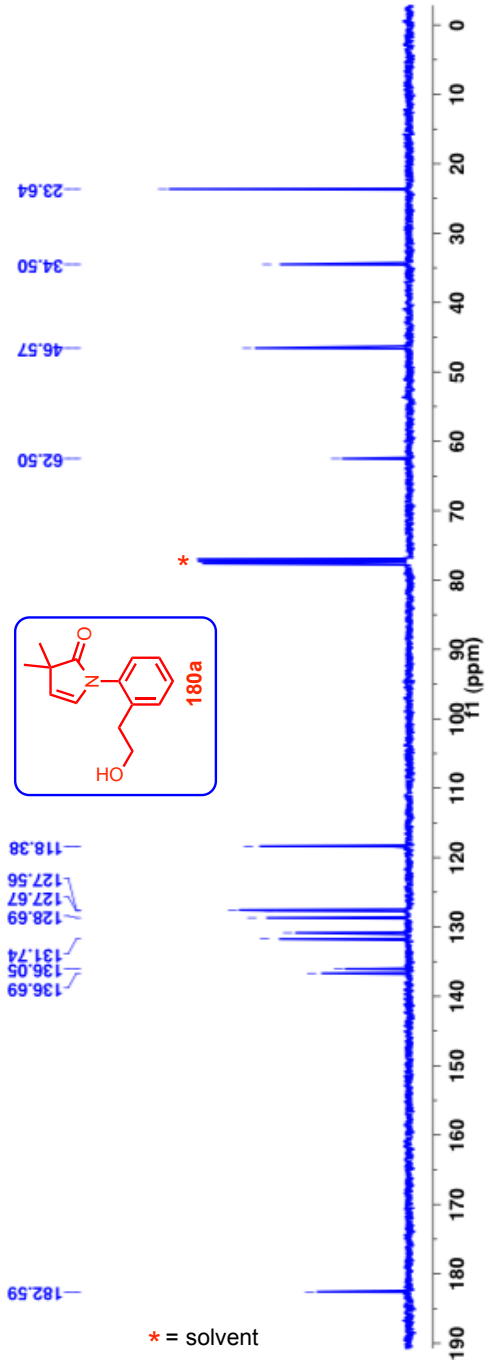

Figure 3.113: ^{13}C-NMR (100 MHz, $CDCl_3$, δ ppm) of 6-hydroxyethyl-pyrrolone derivative **180a**.

HRMS-ESI (m/z) ([M + Na]$^+$):

Calculated : 254.1151

Observed : 254.1144

|Δm| : 2.7 ppm

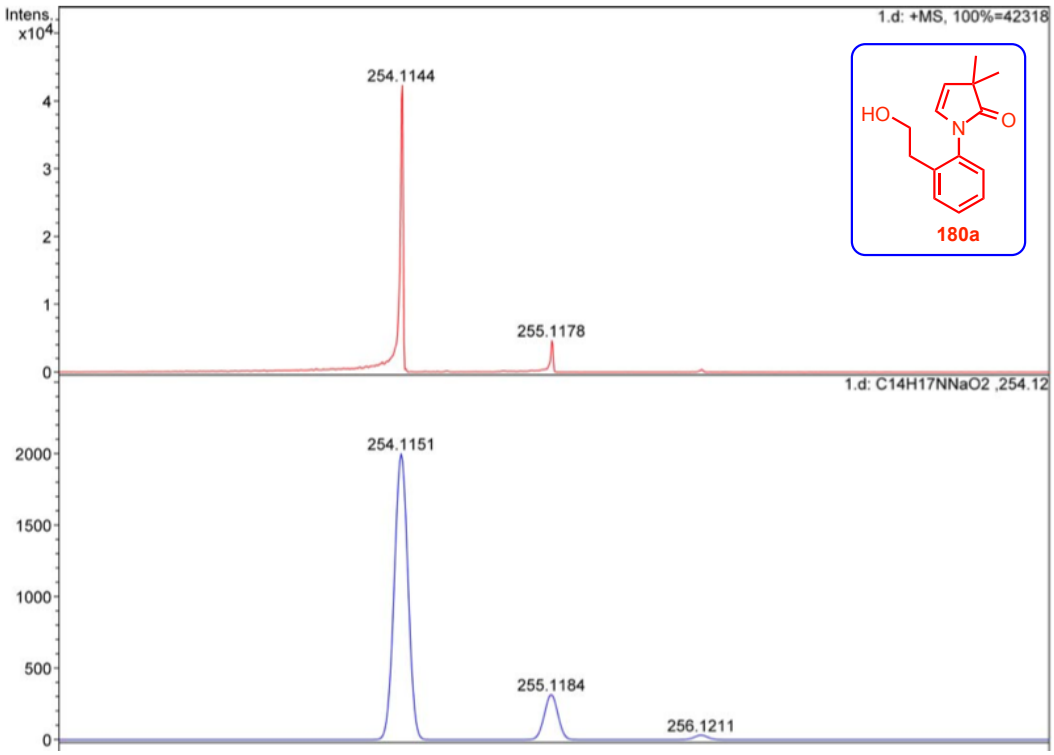

Figure 3.114: HRMS of 6-hydroxyethyl-pyrrolone derivative **180a**.

R*f* = 0.35 (50% hexanes:50% ethyl acetate) for **180b** (Yield = 82%).

^{1}H-NMR (400 MHz, $CDCl_3$, δ ppm): 7.34-7.23 (m, 3H), 7.12-7.10 (m, 1H), 6.43 (d, *J*= 4.8 Hz, 1H), 5.47 (d, *J*= 4.8 Hz, 1H), 3.97-3.89 (m, 1H), 2.69 (dd, *J* = 14.0, 4.3 Hz, 1H), 2.55 (dd, *J* = 14.0, 8.7 Hz, 1H), 2.44 (bs, 1H), 1.28 (s, 3H), 1.27 (s, 3H) and 1.16 (d, *J*= 6.4 Hz, 3H).

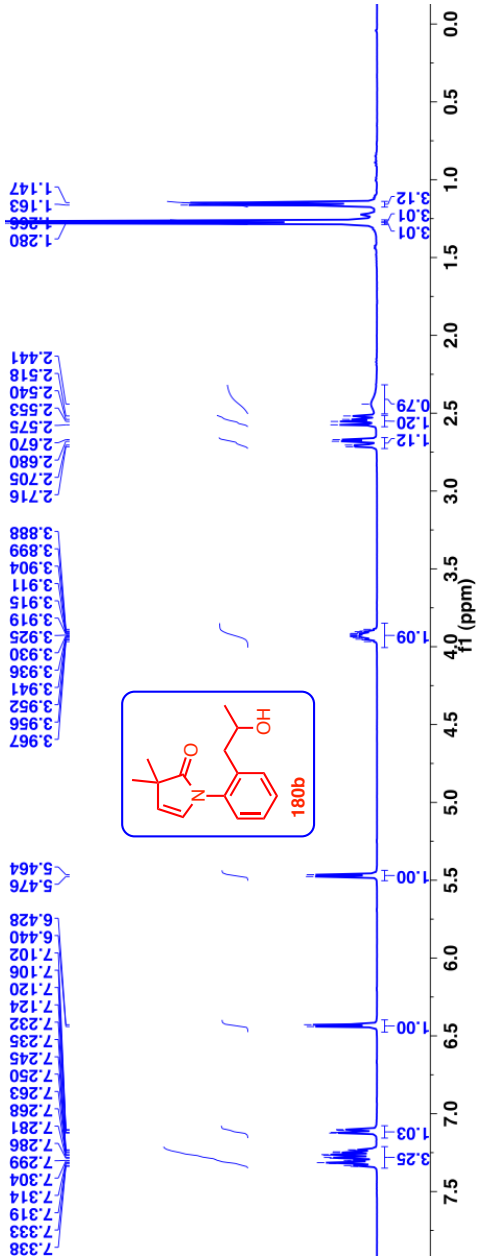

Figure 3.115: ^{1}H-NMR (400 MHz, $CDCl_3$, δ ppm) of 6-hydroxypropyl-pyrrolone derivative **180b**.

^{13}C-NMR (100 MHz, $CDCl_3$, δ ppm): 182.4, 136.8, 136.1, 131.8, 131.3, 128.7, 127.8, 127.7, 118.3, 68.0, 46.5, 41.2, 24.0, 23.7 and 23.6.

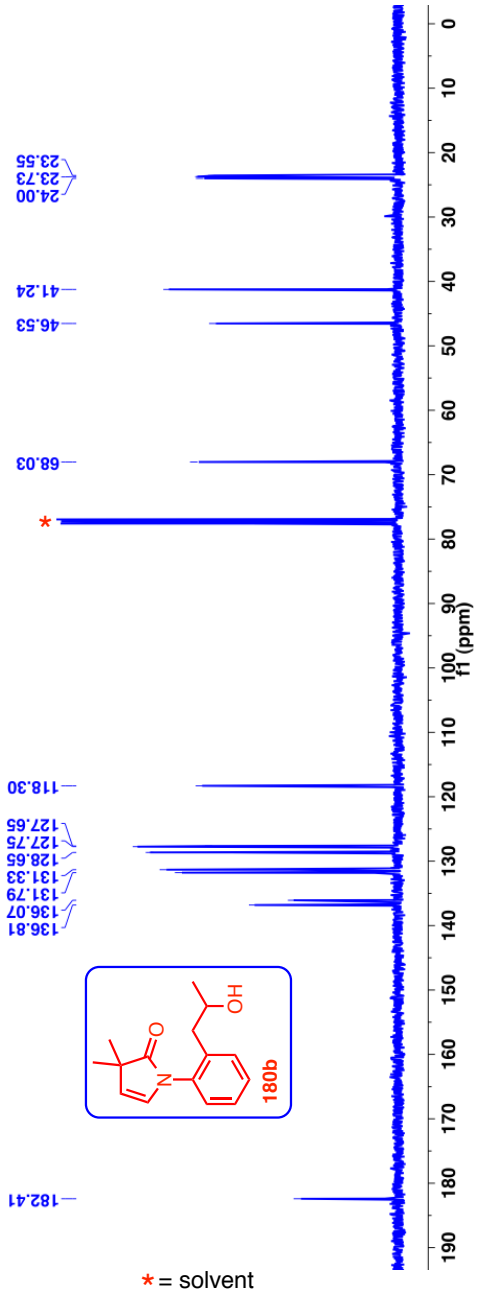

Figure 3.116: ^{13}C-NMR (100 MHz, $CDCl_3$, δ ppm) of 6-hydroxypropyl-pyrrolone derivative **180b**.

HRMS-ESI (m/z) ([M + Na]$^+$):

Calculated : 268.1308

Observed : 268.1313

|Δm| : 1.9 ppm

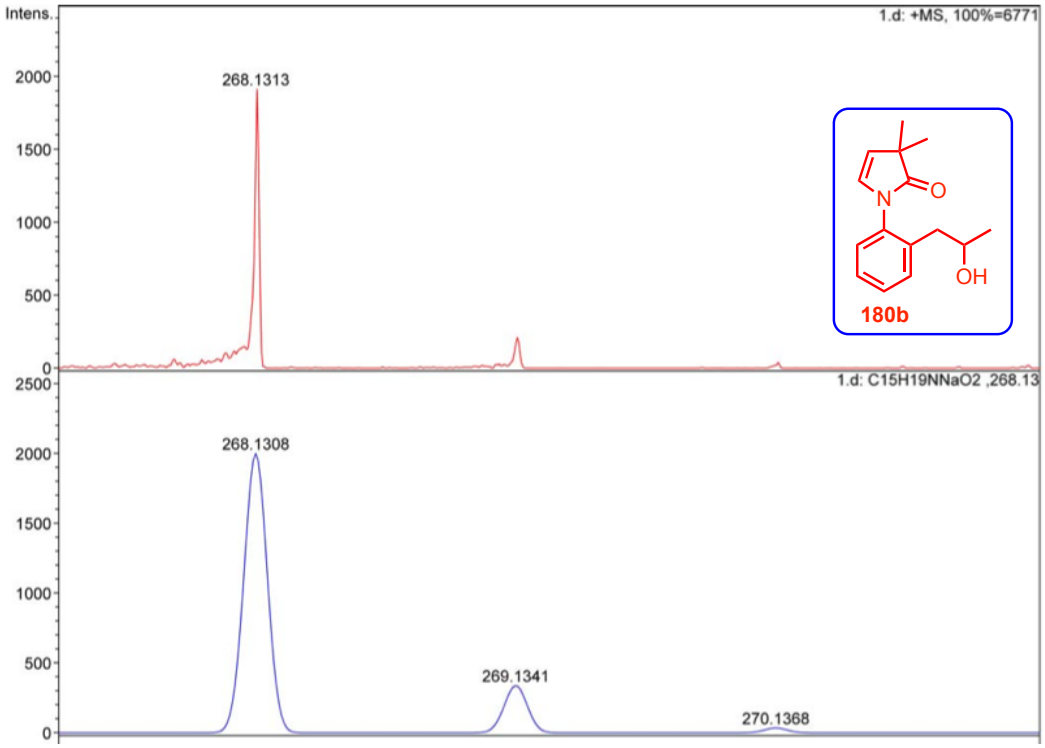

Figure 3.117: HRMS of 6-hydroxypropyl-pyrrolone derivative **180b**.

R*f* = 0.20 (80% hexanes:20% ethyl acetate) for **180c** (Yield = 93%).

^{1}H-NMR (400 MHz, $CDCl_3$, δ ppm): 7.32-7.21 (m, 10H), 7.02 (s, 2H), 6.98 (s, 2H), 6.31 (d, *J* = 4.8 Hz, 1H), 6.17 (d, *J* = 4.8 Hz, 1H), 5.51-5.49 (m, 2H), 4.83-4.78 (m, 2H), 3.46-3.44 (m, 1H), 2.88-2.80 (m, 2H), 2.76-2.68 (m, 2H), 2.48-2.44 (m, 1H), 2.31 (s, 3H), 2.298 (s, 3H), 2.11 (s, 3H), 2.11 (s, 3H), 1.33 (s, 3H), 1.32 (s, 3H), 1.31 (s, 3H) and 1.296 (s, 3H).

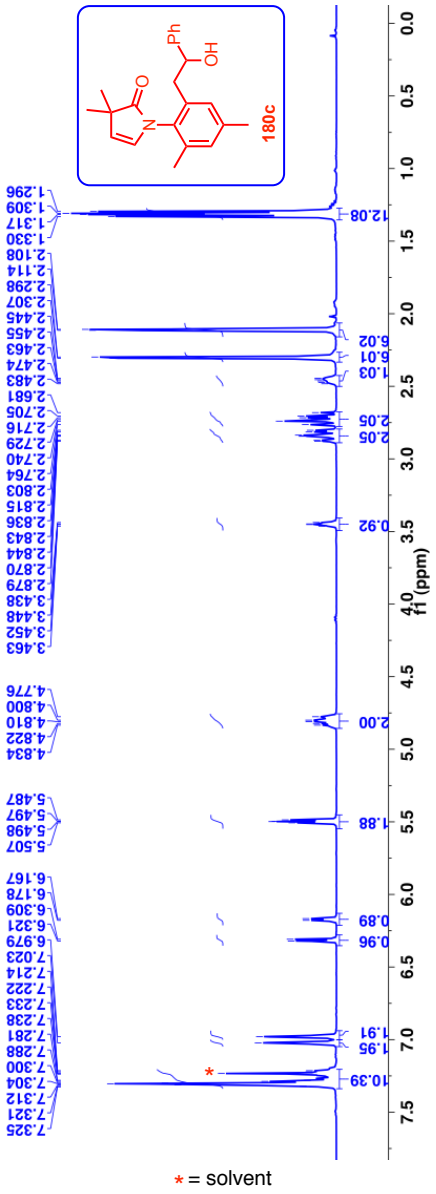

Figure 3.118: ^{1}H-NMR (400 MHz, $CDCl_3$, δ ppm) of 6-hydroxyphenethyl-pyrrolone **180c**.

^{13}C-NMR (100 MHz, $CDCl_3$, δ ppm): 183.2, 182.5, 145.2, 144.7, 138.8, 138.5, 136.96, 136.9, 136.8, 136.5, 132.3, 132.2, 131.7, 131.5, 130.5, 130.4, 130.1, 129.2, 128.5, 128.46, 127.6, 127.4, 125.95, 125.8, 118.5, 118.1, 74.9, 73.7, 46.5, 46.3, 42.2, 41.9, 24.0, 23.7, 23.6, 23.61, 21.3, 18.26 and 18.1.

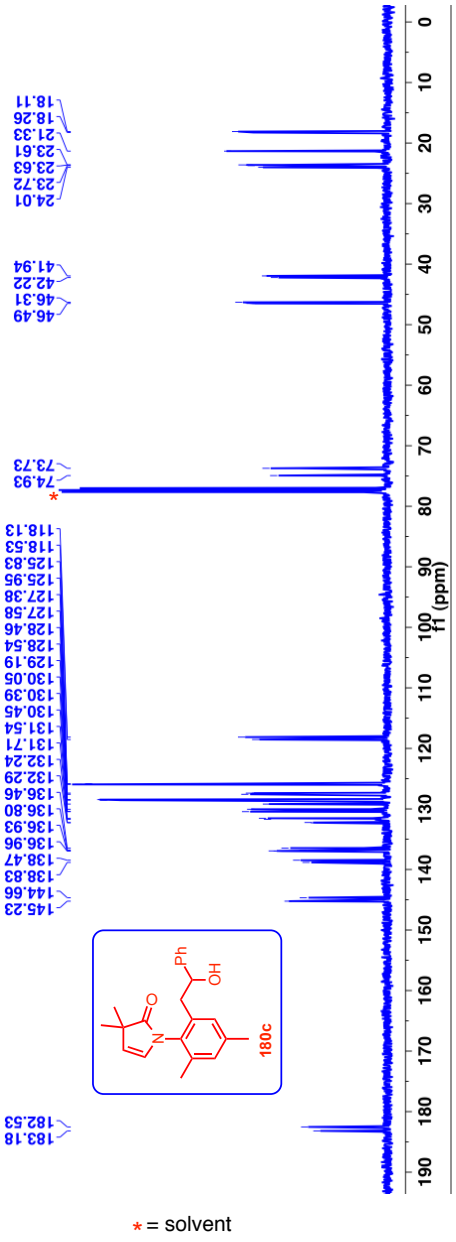

Figure 3.119: ^{13}C-NMR (100 MHz, $CDCl_3$, δ ppm) of 6-hydroxyphenethyl-pyrrolone **180c**.

HRMS-ESI (m/z) ([M + Na]$^+$):

Calculated : 358.1762

Observed : 358.1778

|Δm| : 4.5 ppm

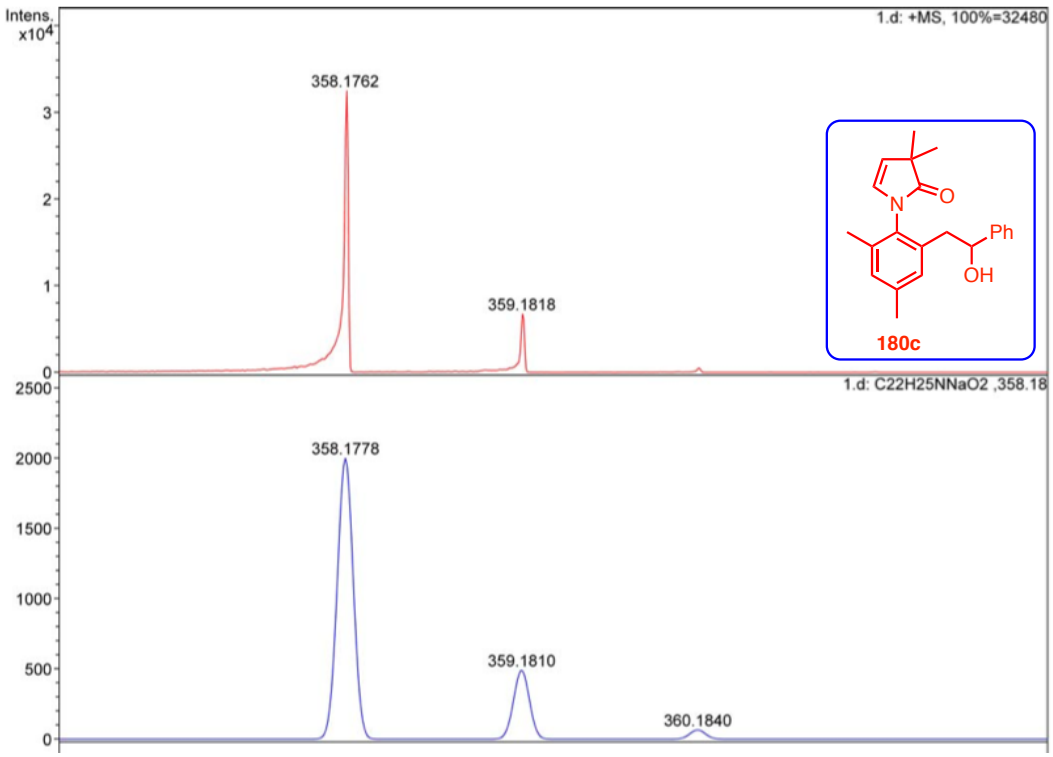

Figure 3.120: HRMS of 6-hydroxyphenethyl-pyrrolone **180c**.

3.11.6. Synthesis of atropisomeric oxo-pyrrol-2-one derivative 174h-i

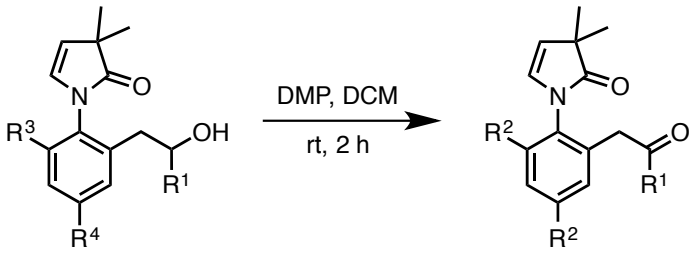

180h-j **174h-j**

h) R^1,R^4= H; R^3= CH_3
i) R^1,R^3= H; R^4= H;
j) R^1= Ph; R^3,R^4= H

Scheme 3.33: Synthesis of atropisomeric oxo-pyrrol-2-one derivative **174h-j**.

To a slurry of Dess-Martin periodinane (1.2 *equiv*) in DCM (20 mL) at 0 ^{o}C, a solution of corresponding alcohol derivative **180h-j** (500 mg, 1.0 *equiv*) in DCM (5 mL) was added. The resulting mixture was warmed to room temperature and stirred for 2 h. The reaction was quenched with 1N NaOH solution (10 mL) and the mixture was extracted with DCM (2 × 15 mL). The combined organic layer was dried over *anhyd.* Na_2SO_4, filtered and the solvent was evaporated under reduced pressure to get the crude product. The crude product was purified by combiflash using a hexanes:ethyl acetate mixture to get the title product.

R*f* = 0.60 (50% hexanes:50% ethyl acetate) for **174h** (Yield = 73%).

^{1}H-NMR (400 MHz, $CDCl_3$, δ ppm): 9.61 (t, *J*= 1.7 Hz, 1H), 7.33-7.23 (m, 3H), 7.18-7.16 (m, 1H), 6.44 (d, *J*= 4.9 Hz, 1H), 5.46 (d, *J*= 4.9 Hz, 1H), 3.60-3.59 (m, 2H) and 1.24 (s, 6H).

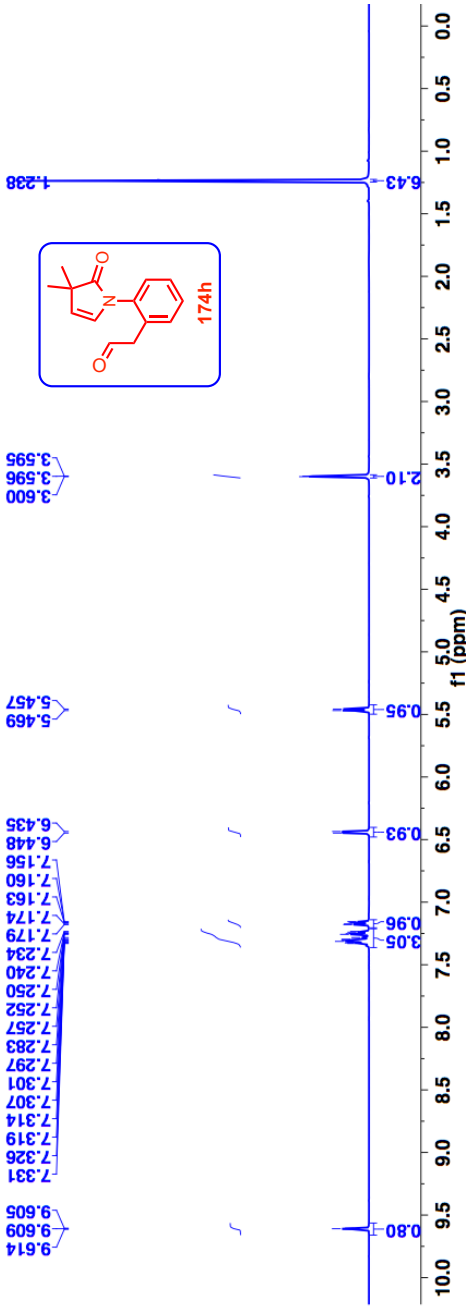

Figure 3.121: ^{1}H-NMR (400 MHz, $CDCl_3$, δ ppm) of 6-acetaldehyde-pyrrolone derivative **174h**.

^{13}C-NMR (100 MHz, $CDCl_3$, δ ppm): 199.2, 181.6, 136.5, 131.8, 131.2, 130.4, 128.9, 128.6, 126.8, 118.8, 47.2, 46.5 and 23.5.

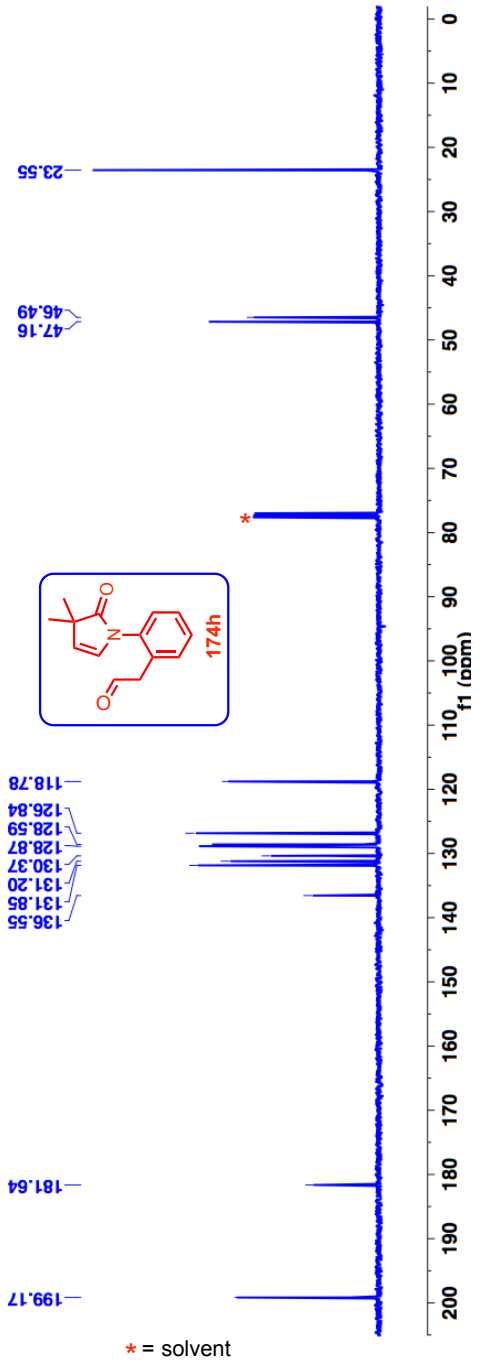

Figure 3.122: ^{13}C-NMR (100 MHz, $CDCl_3$, δ ppm) of 6-acetaldehyde-pyrrolone derivative **174h**.

HRMS-ESI (m/z) ([M + Na]$^+$):

Calculated : 252.0995

Observed : 252.0994

|Δm| : 0.4 ppm

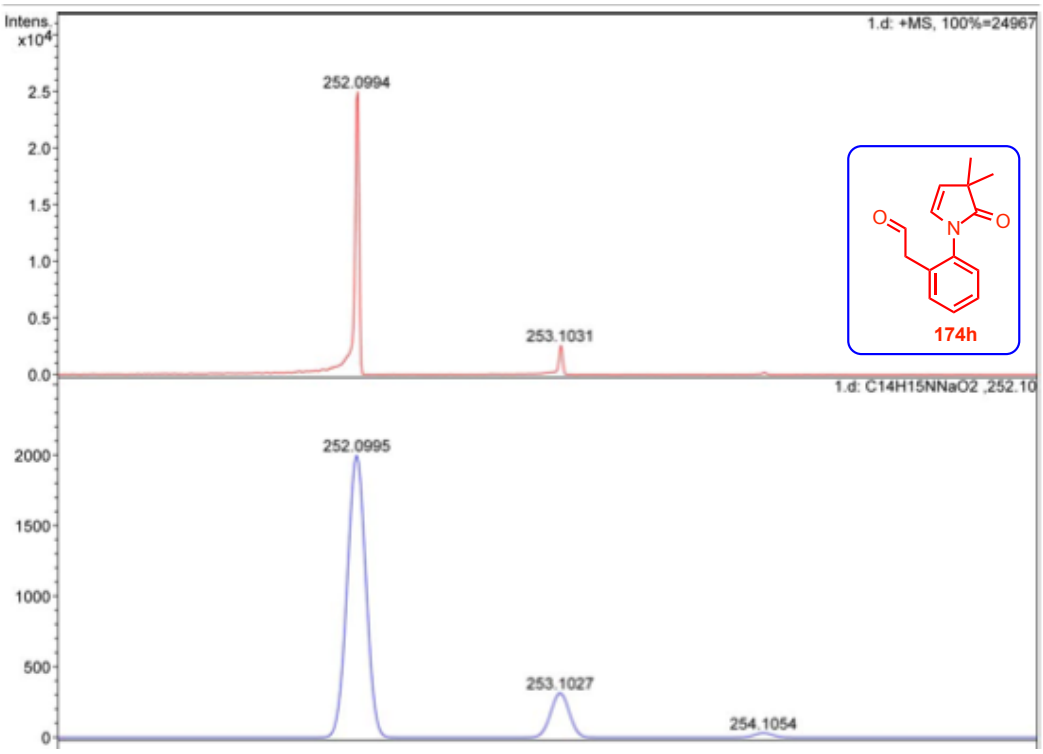

Figure 3.123: HRMS of 6-acetaldehyde-pyrrolone derivative **174h**.

R*f* = 0.50 (50% hexanes:50% ethyl acetate) for **174i** (Yield = 82%).

^{1}H-NMR (400 MHz, $CDCl_3$, δ ppm): 7.27-7.24 (m, 2H), 7.19-7.17 (m, 1H), 7.12-7.09 (m, 1H), 6.39 (d, *J* = 4.8 Hz, 1H), 5.41 (d, *J* = 4.8 Hz, 1H), 3.65 (s, 2H), 2.04 (s, 3H) and 1.22 (s, 6H).

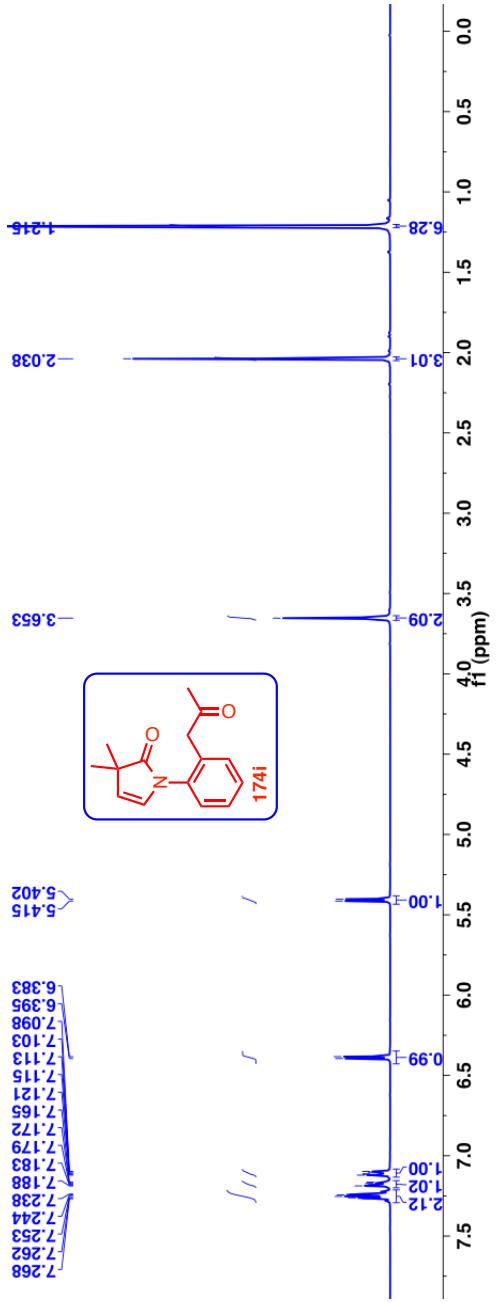

Figure 3.124: ^{1}H-NMR (400 MHz, $CDCl_3$, δ ppm) of 6-acetone-pyrrolone derivative **174i**.

^{13}C-NMR (100 MHz, $CDCl_3$, δ ppm): 205.2, 181.3, 136.2, 132.2, 131.7, 131.3, 128.3, 126.8, 118.2, 47.3, 46.2, 29.5 and 23.5.

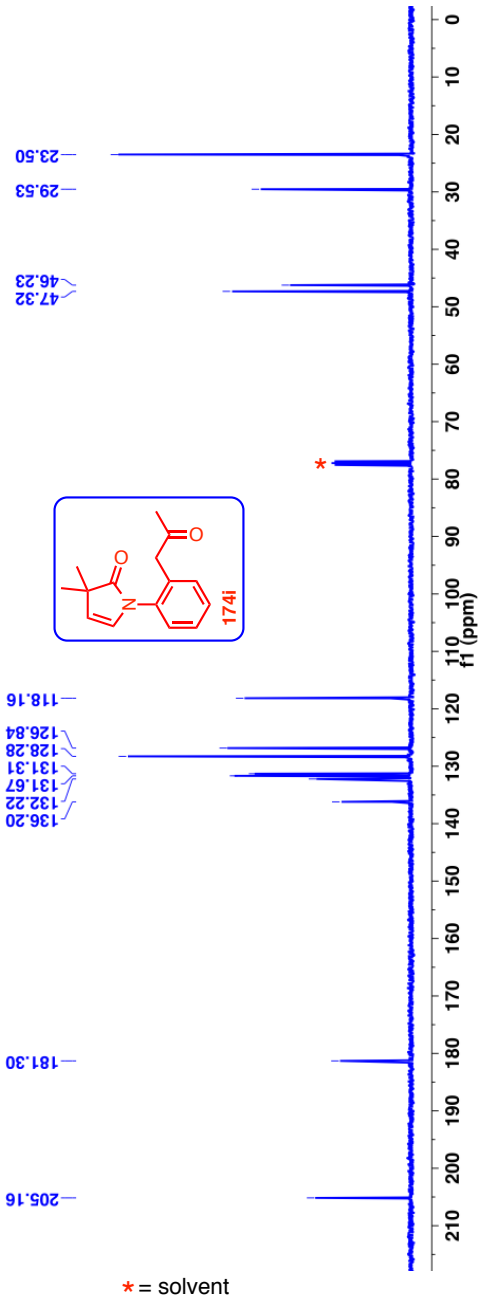

Figure 3.125: ^{13}C-NMR (100 MHz, $CDCl_3$, δ ppm) of 6-acetone-pyrrolone derivative **174i**.

HRMS-ESI (m/z) ([M + Na]$^+$):

Calculated : 266.1151

Observed : 266.1146

|Δm| : 1 .9 ppm

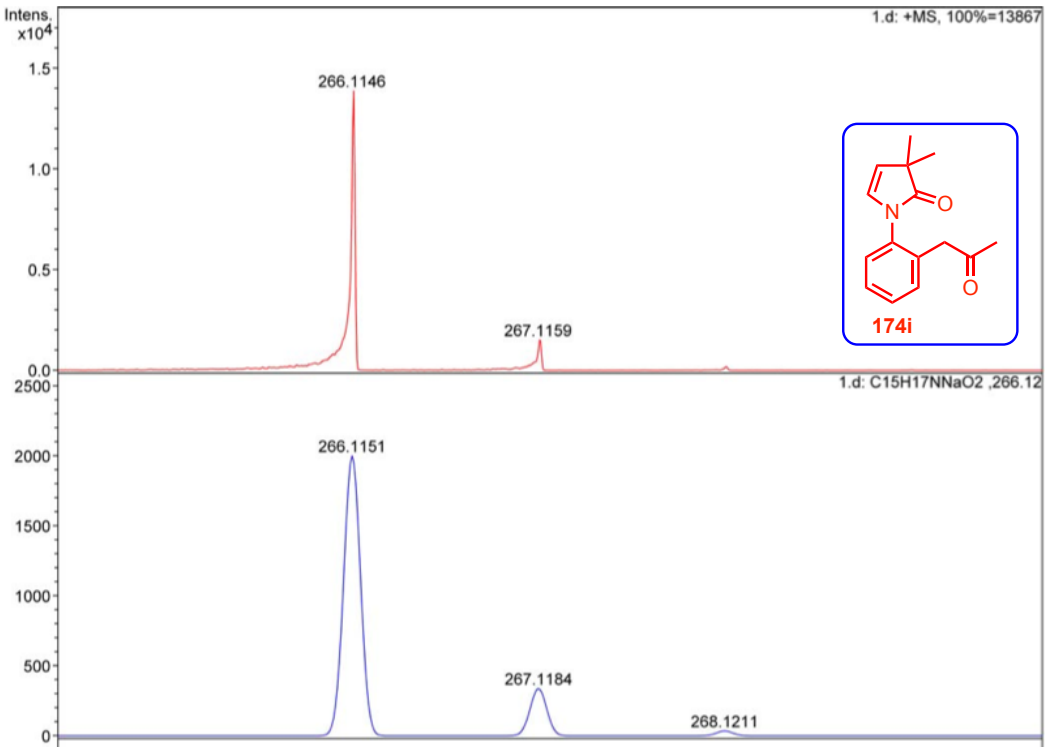

Figure 3.126: HRMS of 6-acetone-pyrrolone derivative **174i**.

R*f* = 0.55 (80% hexanes:20% ethyl acetate) for **174j** (Yield = 68%).

^{1}H-NMR (400 MHz, $CDCl_3$, δ ppm): 7.93-7.91 (m, 2H), 7.53-7.49 (m, 1H), 7.43-7.39 (m, 2H), 6.997 (s, 1H), 6.896 (s, 1H), 6.26 (d, *J* = 4.8 Hz, 1H), 5.31 (d, *J* = 4.8 Hz, 1H), 4.34 (d, *J* = 17.4 Hz, 1H), 4.01 (d, *J* = 17.4 Hz, 1H), 2.28 (s, 3H), 2.11 (s, 3H), 1.22 (s, 3H) and 0.96 (s, 3H).

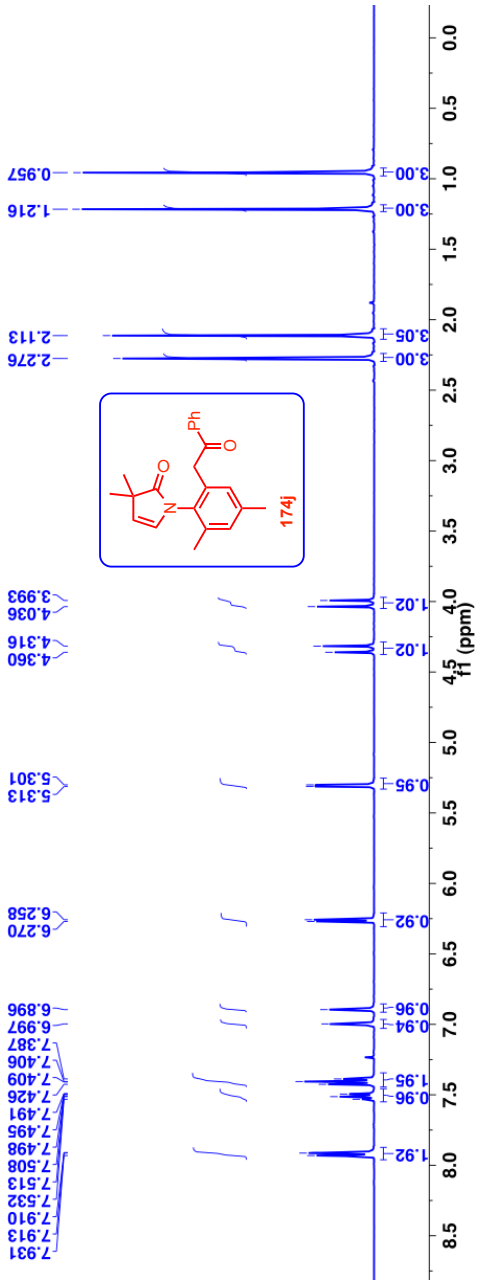

Figure 3.127: ^{1}H-NMR (400 MHz, $CDCl_3$, δ ppm) of 6-acetophenone-pyrrolone derivative **174j**.

^{13}C-NMR (100 MHz, $CDCl_3$, δ ppm): 197.6, 181.8, 138.7, 136.9, 136.4, 133.8, 133.5, 132.5, 131.9, 131.0, 129.9, 128.8, 128.4, 117.7, 46.0, 42.5, 23.8, 23.5, 21.3 and 18.1.

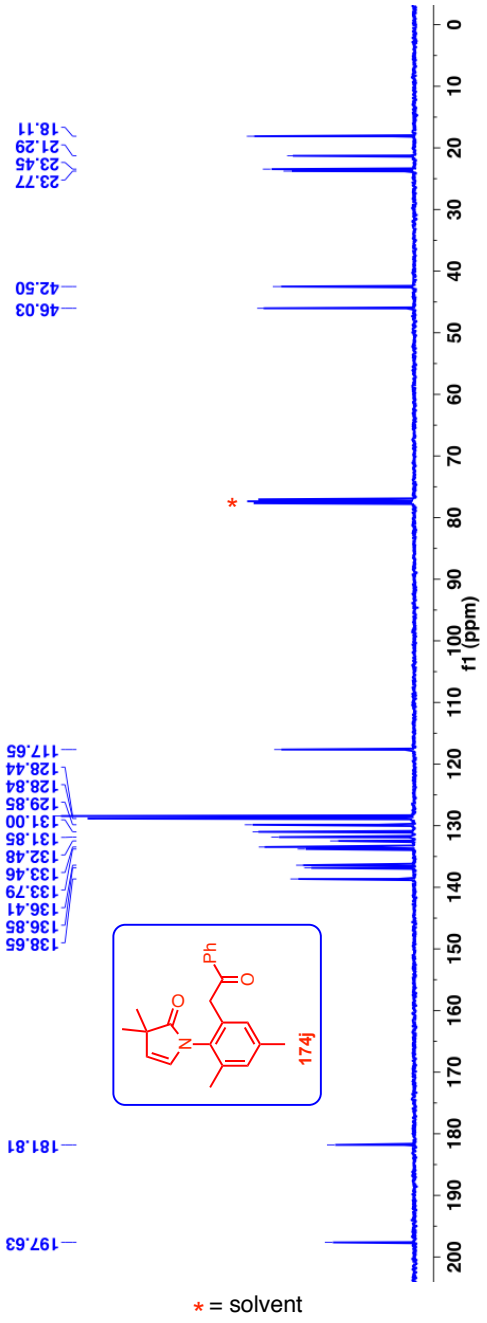

Figure 3.128: ^{13}C-NMR (400 MHz, $CDCl_3$, δ ppm) of 6-acetophenone-pyrrolone derivative **174j**.

HRMS-ESI (m/z) ([M + Na]$^+$):

Calculated : 358.1621

Observed : 358.1623

|Δm| : 0.6 ppm

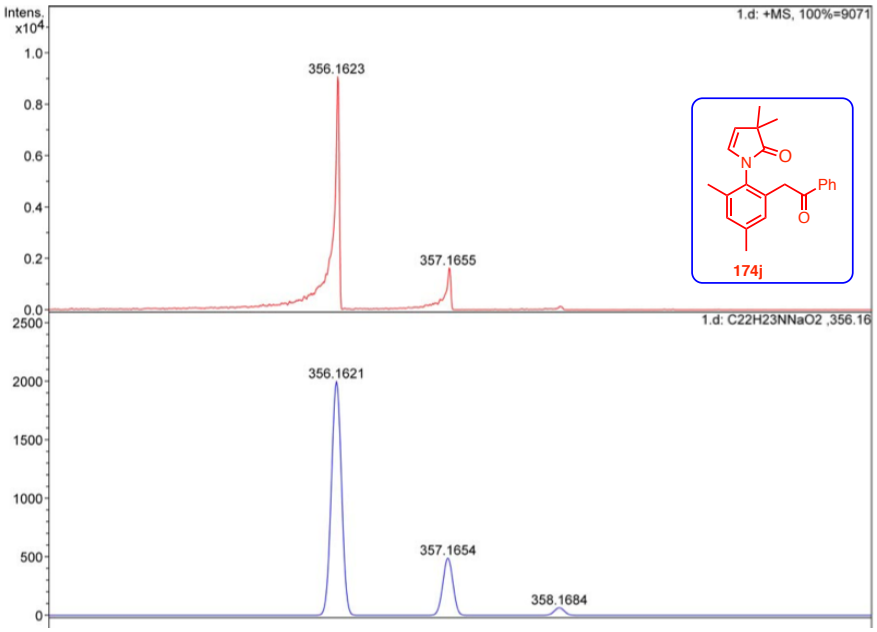

Figure 3.129: HRMS of 6-acetophenone-pyrrolone derivative **174j**.

HPLC analysis conditions:

For analytical conditions,

I). Column : RR-WHELK-01 10/100 FEC

Abs. detector wavelength : 254 nm and 270 nm

Mobile phase : Hexanes:2-propanol = 70:30

Flow rate : 1.5 mL/min

Retention times (min) : ~ 6.77 [(-)-**174j**] and ~ 13.64 [(+)-**174j**

For preparative conditions,

I). Column : CHIRALPAK-ADH

Abs. detector wavelength : 254 nm and 270 nm

Mobile phase : Hexanes:2-propanol = 80:20

Flow rate : 3.0 mL/min

Retention times (min) : ~ 18.08 [(-)-**174j** and ~ 36.35 [(+)-**174j**]

Optical rotation $[\alpha]_D^{24}$:

HPLC retention time (RR-WHELK) at ~ 18.08 min, (*c* = ~1.4 %, MeOH) = -113.68 deg.

HPLC retention time (RR-WHELK) at ~ 36.35 min, (*c* = ~1.4 %, MeOH) = +116.16 deg.

3.11.7. Synthesis of 6-methyl-2-allyl-N-cyclohexenyl acetamides 174k

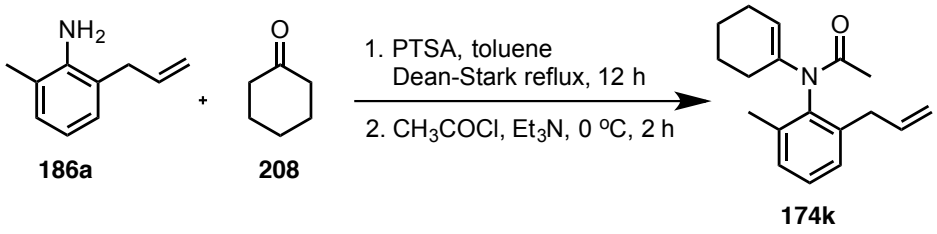

186a **208** **174k**

Scheme 3.34: Synthesis of atropisomeric N-cyclohexenyl acetamide **174k**.

A mixture of aniline **186a** (1.0 g, 6.79 mmol), *p*-toluenesulfonic acid (130 mg, 0.1 *equiv.*) and cyclohexanone **208** (3.51 mL, 33.9 mmol) in dry toluene (30 mL) was refluxed with Dean-Stark apparatus for 12 h. The reaction was concentrated under 25 ^{o}C under reduced pressure. The crude was taken in toluene (10 mL) and cooled to 0 ^{o}C, to which acetyl chloride (0.97 mL, 13.6 mmol) and triethylamine (2.84 mL, 20.4 mmol) was added. The resulting mixture was stirred at 0 ^{o}C for 2 h. After the reaction, DI water (15 mL) was added and the mixture was extracted with ethyl acetate (2 × 15 mL). The combined organic layer was washed with brine solution (10 mL), dried under saturated Na_2SO_4, filtered and the solvent was evaporated under reduced pressure to get the crude product. The crude was purified by combiflash using hexanes and ethyl acetate mixture (90:10).

R*f* = 0.35 (80% hexanes:20% ethyl acetate) for **174k** (Yield = 50%).

^{1}H-NMR (400 MHz, $CDCl_3$, δ ppm): 7.18-7.04 (m, 3H), 5.899-5.79 (m, 1H), 5.09-4.99 (m, 3H), 3.26 (d, *J*= 6.8 Hz, 2H), 2.57-2.40 (m, 2H), 2.18 (s, 3H), 1.97-1.967 (m, 2H), 1.68 (s, 3H) and 1.63-1.52 (m, 4H).

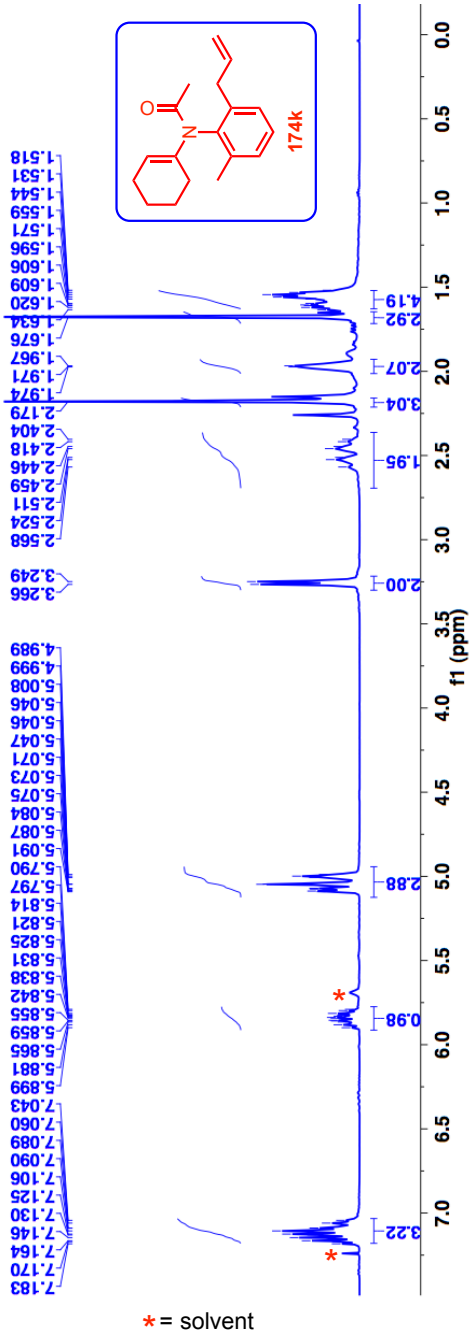

Figure 3.130: ^{1}H-NMR (400 MHz, $CDCl_3$, δ ppm) of 6-allyl-cyclohexenylenamide **174k**.

^{13}C-NMR (100 MHz, $CDCl_3$, δ ppm): 170.3, 140.8, 139.4, 138.2, 136.7, 136.2, 129.4, 128.3, 128.1, 118.6, 117.0, 35.6, 28.3, 24.8, 24.1, 23.4, 22.2 and 18.4.

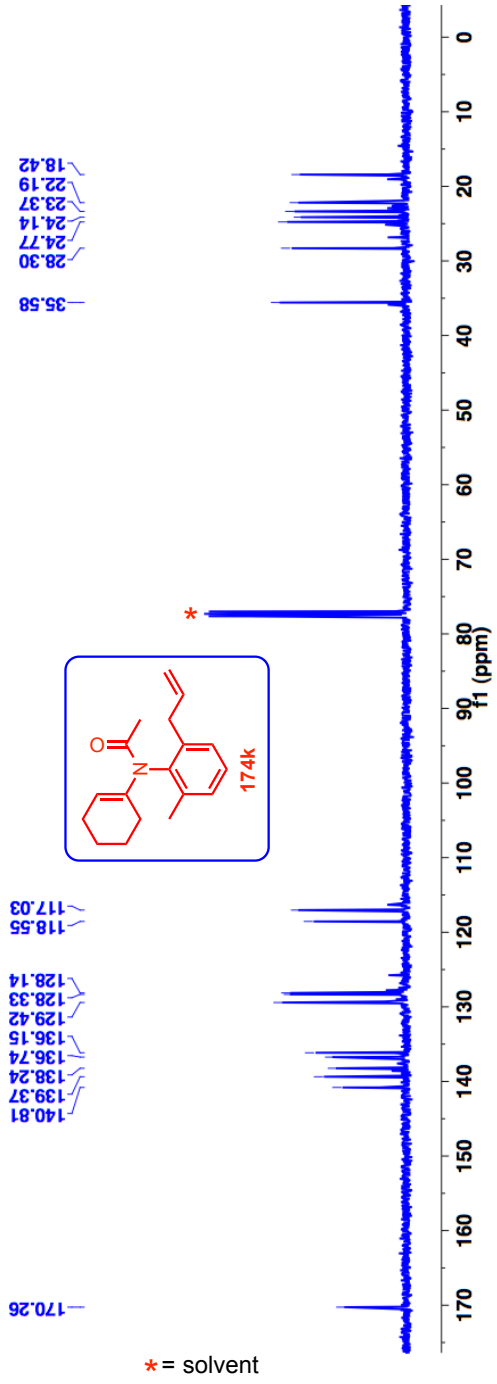

Figure 3.131: ^{13}C-NMR (100 MHz, $CDCl_3$, δ ppm) of 6-allyl-cyclohexenylacetamide **174k**.

HRMS-ESI (m/z) ([M + Na]$^+$):

Calculated : 292.1672

Observed : 292.1663

|Δm| : 3.1 ppm

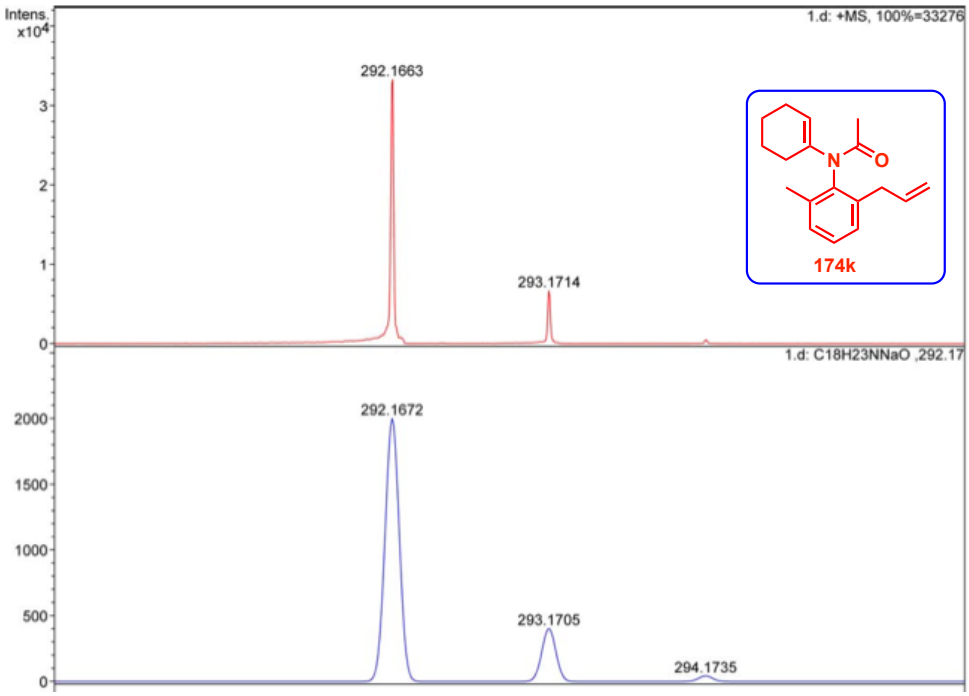

Figure 3.132: HRMS of 6-allyl-cyclohexenylenamide **174k**.

HPLC analysis conditions:

For analytical conditions,

I). Column : CHIRALPAK-IC

Abs. detector wavelength : 254 nm and 270 nm

Mobile phase : Hexanes:2-propanol = 95:5

Flow rate : 1.0 mL/min

Retention times (min) : ~ 20.65 [(A)-**174k**] and ~ 22.33 [(B)-**174k**]

For preparative conditions,

I). Column : CHIRALPAK-IC

Abs. detector wavelength : 254 nm and 270 nm

Mobile phase : Hexanes:2-propanol = 99:1

Flow rate : 4.0 mL/min

Retention times (min) : ~ 57.38 [(A)-**174k**] and ~ 63.17 [(B)-**174k**]

(A and B refers to the order of elution for a given pair of isomers on HPLC)

3.11.8. Synthesis of atropisomeric 6-methyl-2-allyl-N-vinyl acetamide 174l

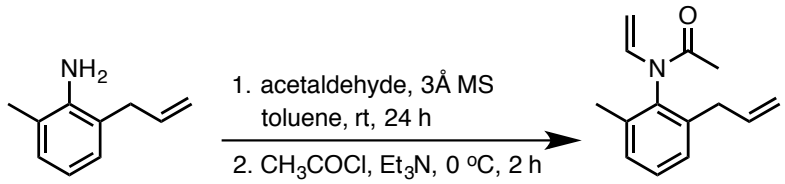

186a **174l**

Scheme 3.35: Synthesis of atropisomeric *N*-vinyl enamide derivative **174l**.

To a mixture of aniline **186a** (1.0 g, 6.79 mmol) and 3Å molecular sieves (1.0 g) in dry toluene (10 mL) at 0 ^{o}C, acetaldehyde (0.76 mL, 13.6 mmol) was added and the resulting mixture was stirred at room temperature for 24 h. After the reaction, the mixture was filtered through celite and concentrated at 25 ^{o}C under reduced pressure. The resulting crude was taken in toluene (10 mL) and cooled to 0 ^{o}C, to which acetyl chloride (0.73 mL, 10.2 mmol) and triethylamine (2.4 mL, 17 mmol) was added. The resulting mixture was stirred at 0 ^{o}C for 2 h. After the reaction, DI water (15 mL) was added and the mixture was extracted with ethyl acetate (2 × 15 mL). The combined organic layer was washed with brine solution (10 mL), dried under saturated Na_2SO_4, filtered and solvent was evaporated under reduced pressure to get the crude product. The crude was purified by combiflash using hexanes and ethyl acetate mixture (90:10).

R*f* = 0.55 (80% hexanes:20% ethyl acetate) for **174l** (Yield = 41%).

^{1}H-NMR (400 MHz, $CDCl_3$, δ ppm): 7.63 (dd, *J* = 16.0, 8.8 Hz, 1H), 7.27-7.23 (m, 1H), 7.19-7.15 (m, 2H), 5.87-5.77 (m, 1H), 5.09-5.03 (m, 2H), 4.30 (d, *J* = 8.8 Hz, 1H), 3.75 (d, *J* = 16.0 Hz, 1H), 3.18 – 3.16 (m, 2H), 2.11 (s, 3H) and 1.73 (s, 3H).

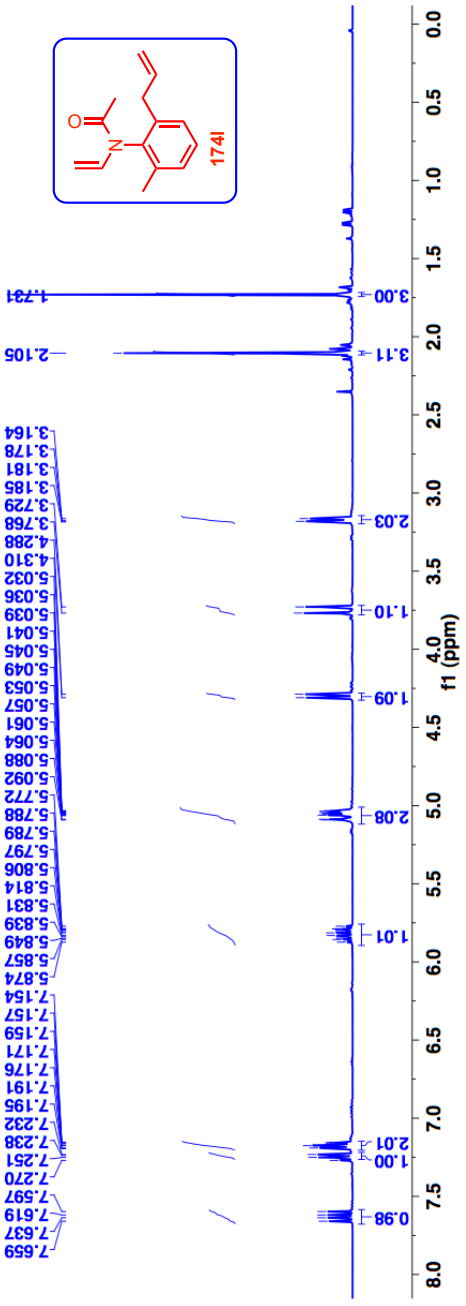

Figure 3.133: ^{1}H-NMR (400 MHz, $CDCl_3$, δ ppm) of 6-allyl-vinylacetamide derivative **174l**.

^{13}C-NMR (100 MHz, $CDCl_3$, δ ppm): 169.4, 138.6, 136.7, 136.2, 136.0, 131.3, 129.7, 129.1, 128.4, 117.1, 95.4, 35.3, 22.8 and 17.6.

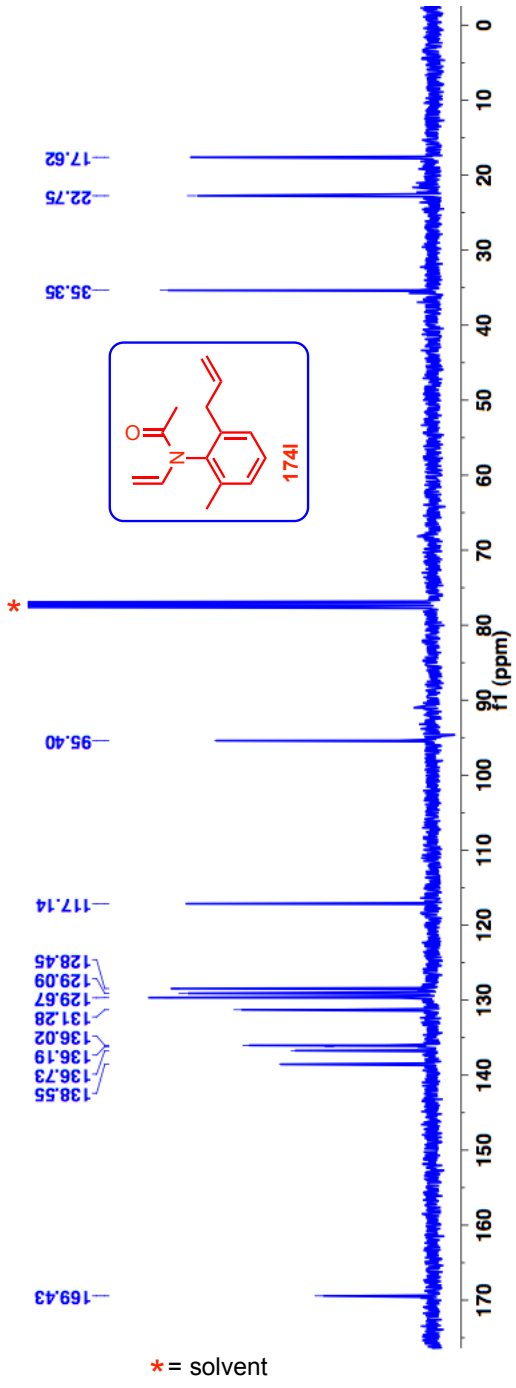

Figure 3.134: ^{13}C-NMR (100 MHz, $CDCl_3$, δ ppm) of 6-allyl-vinylacetamide derivative **174l**.

HRMS-ESI (m/z) ([M + Na]$^+$):

Calculated : 238.1202

Observed : 238.1197

|Δm| : 2.1 ppm

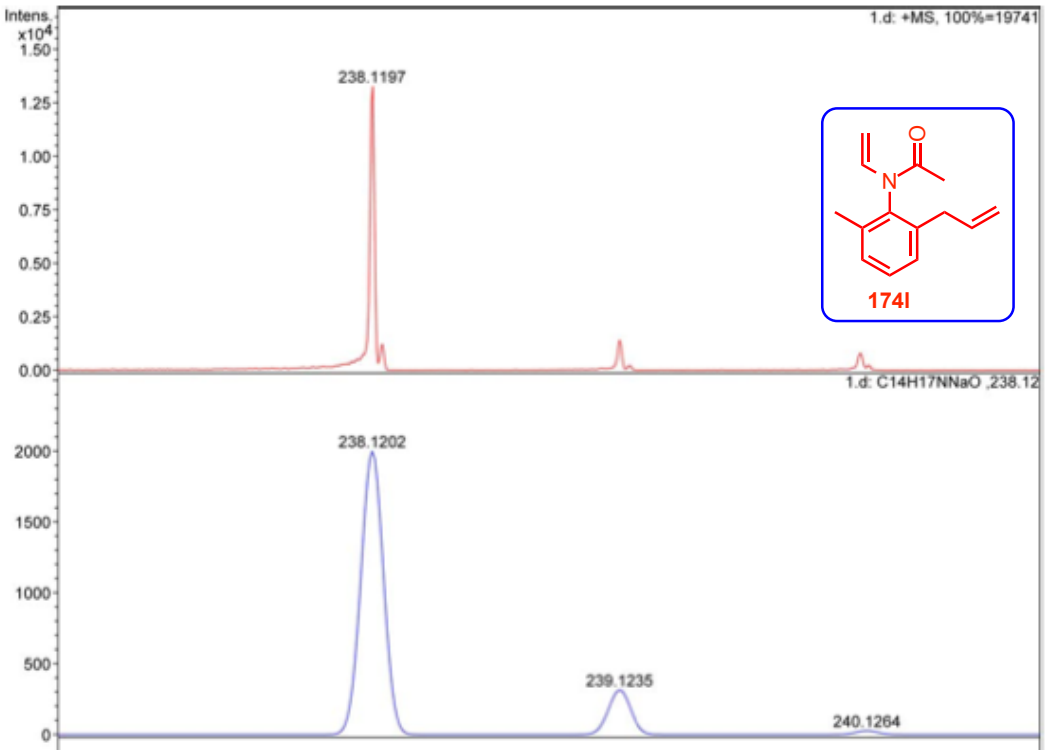

Figure 3.135: HRMS of 6-allyl-vinylacetamide derivative **174l**.

HPLC analysis conditions:

For analytical conditions,

I). Column : CHIRALPAK-IC

Abs. detector wavelength : 254 nm and 270 nm

Mobile phase : Hexanes:2-propanol = 90:10

Flow rate : 1.0 mL/min

Retention times (min) : ~ 6.35 [(A)-**174l**] and ~ 6.77 [(B)-**174l**]

(A and B refers to the order of elution for a given pair of isomers on HPLC)

3.12. General irradiation procedures and characterization of photoproducts

3.12.1. Process for photoreaction of atropisomeric enamides 174a-j

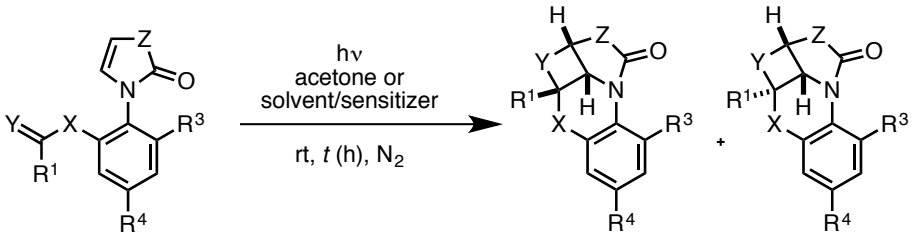

174a-j **175a-j** **176a-j**

R1 = H, Me, Ph; **R2** = H, Me
X = CH_2, CH_2-CH_2, O-CH_2
Y = CH_2, O; **Z =** CMe_2, CH_2-CH_2

Scheme 3.36: General irradiation procedure for atropisomeric enamides **174a-j**.

A solution of optically pure atropisomeric enamides **174a-j** (~2.0-4.0 mM or ~1 mg/1 mL) in acetone or with the combination of methanol/MeCN and the sensitizer (xanthone or acetophenone) were irradiated at -30 ^{o}C for a given time interval in Pyrex tube using a 450 W medium-pressure mercury lamp under constant flow of nitrogen. After irradiation, the solvent was evaporated under reduced pressure and the photoproducts were isolated by preparative thin layer chromatography and characterized by NMR spectroscopy, mass spectrometry, single crystal XRD, CD, $[\alpha]_D$ and by HPLC. HPLC analysis of the photoproduct on chiral stationary phases gave the optical purity of the photoproducts.

3.12.2. Conversion and mass balance after photoreactions in enamides 174a-c

Conversion and mass balance was obtained by irradiating the racemic mixture of enamides (2.23 mM for **174a** and 1.95 mM **174b-c)** in acetone or with the combination of methanol and the sensitizer (xanthone or acetophenone) in Pyrex test tube with a 450 W medium-pressure mercury lamp for given time interval and temperature under constant flow of nitrogen. After irradiation, a stock solution of internal standard in chloroform (triphenylmethane, 4.09 mM) was added to the reaction mixture. The solvent from the mixture with the internal standard was completely evaporated under reduced pressure. The residue was dissolved in 1 mL

of deuterated chloroform and ^{1}H-NMR was recorded. From the integral value of respective peaks, the % conversion and mass balance was calculated using the formula given in equation 2.12.

Table 3.8: Conversion and mass balance in photoreactions of enamides **174a-c**.[a]

Entry	Compd	Solvent	Sensitizer	*T* (^{o}C)	*t* (h)	(%) Convn	(%) MB
1	**174a**	Acetone	Acetone	-30	3	70	96[b]
2		Methanol	xanthone	-30	3	76	89
3		Methanol	Acetophenone	-30	3	29	92
4	**174b**	Acetone	Acetone	-30	24	39	79
5		Methanol	xanthone	-30	3	21	82
6		Methanol	Acetophenone	-30	12	20	87
7	**174c**	Acetone	Acetone	25	2.5	90	77
8		Methanol	xanthone	25	2.5	92	84
9		Methanol	Acetophenone	25	12	33	86

[a] Reported values carry an error of $\pm$5%.[b] 8-10 % of uncharacterized impurity was observed incase of **174a** and **174c**. Convn – conversion; MB- mass balance. Longer irradiation of xanthone sensitizer leads to decomposition, so the irradiation time was limited to 3 h.

While the *ee* values in the photoproducts remained the same at both -30 ^{o}C and at 25 ^{o}C, the conversion and mass balance of the photoreaction was affected significantly. For compounds **174a-b,** the reactions at 25 ^{o}C showed good conversion with poor mass balance. On the other hand, at -30 ^{o}C there was excellent mass balance and conversion. In the case of **174c** the uncharacterized side product was higher at -30 ^{o}C than the photoproduct. But at -30 ^{o}C the uncharacterized side product was less than 8%. Prolonged irradiation after consumption of the reactants **174a-c** (>80% conversion) led to decomposition.

^{1}H-NMR (400 MHz, $CDCl_3$, δ ppm): 7.12-7.03 (m, 2H), 6.96-6.94 (m, 1H), 3.99-3.96 (t, *J* = 8.4 Hz, 1H), 2.99-2.89 (m, 1H), 2.86-2.81 (m, 1H), 2.70-2.60 (m, 1H), 2.57-2.45 (m, 3H), 2.43-2.36 (m, 1H), 2.34-2.24 (m, 1H), 2.21 (s, 3H), 1.94-1.84 (m, 1H) and 1.74-1.68 (m, 1H).

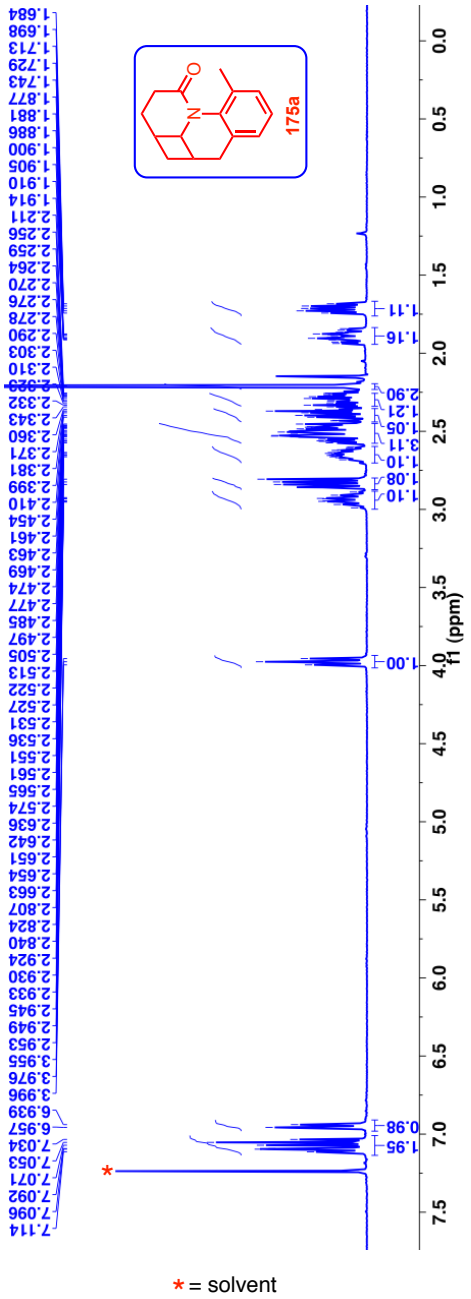

Figure 3.136: ^{1}H-NMR (400 MHz, $CDCl_3$, δ ppm) of cyclobutane photoproduct **175a**.

^{13}C-NMR (100 MHz, $CDCl_3$, δ ppm): 169.7, 137.6, 135.9, 135.2, 129.1, 126.5, 124.98, 55.3, 36.2, 34.2, 32.7, 30.5, 29.8, 28.6 and 18.8.

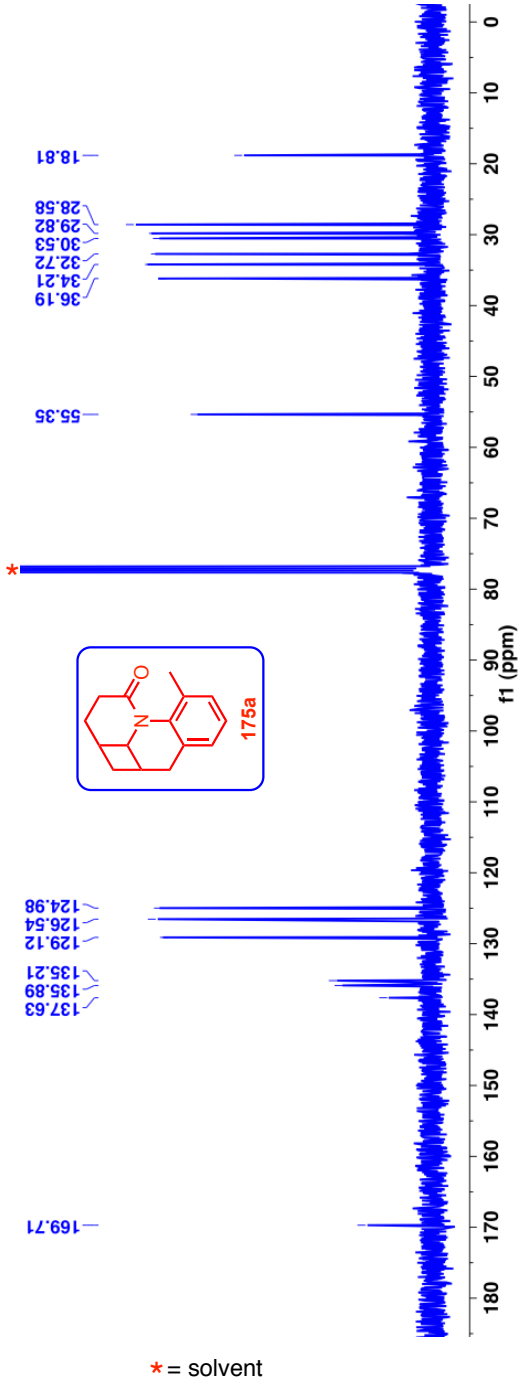

Figure 3.137: ^{13}C-NMR (100 MHz, $CDCl_3$, δ ppm) of cyclobutane photoproduct **175a**.

HRMS-ESI (m/z) ([M + Na]$^+$):

Calculated : 250.1202

Observed : 250.1211

|Δm| : 3.6 ppm

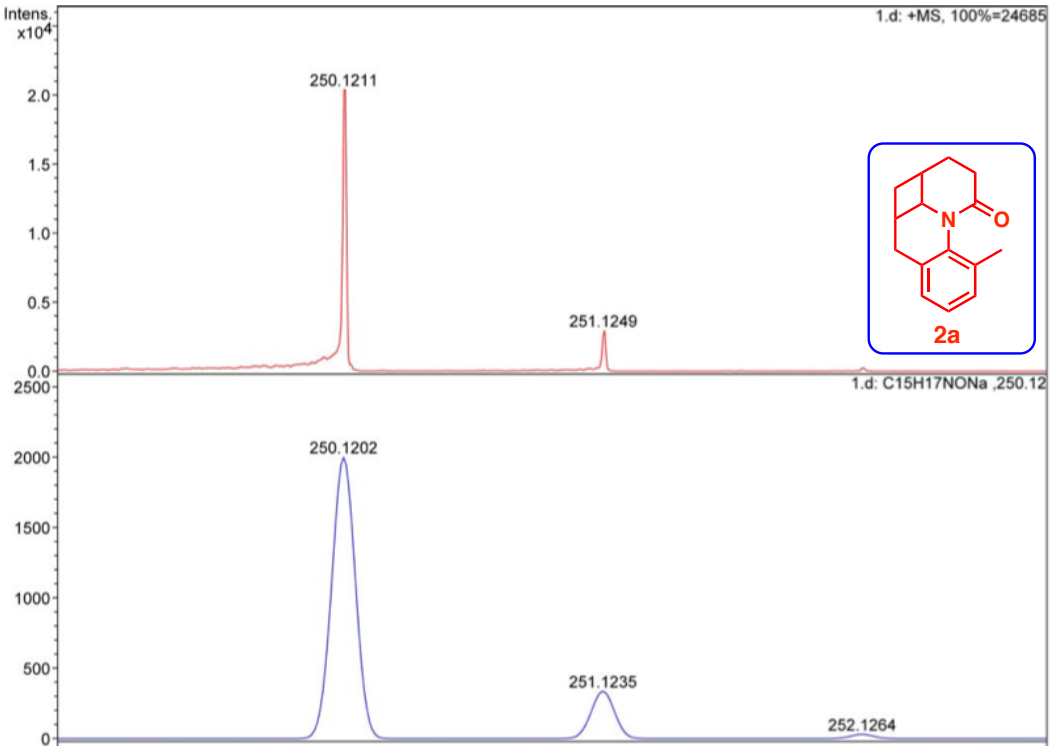

Figure 3.138: HRMS of cyclobutane photoproduct **175a**.

HPLC analysis conditions:

For analytical conditions,

I). Column : RR-WHELK-01 10/100 FEC

Abs. detector wavelength : 254 nm and 270 nm

Mobile phase : Hexanes:2-propanol = 80:20

Flow rate : 1.0 mL/min

Retention times (min) : ~ 19.20 [(+)-(*S,S,S)*-**175a**] and ~ 34.63 [(-)-(*R,R,R)*-**175a**]

Compound **174a**: Optical Rotation $[\alpha]_D^{26}$

HPLC Rt (RR-WHELK-01) at ~19.20 min, (*c* ~0.725%, MeOH) = +126.6 deg.

HPLC Rt (R-WHELK-01) at ~ 34.63 min, (*c* ~0.725%, MeOH) = -126.3 deg.

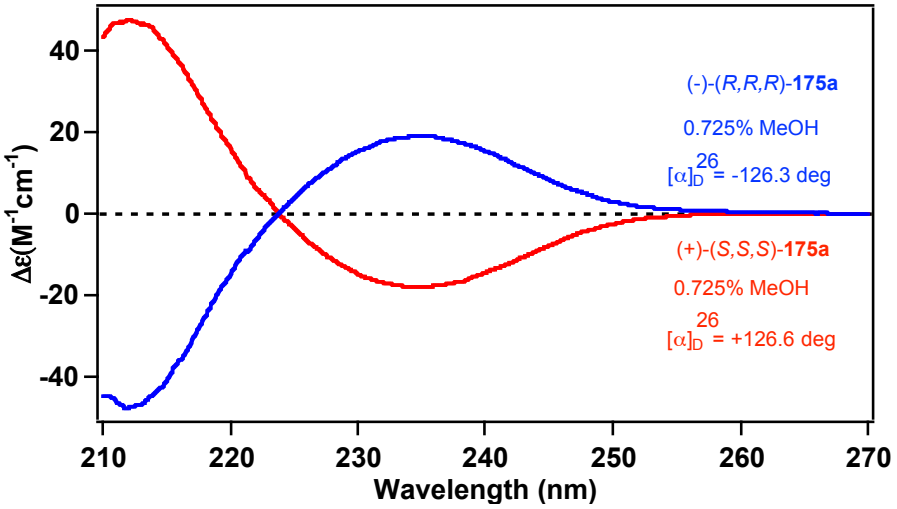

Figure 3.139: CD spectra of cyclobutane photoproduct **175a** measured in MeOH (*c* ~ 0.048 mM).

^{1}H-NMR (400 MHz, $CDCl_3$, δ ppm): 7.098-7.02 (m, 2H), 6.96-6.94 (m, 1H), 4.09-4.05 (t, *J*= 8.4 Hz, 1H), 2.63-2.57 (m, 1H), 2.54-2.42 (m, 3H), 2.296-2.22 (m, 2H), 2.21 (m, 3H), 2.12-2.05 (m, 1H), 1.99-1.89 (m, 1H), 1.24 (s, 3H) and 1.06 (m, 3H).

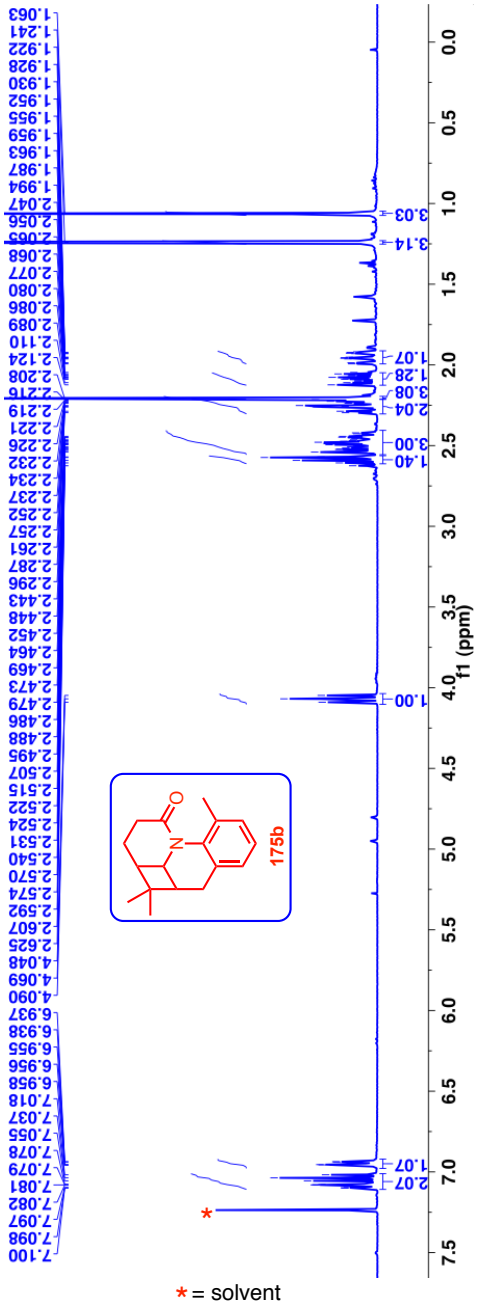

Figure 3.140: ^{1}H-NMR (400 MHz, $CDCl_3$, δ ppm) of cyclobutane photoproduct **175b**.

^{13}C-NMR 100 MHz, $CDCl_3$, δ ppm): 170.2, 137.4, 136.1, 135.3, 129.0, 126.4, 124.8, 51.1, 49.1, 42.6, 33.5, 33.4, 32.97, 29.3, 24.2, 18.9 and 18.8.

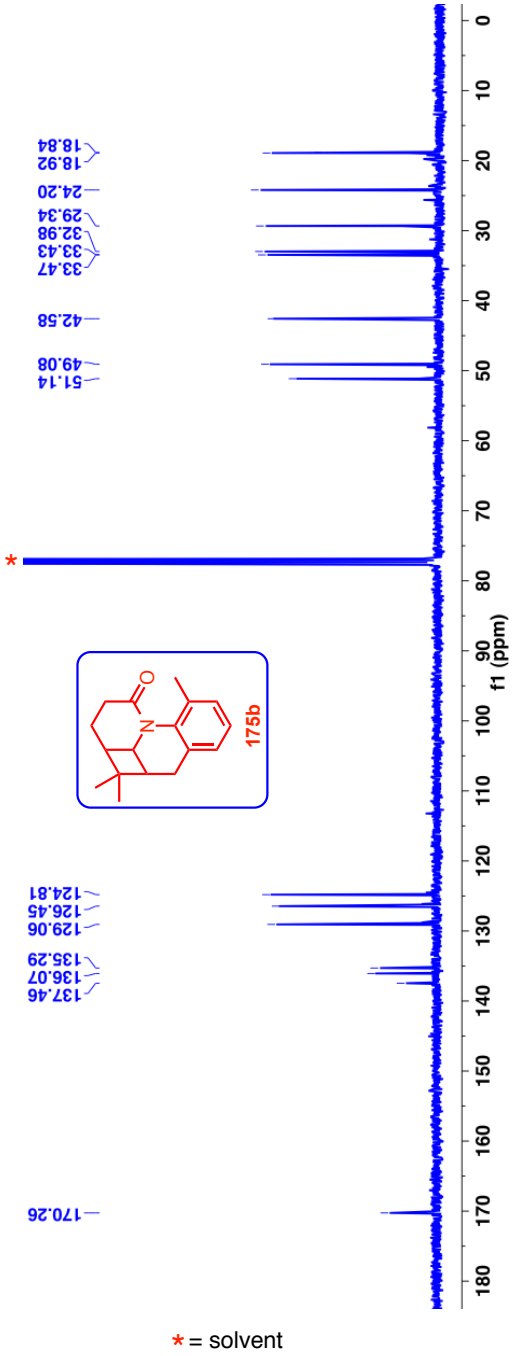

Figure 3.141: ^{13}C-NMR (100 MHz, $CDCl_3$, δ ppm) of cyclobutane photoproduct **175b**.

HRMS-ESI (m/z) ([M + Na]$^+$):

Calculated : 278.1515

Observed : 278.1514

|Δm| : 0.4 ppm

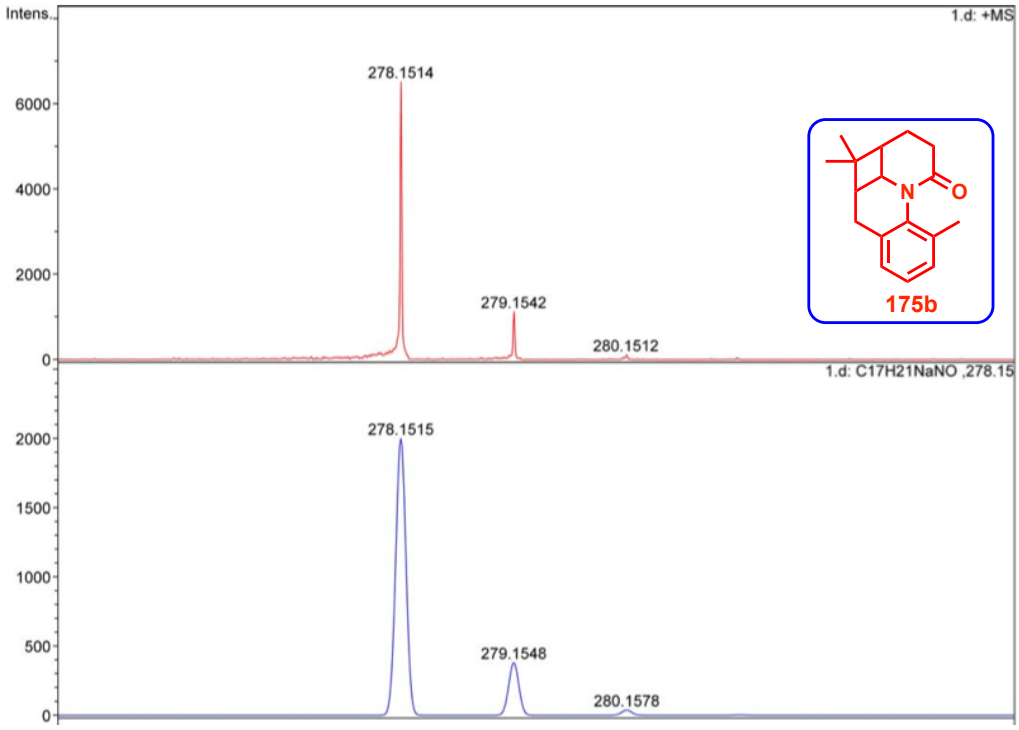

Figure 3.142: HRMS of cyclobutane photoproduct **175b**.

HPLC analysis conditions:

For analytical conditions,

I). Column : CHIRALPACK® IC

Abs. detector wavelength : 254 nm and 270 nm

Mobile phase : Hexanes:2-propanol = 95:5

Flow rate : 1.0 mL/min

Retention times (min) : ~ 55.32 [(+)-**175b**] and ~ 57.64 [(-)-**175b**]

Optical Rotation $[\alpha]_D^{26}$:

HPLC Rt (CHIRALPACK® IC) at ~ 55.32 min, (*c* ~0.854%, MeOH) = +81.1 deg

HPLC Rt (CHIRALPACK® IC) at ~ 57.64 min, (*c* ~0.854%, MeOH) = -80.5 deg.

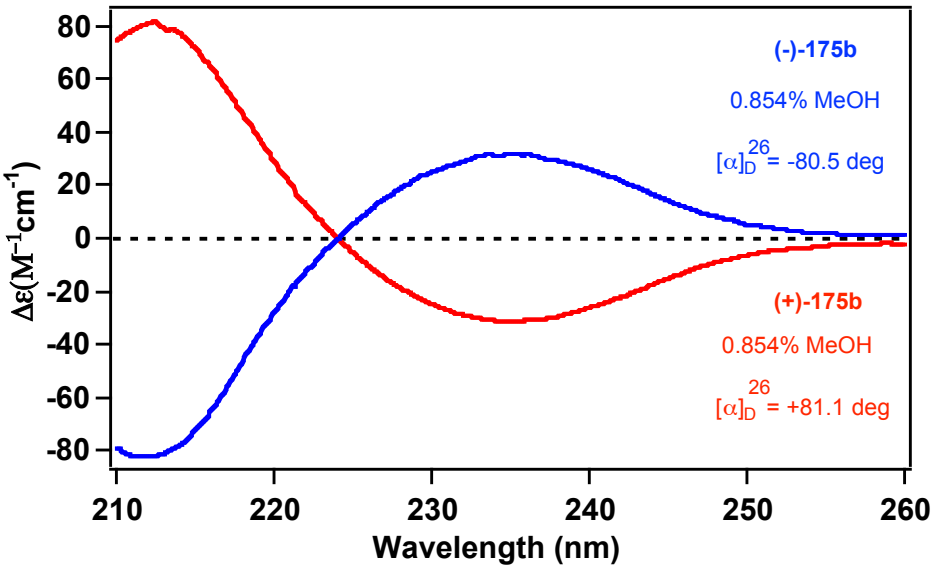

Figure 3.143: CD spectra of cyclobutane photoproduct **175b** measured in MeOH (c ~ 0.035 mM).

^{1}H-NMR (400 MHz, $CDCl_3$, δ ppm): 7.08-7.06 (m, 1H), 7.01-6.95 (m, 2H), 3.66 - 3.62 (m, 1H), 2.94-2.81 (m, 2H), 2.73-2.62 (m, 2H), 2.37-2.25 (m, 2H), 2.16 (s, 3H) 1.96-1.84 (m, 2H), 1.19 (s, 3H), 1.13 (s, 3H).

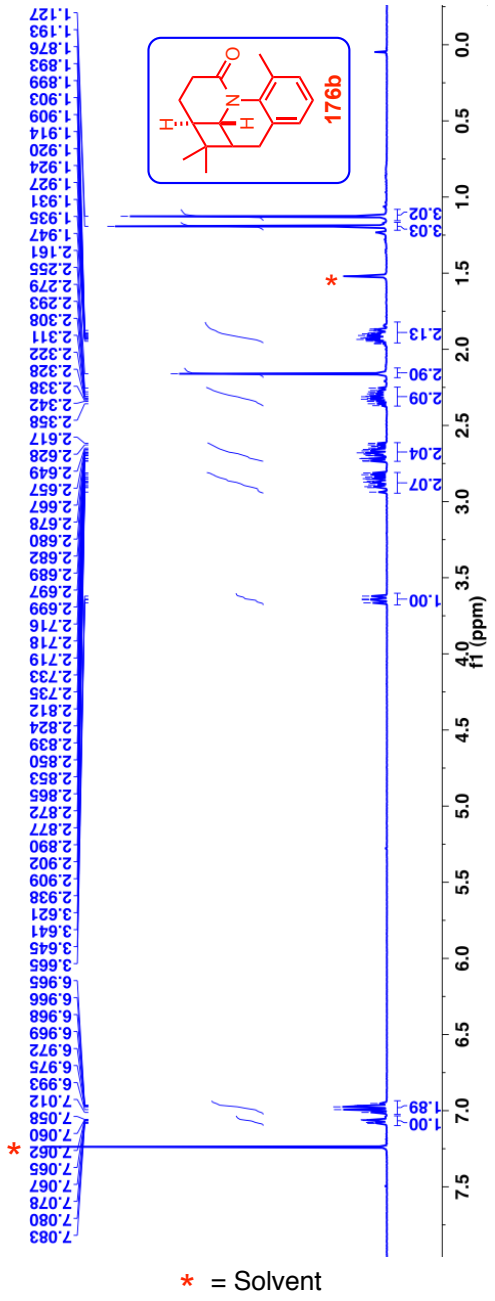

Figure 3.144: ^{1}H-NMR (400 MHz, $CDCl_3$, δ ppm) of cyclobutane photoproduct **176b**.

^{13}C-NMR (100 MHz, $CDCl_3$ and DMSO, δ ppm): 169.1, 136.5, 133.6, 133.3, 126.6, 126.4, 125.5, 52.8, 50.2, 45.5, 39.1, 35.4, 28.1, 23.9, 23.2, 21.7 and 19.8.

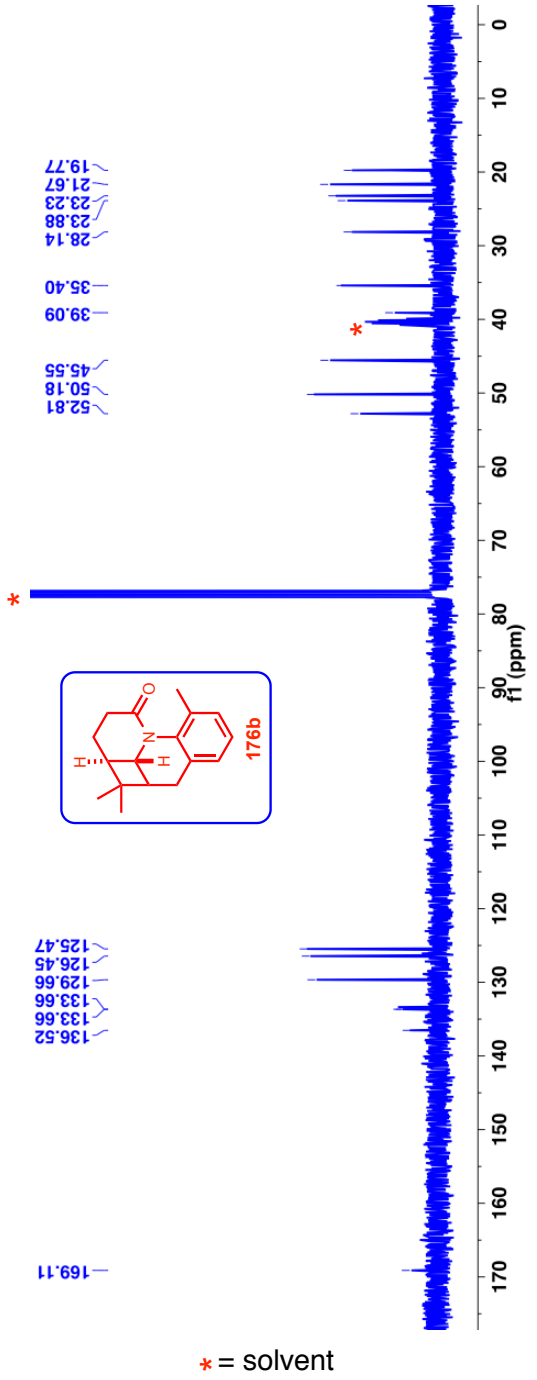

Figure 3.145: ^{13}C-NMR (100 MHz, $CDCl_3$, δ ppm) of cyclobutane photoproduct **176b**.

HRMS-ESI (m/z) ([M + Na]$^+$):

Calculated : 278.1515

Observed : 278.1519

|Δm| : 1.4 ppm

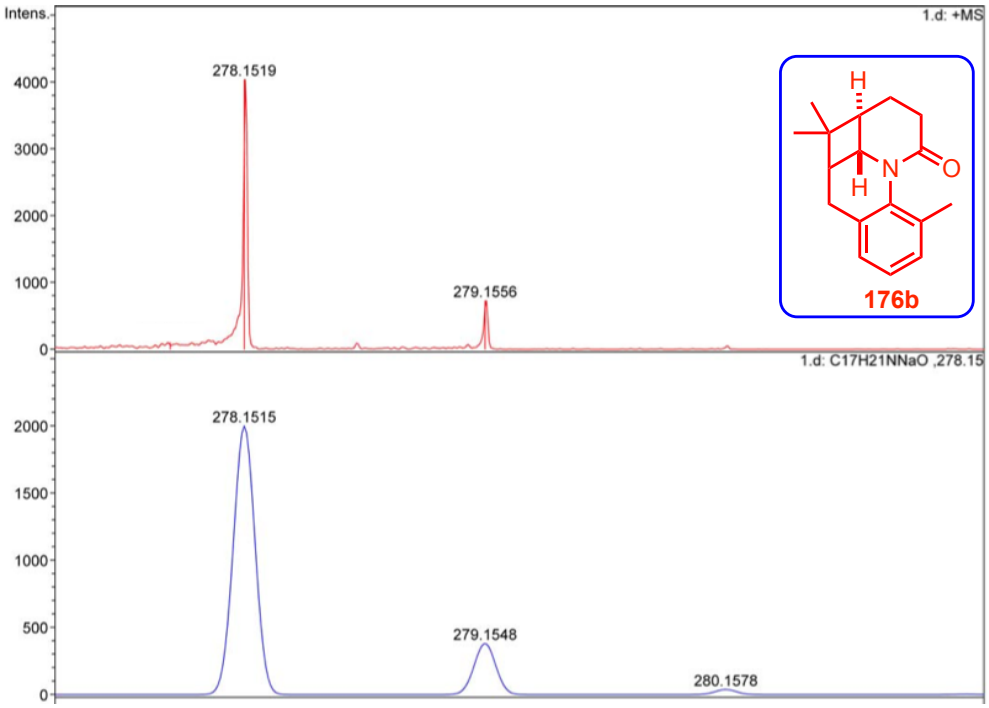

Figure 3.146: HRMS of cyclobutane photoproduct **176b**.

HPLC analysis conditions:

For analytical conditions,

I). Column : CHIRALPACK® IC

Abs. detector wavelength : 254 nm and 270 nm

Mobile phase : Hexanes:2-propanol = 95:5

Flow rate : 1.0 mL/min

Retention times (min) : ~ 37.62 [(+)-**176b**] and ~ 54.03 [(-)-**176b**]

Compound **176b**: Optical Rotation $[\alpha]_D^{26}$:

HPLC Rt (CHIRALPACK® IC) at ~ 37.62 min, (*c* ~0.172%, MeOH) = +15.53 deg

HPLC Rt (CHIRALPACK® IC) at ~ 57.64 min, (*c* ~0.172%, MeOH) = -15.46 deg.

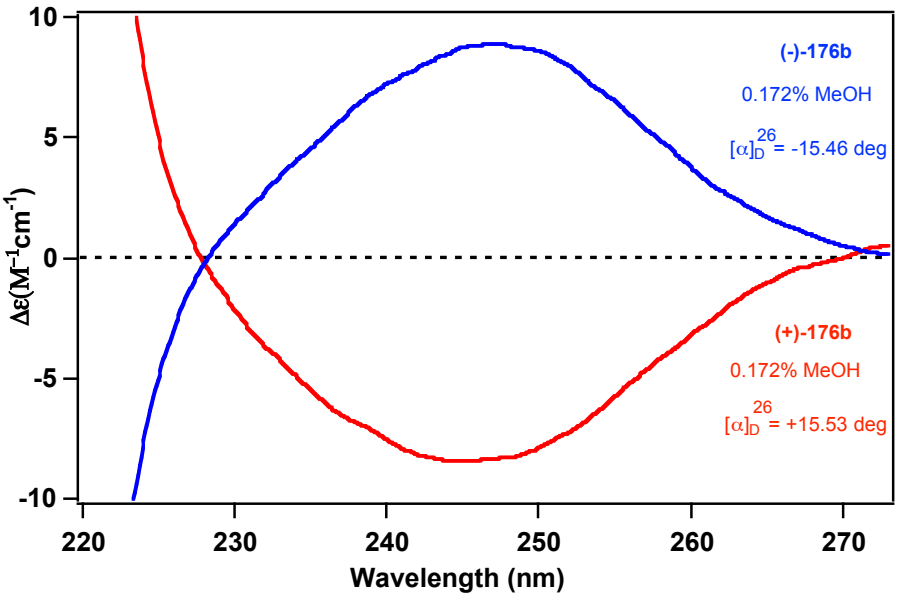

Figure 3.147: CD spectra of cyclobutane photoproduct **176b** measured in MeOH (c ~ 0.086 mM).

^{1}H-NMR (400 MHz, $CDCl_3$, δ ppm): 6.92 (s, 1H), 6.75 (s, 1H), 3.44-3.42 (d, *J*= 8.4 Hz, 1H), 2.94-2.87 (m, 1H), 2.65-2.62 (m, 1H), 2.54-2.48 (m, 1H), 2.39-2.26 (m, 3H), 2.25 (s, 3H), 2.16 (s, 3H), 2.12-2.06 (m, 1H), 1.89-1.82 (m, 2H) and 0.93 (s, 3H).

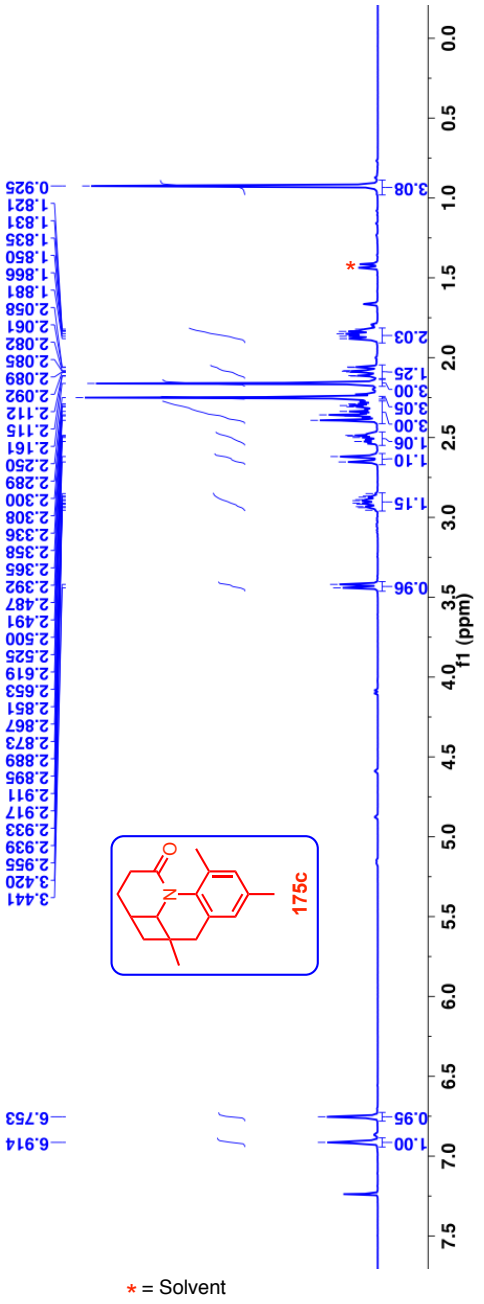

Figure 3.148: ^{1}H-NMR (400 MHz, $CDCl_3$, δ ppm) of cyclobutane photoproduct **175c**.

^{13}C-NMR (100 MHz, $CDCl_3$, δ ppm): 169.5, 135.9, 135.3, 134.5, 134.47, 129.7, 126.5, 61.6, 41.6, 41.1, 37.1, 32.6, 28.4, 27.1, 26.1, 21.2 and 18.7.

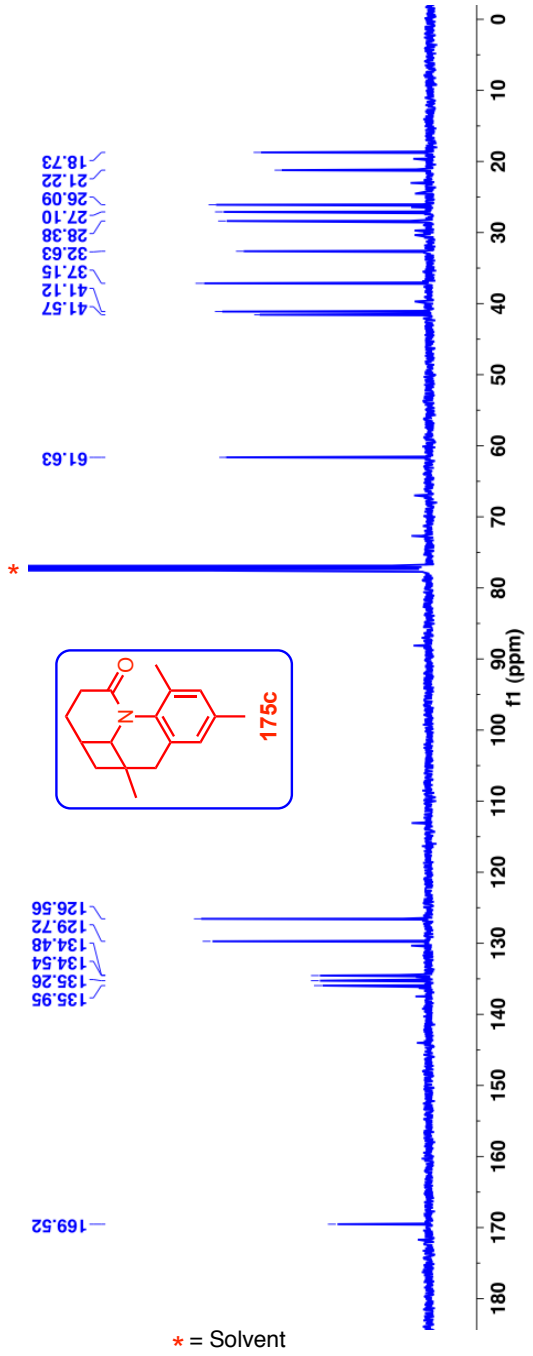

Figure 3.149: ^{13}C-NMR (100 MHz, $CDCl_3$, δ ppm) of cyclobutane photoproduct **175c**.

HRMS-ESI (m/z) ([M + Na]$^+$):

Calculated : 278.1515

Observed : 278.1514

|Δm| : 0.4 ppm

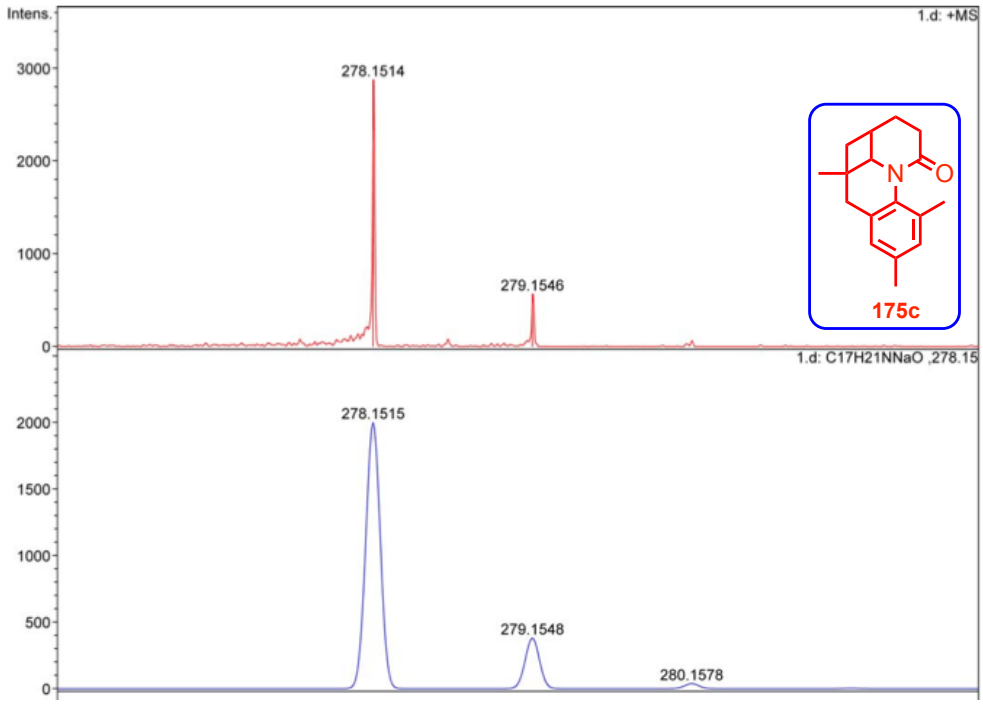

Figure 3.150: HRMS of cyclobutane photoproduct **175c**.

HPLC analysis conditions:

For analytical conditions,

I). Column : CHIRALPAK IC

Abs. detector wavelength : 254 nm and 270 nm

Mobile phase : Hexanes:2-propanol = 90:10

Flow rate : 1.0 mL/min

Retention times (min) : ~ 81.63 [(+)-*S,S,S*-**175c**] and ~ 89.90 [(-)-*R,R,R*-**175c**]

II). Column : RR-WHELK-01 10/100 FEC

Abs. detector wavelength : 254 nm and 270 nm

Mobile phase : Hexanes:2-propanol = 90:10

Flow rate : 1.0 mL/min

Retention times (min) : ~ 39.35 [(+)-*S,S,S*-**175c**] and ~ 79.74 [(-)-*R,R,R*-**175c**]

Compound **175c**: Optical Rotation $[\alpha]_D^{26}$:

HPLC Rt (CHIRALPACK® IC) at ~ 39.35 min, (*c* = 1.04%, MeOH) = +156.9 deg

HPLC Rt (CHIRALPACK® IC) at ~ 79.74 min, (*c* = 1.04%, MeOH) = -156.4 deg.

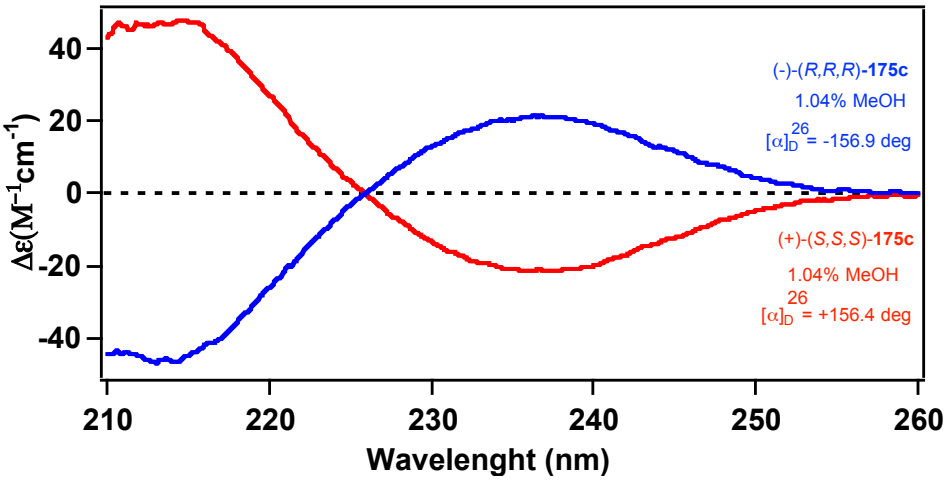

Figure 3.151: CD spectra of cyclobutane photoproduct **175c** measured in MeOH (*c* ~ 0.052 mM).

^{1}H-NMR (400 MHz, $CDCl_3$, δ ppm): 7.08-7.02 (m, 2H), 6.92-6.90 (m, 1H), 3.98-3.94 (m, 1H), 2.98-2.85 (m, 2H), 2.75-2.696 (m, 1H), 2.59-2.51 (m, 1H), 2.398 (d, *J*= 14Hz, 1H), 2.27 (s, 3H), 1.86-1.79 (m, 1H), 1.22 (s, 3H) and 1.14 (m, 3H).

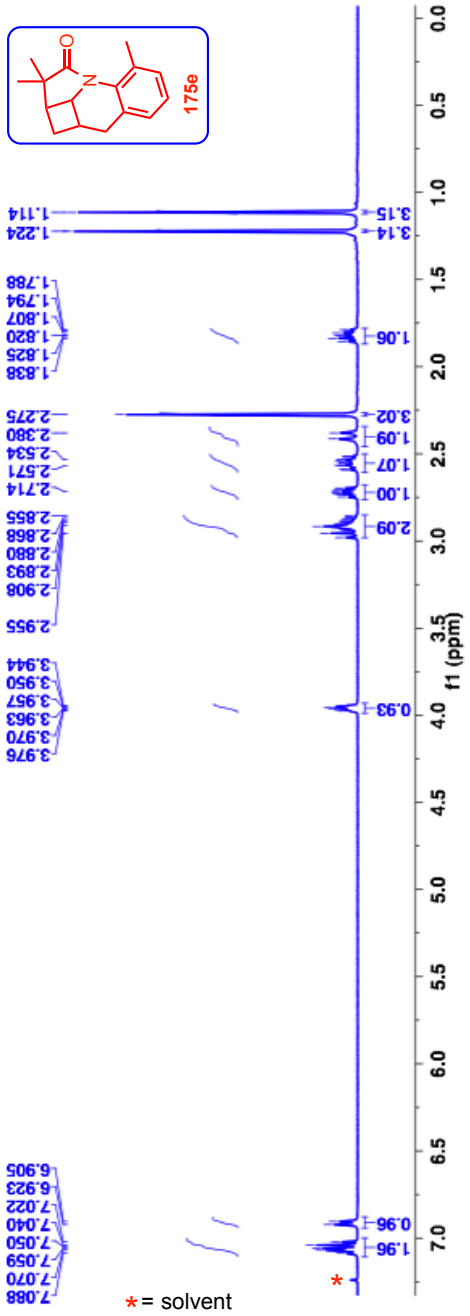

Figure 3.152: ^{1}H-NMR (400 MHz, $CDCl_3$, δ ppm) of cyclobutane photoproduct **175e**.

^{13}H-NMR (100 MHz, $CDCl_3$, δ ppm): 178.02, 135.3, 134.5, 134.3, 128.6, 126.4, 126.2, 55.4, 43.9, 41.8, 32.1, 31.9, 31.6, 25.7, 18.3 and 18.1

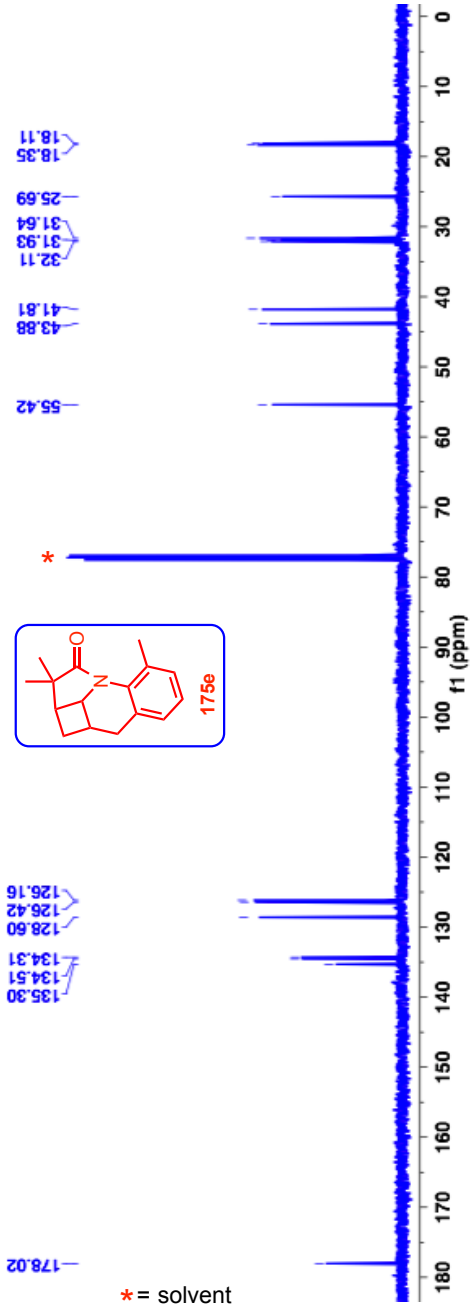

Figure 3.153: ^{13}C-NMR (100 MHz, $CDCl_3$, δ ppm) of cyclobutane photoproduct **175e**.

HRMS-ESI (m/z) ([M + Na]$^+$):

Calculated : 264.1359

Observed : 264.1358

|Δm| : 0.4 ppm

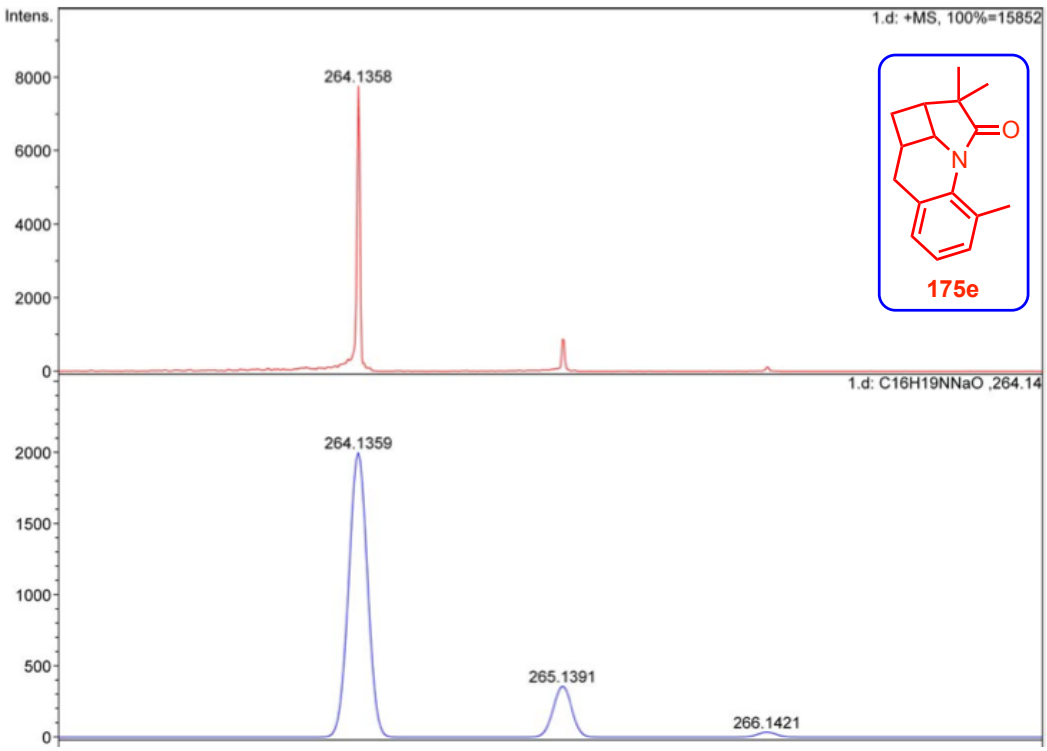

Figure 3.154: HRMS of cyclobutane photoproduct **175e**.

HPLC analysis conditions:

For analytical conditions,

I). Column : CHIRALPAK-AS-H

Abs. detector wavelength : 254 nm and 270 nm

Mobile phase : Hexanes:2-propanol = 95:5

Flow rate : 1.0 mL/min

Retention times (min) : ~ 5.90 [(+)-**175e**] and ~ 9.97 [(-)-**175e**]

Optical rotation $[\alpha]_D^{26}$:

HPLC Rts (CHIRALPAK-AS-H) at ~ 5.90 min, (*c* ~ 0.841 %, MeOH) = +73.76 deg

HPLC Rts (CHIRALPAK-AS-H) at ~ 9.97 min, (*c* ~ 0.841 %, MeOH) = -75.14 deg

^{1}H-NMR (400 MHz, $CDCl_3$, δ ppm): 7.11-7.06 (m, 2H), 7.01-6.99 (m, 1H), 4.02-3.98 (m, 1H), 3.08-3.01 (m, 1H), 2.68-2.60 (m, 2H), 2.45-2.398 (m, 1H), 2.21-2.14 (m, 1H), 2.13 (s, 3H), 2.03-1.97 (m, 1H), 1.62-1.47 (m, 2H), 1.174 (s, 3H) and 1.171 (s, 3H).

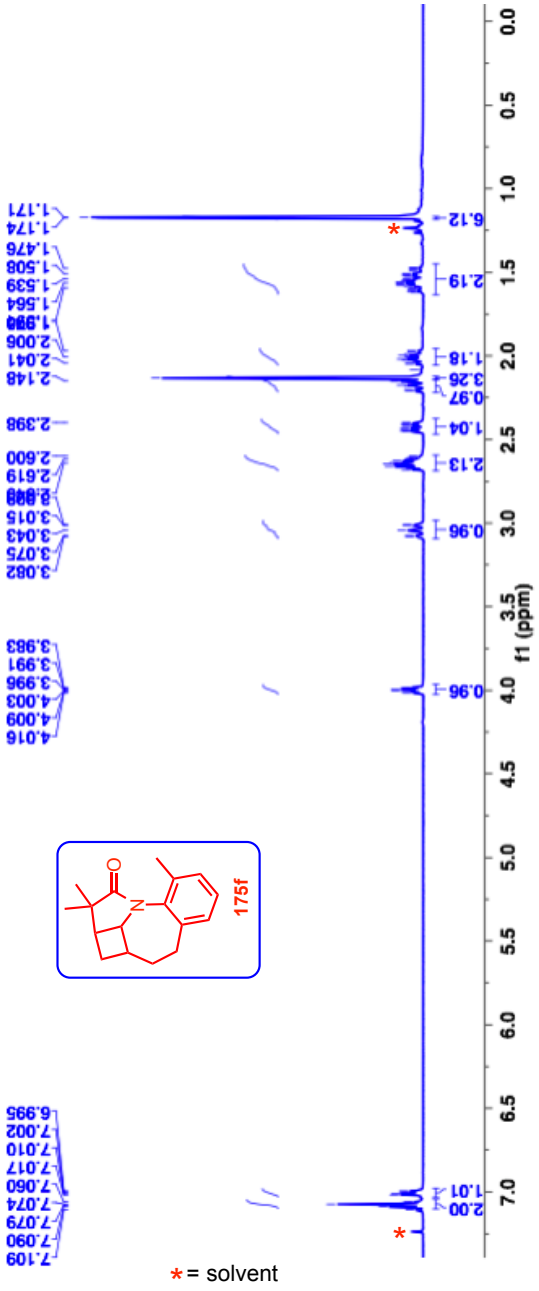

Figure 3.155: ^{1}H-NMR (400 MHz, $CDCl_3$, δ ppm) of cyclobutane photoproduct **175f**.

^{13}C-NMR (100 MHz, $CDCl_3$, δ ppm): 178.1, 141.9, 136.3, 136.1, 128.98, 128.05, 127.2, 57.89, 43.5, 42.5, 34.0, 28.7, 26.7, 25.5, 24.7, 18.3 and 17.7.

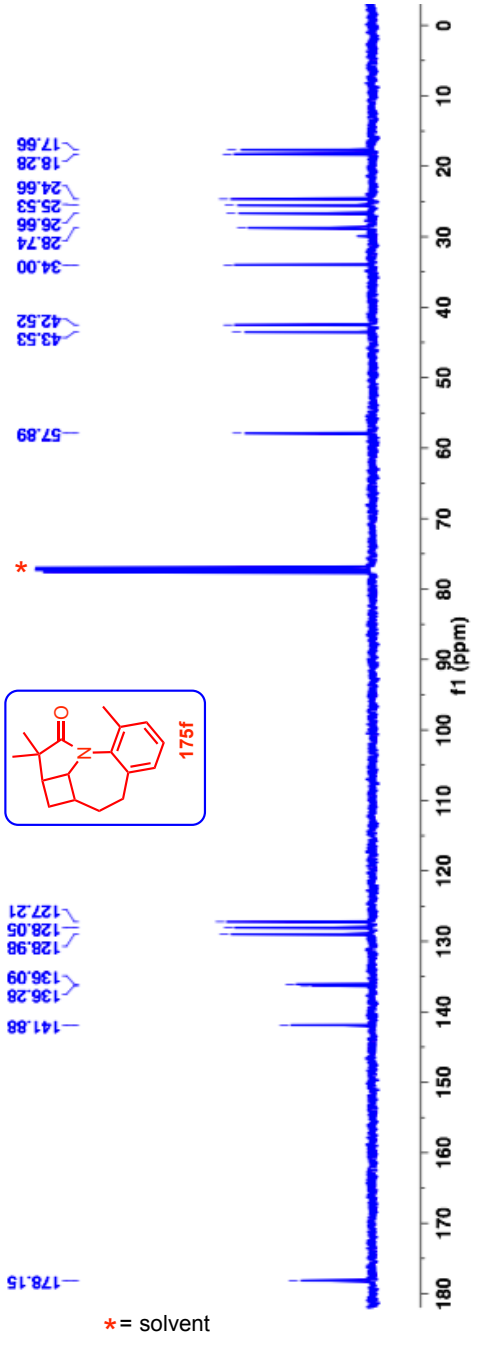

Figure 3.156: ^{13}C-NMR (100 MHz, $CDCl_3$, δ ppm) of cyclobutane photoproduct **175f**.

HRMS-ESI (m/z) ([M + Na]$^+$):

Calculated : 278.1515

Observed : 278.1505

|Δm| : 3.6 ppm

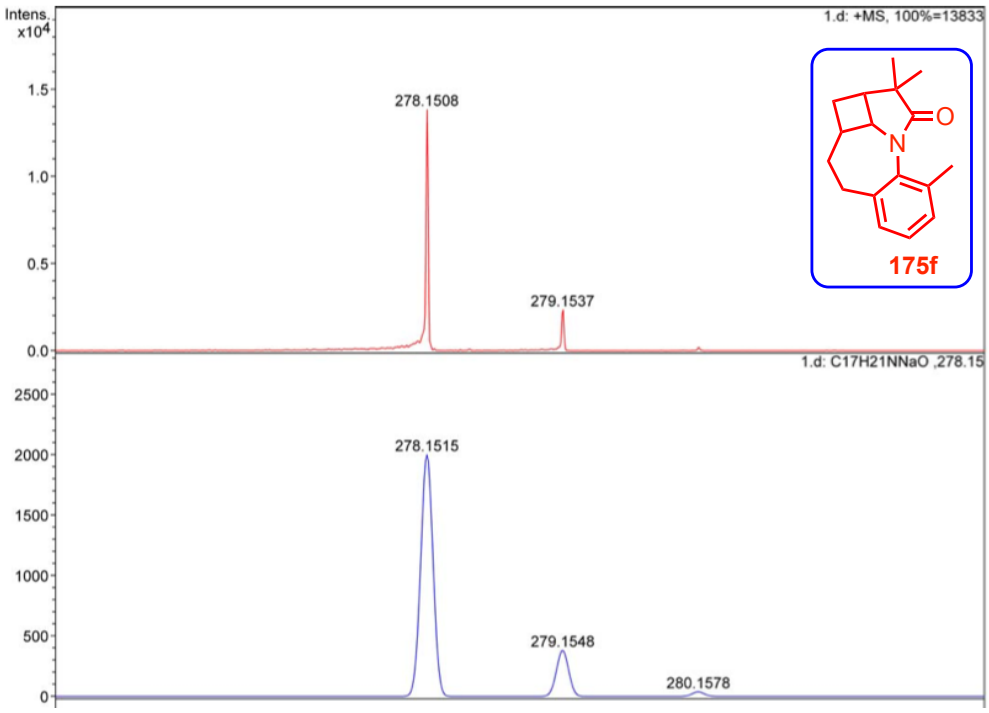

Figure 3.157: HRMS of cyclobutane photoproduct **175f**.

HPLC analysis conditions:

For analytical conditions,

I). Column : CHIRALPAK-AS-H

Abs. detector wavelength : 254 nm and 270 nm

Mobile phase : Hexanes:2-propanol = 90:10

Flow rate : 1.0 mL/min

Retention times (min) : ~ 5.34 [(+)-**175f**] and ~ 7.87 [(-)-**175f**

Optical rotation $[\alpha]_D^{22}$:

HPLC Rts (CHIRALPAK-AS-H) at ~ 5.34 min, (*c* ~ 0.657 %, MeOH) = +62.81 deg

HPLC Rts (CHIRALPAK-AS-H) at ~ 7.87 min, (*c* ~ 0.657%, MeOH) = -63.97 deg.

^{1}H-NMR (400 MHz, $CDCl_3$, δ ppm): 7.097-7.06 (m, 1H), 6.95-6.93 (m, 1H), 6.88-6.86 (m, 1H), 4.17-4.04 (m, 1H), 4.07 (dd, *J* = 12.8, 2.8 Hz, 1H), 3.66 (dd, *J* = 13.2, 3.2 Hz, 1H), 2.72-2.66 (m, 1H), 2.59-2.54 (m, 1H), 2.36-2.28 (m, 1H), 2.15 (m, 3H), 2.12-2.05 (m, 1H), 1.16 (s, 3H) and 1.14 (s, 3H).

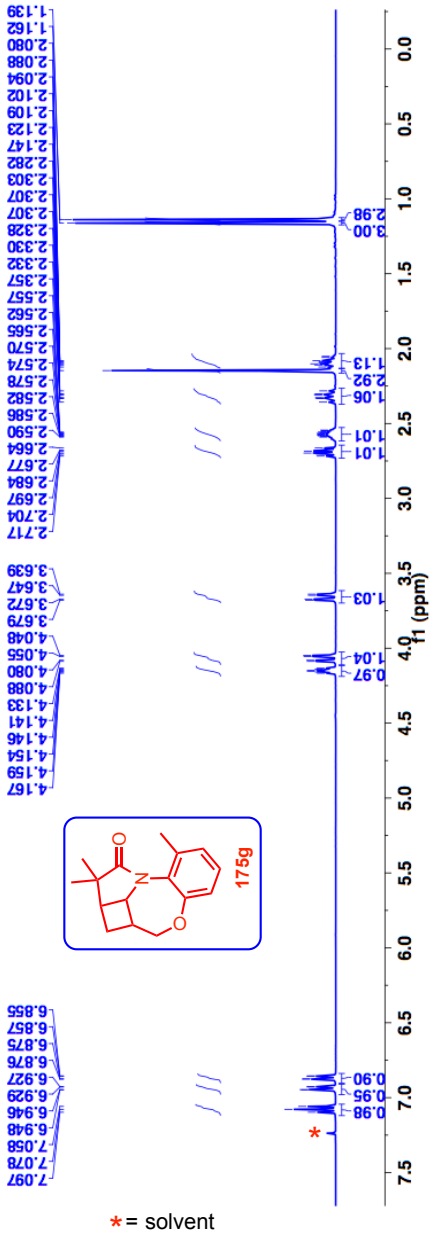

Figure 3.158: ^{1}H-NMR (400 MHz, $CDCl_3$, δ ppm) of cyclobutane photoproduct **175g**.

^{13}C-NMR (100 MHz, $CDCl_3$, δ ppm): 178.2, 157.0, 137.8, 130.2, 128.7, 126.1, 119.7, 70.6, 57.1, 43.4, 42.2, 36.0, 25.5, 23.6, 18.2 and 17.8.

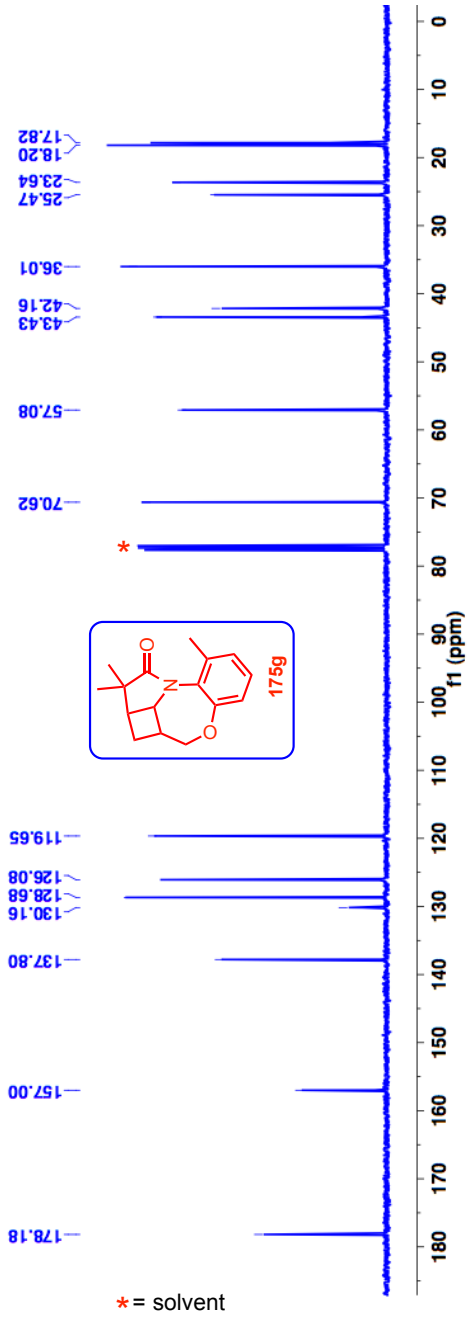

Figure 3.159: ^{13}C-NMR (100 MHz, $CDCl_3$, δ ppm) of cyclobutane photoproduct **175g**.

HRMS-ESI (m/z) ([M + Na]$^+$):

Calculated : 280.1308

Observed : 230.1301

|Δm| : 2.5 ppm

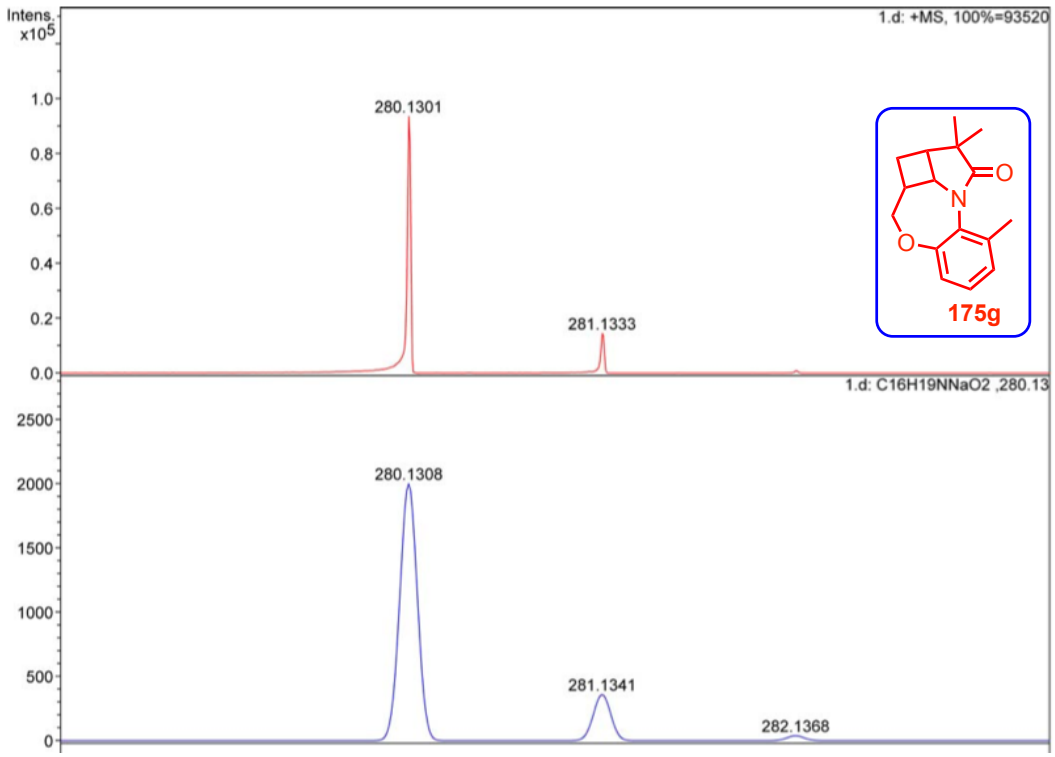

Figure 3.160: HRMS of cyclobutane photoproduct **175g**.

HPLC analysis conditions:

For analytical conditions,

I). Column : CHIRALPAK-AD-H

Abs. detector wavelength : 254 nm and 270 nm

Mobile phase : Hexanes:2-propanol = 95:5

Flow rate : 1.0 mL/min

Retention times (min) : ~ 5.34 [(-)-**175g**] and ~ 7.87 [(+)-**175g**

^{1}H-NMR (400 MHz, $CDCl_3$, δ ppm): 7.39-7.37 (m, 1H), 7.29-7.24 (m, 1H), 7.18-7.15 (m, 1H), 7.12-7.10 (m, 1H), 5.39-5.35 (m, 1H), 4.87-4.86 (m, 1H), 4.23-4.21 (m, 1H), 3.10 (dd, *J*= 18, 8.4 Hz, 1H), 3.10 (dd, *J*= 17.6, 8.4 Hz, 1H), 2.68 (d, *J*= 17.6 Hz, 1H), 1.20 (s, 3H) and 1.15 (s, 3H).

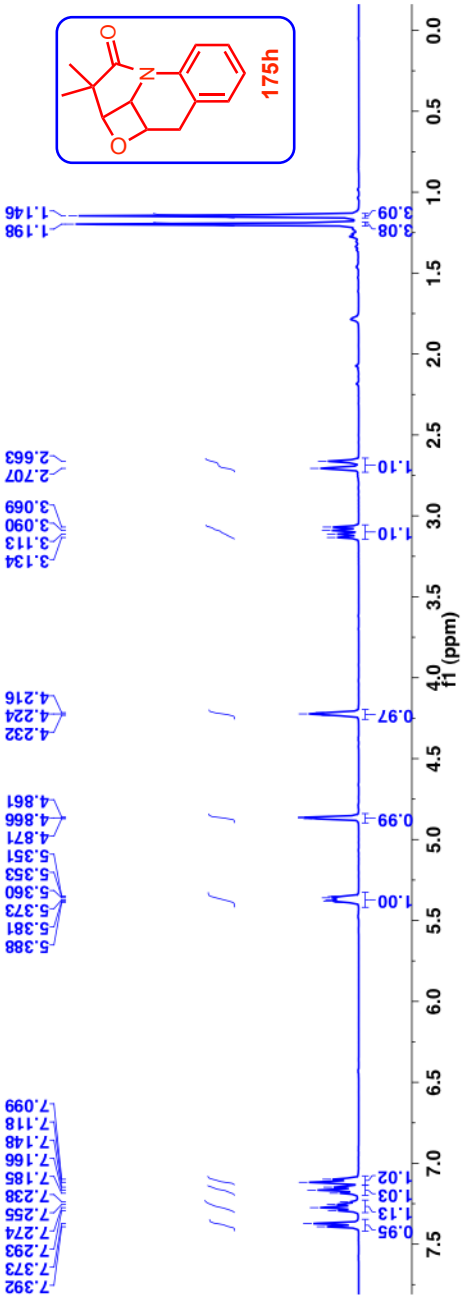

Figure 3.161: ^{1}H-NMR (400 MHz, $CDCl_3$, δ ppm) of cyclobutane photoproduct **175h**.

^{13}C-NMR (100 MHz, $CDCl_3$, δ ppm): 179.7, 135.8, 131.8, 129.0, 127.3, 126.98, 126.1, 84.8, 80.4, 55.1, 45.3, 32.7, 21.6 and 16.3.

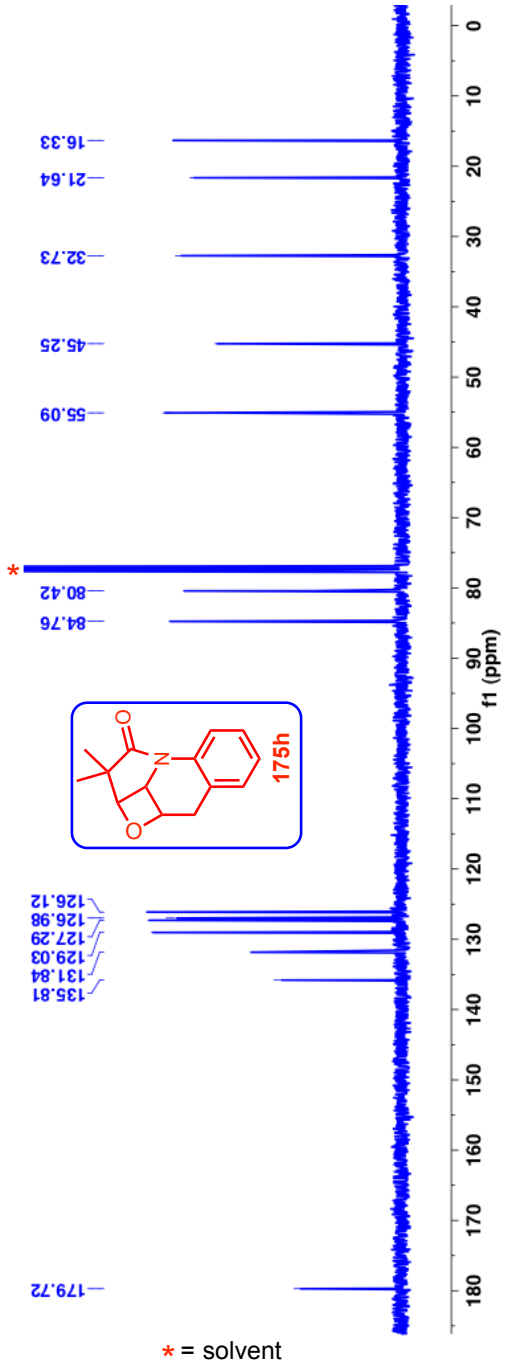

Figure 3.162: ^{13}C-NMR (100 MHz, $CDCl_3$, δ ppm) of cyclobutane photoproduct **175h**.

HRMS-ESI (m/z) ([M + Na]$^+$):

Calculated : 252.0995

Observed : 252.0997

|Δm| : 0.8 ppm

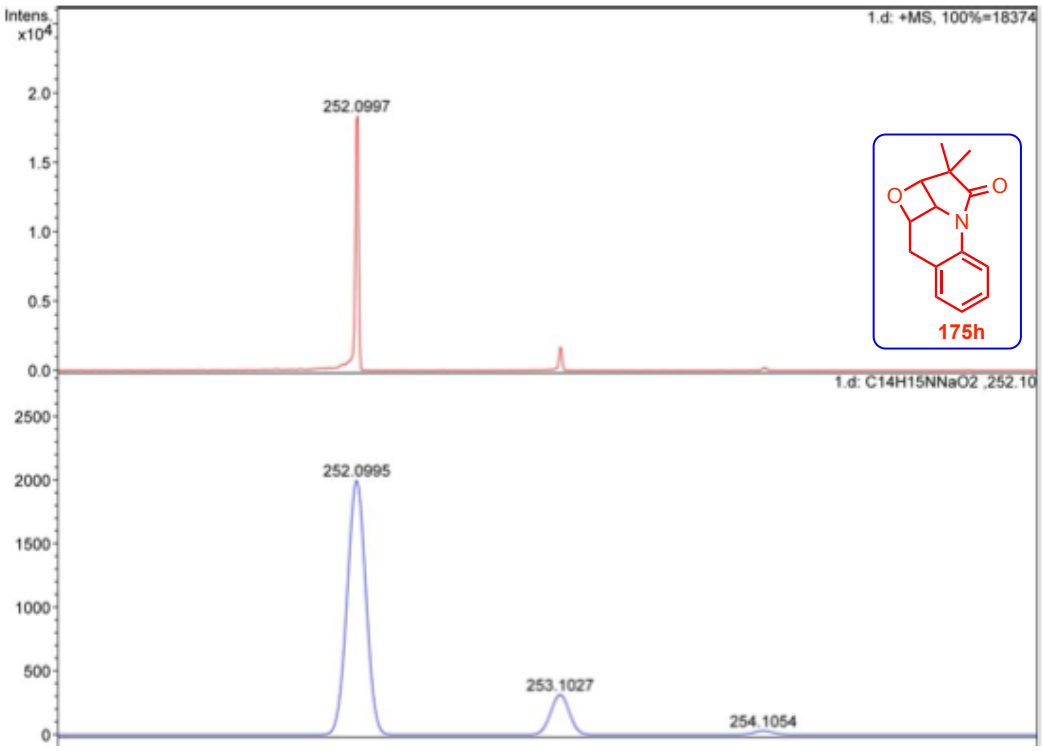

Figure 3.163: HRMS of cyclobutane photoproduct **175h**.

^{1}H-NMR (400 MHz, $CDCl_3$, δ ppm): 7.38-7.35 (m, 1H), 7.31-7.27 (m, 1H), 7.19-7.16 (m, 1H), 7.12-7.097 (m, 1H), 4.79 (d, *J* = 3.8 Hz, 1H), 3.92 (d, *J* = 3.8 Hz, 1H), 2.86 (d, *J* = 16.4 Hz, 1H), 2.76 (d, *J* = 16.4 Hz, 1H), 1.61 (s, 3H), 1.21 (s, 3H) and 1.16 (s, 3H).

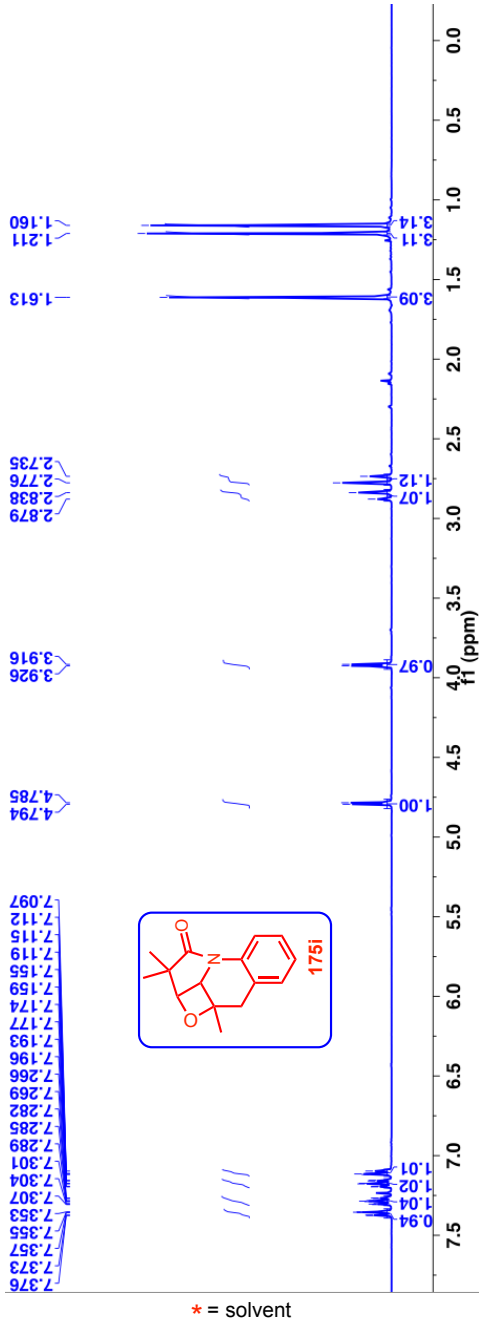

Figure 3.164: ^{1}H-NMR (400 MHz, $CDCl_3$, δ ppm) of cyclobutane photoproduct **175i**.

^{13}C-NMR (100 MHz, $CDCl_3$, δ ppm): 179.9, 136.3, 132.6, 128.9, 127.5, 127.2, 126.0, 88.5, 82.4, 59.7, 45.3, 40.9, 25.3, 22.1 and 16.6.

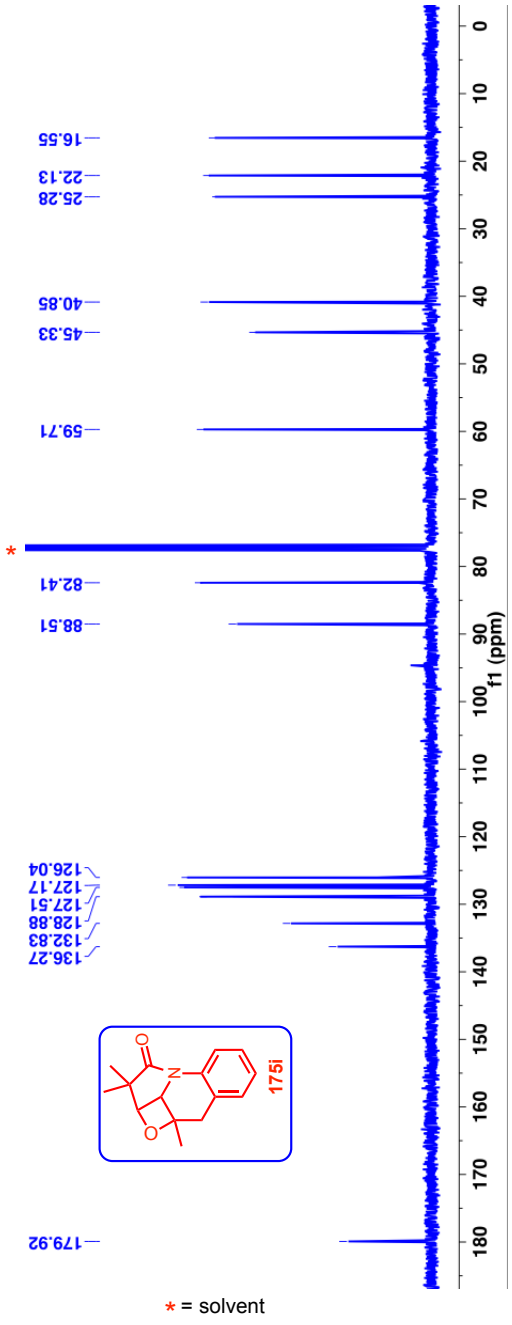

Figure 3.165: ^{13}C-NMR (100 MHz, $CDCl_3$, δ ppm) of cyclobutane photoproduct **175i**.

HRMS-ESI (m/z) ([M + Na]$^+$):

Calculated : 266.1151

Observed : 266.1142

|Δm| : 3.4 ppm

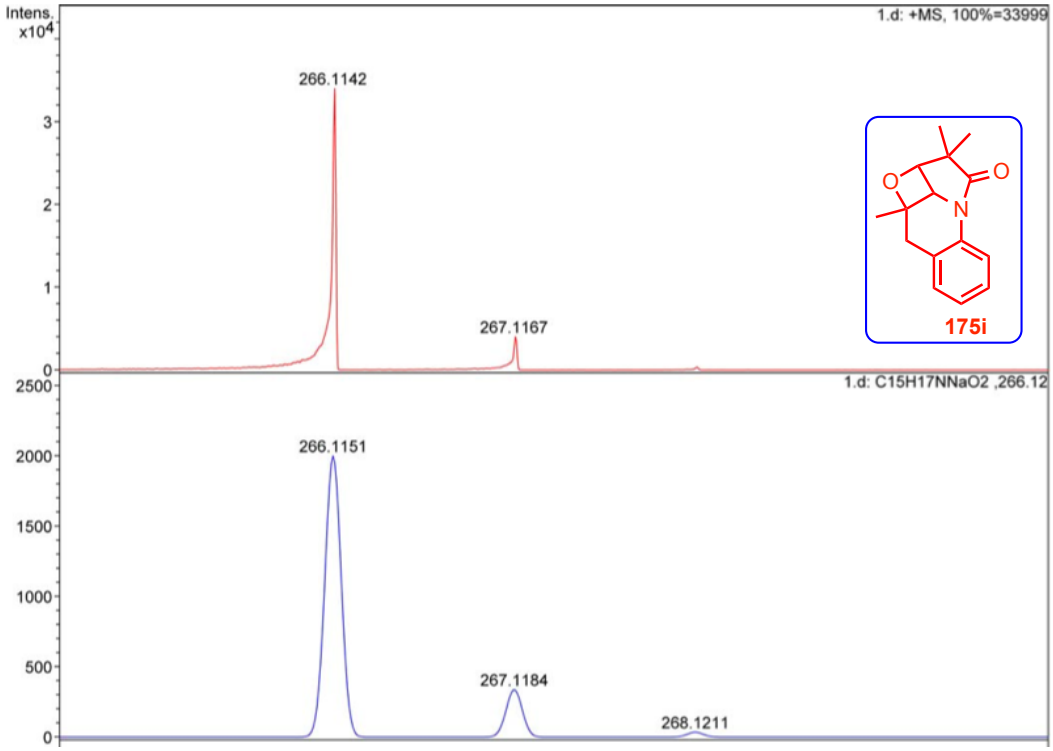

Figure 3.166: HRMS of cyclobutane photoproduct **175i**.

^{1}H-NMR (400 MHz, $CDCl_3$, δ ppm): 7.39-7.26 (m, 5H), 7.02 (s, 1H), 6.82 (s, 1H), 4.87 (d, *J* = 3.6 Hz, 1H), 4.06 (d, *J* = 4.0 Hz, 1H), 3.11 (d, *J* = 16.0 Hz, 1H), 3.03 (d, *J* = 16.0 Hz, 1H), 2.32 (s, 3H), 2.30 (s, 3H), 1.33 (s, 3H) and 1.16 (s, 3H)

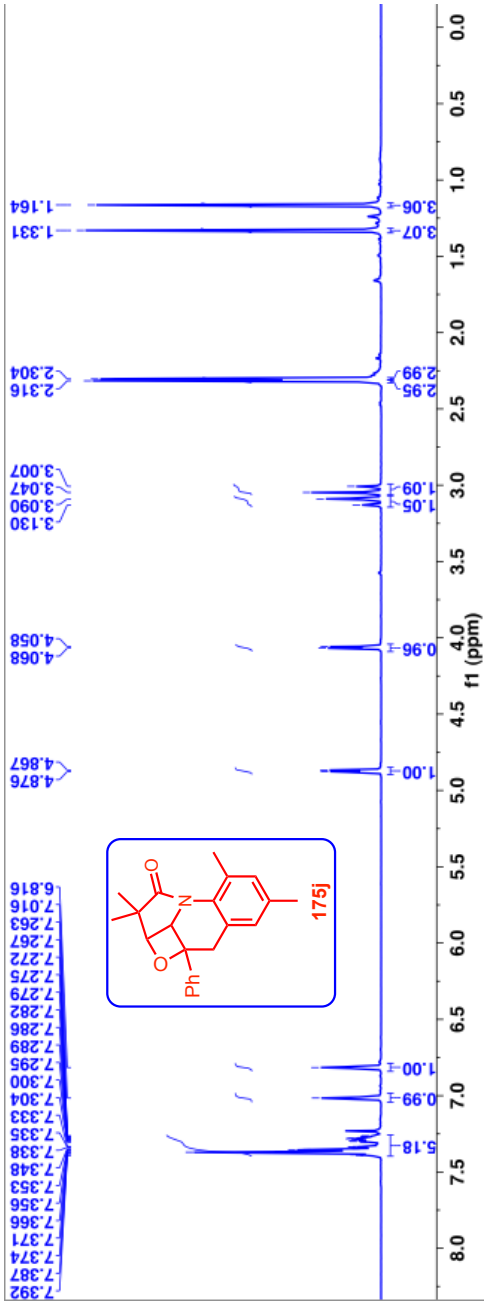

Figure 3.167: ^{1}H-NMR (400 MHz, $CDCl_3$, δ ppm) of cyclobutane photoproduct **175j**.

^{13}C-NMR (100 MHz, $CDCl_3$, δ ppm): 179.5, 143.98, 137.4, 134.94, 133.4, 133.3, 129.95, 128.9, 127.8, 126.7, 124.1, 91.5, 83.1, 62.3, 45.5, 43.4, 22.3, 21.4, 17.6 and 16.5.

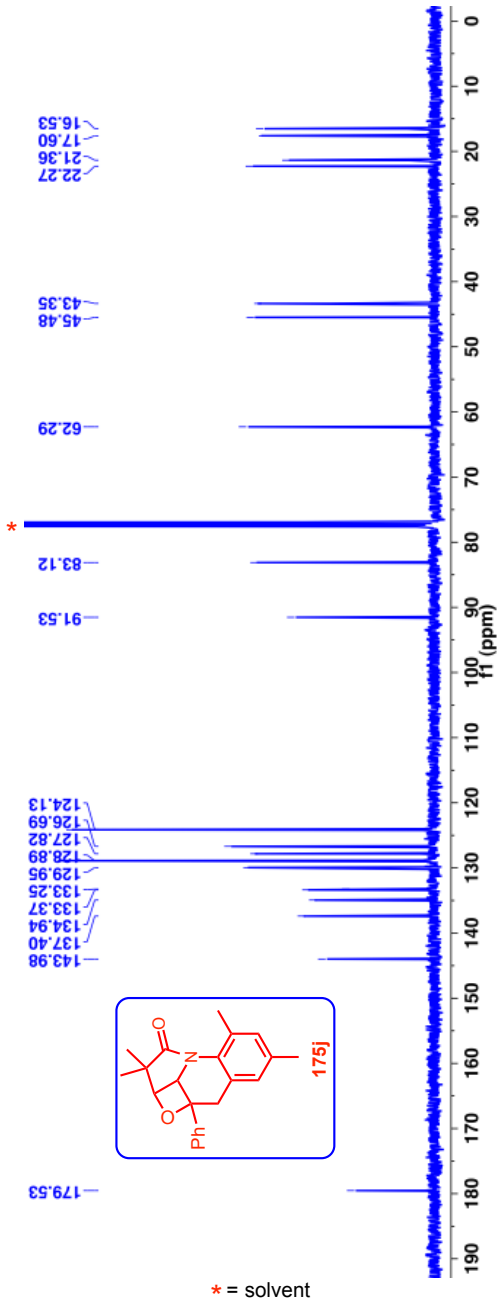

Figure 3.168: ^{13}C-NMR (100 MHz, $CDCl_3$, δ ppm) of cyclobutane photoproduct **175j**.

HRMS-ESI (m/z) ([M + Na]$^+$):

Calculated : 356.1621

Observed : 356.1608

|Δm| : 3.7 ppm

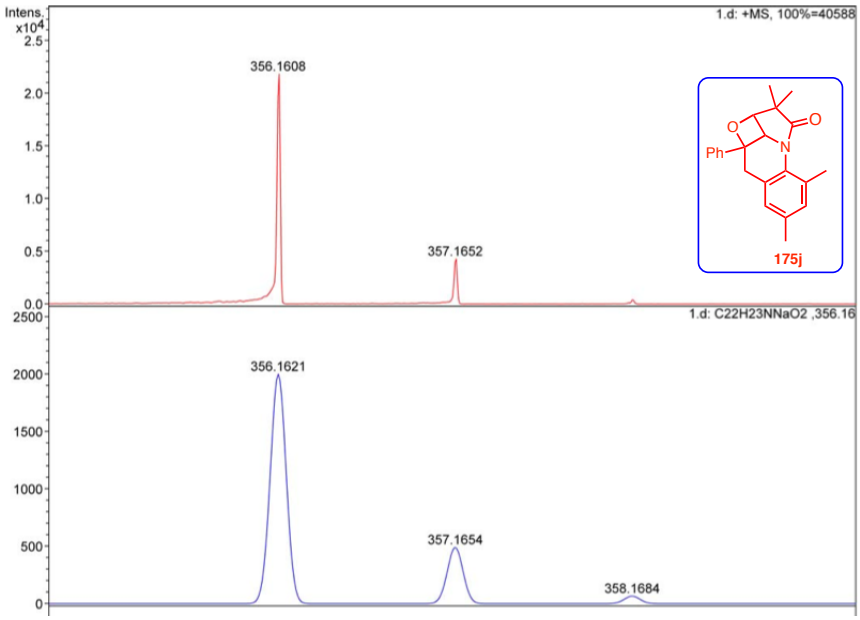

Figure 3.169: HRMS of cyclobutane photoproduct **175j**.

HPLC analysis conditions:

For analytical conditions,

I). Column : RR-WHELK-01 10/100 FEC

Abs. detector wavelength : 254 nm and 270 nm

Mobile phase : Hexanes:2-propanol = 80:20

Flow rate : 1.0 mL/min

Retention times (min) : ~ 9.23 [(+)-**175j**] and ~ 19.00 [(-)-**175j**]

For preparative conditions,

I). Column : RR-WHELK-01 10/100 FEC

Abs. detector wavelength : 254 nm and 270 nm

Mobile phase : Hexanes:2-propanol = 90:10

Flow rate : 1.0 mL/min

Retention times (min) : ~ 18.05 [(+)-**175j**] and ~ 36.69 [(-)-**175j**]

Optical rotation $[\alpha]_D^{24}$:

HPLC retention time (RR-WHELK) at ~ 9.23 min, (*c* ~1.9 %, MeOH) = +64.86 deg

HPLC retention time (RR-WHELK) at ~ 19.00 min, (*c* ~1.9%, MeOH) = -64.82 deg.

3.13. Cleavage of photoproducts of atropisomeric enamides

3.13.1. Cleavage of enamide photoproduct 175g using BBr_3

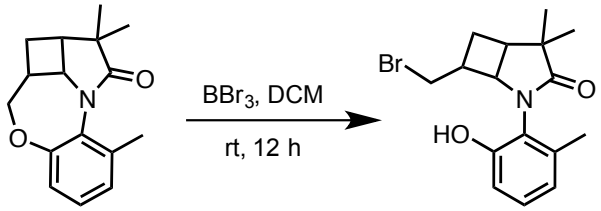

175g **177**

Scheme 3.37: Cleavage of photoproduct **175g** using BBr_3.

To a solution of photoproduct **175g** (100 mg, 0.39 mmol) in dry DCM (20 mL) at -78 ^{o}C under N_2 atmosphere added BBr_3 (1M solution in DCM, 3.11 mmol). The resulting mixture was allowed to warm to room temperature and stirred for 24 h. After the reaction, the solution was cooled to 0 ^{o}C and quenched with saturated $NaHCO_3$ solution. The aqueous layer was extracted with DCM (2 X 10mL). The combined organic layer was washed with brine solution (20 mL), dried over *anhyd.* Na_2SO_4, filtered and the solvent was removed under reduced pressure to get the crude product. The product was purified by combiflash using hexanes:ethyl acetate mixture.

R*f* = 0.35 (80% hexanes:20% ethyl acetate) for **177** (Yield = 71%).

^{1}H-NMR (400 MHz, $CDCl_3$, δ ppm): 7.21-7.08 (m, 1H), 6.91-6.89 (m, 1H), 6.79-6.77 (m, 1H), 4.74-4.70 (m, 1H), 3.17 (dd, *J* = 10.0, 8.0 Hz, 1H), 3.03 (dd, *J* = 10.0, 8.2 Hz, 1H), 2.77-2.65 (m, 1H), 2.28-2.199 (m, 1H), 2.23 (s, 3H) 1.85-1.78 (m, 1H), 1.21 (s, 3H) and 1.20 (s, 3H).

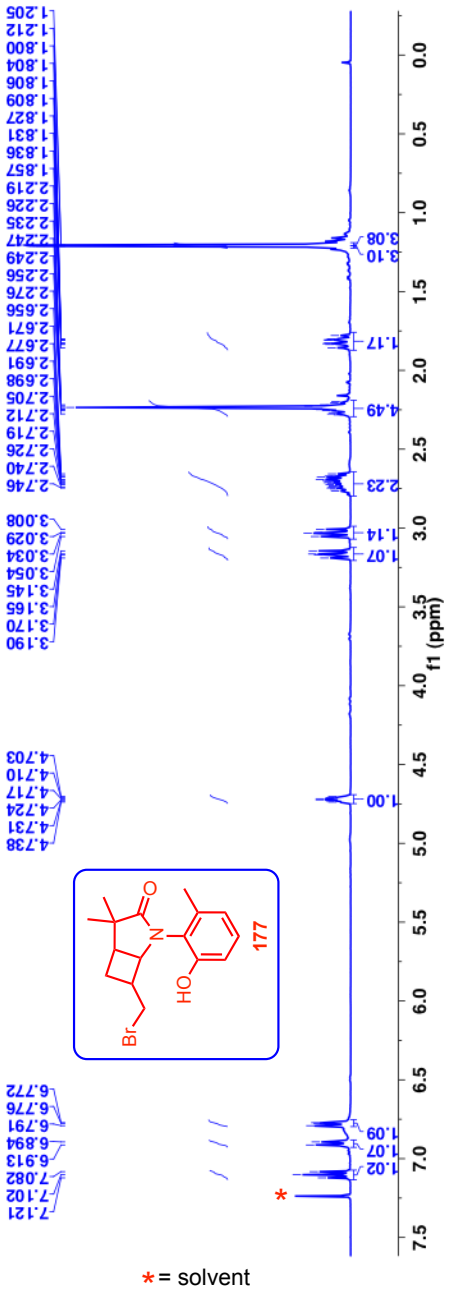

Figure 3.170: ^{1}H-NMR (400 MHz, $CDCl_3$, δ ppm) of cleavage product **177**.

^{13}C-NMR (100 MHz, $CDCl_3$, δ ppm): 182.2, 152.4, 134.2, 128.9, 126.7, 124.5, 118.2, 58.7, 43.1, 40.8, 40.1, 31.5, 28.1, 26.5, 19.5 and 18.2.

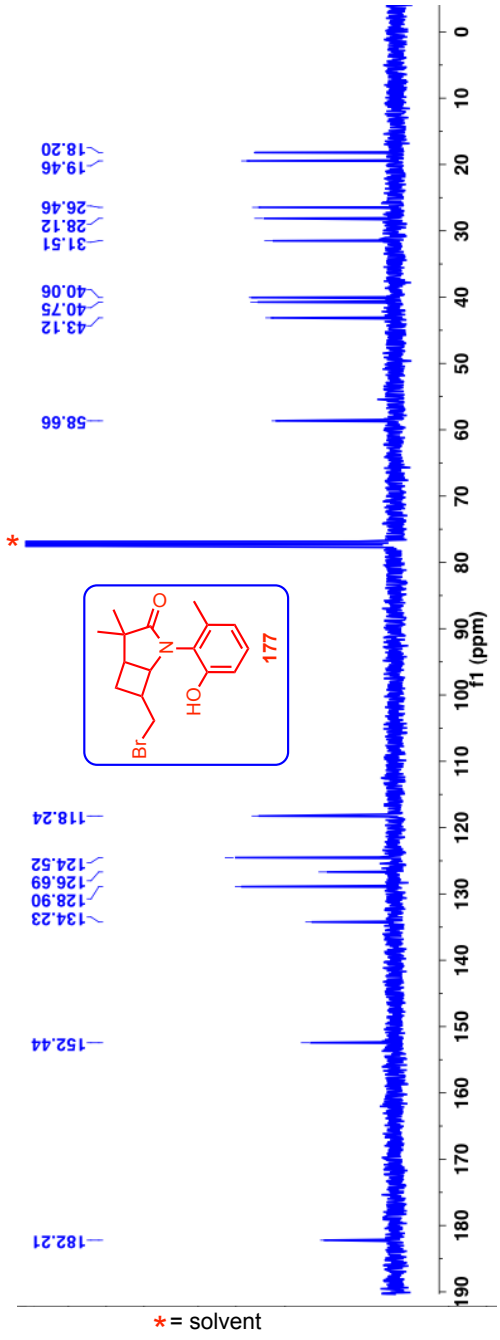

Figure 3.171: ^{13}C-NMR (100 MHz, $CDCl_3$, δ ppm) of cleavage product **177**.

HRMS-ESI (m/z) ([M + Na]$^+$):

Calculated : 360.0570

Observed : 360.0573

|Δm| : 0.8 ppm

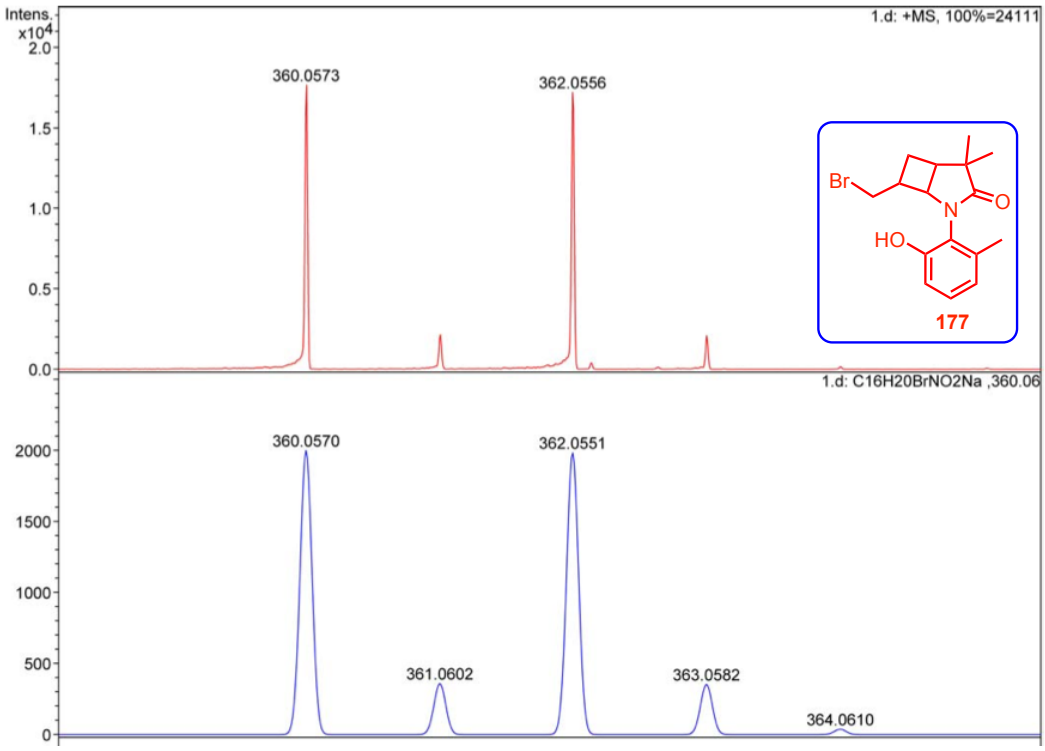

Figure 3.172: HRMS of cleavage product **177**.

3.13.2. Cleavage of enamide photoproduct 175j using $Pd(OH)_2$

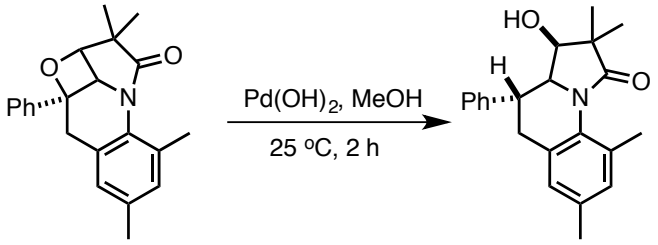

175j **178**

Scheme 3.38: Cleavage of photoproduct **175j** using $Pd(OH)_2$.

The ring opening of oxetane was achieved following a literature reported procedure.[8] A mixture of oxetane **175j** (30 mg, 0.09 mmol) and $Pd(OH)_2$ (20 wt% in charcoal, mg, mmol) in methanol (5 mL) was stirred under H_2 atmosphere for 2 h. After the reaction, the mixture was filtered through the celite and the solid was washed with methanol (10 mL). The combined organic layer was concentrated to get the crude product. The crude was purified by combiflash using hexanes:ethyl acetate mixture.

R*f* = 0.25 (80% hexanes:20% ethyl acetate) for **178** (Yield = 93%).

^{1}H-NMR (400 MHz, $CDCl_3$, δ ppm): 7.36-7.34 (m, 2H), 7.28-7.24 (m, 2H), 7.18-7.14 (m, 1H), 6.87 (s, 1H), 6.82 (s, 1H), 4.737 (d, *J*= 5.2 Hz, 1H), 4.58-4.55 (m, 1H), 3.49 (t, J = 4 Hz, 1H), 3.29-3.21 (m, 2H), 2.76-2.72 (m, 1H), 2.21 (s, 3H), 2.09 (s, 3H), 1.10 (s, 3H) and 0.797 (s, 3H)

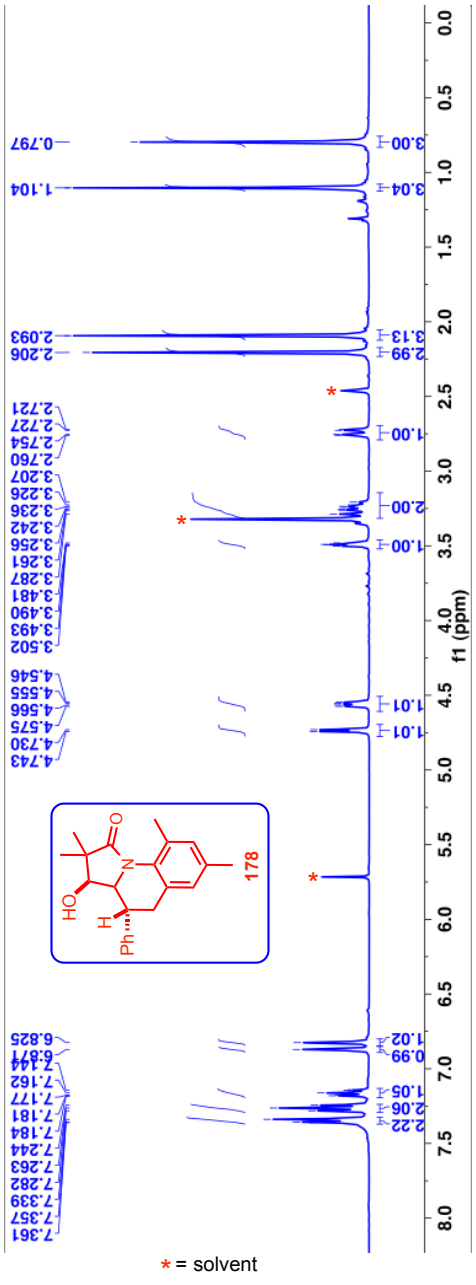

Figure 3.173: ^{1}H-NMR (400 MHz, $CDCl_3$, δ ppm) hydroxy-tetrahydro-pyrroloquinolinone **178**.

^{13}C-NMR (100 MHz, $CDCl_3$, δ ppm): 181.8, 145.5, 141.3, 139.5, 137.8, 137.0, 134.5, 133.7, 133.0, 131.3, 130.9, 82.2, 65.2, 51.8, 49.4, 36.5, 27.8, 26.0, 24.1 and 23.4.

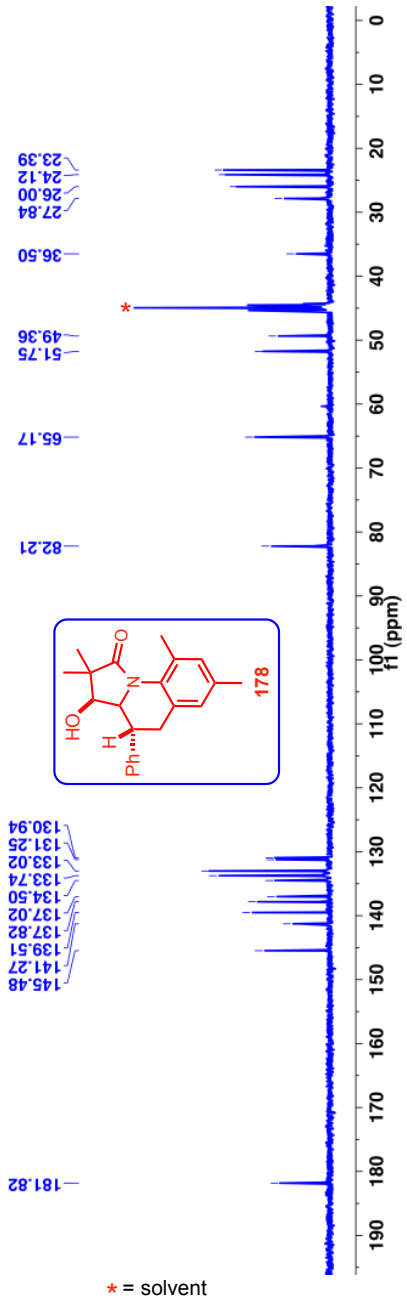

Figure 3.174: ^{13}C-NMR (100 MHz, $CDCl_3$, δ ppm) of hydroxy-tetrahydro-pyrroloquinolinone **178**.

HRMS-ESI (m/z) ([M + Na]$^+$):

Calculated : 358.1783

Observed : 358.1781

|Δm| : 0.6 ppm

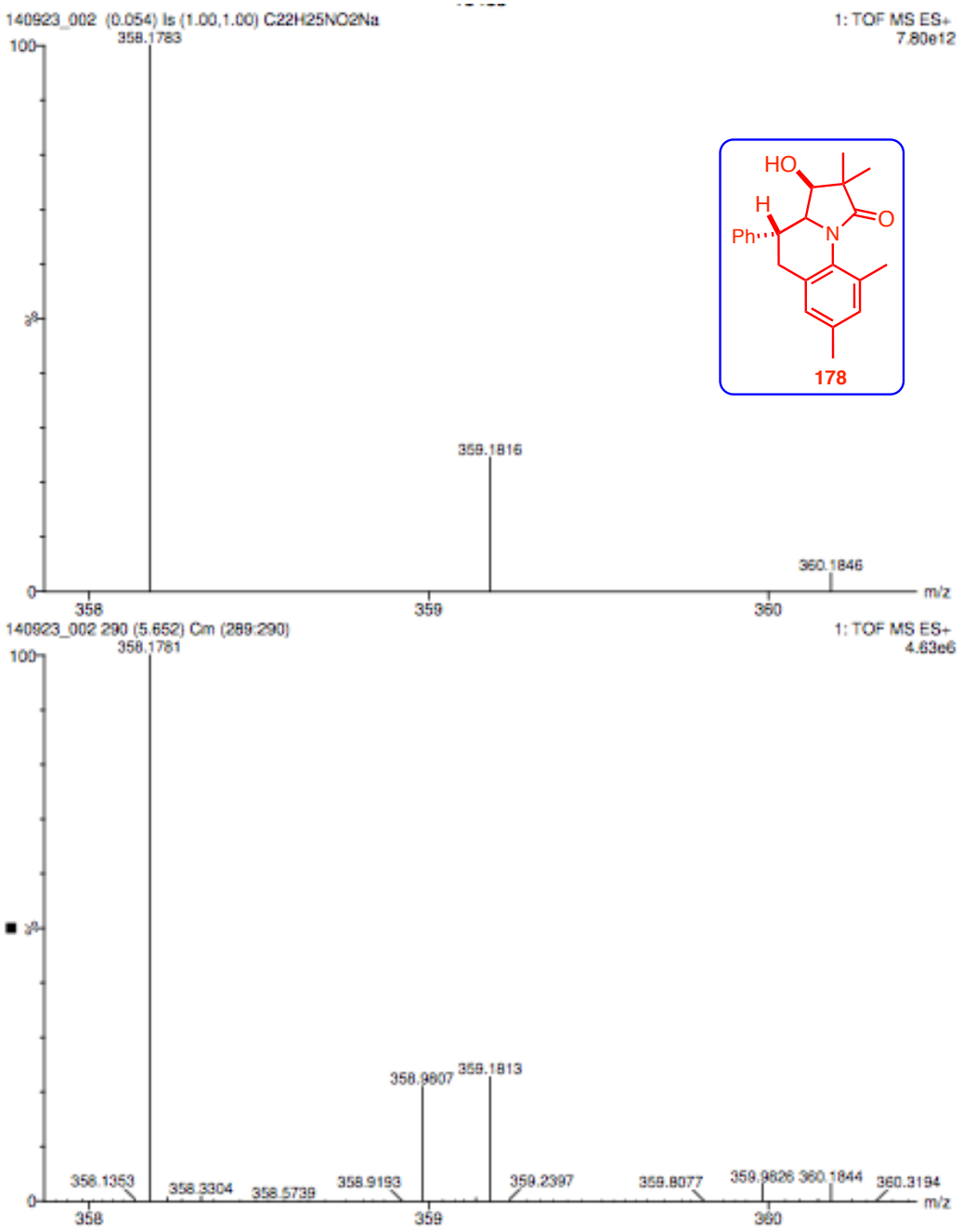

Figure 3.175: HRMS of hydroxy-tetrahydro-pyrroloquinolinone **178**.

3.14. UV-Vis spectrum of non-biaryl atropisomeric enamides 174a-c and its photoproducts.

The UV-Vis spectra of atropisomeric enamides **174a-c** and its photoproducts were measured in methanol (c ~ 0.1 mM).

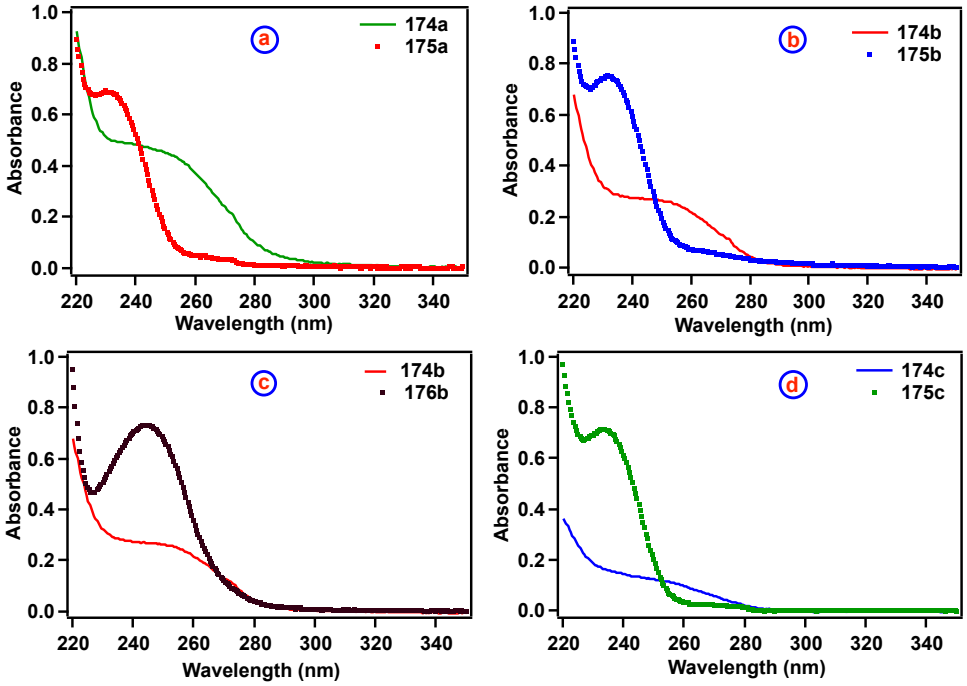

Figure 3.176: UV-Vis spectra of **174a-c, 175a-c** and **176b** in methanol (*c* ~ 0.1 mM).

3.15. Variable temperature NMR (VT-NMR) of enamide photoproduct 175a.

To ascertain the enantiomeric nature of the individual photoproduct **175**, variable temperature ^{1}H-NMR was carried out. Enantiopure photoproduct [(-)-(*R,R,R*)-**175a**] was dissolved in $CDCl_3$ and ^{1}H-NMR was recorded at different temperatures *viz*, 50, 25, -25 and -50 ^{o}C. There was no observable diastereomeric protons in the temperature range investigated (50 to -50 ^{o}C) indicating the lack of chiral conformers in the photoproduct.

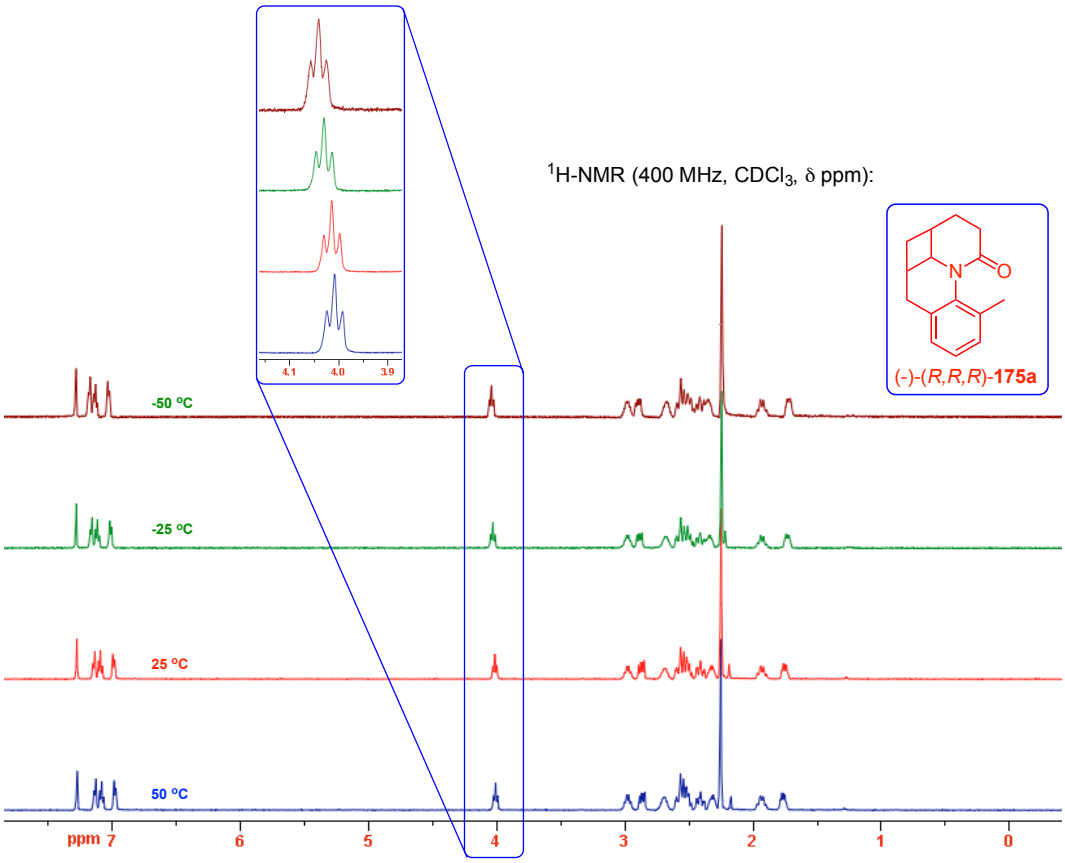

Figure 3.177: Variable temperature ^{1}H-NMR on enantiopure (-)-(*R,R,R*)-**175a** at various temperatures.

3.16. References

(1) Schreiber, S. L. [2 + 2] photocycloadditions in the synthesis of chiral molecules. *Science* **1985**, *227*, 857-863.

(2) Oppolzer, W. The intramolecular [2 + 2] photoaddition/cyclobutane-fragmentation sequence in organic synthesis. *Acc. Chem. Res.* **1982**, *15*, 135-141.

(3) Bach, T. Stereoselective Intermolecular [2+2]-Photocycloaddition Reactions and Their Application in Synthesis. *Synthesis* **1998**, 683.

(4) Sahn, J. J.; Comins, D. L. [2 + 2] Photochemical Cycloaddition/Ring Opening of 6-Alkenyl-2,3-dihydro-4-pyridones. *J. Org. Chem.* **2010**, *75*, 6728-6731.

(5) Comins, D. L.; Zheng, X.; Goehring, R. R. Total Synthesis of the Putative Structure of the Lupin Alkaloid Plumerinine. *Org. Lett.* **2002**, *4*, 1611-1613.

(6) Brimioulle, R.; Bach, T. Enantioselective Lewis Acid Catalysis of Intramolecular Enone [2+2] Photocycloaddition Reactions. *Science* **2013**, *342*, 840-843.

(7) Carbery, D. R. Enamides: valuable organic substrates. *Org. Biomol. Chem.* **2008**, *6*, 3455-3460.

(8) Bach, T.; Bergmann, H.; Brummerhop, H.; Lewis, W.; Harms, K. The [2+2]-Photocycloaddition of Aromatic Aldehydes and Ketones to 3,4-Dihydro-2-pyridones: Regioselectivity, Diastereoselectivity, and Reductive Ring Opening of the Product Oxetanes. *Chem. Eur. J.* **2001**, *7*, 4512-4521.

(9) Bach, T.; Schröder, J.; Harms, K. Diastereoselective photocycloaddition of an axial chiral enamide. *Tetrahedron Lett.* **1999**, *40*, 9003-9004.

(10) Vogt, F.; Jödicke, K.; Schröder, J.; Bach, T. Paternò-Büchi Reactions of Silyl Enol Ethers and Enamides. *Synthesis* **2009**, 4268-4273.

(11) Kitagawa, O.; Fujita, M.; Kohriyama, M.; Hasegawa, H.; Taguchi, T. Stereoselective synthesis of diastereomeric atropisomeric lactam with various ring sizes and their structural characterization. *Tetrahedron Lett.* **2000**, *41*, 8539-8544.

(12) Morris, J. V.; Mahaney, M. A.; Huber, J. R. Fluorescence quantum yield determinations. 9,10-Diphenylanthracene as a reference standard in different solvents. *J. Phys. Chem.* **1976**, *80*, 969-974.

(13) Hembury, G. A.; Borovkov, V. V.; Inoue, Y. Chirality-Sensing Supramolecular Systems. *Chem. Rev.* **2007**, *108*, 1-73.

(14) Görl, C.; Alt, H. G. Iron complexes with ω-alkenyl substituted bis(arylimino)pyridine ligands as catalyst precursors for the oligomerization and polymerization of ethylene. *J. Mol. Catal. A: Chem.* **2007**, *273*, 118-132.

(15) Hennion, G. F.; Boisselle, A. P. Preparation of t-Acetylenic Chlorides. *J. Org. Chem.* **1961**, *26*, 725-727.

(16) Cooper, M. A.; Lucas, M. A.; Taylor, J. M.; Ward, A. D.; Williamson, N. M. A Convenient Method for the Aromatic Amino-Claisen Rearrangement of N-(1,1-Disubstituted-allyl)anilines. *Synthesis* **2001**, 621.

(17) Kajigaeshi, S.; Kakinami, T.; Yamasaki, H.; Fujisaki, S.; Okamoto, T. Halogenation Using Quarternary Ammonium Polyhalides. *Bull. Chem. Soc. Jpn.* **1988**, *61*, 600.

(18) Tidwell, J. H.; Buchwald, S. L. Synthesis of Polysubstituted Indoles and Indolines by Means of Zirconocene-Stabilized Benzyne Complexes. *J. Am. Chem. Soc.* **1994**, *116*, 11797-11810.

(19) Yip, K.-T.; Yang, M.; Law, K.-L.; Zhu, N.-Y.; Yang, D. Pd(II)-Catalyzed Enantioselective Oxidative Tandem Cyclization Reactions. Synthesis of Indolines through C-N and C-C Bond Formation. *J. Am. Chem. Soc.* **2006**, *128*, 3130-3131.

(20) Garro-Helion, F.; Merzouk, A.; Guibe, F. Mild and selective palladium(0)-catalyzed deallylation of allylic amines. Allylamine and diallylamine as very convenient ammonia equivalents for the synthesis of primary amines. *J. Org. Chem.* **1993**, *58*, 6109-6113.

(21) Muchowski, J. M.; Venuti, M. C. Ortho functionalization of N-(tert-butoxycarbonyl)aniline. *J. Org. Chem.* **1980**, *45*, 4798-4801.

(22) Hogan, A.-M. L.; O'Shea, D. F. Carbolithiation of o-Amino-(E)-Stilbenes: Diastereoselective Electrophile Substitution with Applications to Quinoline Synthesis. *J. Org. Chem.* **2007**, *72*, 9557-9571.

(23) Trost, B. M.; Li, Y. A New Catalyst for a Pd Catalyzed Alder Ene Reaction. A Total Synthesis of (+)-Cassiol. *J. Am. Chem. Soc.* **1996**, *118*, 6625-6633.

(24) Kumarasamy, E.; Jesuraj, J. L.; Omlid, J. N.; Ugrinov, A.; Sivaguru, J. Light-Induced Enantiospecific 4π Ring Closure of Axially Chiral 2-Pyridones: Enthalpic and Entropic Effects Promoted by H-Bonding. *J. Am. Chem. Soc.* **2011**, *133*, 17106-17109.

CHAPTER 4: STEREOSPECIFIC INTRAMOLECULAR [2+2]-PHOTOCYCLOADDITION OF ATROPISOMERIC MALEIMIDES

4.1. Introduction

Maleimides are versatile reactants that find wide application in the ground state (thermal transformations) as well as in the excited state (photochemical transformations). The presence of electron deficient double bond that is in conjugation with imides carbonyls (conjugate acceptor) makes it both a reactive and a functionalizable chromophore.

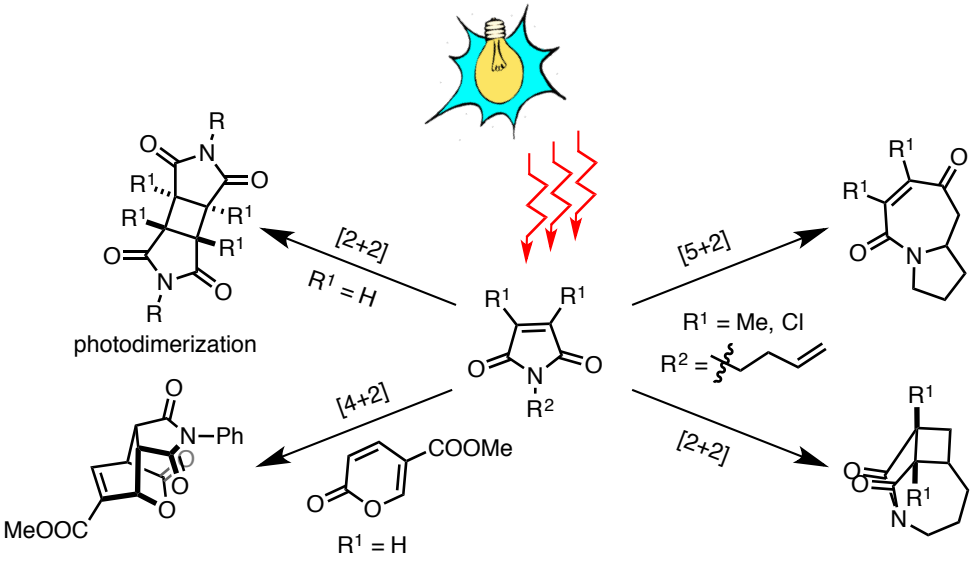

Scheme 4.1: Various photochemical transformations of maleimides.

Photocycloaddition of maleimides is the widely known photoreactivity of the maleimides. Some of the variants of photocycloaddition includes [2+2][1], [4+2][2] and [5+2][3,4] as shown in scheme 4.1.

The material in this chapter was co-authored by Elango Kumarasamy (EK), Ramya Raghunathan (RR), Dr. Steffen Jockusch (SJ), Dr. Angel Ugrinov (AU) and Dr. J. Sivaguru (JS). EK and RR in consultation with JS synthesized all the compounds and carried out all the experiments. A part of the results based on the atropisomeric maleimide system that is not reported in this thesis will be part of RR's thesis. AU recorded XRD data and solved the structures reported in this chapter. SJ performed photophysical studies detailed in this chapter. EK, RR, SJ and JS came up with the mechanistic rationale and the conclusion described in this chapter.

Despite the success of atropisomeric maleimides in thermal chemistry, the photochemical studies were not investigated extensively. This provided a perfect platform for us to evaluate the influence of axial chirality in promoting stereospecific [2+2]-photocycloaddition reactions in atropisomeric maleimides. Milburn and other research groups have evaluated the photochemistry of maleimides and thiomaleimides and showed that the reaction proceed smoothly to yield cyclobutane photoproducts (Scheme 4.2 and 4.3).[1,5,6] Interestingly, N-alkyl maleimides **209** provided an access to chemoselective products depending on the type of irradiation conditions.[6]

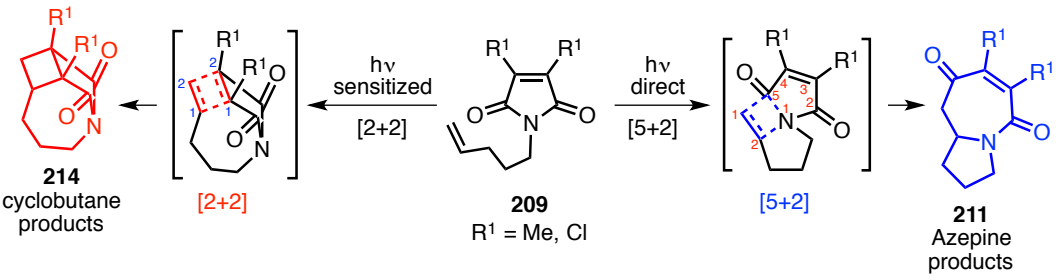

Scheme 4.2: Chemoselectivity in the photochemical transformation of *N*-alkyl maleimides **209.**

The direct irradiation of *N*-alkylmaleimide in acetonitrile resulted in [5+2]-photocycloaddition by the cleavage to N-CO bond leading to azepine products **211** (scheme 4.2). On the other hand, benzophenone sensitized irradiation in acetonitrile led to [2+2]-photocycloaddition resulting in cyclobutane products **214**. Such diversity in the maleimides makes them very useful synthetic building blocks. Similarly, Baker and coworkers reported intra and intermolecular [2+2]-photocycloaddition of thiomaleimides **215** leading to cyclobutane products **216** in excellent yield (Scheme 4.3).[1]

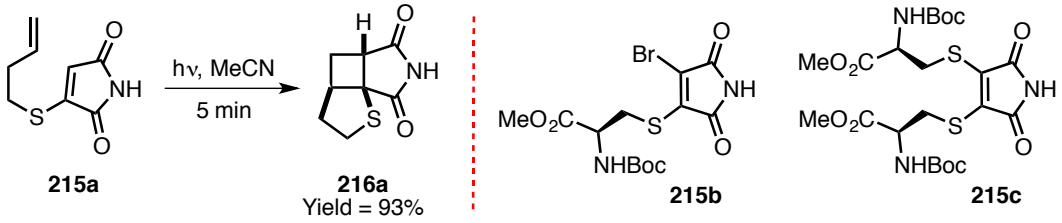

Scheme 4.3: [2+2]-Photocycloaddition of thiomaleimides **215.**

The sulfur substitution on the maleimides caused bathochromic shift along with increase in the extinction coefficient in UV-vis spectrum (maleimide with λ_{max} of 273 nm, mono thiomaleimides **215b** with λ_{max} of 339 nm and dithiomaleimide **215c** with λ_{max} of 393 nm) allowing for efficient reaction. Despite their synthetic utility, stereoselective phototransformations of maleimides in the literature were scarce. In one such example, Milburn and coworkers reported a diastereoselective intramolecular [2+2]-photocycloaddition of valinol, phenylglycinol derived tetrahydrophthalimides **217** that was attached to a cleavable temporary tether.[5] The diastereoselectivity between the *endo* and *exo* photoproduct **218** was moderate to good in some cases.

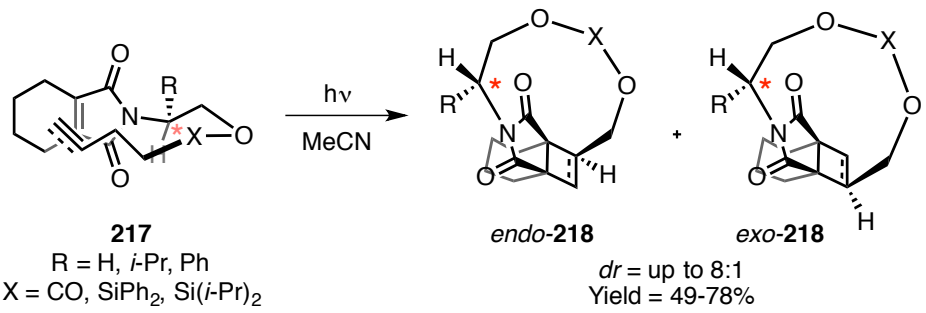

217 *endo*-**218** *exo*-**218**

Scheme 4.4: [2+2]-Photocycloaddition of chiral auxiliary, temporary tether appended tetrahydrophthalimide **217** (reproduced from reference 5, copyright© Elsevier Ltd, 2007)**.**

The presence of temporary tether allowed them for further synthetic modifications to useful building blocks. Based on the literature precedence and the importance of maleimide scaffold in the organic synthesis, we designed atropisomeric maleimides to evaluate them towards stereospecific phototransformation. The atropisomeric maleimides and their intermediates listed in the following chart were synthesized according to the procedure reported in literature.

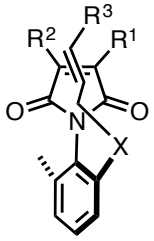

219a-g

a) R^1 = Me; R^2-R^3 = H; X = O
b) R^1,R^3 = Me; R^2 = H; X = O
c) R^1= Me; R^2-R^3 = H; X = SiO_2Ph_2
d) R^1 = Me; R^2-R^3 = H; X = CH_2
e) R^1 = Ph; R^2-R^3 = H; X = O
f) R^1 = Br; R^2-R^3 = H; X = CH_2
g) R^1 = Me; R^2 = Br; R^3 = H; X = O

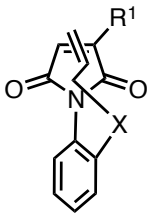

219h-i
h) R^1 = Me; X = O;
i) R^1 = Ph; X = O;

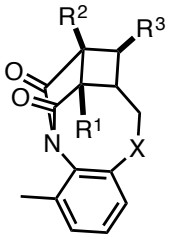

220a-g

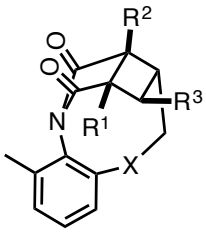

221a-g

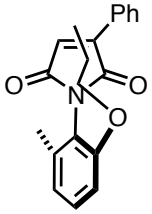

222e
R^1 = Ph

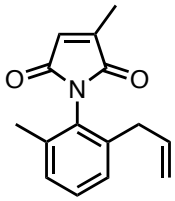

223

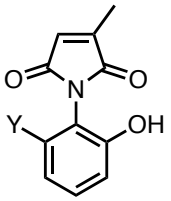

224a-b

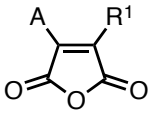

225a-d
R^1 = Me, Ph, Br;
A = H, Br

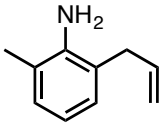

226d
186b = **225b**

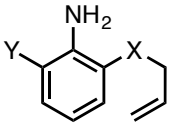

226a-c
186b = **225c**

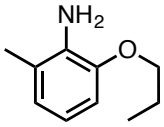

227

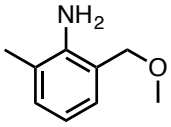

193

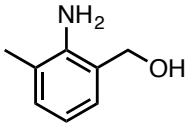

194

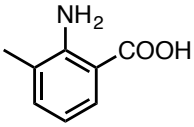

195

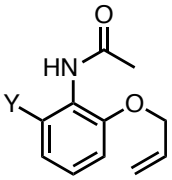

228a-b
a) Y = Me; X=O
b) Y = H; X=O

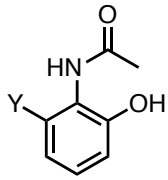

229a-b

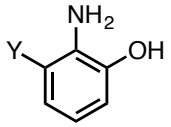

196a-b
a) Y = Me
b) Y = H

Chart 4.1: Structures of **i**mine derived maleimides, their photoproducts and compounds used for their synthesis.

4.2. Reactivity of N-aryl atropisomeric maleimides in photocycloaddition reaction

The *N*-alkenyl maleimides (with suitable chain length) are known to undergo chemoselective [2+2] or [5+2]-photocycloaddition depending on the irradiation conditions.[6] We were interested in evaluating the newly synthesized atropisomeric maleimides towards photocycloaddition reaction. In our study, irrespective of the irradiation conditions, the chemoselectivity was completely dictated by the chain length of alkenyl tether (Scheme 4.5). For example, when maleimide **219a** (that had butenyl chain length) was subjected to photoreaction, only [2+2]-photocycloaddition was observed (direct or sensitized). On the other hand, when the maleimide derivative **223** that had allyl chain length subjected to direct irradiation conditions only [5+2]-photocycloaddition was observed, while sensitized irradiation resulted in the isomerization of allyl chain double bond leading to styrene type products.

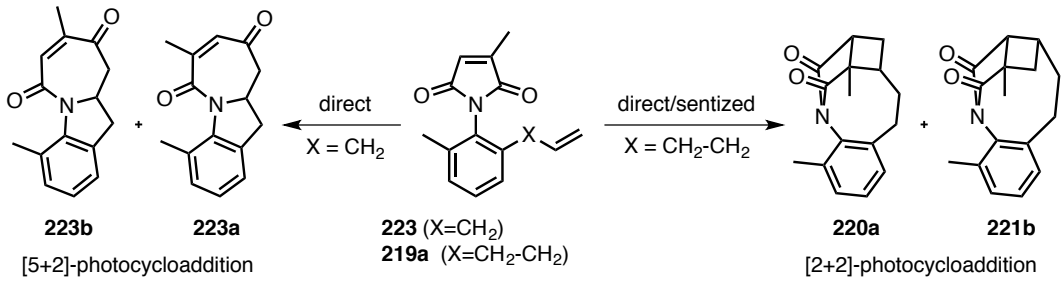

Scheme 4.5: Chain length dependent chemoselectivity of atropisomeric maleimides in photocycloaddition reaction.

This chain length dependent chemoselectivity, we believe was the consequence of molecular constraints imposed on the maleimides and the kinetics of the individual reaction ([2+2] vs [5+2]) that forced it to undergo one reaction pathway vs. another. For example, the length of the allyl substituent in the maleimide **223** was short that prevented it from reaching to maleimide double bond to form [2+2]-adduct. So, the excited maleimide underwent facile N-CO bond cleavage resulting in the insertion of allyl double bond leading to [5+2]-adduct. On the other hand, the butenyl-substituted maleimide **219a** is too long to undergo [5+2]-adduct. So, the excited maleimide was instantly quenched by the butenyl substituent to form [2+2]-adduct.

4.3. Racemization barrier in atropisomeric maleimides

N-Aryl maleimides are known to be inherently twisted owing to the steric congestion between imide carbonyls and the *ortho* hydrogens of the phenyl ring.[7,8] However, the simple hydrogen substitutions do not present enough sterics to have a stable chiral axis. Thus, in the newly synthesized maleimides **219**, the presence of methyl group at the *ortho* position (6-position of maleimide) was indispensible to have higher energy barrier for rotation. The maleimides that lacked this methyl group (**219h-i**) were not axially chiral at room temperature. So, we carried out racemization kinetics to evaluate the strength of energy barrier towards racemization. Racemization kinetics of optically pure atropisomeric maleimides **219a-b** and **219e** was carried at 100 °C in toluene. The course of racemization (% *ee*) was monitored by HPLC analyses on a chiral stationary phase at various time intervals. The activation energy barrier is provided in the table 4.1.

Table 4.1: Rate constant, half-life and energy barrier for racemization on atropisomeric maleimides

Entry	Compound	Parameters		
		$\tau_{1/2}$ (days)	k_{rac} (s^{-1})	$\Delta G^{\ddagger}_{rac}$ (kcal·mol^{-1})
1	**219a**	3.5	2.27×10^{-6}	31.6
2	**219b**	3.5	2.33×10^{-6}	31.6
3	**219e**	3.5	2.40×10^{-6}	31.6

The racemization kinetics was followed by HPLC analysis on a chiral stationary phase. Values carry an error of ±5%.

Analysis of the kinetic parameters on atropisomeric maleimides **219** provided insights into the energy barrier to rotation around the N-C_{aryl} chiral axis (Table 4.1). For example, in the case of **219a**, the half-life for racemization ($\tau_{1/2}$) was 3.5 days at 100 °C, corresponding to a racemization rate constant (k_{rac}) of 2.27×10^{-6} s^{-1} and an activation energy barrier ($\Delta G^{\ddagger}_{rac}$) of 31.6 kcal·$mol^{-1}$. These results clearly show that the newly synthesized atropisomeric maleimides have sufficiently high-energy barriers to be employed for stereospecific photoreactions at without the loss of absolute configuration.

4.4. Intramolecular [2+2]-photocycloaddition of atropisomeric maleimides

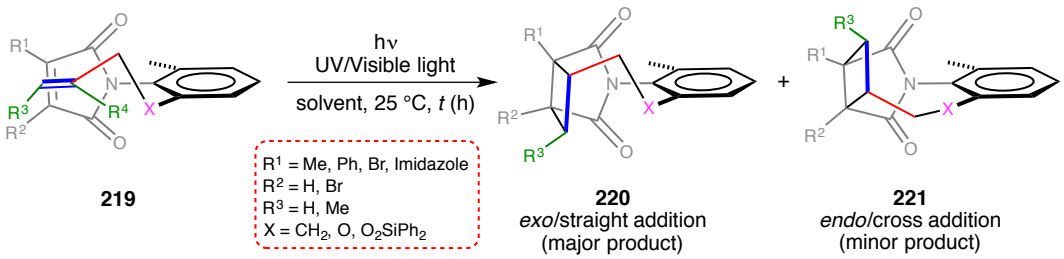

Scheme 4.6: [2+2]-Photocycloaddition of atropisomeric maleimides **219**.

The photoreactions of newly synthesized atropisomeric maleimides **219** were evaluated under different irradiation conditions and solvent that proceeded smoothly to furnish [2+2]-photoadduct(s) in excellent isolated yield and mass balance. Three different sets of irradiation conditions were tested: (a) direct irradiation; (b) sensitized irradiation under UV light (e.g., using xanthone as a sensitizer); and (c) metal-free sensitized irradiation under visible-light (e.g., using thioxanthone as a sensitizer). After the photoreaction, the solvent was evaporated under reduced pressure, and the product(s) were purified by column chromatography. The NMR, HPLC and X-ray diffraction (XRD) analyses revealed that the presence of two diastereomeric photoproducts viz., *exo*-photoadduct **220** and *endo*-photoadduct **221**. In the major *exo*-photoproduct **220**, the terminal carbon of the alkene tether was oriented away from the carbon bearing the R^1 substituent of the maleimide. Where as in the minor *endo*-photoproduct **221**, the terminal carbon of the alkene tether was oriented toward the carbon bearing the R^1 substituent of the maleimide. The atropisomeric maleimide **219a** was chosen as a model system to optimize the irradiation conditions.

4.4.1. Control studies towards stereospecific [2+2]-photocycloaddition of atropisomeric maleimides

The optimized conditions for the photoreactions were obtained after several screening reactions carried out on atropisomeric maleimide **219a**. These reactions provided crucial information about the solvents, type of irradiations, sensitizers, temperature and time. The following table provides the list of those trial experiments.

Table 4.2: Control experiments on atropisomeric maleimide **219** for optimization of photoreactions

Entry	Compd	Solvent	Conditions	*dr* (**220:221**)	Convn (%)	MB (%)
1	**219a**	MeCN	bb, rt, 12 h	79:21	> 98	-
2	**219a**	MeCN	~350 nm, rt, 2 h	No reaction		
3	**219a**	MeCN	Xanthone, 350 nm, rt, 1 h	79:21	> 99	-
4	**219a**	MeCN	Thioxanthone, 420 nm, rt, 1 h	79:21	> 98	95
5	**219a**	MeCN	~300 nm, rt, N_2, 6 h	-	93	97
6	**219a**	MeCN	~300 nm, rt, O_2, 6 h	-	88	92
7	**219a**	MeCN	~300 nm, -30 ^oC, 12 h	79:21	-	-
8	**219a**	Methanol	~300 nm, -60 ^oC, 12 h	79:21	-	-
9	**219a**	Toluene	~300 nm, -60 ^oC, 12 h	**219a** crashed out		
10	**219e**	Acetone	bb, rt, 12 min	>99:1	> 98	55 [a]
11	**219e**	MeCN	~350 nm, rt, 12 h	>99:1	92	80

Note: MeCN- acetonitrile; bb- broad band (450W mercury lamp); rt- room temperature; The reactions were run with ~3.9 mM concentration either under constant bubbling of N_2 or N_2 degassed solution (except for entry 6). Convn- conversion, MB- mass balance. ~300, ~350 and ~420 nm irradiations were carried out in a Rayonet reactor. [a] Isolated yield.

The analysis of table 4.2 clearly indicated that the photocycloaddition reaction proceeded smoothly under sensitization. For example under xanthone and thioxanthone sensitized reaction completed within 1 h (entry 3 and 4). The reaction proceeded to similar conversions both under O_2 and N_2 atmospheres (entry 5 and 6) and the temperature or solvent did not have any influence on the *dr* of the photoproducts (entry 7 and 8).

4.4.2. Solvent screening for the UV/Visible light mediated photoreaction of maleimides 219a and 219e

Various solvents were investigated for the xanthone and thioxanthone sensitized photoreaction of atropisomeric maleimide **219a**. In a standard experiment, maleimide **219a** with 30 mol % of sensitizer in a respective solvent (~3.9 mM concentration) was degassed with N_2 for 15 min and then sealed. This solution was irradiated in a Rayonet reactor (~350 nm for xanthone and ~420 nm for thioxanthone, respectively) for 1 h. After the reaction, a stock solution of internal standard (triphenylmethane) was added and the solution was concentrated under reduced pressure to obtain the crude reaction mixture. ^{1}H-NMR spectroscopy was recorded on the crude reaction mixture and from the integral values the conversion and mass balance were calculated.

Table 4.3: Solvent screening for sensitized photoreaction of **219a**

Entry	Solvent	% Conversion (% mass balance)	
		Xanthone	Thioxanthone
1	Methanol	> 98 (> 98)	> 98 (> 98)
2	Acetonitrile	> 98 (> 98)	> 98 (> 98)
3	Ethyl acetate	> 98 (95)	83 (> 98)
4	THF	Decomposed	-
5	Chloroform	> 98 (81)	> 98 (> 98)
6	Dichloromethane	> 98 (> 98)	> 98 (> 98)
7	Benzene	44 (78)	73 (> 98)
8	Toluene	- (36)	41 (> 98)
9	MCH	27 (> 98)	26 (> 98)

Note: The reported value carry an error of ±5%.

The photoreaction with xanthone and thioxanthone in various solvents proceeded with good conversion and excellent mass balance. However, in certain solvents such as benzene toluene and methylcyclohexane (MCH) poor conversion and mass balance was observed. In THF however complete decomposition was observed with no trace of either starting material or photoproduct.

4.4.3. Visible light photocatalysis - Sensitizer loading for photoreaction of maleimide 219a and 219e

The efficiency of visible light photoreaction with 30 mol% of the thioxanthone was high (reaction completed in 1 h). So, to evaluate the % of conversion in **219a** with respect to mol% of sensitizer, we conducted visible light photoreaction with varying mol % of the thioxanthone. In a typical reaction, the maleimides were taken in acetonitrile (*c* ~ 3.9 mM) and desired mol% of thioxanthone was added and the solution was degassed with N_2 for ~15 min, sealed and irradiated at ~420 nm in a rayonet reactor for 1 h. After the reaction, a stock solution of internal standard was added and the solvent was evaporated. ^{1}H-NMR was recorded on the crude reaction mixture and from the integral values of the peaks conversion and mass balance were calculated (refer to section 4.11).

Table 4.4: Sensitizer loading for thioxanthone sensitized photoreaction of maleimides **219a** and **219e**

Entry	Compd	Sensitizer (mol%)	Conversion (%)	Mass balance (%)
1	**219a**	5	60	> 98
2		10	81	> 98
3		15	86	> 98
4		20	100	88
5	**219e**	5	40	> 98
6		10	71	87
7		15	100	> 98
8		20	100	> 98

Note: The reported value carry an error of ±5%.

The result clearly showed that the thioxanthone was extremely efficient in promoting the visible light photoreaction. For example, even with 5 mol% sensitizer loading 60% conversion was achieved in 1 h. However, the sensitizer loading was maintained at 30 mol%, to ensure that the catalyst always absorb the light thus acting as an optical shield to prevent decomposition of starting material or photoproduct.

4.4.4. Analysis of *dr* in the photoproducts for maleimides 219a and 219d in various solvents under direct irradiation

The photoreaction of atropisomeric maleimides resulted in the formation of mixture of diastereomeric products **220** and **221**. We screened atropisomeric maleimides **219a** and **219d** in various solvents *viz.,* toluene, MCH, acetone, acetonitrile and methanol ($c \sim 3.88$ mM) to ascertain the role of solvent in biasing one product over the other. In a typical experiment, a solution of atropisomeric maleimide **219a** and **219d** in a given solvent was irradiated with a 450W medium-pressure mercury lamp under constant flow of nitrogen for 5 h at 25 °C. After 5 h of irradiation, the solvent was evaporated under reduced pressure and the NMR of the crude reaction mixture was recorded in $CDCl_3$. From the integral values, diastereomeric ratio (*dr)* between **220** and **221** was analyzed.

Table 4.5: Analysis of *dr* in the photoproducts of maleimides **219a** and **219d** in various solvents.

Entry	Compd	Solvents				
		Toluene	MCH	Acetone	Acetonitrile	Methanol
1	**219a**	73:27	77:23	79:21	78:22	73:27
2	**219d**	77:23	78:22	74:26	79:21	71:29

Note: The results are an average of 2 runs with ±5 error limit. MCH- methylcyclohexane.

The result showed that the solvent plays a minimal role in dictating the *dr* in the photoproducts. Screening from non-polar solvent such as MCH to polar solvent such as methanol resulted in similar *dr* values. Also, from the low temperature (-60 °C) screening studies, it was revealed that the temperature also had only minimum influence over the *dr* in the photoproducts.

4.4.5. Stereospecific [2+2]-photocycloaddition of atropisomeric maleimides 219

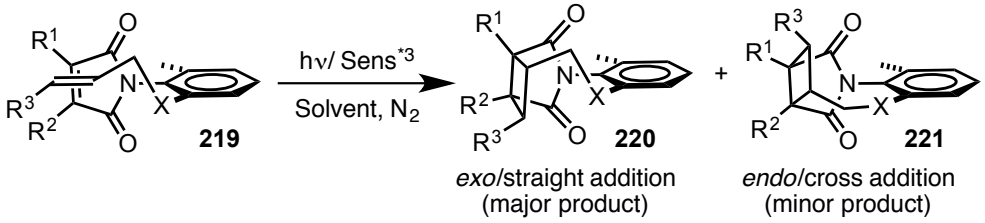

Scheme 4.7: Stereospecific [2+2]-photocycloaddition of atropisomeric maleimides **219a-g**.

The photoreaction of maleimides was performed under optimized conditions to evaluate the enantiomeric excess and diastereomeric ratio in the product (Scheme 4.7). The photoreaction was performed under the given conditions in table 4.6 until complete consumption of starting material as observed in thin layer chromatography (TLC). After the reaction, the products were isolated either in preparative TLC or column chromatography. The NMR analysis of the crude and the HPLC analysis revealed the *dr* and enantiomeric excess in the photoproducts respectively.

Analysis of Table 4.6 disclosed several interesting characteristics in the [2+2]-photocycloaddition reaction of atropisomeric maleimides. The enantiomeric excess in the photoproduct of all the maleimides analyzed were >98% (**219a-b** and **219e**). This was a clear indication of the influence of stable chiral axis that enabled efficient chirality transfer resulting in enantioenriched photoproducts.

The diastereomeric ratio in the photoproduct was affected by the substituents at the alkenyl tether (R^2-R^3) and the maleimide double bond (R^1). So, we systematically changed the substituents R^1-R^3 and X to evaluate the influence of substituents in determining the *dr* in the photoproducts. The X substituent that connects the alkene tether (O, CH_2 and $O_2Si_2Ph_2$) and *N*-phenyl ring had only minimal influence over the *dr*. For example, comparing **219a** and **219d** shows that the *dr* was only minimally affected up on changing the X group from O to CH_2. Even increasing the chain length as in the case of **219c** (X = O-($SiPh_2$)-O) did not improve the *dr* in the photoproduct. This result was a slight surprise as the literature precedence shows that silyl tether had good control over the *dr*.[5] When the R^1 group was changed to bromine, further decrease in

the *dr* was noted (61:39). To our surprise, when a bulky substituent was employed for the photoreaction as in the case of **219e** (R^1 = Ph), complete control over the *dr* was obtained. When the optically pure **219e** was employed for photoreaction, complete enantio- and diastereomeric control was achieved. If the maleimide double bond contained disubstitution as in the case of **219g** (R^1= Me, R^2= Br), slight reversal in the *dr* was observed that favors *endo* photoproduct (**220:221** = 42:58).

Table 4.6: Intramolecular [2+2]-photocycloaddition of atropisomeric maleimides[a]

Entry	Substrate	Major photoproduct	Isolated yield *dr* (**220:221**),[b] % ee [c]
1	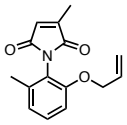	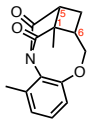	84 (79:21)
	(+)-**219a**	(-)-(1*R*,5*S*,6*R*)-**220a**	> 98% *ee*
	(-)-**219a**	(+)-(1*S*,5*R*,6*S*)-**220a**	> 98% *ee*
2	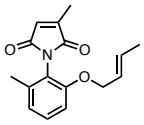	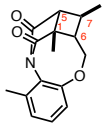	84 (87:13)
	(+)-**219b**	(-)-(1*R*,5*S*,6*R*,7*R*)-**220b**	> 98% *ee*
	(-)-**219b**	(+)-(1*S*,5*R*,6*S*,7*S*)-**220b**	> 98% *ee*
3	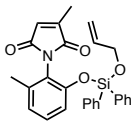	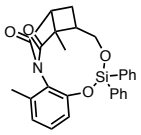	76 (77:23)
	219c	**220c**	
4	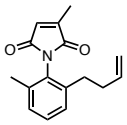	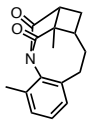	88 (74:26)
	219d	**220d**	

Entry	Substrate	Major photoproduct	Isolated yield [%] *dr* (**220:221**),[b] % ee [c]
5	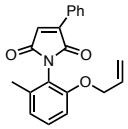	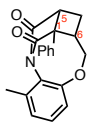	90 (>99:1)
	(+)-**219e**	(-)-(1*R*,5*S*,6*R*)-**220e**	> 98% *ee*
	(-)-**219e**	(+)-(1*S*,5*R*,6*S*)-**220e**	> 98% *ee*
6	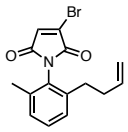	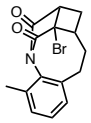	80 (61:39)
	219f	**220f**	
7	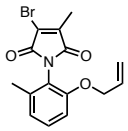	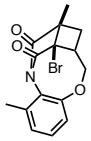	94 (42:58)
	219g	**220g**	

[a] Irradiations of **219e** was performed with 30 mol % thioxanthone as the triplet sensitizer in acetonitrile solvent at room temperature using a Rayonet reactor equipped with 420 nm lamps. For all other substrates, the photoreactions were performed in acetone at room temperature using a 450 W medium-pressure Hg lamp with a Pyrex cutoff filter. [b] The ratios were determined by ^{1}H-NMR spectroscopy of the crude samples. [c] The *ee* values were obtained from HPLC analysis on a chiral stationary phase, and the results are averages of three runs with an error of ±3%. The absolute configuration was determined by XRD with Flack parameters.

These results clearly indicate that the [2+2]-photocycloaddition of maleimides undergoes highly stereospecific phototransformations under ambient conditions. The *dr* ratio in the photoproduct is dictated by the R^1 substituent to a major extent, while the R^3 and X has only

minimal influence. The presence of oxygen at the alkenyl tether allowed us to cleavage the tether after the photoreaction, revealing the enantioenriched building blocks.

4.4.6. Continuous flow visible-light photocatalysis of atropisomeric maleimides 219a

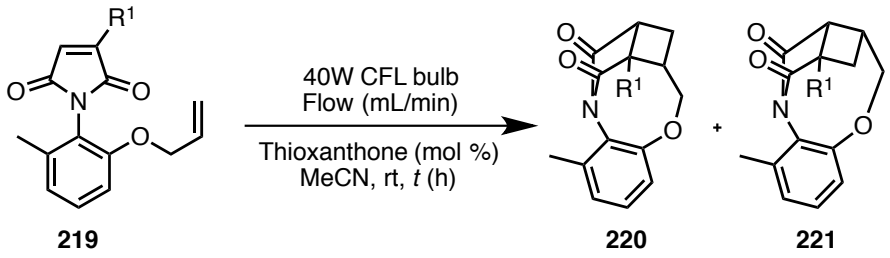

219 **220** **221**

Scheme 4.8: General irradiation procedure for maleimides **219a**.

The efficiency of thioxanthone in effecting the [2+2]-phototransformations provided us an opportunity to evaluate the reaction under visible light using household light (**C**ompact **F**luorescent **L**ight bulbs). This idea was appealing, as the reaction condition was redox-neutral and metal- free. Apart from using visible-light, we also attempted to run the reaction under flow condition so that our methodology could be easily scaled up with increased efficiency. With the simplest set up available in our lab, we designed a flow set up and optimized the irradiation conditions. In a typical reaction, a N_2 degassed acetonitrile solution of maleimide ($c \sim 3.9$ mM) and thioxanthone (10 mol%) in a 100 mL round bottom flask was pumped through a peristaltic pump (8 RPM = ~ 0.83mL/min and 4 RPM = ~0.45mL/min) into FEP tubing that was coiled around a 40W CFL bulb. The solution after the irradiation was collected at the end in a round bottom flask, concentrated under reduced pressure, analyzed by ^{1}H-NMR and was purified by combiflash.

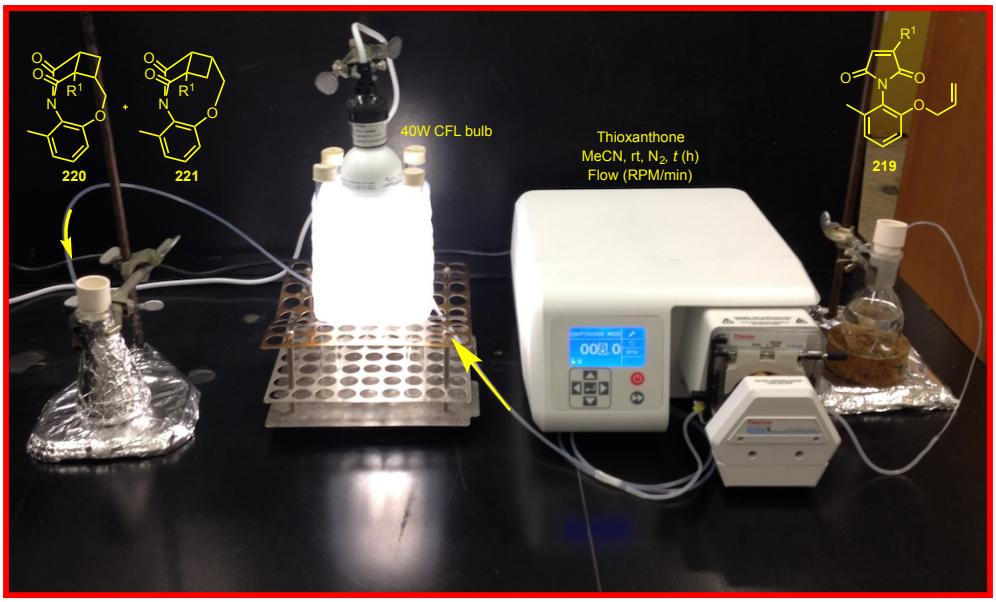

Figure 4.1: Flow set up for visible light photocatalysis of maleimides **219a**.

Several trial runs were carried out to optimize the best conditions for flow photolysis. The following table summarizes the trials.

Table 4.7: Reaction optimization for flow photolysis of **219a** under visible light conditions.[a]

Entry	Compd	Parameters			*t* (min)	Conversion (%)
		Lamp	Flow (RPM)	Sens. (mol%)		
1	**219a**	13W	4	30	15	50
2	**219a**	13W	4	100	15	30
3	**219a**	20W	4	30	15	50
4	**219a**	20W	8	30	35	72
5	**219a**	40W	8	10	35	> 98
6	**219a**	40W	Batch mode	10	35	21
7	**219a**	40W	Batch mode	10	180	63

[a] Entries 1-3 were tested on a FEP tubing with dimension 1/16×0.03×20ft that had internal volume ~3 mL around the lamp. *t* is the residence time of the solution during irradiation. Sens.- sensitizer loading for a given reaction. Conversion was calculated by NMR spectroscopy analysis of the crude sample. Batch mode was conducted using a test tube placed at ~ 2.5 cm from the lamp (the similar distance for the FEP tubing from the lamp).

Complete conversion of maleimide **219a** was observed achieved (3.9 mM with 10 mol % sensitizer and a flow rate of 0.83 mL/min) within 35 min of irradiation, while the batch mode for the similar scale only resulted in 23% conversion in 35 min. These results clearly demonstrate the efficacy of [2+2] photoreactions of maleimides even under visible-light conditions.

4.5. Photophysical studies on atropisomeric maleimides

To understand the nature of excited states and the reactivity of atropisomeric maleimides, we carried out detailed photophysical studies. However, the maleimides with alkenyl tether found to be too reactive to provide any significant information about the excited states even at 77 K. To avoid the photochemical reaction and to understand its photophysical properties, atropisomeric maleimide **222e** was synthesized wherein the alkenyl part of the maleimide was saturated while retaining the chromophore part of the maleimide intact. This approach completely avoided the photoreaction thus providing more information about the excited states.

4.5.1. Triplet-triplet absorbance studies on atropisomeric maleimides 222e and 219e

Lase flash photolysis studies were carried out on maleimides whose alkenyl tether was saturated and unsaturated (**222e** and **219e**) in acetonitrile solution. The saturated alkenyl tether was evaluated to prevent the fast [2+2]-photocycloaddition reaction.

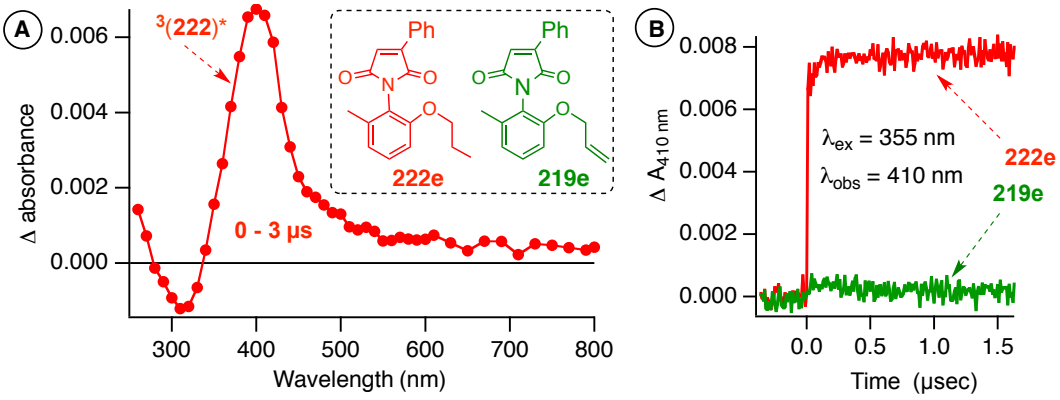

Figure 4.2: (A): Transient absorption spectrum monitored 0-3 µs after pulsed laser excitation (355 nm, 7 ns pulse length) of argon saturated MeCN solution of **222e**. (B): Absorbance kinetic traces monitored at 410 nm of argon saturated MeCN solution of **222e** (red) and **219e** (green) with matching absorbance of 0.3 at 355 nm. (Reproduced from reference 9, with permission from American Chemical Society, 2014).

To obtain the triplet-triplet absorption (TTA) spectrum of maleimide **222e** under direct excitation, an argon purged acetonitrile solution of the maleimide **222e** that had an absorbance of 0.3 (1 cm path length) at the excitation wavelength (355 nm) was placed in a 1×1 cm quartz cell with reservoir. Kinetic traces at varying probe wavelength (260 – 800 nm) were measured after pulsed laser excitation (Ex = 355 nm, 7 ns pulse length). From these kinetic traces the transient absorption was plotted (figure 4.1).

The transient absorption of **222e** was centered on 400 nm that decayed with a lifetime of 50 µs. The transient was quenched by molecular oxygen (k_q = 2 × 10^{-9} M^{-1}·s^{-1}), and was assigned to the TTA of the maleimide chromophore. The triplet transient absorption of **222e** was further ascertained by its generation from excited thioxanthone (TX) sensitizer through triplet energy transfer. Similar TTA studies carried out on **219e** (maleimide with an alkenyl tether) revealed that the triplet lifetime of maleimide was only 450 ns.

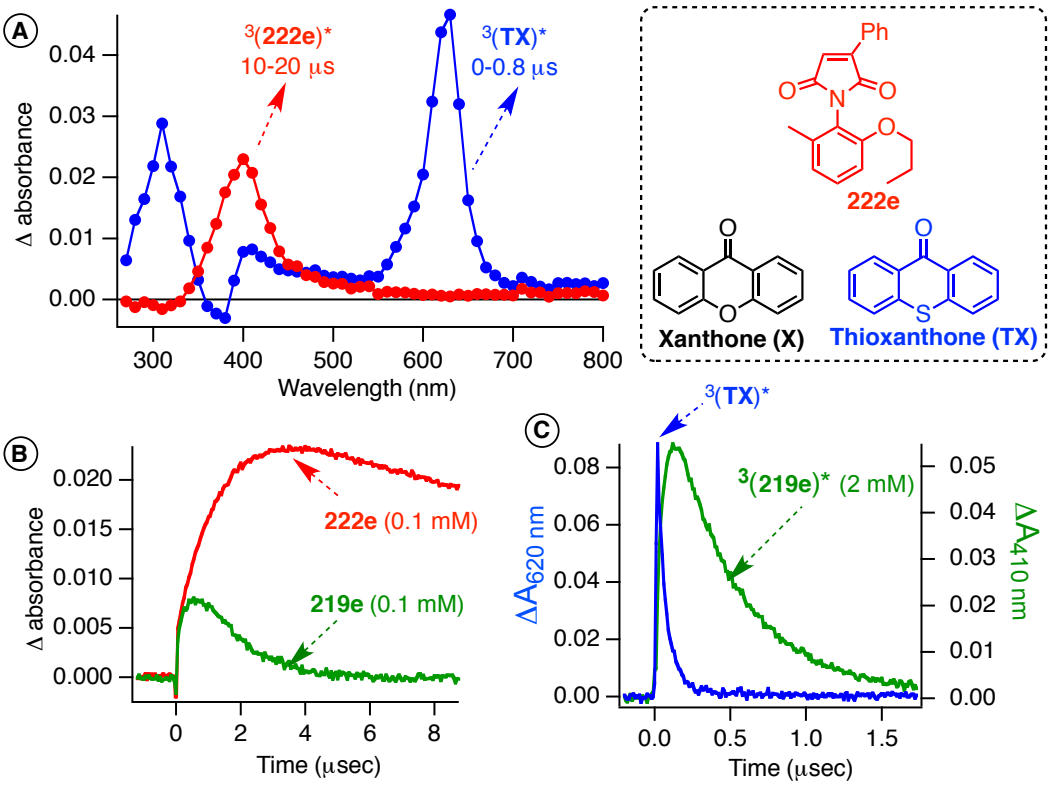

Figure 4.3: (A): Transient absorption spectra monitored 0-0.8 μs (blue) and 10-20 μs (red) after pulsed laser excitation (355 nm, 7 ns pulse length) of argon saturated MeCN solutions of **TX** and **222e** (0.05 mM). (B): Absorbance kinetic traces monitored at 410 nm of argon saturated MeCN solutions of **TX** containing 0.1 mM of **222e** (red) or **219e** (green). (C): Absorbance kinetic traces monitored at 620 nm (blue) and 410 nm (green) after pulsed laser excitation using front face geometry and a 2 mm optical path length. (Reproduced from reference 9, with permission from American Chemical Society, 2014).

Comparison of the TTA at 410 nm upon laser excitation at 355 nm between the maleimide with a saturated alkyl tether (**222e**) and the maleimide with alkenyl tether (**219e**) revealed the efficiency of the photoreaction. For example, the lifetime of **222e** and **219e** was 50 μs and 450 ns respectively suggesting that the excited state of **219e** (^{3}**219e***) is highly deactivated by the [2+2]-photocycloaddition reaction.

Similarly, the TTA studies were carried out on thioxanthone sensitizer TX in Argon-saturated acetonitrile solution in the presence of maleimide to understand the interaction between the sensitizer and the maleimide. Excitation of TX (Ex = 355 nm, 7 ns pulse length) resulted in the transient absorbance monitored at 620 nm. This initial triplet absorption was quenched by maleimide **222e** (decay of the absorbance at 620 nm) to generate ^{3}**222e** * (rise in absorbance at 420 nm) that was monitored at 420 nm. This suggested that the excited state TX acted as a donor, while the maleimide acted as an acceptor.

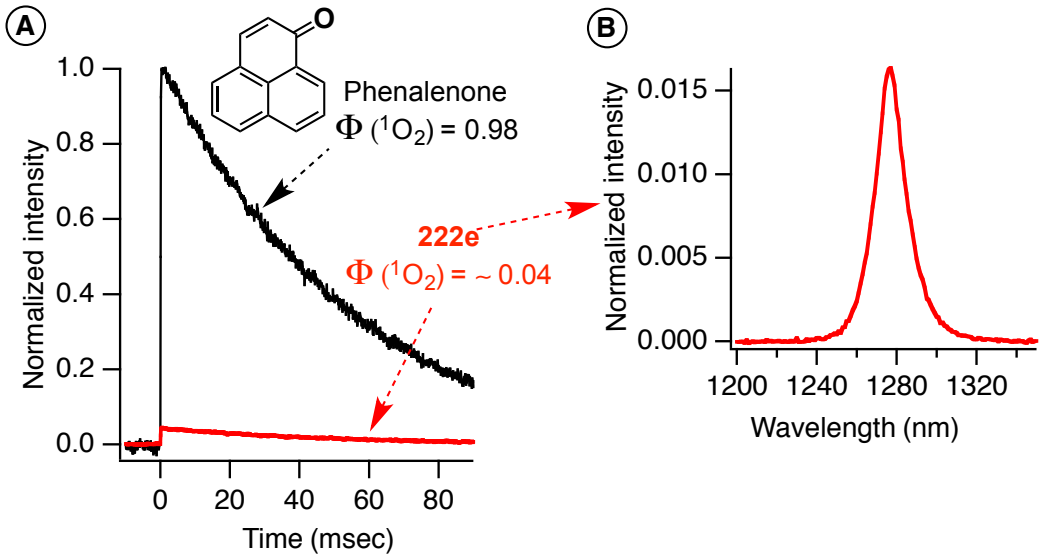

Figure 4.4: (A): Singlet oxygen phosphorescence decay traces monitored at 1270 nm generated by pulsed laser excitation (355 nm, 7 ns pulse length) of air saturated CCl_4 solutions of **222e** or phenalenone with matching absorbance of 0.3 at 355 nm. (B): Normalized singlet oxygen phosphorescence spectrum generated by steady-state irradiation (355 nm) of **222e** in air saturated CCl_4 solution. (Reproduced from reference 9, with permission from American Chemical Society, 2014).

Once the involvement of triplet transient of maleimide **222e** was confirmed, we attempted to evaluate the triplet quantum yield of maleimide **222e** by the generation of singlet oxygen. The singlet oxygen generation was carried out by pulsed irradiation of an aerated CCl_4 solution of maleimide. The relative triplet quantum yield of the maleimide ($\Phi_{1O2} \approx 0.04$) was calculated by comparing the efficiency with phenalenone as the reference standard ($\Phi_{1O2} = 0.98$).[10] The result revealed that the maleimides had very poor intersystem crossing quantum yield and produce very low amounts of the triplet upon direct irradiation.

4.6. Mechanistic rationale for stereospecific [2+2]-photocycloaddition

On the basis of photochemical and photophysical investigations, we postulated that the intramolecular [2+2]-photocycloaddition proceeded via triplet manifold. We believe that the electron rich alkene likely interacts with the half-filled π orbital of the $\pi\pi^*$ excited state of the maleimide.[11] As the triplet reaction goes through spin inversion, we believe the photoproduct formed via two-step process (scheme 4.9). The initial step was the formation of triplet 1,4-diradical (labeled as DR1-DR4) that was followed by the cyclization step, in which the triplet 1,4-diradical intersystem crosses to the corresponding singlet 1,4-diradical and recombines to form the cyclobutane photoproduct **220** or **221**.

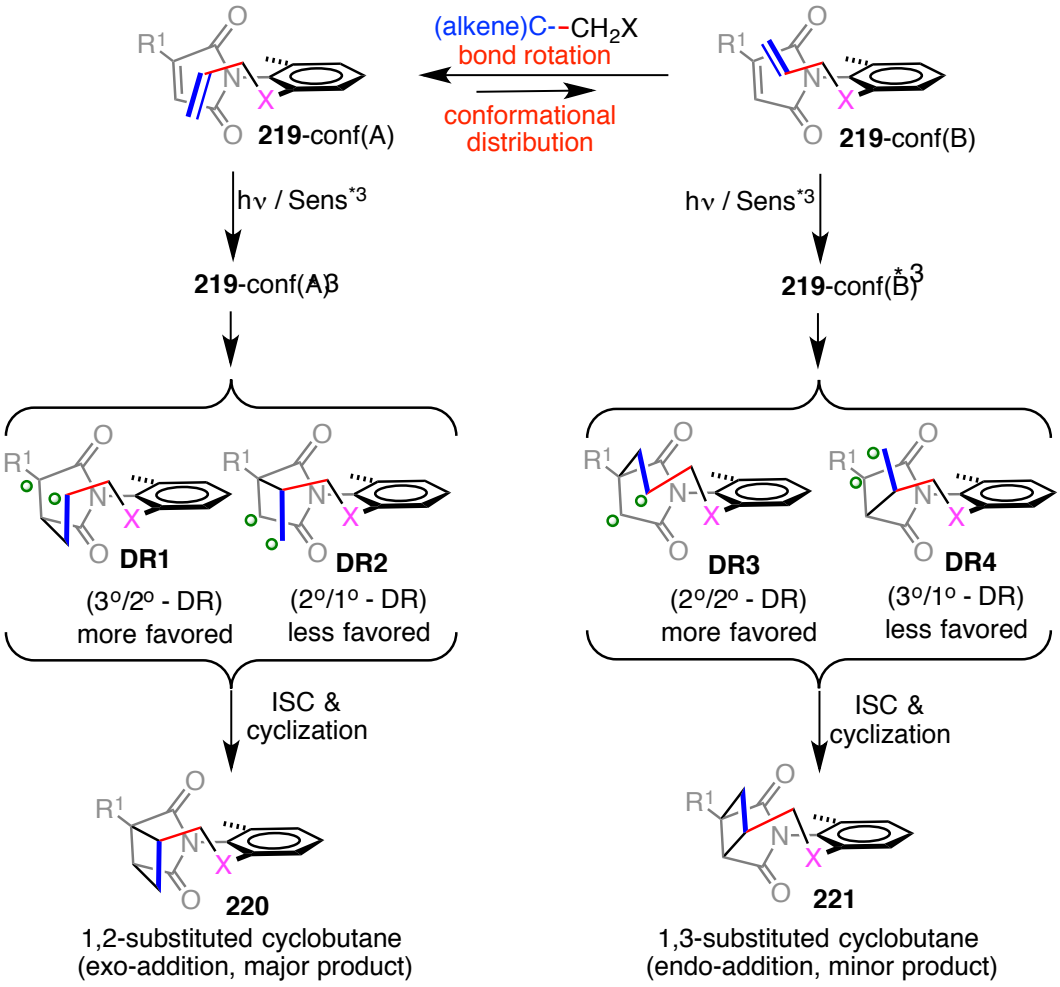

Scheme 4.9: Mechanistic rationale for [2+2]-photocycloaddition of atropisomeric maleimides **219**. (Reproduced from reference 9, with permission from American Chemical Society, 2014).

While the formation of the *exo* and *endo*-photoproduct can be explained based on the general two-step process, the conformational equilibrium and the type of diradical formed that dictates the *exo*-*endo* selectivity needs further substantiation. In the case of maleimides, the *exo*-photoproduct could have originated from the conformer "**219**-*conf*(A)" in which the CH_2 group of the alkenyl tether is positioned away from the R^1 substituent of the maleimide double bond. The initial step of the photoreaction could have led to the formation of either DR1 or DR2. Similarly, the formation of *endo*-photoproduct could have formed from the conformer "**219**-*conf*(B)" in which the CH_2 group of the alkenyl tether is positioned towards the R^1 substituent of the maleimide double bond. In this case, the initial step of the photoreaction could have led to either DR3 or

DR4. These triplet 1,4-diradicals then intersystem cross to singlet 1,4-diradicals and cyclize to form the photoproducts.

To gain more insight into the formation of preferred triplet 1,4-diradical, we carried out scrambling studies in **219b**. The maleimide **219b** has a methyl substituent at the terminal carbon of the alkenyl tether. The analysis of photoproducts revealed that the no products corresponding to the scrambling of the alkenes was observed. For example, irradiation of **219b** only resulted in *exo*- and *endo*-adduct (**220b** and **221b**) with only trace of scrambled photoproduct (scheme 4.10).

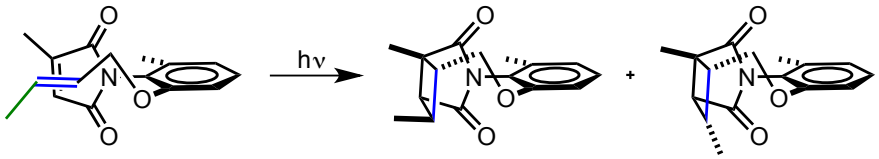

Scheme 4.10: Scrambling studies with maleimides **219b** (for clarity the *endo* photoproduct is omitted in the scheme).

The absence of scrambling could be the result of two scenarios. In the first scenario, the 1,4-diradical DR1 was likely preferred over DR2 resulting in major photoproduct. In the second scenario, the 1,4-diradical DR2 that was formed in the initial step cyclized at a much higher rate compared to bond rotation (responsible for the scrambling products) retaining the stereospecificity of the reaction. However, this was unlikely as the reaction proceeds in a triplet manifold, the 1,4-diradical DR2 will be in triplet state. In order to cyclize, the triplet diradical has to intersystem cross, which presents sufficient time for the 1,4-diradical DR2 to scramble. Although, this assertion could have exceptions, the absence of scrambling products suggests that the first scenario is the likely operating mechanism.

Also, the mechanistic rationale for the direct irradiation was assumed to undergo singlet pathway. This assertion is based on the photophysical studies and literature precedence. [12] The photophysical data indicated that the maleimides have poor inter system crossing efficiency. Also, the similar conversions in presence of both N_2 and O_2 (oxygen known to quench to triplet states efficiently) confirmed the presence of singlet-excited state. The literature precedence supports the involvement of singlet excited state in intramolecular photodimerization of maleimides that occurs

via exciplex formation.[12] The *exo/endo* selectivity in the photoproducts again was dictated by the orbital interaction between the electron rich alkene tether and the maleimide double bond that is dictate by the R^1 substituent.

The atropisomeric *N*-phenyl substituted maleimides present new findings that complement the existing reports wherein the irradiation conditions dictate the product outcome. For example, the *N*-alkenyl maleimides form [5+2]-product up on direct irradiation and [2+2]-product up on sensitized irradiation. Where as in the case of atropisomeric maleimides, it is the chain length that dictated the chemoselectivity in the product. This chemoselectivity was the result of molecular constraints imposed on the reacting alkene tether.

4.7. X-Ray crystal structure data for atropisomeric maleimides and its photoproducts

Structure determination: Single crystal X-ray diffraction data of the compounds **219, 220** and **221** were collected on a Bruker Apex Duo diffractometer with a Apex 2 CCD area detector at T = 100K. Cu radiation was used. All structures were process with Apex 2 v2010.9-1 software package (SAINT v. 7.68A, XSHELL v. 6.3.1). Direct method was used to solve the structures after multi-scan absorption corrections. Details of data collection and refinement are given in the table below.

Table 4.8: Crystal structure data for atropisomeric maleimides and its photoproducts

	219e	(*1R,5S,6R*) -**220a**	(*1S,5R,6S*) -**220a**	(*1R,5S,7S*) -**221a**	(*1S,5R,7R*) -**221a**	(*1R,5S,6R,7R*) -**220b**
Formula	$C_{20}H_{17}NO_3$	$C_{15}H_{15}NO_3$	$C_{15}H_{15}NO_3$	$C_{15}H_{15}NO_3$	$C_{15}H_{15}NO_3$	$C_{16}H_{17}NO_3$
FW	319.35	257.28	257.28	257.28	257.28	271.30
cryst. size_max	0.27	0.26	0.227	0.206	0.244	0.196
cryst. size_mid	0.22	0.09	0.185	0.168	0.084	0.13
cryst. size_min	0.07	0.05	0.13	0.114	0.045	0.085
cryst. system	Orthorhombic	Monoclinic	Orthorhombic	Orthorhombic	Orthorhombic	Monoclinic
Space Group, Z	'P b c a', 8	$P12_121$, 8	$P2_12_12_1$, 4	$P2_12_12_1$, 4	$P2_12_12$, 4	'$P12_11$', 2
a [Å]	10.9776(3)	14.5256(3)	7.2608(2)	10.9054(3)	10.9133(2)	10.0478(3)
b [Å]	9.9868(3)	6.9706(2)	12.2775(4)	17.4588(4)	17.4560(4)	7.4742(2)
c [Å]	28.5806(8)	24.6411(6)	13.9906(5)	6.6865(2)	6.68560(10)	10.4273(3)
α [Å]	90	90	90	90	90	90
ß [Å]	90	92.0890(10)	90	90	90	117.9950(10)
γ [Å]	90	90	90	90	90	90
V [$Å^3$]	3133.32(5)	2493.31(11)	1247.18(7)	1273.08(6)	1273.62(4)	691.45(3)
ρ_{calc} [g/cm^3]	1.354	1.371	1.370	1.395	1.389	1.303
μ [mm^{-1}]	0.739	0.784	0.784	0.816	0.815	0.733
Radiation Type	Cu	Cu	Cu	Cu	Cu	Cu
F(000)	1344	1088	544	568	564	288
no of measured refl.	20129	35878	8134	7147	9437	9074
no of indep. refl.	2756	8708	2189	2197	2245	2430
no of refl. (I ≥ 2σ)	2623	8348	2164	2124	2202	2413
Resolution [Å]	0.84	0.84	0.84	0.84	0.84	0.84
R1/wR2 (I ≥ 2σ)[a] [%]	3.24/8.03	2.79/6.82	2.55/6.66	3.27/8.94	3.37/9.69	2.48/6.56
R1/wR2 (all data)	3.39/8.14	2.97/6.95	2.58/6.75	3.42/9.08	3.43/9.75	2.50/6.59

Table 4.8: Crystal structure data for atropisomeric maleimides and its photoproducts (continued)

	(*1S,5R,6S,7S*)-**220b**	(*1S,5R,6S*)-**220d**	(*1R,5S,6S*)-**221d**	(*1R,5S,6R*)-**220e**	(*1S,5R,6S*)-**220e**
Formula	$C_{16}H_{17}NO_3$	$C_{16}H_{17}NO_2$	$C_{16}H_{17}NO_2$	$C_{20}H_{17}NO_3$	$C_{20}H_{17}NO_3$
FW	271.30	255.30	255.30	319.35	319.35
cryst. size_max [mm]	0.28	0.11	0.22	0.21	0.238
cryst. size_mid [mm]	0.134	0.1	0.1	0.077	0.164
cryst. size_min [mm]	0.054	0.042	0.08	0.04	0.07
cryst. system	Monoclinic	Orthorhombic	Orthorhombic	Monoclinic	Monoclinic
Space Group, Z	'$P12_11$', 2	$P2_12_12_1$, 4	$P2_12_12_1$, 4	'$P12_11$', 2	'$P12_11$', 2
a [Å]	10.0586(15)	10.5289(2)	10.4120(3)	10.5871(2)	10.5863(5)
b [Å]	7.4726(11)	10.8797(2)	11.0795(3)	7.2845(2)	7.2819(3)
c [Å]	10.4252(15)	11.1329(2)	11.1114(4)	10.7784(3)	10.7905(5)
α [Å]	90	90	90	90	90
ß [Å]	117.968(5)	90	90	112.488(2)	112.547(2)
γ [Å]	90	90	90	90	90
V [$Å^3$]	692.08(18)	1275.29(4)	1281.81(7)	768.04(3)	768.24(6)
ρ_{calc} [g/cm^3]	1.302	1.330	1.323	1.381	1.381
μ [mm^{-1}]	0.732	0.700	0.696	0.754	0.753
Radiation Type	Cu	Cu	Cu	Cu	Cu
F(000)	288	544	544	336	336
no of measured refl.	7545	7617	10517	10176	9986
no of indep. refl.	2334	2173	2235	2675	2684
no of refl. (I ≥ 2σ)	2310	1985	2127	2580	2661
Resolution [Å]	0.84	0.84	0.84	0.84	0.84
R1/wR2 (I ≥ 2σ)[a] [%]	2.64/6.81	3.43/7.82	4.13 / 11.07	2.63/6.49	2.48/6.40
R1/wR2 (all data) [%]	2.67/6.83	3.94/8.08	4.35 / 11.24	2.79/6.60	2.49/6.42

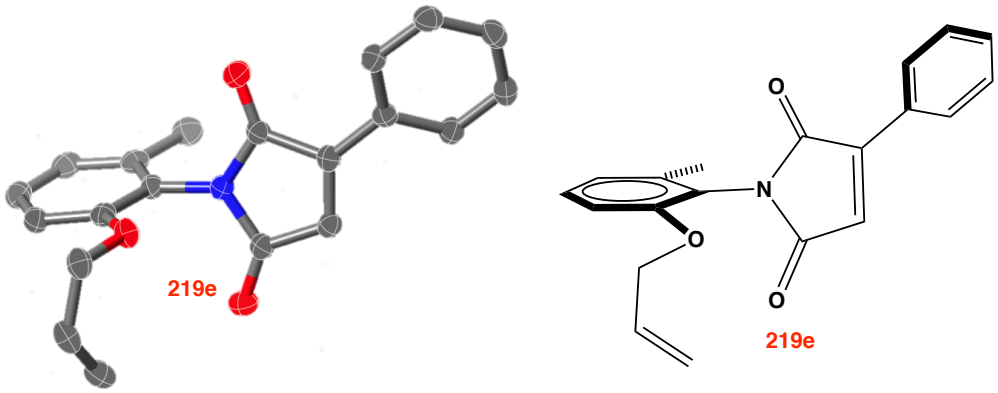

Figure 4.5: Atropisomeric maleimide **219e** (crystallized from hexanes/2-propanol).

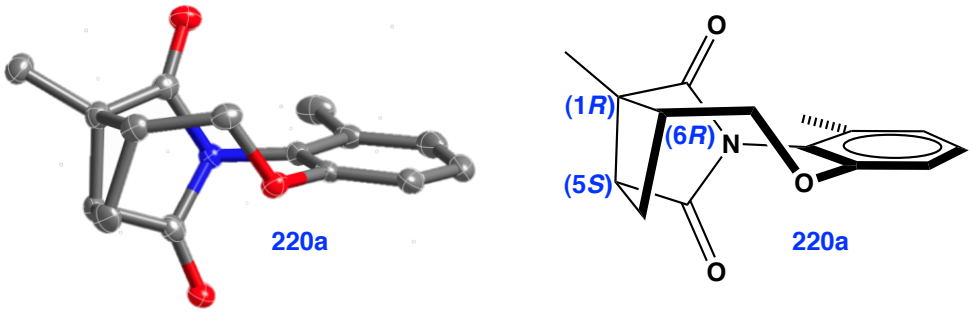

Figure 4.6: Photoproduct (-)-(1R,5S,6R)-**220a** (crystallized from hexanes/$CHCl_3$).

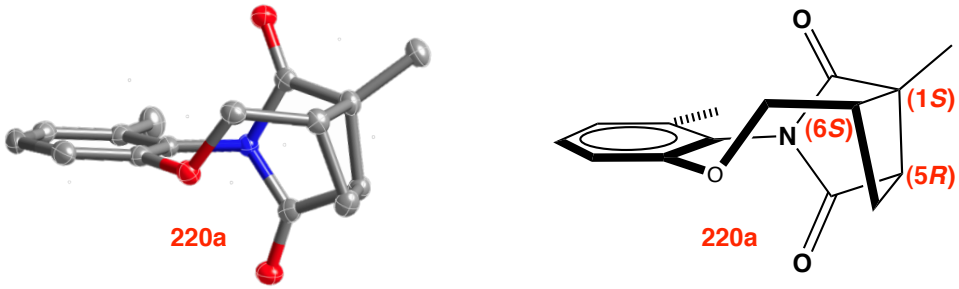

Figure 4.7: Photoproduct (+)-(1S,5R,6S)-**220a** (crystallized from hexanes/$CHCl_3$).

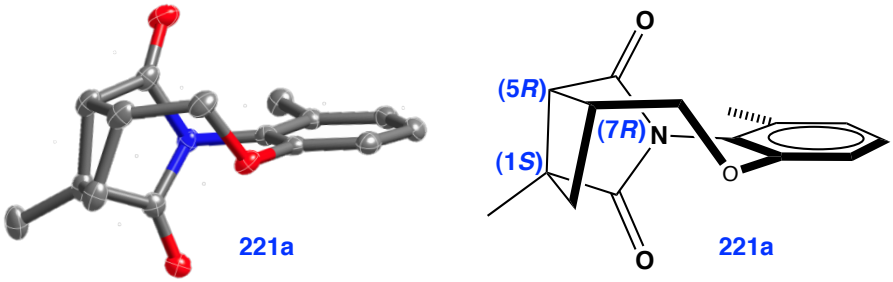

(B is the second isomer that elutes from chiral stationary phase in HPLC analysis)

Figure 4.8: Photoproduct (B)-(1S,5R,7R)-**221a** (crystallized from hexanes/$CHCl_3$).

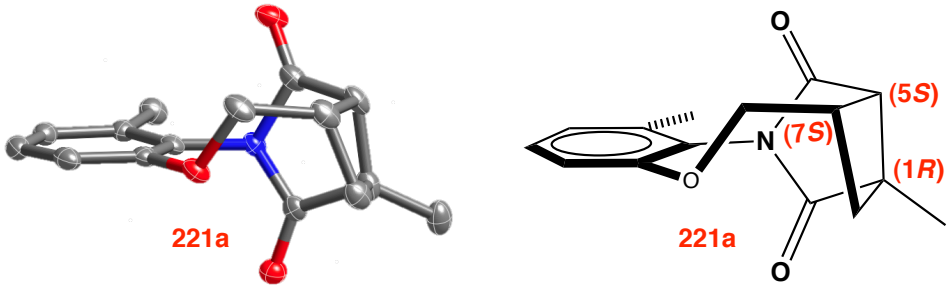

(A is the first isomer that elutes from chiral stationary phase in HPLC analysis)

Figure 4.9: Photoproduct (A)-(1R,5S, 7S)-**221a** (crystallized from hexanes/$CHCl_3$).

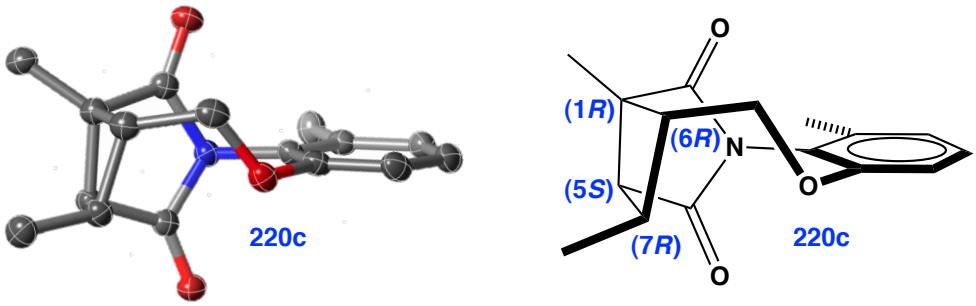

Figure 4.10: Photoproduct (-)-(1R,5S,6R,7R)-**220b** (crystallized from hexanes/$CHCl_3$).

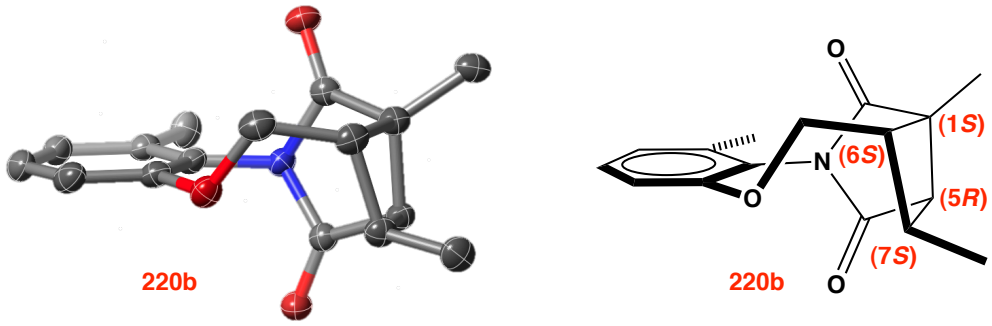

Figure 4.11: Photoproduct (+)-(1S,5R,6S,7S)-**220b** (crystallized from hexanes/$CHCl_3$).

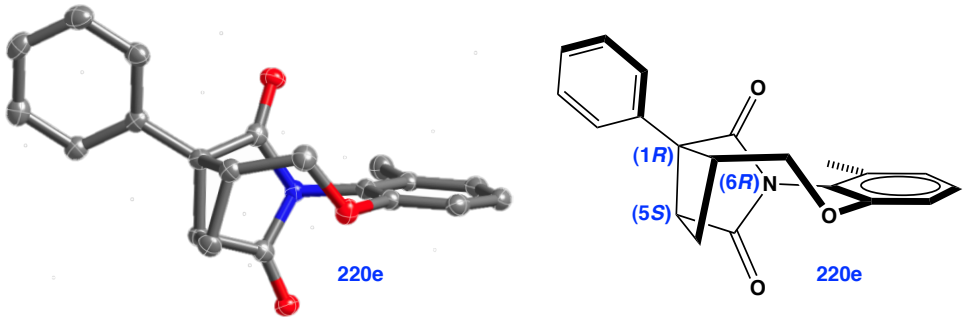

Figure 4.12: Photoproduct (-)-(1R,5S,6R)-**220e** (crystallized from hexanes/$CHCl_3$).

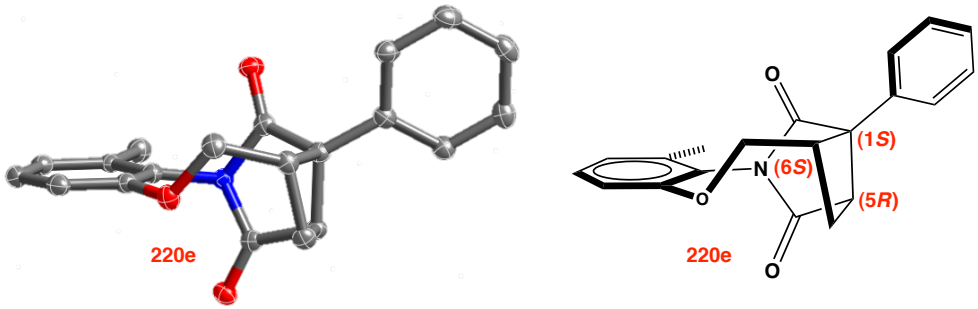

Figure 4.13: Photoproduct (+)-(1S,5R,6S)-**220e** (crystallized from hexanes/$CHCl_3$).

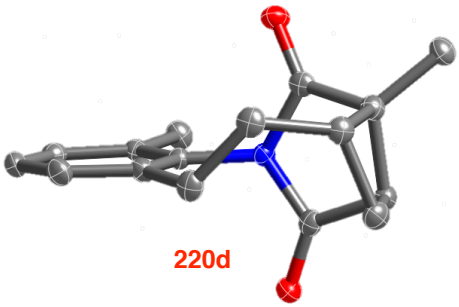

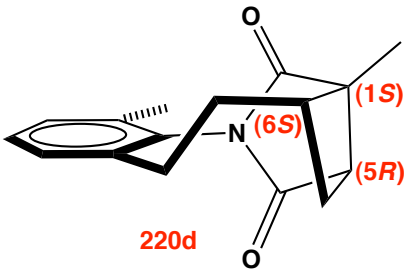

(A is the first isomer that elutes from chiral stationary phase in HPLC analysis)

Figure 4.14: Photoproduct (A)-(1S,5R,6S)-**220d** (crystallized from hexanes/2-propanol).

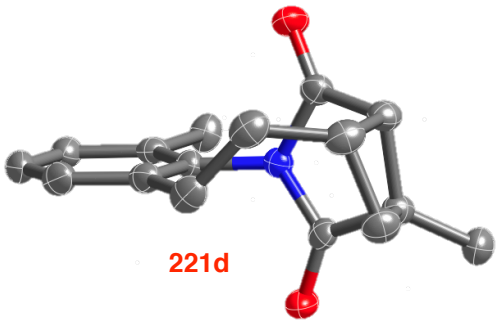

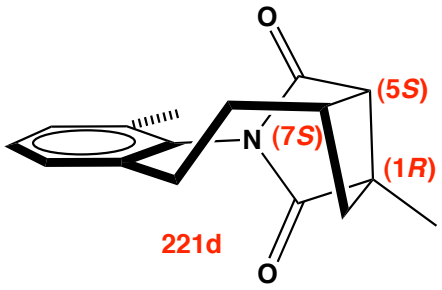

Figure 4.15: Photoproduct (1R,5S,7S)-**221d** (crystallized from hexanes/$CHCl_3$).

4.8. Summary and outlook

The [2+2]-photocycloaddition of atropisomeric maleimides revealed several unique features of atropisomeric maleimides towards photocycloaddition reaction. On contrary to *N*-alkenyl maleimides, the atropisomeric maleimides, irrespective of irradiation conditions, the chemoselectivity between [2+2] vs. [5+2]-photocycloaddition was dictated by length of the alkenyl tether. The reaction proceeded smoothly under direct and sensitized irradiation to result in regioisomeric products (*exo* and *endo* photoadduct). The regioselectivity in the photoreaction was highly affected by the substituents on the alkenyl tether and the maleimide double bond but only minimally influenced by solvent or temperature. The photoreaction was very efficient under both UV and visible light irradiation conditions thus allowing us to use household lamp to perform reactions. Integrating visible light photoreaction with continuous flow setup provided opportunity to scale up the photoreactions. Detailed photophysical studies carried out on the maleimides provided crucial insights about the nature of excited states and their lifetime, which helped to explain the photoreactivity of atropisomeric maleimides.

4.9. Experimental section

4.9.1. General methods

All commercially obtained reagents/solvents were used as received; chemicals were purchased from Alfa Aesar®, Sigma-Aldrich®, Acros organics®, TCI America®, Mallinckrodt®, and Oakwood® Products, and were used as received without further purification. Unless otherwise stated, reactions were conducted in oven-dried glassware under nitrogen atmosphere. ^{1}H-NMR and ^{13}C-NMR spectra were recorded on Varian 400 MHz (100 MHz for ^{13}C) and on 500 MHz (125 MHz for ^{13}C) spectrometers. Data from the ^{1}H-NMR spectroscopy are reported as chemical shift (δ ppm) with the corresponding integration values. Coupling constants (*J*) are reported in hertz (Hz). Standard abbreviations indicating multiplicity are used as follows: s (singlet), b (broad), d (doublet), t (triplet), q (quartet), m (multiplet) and virt (virtual). Data for ^{13}C NMR spectra are reported in terms of chemical shift (δ ppm). High-resolution mass spectrum data in Electrospray Ionization mode were recorded on a Bruker – Daltronics® BioTof mass spectrometer in positive (ESI+) ion mode. HPLC analyses were performed on Waters® HPLC equipped with 2525 pump or

on Dionex® Ultimate 3000 HPLC. Waters® 2767 sample manager was used for automated sample injection on Waters® HPLC Ultimate 3000 sample injector was used for injection on Dionex® HPLC. All HPLC injections were monitored using a Waters® 2487 dual wavelength absorbance detector at 254 and 270 nm or on Dionex® HPLC were monitored using a diode array detector (DAD3000125). Analytical and semi-preparative injections were performed on chiral stationary phase using various columns as indicated below.

i) Regis® PIRKLE COVALENT (*R*,*R*) WHELK–01
   a) 25 cm x 4.6 mm column for analytical injections.
   b) 25 cm x 10 mm column for semi-preparative injections.

ii) CHIRALCEL® OD-H
   a) 0.46 cm x 25 cm column for analytical injections.
   b) 10 mm x 25 cm column for semi-preparative injections.

iii) CHIRALPAK® AD-H
   a) 0.46 cm x 25 cm column for analytical injections.
   b) 10 mm x 25 cm column for semi-preparative injections

Masslynx software version 4.1 was used to monitor/analyze the HPLC injections on Waters® and to process HPLC traces. Chromeleon 7 software was used to monitor and process HPLC injections on Dionex® HPLC. Igor Pro® Software version 6.0 was used to process the HPLC graphics. Optical activity values were recorded on JASCO® DIP – 370 digital polarimeter. CD spectra were recorded on JASCO® J-815 with JASCOPTC-423S/15 temperature controller maintained by liquid nitrogen. When necessary, the compounds were purified by combiflash equipped with dual wavelength UV-Vis absorbance detector (Teledyne ISCO) using hexanes:ethyl acetate as the mobile phase and Redisep® cartridge filled with silica (Teledyne ISCO) as stationary phase. In some cases, compounds were purified by column chromatography on silica gel (Sorbent Technologies®, silica gel standard grade: porosity 60 Å, particle size: 230 x 400 mesh, surface area: 500 – 600 m^2/g, bulk density: 0.4 g/mL, pH range: 6.5 – 7.5). Unless indicated, the Retardation Factor (R*f*) values were recorded using a 5-50% hexanes:ethyl acetate as mobile phase and on Sorbent Technologies®, silica Gel TLC plates (200 mm thickness w/UV_{254}).

The plot of CD spectrum was carried out using molar ellipticity vs wavelength (nm) and the molar ellipticity was calculated using the formula,[13]

Molar ellipticity $[\Delta\varepsilon] = [\theta] / 32980cl$

Where,

c = Concentration in mols/lit; l = Path length in cm; θ = Ellipticity measured in millidegrees.

Photophysical Methods:

Spectrophotometric solvents (Sigma-Aldrich®) were used when ever necessary unless mentioned otherwise. UV quality fluorimeter cells (with range until 190 nm) were purchased from Luzchem®. Absorbance measurements were performed using a Shimadzu® UV-2501PC UV-Vis spectrophotometer. Laser flash photolysis (LFP) experiments employed the pulses from a Spectra Physics GCR-150-30 Nd:YAG laser (355 nm, ca 5 mJ/pulse, 7 ns pulse length) and a computer controlled system that has been described elsewhere.[14]

Information about photoreactor with flow set up:

Peristaltic pump: The peristaltic pump employed was purchased from Fischer Scientific® (model No: 72-320-048). The pump can dispense liquid ranging from 4-200 RPM (This can be manually calibrated to mL/min by collecting the amount of liquid pumped per minute).

40W CFL bulb: The light bulb was purchased from Grainger® (Lumapro; item no: 2CUU4) and delivers 2400 lumens of brightness.

FEP tubing: The FEP (Fluorinated ethylene propylene tubing) tubing was purchased from IDEX-Health & Science® (product no: 1521L, natural) with the dimension of 1/8×0.062×50ft. The tube was rapped around a test tube stand in a rectangular fashion surrounding the lamp. The total volume of solvent in the tube that is exposed to the light was around 28-30 mL. The residence time was dependent on the flow rate (with 8RPM, *i.e.* 0.83mL/min the residence time was about 35 min).

4.10. General procedure for synthesis atropisomeric maleimide derivatives 219a-q and their precursors

4.10.1. Synthesis of acetamide derivative 229a-b

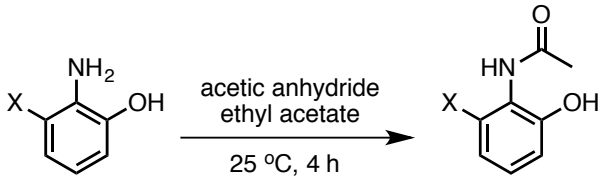

196a-b
X = H, Me

229a-b
X = H, Me

Scheme 4.11: Synthesis of acetamide derivative **229a-b**.

The acetamide derivative was synthesized according to a procedure reported in the literature.[15] To a solution of corresponding aniline **196a-b** (3.0 g, 1.0 *equiv.*) in ethyl acetate (30 mL) at 0 °C, acetic anhydride (2.3 *equiv.*) was added slowly over 15 min. The mixture was allowed to warm to room temperature over 4 h during which a solid started to precipitate out of the solution. The mixture was concentrated under reduced pressure to leave ~10% of the initial ethyl acetate. To this slurry, hexanes (50 mL) was added, stirred for 10 min and filtered. The solid residue was washed with hexanes (15 mL), dried and directly taken for the next step without further purification.

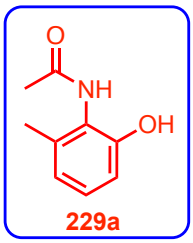

229a

R*f* = 0.20 (50% hexanes:50% ethyl acetate), Yield for **229a** = 94%

^{1}H-NMR (400 MHz, CD_3OD, δ ppm): 7.00-6.96 (m, 1H), 6.699-6.68 (m, 2H), 2.16 (s, 3H) and 2.14 (s, 3H).

^{13}C-NMR (100 MHz, CD_3OD, δ ppm): 175.7, 156.7, 140.3, 131.5, 127.1, 125.0, 117.6, 25.3 and 20.9.

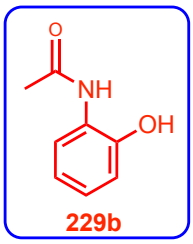

229b

R*f* = 0.25 (50% hexanes:50% ethyl acetate), Yield for **229b** = 98%

^{1}H-NMR (400 MHz, CD_3OD, δ ppm): 7.56-7.53 (m, 1H), 6.99-6.95 (m, 1H), 6.84 (m, 2H) and 2.14 (s, 3H).

^{13}C-NMR (100 MHz, CD_3OD, δ ppm): 174.9, 152.5, 129.8, 129.5, 126.7, 123.3, 120.0 and 26.2.

4.10.2. Synthesis of *o*-allylated acetamide derivative 228a-b

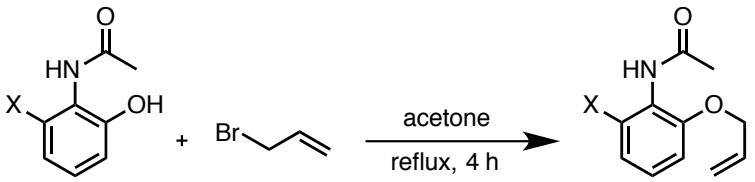

229a-b
X = H, Me

228a-b
X = H, Me

Scheme 4.12: Synthesis of *o*-allylated acetamide derivative **228a-b**.

To a solution of acetamide derivative **229** (3.5 g, 1 *equiv*) in dry acetone (35 mL) *anhyd.* potassium carbonate (3.0 *equiv*) and allyl bromide (2.5 *equiv*) were added at 25 ^{o}C. The resulting mixture was refluxed for 4 h. After the completion of the reaction, the mixture was cooled to 25 ^{o}C, filtered through celite and the solid was washed with acetone (15 mL). The combined organic layer was concentrated and the residue was taken up in DCM (50 mL) and washed with DI water (2 × 15 mL) and brine solution (1 × 15 mL). The organic layer was dried over *anhyd.* Na_2SO_4, filtered and the solvent was removed under reduced pressure to get the crude product. The crude product was directly taken to next step without further purification.

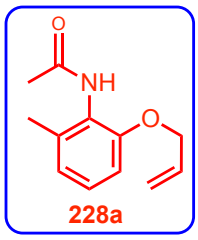

228a

R*f* = 0.75 (95% DCM:5% methanol), Yield for **228a** = 88%

^{1}H-NMR (400 MHz, CD_3OD, δ ppm): 7.12-7.06 (m, 1H), 6.82-6.797 (m, 2H), 6.07-5.97 (m, 1H), 5.41-5.35 (m, 1H), 5.22-5.19 (m, 1H), 4.52-4.499 (m, 2H), 2.17 (m, 3H) and 2.12 (m, 3H).

^{13}C-NMR (100 MHz, CD_3OD, δ ppm): 175.2, 158.2, 141.1, 137.6, 131.5, 128.6, 126.2, 119.8, 114.2, 72.9, 25.3 and 20.9.

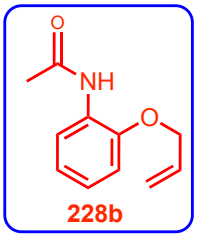

228b

R*f* = 0.70 (50% hexanes:50% ethyl acetate), Yield for **228b** = 87%

^{1}H-NMR (400 MHz, CD_3OD, δ ppm): 8.34-8.32 (m, 1H), 7.78 (bs, 1H), 6.99-6.90 (m, 2H), 6.84-6.82 (m, 1H), 6.08-5.99 (m, 1H), 5.39-5.347 (dd, *J* =17.2, 1.2 Hz, 1H), 5.31-5.28 (dd, *J* =10.4, 1.2 Hz, 1H), 4.56 (d, *J* = 4.8 Hz, 2H) and 2.16 (s, 3H).

^{13}C-NMR (100 MHz, CD_3OD, δ ppm): 168.3, 146.9, 133.0, 128.2, 123.7, 121.5, 120.2, 118.4, 111.6, 69.7 and 25.1.

4.10.3. Synthesis of *o*-allylated aniline derivative 226a-b

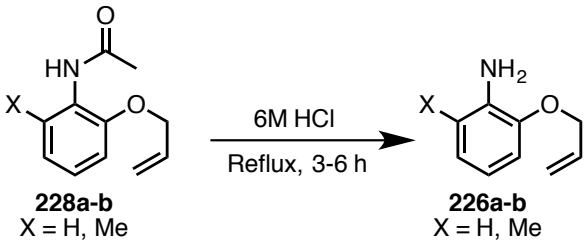

228a-b
X = H, Me

226a-b
X = H, Me

Scheme 4.13: Synthesis of *o*-allylated aniline derivative **226a-b**.

To *o*-allylated acetamide derivative **228** (2.9 g), 6M HCl (7 mL) was added at 25 ^{o}C. The resulting mixture was refluxed for 3-6 h. After the completion of the reaction, the mixture was cooled to 0 ^{o}C. The pH of the reaction mixture was adjusted to 14 by slowly adding 4M NaOH solution without allowing the internal temperature to rise above 10 ^{o}C. The aqueous layer was extracted with ethyl acetate. The combined organic layer was dried over *anhyd.* Na_2SO_4, filtered and the solvent was removed under reduced pressure to get the crude product. The crude product was purified by combiflash using hexanes: ethyl acetate mixture (80:20).

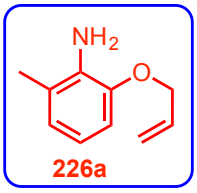

226a

R*f* = 0.80 (80% hexanes: 20% ethyl acetate), Yield for **226a** = 78%

^{1}H-NMR (400 MHz, $CDCl_3$, δ ppm): 6.74-6.43 (m, 3H), 6.15-6.04 (m, 1H), 5.44-5.39 (m, 1H), 5.30-5.27(m, 1H), 4.57-4.55 (m, 2H), 3.79 (bs, 2H) and 2.19 (s, 3H).

^{13}C-NMR (100 MHz, $CDCl_3$, δ ppm): 146.1, 134.8, 133.9, 123.1, 123.0, 117.7, 117.5, 109.9, 69.6 and 17.4.

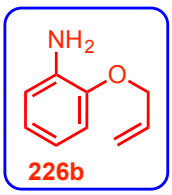

226b

R*f* = 0.80 (80% hexanes: 20% ethyl acetate), Yield for **226b** = 70%

^{1}H-NMR (400 MHz, $CDCl_3$, δ ppm): 6.89-6.84 (m, 2H), 6.79-6.74 (m, 2H), 6.19-6.09 (m, 1H), 5.50-5.44 (qd, *J* = 17.6, 1.6 Hz, 1H), 5.36-5.32 (qd, *J* = 10.8, 1.6 Hz, 1H), 4.61-4.58 (m, 2H) and 3.33 (bs, 2H).

^{13}C-NMR (100 MHz, $CDCl_3$, δ ppm): 146.5, 136.9, 133.9, 121.7, 118.6, 117.6, 115.5, 112.4, and 69.4.

4.10.4. Synthesis of 2-methyl-6-propoxyaniline 227

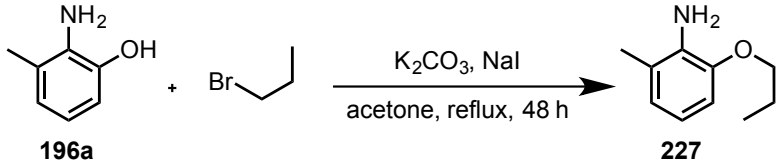

196a **227**

Scheme 4.14: Synthesis of 2-methyl-6-propoxyaniline **227**.

Bromopropane (3.7 mL, 40.5 mmol) was added to a mixture of aniline **196a** (2.0 g, 16.2 mmol), *anhyd*. K_2CO_3 (6.7 g, 48.6 mmol) and NaI (0.2 g, 1.62 mmol) in dry acetone (25 mL) at room temperature. The resulting mixture was refluxed for 48 h. After the reaction, the mixture was cooled to room temperature, filtered through celite and the solid was washed with acetone. The combined organic layer was concentrated under reduced pressure to get the crude product. The crude was purified by combiflash using a hexanes:ethyl acetate mixture.

R*f* = 0.50 (80% hexanes: 20% ethyl acetate), yield for **227** = 40%.

^{1}H-NMR (400 MHz, $CDCl_3$, δ ppm): 6.75-6.66 (m, 3H), 3.98 (t, *J* = 6.5 Hz, 2H), 3.79 (bs, 2H), 2.21 (s, 3H), 1.87 (dq, *J* = 14.0, 7.1 Hz, 2H) and 1.09 (t, *J* = 7.4 Hz, 3H).

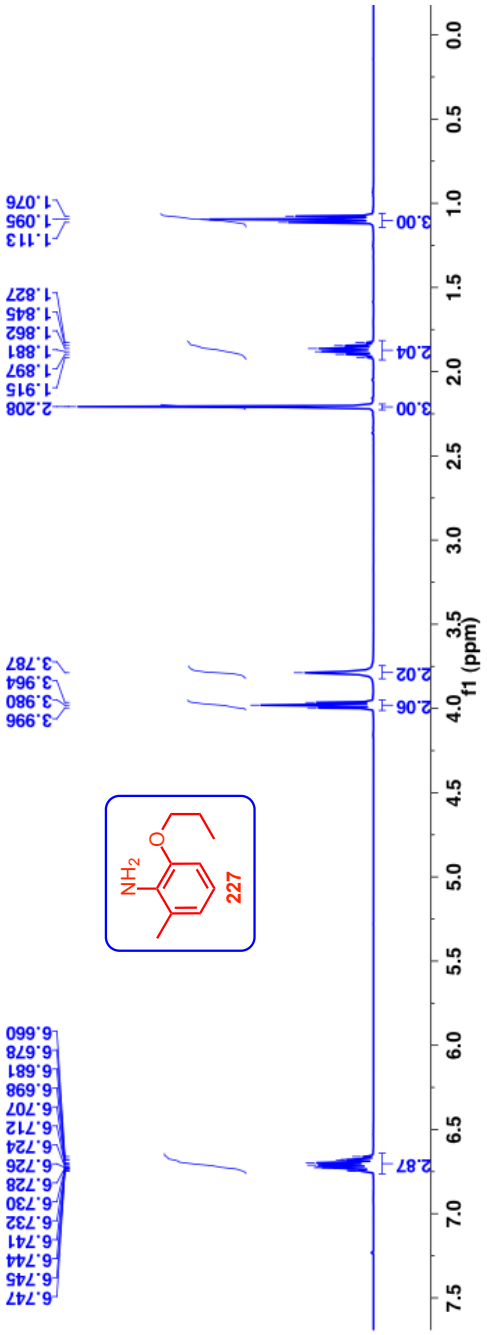

Figure 4.16: ^{1}H-NMR (400 MHz, $CDCl_3$, δ ppm) spectrum of 2-methyl-6-propyloxyaniline **227**.

^{13}C-NMR (100 MHz, $CDCl_3$, δ ppm): 146.6, 134.7, 122.8, 122.7, 117.8, 109.4, 70.1, 23.0, 17.5 and 10.9.

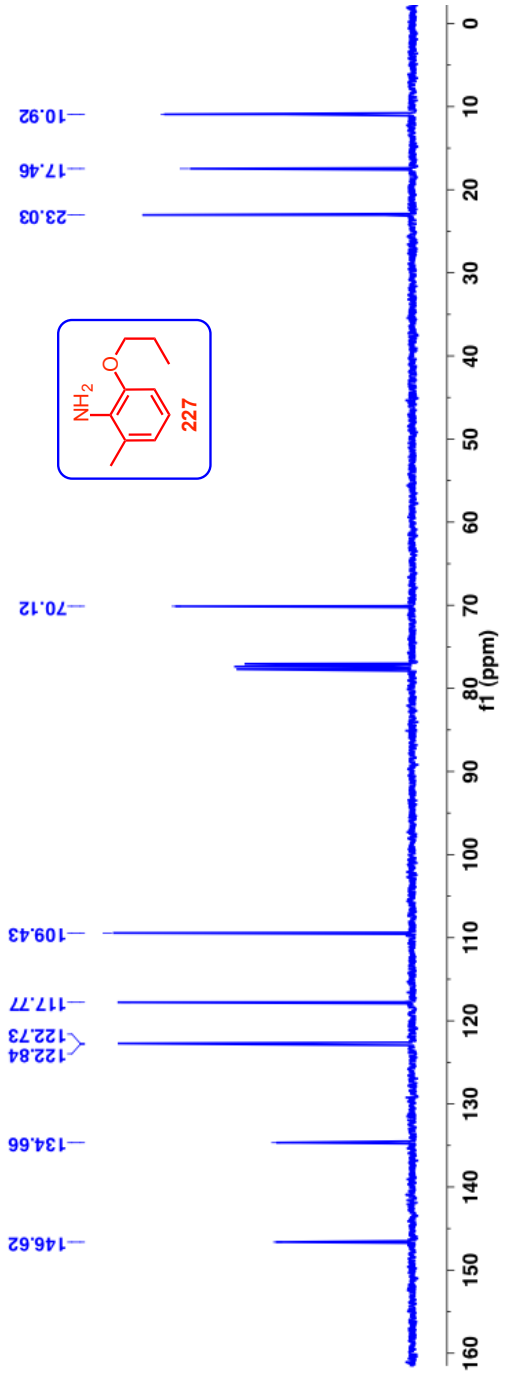

Figure 4.17: ^{13}C-NMR (100 MHz, $CDCl_3$, δ ppm) spectrum of 2-methyl-6-propyloxyaniline **227**.

HRMS-ESI (m/z) ([M + H]$^+$):

Calculated : 166.1226

Observed : 166.1229

|Δm| : 1.8 ppm

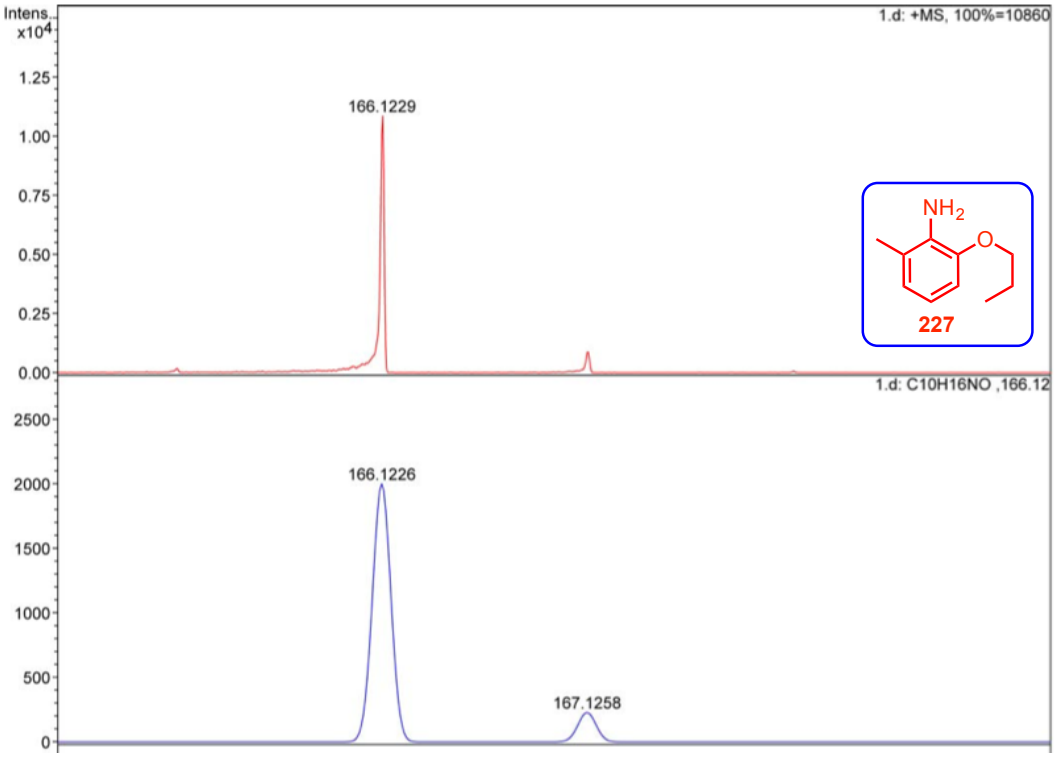

Figure 4.18: HRMS of 2-methyl-6-propyloxyaniline **227**.

4.10.5. Synthesis of citraconicimide derivative 224a-b

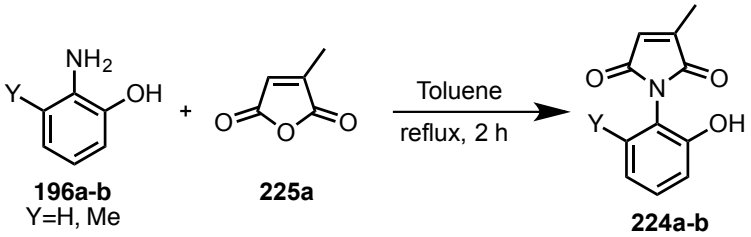

196a-b
Y=H, Me

225a

224a-b

Scheme 4.15: Synthesis of citraconicimide derivative **224a-b**.

To a solution of aniline **196a-b** (5.0 g, 40.6 mmol) in toluene (25 mL) at 25 ^{o}C, citraconic anhydride **225a** (5.46 g, 48.7 mmol) was added with stirring in a round bottom flask. The resulting mixture was refluxed for 2 h after which it was cooled to room temperature and the mixture was diluted with hexanes (50 mL). The precipitated solid was filtered and washed with hexanes (20 mL) and dried under vacuum. The crude product was directly taken to next step without further purification.

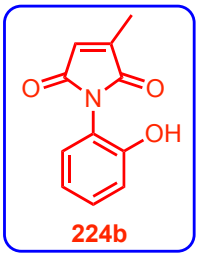

224b

R*f* = 0.40 (50% hexanes: 50% ethyl acetate), Yield for **224a** = 94%.

R*f* = 0.60 (90% DCM: 10% MeOH), yield for **224b** = 51%.

^{1}H-NMR (400 MHz, CD_3OD, δ ppm): 7.25-7.21 (m, 1H), 7.06-7.04 (m, 1H), 6.92-6.85 (m, 1H), 6.53 (s, 1H) and 2.07 (s, 3H).

^{13}C-NMR (100 MHz, CD_3OD, δ ppm): 175.4, 174.5, 157.96, 150.4, 134.1, 134.03, 131.6, 123.4, 123.0, 120.2 and 13.8.

^{1}H-NMR (400 MHz, CD_3OD, δ ppm): 7.14-7.098 (m, 1H), 6.74-6.72 (m, 2H), 6.58 (s, 1H), 2.11 (s, 3H) and 2.04 (s, 3H).

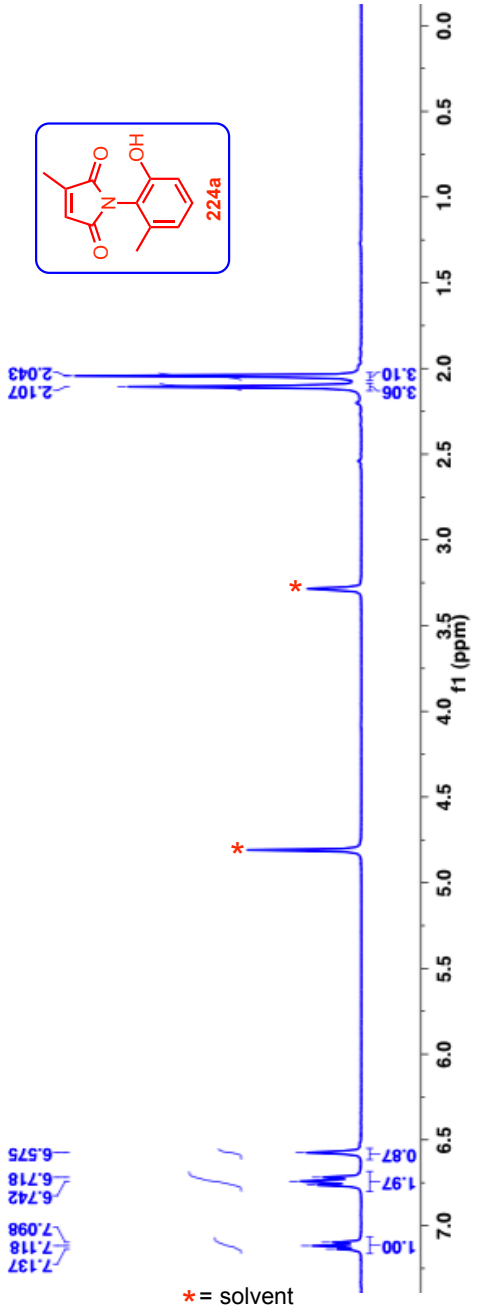

Figure 4.19: ^{1}H-NMR (400 MHz, CD_3OD, δ ppm) spectrum of 6-hydroxy-citraconicimide **224a**.

^{13}C-NMR (100 MHz, CD_3OD, δ ppm): 175.4, 174.5, 158.3, 150.5, 142.7, 133.7, 131.7, 124.8, 122.3, 117.3, 20.5 and 13.7.

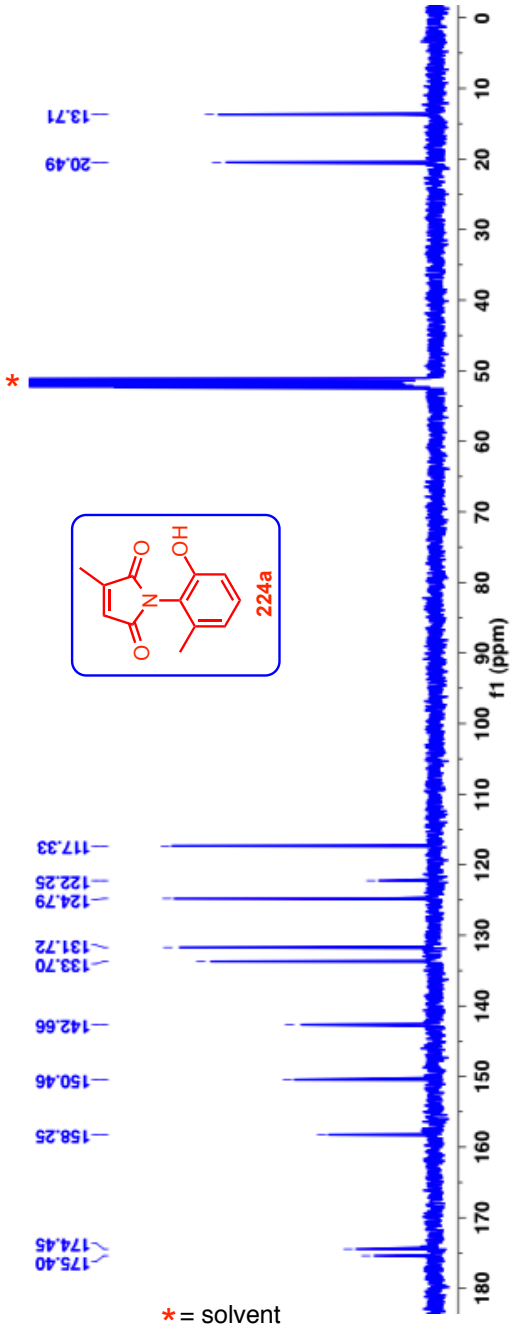

Figure 4.20: ^{13}C-NMR (100 MHz, CD_3OD, δ ppm) spectrum of 6-hydroxy-citraconicimide **224a**.

HRMS-ESI (m/z) ([M + Na]$^+$):

Calculated : 240.0631

Observed : 240.0639

|Δm| : 3.3 ppm

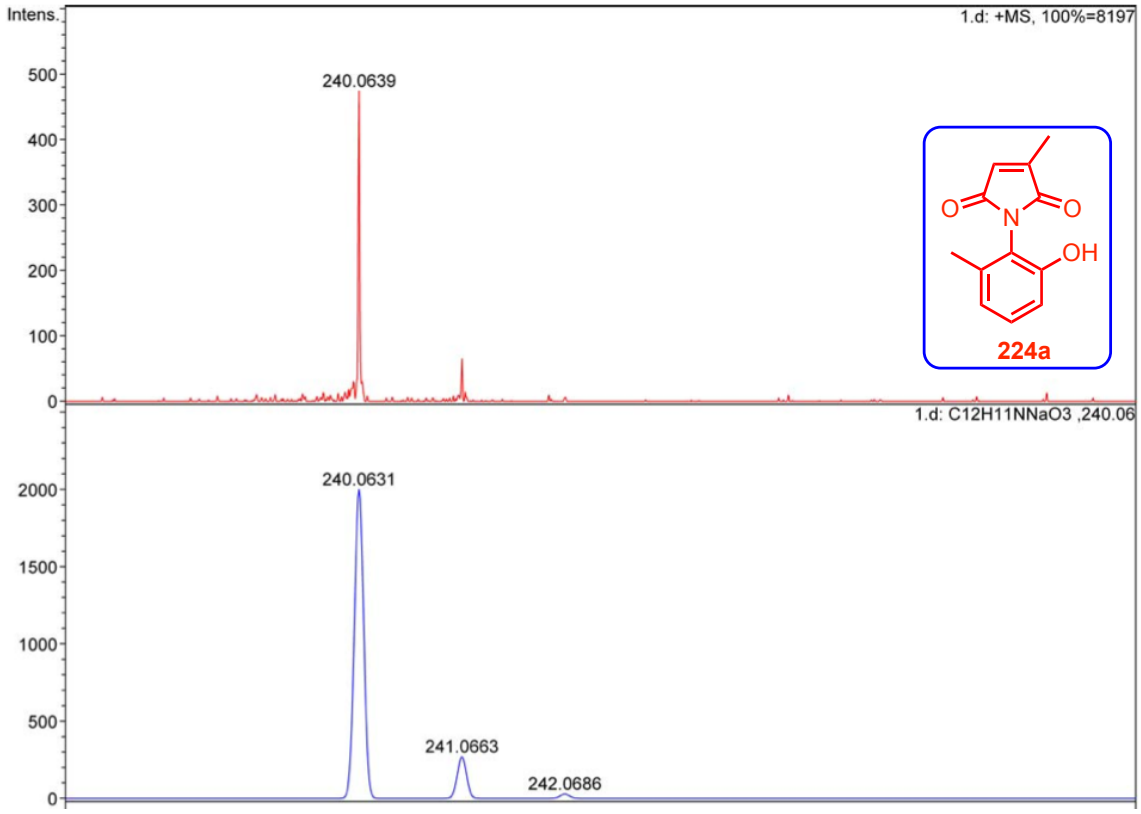

Figure 4.21: HRMS of 6-hydroxy-citraconicimide derivative **224a**.

4.10.6. Synthesis of atropisomeric maleimide derivatives 219a-b

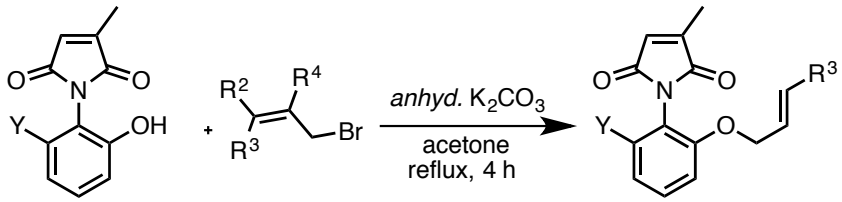

Scheme 4.16: Synthesis of atropisomeric maleimide derivative **219a-b**.

To a mixture of citraconicimide derivative **224a** (1.0 g, 1.0 *equiv.*) and *anhyd.* potassium carbonate (3.0 *equiv.*) in dry acetone (10 mL), corresponding allyl bromide (2.5 *equiv.*) was added in a round bottom flask. The resulting mixture was refluxed for 4 h or until the complete consumption of citraconicimide. The reaction mixture was cooled to room temperature and filtered through celite bed. The solid was washed with acetone and the combined organic layer was concentrated to get the crude product. The crude product was purified by combiflash using a hexanes:ethyl acetate mixture.

^{1}H-NMR (400 MHz, $CDCl_3$, δ ppm): 7.24-7.19 (m, 1H), 6.88-6.86 (m, 1H), 6.78-6.76 (m, 1H), 6.46-6.45 (q, *J* =1.6 Hz, 1H), 5.91-5.82 (m, 1H), 5.26-5.14 (m, 2H), 4.48-4.46 (m, 2H), 2.14 (s, 3H) and 2.13 (s, 3H).

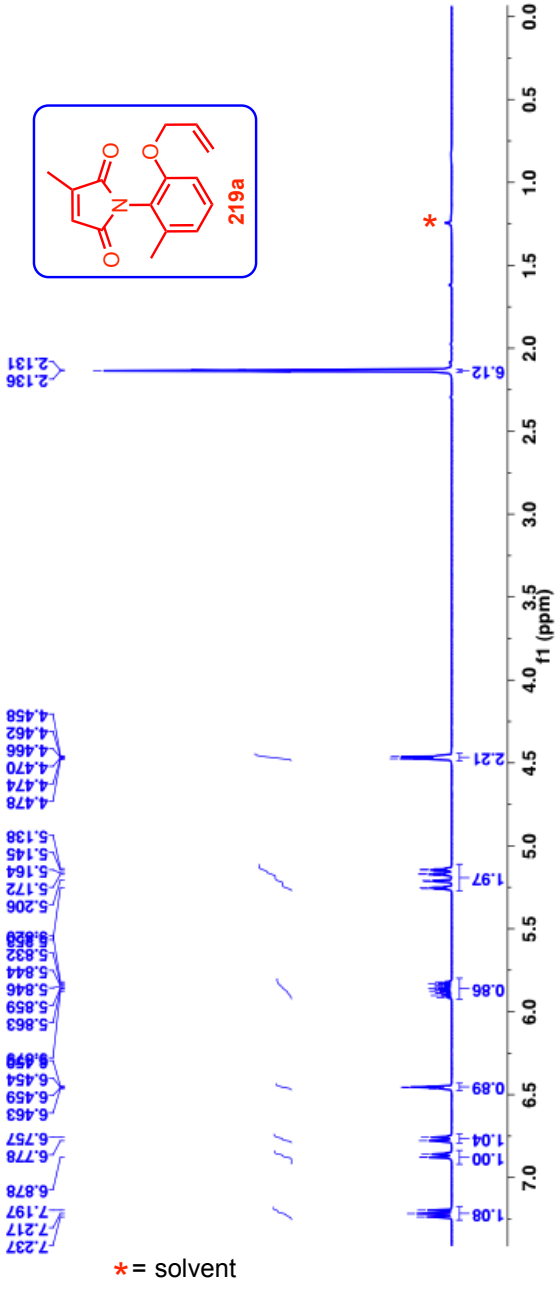

Figure 4.22: ^{1}H-NMR (400 MHz, $CDCl_3$, δ ppm) spectrum of 6-allyloxy-citraconicimide **219a**.

^{13}C-NMR (100 MHz, $CDCl_3$, δ ppm): 171.1, 170.0, 154.9, 146.2, 139.1, 132.96, 130.1, 128.1, 122.9, 119.98, 117.2, 110.7, 69.2, 17.97 and 11.4.

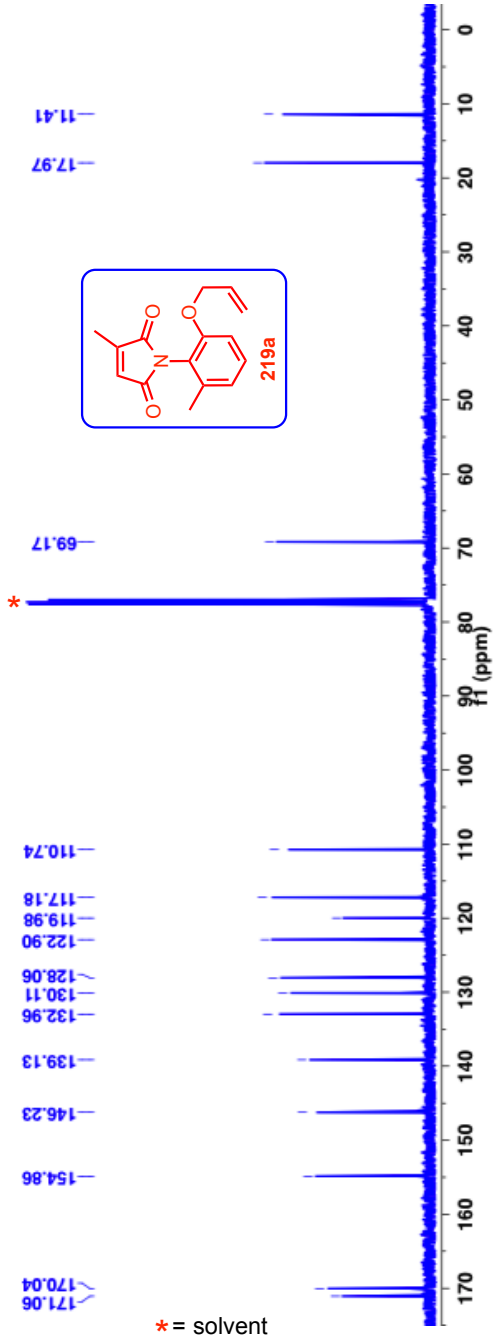

Figure 4.23: ^{13}C-NMR (100 MHz, $CDCl_3$, δ ppm) spectrum of 6-allyloxy citraconicimide **219a**.

HRMS-ESI (m/z) ([M + Na]$^+$):

Calculated : 280.0944

Observed : 280.0954

|Δm| : 3.6 ppm

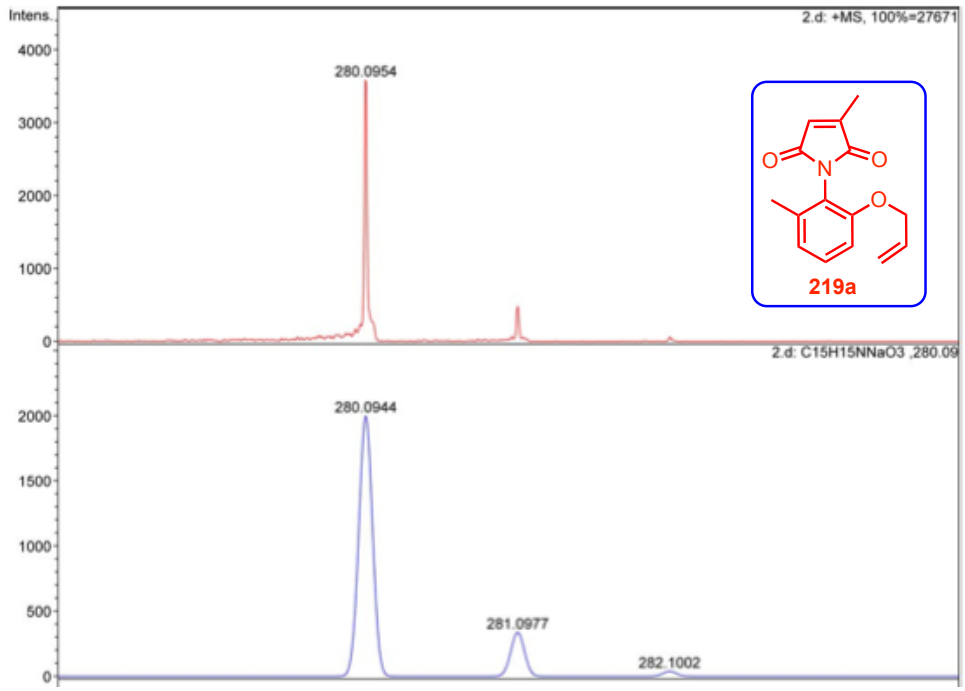

Figure 4.24: HRMS of 6-allyloxy citraconicimide derivative **219a**.

HPLC analysis conditions:

For analytical conditions,

I). Column : CHIRALPAK-ADH

Abs. detector wavelength : 254 nm and 270 nm

Mobile phase : Hexanes:2-propanol = 98:2

Flow rate : 1.0 mL/min

Retention times (min) : ~ 15.09 [(+)-**219a**] and ~ 17.40 [(-)-**219a**]

For preparative conditions,

I). Column : CHIRALPAK-ADH

Abs. detector wavelength : 254 nm and 270 nm

Mobile phase : Hexanes:2-propanol = 99.4:0.6

Flow rate : 3.0 mL/min

Retention times (min) : ~ 45.60 [(+)-**219a** and ~ 54.99 [(-)-**219a**]

Optical rotation $[\alpha]_D^{22}$:

HPLC retention time (CHIRALPAK-ADH) at ~ 15.09 min, (*c* ~ 0.308 %, MeOH) = +57.45 deg

HPLC retention time (CHIRALPAK-ADH) at ~ 17.40 min, (*c* ~ 0.308 %, MeOH) = -59.45 deg.

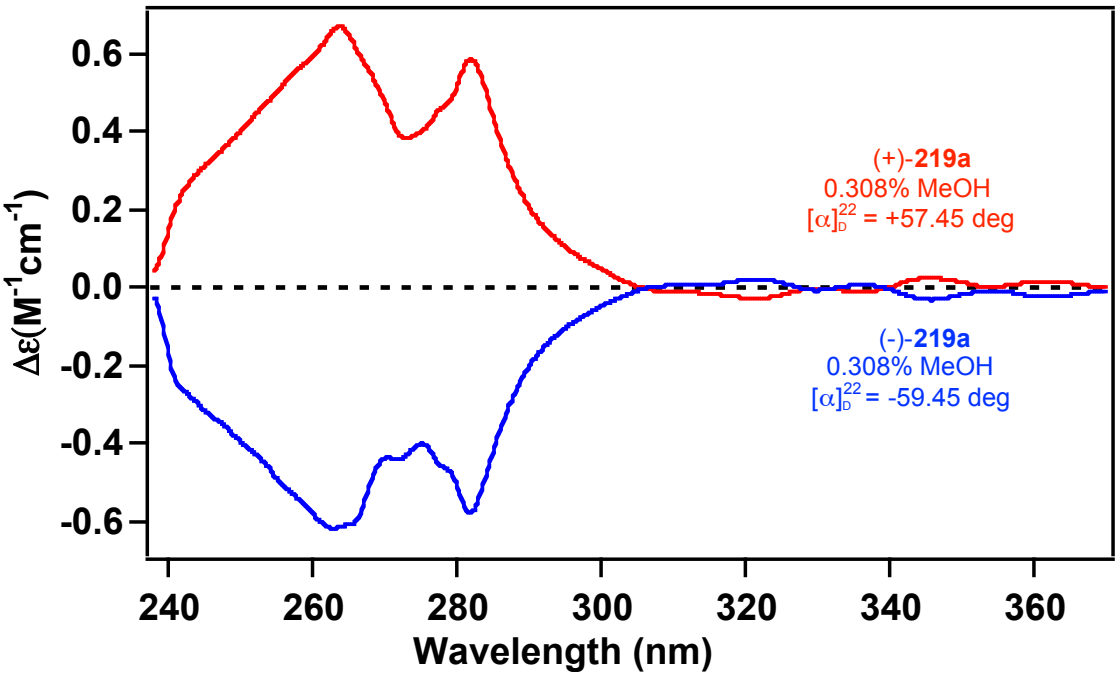

Figure 4.25: CD spectra of 6-allyloxy citraconicimide **219a** measured in methanol (*c* ~ 1.7 mM).

^{1}H-NMR (400 MHz, $CDCl_3$, δ ppm): 7.24-7.19 (m, 1H), 6.85-6.84 (m, 1H), 6.79-6.76 (m, 1H), 6.46-6.45 (m, 1H), 5.73-5.64 (m, 1H), 5.55-5.48 (m, 1H), 4.40-4.39 (m, 2H), 2.15-2.14 (m, 3H), 2.13 (s, 3H) and 1.67-1.65 (m, 3H).

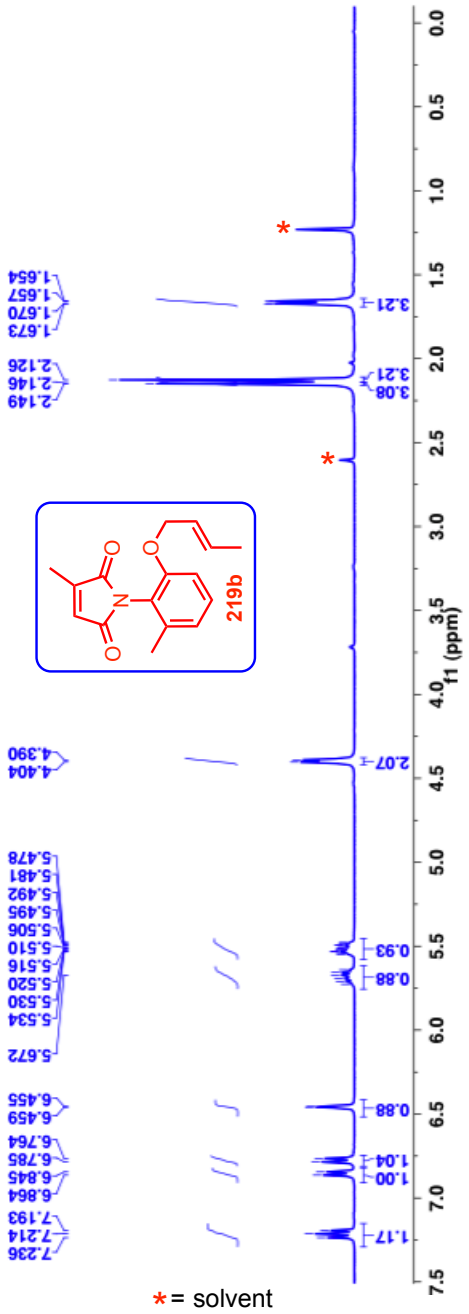

Figure 4.26: ^{1}H-NMR (400 MHz, $CDCl_3$, δ ppm) spectrum of 6-crotyloxy citraconicimide **219b**.

^{13}C-NMR (100 MHz, $CDCl_3$, δ ppm): 171.1, 170.1, 155.1, 146.2, 139.0, 130.1, 129.7, 128.1, 125.97, 122.7, 120.1, 110.97, 69.4, 17.99, 17.97 and 11.4.

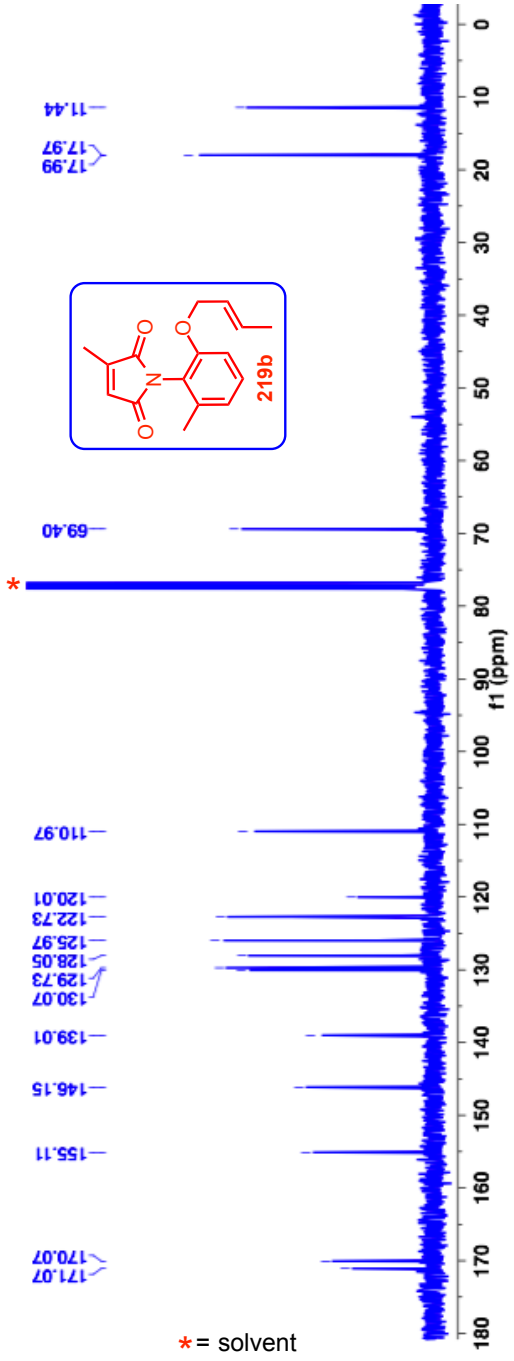

Figure 4.27: ^{13}C-NMR (100 MHz, $CDCl_3$, δ ppm) spectrum of 6-crotyloxy citraconicimide **219b**.

HRMS-ESI (m/z) ([M + Na]$^+$):

Calculated : 294.1101

Observed : 294.1099

|Δm| : 0.7 ppm

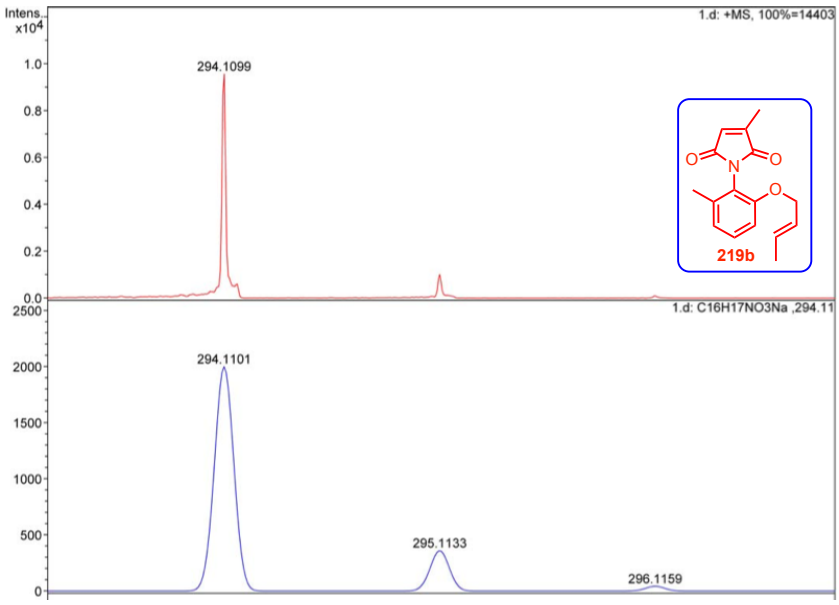

Figure 4.28: HRMS of 6-crotyloxy citraconicimide **219b**.

HPLC analysis conditions:

For analytical conditions,

I). Column : CHIRALPAK-ADH

Abs. detector wavelength : 254 nm and 270 nm

Mobile phase : Hexanes:2-propanol = 95:5

Flow rate : 1.0 mL/min

Retention times (min) : ~ 12.15 [(+)-**219b**] and ~ 14.97 [(-)-**219b**

For preparative conditions,

I). Column : CHIRALPAK-ADH

Abs. detector wavelength : 254 nm and 270 nm

Mobile phase : Hexanes:2-propanol = 99:1

Flow rate : 3.0 mL/min

Retention times (min) : ~ 41.78 [(+)-**219b** and ~ 57.07 [(-)-**219b**

Optical rotation $[\alpha]_D^{24}$:

HPLC retention time (CHIRALPAK-ADH) at ~ 12.15 min, (c ~ 1.25 %, MeOH) = +42.53 deg

HPLC retention time (CHIRALPAK-ADH) at ~ 14.97 min, (c ~ 1.25 %, MeOH) = -42.84 deg.

4.10.7. Synthesis of atropisomeric maleimide derivative 219c

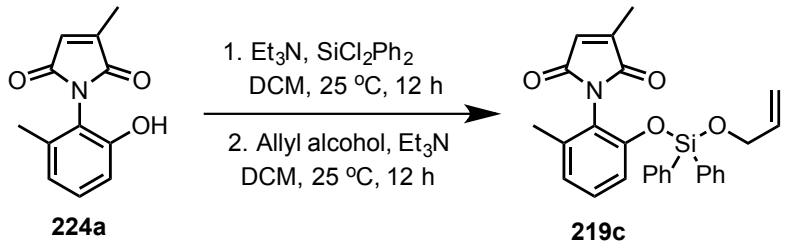

224a **219c**

Scheme 4.17: Synthesis of atropisomeric maleimide derivative **219c**.

The silyl derivative of atropisomeric maleimide **219c** was synthesized according to a procedure reported in the literature.[5] To a solution of citraconicimide **224a** (0.5 g, 2.30 mmol) derivative in DCM (10 mL) under N_2 atmosphere at 25 ^oC, triethylamine (0.64 mL, 4.60 mmol) was added. The resulting mixture was stirred for 20 min followed by the addition of dichlorodiphenylsilane (0.97 mL, 4.60 mmol). After stirring for 12 h, the solvent was removed under reduced pressure and the crude product was directly taken to the next step without further purification.

To a mixture of allyl alcohol (1.20 mL, 17.25 mmol) and triethylamine (2.40 mL, 17.25 mmol) in DCM (20 mL), a solution of the crude product from the above reaction in DCM (30 mL) was added over a period of 15 min and the mixture was further stirred for 12 h. After the reaction, the solvent was completely removed under reduced pressure. The residue was taken in a saturated $NaHCO_3$ solution and extracted with diethyl ether. The combined organic layer was dried under *anhyd.* Na_2SO_4, filtered and concentrated at 35 ^oC to the yield crude product. The crude product was purified by combiflash using a hexanes:ethyl acetate mixture.

^{1}H-NMR (400 MHz, $CDCl_3$, δ ppm): 7.61-7.59 (m, 4H), 7.39-7.38 (m, 2H), 7.35-7.30 (m, 4H), 7.07-7.03 (m, 1H), 6.88-6.83 (m, 2H), 6.45-6.43 (q, *J* = 1.6 Hz, 1H), 5.92-5.83 (m, 1H), 5.31-5.25 (m, 1H), 5.09-5.06 (m, 1H), 4.31-4.29 (m, 2H), 2.16 (s, 3H) and 2.094 (d, *J* = 2 Hz, 3H).

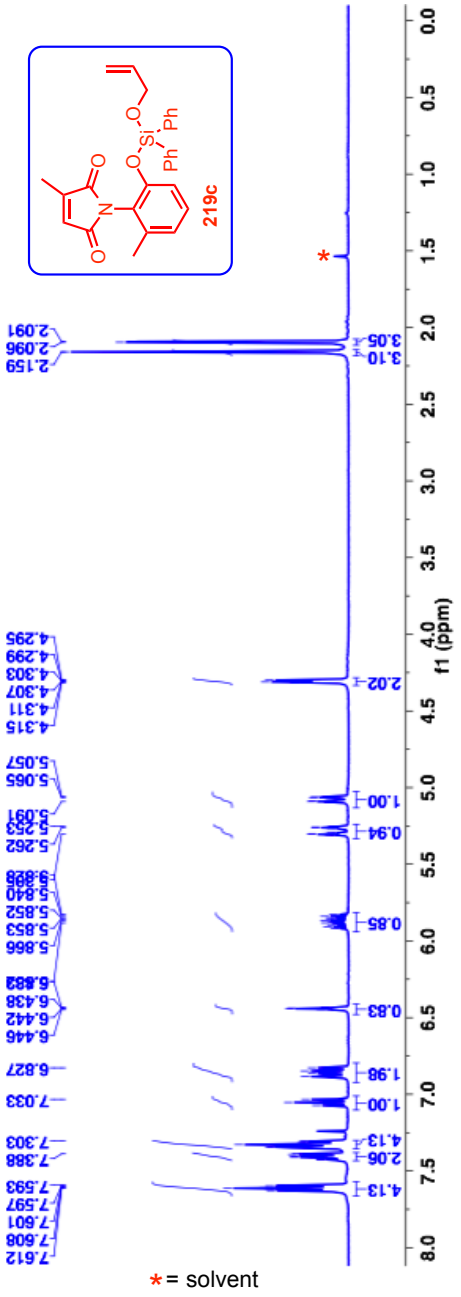

Figure 4.29: ^{1}H-NMR (400 MHz, $CDCl_3$, δ ppm) spectrum of 6-silyloxy citraconicimide **219c**.

^{13}C-NMR (100 MHz, $CDCl_3$, δ ppm): 170.8, 169.9, 151.1, 146.4, 139.1, 136.1, 134.97, 134.9, 131.7, 131.66, 130.9, 129.99, 128.1, 128.0, 123.8, 121.7, 117.0, 115.3, 64.6, 18.2 and 11.4.

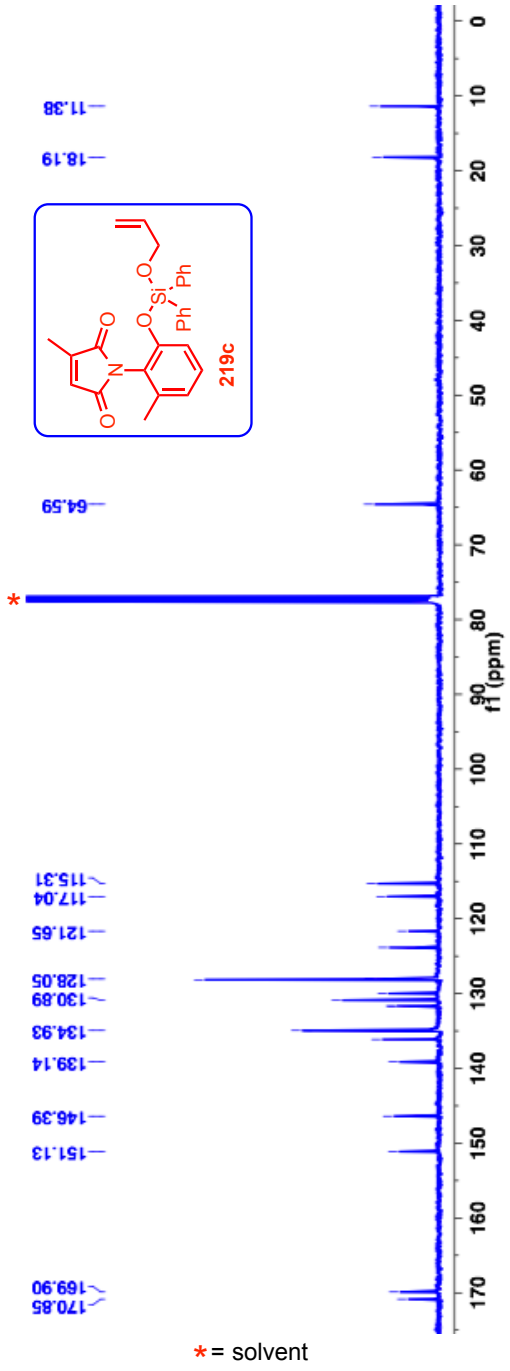

Figure 4.30: ^{13}C-NMR (100 MHz, $CDCl_3$, δ ppm) spectrum of 6-silyloxy citraconicimide **219c**.

HRMS-ESI (m/z) ([M + Na]$^+$):

Calculated : 478.1445

Observed : 478.1427

|Δm| : 3.8 ppm

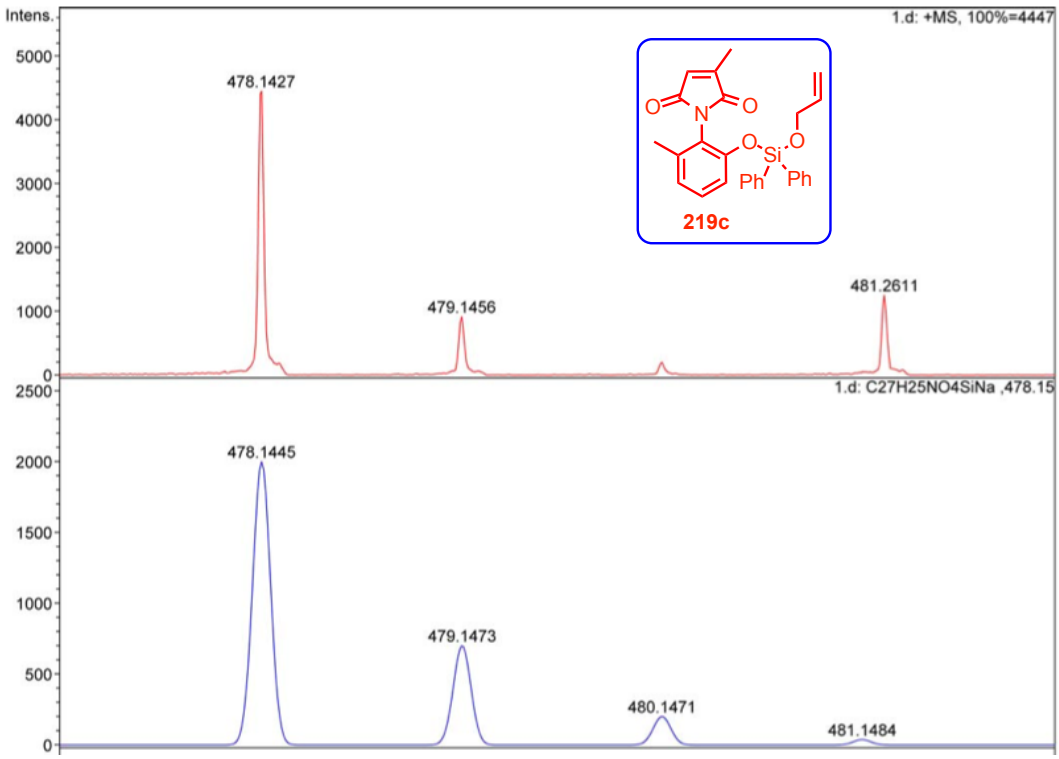

Figure 4.31: HRMS of 6-silyloxy citraconicimide derivative **219c**.

HPLC analysis conditions:

For analytical conditions,

I). Column : CHIRALPAK-ODH

Abs. detector wavelength : 254 nm and 270 nm

Mobile phase : Hexanes:2-propanol = 98:2

Flow rate : 1.0 mL/min

Retention times (min) : ~ 7.43 [**PkA**] and ~ 8.39 [**PkB**]

(**PkA** and **PkB** refers to the order of elution of the isomers on the chiral stationary phase)

4.10.8. Synthesis of atropisomeric maleimide derivatives 219d,f,h

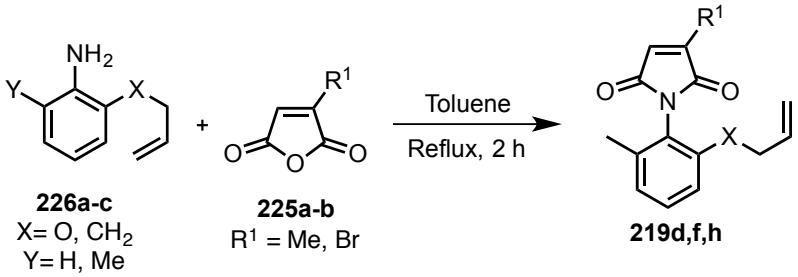

Scheme 4.18: Synthesis of axially chiral maleimide derivative **219d,f,h**.

A mixture of aniline **226a,c** (1.0 g, 1.0 *equiv.*) and anhydride **225a-b** (1.1 *equiv.*) in toluene (5 mL) was refluxed for 2 h. The reaction mixture was cooled to room temperature and the solvent was evaporated to get the crude product. The crude product was purified by combiflash using a hexanes:ethyl acetate mixture.

^{1}H-NMR (400 MHz, $CDCl_3$, δ ppm): 7.27-7.24 (m, 1H), 7.15-7.13 (m, 2H), 6.48-6.47 (m, 1H), 5.81-5.71 (m, 1H), 4.99-4.91 (m, 2H), 2.49-2.45 (m, 2H), 2.26-2.21 (m, 2H), 2.16-2.15 (q, *J* = 2 Hz, 3H) and 2.08 (s, 3H).

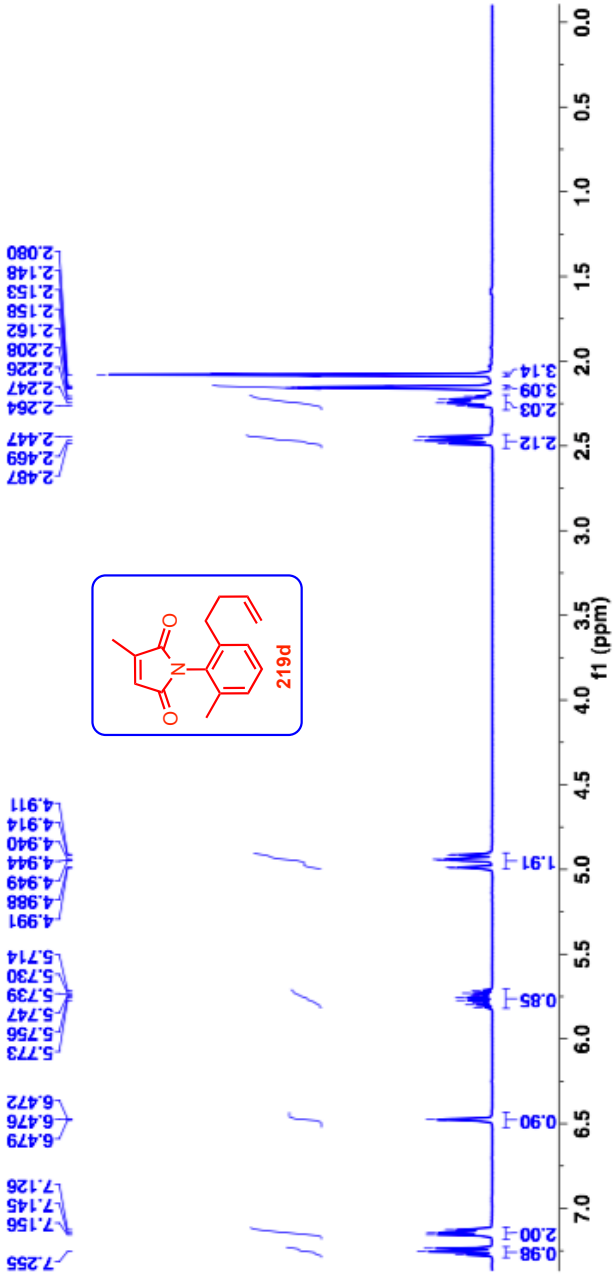

Figure 4.32: ^{1}H-NMR (400 MHz, $CDCl_3$, δ ppm) spectrum of 6-butenyl citraconicimide **219d**.

^{13}C-NMR (100 MHz, $CDCl_3$, δ ppm): 171.1, 170.2, 146.1, 141.0, 137.96, 137.3, 129.6, 129.5, 128.9, 127.8, 127.6, 115.3, 34.4, 31.4, 18.2 and 11.4.

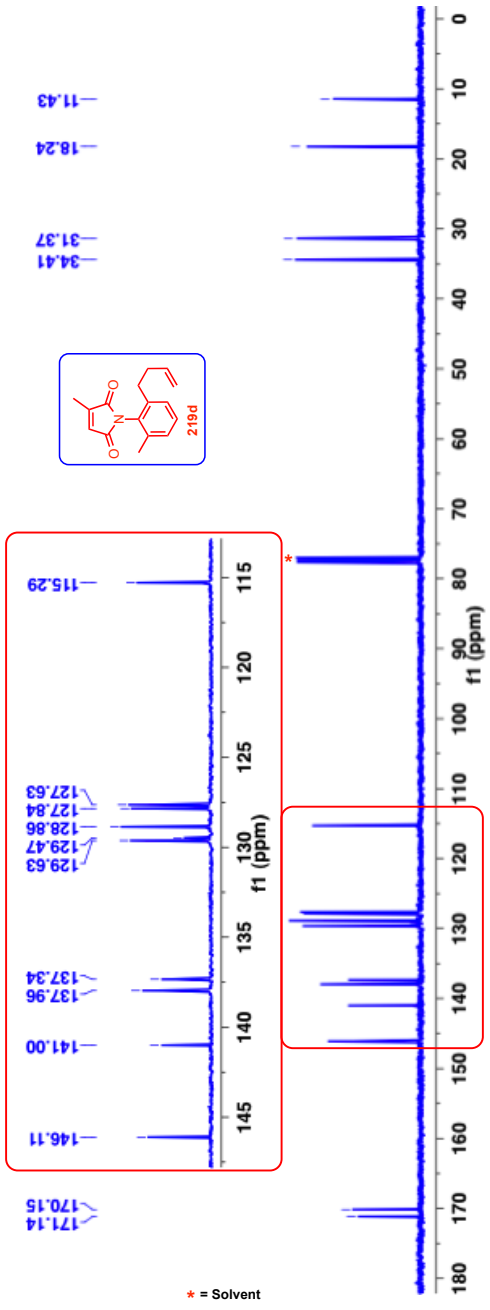

Figure 4.33: ^{13}C-NMR (100 MHz, $CDCl_3$, δ ppm) spectrum of 6-butenyl citraconicimide **219d**.

HRMS-ESI (m/z) ([M + Na]$^+$):

Calculated : 278.1151

Observed : 278.1150

|Δm| : 0.4 ppm

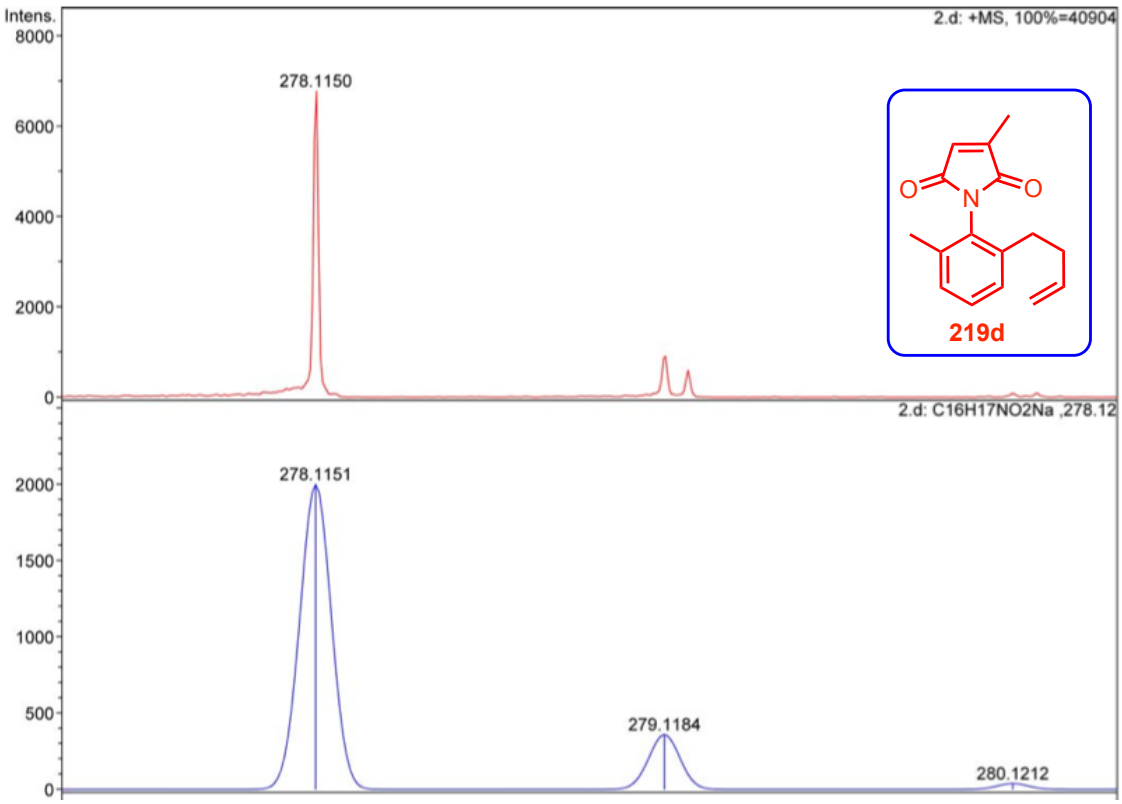

Figure 4.34: HRMS of 6-butenyl citraconicimide derivative **219d**.

^{1}H-NMR (400 MHz, $CDCl_3$, δ ppm): 7.30-7.26 (m, 1H), 7.17-7.14 (m, 2H), 7.02 (s, 1H), 5.81-5.71 (m, 1H), 5.00-4.93 (m, 2H), 2.49-2.45 (m, 2H), 2.27-2.12 (m, 2H) and 2.09 (s, 3H).

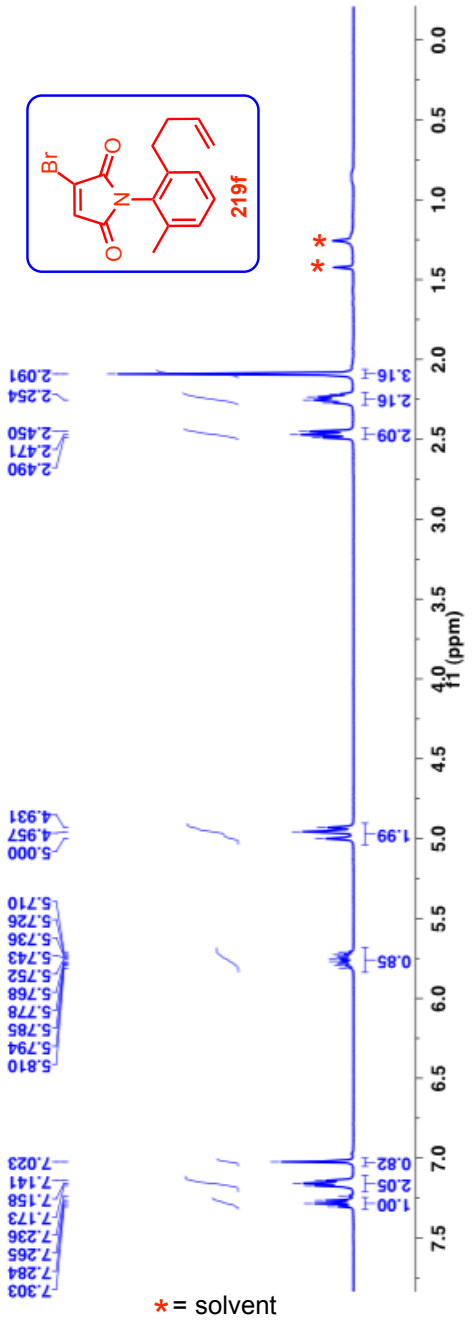

Figure 4.35: ^{1}H-NMR (400 MHz, $CDCl_3$, δ ppm) spectrum of 6-butenyl bromomaleimide **219f**.

^{13}C-NMR (100 MHz, $CDCl_3$, δ ppm): 167.9, 164.6, 140.9, 137.7, 137.3, 132.4, 131.8, 130.1, 129.0, 128.8, 127.8, 115.6, 34.3, 31.3 and 18.3.

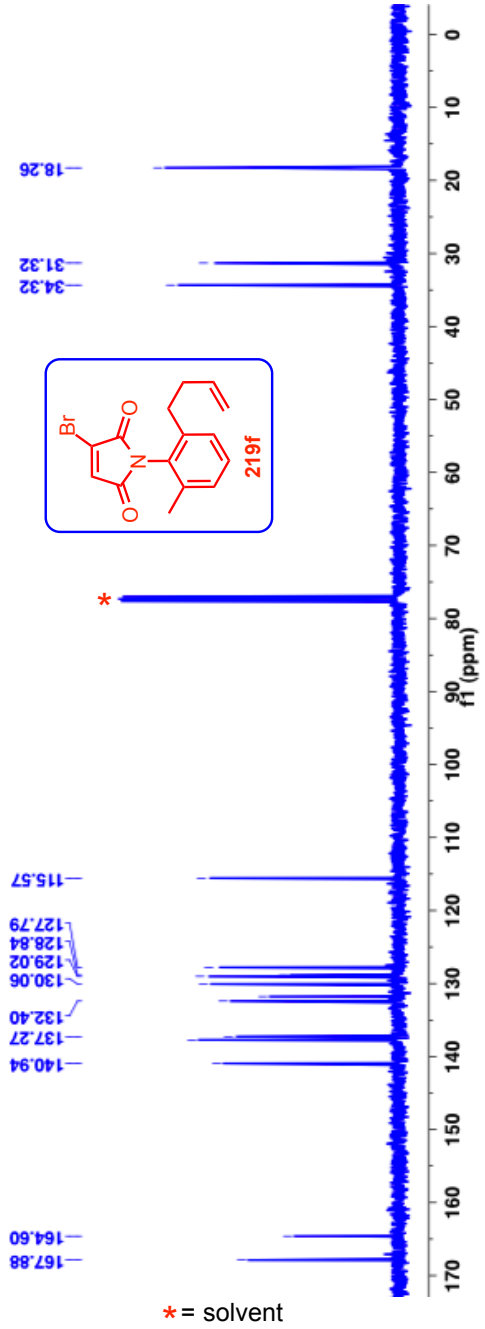

Figure 4.36: ^{13}C-NMR (100 MHz, $CDCl_3$, δ ppm) spectrum of 6-butenyl bromomaleimide **219f**.

HRMS-ESI (m/z) ([M + Na]$^+$):

Calculated : 342.0100

Observed : 342.0101

|Δm| : 0.3 ppm

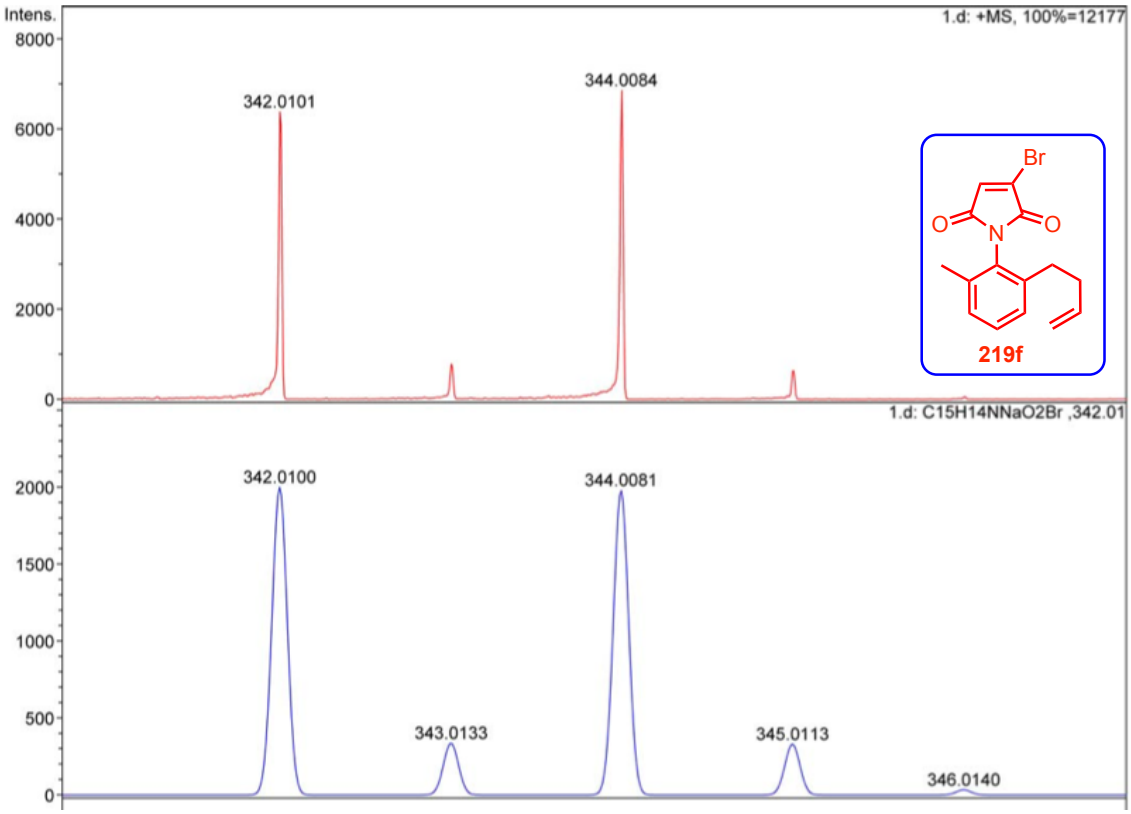

Figure 4.37: HRMS of 6-butenyl bromomaleimide derivative **219f**.

^{1}H-NMR (400 MHz, $CDCl_3$, δ ppm): 7.34-7.29 (m, 1H), 7.16-7.14 (m, 1H), 7.01-6.94 (m, 2H), 6.44-6.43 (m, 1H), 5.94-5.84 (m, 1H), 5.29-5.16 (m, 2H), 4.51-4.49 (m, 2H), 2.10 (d, *J* = 1.6 Hz, 3H).

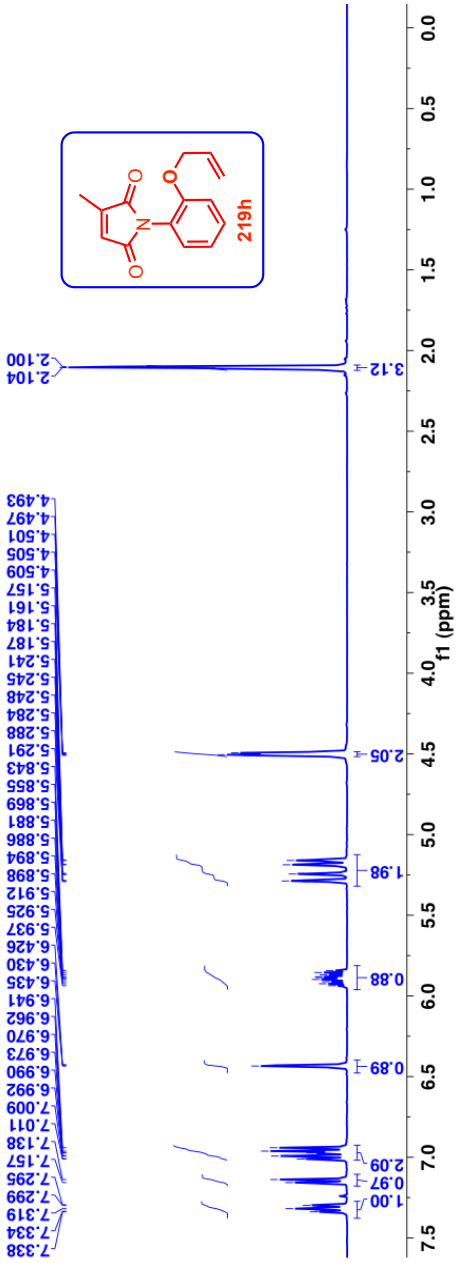

Figure 4.38: ^{1}H-NMR (400 MHz, $CDCl_3$, δ ppm) spectrum of 6-allyloxy-citraconicimide **219h**.

^{13}C-NMR (100 MHz, $CDCl_3$, δ ppm): 170.98, 169.9, 154.6, 146.2, 132.9, 130.5, 130.3, 127.97, 121.2, 120.9, 117.4, 113.7, 69.3 and 11.4.

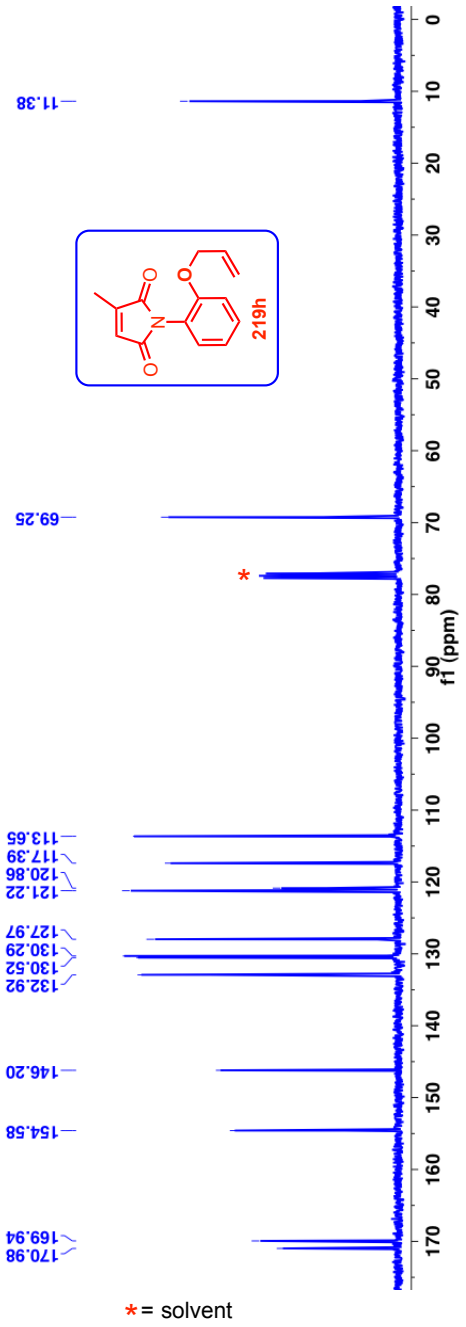

Figure 4.39: ^{13}C-NMR (100 MHz, $CDCl_3$, δ ppm) spectrum of 6-allyloxy-citraconicimide **219h**.

HRMS-ESI (m/z) ([M + Na]$^+$):

Calculated : 266.0788

Observed : 266.0786

|Δm| : 0.8 ppm

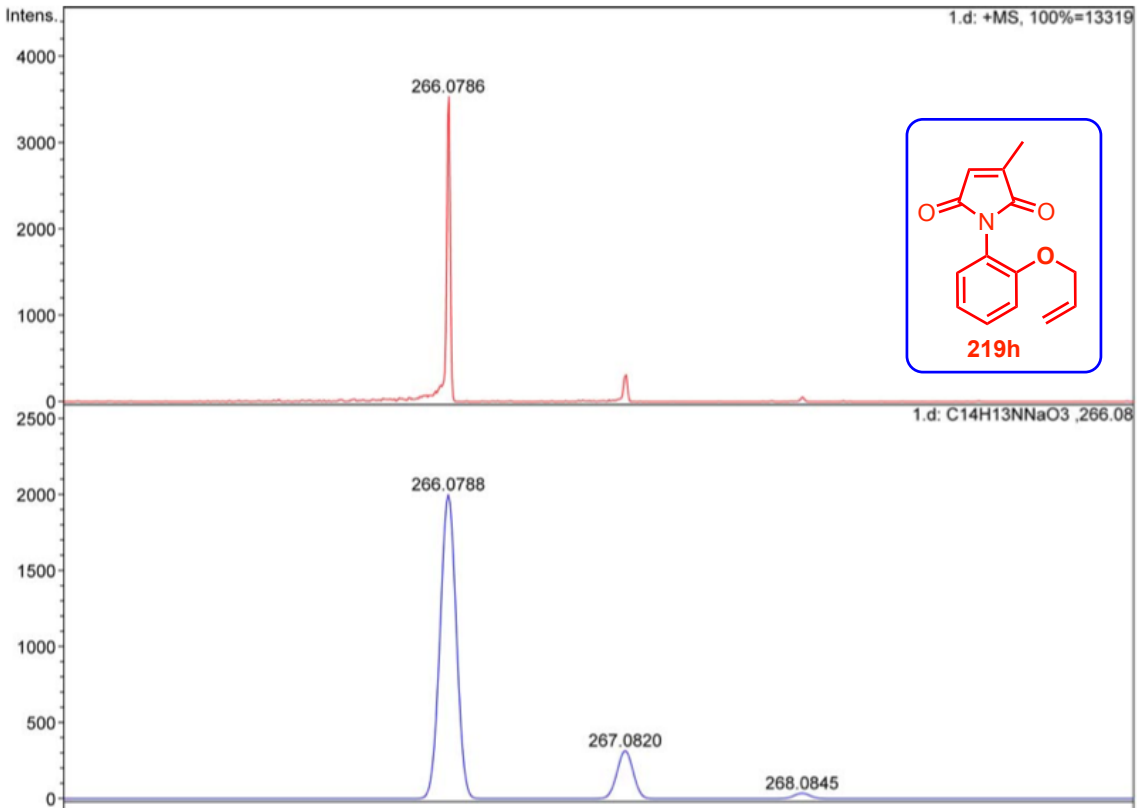

Figure 4.40: HRMS of 6-allyloxy-citraconicimide derivative **219h**.

4.10.9. Synthesis of maleimide derivatives 219e,i

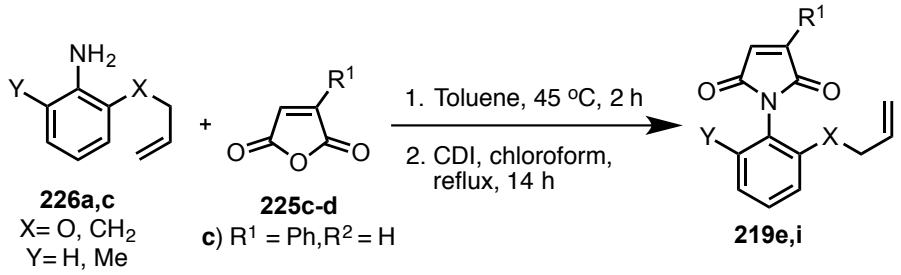

226a,c
X= O, CH_2
Y= H, Me

225c-d
c) R^1 = Ph,R^2 = H

219e,i

Scheme 4.19: Synthesis of maleimide derivatives **219e,i**.

To a solution of corresponding aniline derivative **226a-c** (10 mmol) in toluene (20 mL) at 25 ^oC, substituted maleic anhydride **225c-d** (10.1 mmol) was added. The resulting mixture was heated to 45 ^oC and maintained for 2 h. After the reaction, the mixture was cooled to room temperature and the residue was diluted with hexanes (50 mL). The precipitated solid was filtered, washed with hexanes (20 mL) and dried under vacuum. The crude product was directly taken to next step without further purification.

To the crude product from above reaction dissolved in chloroform under N_2 atmosphere 1,1'-carbonyldiimidazole (12 mmol) was added. The resulting solution was refluxed for 14 h. After the reaction, the solution was cooled to room temperature and DI water was added. The mixture was stirred and the layers were separated. The organic layer was washed with DI Water (2 × 100 mL), cold aqueous 2N HCl (2 × 75 mL or until the imidazole byproduct was removed) and brine solution (1 × 100 mL). The organic layer was dried over *anhyd.* Na_2SO_4, filtered and the solvent was evaporated under reduced pressure to get the crude product. The crude product was purified by combiflash using a hexanes:ethyl acetate mixture (90:10).

Note: During the addition of 1,1'-carbonyldiimidazole evolution of CO_2 gas was observed.

^{1}H-NMR (400 MHz, $CDCl_3$, δ ppm): 8.03-7.99 (m, 2H), 7.49-7.44 (m, 3H), 7.29-7.24 (m, 1H), 6.94-6.91 (m, 1H), 6.83-6.81 (m, 1H), 5.94-5.85 (m, 1H), 5.31-5.24 (m, 1H), 5.18-5.14 (m, 1H), 4.52-4.499 (m, 2H) and 2.22 (m, 3H).

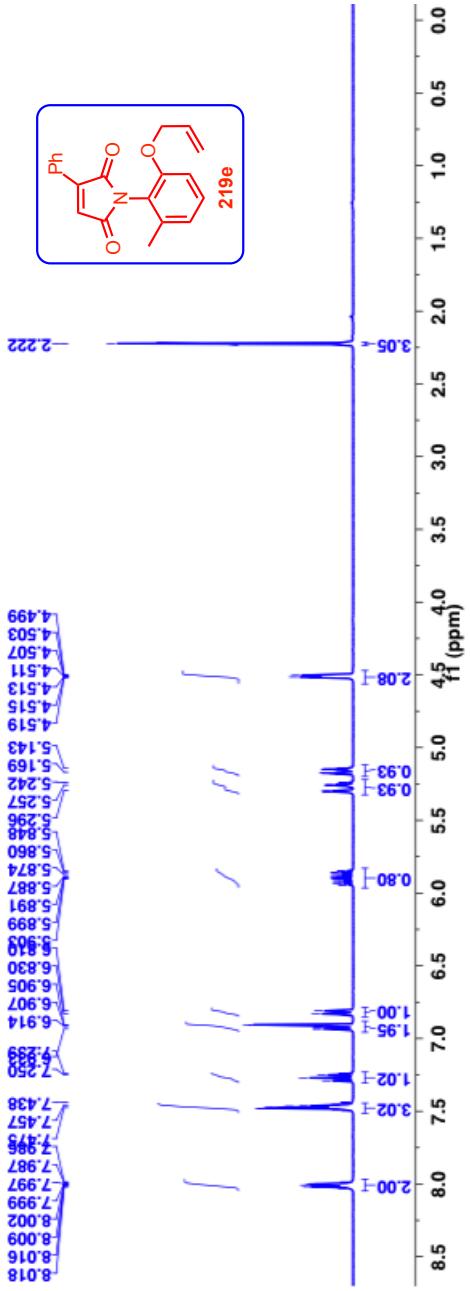

Figure 4.41: ^{1}H-NMR (400 MHz, $CDCl_3$, δ ppm) spectrum of 6-silyloxy citraconicimide **219e**.

^{13}C-NMR (100 MHz, $CDCl_3$, δ ppm): 169.9, 169.6, 154.9, 144.2, 139.2, 132.96, 131.4, 130.3, 129.2, 129.1, 129.0, 124.7, 122.98, 119.96, 117.3, 110.8, 69.2 and 18.1.

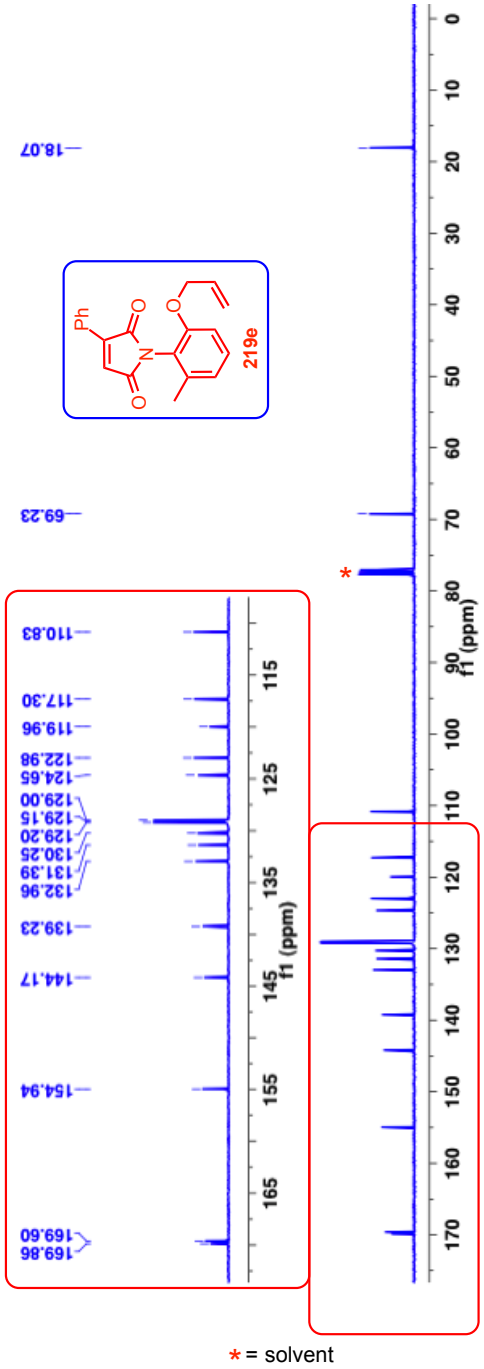

Figure 4.42: ^{13}C-NMR (100 MHz, $CDCl_3$, δ ppm) spectrum of 6-silyloxy citraconicimide **219e**.

HRMS-ESI (m/z) ([M + Na]$^+$):

Calculated : 342.1101

Observed : 342.1093

|Δm| : 2.3 ppm

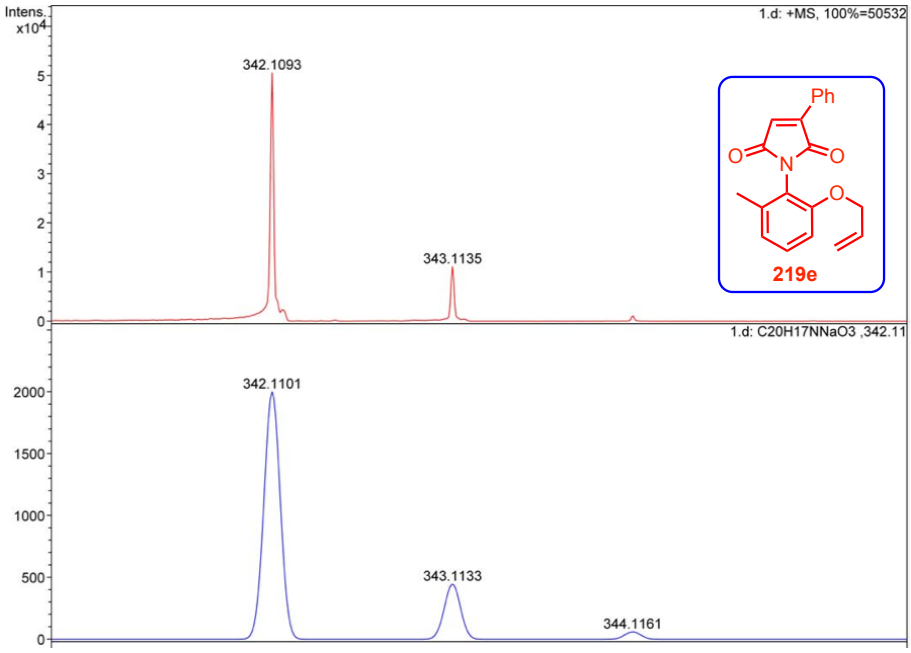

Figure 4.43: HRMS of 6-silyloxy citraconicimide derivative **219e**.

HPLC analysis conditions:

For analytical conditions,

I). Column : CHIRALPAK-ADH

Abs. detector wavelength : 254 nm and 270 nm

Mobile phase : Hexanes:2-propanol = 90:10

Flow rate : 1.0 mL/min

Retention times (min) : ~ 13.32 [(+)-**219e**] and ~ 16.95 [(-)-**219e**

For preparative conditions,

I). Column : CHIRALPAK-ADH

Abs. detector wavelength : 254 nm and 270 nm

Mobile phase : Hexanes:2-propanol = 97:3

Flow rate : 3.0 mL/min

Retention times (min) : ~ 37.55 [(+)-**219e** and ~ 52.30 [(-)-**219e**]

Optical rotation $[\alpha]_D^{22}$:

HPLC retention time (CHIRALPAK-ADH) at ~ 13.32 min, (*c* ~ 0.292 %, MeOH) = +30.49 deg

HPLC retention time (CHIRALPAK-ADH) at ~ 16.95 min, (*c* ~ 0.292 %, MeOH) = -29.47 deg.

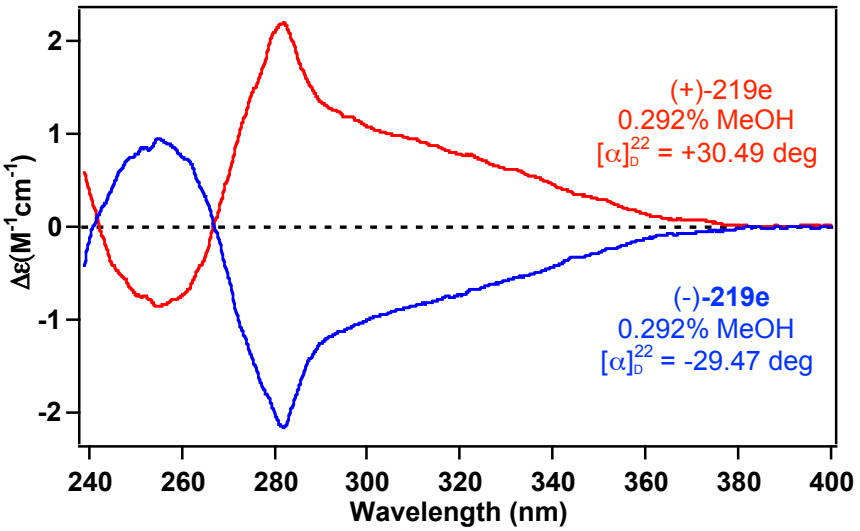

Figure 4.44: CD spectra of 2-allyloxy-phenylmaleimides **219e** measured in MeOH (c ~ 0.4 mM).

^{1}H-NMR (400 MHz, $CDCl_3$, δ ppm): 7.998-7.97 (m, 2H), 7.47-7.45 (m, 3H), 7.397-7.35 (m, 1H), 7.26-7.24 (m, 1H), 7.07-6.989 (m, 2H), 6.88 (s, 1H), 5.97-5.88 (m, 1H), 5.34-5.28 (m, 1H), 5.20-5.17 (m, 1H) and 4.56-4.53 (m, 2H).

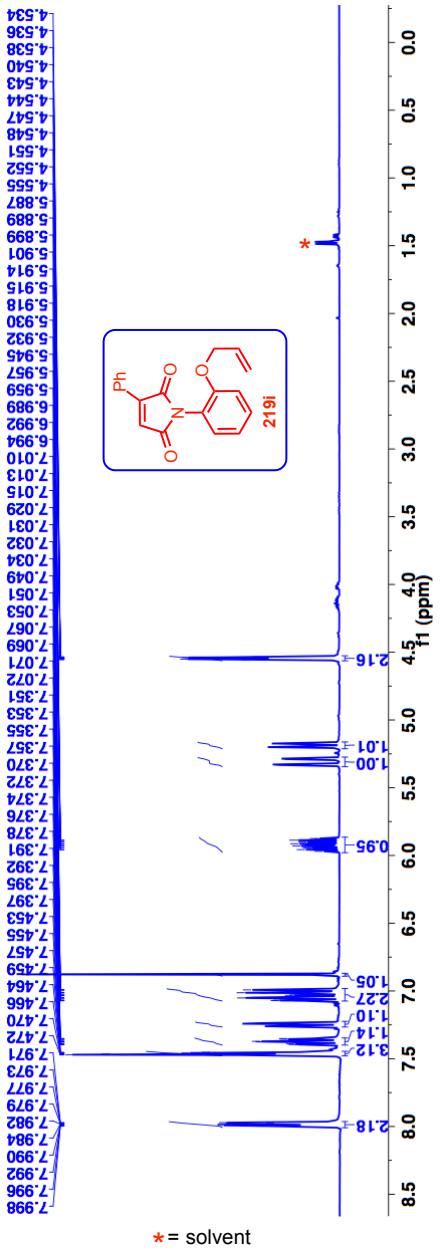

Figure 4.45: ^{1}H-NMR (400 MHz, $CDCl_3$, δ ppm) spectrum of 6-allyloxy-phenylmaleimide **219i**.

^{13}C-NMR (100 MHz, $CDCl_3$, δ ppm): 169.8, 169.5, 154.7, 144.1, 132.9, 131.4, 130.7, 130.4, 129.2, 129.1, 128.99, 124.6, 121.3, 120.8, 117.5, 113.7 and 69.3.

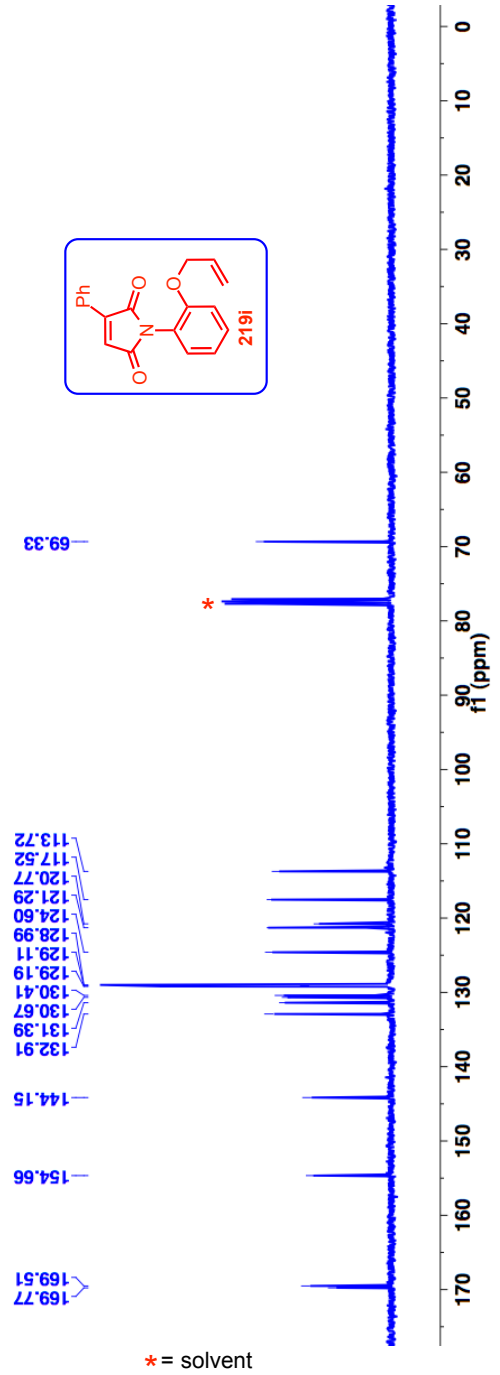

Figure 4.46: ^{13}C-NMR (100 MHz, $CDCl_3$, δ ppm) spectrum of 6-allyloxy-phenylmaleimide **219i**.

HRMS-ESI (m/z) ([M + Na]$^+$):

Calculated : 328.0944

Observed : 328.0942

|Δm| : 0.6 ppm

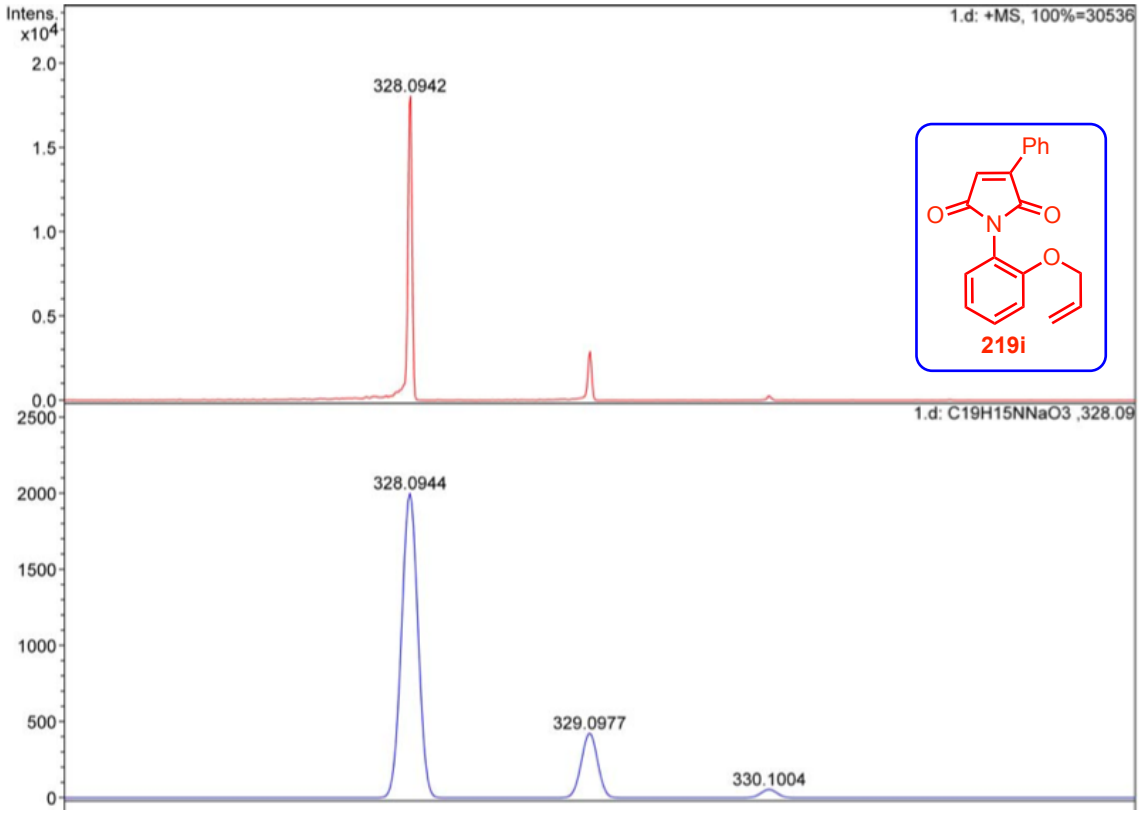

Figure 4.47: HRMS of 6-allyloxy-phenylmaleimide derivative **219i**.

4.10.10. Synthesis of atropisomeric maleimide derivatives 219g

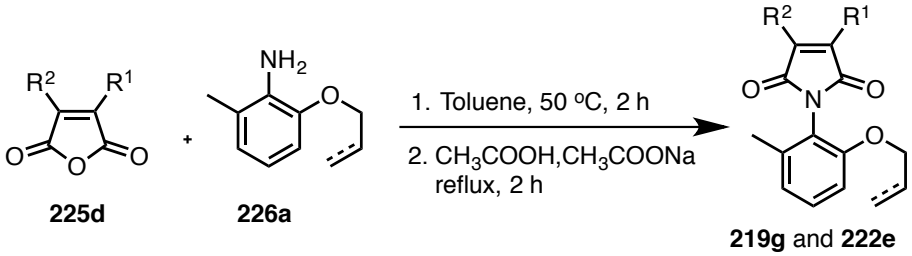

225d **226a** **219g** and **222e**

Scheme 4.20: Synthesis of atropisomeric maleimide derivative **219g**.

Synthesis of bromocitraconic anhydride 225d: The bromocitraconic anhydride **225d** was synthesized according a procedure reported in the literature.[16] A mixture of citraconic anhydride **225a** (1.0 g, 8.92 mmol), bromine (0.46 mL, 8.92 mmol) and aluminum bromide (27 mg, 0.098 mmol) in a sealed vial was heated to 120 °C for 12 h. After the reaction, the mixture was cooled to room temperature, diluted with ethyl acetate (30 mL), filtered through celite and washed with DI water (2 x 15 mL) and saturated NaCl solution. The combined organic layer was dried over *anhyd.* Na_2SO_4, filtered and concentrated under reduced pressure to yield crude product. The crude product was sufficiently pure to be taken to next step.

To a solution of aniline derivative **226a** (500 mg, 1.1 *equiv.*) in toluene (5 mL) corresponding anhydride **225d** (1.0 *equiv.*) was added and the resulting mixture was heated to 50 °C for 2 h. After the reaction, the solvent was concentrated and the residue was directly taken to next step.

To the residue from the above reaction in glacial acetic acid (5 mL), *anhyd.* sodium acetate (236 mg, 2.88 mmol) was added. The resulting mixture was refluxed for 2 h. After the reaction, the mixture was cooled to room temperature and diluted with ethyl acetate (20 mL). The organic layer was washed with DI water (2 x 15 mL), saturated $NaHCO_3$ solution (2 × 15 mL), dried over *anhyd.* Na_2SO_4, filtered and concentrated under reduced pressure to yield crude product. The crude product was purified by combiflash using a hexanes:ethyl acetate mixture.

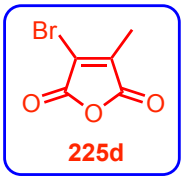

225d

(Yield = 80%). ^{1}H-NMR (400 MHz, $CDCl_3$, δ ppm): 2.11 (s, 3H).

^{13}C-NMR (100 MHz, $CDCl_3$, δ ppm): 163.7, 160.3, 145.8, 127.0 and 11.6.

^{1}H-NMR (400 MHz, $CDCl_3$, δ ppm): 7.25-7.21 (m, 1H), 6.89-6.86 (m, 1H), 6.78-6.76 (m, 1H), 5.91-5.82 (m, 1H), 5.25-5.16 (m, 2H), 4.48 (d, J = 4.8 Hz, 2H), 2.14 (s, 3H) and 2.12 (s, 3H).

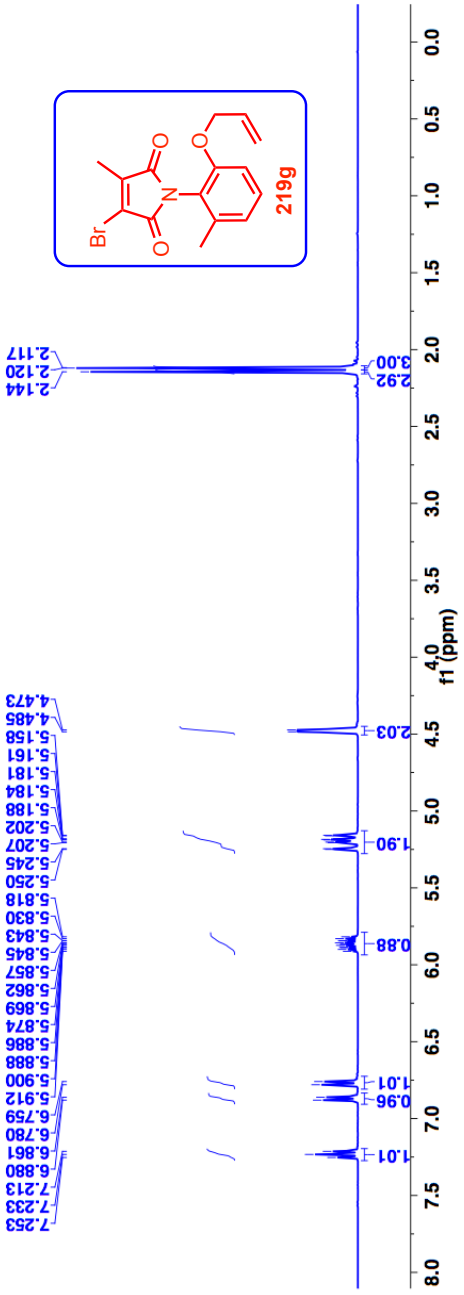

Figure 4.48: ^{1}H-NMR (400 MHz, $CDCl_3$, δ ppm) spectrum of 6-allyloxy bromo-citraconicimide **219g**.

^{13}C-NMR (100 MHz, $CDCl_3$, δ ppm): 168.6, 164.7, 154.8, 142.95, 139.1, 132.8, 130.4, 125.7, 122.95, 119.7, 117.4, 110.8, 69.2, 18.0 and 11.2.

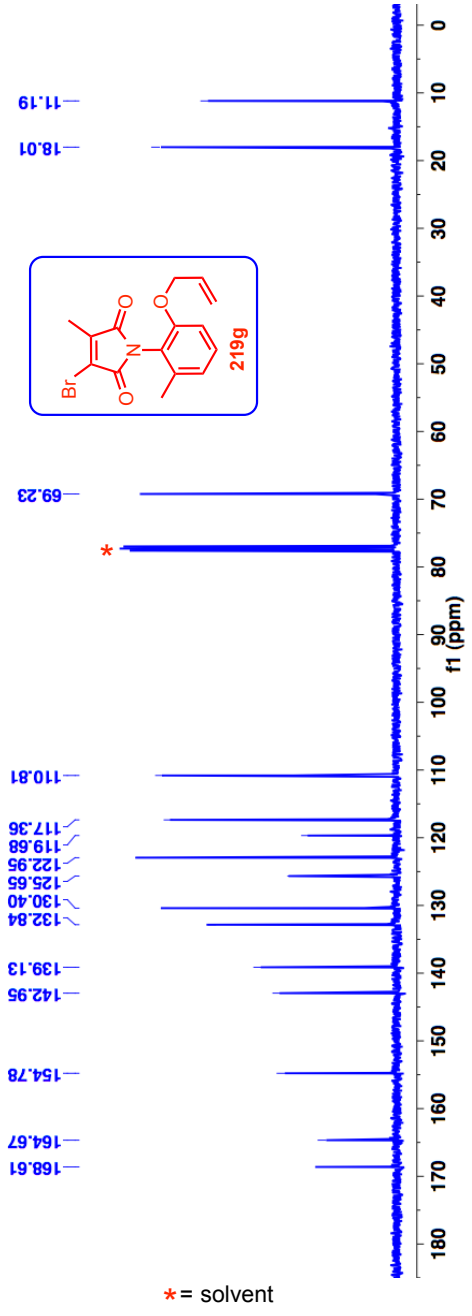

Figure 4.49: ^{13}C-NMR (100 MHz, $CDCl_3$, δ ppm) spectrum of 6-allyloxy bromo-citraconicimide **219g**.

HRMS-ESI (m/z) ([M + Na]$^+$):

Calculated : 358.0049

Observed : 358.0053

|Δm| : 1.1 ppm

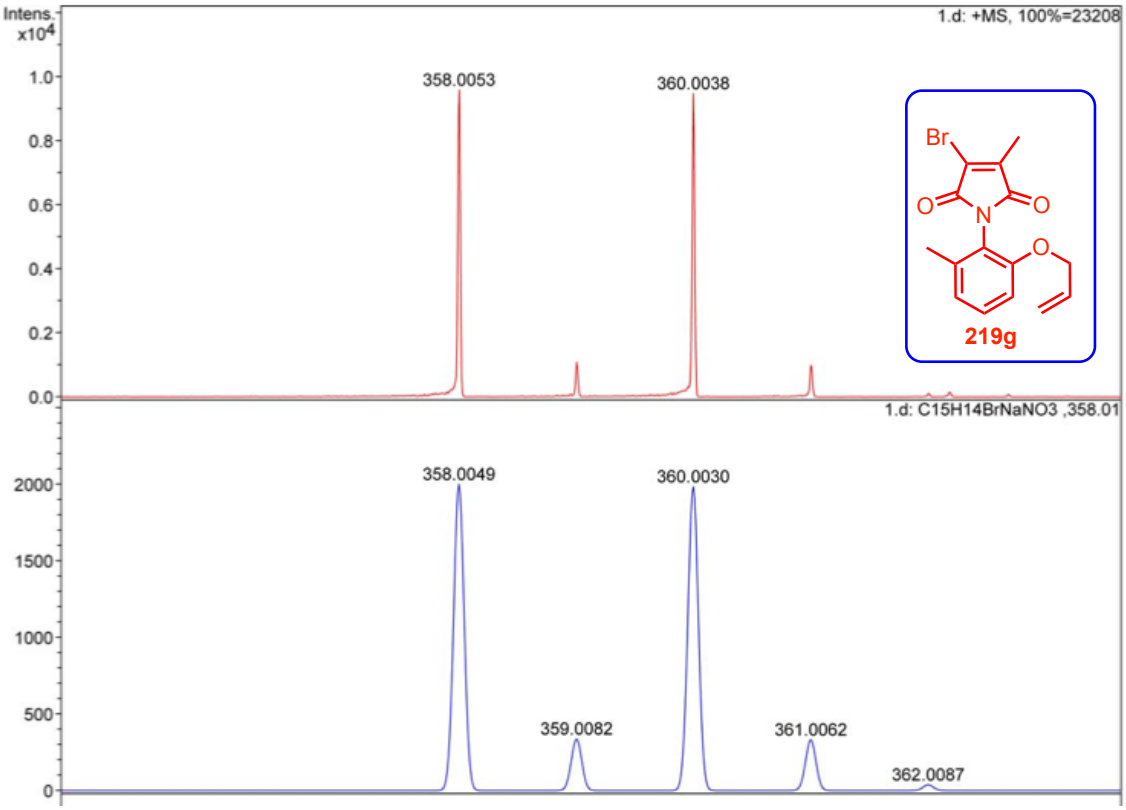

Figure 4.50: HRMS of 6-allyloxy bromo-citraconicimide derivative **219g**.

HPLC analysis conditions:

For analytical conditions,

I). Column : CHIRALPAK-ADH

Abs. detector wavelength: 254 nm and 270 nm

Mobile phase : Hexanes:2-propanol = 95:5

Flow rate : 1.0 mL/min

Retention times (min) : ~ 7.40 [**PkA**] and ~ 8.20 [**PkB**]

(**PkA** and **PkB** refers to the order of elution of the isomers in HPLC on a chiral stationary phase)

^{1}H-NMR (400 MHz, $CDCl_3$, δ ppm): 8.02-7.99 (m, 2H), 7.47-7.46 (m, 3H), 7.26-7.23 (m, 1H), 6.91-6.88 (m, 2H), 6.82-6.799 (m, 1H), 3.89 (t, *J* = 6.3 Hz, 2H), 2.21 (s, 3H), 1.66 (h, *J* = 7.3 Hz, 2H) and 0.89 (t, *J* = 7.4 Hz, 3H).

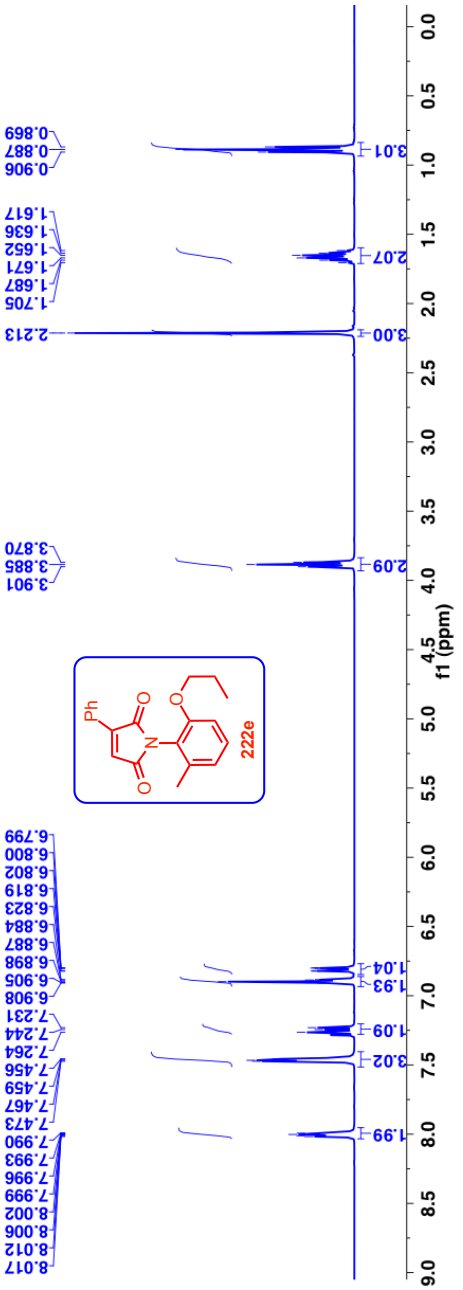

Figure 4.51: ^{1}H-NMR (400 MHz, $CDCl_3$, δ ppm) spectrum of 6-propyloxy-phenylmaleimide **222e**.

^{13}C-NMR (100 MHz, $CDCl_3$, δ ppm): 169.98, 169.7, 155.4, 144.1, 139.1, 131.4, 130.3, 129.2, 129.17, 128.97, 124.6, 122.6, 119.9, 110.3, 70.15, 22.7, 18.0 and 10.6.

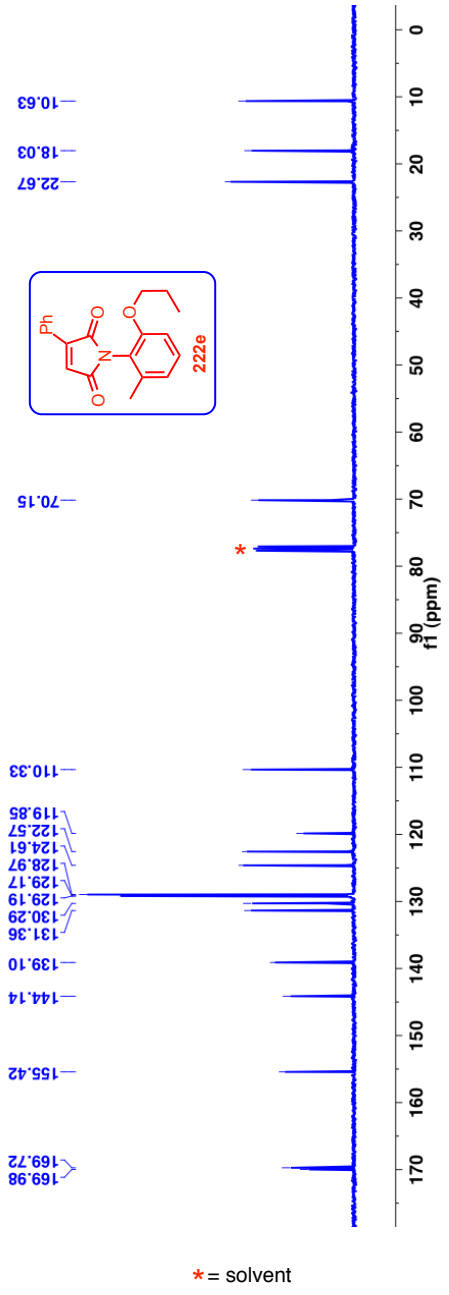

Figure 4.52: ^{13}C-NMR (100 MHz, $CDCl_3$, δ ppm) spectrum of 6-propyloxy-phenylmaleimide **222e**.

HRMS-ESI (m/z) ([M + Na]$^+$):

Calculated : 344.1257

Observed : 344.1252

|Δm| : 1.5 ppm

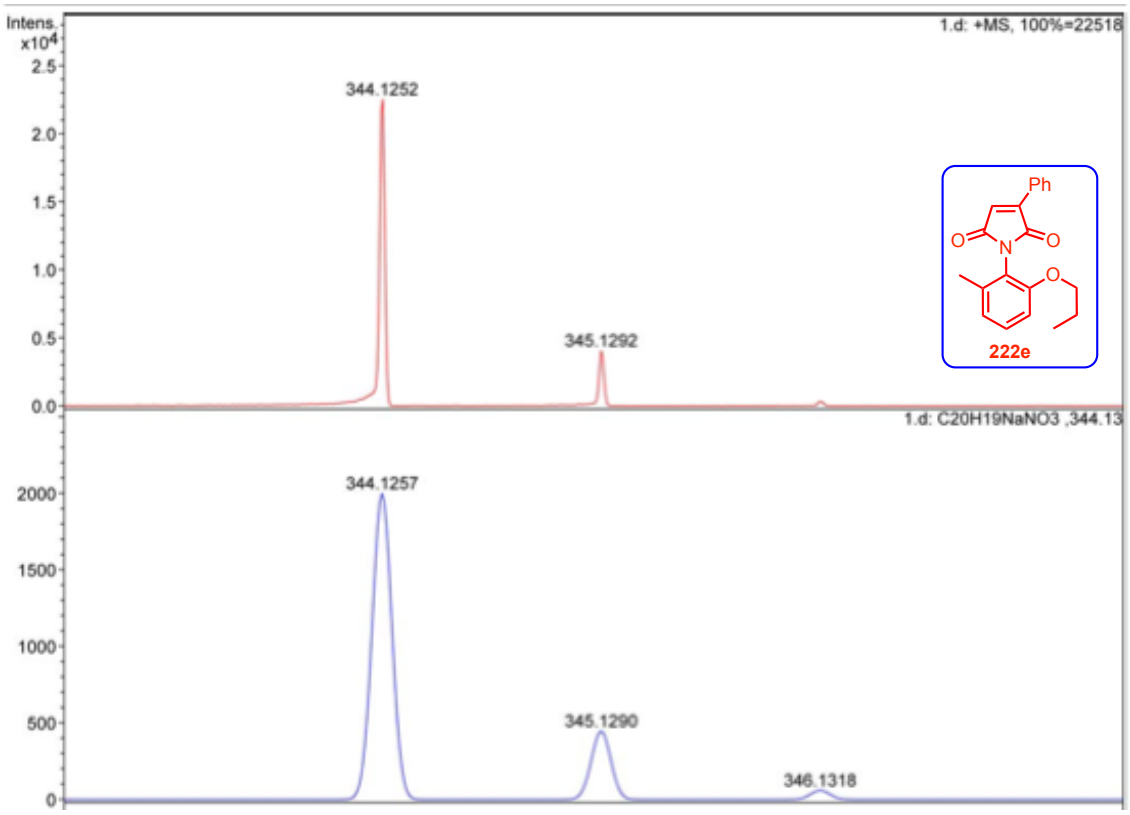

Figure 4.53: HRMS of 6-propyloxy-phenylmaleimide derivative **222e**.

4.11. Process for photoreaction of atropisomeric maleimides 219a-g

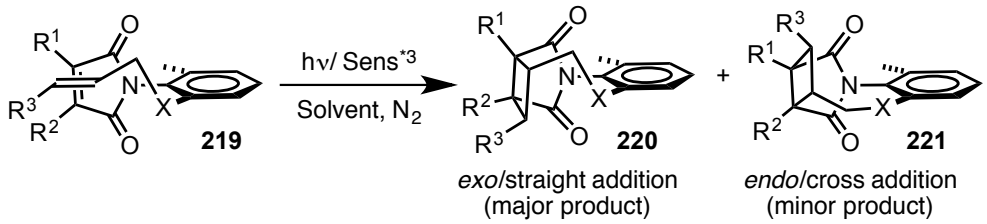

Scheme 4.21: General irradiation procedure for maleimides **219a-g**.

Enantiospecific reactions: A solution of optically pure atropisomeric maleimides obtained from HPLC preparative separation on a chiral stationary phase (2.5-4.0 mM or 1 mg/1 mL) in appropriate solvent (acetone or MeCN) or with the combination of MeCN/30 mol% sensitizer (xanthone or thioxanthone) was irradiated in either one of the following procedures. a) The solution in a Pyrex tube was irradiated with a 450W medium-pressure mercury lamp under constant flow of nitrogen for a given time interval. b) Irradiated in a Rayonet reactor fitted with bulb of desired wavelength. After the irradiation, the solvent was evaporated under reduced pressure and the photoproducts were isolated by preparative thin layer chromatography and characterized by NMR spectroscopy, mass spectrometry, single crystal XRD, CD, $[\alpha]_D$ and by HPLC. HPLC analysis of the photolysate on a chiral stationary phase gave the optical purity of the photoproducts.

Large-scale reactions: Large-scale reactions were carried out on racemic maleimides as batches (4 × 20 mL test tubes per batch). After the irradiation, the solutions were combined and the solvent was evaporated under reduced pressure. The residue was purified by combiflash using a hexanes:ethyl acetate mixture as mobile phase.

In some cases (**219e**) N_2 degassed solutions of maleimide placed in a merry-go-round (8 x 10 mL test tubes) were irradiated in a Rayonet reactor for given time period. After the irradiation, the solutions were combined and the solvent was evaporated under reduced pressure. The residue was purified by combiflash using a hexanes:ethyl acetate mixture as mobile phase.

Conversion and mass balance were obtained from NMR integration of the crude photosylate against triphenylmethane as an internal standard using the following formula

$$mol_a = mol_i \; X \left(\frac{\text{Integral of analyte}}{\text{Integral of Int. Std}} \right) X \frac{N_a}{N_i} \qquad \textbf{Equation 2:12}$$

Where, N_a and N_i are the number of nuclei giving rise to the relevant analyte and internal standard signals respectively. Similarly mol_a and mol_i are the molarity of analyte and the internal standard in deuterated chloroform, respectively. The *dr* of the photoproducts **220** and **221** were calculated from the crude reaction mixture after the photoreaction.

^{1}H-NMR (400 MHz, $CDCl_3$, δ ppm): 7.21-7.18 (m, 1H), 7.08-7.06 (m, 1H), 6.97-6.95 (m, 1H), 4.40-4.36 (dd, *J* = 14, 4.8 Hz, 1H), 3.72 (d, *J* = 14 Hz, 1H), 3.09-3.01 (m, 2H), 2.64-2.51 (m, 2H), 2.36 (s, 3H) and 1.57 (s, 3H).

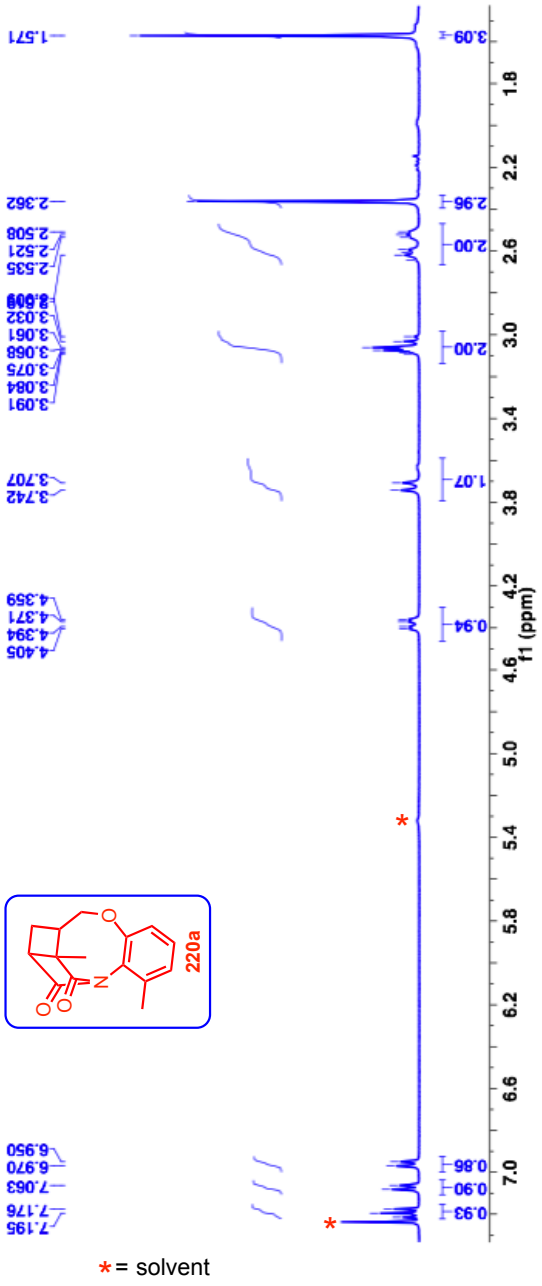

Figure 4.54: ^{1}H-NMR (400 MHz, $CDCl_3$, δ ppm) spectrum of cyclobutane photoproduct **220a**.

^{13}C-NMR (100 MHz, $CDCl_3$, δ ppm): 182.2, 181.8, 156.4, 139.4, 132.4, 129.8, 126.7, 120.4, 74.5, 52.4, 48.6, 43.1, 23.9, 17.6 and 15.7.

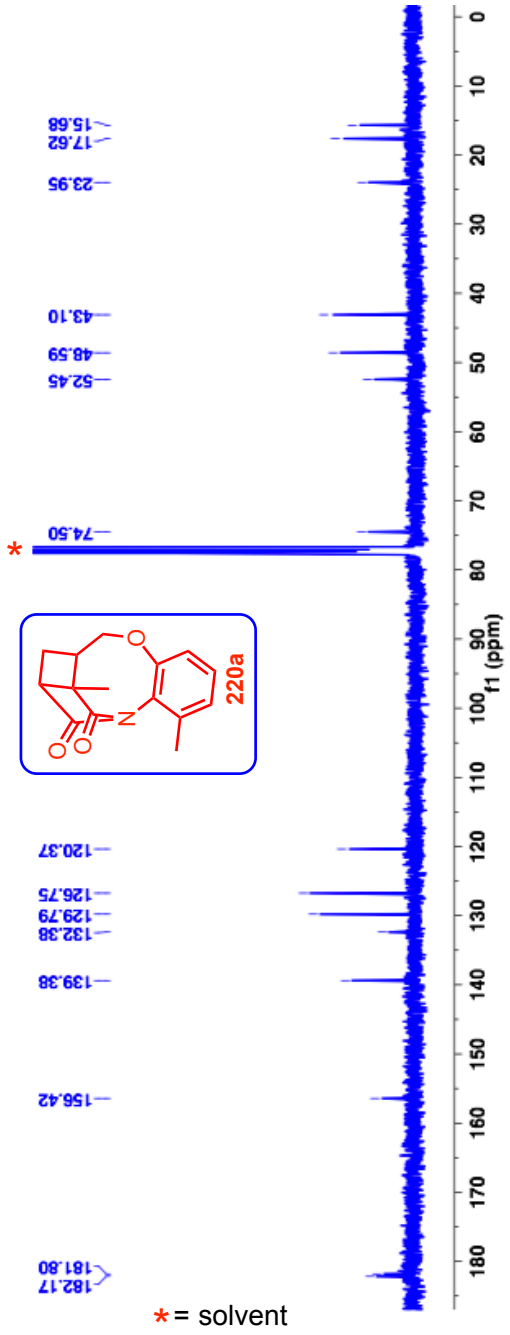

Figure 4.55: ^{13}C-NMR (100 MHz, $CDCl_3$, δ ppm) spectrum of cyclobutane photoproduct **220a**.

HRMS-ESI (m/z) ([M + Na]$^+$):

Calculated : 280.0944

Observed : 280.0941

|Δm| : 1.1 ppm

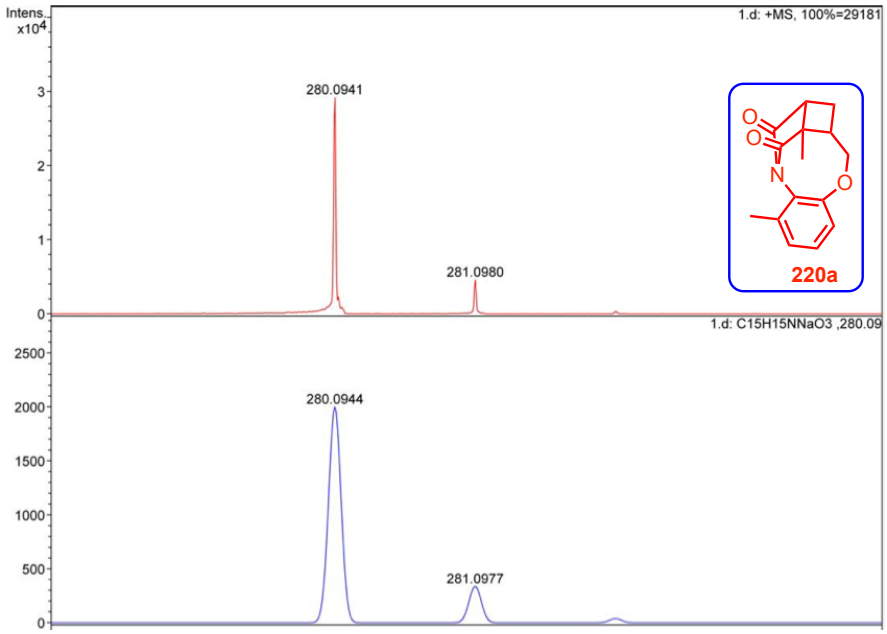

Figure 4.56: HRMS of cyclobutane photoproduct **220a**.

HPLC analysis conditions:

For analytical conditions,

I). Column : CHIRALPAK-OD-H

Abs. detector wavelength : 254 nm and 270 nm

Mobile phase : Hexanes:2-propanol = 90:10

Flow rate : 1.0 mL/min

Retention times (min) : ~15.87 [(-)(*1R,5S,6R*)-**220a**] & ~20.57 [(+)-(*1S,5R,6S*)-**220a**

For preparative conditions,

I). Column : CHIRALPAK-OD-H

Abs. detector wavelength : 254 nm and 270 nm

Mobile phase : Hexanes:2-propanol = 95:5

Flow rate : 3.0 mL/min

Retention times (min) : ~35.30 [(-)(*1R,5S,6R*)-**220a**] & ~45.40 [(+)-(*1S,5R,6S*)-**220a**

Optical rotation $[\alpha]_D^{23}$:

HPLC retention time (CHIRALPAK-ODH) at ~ 15.87 min, (*c* ~ 0.208 %, $CHCl_3$) = -23.85 deg

HPLC retention time (CHIRALPAK-ODH) at ~ 20.57 min, (*c* ~ 0.208 %, $CHCl_3$) = 24.27 deg.

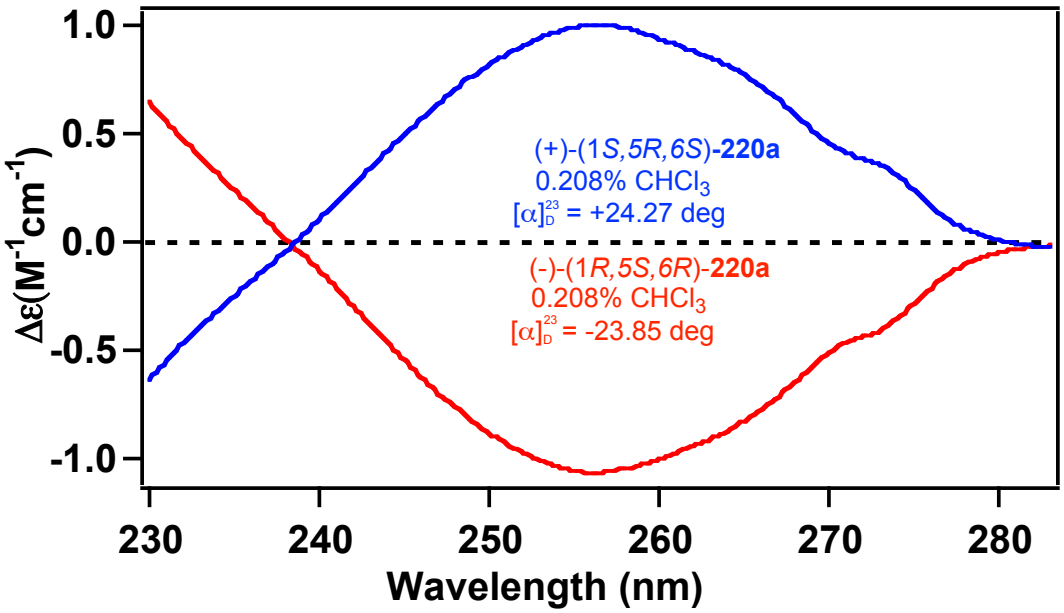

Figure 4.57: CD spectrum of cyclobutane photoproduct **220a** measured in MeOH (*c* ~ 1.8 mM).

^{1}H-NMR (400 MHz, $CDCl_3$, δ ppm): 7.22-7.18 (m, 1H), 7.08-7.06 (m, 1H), 6.97-6.95 (m, 1H), 4.40 (dd, *J* = 13.6, 4.8 Hz, 1H), 3.71 (d, *J* = 13.6 Hz, 1H), 3.45 (d, *J* = 8.8 Hz, 1H), 2.99-2.92 (m, 1H), 2.79-2.76 (m, 1H), 2.65-2.59 (m, 1H), 2.34 (s, 3H) and 1.52 (s, 3H).

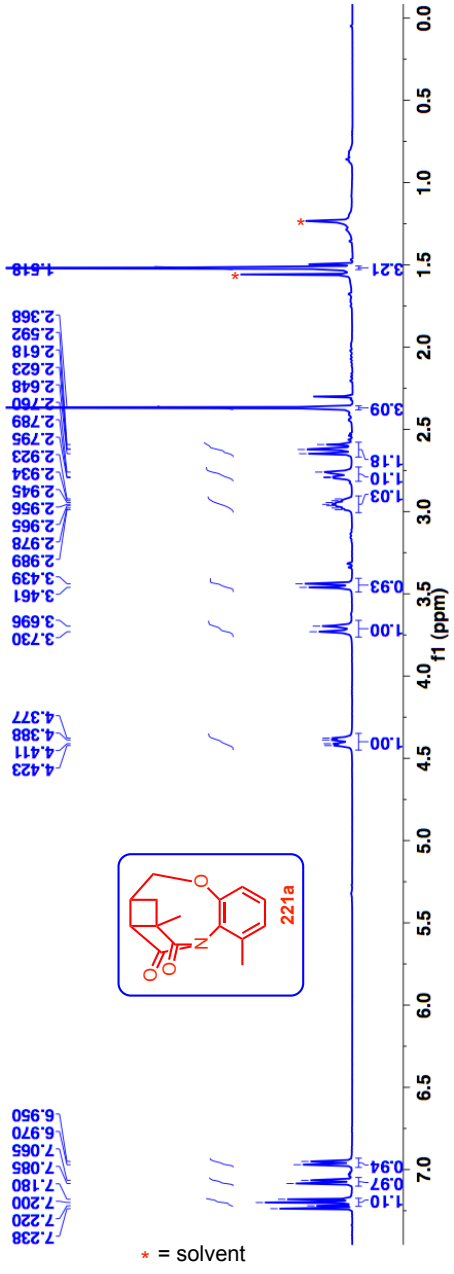

Figure 4.58: ^{1}H-NMR (400 MHz, $CDCl_3$, δ ppm) spectrum of cyclobutane photoproduct **221a**.

^{13}C-NMR (100 MHz, $CDCl_3$, δ ppm): 185.1, 179.8, 156.4, 139.3, 132.3, 129.8, 126.7, 120.4, 74.3, 51.76, 45.3, 37.4, 33.2, 19.6 and 17.6.

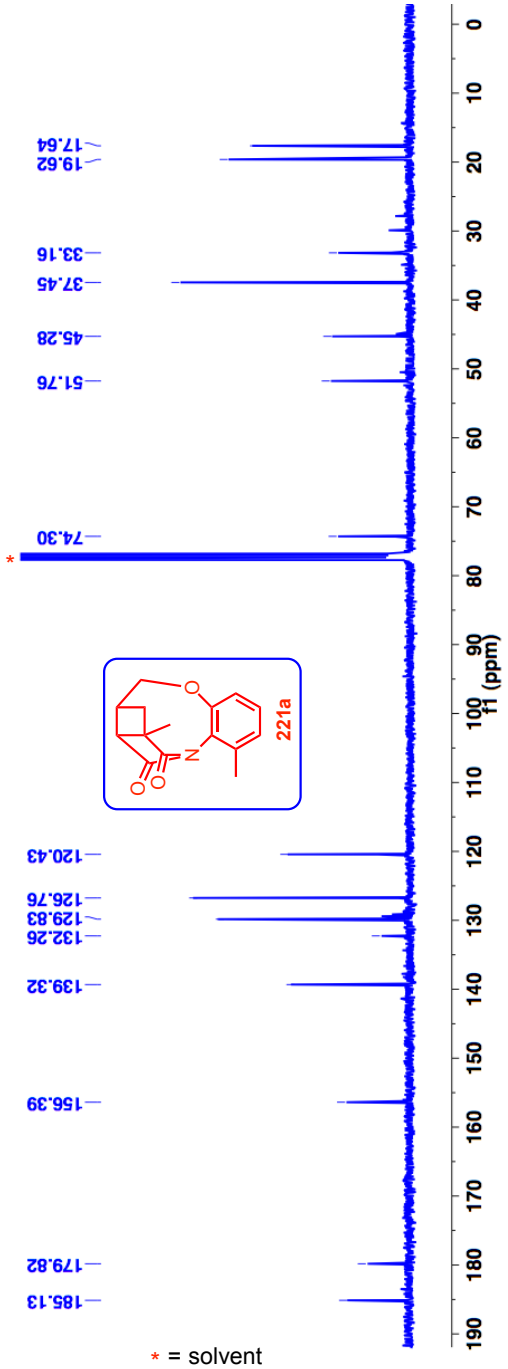

Figure 4.59: ^{13}C-NMR (100 MHz, $CDCl_3$, δ ppm) spectrum of cyclobutane photoproduct **221a**.

HRMS-ESI (m/z) ([M + Na]$^+$):

Calculated : 280.0944

Observed : 280.0942

|Δm| : 0.7 ppm

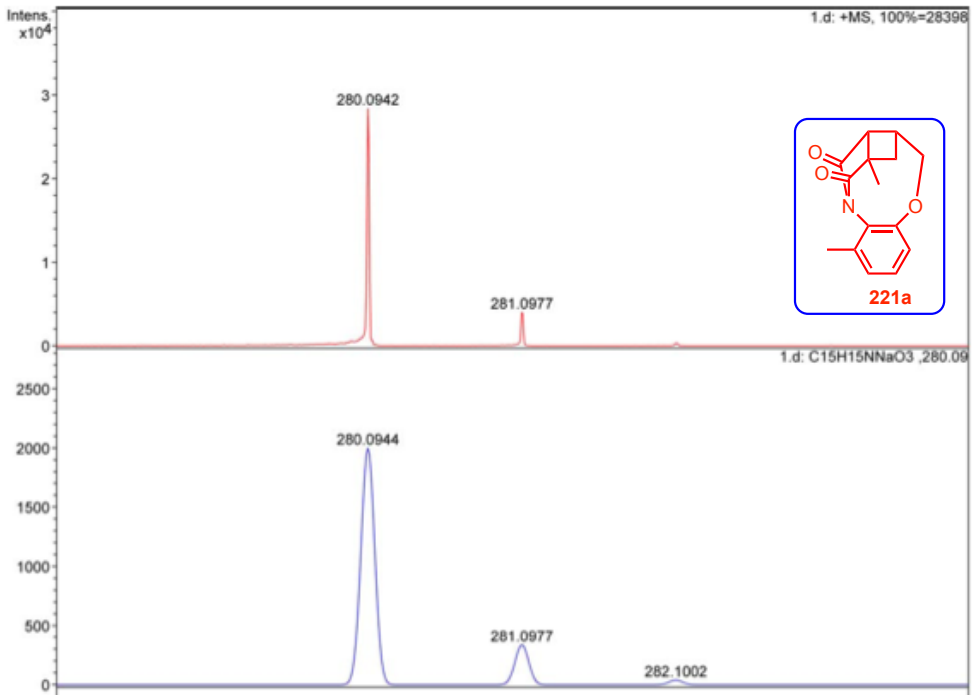

Figure 4.60: HRMS of cyclobutane photoproduct **221a**.

HPLC analysis conditions:

For analytical conditions,

I). Column : CHIRALPAK-OD-H

Abs. detector wavelength: 254 nm and 270 nm

Mobile phase : Hexanes:2-propanol = 90:10

Flow rate : 1.0 mL/min

Retention times (min) : ~10.92 [(*1R,5S,7S*)-**221a**] & ~12.64 [(*1S,5R,7R*)-**221a**]

For preparative conditions,

I). Column : CHIRALPAK-OD-H

Abs. detector wavelength : 254 nm and 270 nm

Mobile phase : Hexanes:2-propanol = 95:5

Flow rate : 3.0 mL/min

Retention times (min) : ~ 24.83 [(*1R,5S,7S*)-**221a**] & ~28.62 [(*1S,5R,7R*)-**221a**]

^{1}H-NMR (400 MHz, $CDCl_3$, δ ppm): 7.20-7.16 (m, 1H), 7.07-7.05 (m, 1H), 6.94-6.92 (m, 1H), 4.41 (dd, *J* = 13.6, 4.8 Hz, 1H), 3.69 (d, *J* = 13.6 Hz, 1H), 3.02-2.97 (m, 1H), 2.82 (s, 1H), 2.35 (s, 3H), 2.17-2.15 (m, 1H), 1.64 (s, 3H) and 1.55 (d, *J* = 7.6 Hz, 3H).

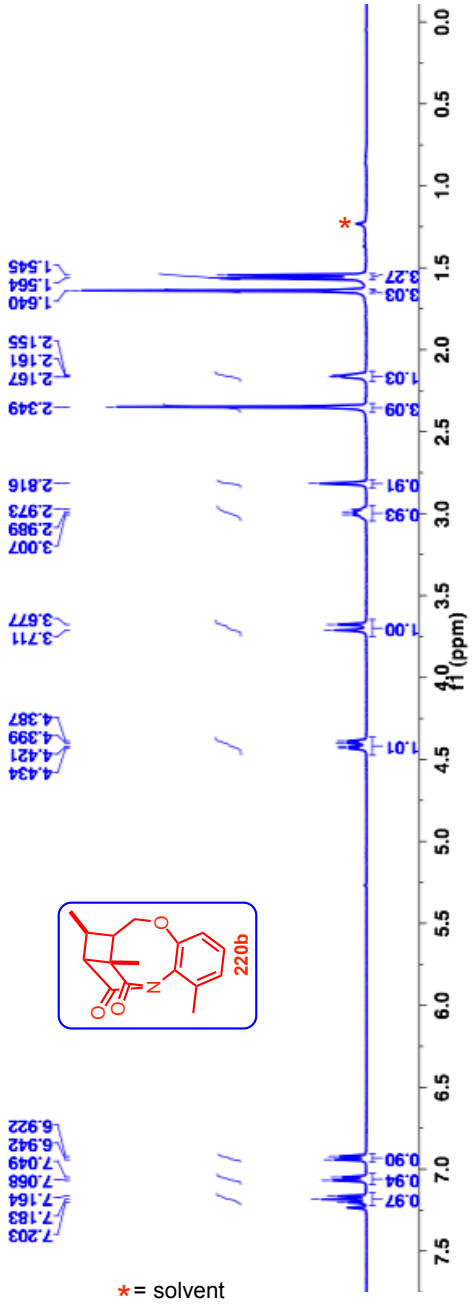

Figure 4.61: ^{1}H-NMR (400 MHz, $CDCl_3$, δ ppm) spectrum of cyclobutane photoproduct **220b**.

^{13}C-NMR (100 MHz, $CDCl_3$, δ ppm): 182.5, 181.6, 156.4, 139.4, 132.1, 129.8, 126.7, 120.4, 73.7, 55.3, 50.3, 49.2, 33.5, 21.4, 17.6 and 17.5.

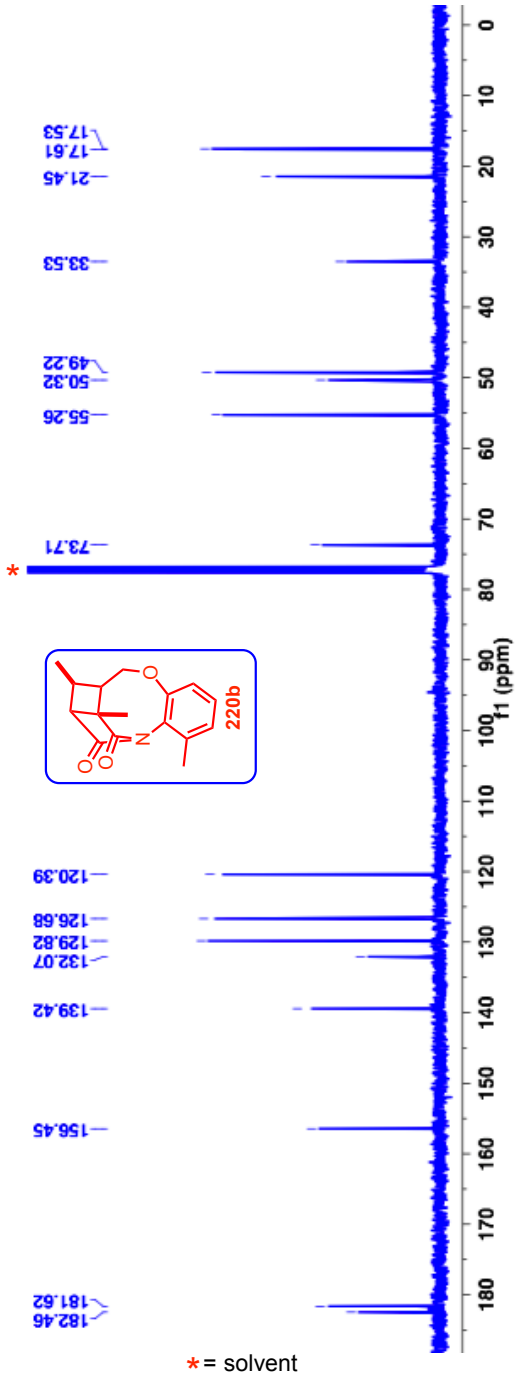

Figure 4.62: ^{13}C-NMR (100 MHz, $CDCl_3$, δ ppm) spectrum of cyclobutane photoproduct **220b**.

HRMS-ESI (m/z) ([M + Na]$^+$):

Calculated : 294.1101

Observed : 294.1094

|Δm| : 2.4 ppm

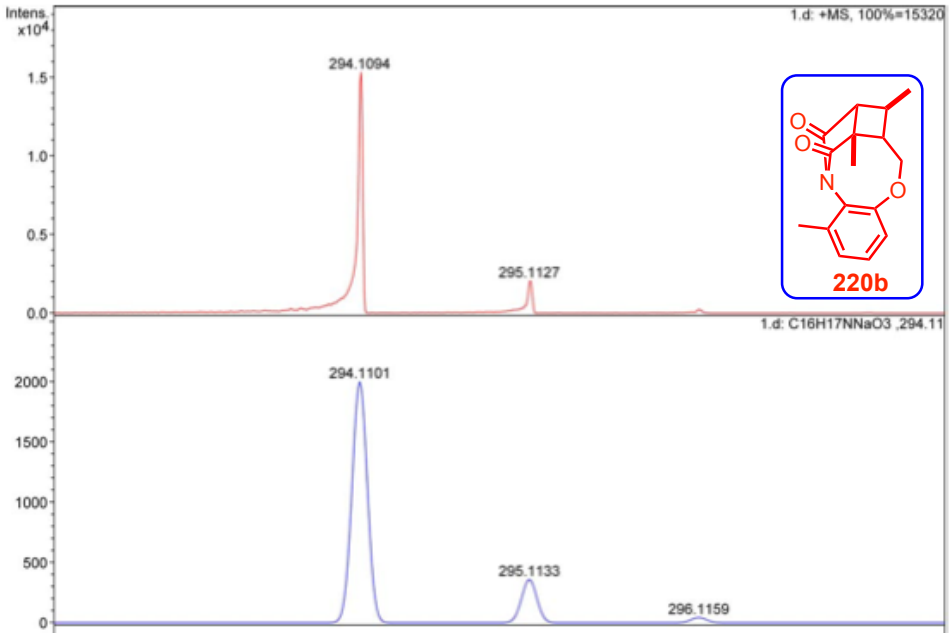

Figure 4.63: HRMS of cyclobutane photoproduct **220b**.

HPLC analysis conditions:

For analytical conditions,

I). Column : CHIRALPAK-AD-H

Abs. detector wavelength : 254 nm and 270 nm

Mobile phase : Hexanes:2-propanol = 95:5

Flow rate : 1.0 mL/min

Ret. tim. (min): ~14.03 [(-)-(*1R,5S,6R,7R*)- **220b**] and ~15.20 [(+)-(*1S,5R,6S,7S*)- **220b**]

For preparative conditions,

I). Column : CHIRALPAK-AD-H

Abs. detector wavelength : 254 nm and 270 nm

Mobile phase : Hexanes:2-propanol = 97:3

Flow rate : 3.0 mL/min

Ret. tim. (min): ~ 28.53 [(-)-(*1R,5S,6R,7R*)- **220b**] and ~40.17 [(+)-(*1S,5R,6S,7S*)- **220b**]

Optical rotation $[\alpha]_D^{27}$:

HPLC retention time (CHIRALPAK-ADH) at ~ 14.03 min, (*c* ~ 1.1%, $CHCl_3$) = -21.26 deg

HPLC retention time (CHIRALPAK-ADH) at ~ 15.20 min, (*c* ~ 1.1%, $CHCl_3$) = +21.27 deg.

^{1}H-NMR (400 MHz, $CDCl_3$, δ ppm): 7.71-7.66 (m, 2H, Major+minor), 7.56-7.51 (m, 2H, Major+minor), 7.46-7.24 (m, 6H, Major+minor), 7.09-7.06 (m, 1H, Major+minor), 6.87-.6.84 (m, 1H, Major+minor), 6.80-6.77 (m, 1H, Major+minor), 4.20-4.16 (m, 1H, Major+minor), 3.77-3.73 (m, 1H, Major+minor), 3.25-3.23 (m, 1H, minor), 2.99-2.94 (m, 1H, Major+minor), 2.93-2.90 (m, 1H, minor), 2.75-2.61 (m, 2H, major), 2.57-2.52 (m, 1H, major), 2.36-2.30 (m, 1H, minor), 2.07 (s, 3H, major), 2.06 (s, 3H, minor), 1.54 (s, 3H, major) and 1.52 (s, 3H, minor)

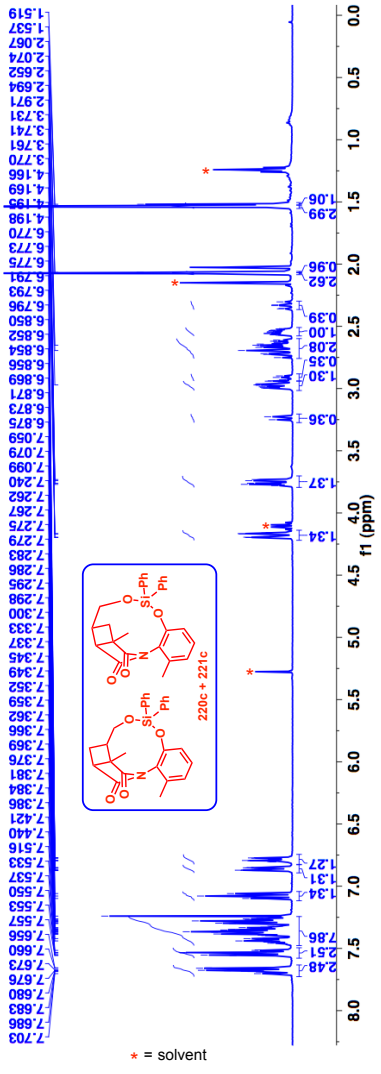

Figure 4.64: ^{1}H-NMR (400 MHz, $CDCl_3$+CD_3OD, δ ppm) spectrum of cyclobutane photoproducts **220c** and **221c**.

^{13}C-NMR (100 MHz, $CDCl_3$, δ ppm): 181.3, 178.7, 177.9, 175.9, 150.8, 137.4, 135.7, 135.5, 135.3, 135.2, 135.2, 134.6, 131.0, 131.0, 130.6, 130.4, 130.3, 130.2, 130.1, 129.7, 128.5, 128.2, 128.2, 128.1, 128.06, 128.0, 124.8, 124.7, 123.0, 122.8, 120.4, 62.7, 62.4, 47.3, 46.9, 44.98, 43.3, 42.4, 33.5, 30.0, 21.8, 20.6, 20.3, 18.3 and 18.1.

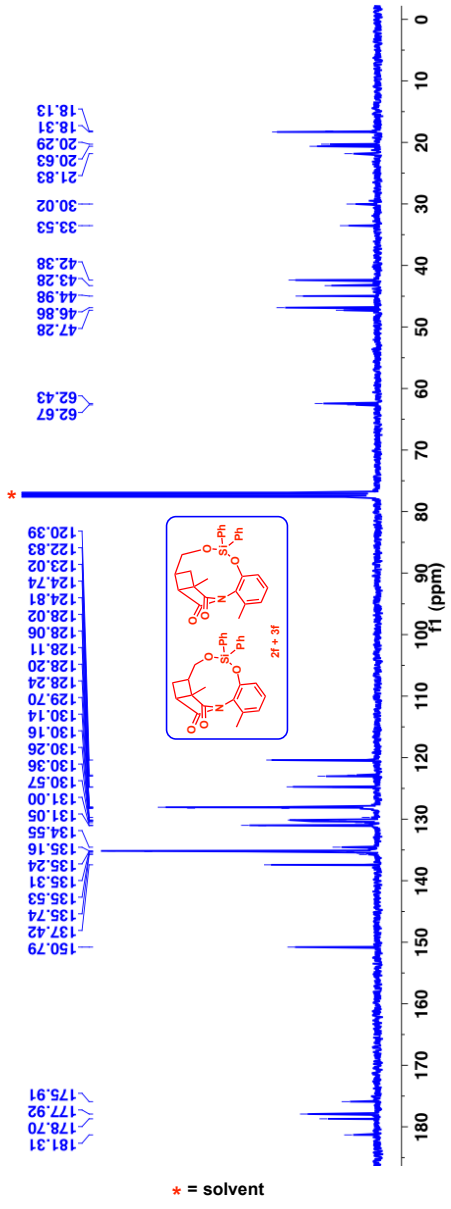

Figure 4.65: ^{13}C-NMR (100 MHz, $CDCl_3$+CD_3OD, δ ppm) spectrum of cyclobutane photoproducts **220c** and **221c**.

HRMS-ESI (m/z) ([M + Na]$^+$):

Calculated : 478.1445

Observed : 478.1442

|Δm| : 0.6 ppm

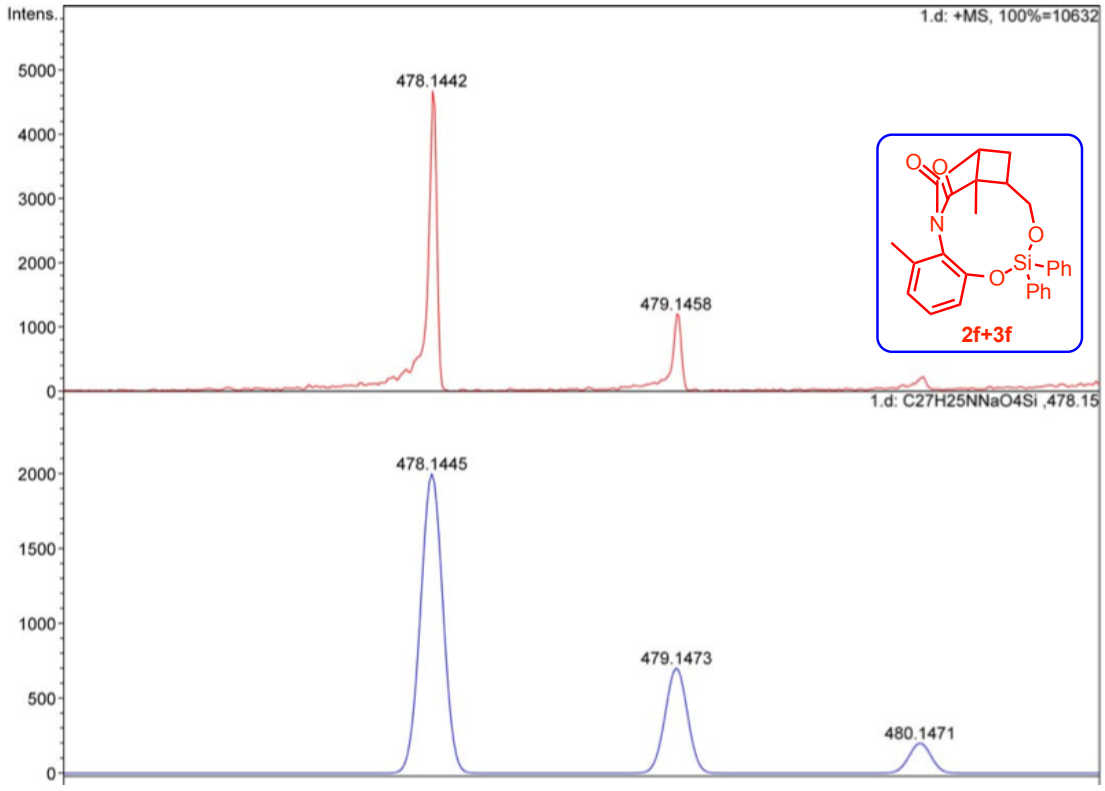

Figure 4.66: HRMS of cyclobutane photoproducts **220c** and **221c**.

^{1}H-NMR (400 MHz, $CDCl_3$+CD_3OD, δ ppm): 7.19-7.16 (m, 2H), 7.07-7.04 (m, 1H), 3.09-2.99 (m, 2H), 2.80-2.59 (m, 3H), 2.25 (s, 3H), 2.21-2.14 (m, 1H), 2.12-2.03 (m, 1H), 1.68-1.62 (m, 1H) and 1.50 (s, 3H).

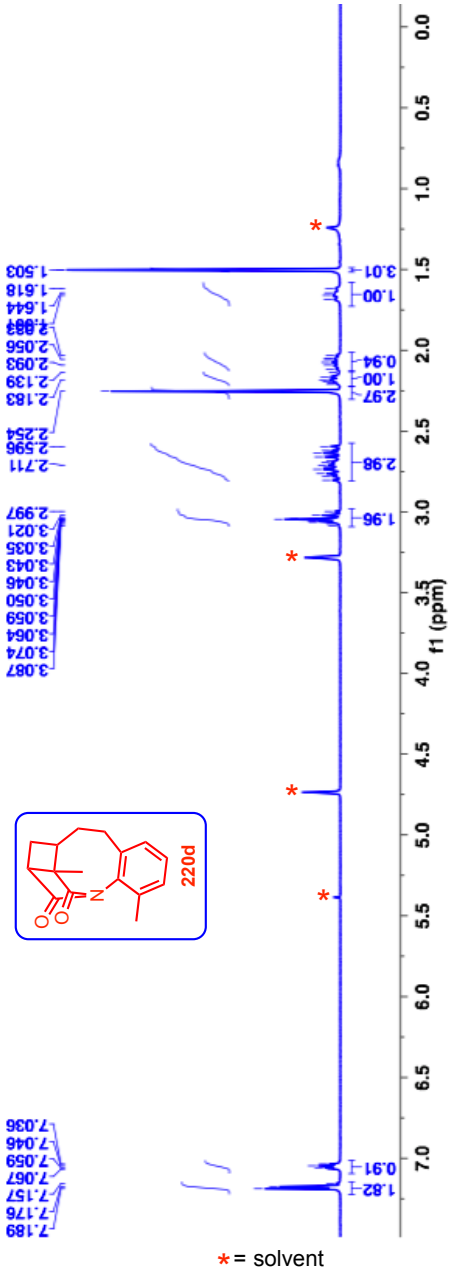

Figure 4.67: ^{1}H (400 MHz, $CDCl_3$, δ ppm) spectrum of cyclobutane photoproduct **220d**.

^{13}C-NMR (100 MHz, $CDCl_3$+CD_3OD, δ ppm): 185.5, 185.3, 145.5, 141.6, 138.4, 133.1, 132.9, 132.8, 54.8, 50.7, 46.6, 33.5, 31.5, 27.2, 20.5 and 18.5.

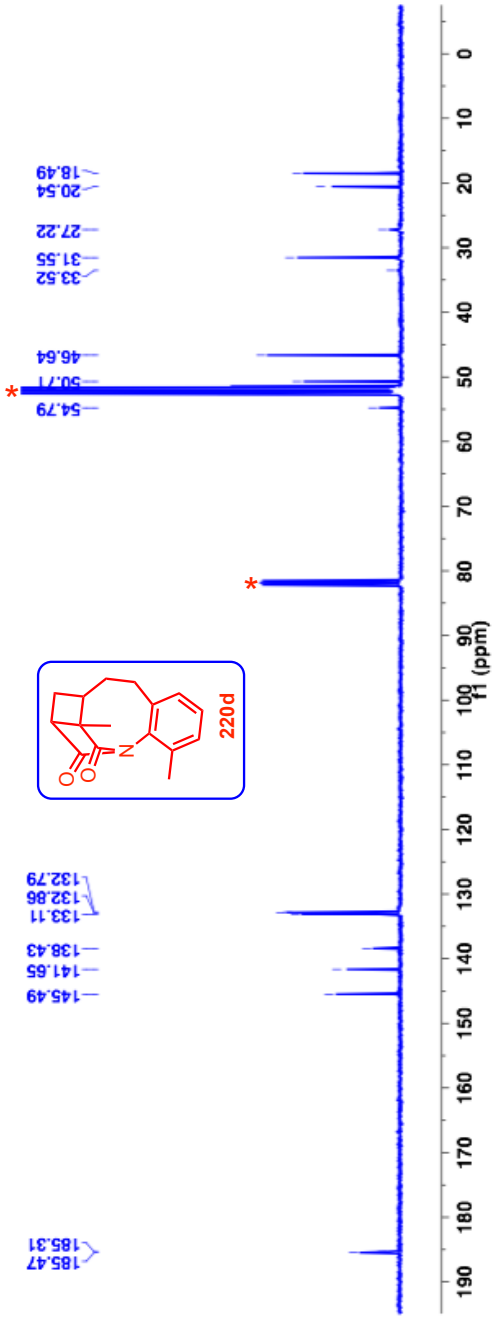

Figure 4.68: ^{13}C-NMR (100 MHz, $CDCl_3$, δ ppm) spectrum of cyclobutane photoproduct **220d**.

HRMS-ESI (m/z) ([M + Na]$^+$):

Calculated : 278.1151

Observed : 278.1158

|Δm| : 2.5 ppm

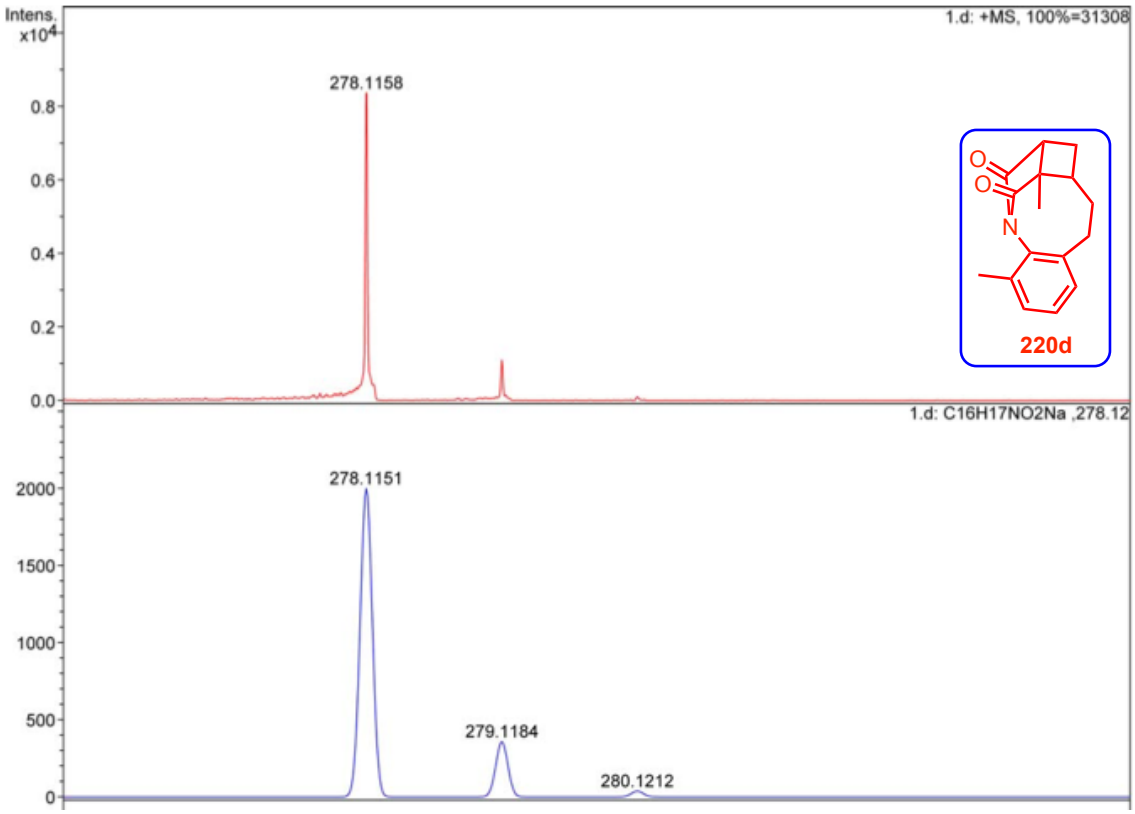

Figure 4.69: HRMS of cyclobutane photoproduct **220d**.

^{1}H-NMR (400 MHz, $CDCl_3$, δ ppm): 7.19-7.16 (m, 2H), 7.04-7.02 (m, 1H), 3.38-3.32 (m, 1H), 3.18-3.12 (m, 1H), 2.79 (dd, *J* = 16.3, 10.4 Hz, 1H), 2.65–2.53 (m, 2H), 2.45-2.41 (m, 1H), 2.30 (s, 3H), 2.11-2.03 (m, 1H), 1.75-1.68 (dd, *J* = 16.0, 10.4 Hz, 1H) and 1.50 (s, 3H).

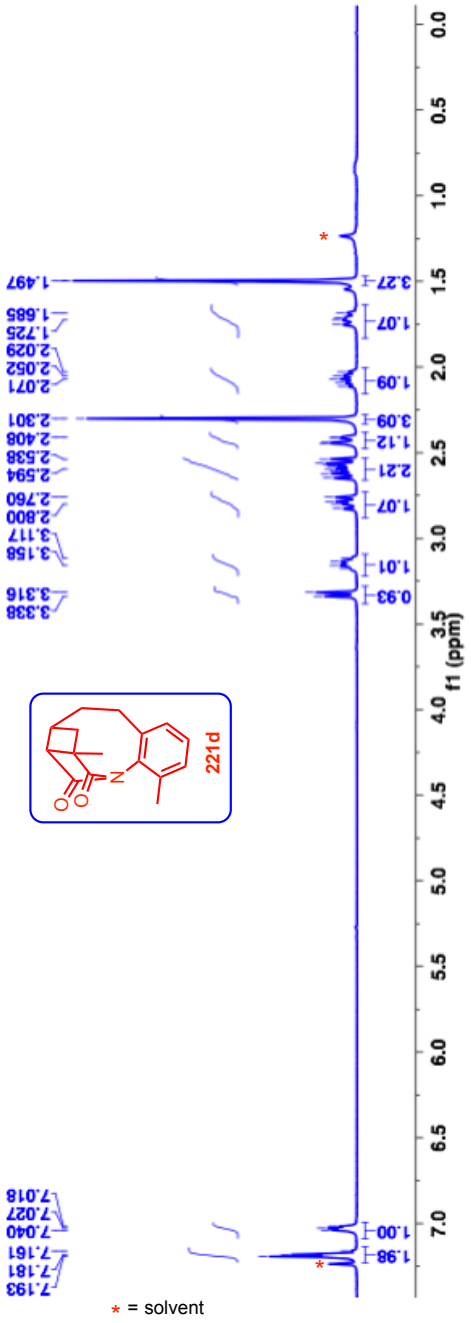

Figure 4.70: ^{1}H-NMR (400 MHz, $CDCl_3$, δ ppm) spectrum of cyclobutane photoproduct **221d**.

^{13}C-NMR (100 MHz, $CDCl_3$, δ ppm): 183.5, 178.7, 150.1, 141.4, 137.8, 134.4, 129.4, 129.1, 50.5, 44.96, 34.9, 33.3, 27.8, 27.4, 19.6 and 17.5.

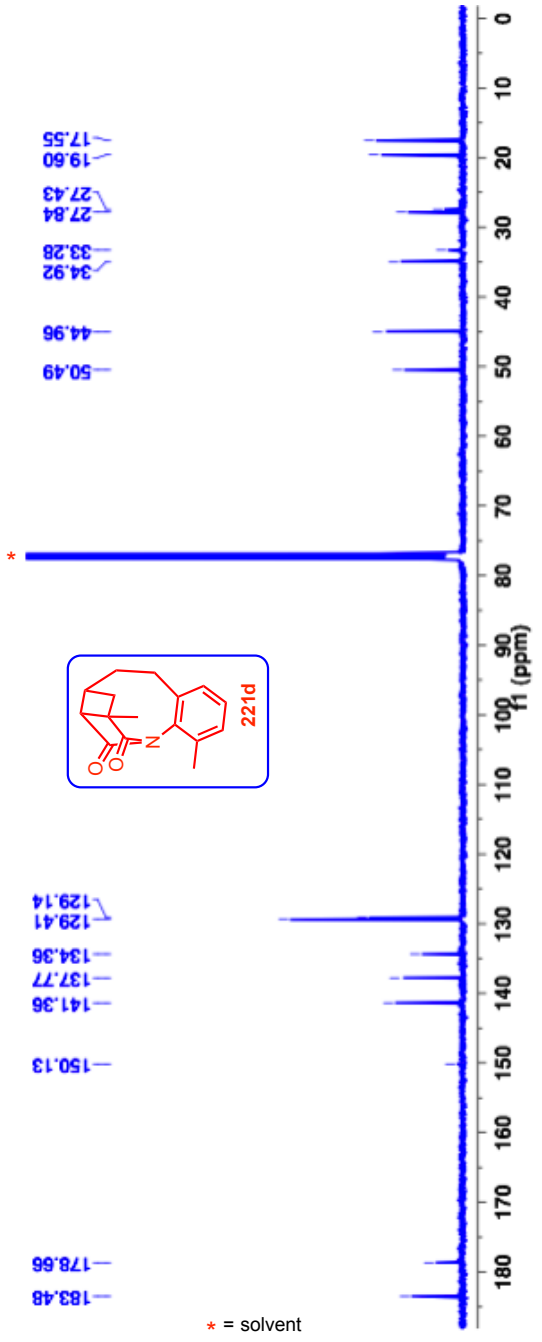

Figure 4.71: ^{13}C-NMR (100 MHz, $CDCl_3$, δ ppm) spectrum of cyclobutane photoproduct **221d**.

HRMS-ESI (m/z) ([M + Na]$^+$):

Calculated : 278.1151

Observed : 278.1153

|Δm| : 0.7 ppm

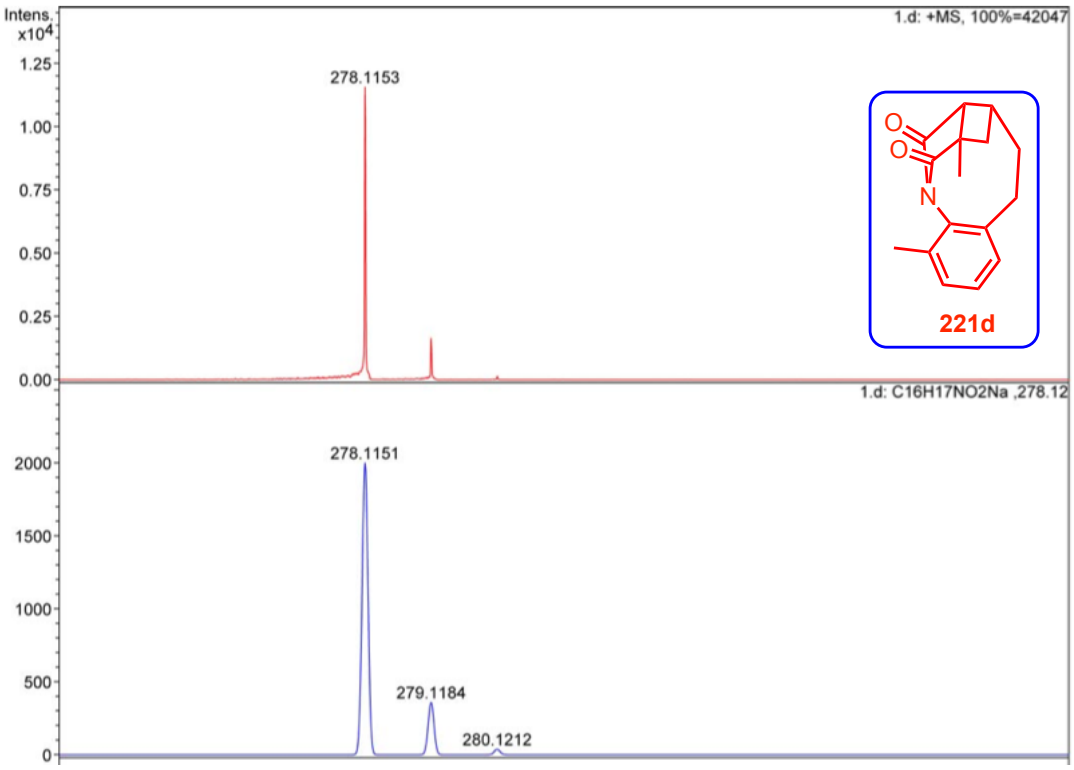

Figure 4.72: HRMS of cyclobutane photoproduct **221d**.

^{1}H-NMR (400 MHz, $CDCl_3$, δ ppm): 7.50-7.42 (m, 4H), 7.37-7.34 (m, 1H), 7.25-7.21 (m, 1H), 7.11-7.07 (m, 1H), 7.03-7.01 (m, 1H), 4.54 (dd, *J* = 14, 4.4 Hz, 1H), 3.98 (d, *J* = 14 Hz, 1H), 3.76-3.74 (m, 1H), 3.17-3.04 (m, 2H), 2.74 (d, *J* =11.6 Hz, 1H) and 2.36 (s, 3H).

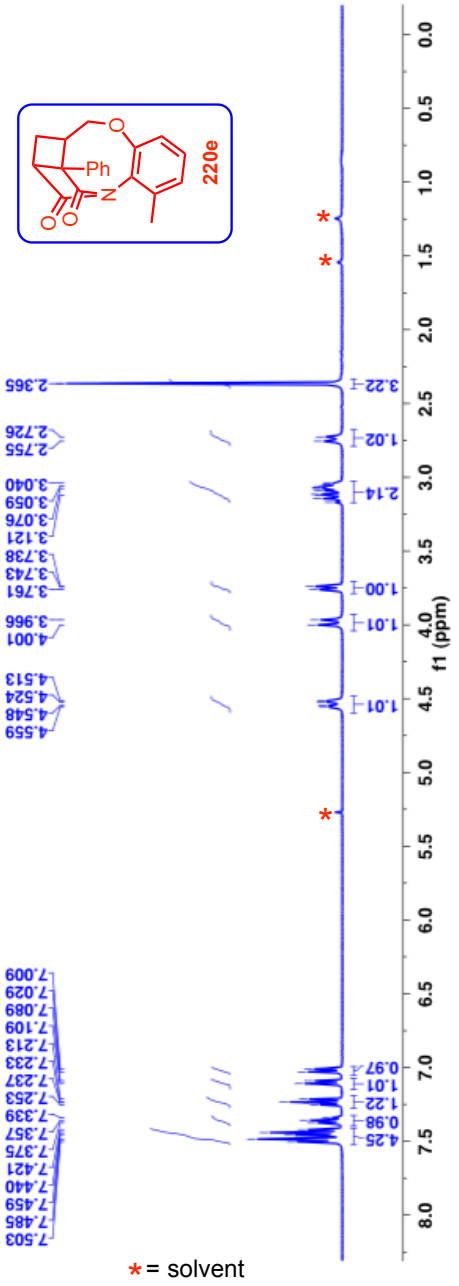

Figure 4.73: ^{1}H-NMR (400 MHz, $CDCl_3$, δ ppm) spectrum of cyclobutane photoproduct **220e**.

^{13}C-NMR (100 MHz, $CDCl_3$, δ ppm): 181.4, 179.3, 156.5, 140.4, 139.5, 135.0, 132.4, 129.9, 129.1, 128.2, 126.9, 120.4, 74.7, 59.5, 50.9, 42.96, 24.9 and 17.6.

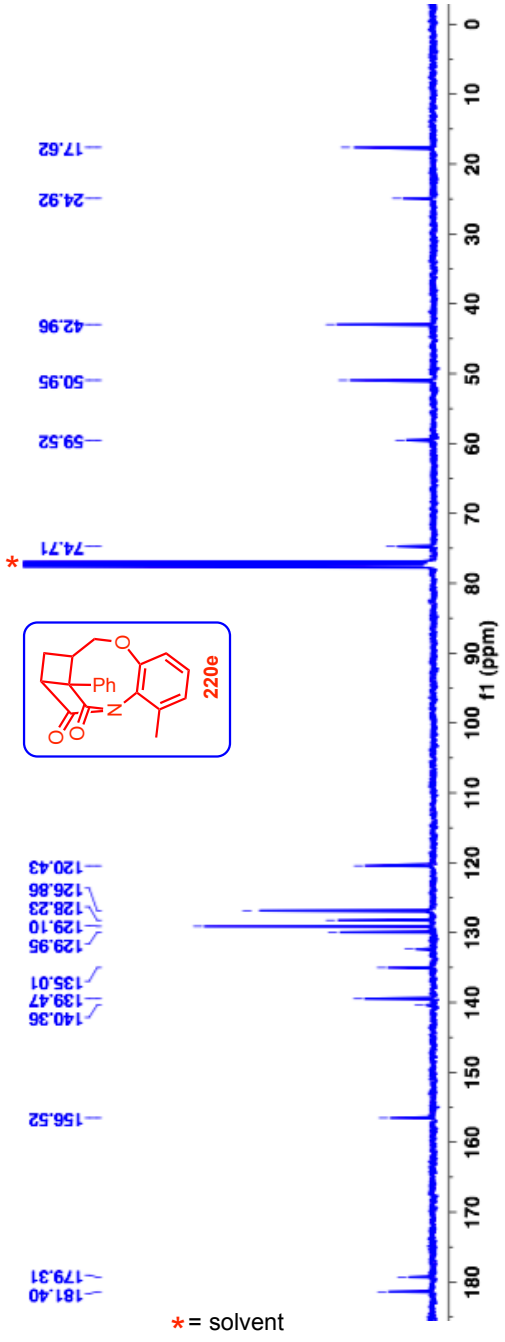

Figure 4.74: ^{13}C-NMR (100 MHz, $CDCl_3$, δ ppm) spectrum of cyclobutane photoproduct **220e**.

HRMS-ESI (m/z) ([M + Na]$^+$):

Calculated : 342.1101

Observed : 342.1094

|Δm| : 2.0 ppm

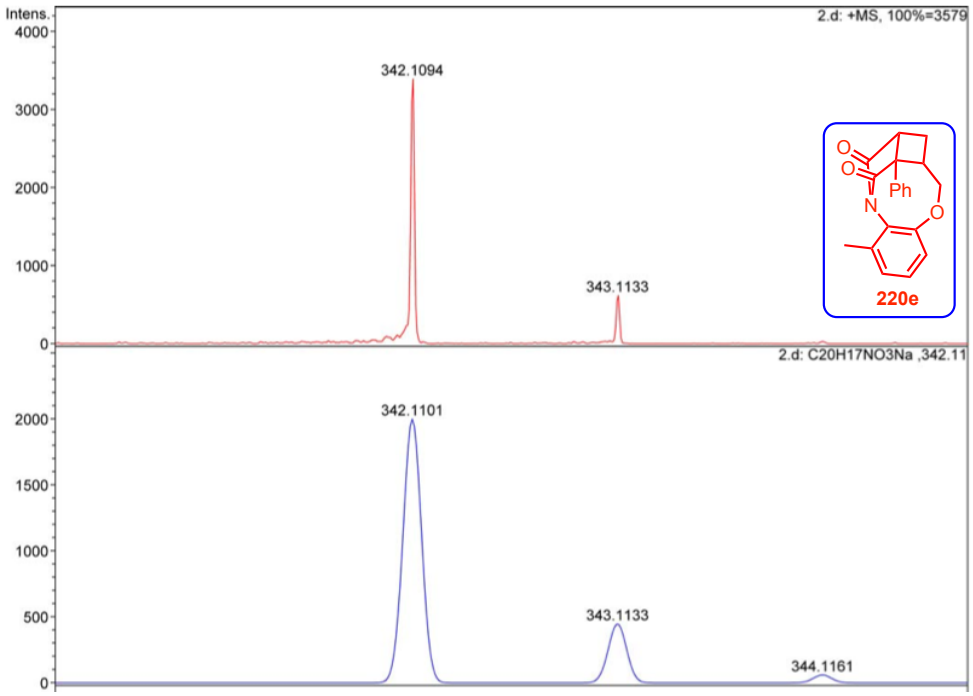

Figure 4.75: HRMS of cyclobutane photoproduct **220e**.

HPLC analysis conditions:

For analytical conditions,

I). Column : CHIRALPAK-AD-H

Abs. detector wavelength : 254 nm and 270 nm

Mobile phase : Hexanes:2-propanol = 90:10

Flow rate : 1.0 mL/min

Retention times (min) : ~11.28 [(-)-(*1R,5S,6R*)-**220e**] & ~16.64 [(+)-(*1S,5R,6S*)-**220e**]

For preparative conditions,

I). Column : CHIRALPAK-AD-H

Abs. detector wavelength : 254 nm and 270 nm

Mobile phase : Hexanes:2-propanol = 97:3

Flow rate : 3.0 mL/min

Retention times (min) : ~ 34.85 [(-)-(*1R,5S,6R*)-**220e**] & ~55.75 [(+)-(*1S,5R,6S*)-**220e**]

Optical rotation $[\alpha]_D^{23}$:

HPLC retention time (CHIRALPAK-ADH) at ~ 11.28 min, (*c* ~ 0.690 %, $CHCl_3$) = -85.22 deg

HPLC retention time (CHIRALPAK-ADH) at ~ 16.64 min, (*c* ~ 0.690 %, $CHCl_3$) = +84.66 deg.

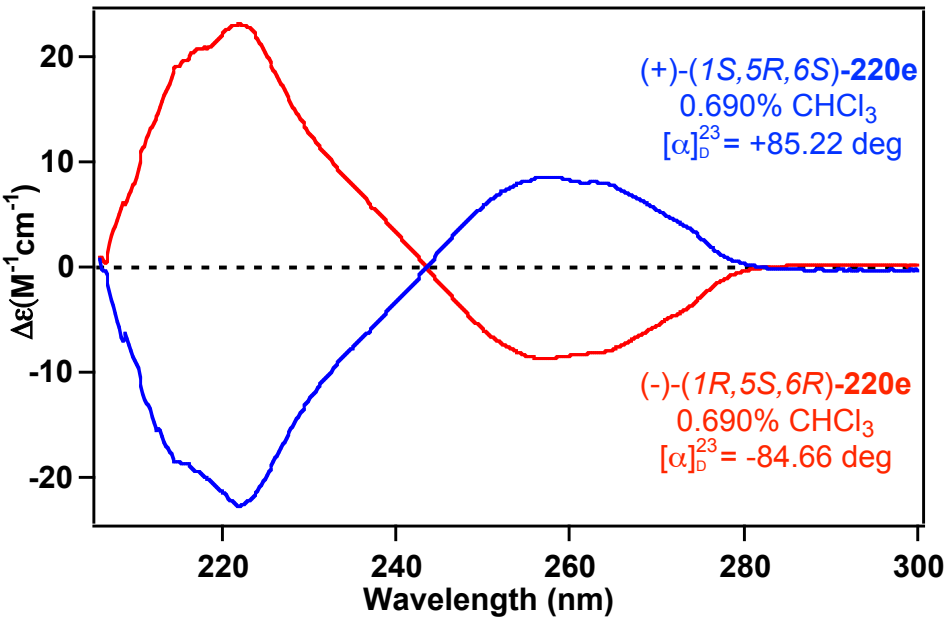

Figure 4.76: CD spectrum of cyclobutane photoproduct **220e** measured in MeOH (c ~ 0.1 mM).

^{1}H-NMR (400 MHz, $CDCl_3$, δ ppm): 7.26–7.16 (m, 2H), 7.04-7.02 (m, 1H), 3.48–3.45 (m, 1H), 3.37–3.28 (m, 2H), 2.82 (dd, *J* = 16.8, 10.4 Hz, 1H), 2.67 (dd, *J* = 16.8, 10.0 Hz, 1H), 2.34-2.32 (m, 1H), 2.31 (s, 3H), 2.12-2.04 (m, 1H) and 1.86 (dd, *J* = 16.7, 10.0 Hz, 1H).

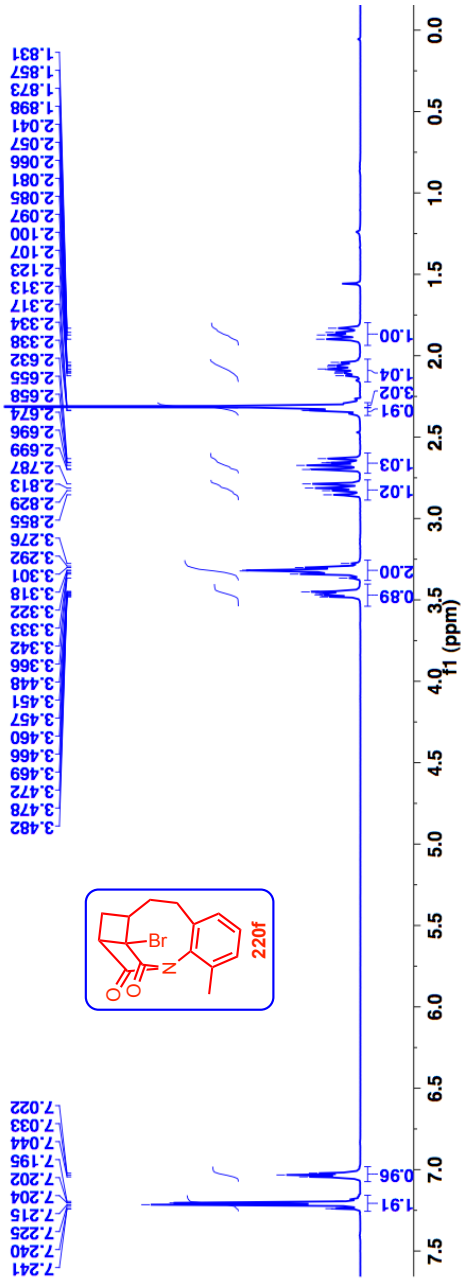

Figure 4.77: ^{1}H-NMR (400 MHz, $CDCl_3$, δ ppm) spectrum of cyclobutane photoproduct **220f**.

^{13}C-NMR (100 MHz, $CDCl_3$, δ ppm): 177.4, 173.9, 140.7, 138.0, 134.2, 129.8, 129.7, 129.2, 55.4, 51.7, 47.3, 27.9, 27.8, 24.5 and 17.6.

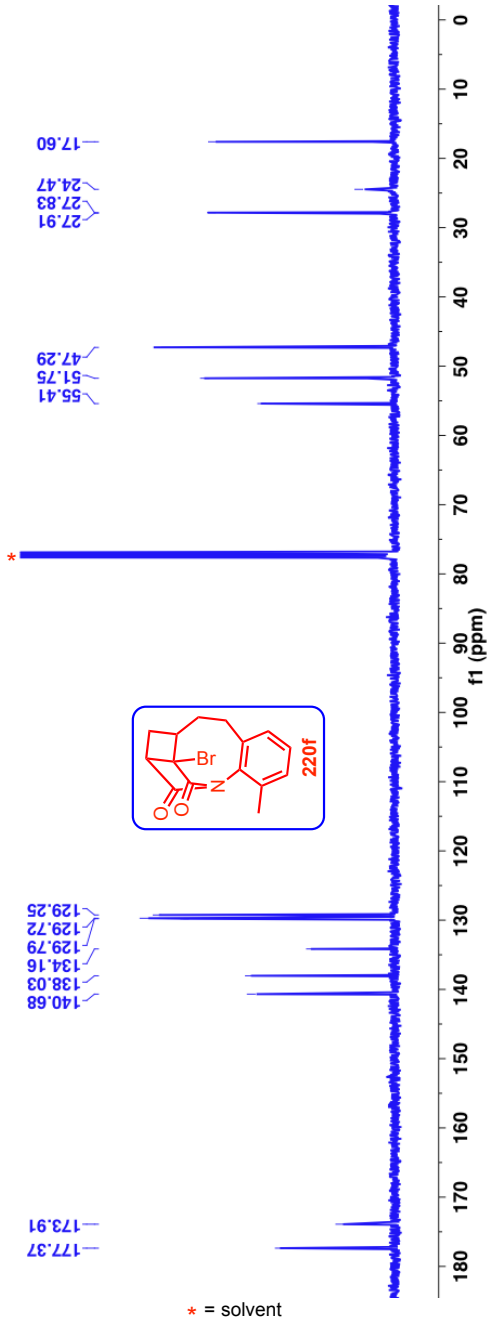

Figure 4.78: ^{13}C-NMR (400 MHz, $CDCl_3$, δ ppm) spectrum of cyclobutane photoproduct **220f**.

HRMS-ESI (m/z) ([M + Na]$^+$):

Calculated : 342.0100

Observed : 342.0098

|Δm| : 0.6 ppm

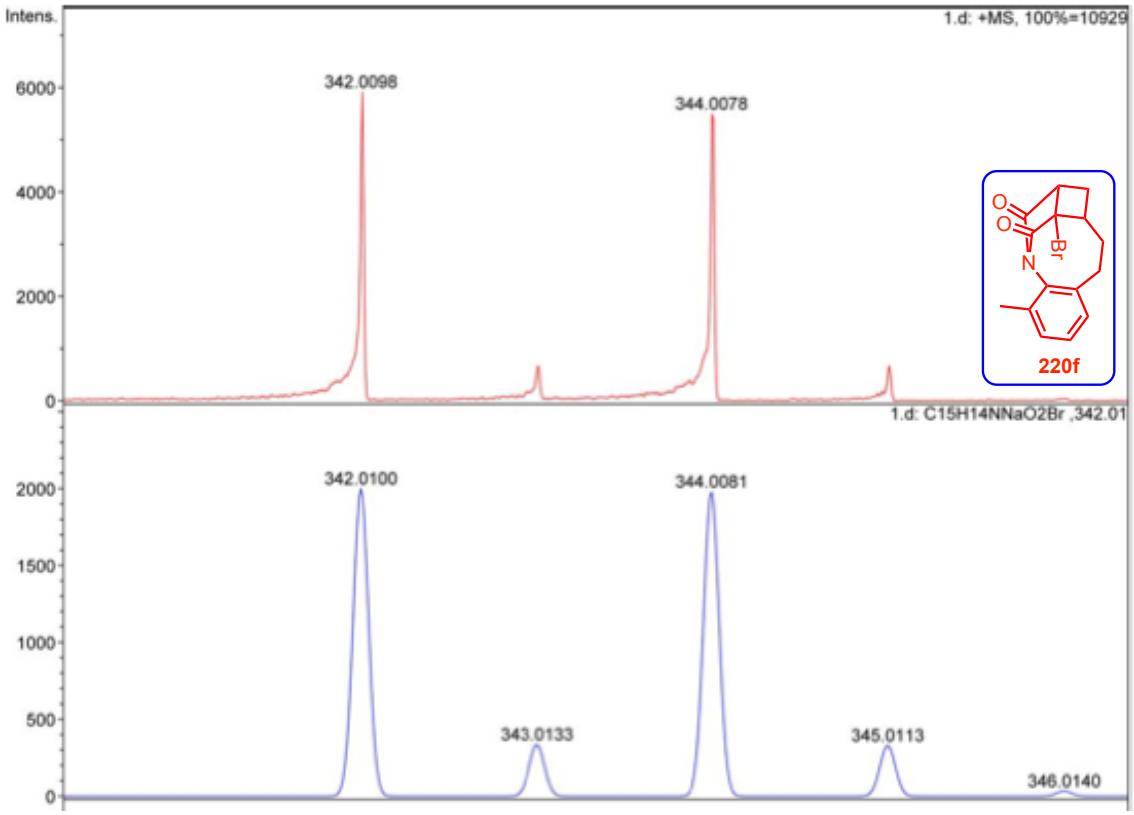

Figure 4.79: HRMS of cyclobutane photoproduct **220f**.

^{1}H-NMR (400 MHz, $CDCl_3$, δ ppm): 7.22-7.20 (m, 2H), 7.04-7.02 (m, 1H), 3.85 (d, *J* = 9.6 Hz, 1H), 3.44-3.37 (m, 1H), 3.16 (dd, *J* = 13.2, 10.8 Hz, 1H), 2.89-2.86 (m, 1H), 2.75-2.61 (m, 2H), 2.33 (s, 3H), 2.16-2.06 (m, 1H) and 1.699-1.61 (m, 1H).

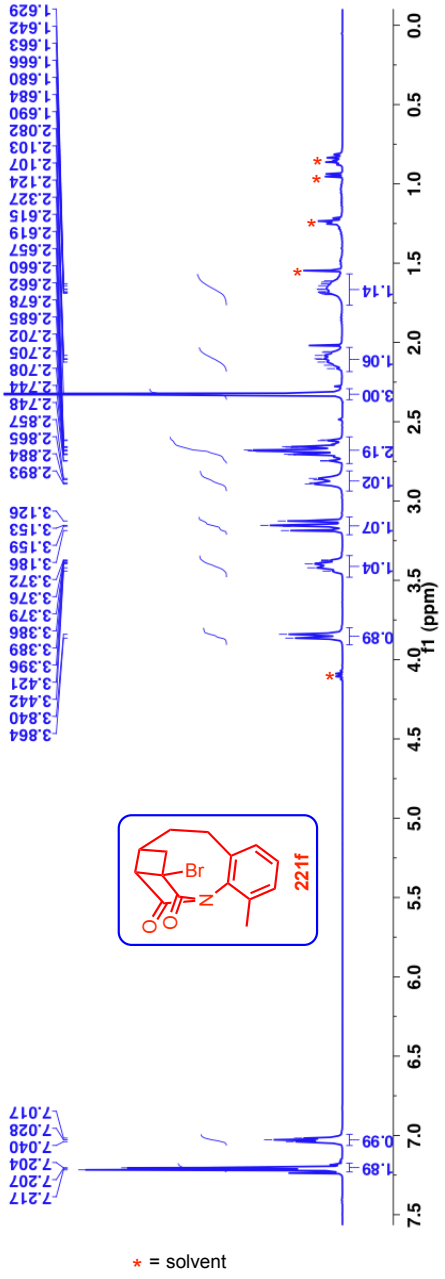

Figure 4.80: ^{1}H-NMR (400 MHz, $CDCl_3$, δ ppm) spectrum of cyclobutane photoproduct **221f**.

^{13}C-NMR (100 MHz, $CDCl_3$, δ ppm): 176.6, 175.5, 140.9, 137.9, 133.8, 129.8, 129.7, 129.2, 54.7, 45.5, 37.2, 36.7, 27.7, 26.8 and 17.6.

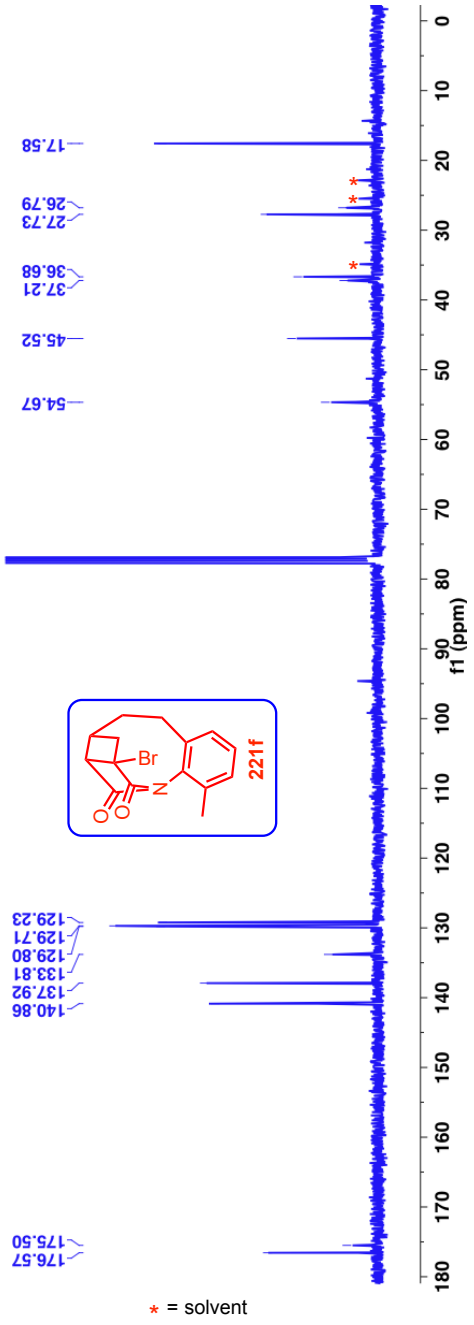

Figure 4.81: ^{13}C-NMR (100 MHz, $CDCl_3$, δ ppm) spectrum of cyclobutane photoproduct **221f**.

HRMS-ESI (m/z) ([M + Na]$^+$):

Calculated : 342.0100

Observed : 342.0096

|Δm| : 1.2 ppm

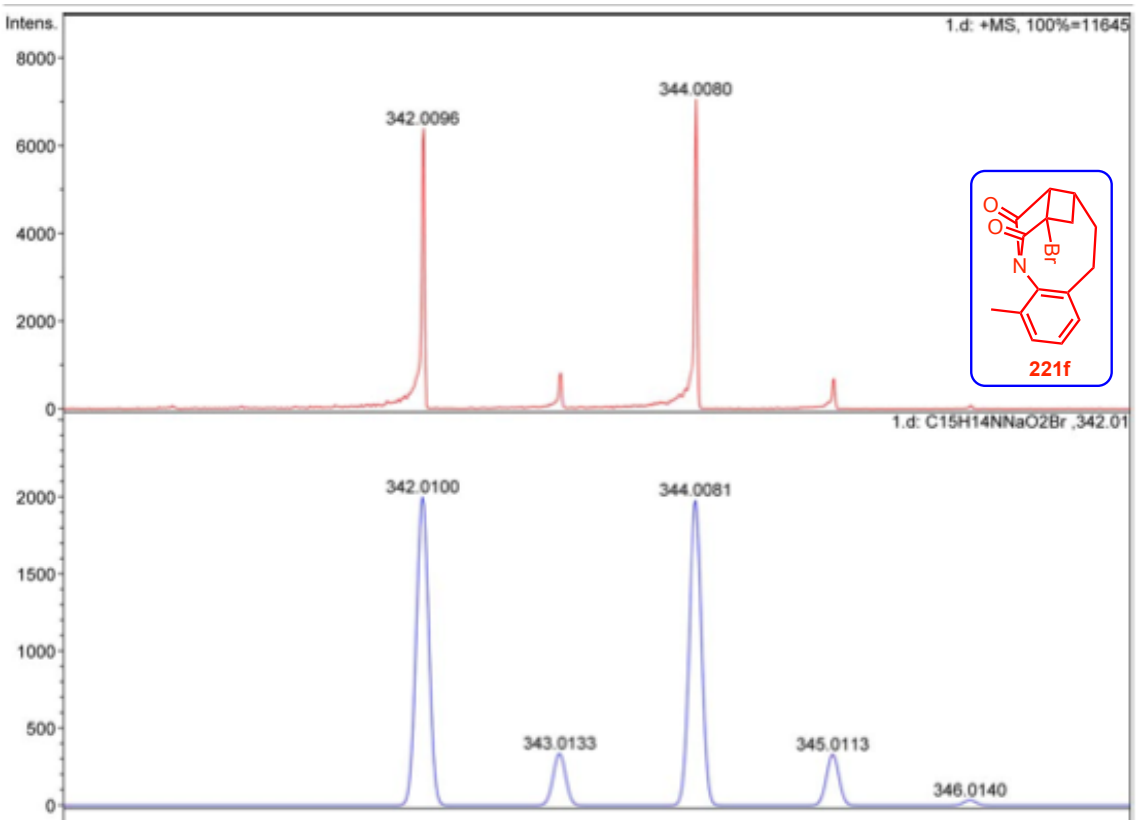

Figure 4.82: HRMS of cyclobutane photoproduct **221f**.

^{1}H-NMR (400 MHz, $CDCl_3$, δ ppm): 7.24-7.20 (m, 1H), 7.10-7.08 (m, 1H), 6.97-6.95 (m, 1H), 4.37 (dd, *J* = 14.0, 5.2 Hz, 1H), 3.86 – 3.73 (m, 1H), 3.05 (m, 1H), 2.82 (m, 2H), 2.37 (s, 3H) and 1.53 (s, 3H).

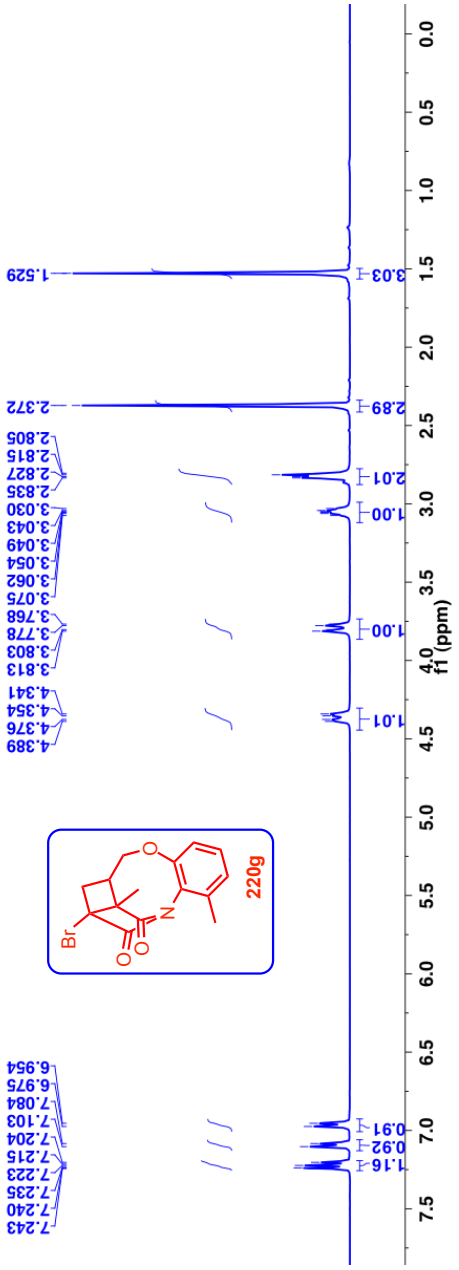

Figure 4.83: ^{1}H-NMR (400 MHz, $CDCl_3$, δ ppm) spectrum of cyclobutane photoproduct **220g**.

^{13}C-NMR (100 MHz, $CDCl_3$, δ ppm): 181.4, 175.0, 156.4, 139.5, 131.5, 130.2, 127.1, 120.4, 73.6, 62.6, 51.0, 49.6, 31.5, 19.2 and 17.7.

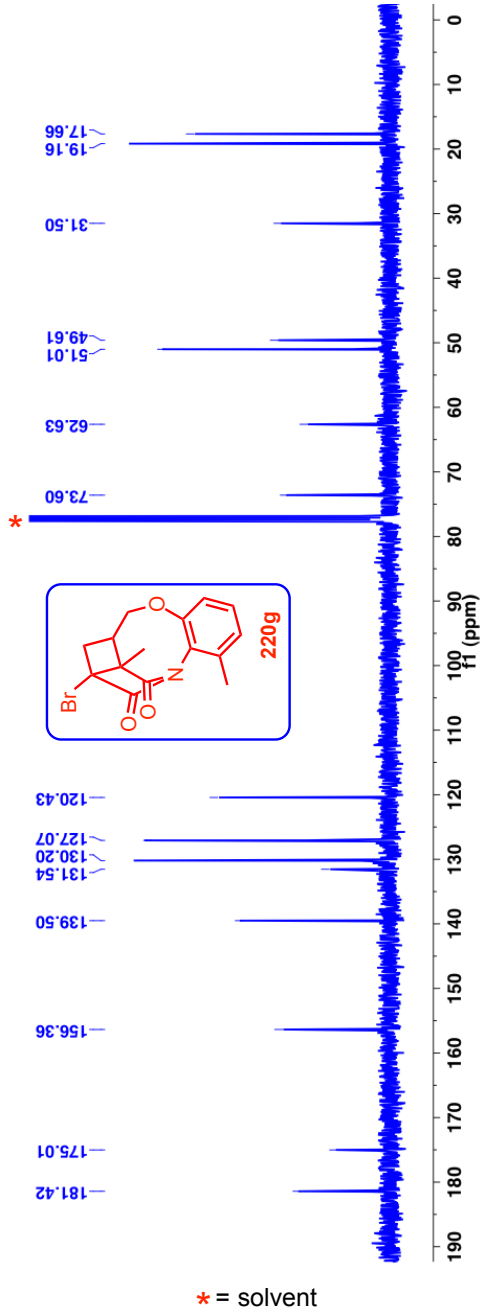

Figure 4.84: ^{13}C-NMR (100 MHz, $CDCl_3$, δ ppm) spectrum of cyclobutane photoproduct **220g**.

HRMS-ESI (m/z) ([M + Na]$^+$):

Calculated : 358.0049

Observed : 358.0055

|Δm| : 1.7 ppm

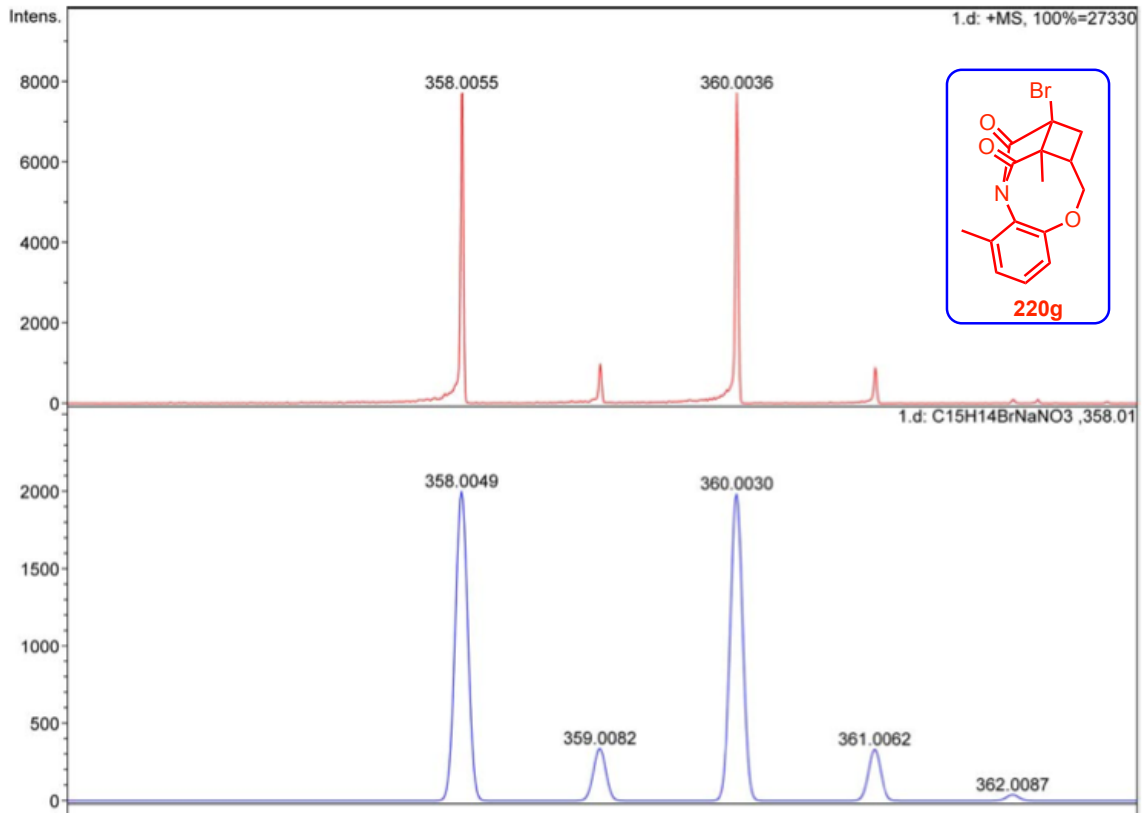

Figure 4.85: HRMS of cyclobutane photoproduct **220g**.

4.12. References

(1) Tedaldi, L. M.; Aliev, A. E.; Baker, J. R. [2 + 2] Photocycloadditions of thiomaleimides. *Chem. Commun.* **2012**, *48*, 4725-4727.

(2) Obata, T.; Shimo, T.; Suishu, T.; Somekawa, K. Stereoselective photo[4+2]-cycloadditions of 2-pyrone-5-carboxylates with maleimides in the solid state and in solution. *J. Heterocycl. Chem.* **1998**, *35*, 1361-1364.

(3) Cubbage, K. L.; Orr-Ewing, A. J.; Booker-Milburn, K. I. First Higher-Order Photocycloaddition to a C-N Bond: 1,3-Diazepines from Maleimides. *Angew. Chem. Int. Ed.* **2009**, *48*, 2514-2517.

(4) Booker-Milburn, K. I.; Anson, C. E.; Clissold, C.; Costin, N. J.; Dainty, R. F.; Murray, M.; Patel, D.; Sharpe, A. Intramolecular Photocycloaddition of N-Alkenyl Substituted Maleimides: A Potential Tool for the Rapid Construction of Perhydroazaazulene Alkaloids. *Eur. J. Org. Chem.* **2001**, 1473-1482.

(5) Gülten, Ş.; Sharpe, A.; Baker, J. R.; Booker-Milburn, K. I. Use of temporary tethers in the intramolecular [2+2] photocycloaddition reactions of tetrahydrophthalimide derivatives: a new approach to complex tricyclic lactones. *Tetrahedron* **2007**, *63*, 3659-3671.

(6) Roscini, C.; Cubbage, K. L.; Berry, M.; Orr-Ewing, A. J.; Booker-Milburn, K. I. Reaction Control in Synthetic Organic Photochemistry: Switching between [5+2] and [2+2] Modes of Cycloaddition. *Angew. Chem. Int. Ed.* **2009**, *48*, 8716-8720.

(7) Miller, C. W.; Jönsson, E. S.; Hoyle, C. E.; Viswanathan, K.; Valente, E. J. Evaluation of N-Aromatic Maleimides as Free Radical Photoinitiators: A Photophysical and Photopolymerization Characterization. *J. Phys. Chem. B* **2001**, *105*, 2707-2717.

(8) Curran, D. P.; Qi, H.; Geib, S. J.; DeMello, N. C. Atroposelective Thermal Reactions of Axially Twisted Amides and Imides. *J. Am. Chem. Soc.* **1994**, *116*, 3131-3132.

(9) Kumarasamy, E.; Raghunathan, R.; Jockusch, S.; Ugrinov, A.; Sivaguru, J. Tailoring Atropisomeric Maleimides for Stereospecific [2+2] Photocycloaddition-Photochemical and Photophysical Investigations Leading to Visible-Light Photocatalysis. *J. Am. Chem. Soc.* **2014**, *136*, 8729-8737.

(10) Schmidt, R.; Tanielian, C.; Dunsbach, R.; Wolff, C. Phenalenone, a universal reference compound for the determination of quantum yields of singlet oxygen O2(1Δg) sensitization. *J. Photochem. Photobiol., A* **1994**, *79*, 11-17.

(11) Turro, N. J.; Ramamurthy, V.; Scaiano, J. C.: *Modern Molecular Photochemistry of Organic Molecules*; University Science Books: Sausalito, CA, 2010.

(12) Put, J.; De Schryver, F. C. Photochemistry of nonconjugated bichromophoric systems. Intramolecular photocycloaddition of N,N'-alkylenedimaleimides in solution. *J. Am. Chem. Soc.* **1973**, *95*, 137-145.

(13) Hembury, G. A.; Borovkov, V. V.; Inoue, Y. Chirality-Sensing Supramolecular Systems. *Chem. Rev.* **2007**, *108*, 1-73.

(14) Yagci, Y.; Jockusch, S.; Turro, N. J. Mechanism of Photoinduced Step Polymerization of Thiophene by Onium Salts: Reactions of Phenyliodinium and Diphenylsulfinium Radical Cations with Thiophene. *Macromolecules* **2007**, *40*, 4481-4485.

(15) Siqueira, F. A.; Taylor, J. G.; Correia, C. R. D. The first intramolecular Heck–Matsuda reaction and its application in the syntheses of benzofurans and indoles. *Tetrahedron Lett.* **2010**, *51*, 2102-2105.

(16) Choi, D.-S.; Huang, S.; Huang, M.; Barnard, T. S.; Adams, R. D.; Seminario, J. M.; Tour, J. M. Revised Structures of N-Substituted Dibrominated Pyrrole Derivatives and Their Polymeric Products. Termaleimide Models with Low Optical Band Gaps. *J. Org. Chem.* **1998**, *63*, 2646-2655.

CHAPTER 5: INTRAMOLECULAR [2+2]-PHOTOCYCLOADDTION OF IMINES TO ENAMIDES

5.1. Introduction

[2+2]-Photocycloaddition that involves carbon-carbon, carbon-oxygen and carbon-sulfur chromophores are frequently encountered in the literature that led to variety of four membered carbocyclic and heterocyclic ring systems. However, the [2+2]-photocycloaddition reaction of carbon-nitrogen analogues are scarcely observed in the literature. The main reason for its scarcity lies in its other reaction pathways such as photoisomerization, photoreduction, photoelimination/fragmentation and electron transfer reaction pathways that makes it harder to engage in [2+2]-photocycloaddition. Occasionally, there are scattered reports on the [2+2]-photocycloaddition of cyclic imines (that cannot undergo photoisomerization) and stabilized imines wherein the imine nitrogen is connected to electron withdrawing substituent which inhibits other electron transfer pathways.[1,2] For example in 1972, Tsuge and coworkers reported the first photocycloaddition of 2,5-diphenyl-1,3,4-oxadiazole **231** to indene **230** and furan in presence of catalytic amount (5 mol%) of iodine (Scheme 5.1). [3,4]

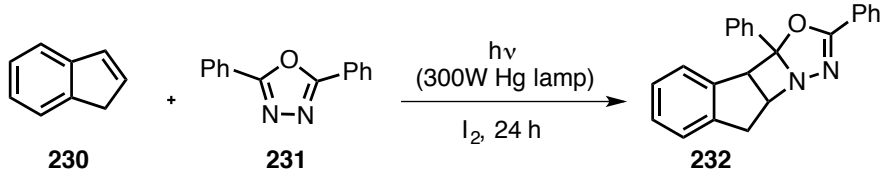

230 **231** **232**

Scheme 5.1: [2+2]-Photocycloaddition of 2,5-diphenyl-1,3,4-oxadiazole with indene.

Similarly, Koch and coworkers reported [2+2]-photocycloaddition of 3-ethoxyisoindolone with various alkenes such as dimethoyethene and cyclohexene (Scheme 5.2).[5-9]

The material in this chapter was co-authored by Elango Kumarasamy (EK), and Dr. J. Sivaguru (JS). EK in consultation with JS synthesized all compounds and carried out all the experiments. Further mechanistic investigations related to this project will be carried out by junior graduate students in JS lab.

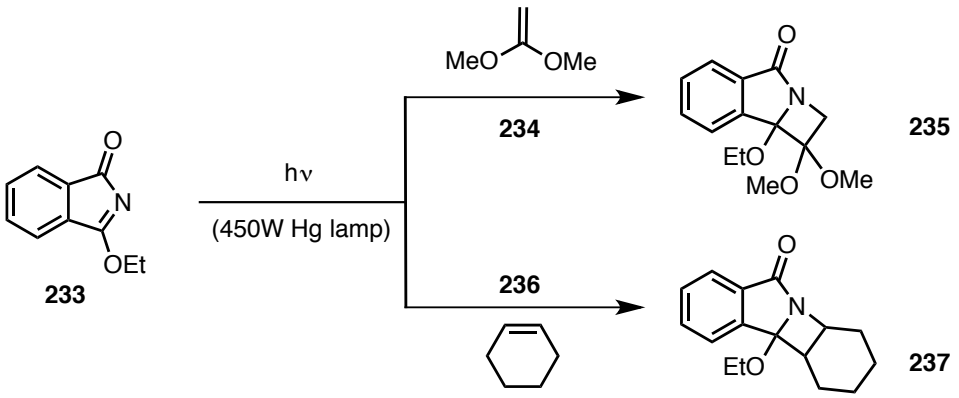

Scheme 5.2: [2+2]-Photocycloaddition of 3-ethoxyisoindolone with olefins.

The structure of **233** was cleverly chosen to resemble α,β-unsaturated ketone whose photochemistry is well understood. The 3-ethoxyisoindolone does not undergo the desired photocycloaddition with electron deficient alkenes such as fumaronitrile. To understand the structural requirement to undergo the desired [2+2]-photocycloaddition, they carried out photoreaction with modified chromophore (Scheme 5.3). For example, they examined the photoreaction of 2-phenyl-2-oxazolin-4-one **238** that underwent smooth photocycloaddition with dimethoxyethene **234** to furnish azetidine derivatives **239**.[8]

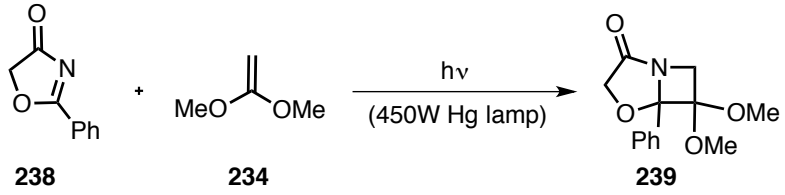

Scheme 5.3: [2+2]-Photocycloaddition of 2-phenyl-2-oxazolin-4-one with dimethoxyethene.

On the contrary, the non-stabilized imine as in the case of oxazinone derivative **240** failed to undergo photoreaction with dimethoxyethene derivative (Scheme 5.4). Based on these results, the authors concluded that the reactive imines that undergo photocycloaddition react from their low lying ππ* excited state. However, the imines that have low lying nπ* excited state do not undergo the desired photoreaction but undergo other reactions characteristics of nπ* excited state such as hydrogen abstraction.[10,11] This was further confirmed by the hydrogen abstraction of oxazinone in the presence of 2-propanol solvent resulting in reductive dimers.

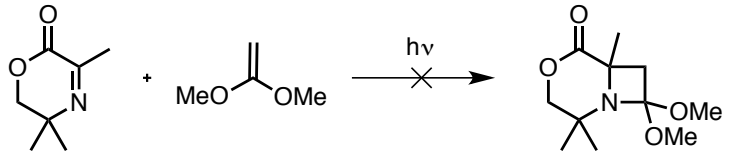

240 **234** **241**

Scheme 5.4: [2+2]-Photocycloaddition of oxazinone with dimethoxyethene

Similarly, other types of stabilized imines are reported to undergo photocycloaddition reaction. For example, Swenton and coworkers reported [2+2]-photocycloaddition of uracil and thymine derivatives (Scheme 5.5).[12,13] The authors attributed the unusual reactivity of **242** towards the conjugation of cyclic imine system to electron withdrawing group that prevent other side reactions. However elaborate photophysical investigations were not carried out to solidify the mechanism of the photoreaction.

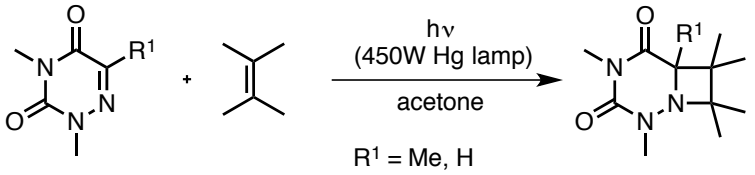

242 **243** **244**

Scheme 5.5: [2+2]-Photocycloaddition of uracil and thymine derivatives with tetramethylethylene.

Sampedro carried out detailed experimental and computational study on the [2+2]-photocycloaddition of isoxazoline derivatives **245** with furan **246** and reiterated the importance of electron withdrawing group in facilitating the photoreaction (Scheme 5.6).[14]

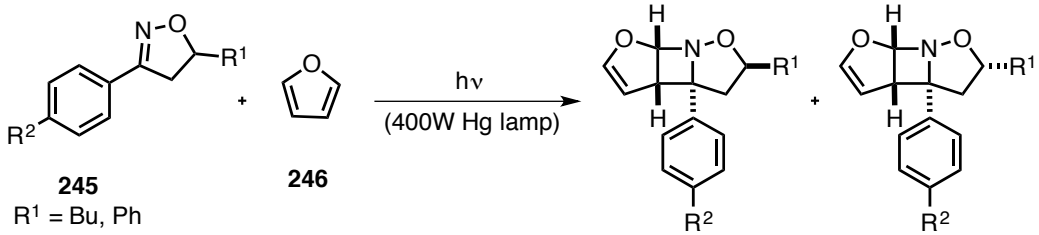

245
R^1 = Bu, Ph
R^2 = CN, CO_2Me

246 **247** **248**

Scheme 5.6: [2+2]-Photocycloaddition of isoxazoline derivatives with furan.

The photocycloaddition of the excited imine competes with deactivation process. The analysis of conical intersection of the reaction revealed that the presence of electron withdrawing group in the system prevented such deactivation process. Also, the substituent (electron withdrawing vs. electron donating) greatly affected the outcome of stereo- and regioselectivity in the reaction. Similar type of experimental study carried out by Mukai and coworkers on isoxazoline derivative revealed the importance of electron withdrawing group on the chromophore.[15] Also, the reaction was observed to undergo via exciplex formation with high regiospecificity.

In all the above examples, the chromophore was constrained in the ring that facilitated the reaction. The acyclic imine in the [2+2]-photocycloaddition reaction has not been reported so far. Milburn and coworkers documented the only report that emerged recently concerning the photocycloaddition of acyclic imines (Scheme 5.7).[16] The stabilized-imine tethered maleimides **249** undergo facile [5+2]-photocycloaddition to furnish 1,3-diazepine derivatives **250**.

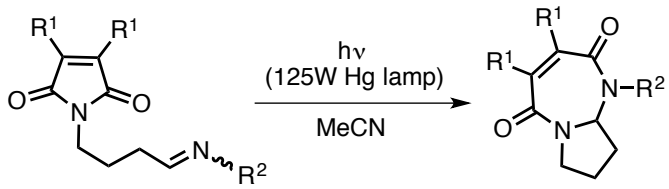

249 **250**

R^1 = Me, Cl, -C_4H_8-
R^2 = NHTs, OH, OMe,
O*t*-Bu, NHCOPh

Scheme 5.7: [5+2]-Photocycloaddition of imine tethered maleimides.

In this higher order photocycloaddition reaction, the *E/Z* mixture of stabilized imine (hydrazones and oximes) which is in the ground state adds to the excited maleimide resulting in the 1,3-diazepine derivatives in good isolated yields. The non-stabilized imines do not engage in the [5+2]-photocycloaddition reaction. With this literature background, we evaluated some stabilized imine derived enamides as an exploratory study to survey the feasibility of [2+2]-photocycloaddition of imines. The following compounds were synthesized according to the procedures reported in the literature.

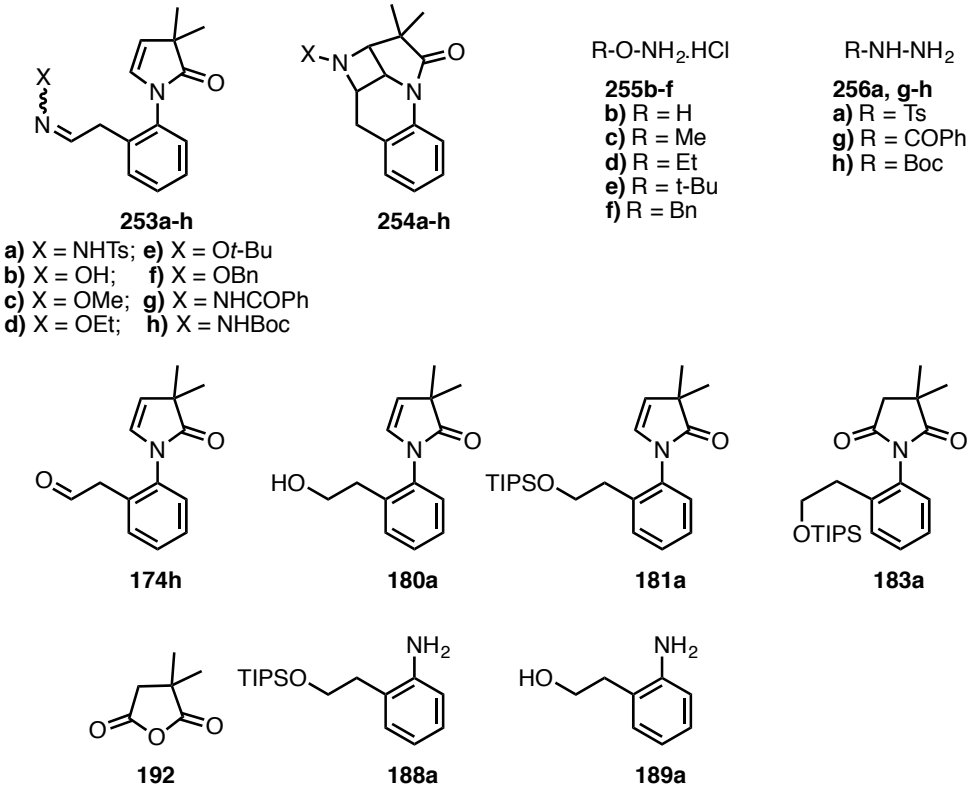

Chart 5.1: Structures of **i**mine derived enamides, their photoproducts and compounds used for their synthesis.

5.2. [2+2]-Photocycloaddition of imine tethered enamides

The initial investigation on the [2+2]-photocycloaddition was carried out on the stabilized imines (hydrazones and oximes). The reaction proceeds smoothly under xanthone-sensitized irradiation with in 1 h in acetonitrile solvent to furnish the desired photocycloadduct **252** (Table 5.1).

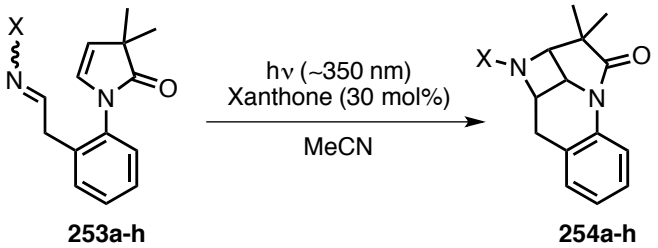

Scheme 5.8: [2+2]-Photocycloaddition of imine tethered enamides.

Table 5.1: [2+2]-Photocycloaddition of imine tethered enamides[a]

Entry	Substrate	Major photoproduct	Isolated yield	Entry	Substrate	Major photoproduct	Isolated yield
1	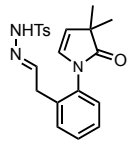 **253a** 1:5.5 (*E*:*Z*)	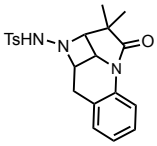 **254a**	(63%)	5	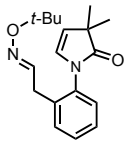 **253e** 1:1.0 (*E*:*Z*)	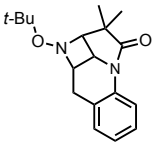 **254e**	(50%)
2	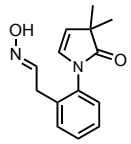 **253b** 1:1.6 (*E*:*Z*)	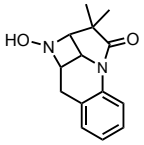 **254b**	(79%)	6	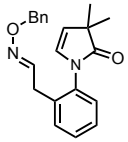 **253f** 1:1 (*E*:*Z*)	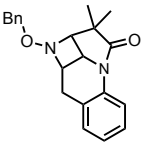 **254f**	(70%)
3	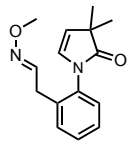 **253c** 1:1.0 (*E*:*Z*)	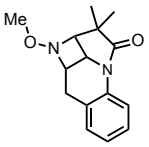 **254c**	(68%)	7	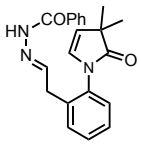 **253g** (E:*Z*)	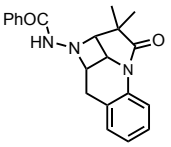 **254g**	(50%)
4	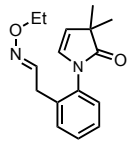 **253d** 1:1.0 (*E*:*Z*)	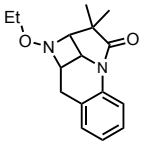 **254d**	(58%)	8	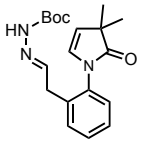 **253h** 1:3.5 (*E*:*Z*)	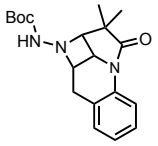 **254h**	(48%)

[a]The photoreaction was performed in MeCN with 30 mol% xanthone as sensitizer in a Rayonet reactor equipped with ~350 nm bulbs using merry-go-round apparatus at room temperature. The reaction usually completes in 1 h and monitored by ^{1}H-NMR and TLC. The ratio of *E:Z* isomers in the starting material were calculated from ^{1}H-NMR of the crude reaction mixture.

While reaction proceeded smoothly under described conditions, longer irradiation or broadband irradiation only resulted in the decomposition of reaction mixture. The reaction was monitored by ^{1}H-NMR spectroscopy and TLC. After the reaction, the solvent was evaporated and the crude product was purified by column chromatography and confirmed by NMR, HRMS and single crystal XRD. Lower wavelength (420 nm) irradiation did not result in the product formation. The reaction tolerates wide substitution pattern in the hydrazone and oximes derived enamides as evident from table 5.1. The *E:Z* ratio in the starting material does not seem to affect the reaction and proceed to completion resulting in single photoproduct. The analysis of the crystal

structure data revealed that the orientation of hydrogens in the newly formed stereocenter are *syn* to each other.

Further investigations such as stereospecific [2+2]-photocycloaddition using atropisomeric chromophores and detailed photophysical studies are to be carried out in order to understand the nature of excited states and the ability of axial chirality in imparting very high chirality transfer. Photophysical studies will provide key information to ascertain the type of excited state (excited enamide vs. excited imine) that initiates the photocycloaddition reaction. These studies are currently underway in our lab by junior graduate students.

5.3. X-ray structure data for photoproduct 252a

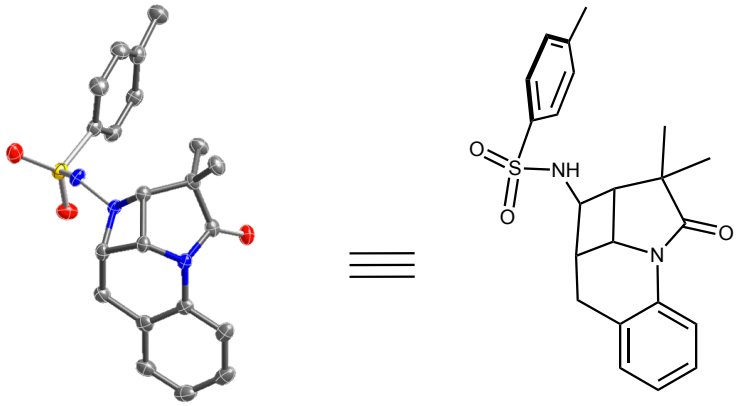

Figure 5.1: X-ray structure of photoproduct **252a** (crystallized from hexanes/DCM).

X-Ray data: Formula = $C_{23}H_{21}N_3O_3S$; FW = 397.48; Cryst. size_max [mm] = 0.24; cryst. size_mid [mm] = 0.1; Cryst. size_min [mm] = 0.052; Cryst. System = Monoclinic; Space Group, Z = 8; a [Å] = 24.7877(6); b [Å] = 10.2096(3); c [Å] = 16.2987(4); α [Å] = 90; β [Å] = 112.7980(10); γ [Å] = 90; V [Å^3] = 3802.51(17); ρ_{calc} [g/cm^3] = 1.389; μ [mm^{-1}] = 1.747; Radiation Type = CuKα (λ = 1.54178); F(000) = 1680.0; no of measured refl. = 27306; no of indep. refl. = 3363 [R_{int} = 0.0353, R_{sigma} = 0.0180]; Resolution [Å] = 0.84; R1/wR2 ($I \geq 2\sigma$)^a [%] = 0.0324/0.0786; R1/wR2 (all data) [%] = 0.037/0.0813.

5.4. Summary and outlook

The initial investigation on the [2+2]-photocycloaddition of imines with maleimides not only provides easy access to azetidine derivatives but also provides a perfect platform to investigate the reactivity of imines in general toward photocycloaddition reaction. Detailed photochemical and photophysical analysis will shed crucial insights into the nature of excited states involved in the reaction and will allow us to tailor make imines chromophores that can undergo facile photocycloaddition reaction.

5.5. Experimental section

5.5.1. General methods

All commercially obtained reagents/solvents were used as received; chemicals were purchased from Alfa Aesar®, Sigma-Aldrich®, Acros organics®, TCI America®, Mallinckrodt®, and Oakwood® Products, and were used as received without further purification. Unless stated otherwise, reactions were conducted in oven-dried glassware under nitrogen atmosphere. ^{1}H-NMR and ^{13}C-NMR spectra were recorded on Varian 400 MHz (100 MHz for ^{13}C) and on 500 MHz (125 MHz for ^{13}C) spectrometers. Data from the ^{1}H-NMR spectroscopy are reported as chemical shift (δ ppm) with the corresponding integration values. Coupling constants (*J*) are reported in hertz (Hz). Standard abbreviations indicating multiplicity were used as follows: s (singlet), b (broad), d (doublet), t (triplet), q (quartet), m (multiplet) and virt (virtual). Data for ^{13}C NMR spectra are reported in terms of chemical shift (δ ppm). High-resolution mass spectrum data in Electrospray Ionization mode were recorded either on a Bruker – Daltronics® BioTof mass spectrometer in positive (ESI+) ion mode or on a Waters® SYNAPT G2-Si connected to ACQUITY UPLC system. HPLC analyses were performed on Waters® HPLC equipped with 2525 pump or on Dionex® Ultimate 3000 HPLC. Waters® 2767 sample manager was used for automated sample injection on Waters® HPLC or Ultimate 3000 sample injector was used for injection on Dionex® HPLC. All HPLC injections on Waters® HPLC were monitored using a Waters® 2487 dual wavelength absorbance detector at 254 and 270 nm or on Dionex®. HPLC were monitored using a diode array detector (DAD3000125). Analytical and semi-preparative injections were performed on chiral stationary phase using various columns as indicated below

i) Regis® PIRKLE COVALENT (*R*,*R*) WHELK–01

a) 25 cm × 4.6 mm column for analytical injections

b) 25 cm × 10 mm column for semi-preparative injections

ii) CHIRACEL® OD-H

a) 0.46 cm × 25 cm column for analytical injections

b) 10 mm × 25 cm column for semi-preparative injections

iii) CHIRALPACK® IC

a) 0.46 cm × 25 cm column for analytical injections

b) 10 mm × 25 cm column for semi-preparative injections

iv) CHIRALPAK® AD-H

a) 0.46 cm × 15 cm column for analytical injections

b) 10 mm × 25 cm column for semi-preparative injections

Masslynx software version 4.1 was used to monitor/analyze the HPLC injections and to process HPLC traces. Igor Pro® Software version 6.0 was used to process the HPLC graphics. UV-Vis spectra were recorded on Shimadzu 2501PC UV-Vis spectrometer using UV quality fluorimeter cells (with range until 190 nm) purchased from Luzchem. Optical activity values were recorded on JASCO® DIP – 370 digital polarimeter. CD spectra were recorded on JASCO® J-815 with JASCOPTC-423S/15 temperature controller maintained by liquid nitrogen. When necessary, the compounds were purified by combiflash equipped with dual wavelength UV-Vis absorbance detector (Teledyn ISCO) using hexanes:ethyl acetate as the mobile phase and Redisep® cartridge filled with silica (Teledyne ISCO) as stationary phase. In some cases, compounds were purified by column chromatography on silica gel (Sorbent Technologies®, silica gel standard grade: porosity 60 Å, particle size: 230 x 400 mesh, surface area: 500 – 600 m^2/g, bulk density: 0.4 g/mL, pH range: 6.5 – 7.5). Unless indicated, the Retardation Factor (R*f*) values were recorded using a 5-50% hexanes:ethyl acetate as mobile phase and on Sorbent Technologies®, silica Gel TLC plates (200 mm thickness w/UV_{254}).

5.5.2. Synthesis of hydrazone derivatives of enamides 251a, g-h

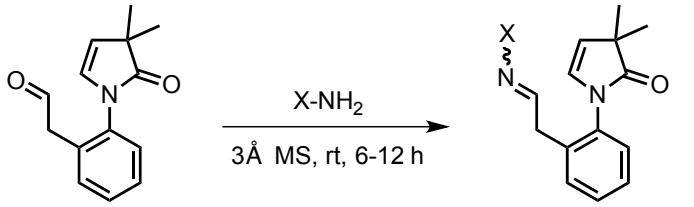

174h **251a, g-h**

a) X = NHTs
g) X = NHBoc
h) X = NHCOPH

Scheme 5.9: Synthesis of hydrazone derivatives of enamides **251a, g-h**.

The hydrazone derivatives of enamides was synthesized according to a procedure reported in the literature.[16] To a mixture of hydrazide (1.1 *equiv.*) and 3 Å molecular sieves (200 mg) in dry DCM (3 mL) at room temperature a solution of aldehyde (100mg, 0.44 mmol, 1.0 *equiv.*) in DCM (2 mL) was slowly added. The resulting mixture was stirred for 6-12 h. The reaction was monitored by TLC and after the reaction the mixture was filtered through celite and washed with DCM (5 mL). The combined organic layer was concentrated under reduced pressure to yield the crude product. The crude was purified by combiflash using hexanes:ethyl acetate mixture to obtain pure product as a mixture of *E:Z* isomers (The ratio of *E:Z* isomers was ascertained from ^{1}H-NMR crude reaction mixture).

^{1}H-NMR (400 MHz, $CDCl_3$, δ ppm): 8.86 (bs, 1H, minor), 8.08 (bs, 1H, major), 7.77-7.75 (m, 2H, minor), 7.72-7.70 (m, 2H, major), 7.27-7.22 (m, 3H, major+minor), 7.19-7.09 (m, 3H, major+minor), 7.01-6.98 (m, 1H, major), 6.80 (t, *J* = 5.2 Hz, 1H, minor) 6.40 (d, *J* = 4.8 Hz, 1H, minor), 6.34 (d, *J* = 4.8 Hz, 2H, major), 5.49 (d, J = 4.8 Hz, 1H, minor), 5.43 (d, *J* = 4.8 Hz, 3H, major), 3.34-3.33 (m, 2H, major+minor), 2.398-2.381 (m, 3H, major+minor) and 1.22-1.21 (m, 6H, major+minor).

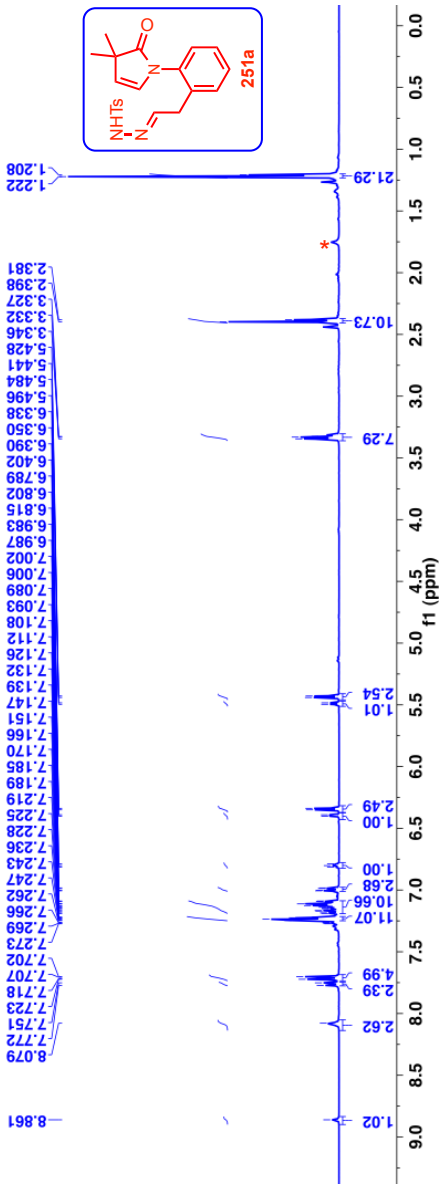

Figure 5.2: ^{1}H-NMR (400 MHz, $CDCl_3$, δ ppm) of N-tosyl imine derivative **251a**.

^{13}C-NMR (100 MHz, $CDCl_3$, δ ppm): 182.4, 182.1, 149.8, 147.1, 144.7, 144.0, 143.9, 135.96, 135.8, 135.7, 133.7, 133.4, 132.6, 131.3, 130.9, 130.3, 130.1, 129.7, 129.66, 128.5, 128.47, 128.3, 128.2, 128.16, 127.2, 126.8, 119.6, 118.6, 46.8, 46.5, 34.7, 31.8, 30.6, 23.6, 23.5 and 21.8.

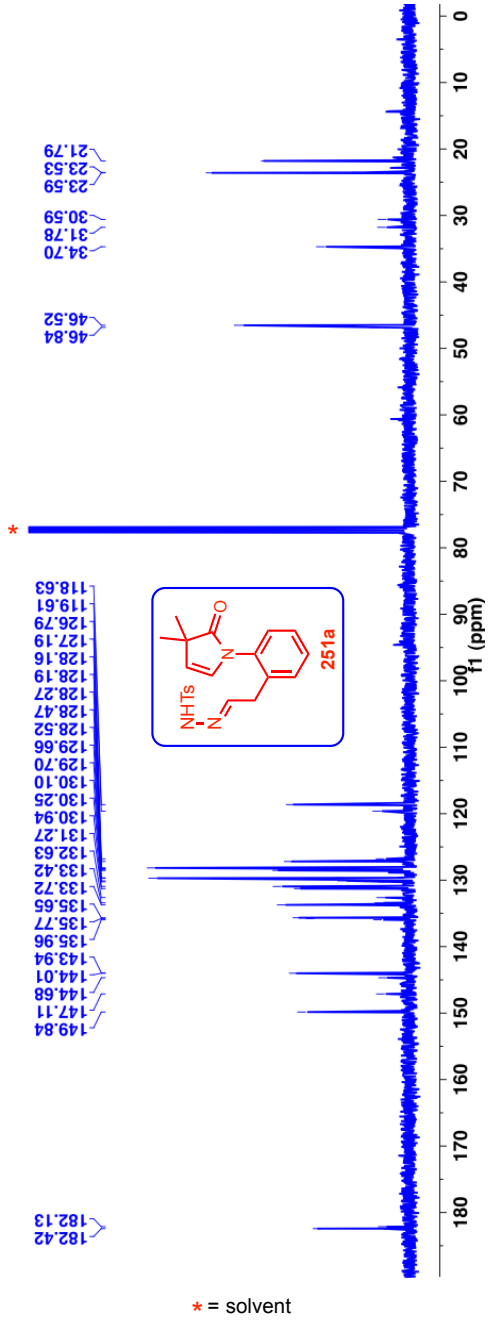

Figure 5.3: ^{13}C-NMR (100 MHz, $CDCl_3$, δ ppm) of N-tosyl imine derivative **251a**.

HRMS-ESI (m/z) ([M + Na]):

Calculated : 420.1352

Observed : 420.1348

|Δm| : 0.9 ppm

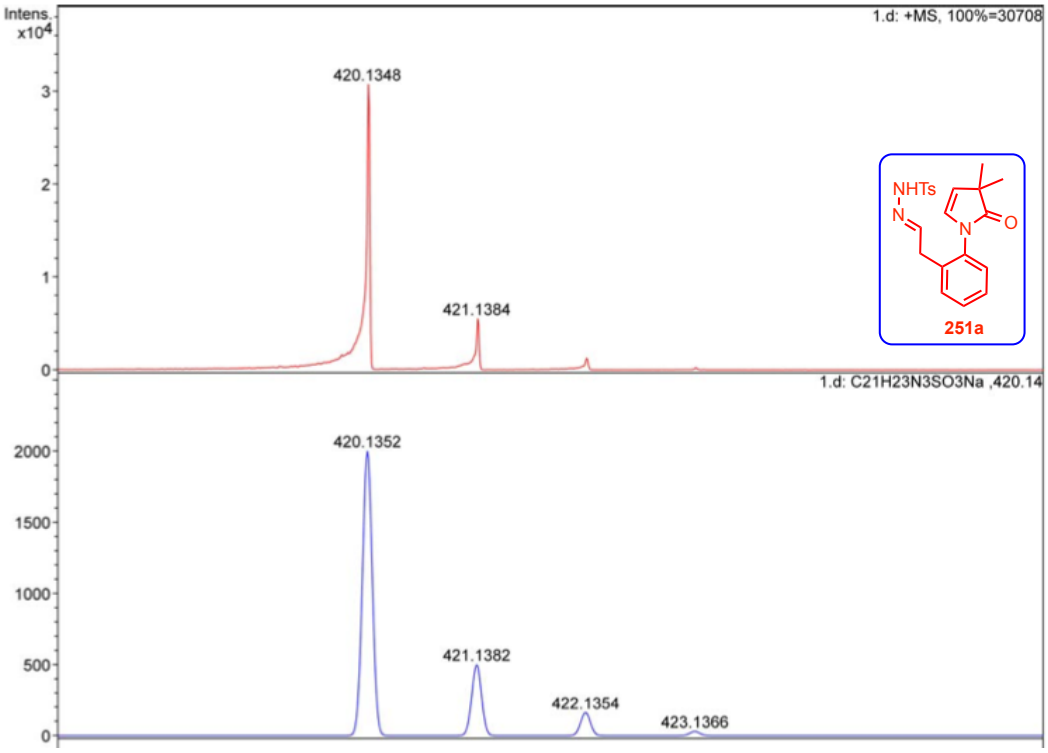

Figure 5.4: HRMS of N-tosyl imine derivative **251a**.

^{1}H-NMR (400 MHz, $CDCl_3$, δ ppm): 8.26 (s, 1H), 7.21-7.206 (m, 3H), 7.13-7.06 (m, 2H), 6.38 (d, *J* = 4.8 Hz, 1H), 5.42 (d, *J* = 4.8 Hz, 1H), 3.40 (d, *J* = 5.6 Hz, 2H), 1.40 (s, 9H) and 1.21 (s, 6H).

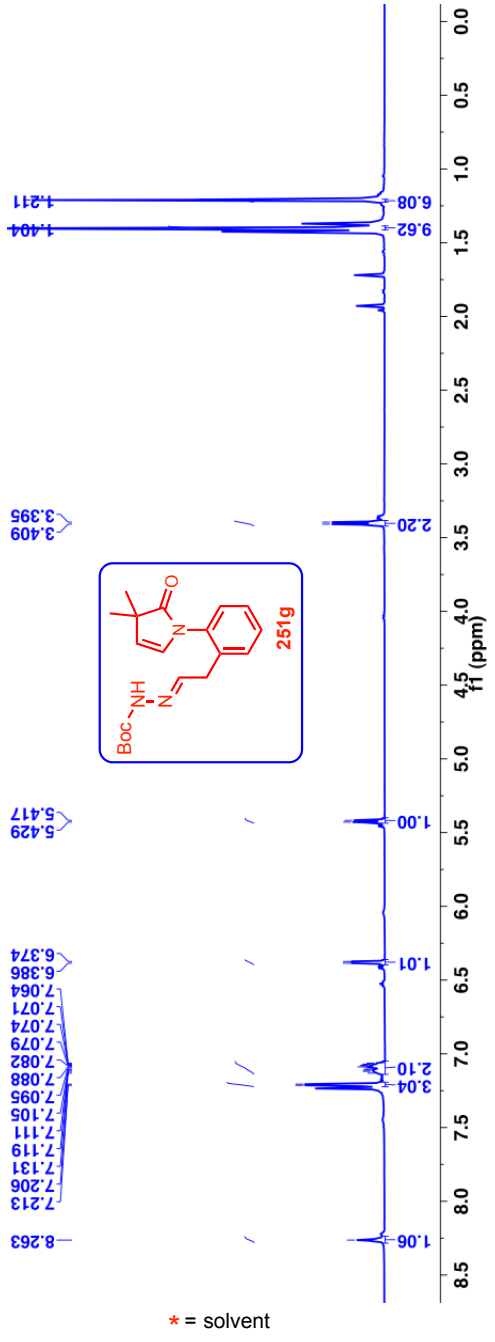

Figure 5.5: ^{1}H-NMR (400 MHz, $CDCl_3$, δ ppm) of N-Boc imine derivative **251g**.

^{13}C-NMR (100 MHz, $CDCl_3$, δ ppm): 182.3, 152.9, 144.97, 135.8, 134.5, 131.3, 131.0, 128.7, 128.1, 127.3, 118.4, 77.6, 46.4, 34.8, 28.5, 28.47 and 23.6.

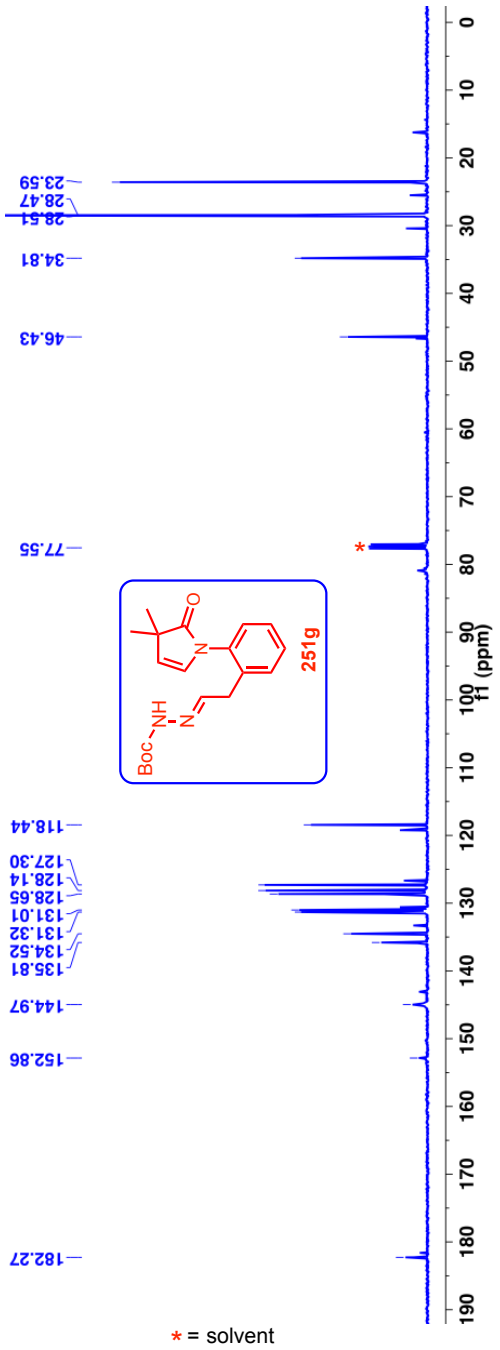

Figure 5.6: ^{13}C-NMR (100 MHz, $CDCl_3$, δ ppm) of N-Boc imine derivative **251g**.

HRMS-ESI (m/z) ([M + Na]$^+$):

Calculated : 366.1794

Observed : 366.1799

|Δm| : 1.4

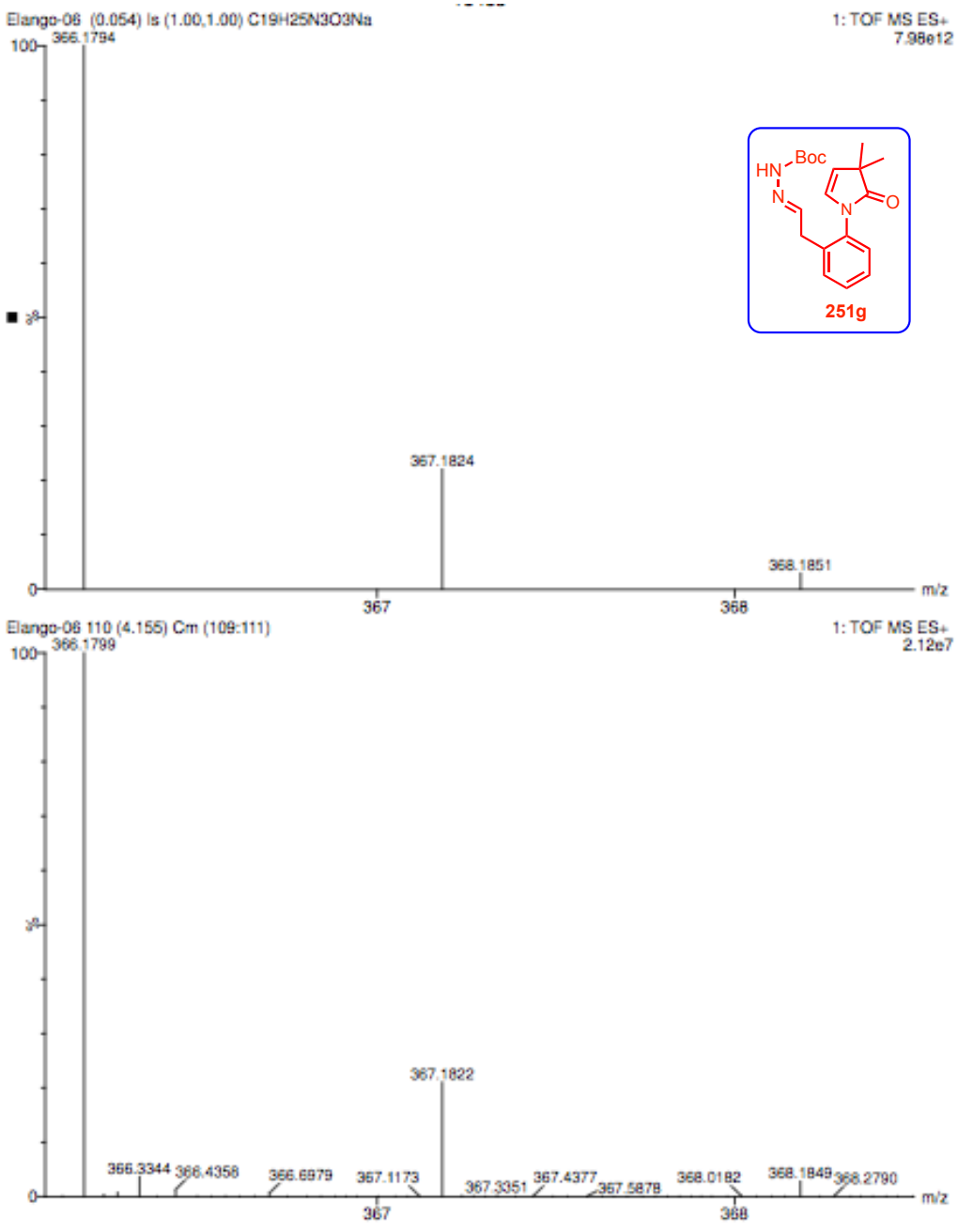

Figure 5.7: HRMS of N-Boc imine derivative **251g**.

^{1}H-NMR (400 MHz, $CDCl_3$, δ ppm): 10.11 (s, 1H), 7.78-7.76 (m, 2H), 7.54-7.51 (m, 1H), 7.43-7.39 (m, 1H), 7.34-7.28 (m, 2H), 7.21-7.19 (m, 3H), 7.06-7.03 (m, 1H), 6.38 (d, *J* = 4.8 Hz, 1H), 5.43 (d, *J* = 4.8 Hz, 1H), 3.44 (d, *J* = 5.6 Hz, 2H) and 1.19 (s, 6H).

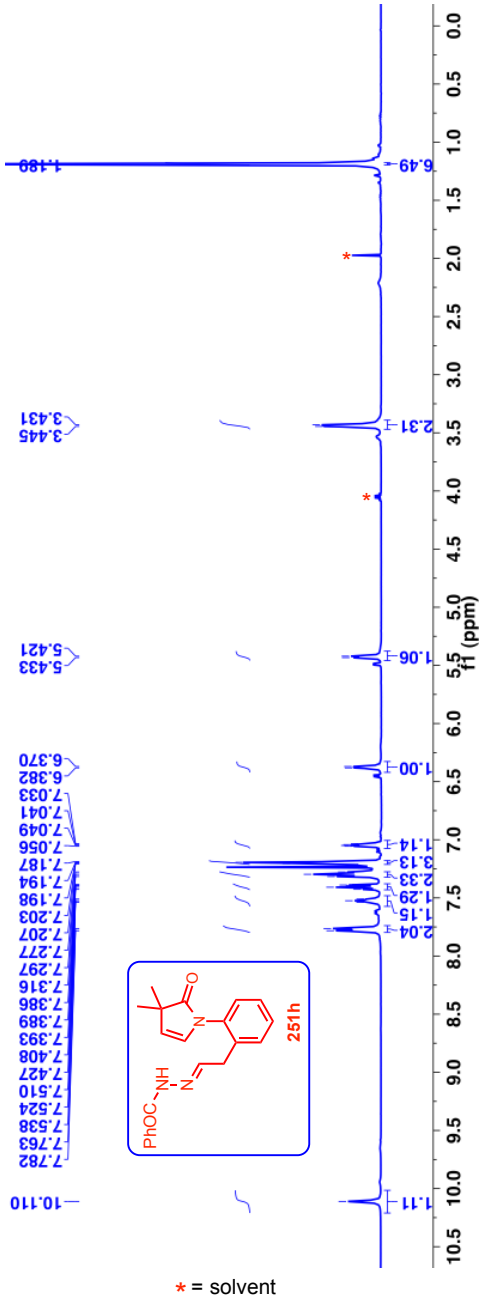

Figure 5.8: ^{1}H-NMR (400 MHz, $CDCl_3$, δ ppm) of N-Benzohydrazide imine derivative **251h**.

^{13}C-NMR (100 MHz, $CDCl_3$, δ ppm): 182.6, 164.4, 150.0, 135.8, 134.1, 133.3, 131.96, 131.2, 131.1, 128.8, 128.7, 128.3, 127.7, 127.3, 118.7, 46.5, 34.9 and 23.5.

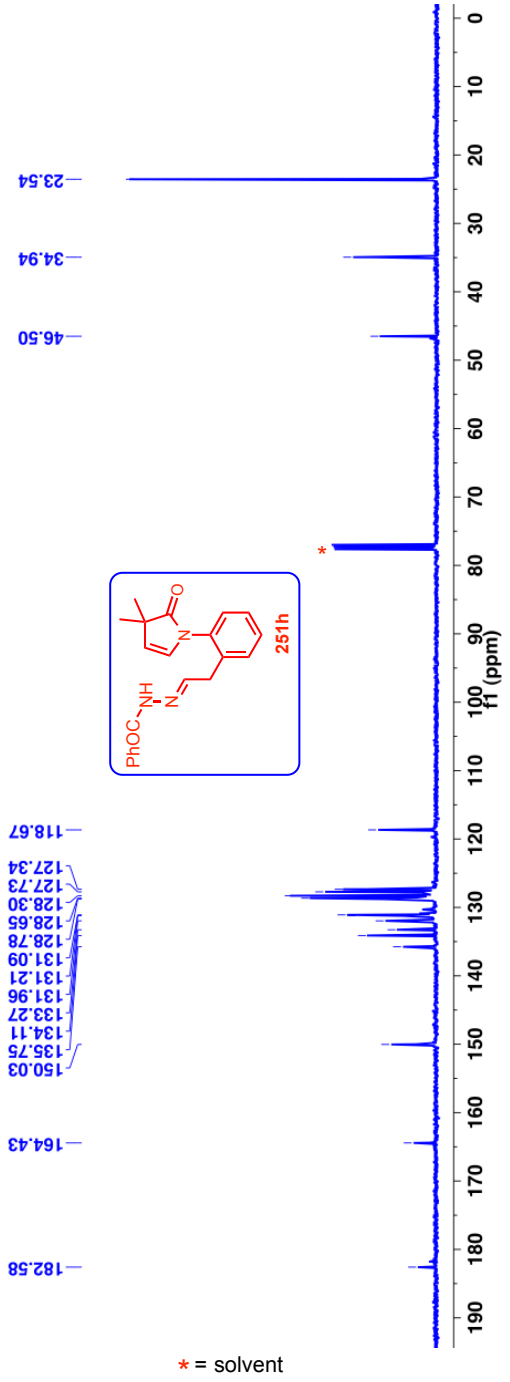

Figure 5.9: ^{13}C-NMR (100 MHz, $CDCl_3$, δ ppm) of N-Benzohydrazide imine derivative **251h**.

HRMS-ESI (m/z) ([M + H]$^+$):

Calculated : 348.1712

Observed : 348.1721

|Δm| : 2.6 ppm

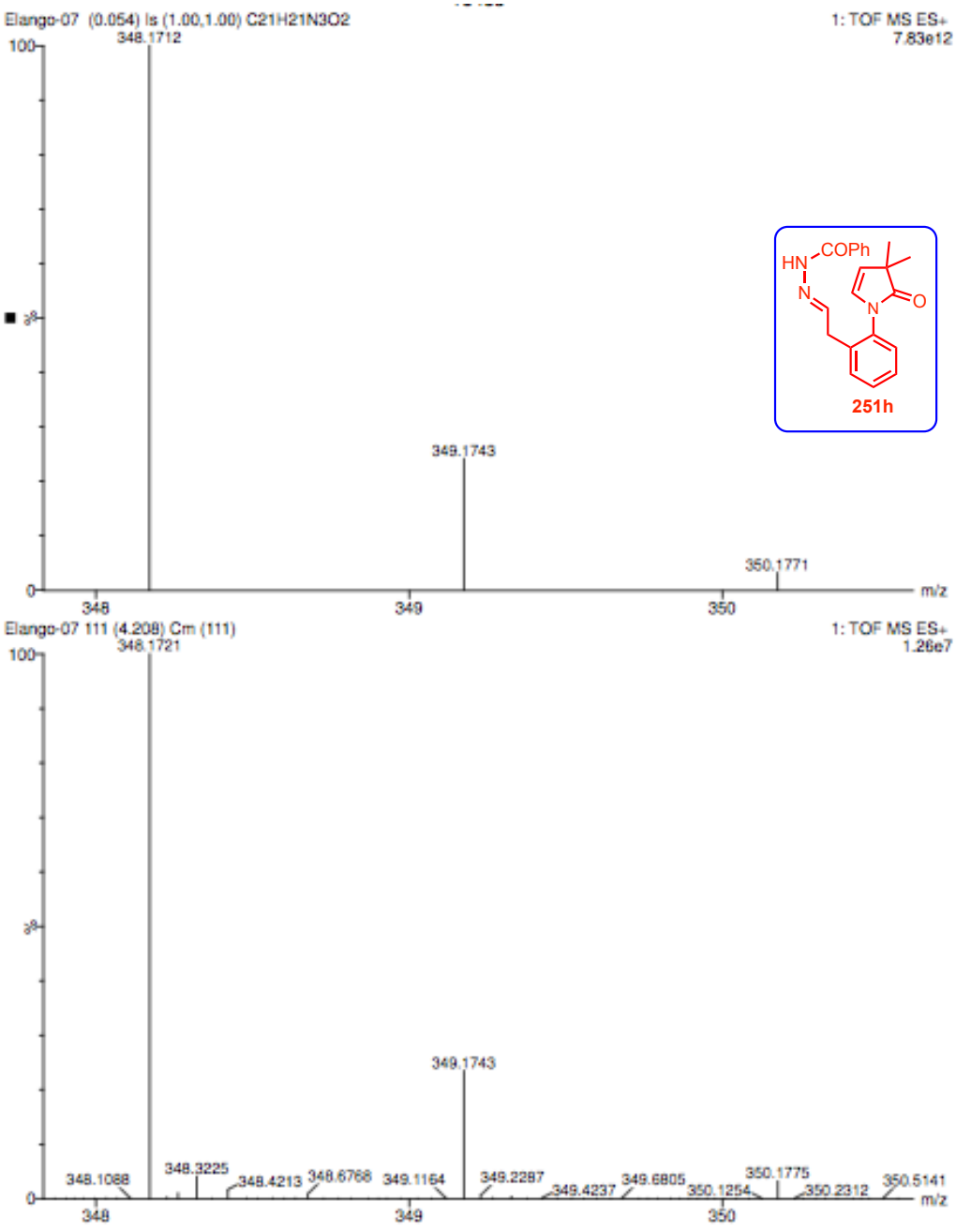

Figure 5.10: HRMS of N-Benzohydrazide imine derivative **251h**.

5.5.3. Synthesis of oxime derivatives of enamides 251b-f

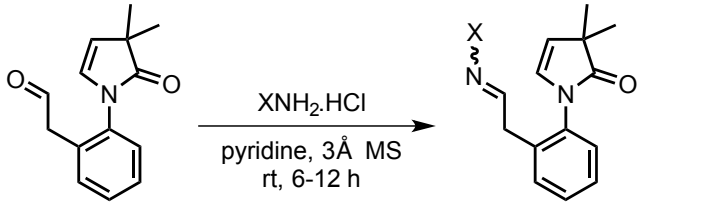

174h **251b-f**

b) X = OH **e**) X = O-*t*-Bu
c) X = OMe **f**) X = OBn
d) X = OEt

Scheme 5.10: Synthesis of oxime derivatives of enamides **251b-f**.

To a mixture of oxime hydrochloride (1.1 *equiv.*), pyridine (1.5 *equiv.*) and 3Å molecular sieves (200 mg) in dry DCM (3 mL) at room temperature a solution of aldehyde (100mg, 0.44 mmol, 1.0 *equiv.*) in DCM (2 mL) was slowly added. The resulting mixture was stirred for 6-12 h. The reaction was monitored by TLC and after the reaction the mixture was filtered through celite and washed with DCM. The combined organic layer was concentrated under reduced pressure to yield the crude product. The crude was purified by combiflash using hexanes:ethyl acetate mixture to obtain pure product as a mixture of *E:Z* isomers (The ratio of *E:Z* isomers was ascertained from ^{1}H-NMR crude reaction mixture).

^{1}H-NMR (400 MHz, $CDCl_3$, δ ppm): 8.46 (bs, 1H, minor), 8.03 (bs, 1H, major), 7.45 (t, *J* = 5.9 Hz, 1H, major), 7.3-7.14 (m, 5H, major+minor) 7.17-7.14 (m, 1H, major+minor), 6.74 (t, *J* = 5.1 Hz, 1H, minor), 6.46-6.44 (m, 1H, major+minor), 5.47 (dd, *J* = 4.9, 1.0 Hz, 1H, major+minor), 3.63 (d, *J* = 5.1 Hz, 2H, minor), 3.44 (d, *J* = 5.9 Hz, 2H, major), 1.28 (s, 3H, major+minor) and 1.27 (s, 3H, major+minor).

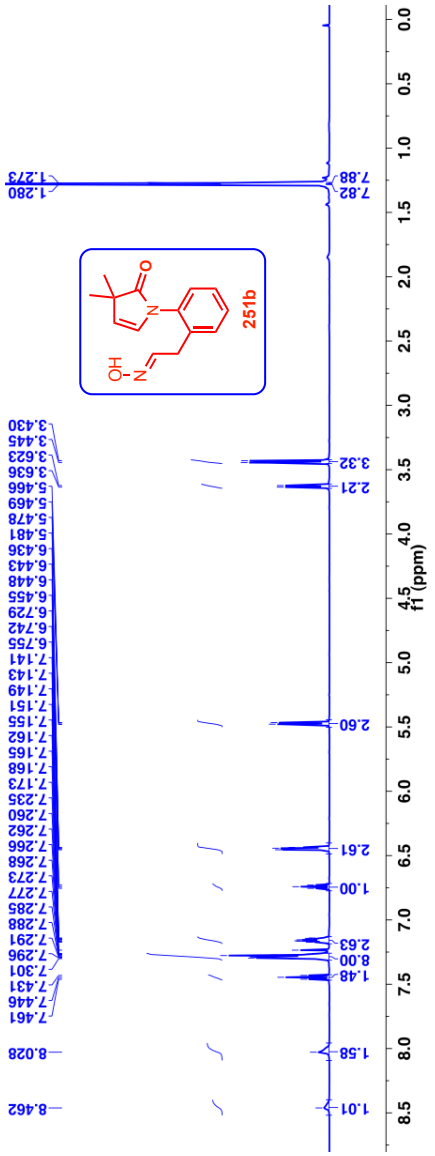

Figure 5.11: ^{1}H-NMR (400 MHz, $CDCl_3$, δ ppm) of N-hydroxy oxime derivative **251b**.

^{13}C-NMR (100 MHz, $CDCl_3$, δ ppm): 181.94, 181.9, 150.0, 149.96, 135.94, 135.9, 134.7, 133.98, 131.4, 131.2, 130.97, 130.9, 128.7, 128.6, 128.3, 128.2, 127.4, 127.3, 118.6, 118.5, 46.51, 46.5, 32.3, 28.3, 23.7 and 23.6.

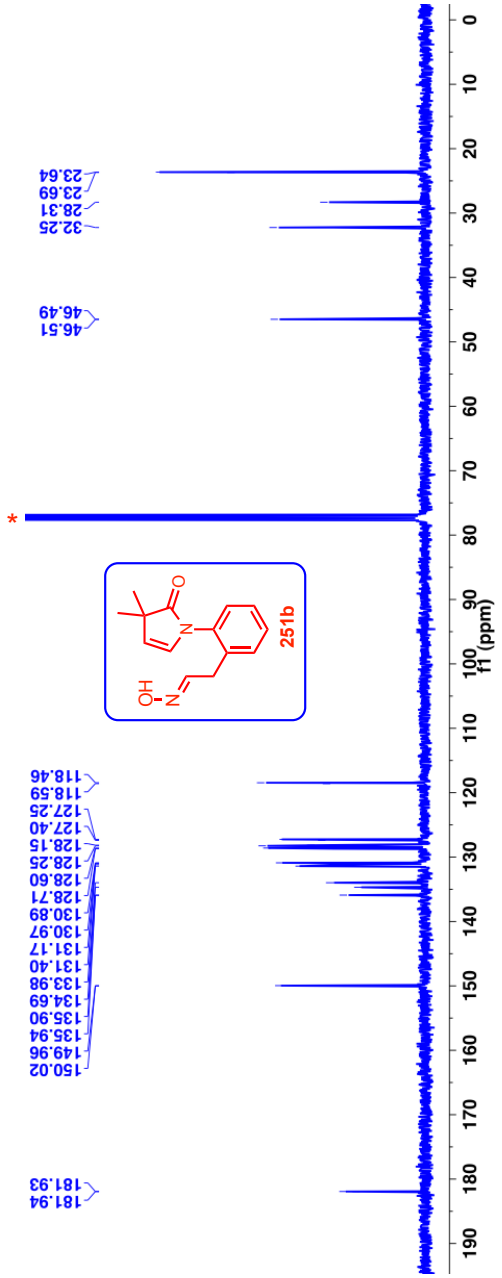

* = solvent
(1:1.6 mixture of *E*:*Z* isomers)

Figure 5.12: ^{13}C-NMR (100 MHz, $CDCl_3$, δ ppm) of N-hydroxy oxime derivative **251b**.

HRMS-ESI (m/z) ([M + Na]$^+$):

Calculated : 267.1104

Observed : 267.1095

|Δm| : 3.4 ppm

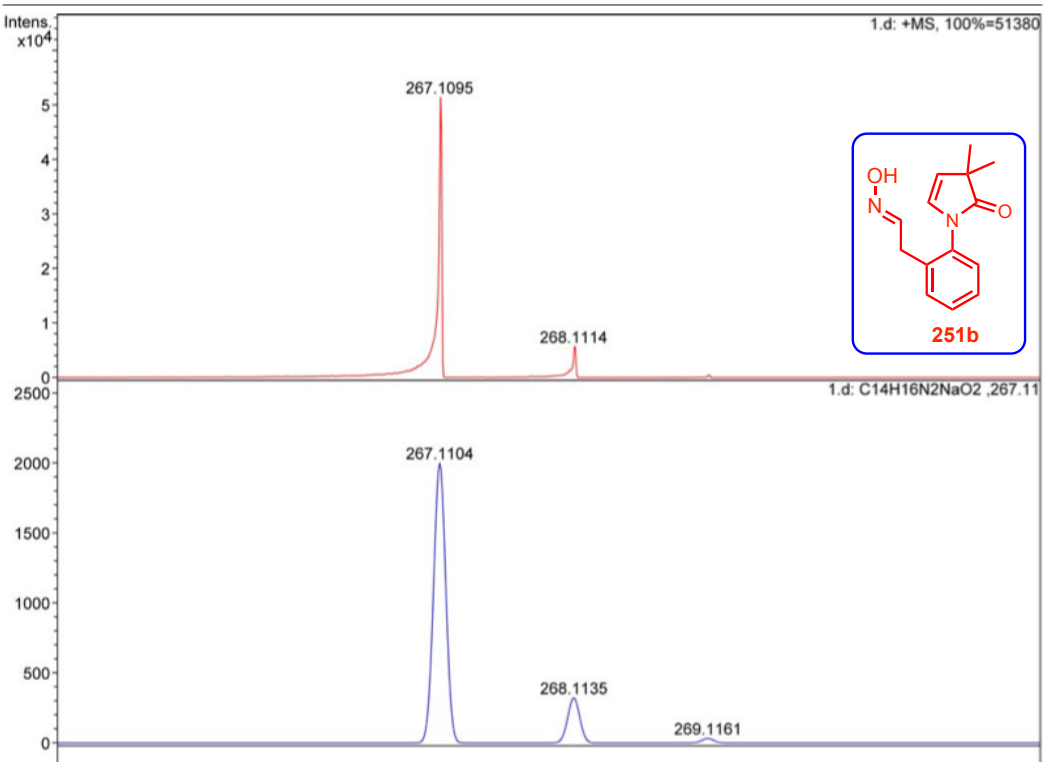

Figure 5.13: HRMS N-hydroxy oxime derivative **251b**.

^{1}H-NMR (400 MHz, $CDCl_3$, δ ppm): 7.37 (t, *J* = 6.2 Hz, 1H, minor), 7.29-7.27 (m, 6H, major+minor), 7.17-7.14 (m, 2H, major+minor), 6.64 (t, *J* = 5.2 Hz, 1H, major), 6.44 (dd, *J* = 4.8, 4.0 Hz, 2H, major+minor), 5.47 (d, *J* = 4.8 Hz, 2H, major+minor), 3.85 (s, 3H, major), 3.78 (s, 3H, major), 3.58 (d, *J* = 5.2 Hz, 2H, major), 3.43 (d, *J* = 6.0 Hz, 2H, minor), 1.29 (s, 6H, minor) and 1.27 (s, 3H, major).

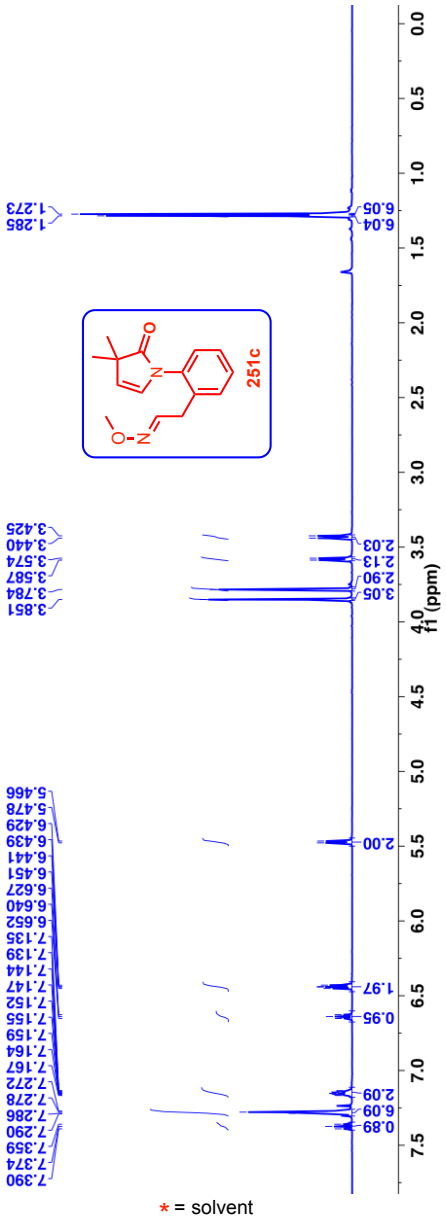

Figure 5.14: ^{1}H-NMR (400 MHz, $CDCl_3$, δ ppm) of N-methoxy oxime derivative **251c**.

^{13}C-NMR (100 MHz, $CDCl_3$, δ ppm): 181.7, 148.96, 148.5, 136.0, 135.95, 134.8, 134.2, 131.4, 131.2, 130.9, 130.8, 128.7, 128.6, 128.2, 128.1, 127.4, 127.2, 118.5, 118.3, 61.9, 61.6, 46.5, 32.3, 29.0, 23.7 and 23.6.

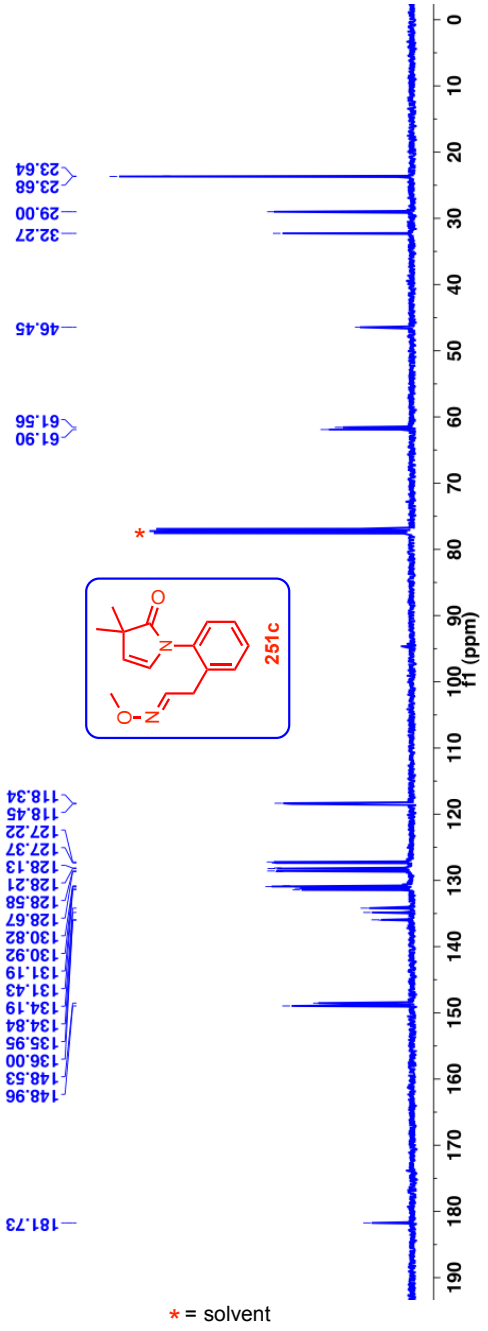

Figure 5.15: ^{13}C-NMR (100 MHz, $CDCl_3$, δ ppm) of N-methoxy oxime derivative **251c**.

HRMS-ESI (m/z) ([M + Na]$^+$):

Calculated : 281.1260

Observed : 281.1253

|Δm| : 2.5 ppm

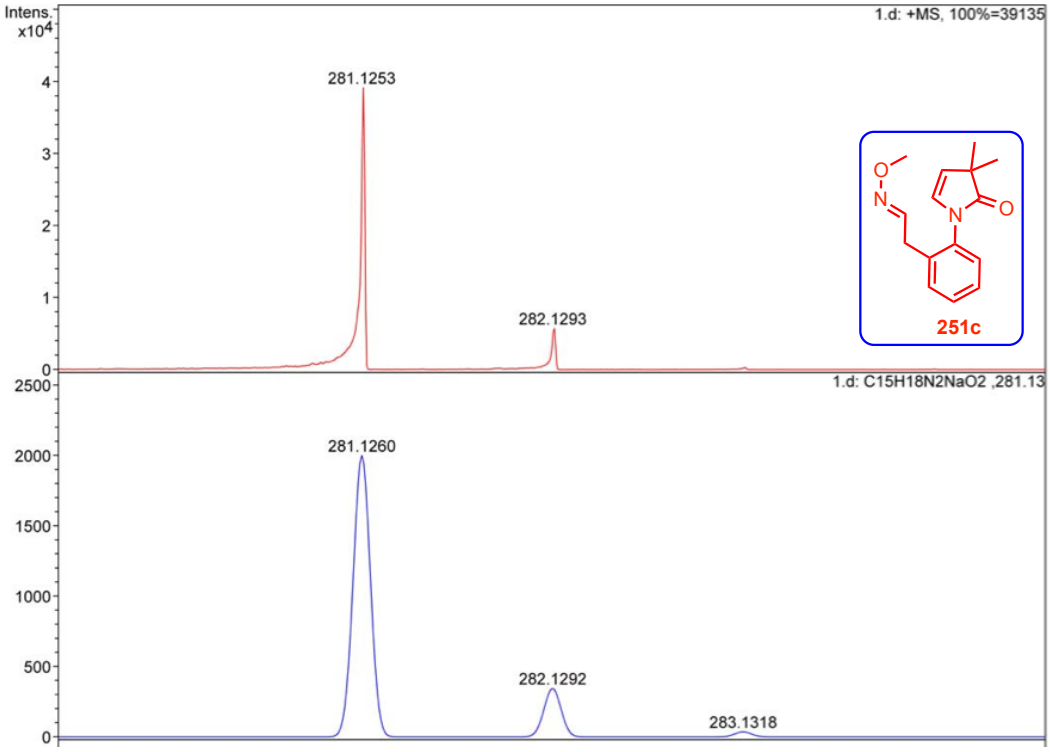

Figure 5.16: HRMS of N-methoxy oxime derivative **251c**.

^{1}H-NMR (400 MHz, $CDCl_3$, δ ppm): 7.38 (t, *J*= 6.2 Hz, 1H, *Z*), 7.27-7.26 (m, 6H, *Z*+*E*), 7.16-7.12 (m, 2H, *Z*+*E*), 6.63 (t, *J*= 5.2 Hz, 1H, *E*), 6.44-6.42 (m, 2H, *Z*+*E*), 5.46-5.45 (m, 2H, *Z*+*E*), 4.09 (q, J= 7.0 Hz, 2H, *Z*), 4.03 (q, J= 7.0 Hz, 2H, *E*), 3.58 (d, *J* = 5.1 Hz, 2H, *Z*), 3.42 (d, *J* = 6.2 Hz, 2H, *E*), 1.27 (s, 6H, *Z*), 1.26 (s, 6H, *E*) and 1.23-1.18 (m, 6H, *E*+*Z*)

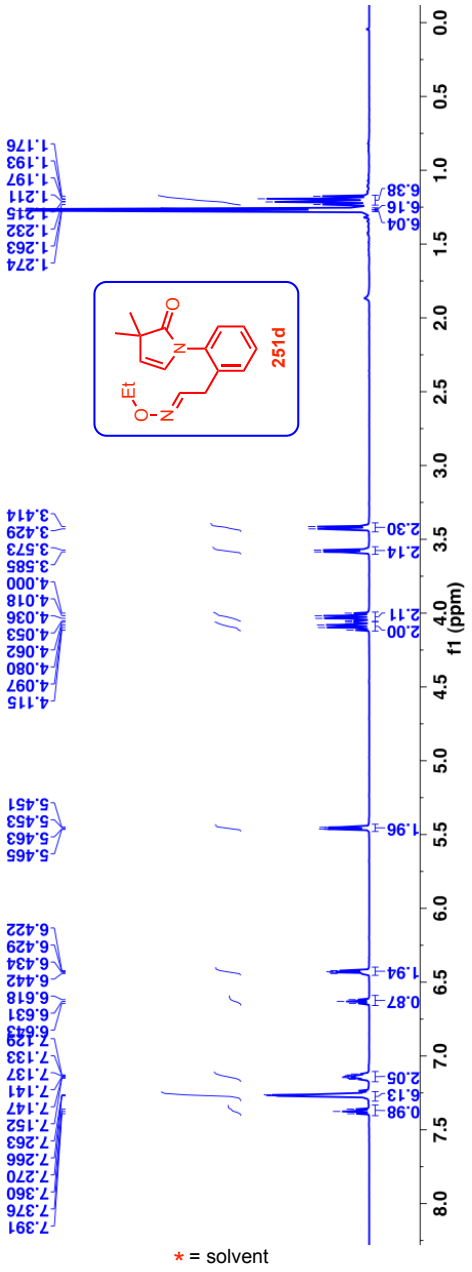

Figure 5.17: ^{1}H-NMR (400 MHz, $CDCl_3$, δ ppm) of N-ethoxy oxime derivative **251d**.

^{13}C-NMR (100 MHz, $CDCl_3$, δ ppm): 181.7, 148.7, 148.2, 135.96, 135.9, 135.0, 134.3, 131.5, 131.2, 130.9, 130.8, 128.6, 128.6, 128.2, 128.1, 127.4, 127.2, 118.4, 118.3, 69.7, 69.3, 46.4, 32.3, 29.1, 23.7, 23.6, 14.8 and 14.7.

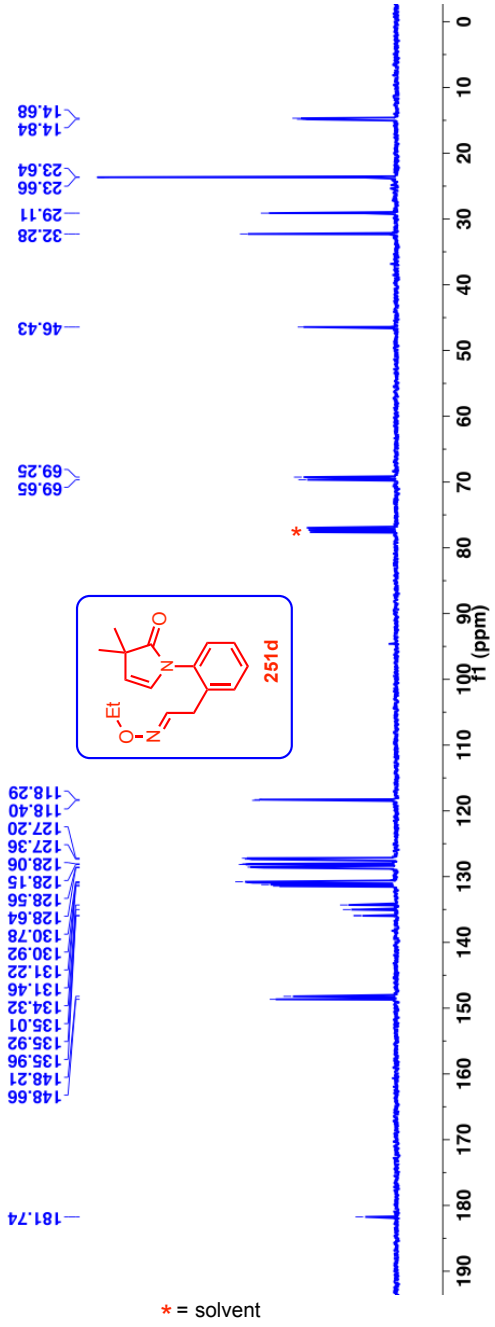

Figure 5.18: ^{1}H-NMR (400 MHz, $CDCl_3$, δ ppm) of N-ethoxy oxime derivative **251d**.

HRMS-ESI (m/z) ([M + H]$^+$):

Calculated	: 273.1603
Observed	: 273.1608
|Δm|	: 1.8 ppm

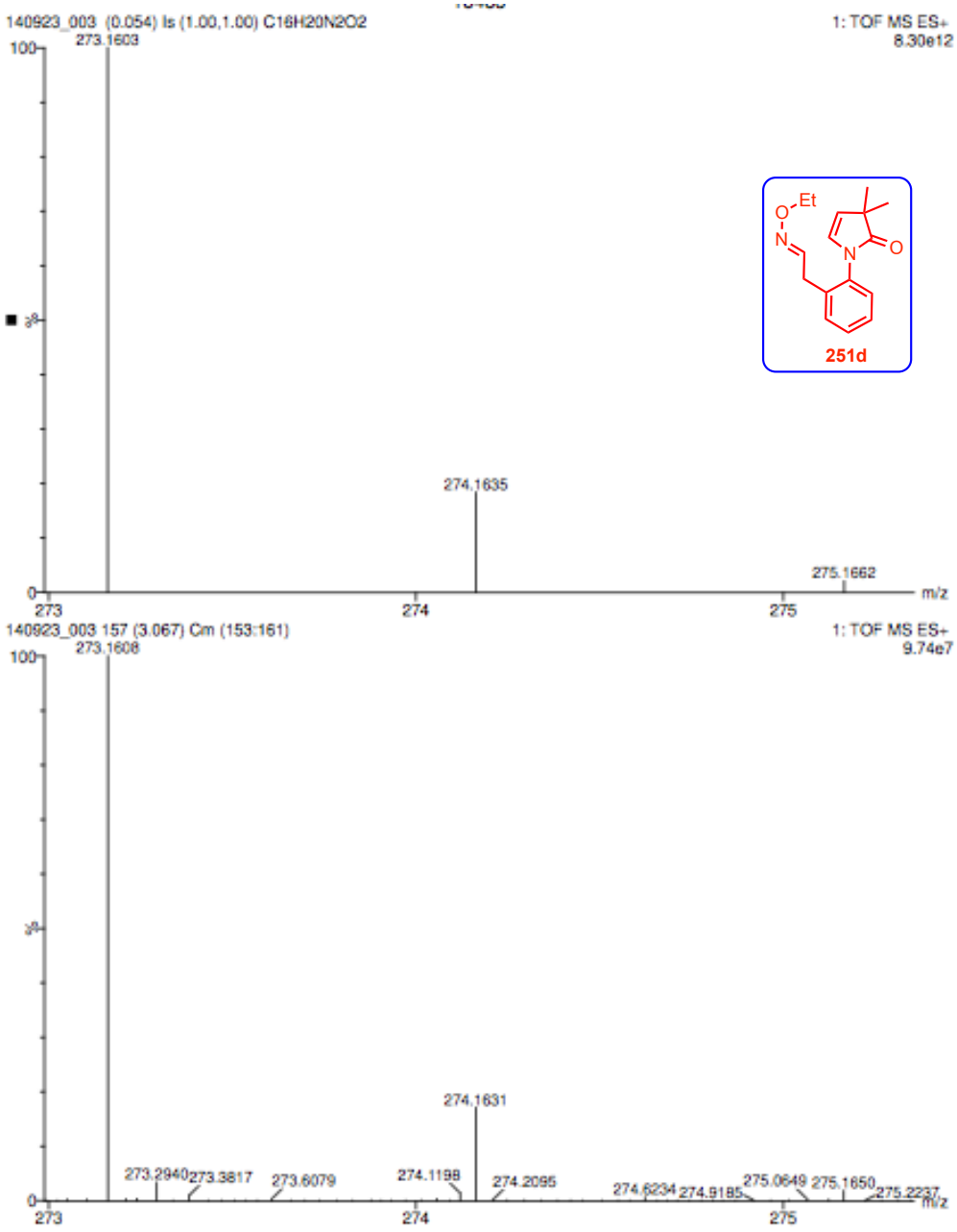

Figure 5.19: HRMS of N-ethoxy oxime derivative **251d**.

^{1}H-NMR (400 MHz, $CDCl_3$, δ ppm): 7.36 (t, *J* = 6.2 Hz, 1H), 7.28-7.26 (m, 6H), 7.17-7.13 (m, 2H), 6.63 (t, *J* = 4.8 Hz, 1H), 6.43 (t, *J* = 4.8 Hz, 2H), 5.45 (d, *J* = 4.8 Hz, 2H), 3.56 (d, *J* = 4.8 Hz, 2H), 3.41 (d, *J* = 6.2 Hz, 2H), 1.28 (s, 6H), 1.27 (s, 6H), 1.24 (s, 9H) and 1.23 (s, 9H).

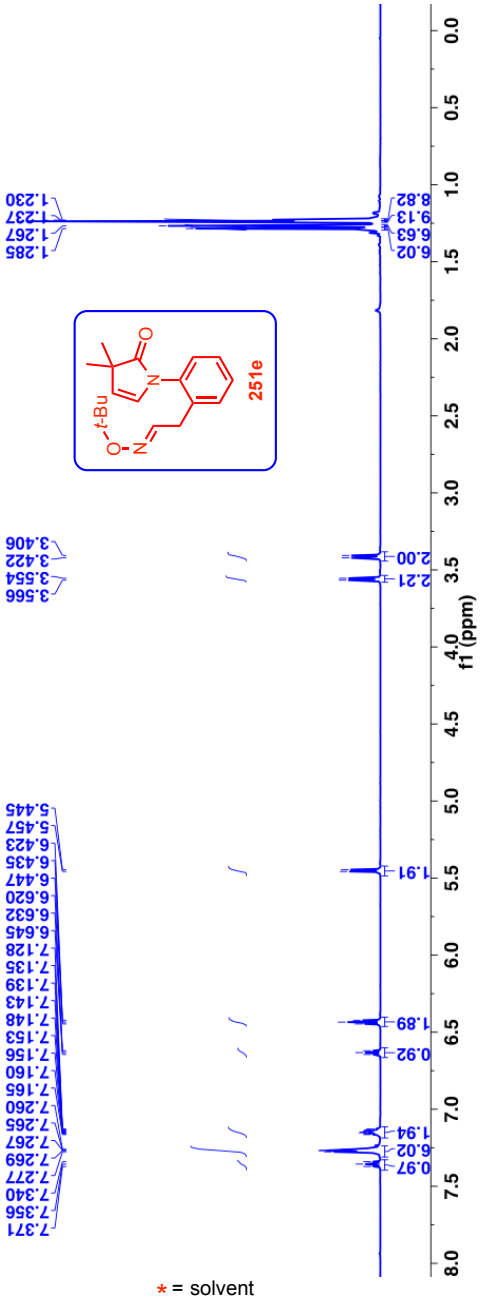

Figure 5.20: ^{1}H-NMR (400 MHz, $CDCl_3$, δ ppm) of N-(*t*-butoxy) oxime derivative **251e**.

^{13}C-NMR (100 MHz, $CDCl_3$, δ ppm): 181.9, 181.8, 147.7, 147.2, 135.9, 135.8, 135.5, 134.7, 131.6, 131.3, 130.95, 130.7, 128.6, 128.5, 127.96, 127.9, 127.4, 127.2, 118.3, 118.1, 78.5, 78.4, 46.4, 32.3, 29.2, 27.8, 27.7 and 23.7.

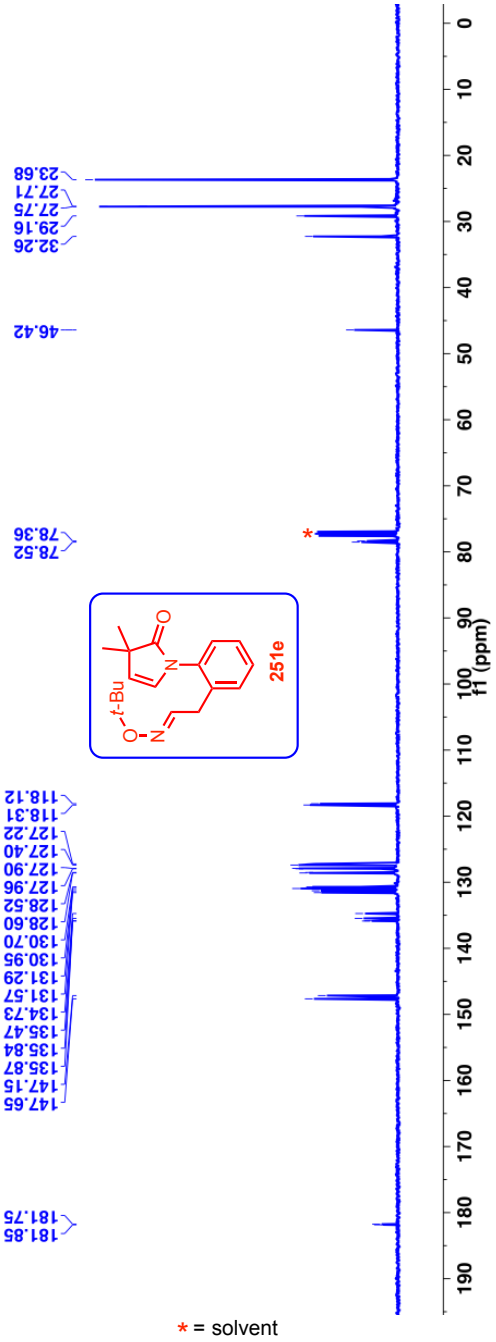

Figure 5.21: ^{13}C-NMR (100 MHz, $CDCl_3$, δ ppm) of N-(*t*-butoxy) oxime derivative **251e**.

HRMS-ESI (m/z) ([M + H]$^+$):

Calculated : 301.1916

Observed : 301.1919

|Δm| : 1.0 ppm

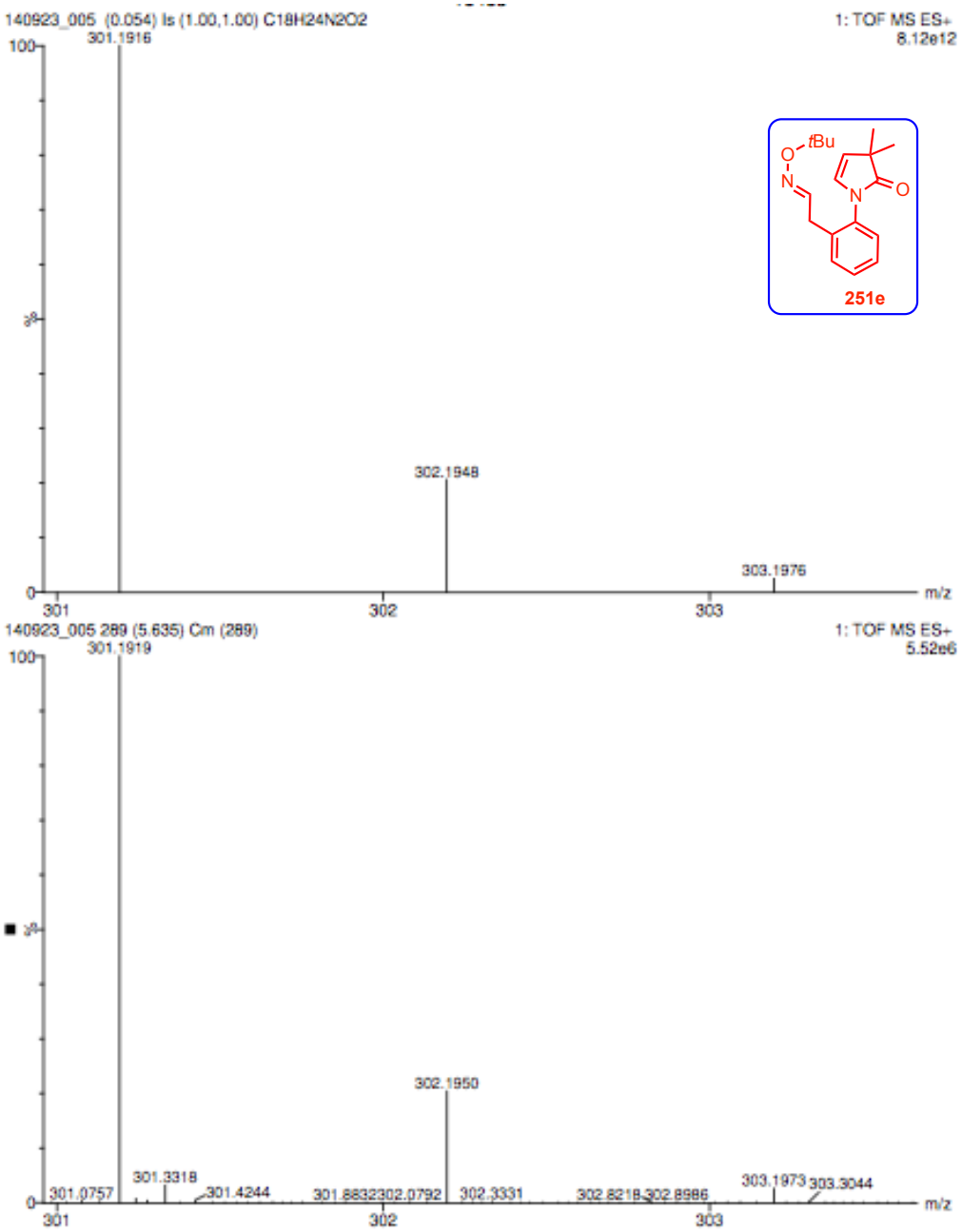

Figure 5.22: HRMS of N-(*t*-butoxy) oxime derivative **251e**.

^{1}H-NMR (400 MHz, $CDCl_3$, δ ppm): 7.49 (t, *J* = 6.2 Hz, 1H), 7.34-7.26 (m, 16H), 7.17-7.14 (m, 2H), 6.73 (t, *J* = 5.0 Hz, 1H), 6.40 (t, *J* = 4.4 Hz, 2H), 5.45 (m, 2H), 5.11 (s, 2H), 5.05 (m, 2H), 3.65 (d, *J* = 5.0 Hz, 2H), 3.45 (d, *J* = 6.2 Hz, 2H), 1.29 (s, 6H) and 1.26 (s, 6H).

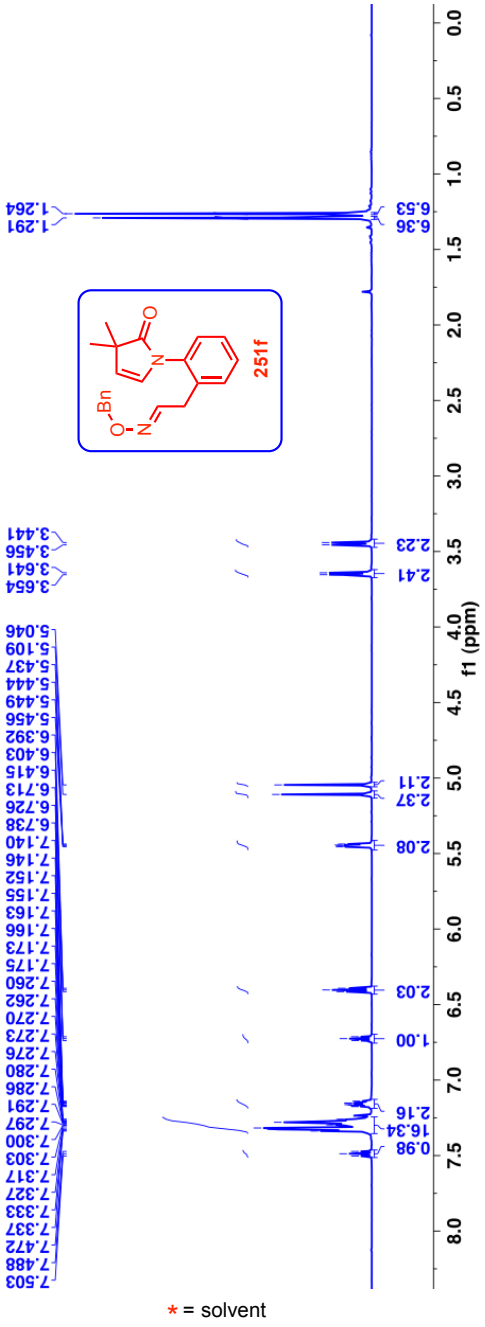

Figure 5.23: ^{1}H-NMR (400 MHz, $CDCl_3$, δ ppm) of N-benzyloxy oxime derivative **251f**.

^{13}C-NMR (100 MHz, $CDCl_3$, δ ppm): 181.8, 181.75, 149.6, 149.3, 138.1, 137.9, 136.0, 135.9, 134.8, 134.2, 131.5, 131.2, 130.96, 130.9, 128.7, 128.6, 128.4, 128.23, 128.2, 128.1, 128.03, 128.0, 127.4, 127.2, 118.5, 118.3, 76.1, 75.9, 46.5, 32.3, 29.3 and 23.7.

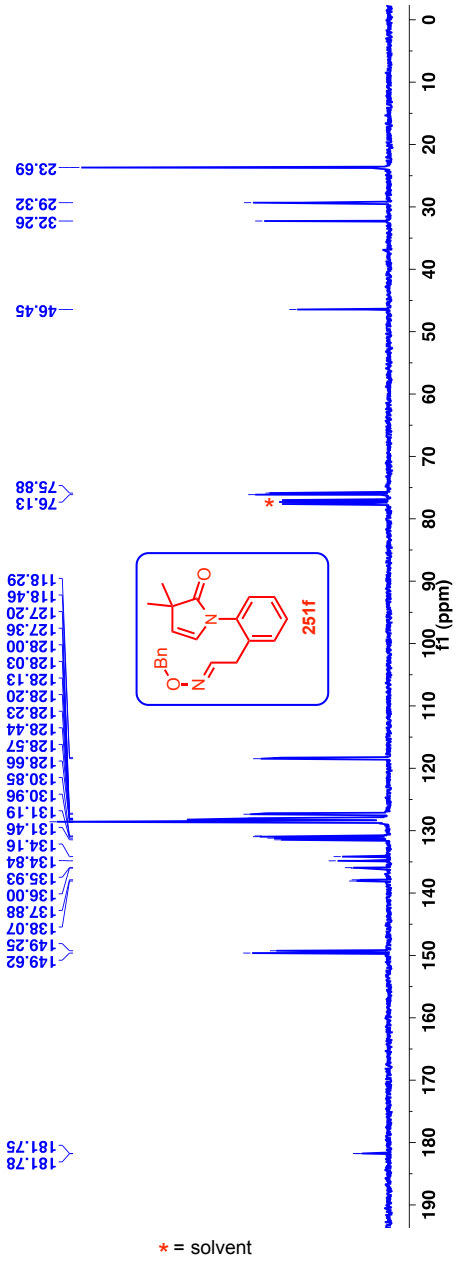

Figure 5.24: ^{13}C-NMR (100 MHz, $CDCl_3$, δ ppm) of N-benzyloxy oxime derivative **251f**.

HRMS-ESI (m/z) ([M + Na]$^+$):

Calculated	: 357.1573
Observed	: 357.1574
|Δm|	: 0.3 ppm

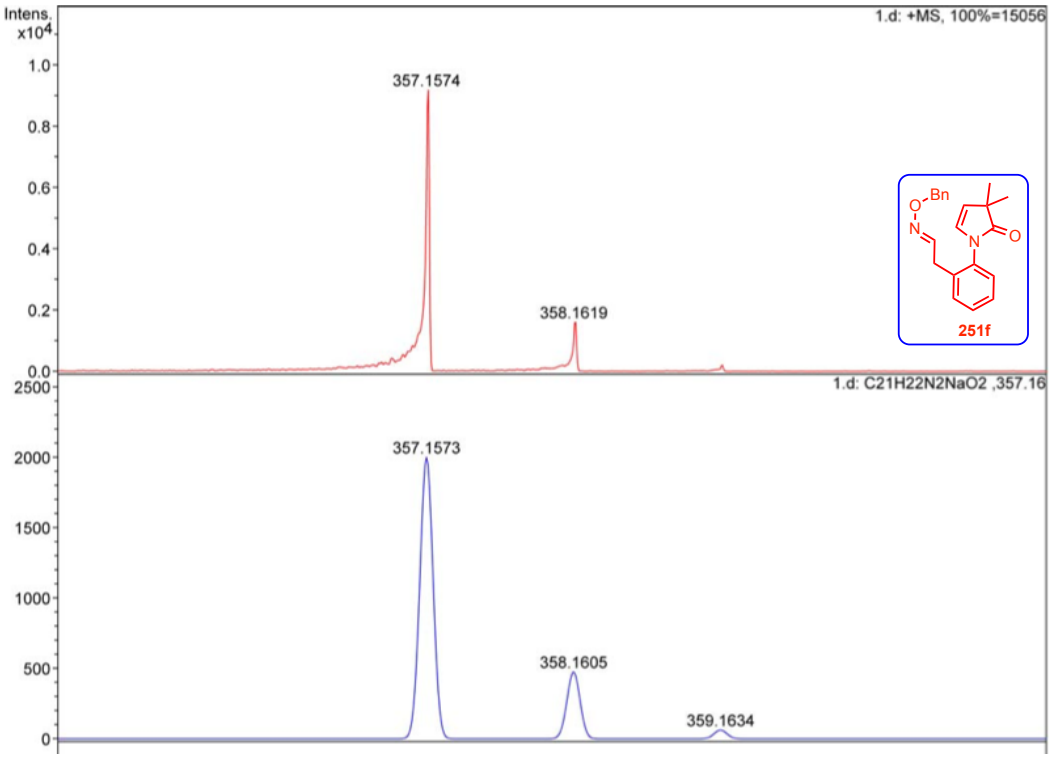

Figure 5.25: HRMS of N-benzyloxy oxime derivative **251f**.

5.5.4. General irradiation procedure for imine derived enamides 251a-f

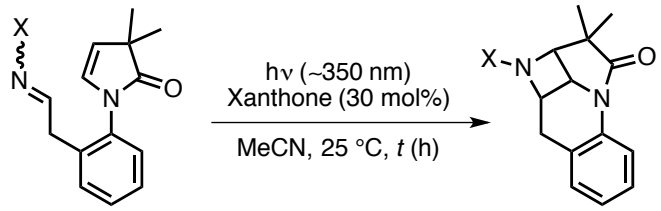

251a-h **252a-h**

Scheme 5.11: Intramolecular [2+2]-photocycloaddition of stabilized imines with enamides.

A N_2 saturated solution of imine derivatives **251a-f** in MeCN (1mg/1mL or 2.5-4.1 mM) with xanthone sensitizer (30 mol%) was irradiated in a Rayonet reactor equipped with ~350 nm bulbs until the reaction is complete as monitored by the ^{1}H-NMR spectroscopy (and TLC). After the reaction, the solvent was evaporated under reduced pressure and the residue was purified by combiflash to get the pure product.

The large-scale photoreactions were performed as batches on the same concentration (8 × 10 mL test tubes per batch) using merry-go-round apparatus. After the reaction, the solvent was evaporated under reduced pressure and the residue was purified by combiflash to get the pure product.

Note: For the given scale (10 mg) the reaction was complete in 1 h. Longer irradiation leads to decomposition of photoproducts. The Rf of most of the photoproducts and their starting materials were same, so ^{1}H-NMR spectroscopy was used to monitor the reaction. A solution of imines undergoes decomposition even when stored in dark, so the operations have to be carried out so as to reduce the pre-irradiation time as less as possible.

^{1}H-NMR (400 MHz, CD_2Cl_2, δ ppm): 7.77-7.34 (m, 2H), 7.41-7.38 (m, 1H), 7.33-7.31 (m, 2H), 7.28-7.24 (m, 1H), 7.18-7.14 (m, 1H), 7.05-7.03 (m, 1H), 6.18 (bs, 1H), 4.06-3.99 (m, 2H), 3.85 (d, *J* = 5.0 Hz, 1H), 2.77 (dd, *J* = 18.4, 8.0 Hz, 1H), 2.46 (m, 3H), 2.39 (d, *J* = 18.8 Hz, 1H), 1.12 (s, 3H) and 0.81 (s, 3H).

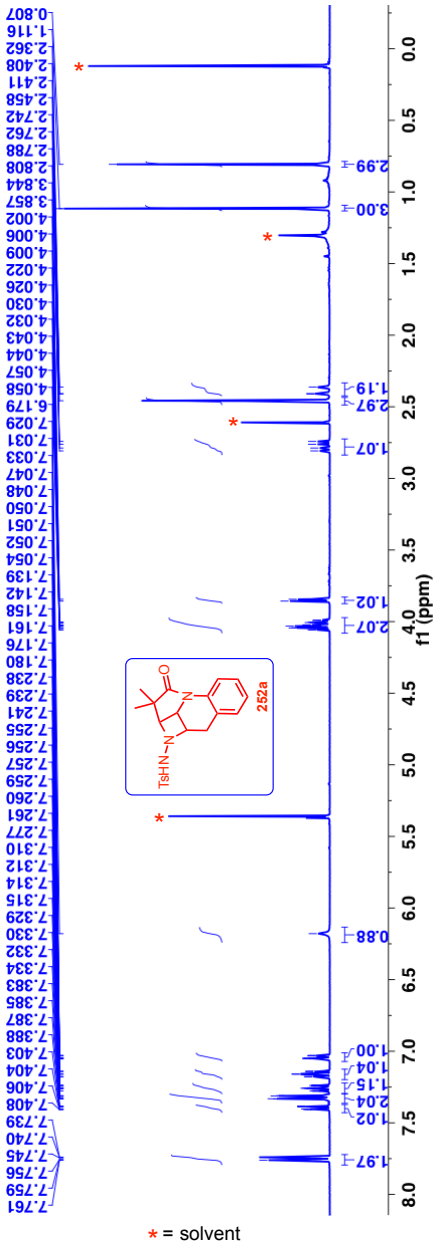

Figure 5.26: ^{1}H-NMR (400 MHz, CD_2Cl_2, δ ppm) of N-tosyl imine photoproduct **252a**.

^{13}C-NMR (100 MHz, CD_2Cl_2, δ ppm): 178.2, 144.6, 135.7, 134.7, 130.5, 129.7, 128.8, 128.5, 126.2, 125.6, 124.9, 76.0, 70.4, 47.4, 44.3, 29.1, 22.3, 21.3 and 16.3.

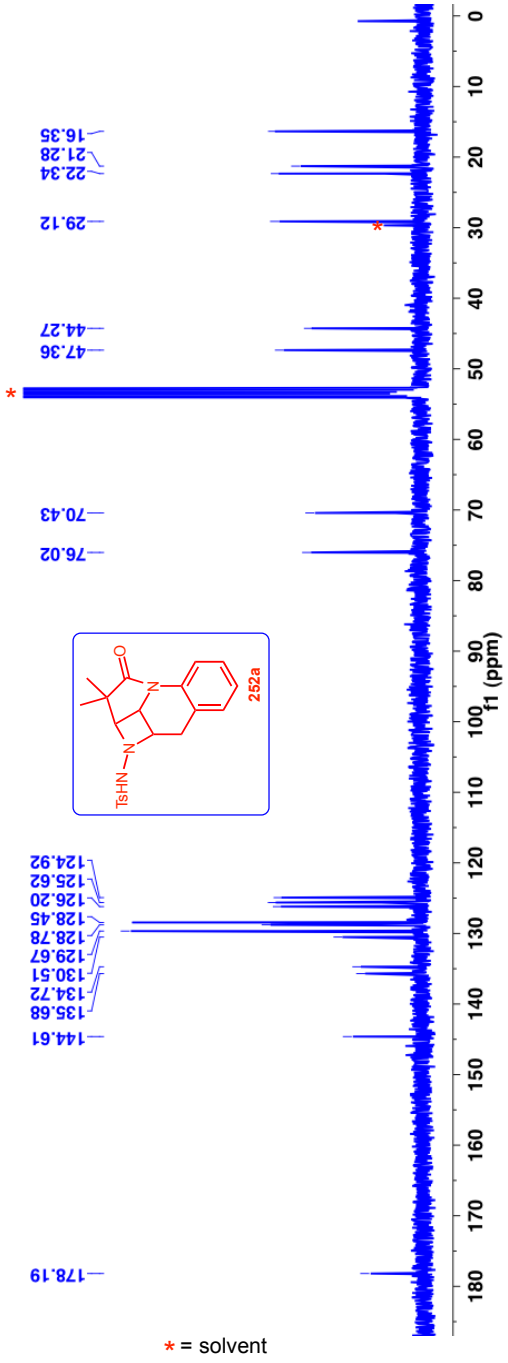

Figure 5.27: ^{13}C-NMR (400 MHz, CD_2Cl_2, δ ppm) of N-tosyl imine photoproduct **252a**.

HRMS-ESI (m/z) ([M + Na]$^+$):

Calculated : 224.1434

Observed : 224.1437

|Δm| : 1.3 ppm

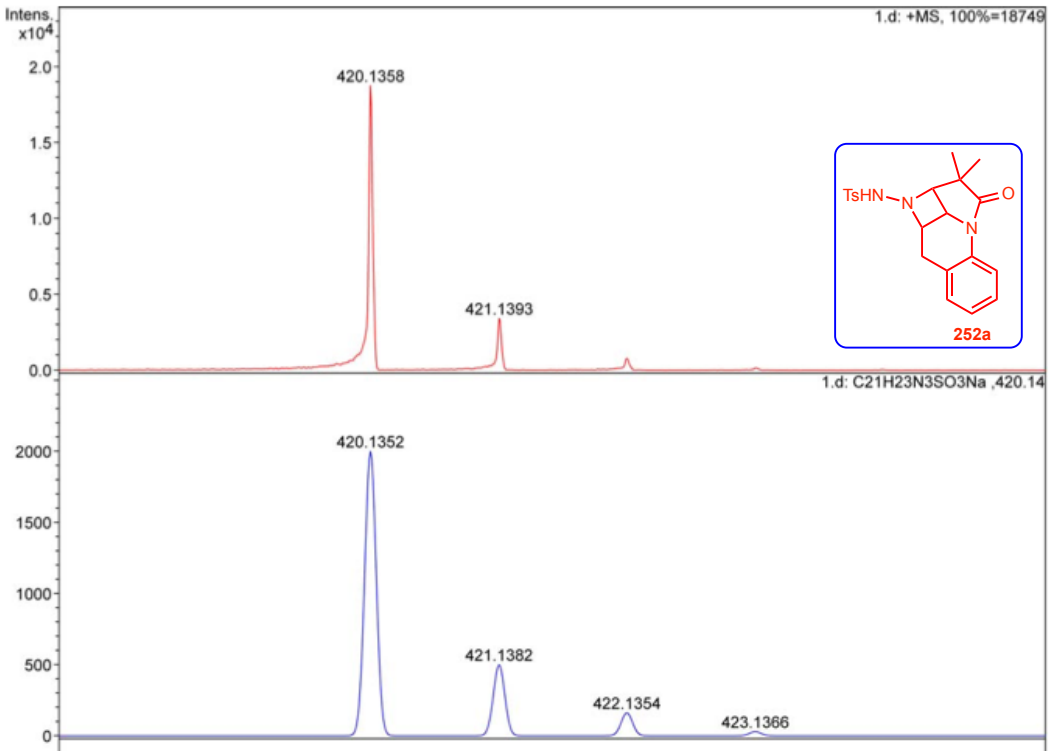

Figure 5.28: HRMS of N-tosyl imine photoproduct **252a**.

^{1}H-NMR (400 MHz, $CDCl_3$, δ ppm): 7.50-7.48 (m, 1H), 7.29-7.25 (m, 1H), 7.17-7.14 (m, 2H), 5.60 (bs, 1H), 4.17 – 4.11 (m, 1H), 4.08-4.04 (m, 1H), 3.83 (d, *J* = 5.2 Hz, 1H), 3.11 (dd, *J* = 18.4, 8.0 Hz, 1H), 2.94 (d, *J* = 18.4 Hz, 1H), 1.28 (s, 3H) and 1.25 (s, 3H).

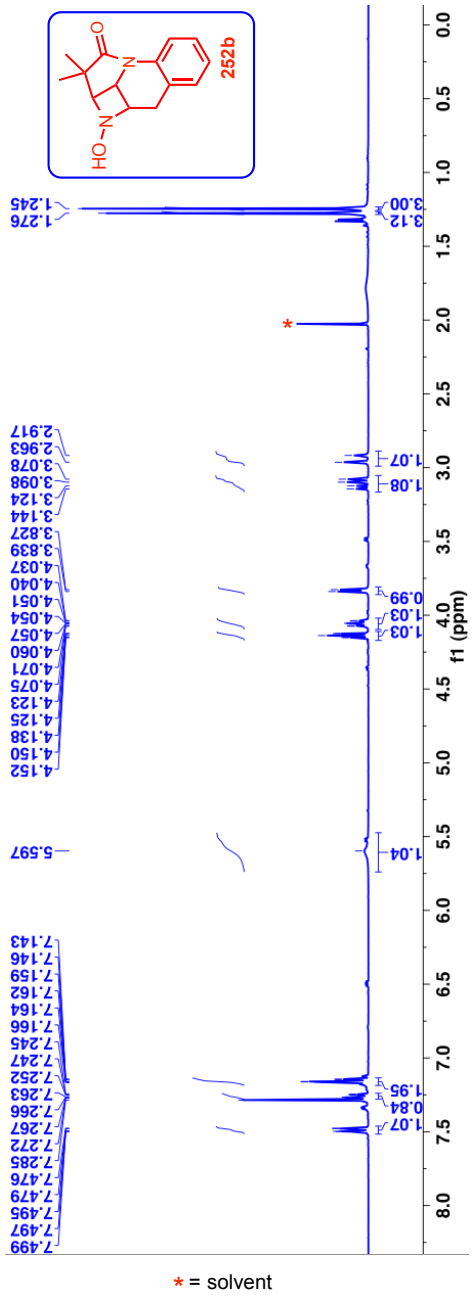

Figure 5.29: ^{1}H-NMR (400 MHz, $CDCl_3$, δ ppm) of N-hydroxy oxime photoproduct **252b**.

^{13}C-NMR (100 MHz, $CDCl_3$, δ ppm): 179.0, 134.7, 129.6, 129.2, 126.6, 125.6, 125.1, 76.1, 66.5, 46.2, 44.3, 29.2, 22.3 and 17.3.

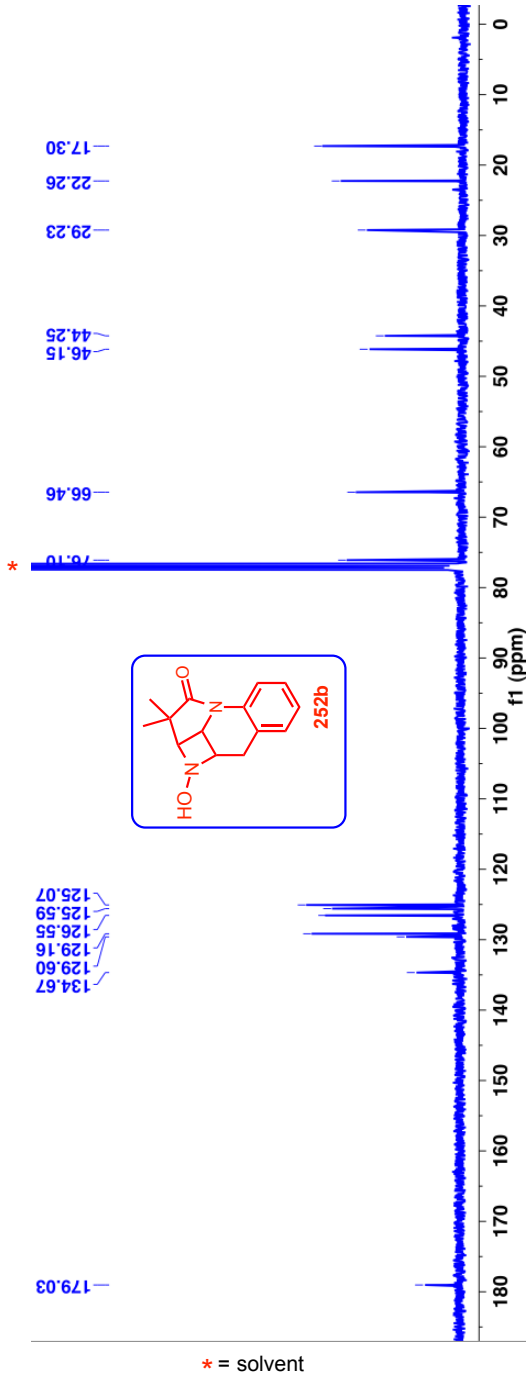

Figure 5.30: ^{13}C-NMR (100 MHz, $CDCl_3$, δ ppm) of N-hydroxy oxime photoproduct **252b**.

HRMS-ESI (m/z) ([M + Na]$^+$):

Calculated : 267.1104

Observed : 267.1103

|Δm| : 0.4 ppm

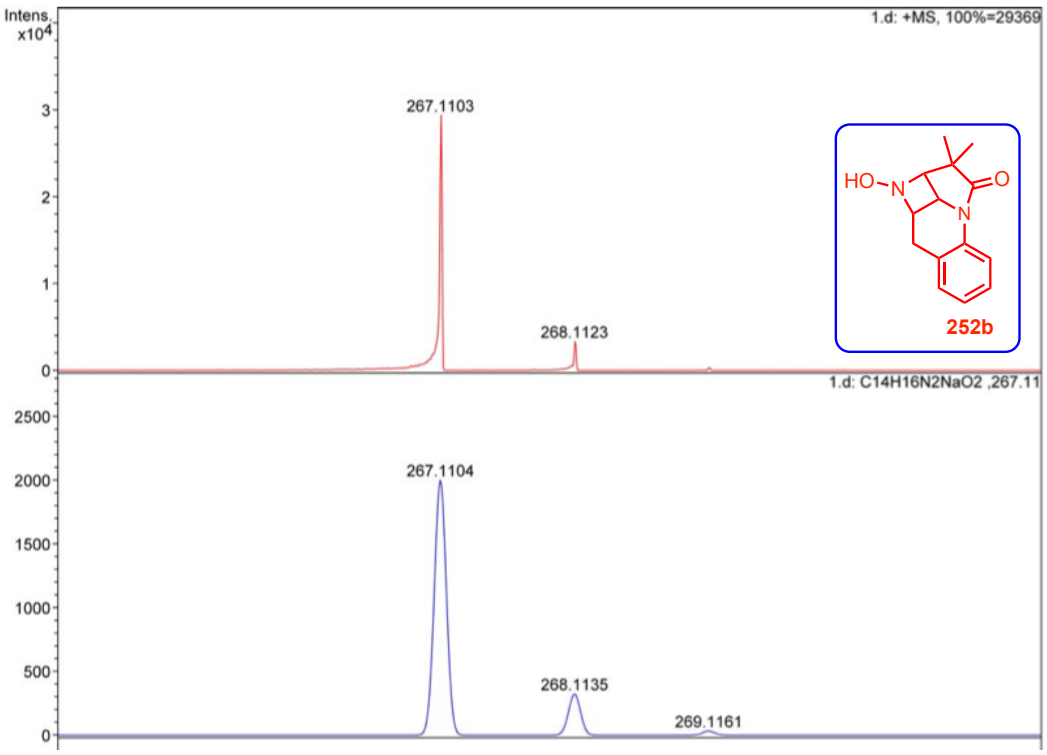

Figure 5.31: HRMS of N-hydroxy oxime photoproduct **252b**.

^{1}H-NMR (400 MHz, $CDCl_3$, δ ppm): 7.46-7.44 (m, 1H), 7.25-7.20 (m, 1H), 7.13-7.08 (m, 2H), 4.08-4.05 (m, 1H), 4.00-3.96 (m, 1H), 3.74 (d, *J* = 5.4 Hz, 1H), 3.49 (s, 3H), 3.14 (dd, *J* = 18.0, 8.0 Hz, 1H), 2.96-2.91 (m, 1H), 1.28 (s, 3H) and 1.20 (s, 3H).

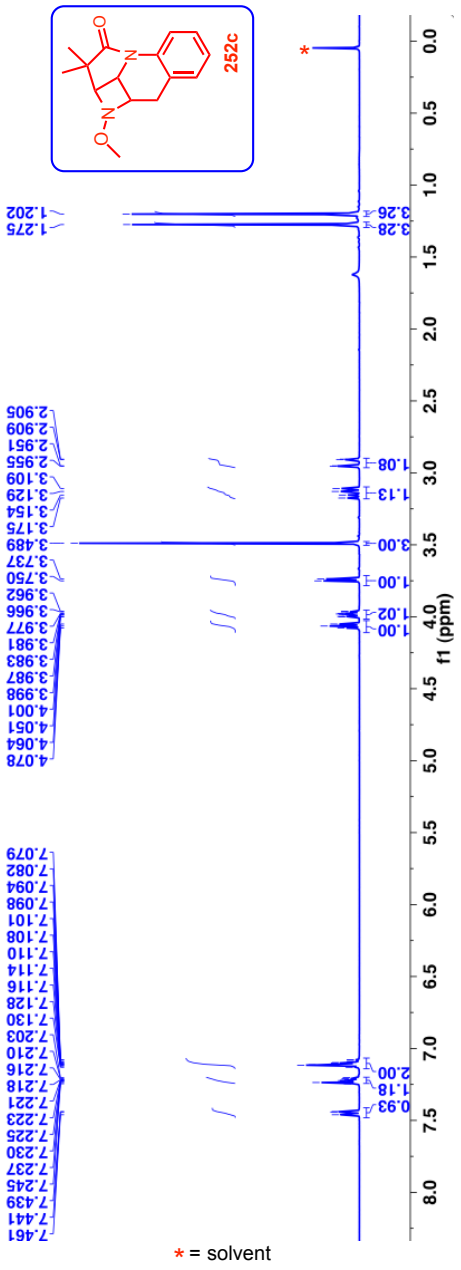

Figure 5.32: ^{1}H-NMR (400 MHz, $CDCl_3$, δ ppm) of N-methoxy oxime photoproduct **252c**.

^{13}C-NMR (100 MHz, $CDCl_3$, δ ppm): 179.1, 134.98, 130.1, 129.2, 126.7, 125.8, 125.2, 75.9, 66.2, 62.0, 46.3, 44.1, 30.7, 22.5 and 18.3.

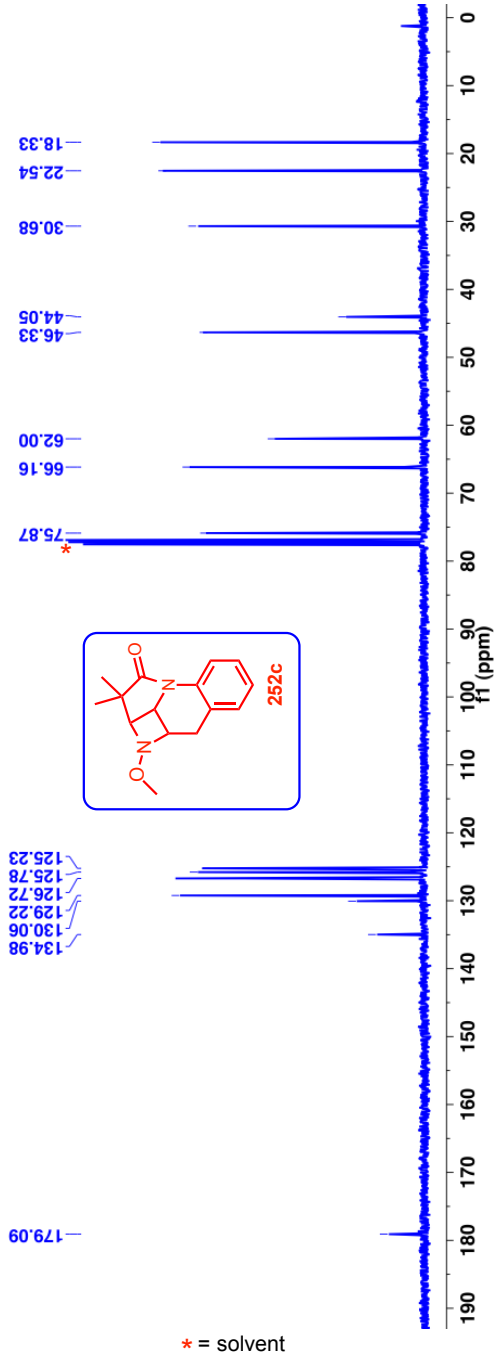

Figure 5.33: ^{13}C-NMR (100 MHz, $CDCl_3$, δ ppm) of N-methoxy oxime photoproduct **252c**.

HRMS-ESI (m/z) ([M + H]$^+$):

Calculated	: 259.1447
Observed	: 259.1451
|Δm|	: 1.5 ppm

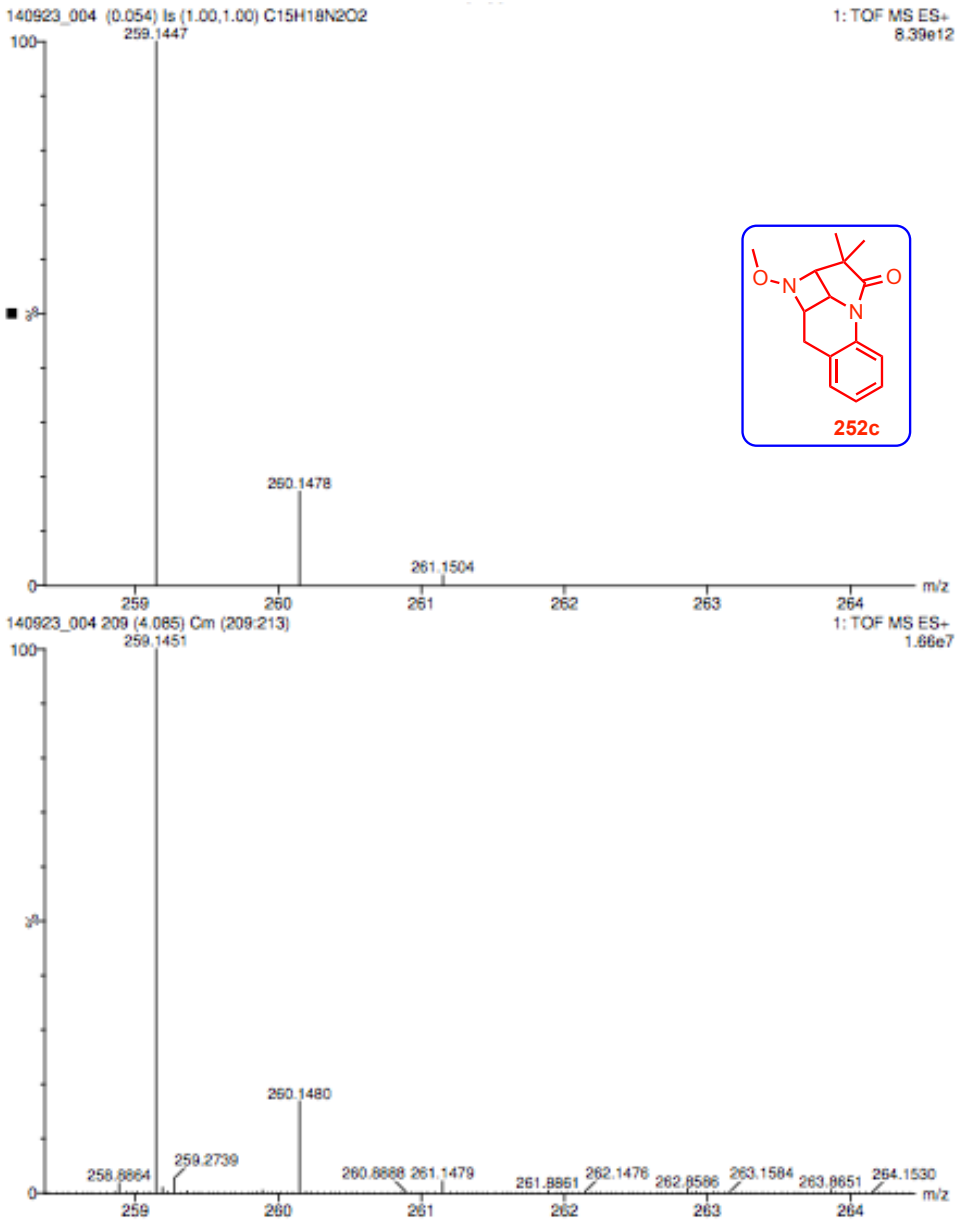

Figure 5.34: HRMS of N-methoxy oxime photoproduct **252c**.

^{1}H-NMR (400 MHz, $CDCl_3$, δ ppm): 7.46-7.44 (m, 1H), 7.24-7.20 (m, 1H), 7.13-7.08 (m, 2H), 4.08-4.06 (m, 1H), 4.00-3.96 (m, 1H), .3.78-3.76 (m, 1H), 3.72-3.61 (m, 2H), 3.11 (dd, *J* = 18.0, 8.4 Hz, 1H), 2.93-2.89 (m, 1H), 1.25 (s, 3H), 1.19 (s, 3H) and 1.11 (t, *J* = 7.0 Hz, 3H).

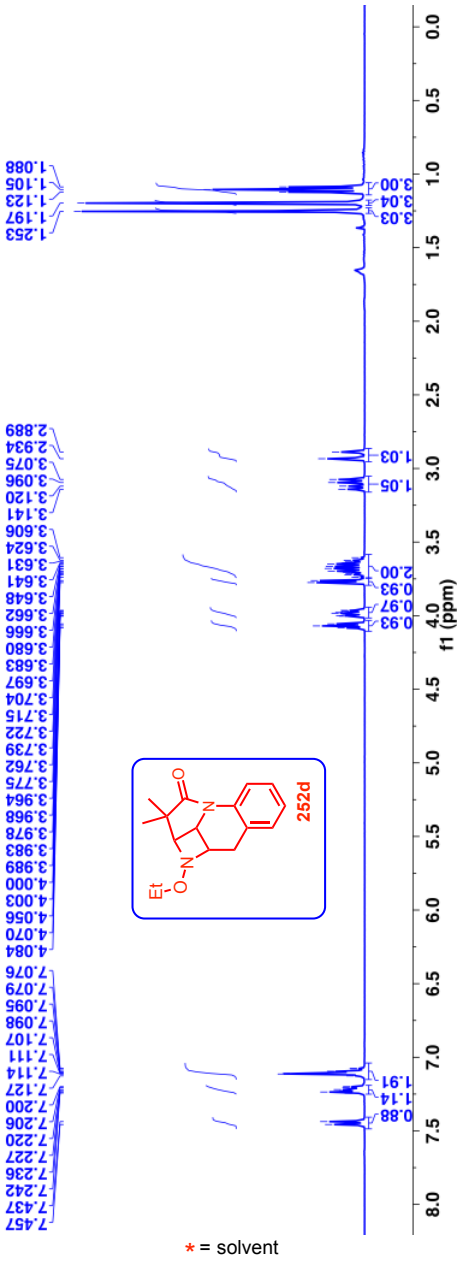

Figure 5.35: ^{1}H-NMR (400 MHz, $CDCl_3$, δ ppm) of N-ethoxy oxime photoproduct **252d**.

^{13}C-NMR (100 MHz, $CDCl_3$, δ ppm): 79.1, 135.0, 130.2, 129.2, 126.7, 125.8, 125.2, 75.98, 69.1, 66.4, 46.5, 44.1, 30.3, 22.6, 18.3 and 14.9.

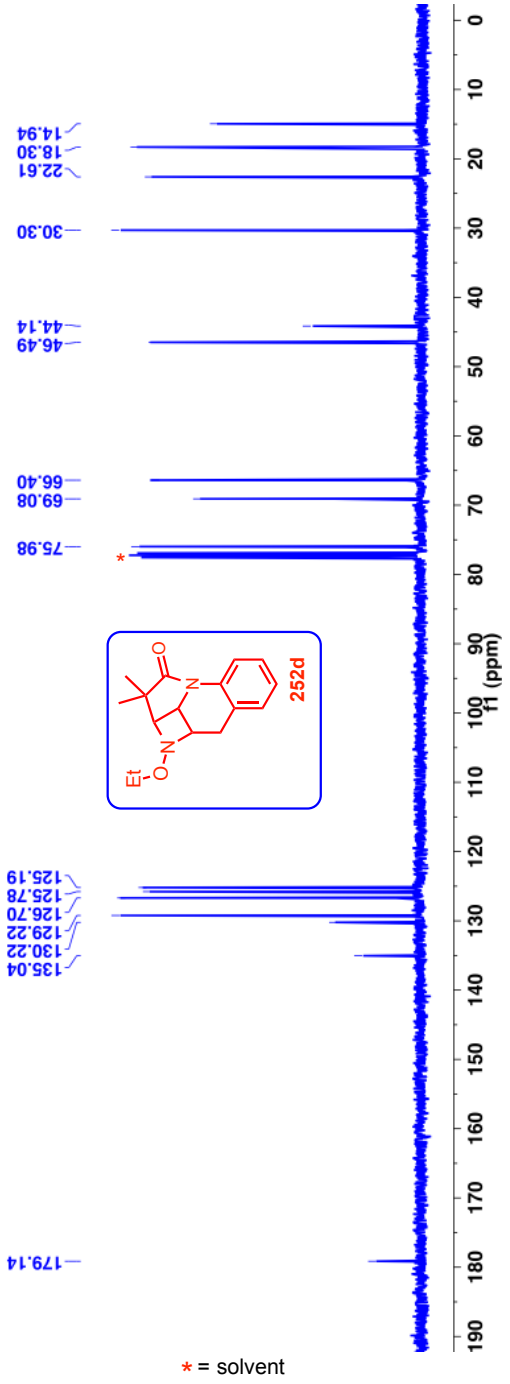

Figure 5.36: ^{13}C-NMR (100 MHz, $CDCl_3$, δ ppm) of N-ethoxy oxime photoproduct **252d**.

HRMS-ESI (m/z) ([M + H]$^+$):

Calculated	: 273.1603
Observed	: 273.1606
|Δm|	: 1.1 ppm

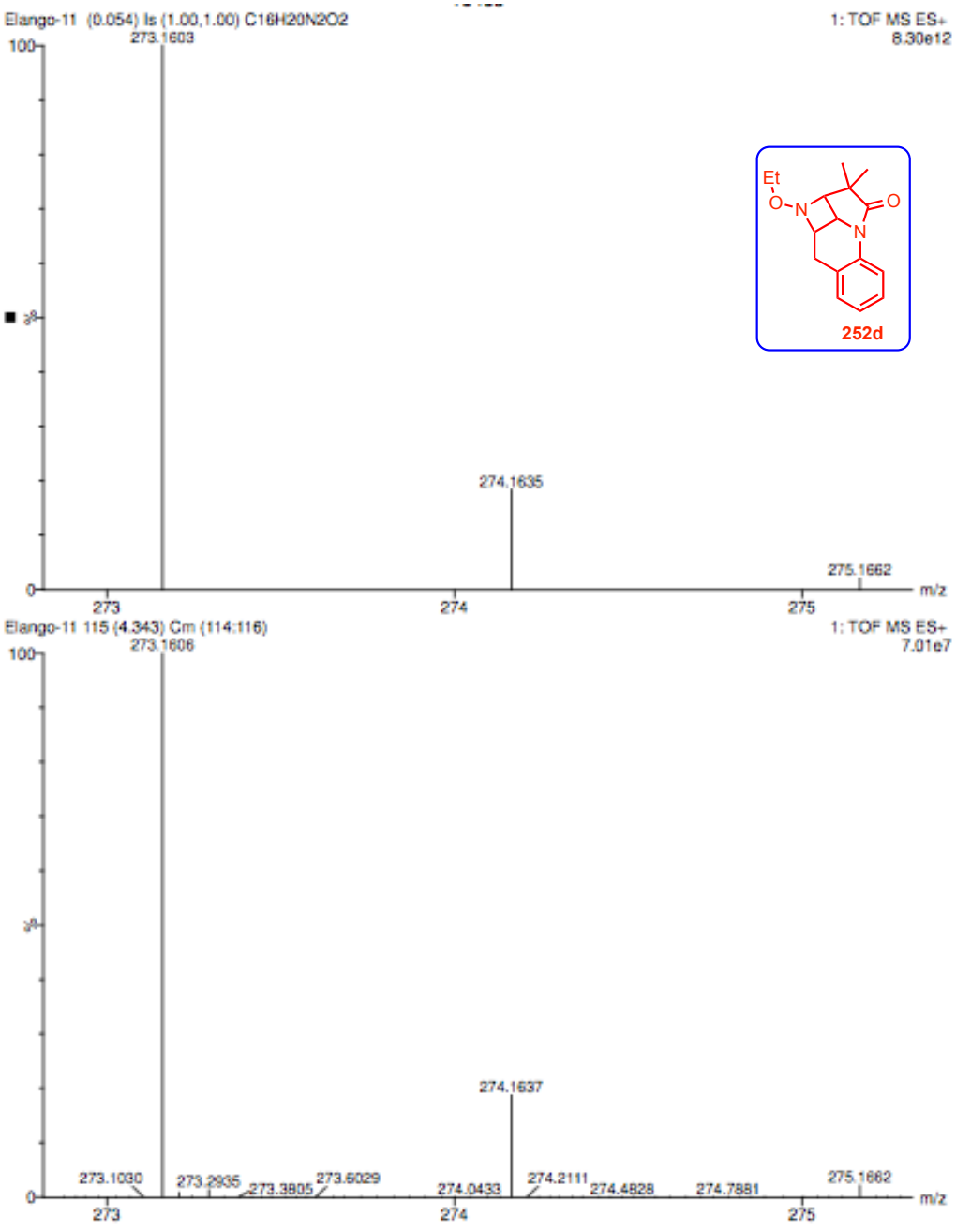

Figure 5.37: HRMS of N-ethoxy oxime photoproduct **252d**.

^{1}H-NMR (400 MHz, $CDCl_3$, δ ppm): 7.43-7.42 (m, 1H), 7.25-7.21 (m, 1H), 7.12-7.11 (m, 2H), 4.15-4.12 (m, 1H), 4.02-3.97 (m, 1H), 3.83-3.82 (m, 1H), 3.09 (dd, *J* = 17.6, 9.0 Hz, 1H), 2.99-2.94 (m, 1H), 1.27 (s, 3H), 1.19 (s, 3H) and 1.14 (s, 9H).

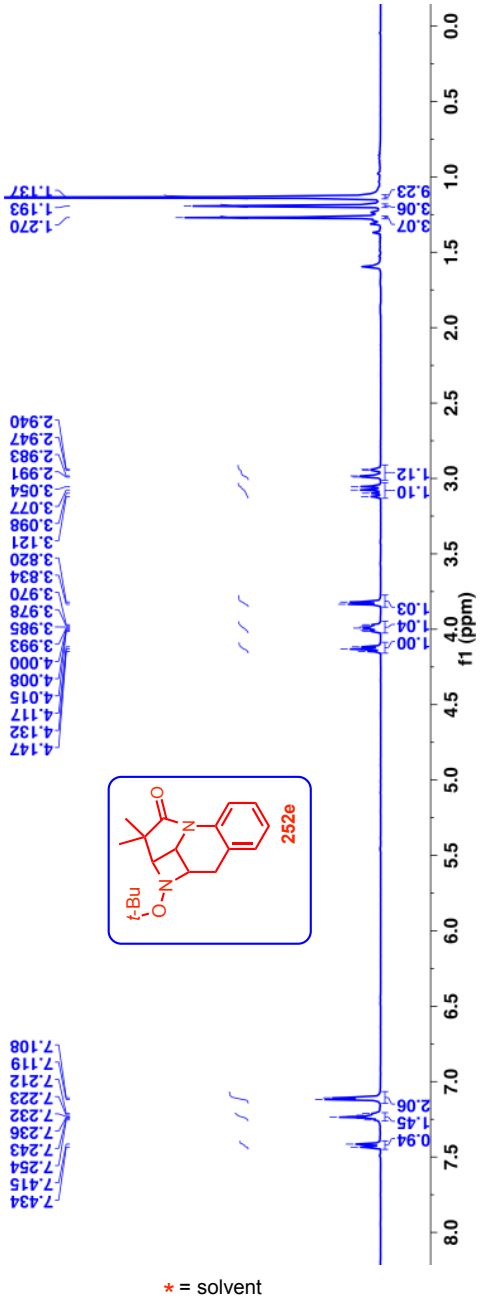

Figure 5.38: ^{1}H-NMR (400 MHz, $CDCl_3$, δ ppm) of N-(*t*-butoxy) oxime photoproduct **252e**.

^{13}C-NMR (100 MHz, $CDCl_3$, δ ppm): 178.8, 135.6, 131.5, 128.9, 126.9, 126.1, 125.0, 77.7, 75.5, 70.0, 48.0, 44.9, 30.9, 28.7, 23.7 and 18.1.

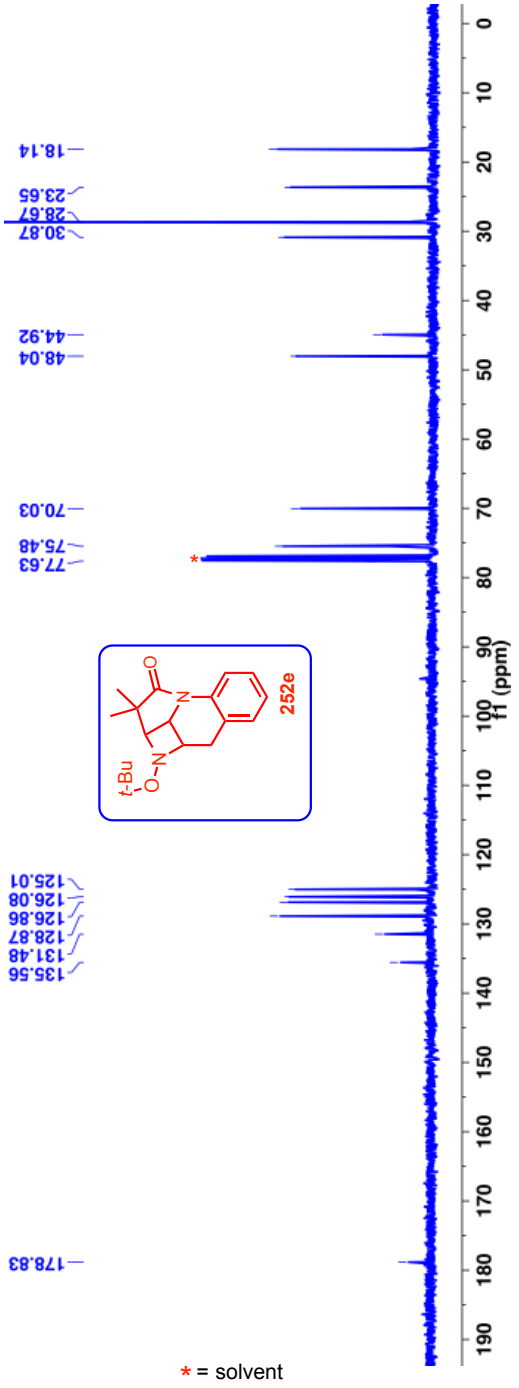

Figure 5.39: ^{13}C-NMR (100 MHz, $CDCl_3$, δ ppm) of N-(*t*-butoxy) oxime photoproduct **252e**.

HRMS-ESI (m/z) ([M + H]$^+$):

Calculated : 301.1916

Observed : 301.1923

|Δm| : 2.3 ppm

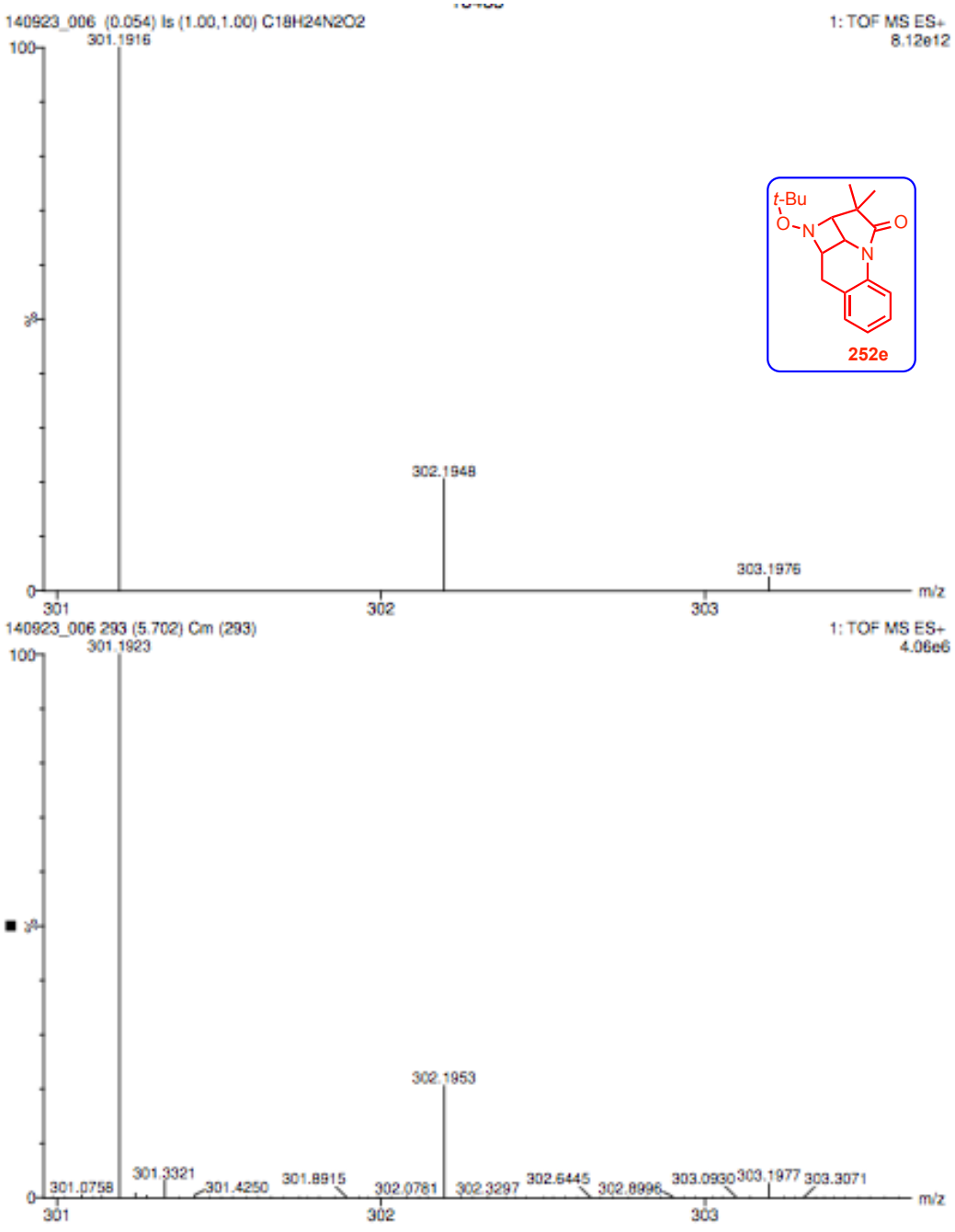

Figure 5.40: HRMS of N-(*t*-butoxy) oxime photoproduct **252e**.

^{1}H-NMR (400 MHz, $CDCl_3$, δ ppm): 7.44-7.41 (m, 1H), 7.32-7.18 (m, 5H), 7.22-7.18 (m, 1H), 7.09-7.04 (m, 1H), 6.99-6.97 (m, 1H), 4.71 (d, *J* = 11.6 Hz, 1H), 4.57 (d, *J* = 11.6 Hz, 1H), 4.05 (t, *J* = 5.6 Hz, 1H), 4.02 – 3.95 (m, 1H), 3.87 (d, *J* = 5.3 Hz, 1H), 2.78 (dd, *J* = 18.4, 8.4 Hz, 1H), 2.31 (d, *J* = 18.3 Hz, 1H), 1.31 (s, 3H) and 1.22 (s, 3H).

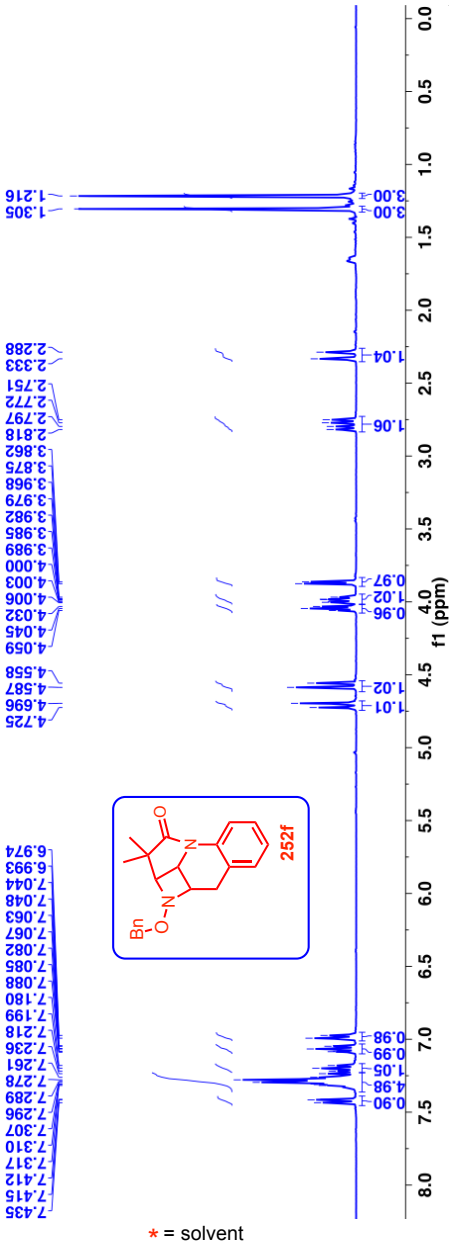

Figure 5.41: ^{1}H-NMR (400 MHz, $CDCl_3$, δ ppm) of N-benzyloxy oxime photoproduct **252f**.

^{13}C-NMR (100 MHz, $CDCl_3$, δ ppm): 179.1, 138.2, 134.9, 130.4, 129.2, 128.9, 128.6, 128.2, 126.6, 125.8, 125.1, 76.4, 75.9, 66.9, 46.6, 44.2, 29.7, 22.6 and 18.4.

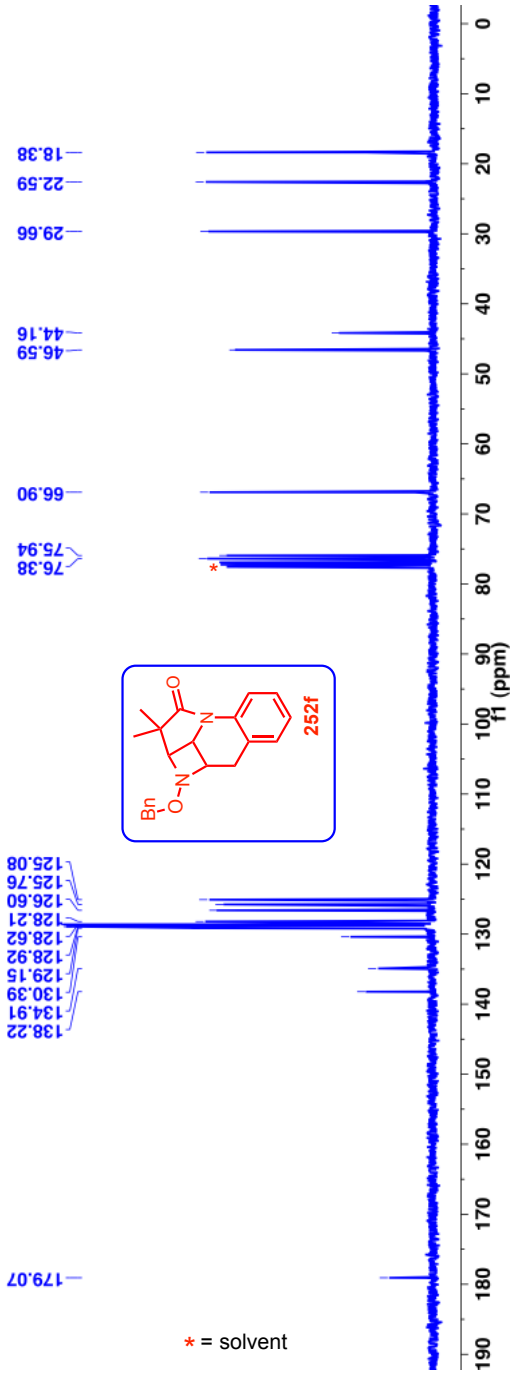

Figure 5.42: ^{13}C-NMR (100 MHz, $CDCl_3$, δ ppm) of N-benzyloxy oxime photoproduct **252f**.

HRMS-ESI (m/z) ([M + H]$^+$):

Calculated : 335.1760

Observed : 335.1762

|Δm| : 0.6 ppm

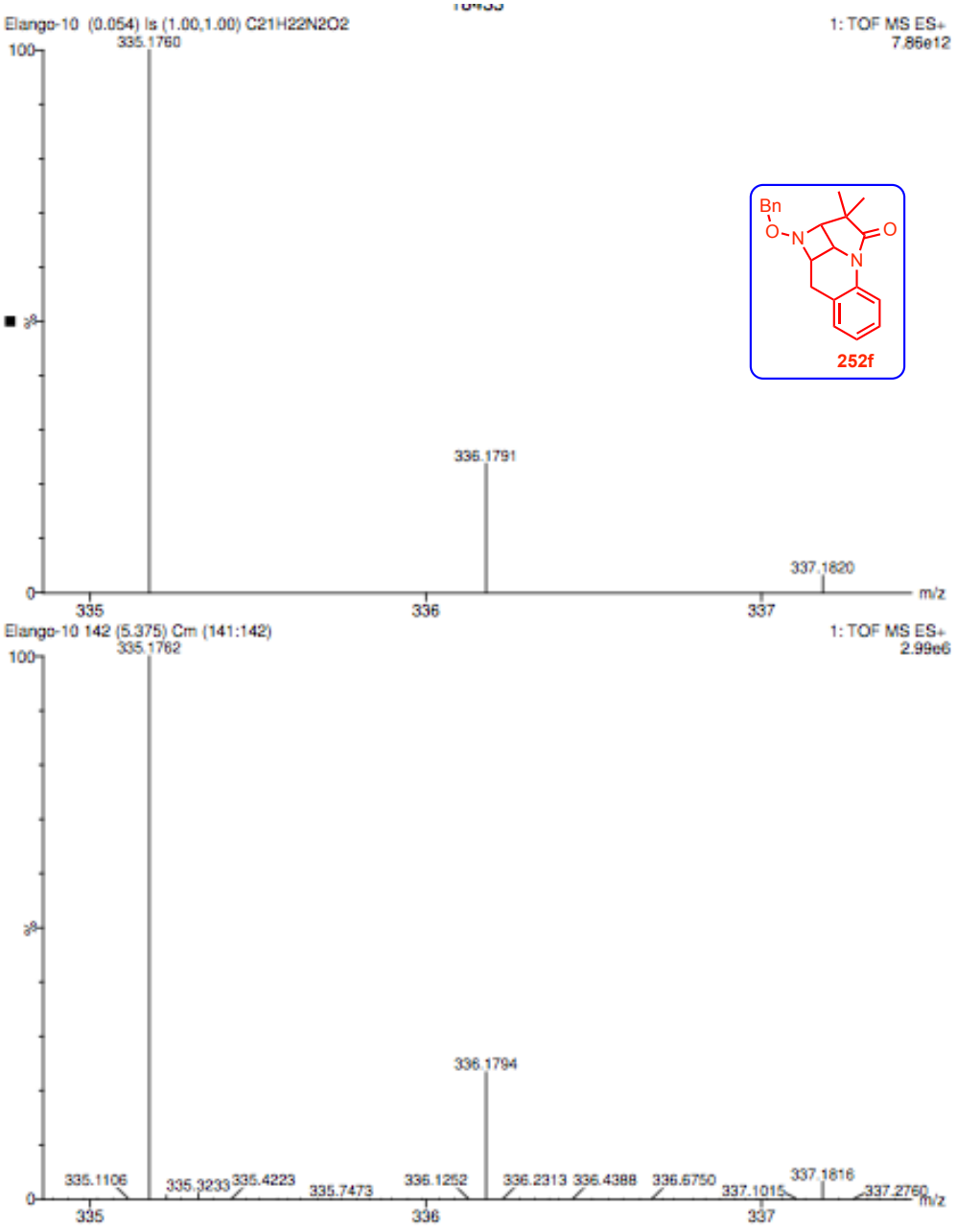

Figure 5.43: HRMS of N-benzyloxy oxime photoproduct **252f**.

^{1}H-NMR (400 MHz, $CDCl_3$, δ ppm): 7.42-7.40 (m, 1H), 7.23-7.19 (m, 1H), 7.10-7.09 (m, 2H), 6.21 (bs, 1H), 4.90 (s, 1H), 4.59 (s, 1H), 4.01 (t, *J* = 5.2 Hz, 1H), 2.96 (dd, *J* = 18.0, 8.0 Hz, 1H), 2.72 (d, *J* = 18.0 Hz, 1H), 1.46 (s, 9H), 1.17 (s, 3H) and 1.16 (s, 3H).

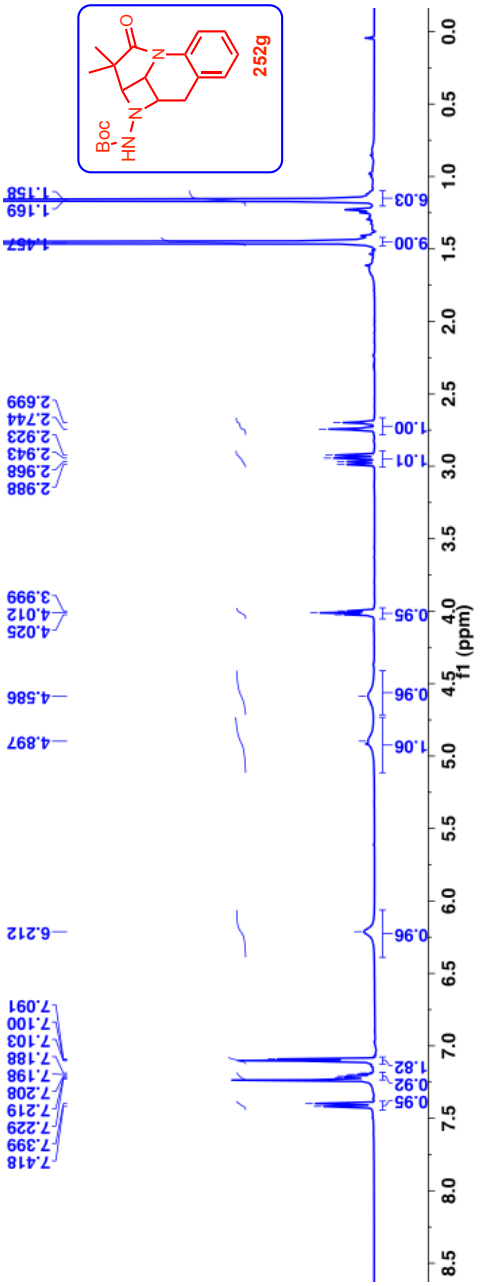

Figure 5.44: ^{1}H-NMR (400 MHz, $CDCl_3$, δ ppm) of N-Boc imine photoproduct **252g**.

^{13}C-NMR (100 MHz, DMSO, δ ppm): 178.7, 154.5, 134.8, 130.4, 129.1, 125.8, 125.1, 124.9, 78.5, 73.0, 63.2, 46.4, 43.9, 28.8, 20.1, 21.8 and 17.2.

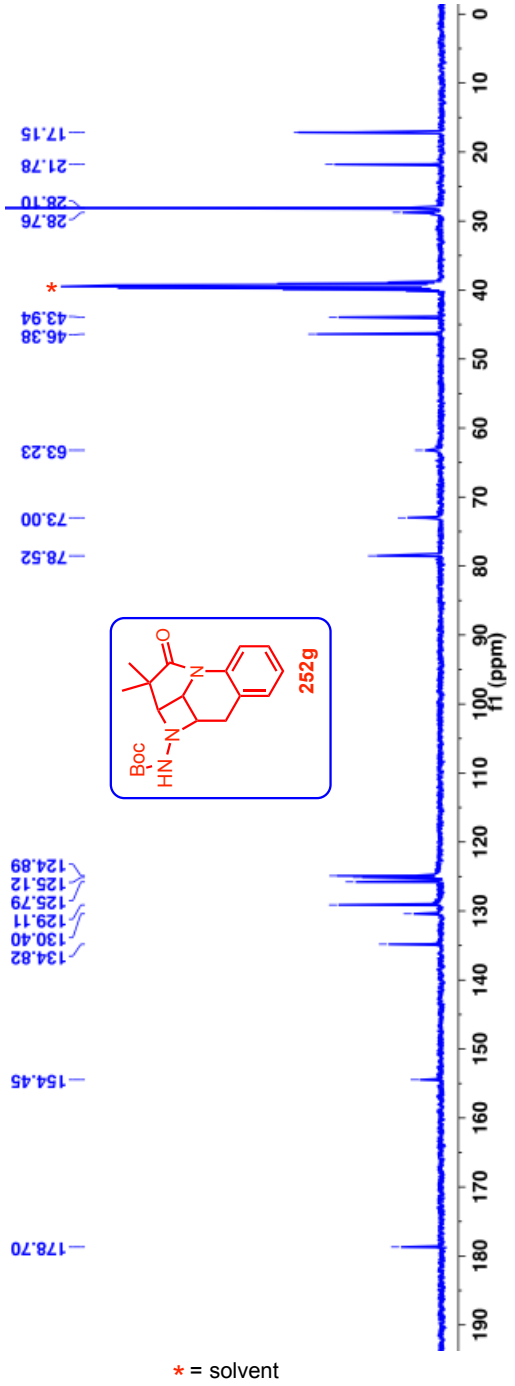

Figure 5.45: ^{13}C-NMR (100 MHz, $CDCl_3$, δ ppm) of N-benzyloxy oxime photoproduct **252g**.

HRMS-ESI (m/z) ([M + Na]$^+$):

Calculated	: 366.1794
Observed	: 366.1790
|Δm|	: 1.1 ppm

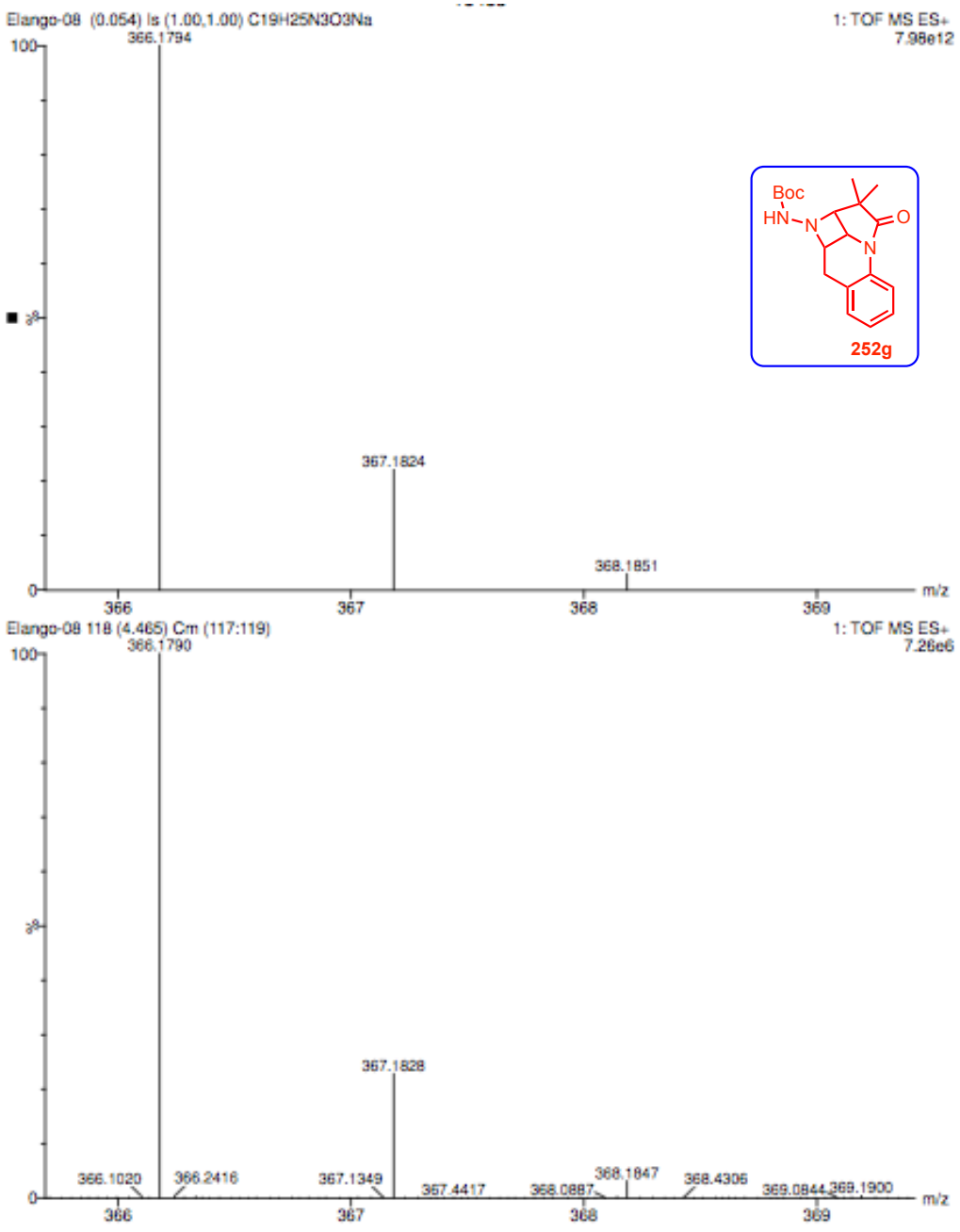

Figure 5.46: HRMS of N-benzyloxy oxime photoproduct **252g**.

^{1}H-NMR (400 MHz, DMSO, δ ppm): 9.91 (bs, 1H), 7.77-7.75 (m, 2H), 7.53-7.49 (m, 1H), 7.45-7.41 (m, 2H), 7.31-7.29 (m, 1H), 7.23-7.095 (m, 3H), 4.61-4.58 (m, 1H), 4.40 (d, *J* = 5.2 Hz, 1H), 4.19 (t, *J* = 4.8 Hz, 1H), 2.99 (dd, *J* = 18.4, 8.0 Hz, 1H), 2.69 (d, *J* = 18.0 Hz, 1H) and 1.07 (s, 6H).

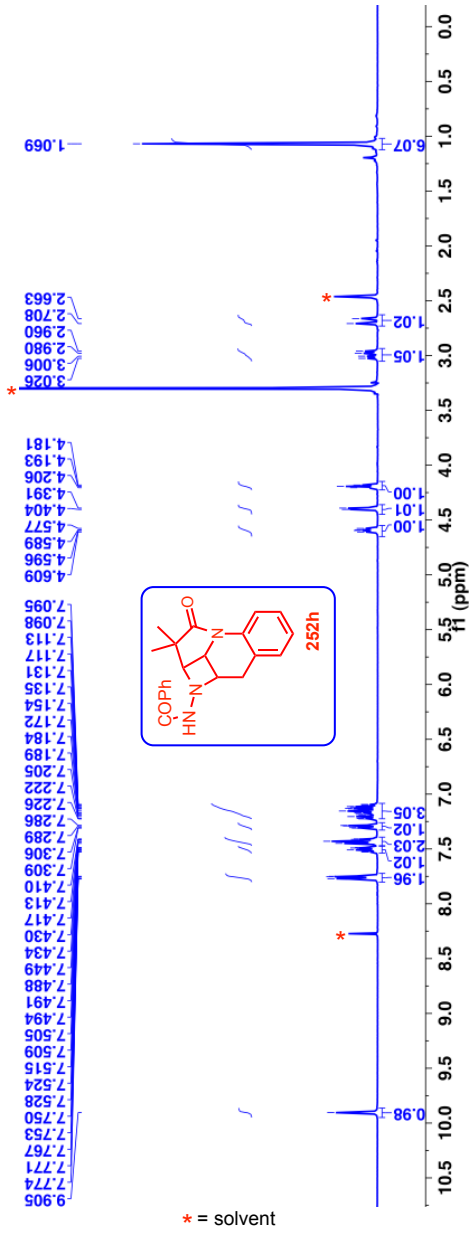

Figure 5.47: ^{1}H-NMR (400 MHz, DMSO, δ ppm) of N-benzoylhydrazide imine photoproduct **252h**.

^{13}C-NMR (100 MHz, DMSO, δ ppm): 184.3, 170.9, 140.3, 138.96, 136.9, 135.97, 134.6, 133.8, 132.6, 131.3, 130.7, 130.4, 77.9, 68.8, 52.3, 49.6, 34.5, 27.2 and 22.6.

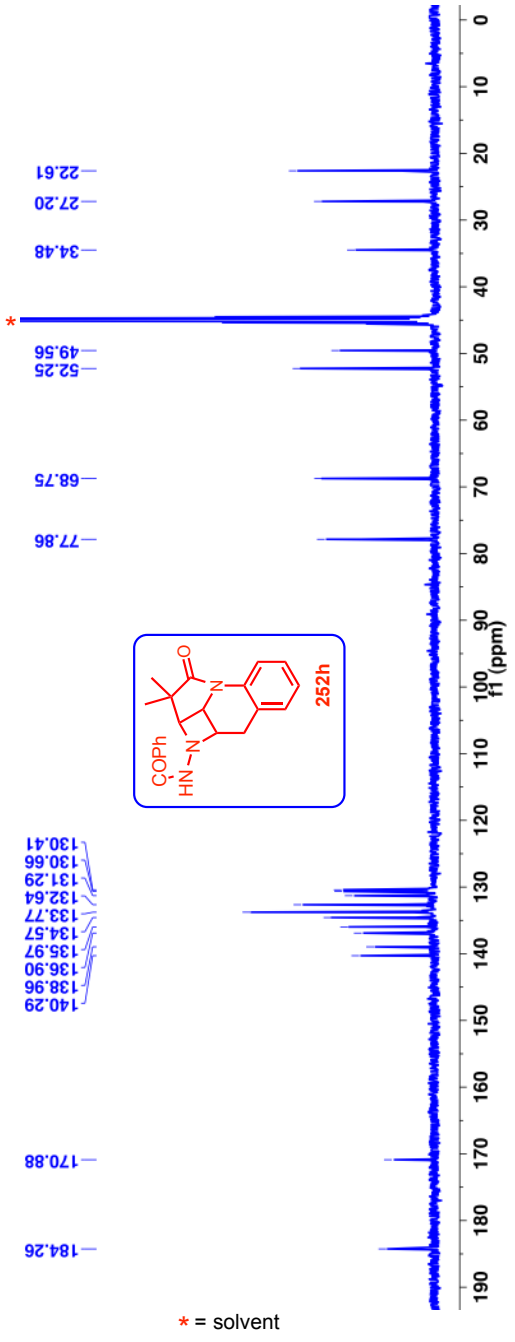

Figure 5.48: ^{1}H-NMR (400 MHz, DMSO, δ ppm) of N-benzoylhydrazide imine photoproduct **252h**.

HRMS-ESI (m/z) ([M + H]$^+$):

Calculated	: 348.1712
Observed	: 348.1714
|Δm|	: 0.6 ppm

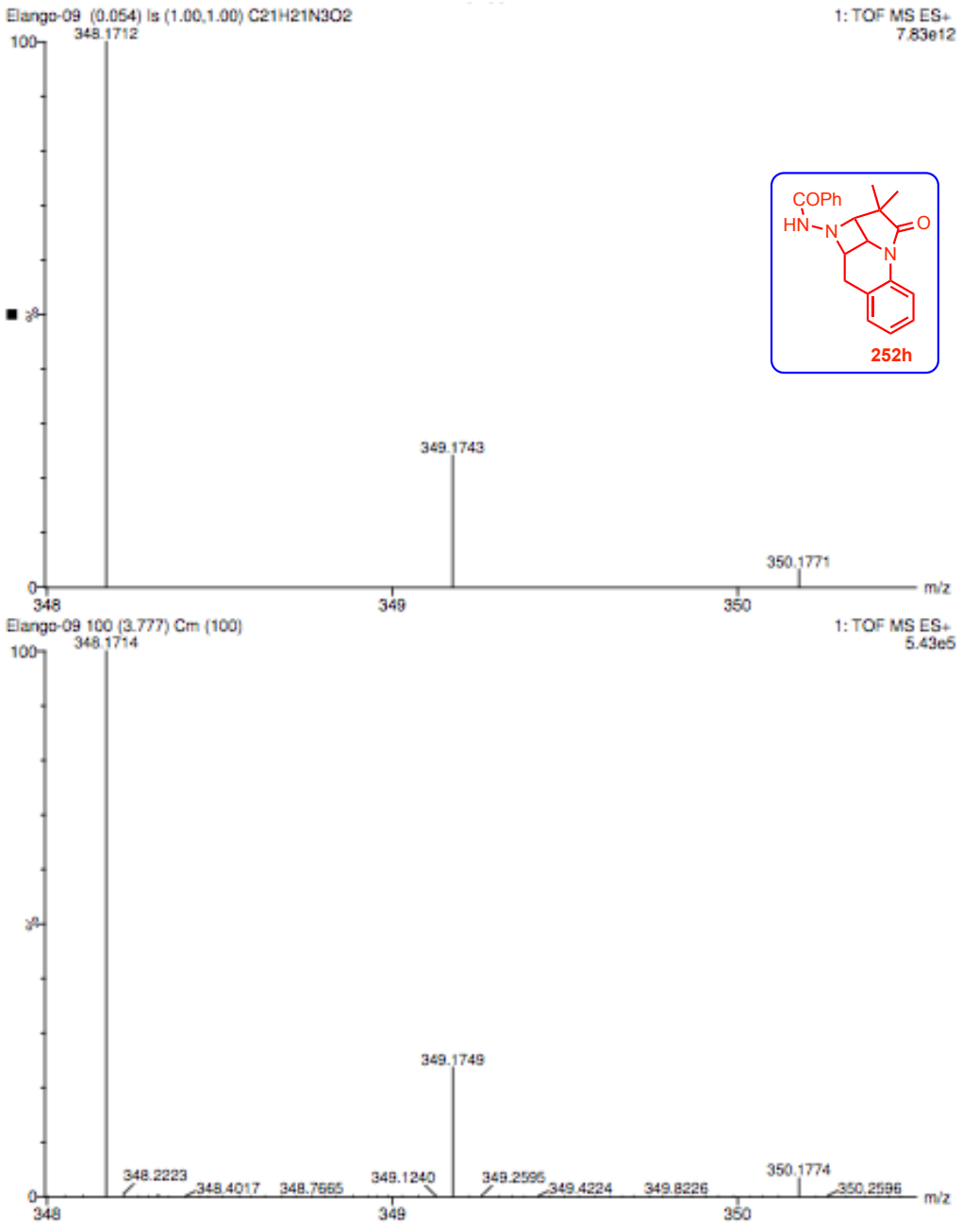

Figure 5.49: HRMS of N-benzoylhydrazide imine photoproduct **252h**.

5.6. References

(1) Padwa, A. Photochemistry of the carbon-nitrogen double bond. *Chem. Rev.* **1977**, *77*, 37-68.

(2) Pratt, A. C. The photochemistry of imines. *Chem. Soc. Rev.* **1977**, *6*, 63-81.

(3) Tsuge, O.; Tashiro, M.; Oe, K. Photochemical reaction of 2,5-diphenyl-1,3,4-oxadiazole with indene. *Tetrahedron Lett.* **1968**, *9*, 3971-3974.

(4) Tsuge, O.; Oe, K.; Tashiro, M. Photochemistry of heterocyclic compounds—II : The photochemical reaction of 2,5-disubstituted 1,3,4-oxadiazoles with furan. *Tetrahedron* **1973**, *29*, 41-46.

(5) Koch, T. H.; Howard, K. H. 2+2 Photocycloaddition to a carbon nitrogen double bond I. 3-ethoxyisoindolone. *Tetrahedron Lett.* **1972**, *13*, 4035-4038.

(6) Koch, T. H.; Rodehorst, R. M. 2+2 Photocycloaddition to a carbon nitrogen double bond II. 2-phenyl-2-oxazolin-4-one. *Tetrahedron Lett.* **1972**, *13*, 4039-4042.

(7) Howard, K. A.; Koch, T. H. Photochemical reactivity of keto imino ethers. V. (2 + 2) Photocycloaddition to the carbon-nitrogen double bond of 3-ethoxyisoindolone. *J. Am. Chem. Soc.* **1975**, *97*, 7288-7298.

(8) Rodehorst, R. M.; Koch, T. H. Photochemical reactivity of keto imino ethers. VI. Type I rearrangement and (2 + 2) photocycloaddition to the carbon-nitrogen double bond of 2-oxazolin-4-ones. *J. Am. Chem. Soc.* **1975**, *97*, 7298-7304.

(9) Saoudi, A.; Hamelin, J.; Benhaoua, H. Elimination reaction over solid supports under microwave irradiation: Synthesis of functionalized alkenes. *Tetrahedron Lett.* **1998**, *39*, 4035-4038.

(10) Koch, T. H.; Olesen, J. A.; DeNiro, J. Unusually weak carbon-carbon single bond. *J. Am. Chem. Soc.* **1975**, *97*, 7285-7288.

(11) Koch, T. H.; Olesen, J. A.; DeNiro, J. Photochemical reactivity of imino lactones. Photoreduction and photoelimination. *J. Org. Chem.* **1975**, *40*, 14-19.

(12) Hyatt, J. A.; Swenton, J. S. Photochemical reactivity of 2,4-dimethyl-1,2,4-triazine-3,5-(2H)-dione (1,3-dimethyl-6-azauracil). *J. Chem. Soc., Chem. Commun.* **1972**, 1144-1145.

(13) Swenton, J. S.; Hyatt, J. A. Photosensitized cycloadditions to 1,3-dimethyl-6-azauracil and 1,3-dimethyl-6-azathymine. Imine linkage unusually reactive toward photocycloaddition. *J. Am. Chem. Soc.* **1974**, *96*, 4879-4885.

(14) Sampedro, D.; Soldevilla, A.; Campos, P. J.; Ruiz, R.; Rodríguez, M. A. Regio- and Stereochemistry of [2 + 2] Photocycloadditions of Imines to Alkenes: A Computational and Experimental Study. *J. Org. Chem.* **2008**, *73*, 8331-8336.

(15) Kawamura, Y.; Kumagai, T.; Murai, T. Photocycloaddition reaction of 3-aryl-2-isoxazolines with indene. Generation of [2+2] cycloadduct stereoisomers. *Chem. Lett.* **1985**, *14*, 1937-1940.

(16) Cubbage, K. L.; Orr-Ewing, A. J.; Booker-Milburn, K. I. First Higher-Order Photocycloaddition to a C-N Bond: 1,3-Diazepines from Maleimides. *Angew. Chem. Int. Ed.* **2009**, *48*, 2514-2517.

CHAPTER 6: CONCLUSIONS

In the quest for newer methodology in the field of asymmetric synthesis to access diverse and stereochemically rich building blocks, phototransformations has offered a definite promise. Photochemistry not only levels with synthetic potential of a methodology but also levels with green chemistry standards that utilize environmentally benign reagent photon. However, in order to take full advantage of its ability, certain fundamental challenges such as controlling the excited state to develop controllable/predictable stereochemistry in a methodology has to be developed. Synthetic strategies that were developed to address this bottleneck have met with varying degree of success.

The introductory chapter explains the principal difference between the asymmetric synthesis carried out under thermal conditions and under photochemical conditions. Also, the failure of synthetic methodologies (successful in thermal chemistry) in photochemical transformations is explained based on the energy profile of the transition states involved in thermal and photochemical transformations. A brief summary of the methodologies developed to address stereoselectivity in the photochemical transformation such as reaction in solid-state, confined media, template mediated reaction, chiral auxiliary tethered substrates …etc and their degree of success is also revealed. The impact of axial chirality in thermal reaction towards asymmetric reactions and the preliminary investigations of axially chiral chromophore in asymmetric phototransformation are also disclosed.

To explore further in the role axial chirality in performing asymmetric phototransformation and in the effort to make it a general established strategy, this thesis describes the asymmetric phototransformation of variety of atropisomeric chromophores. The presence of axial chirality imparts predisposition to the reacting chromophore to undergo highly stereospecific reactions. These molecules are designed to withstand racemization at ambient conditions where the photoreactions are performed. The excited atropisomeric chromophore generally do not undergo racemization obeying Havinga's NEER principle (Non-Equilibrating Excited-state Rotamers) resulting in stereospecific phototransformation, where the product selectivity is dictated by the absolute configuration of the starting material.

The dissertation explores the photoreaction involving 4π-electrons *viz*., 4π-ring closure of 2-pyridones and [2+2]-photocycloaddition of enamides and maleimides. In chapter 2, we disclose enantiospecific 4π-ring closure of 2-pyridones that result in enantioenriched β-lactam photoproducts. The presence of differential axial chirality (with pure sterics or with a blend of sterics and H-bonding) affects the enantiospecificity in the photoreaction as temperature and solvent was varied. This dependence was explained based on the differential activation parameters (differential activation enthalpy and entropy) by performing Eyring plots. The preferred mode of cyclization was deciphered by following the course of reaction through single crystal X-ray diffraction. High-pressure studies carried on racemization and photoreaction provided excellent avenue to perform enantiospecific photoreactions at high temperatures.

Chapter 3 and 4 involves [2+2]-photocycloaddition of atropisomeric enamides and maleimides. The enamides undergo stereospecific photocycloaddition under sensitized irradiation to result in oxetane and cyclobutane products with high *ee*. The reaction proceeds via the excitation of enamides through energy transfer from the sensitizer, which is not reported in the literature so far. Also, analysis on the substitution in the reacting partner (alkenyl and carbonyl) and the ring size of enamides provides excellent mechanistic details, scope and limitations of this approach. The chapter 4 details photocycloaddition of atropisomeric maleimides. The reaction proceeds under variety of conditions including visible light to produce cyclobutane photoproducts in excellent yield. This unprecedented highly stereospecific reaction results in regioisomeric products that are dictated by substitution on the alkenyl tether and at the maleimides double bond. Detailed photophysical analysis provides insights about the nature and lifetime of excited state species involved in the photocycloaddition reaction. Merging flow set up with visible light photoreaction provided an excellent avenue to perform large-scale photoreaction.

Also, results of preliminary investigations of [2+2]-photocycloaddition of enamides to stabilized imines are detailed in chapter 5. In this novel report, unusual photocycloaddition of imines to enamides are observed that result in the formation of azetidine derivatives in good yield. Further mechanistic and photophysical studies will provide crucial details that would allow us to access four membered heterocyclic compounds.

In conclusion, the “axial to point chiral transfer” in photochemical transformation is a cutting edge strategy to access enantiomerically enriched building blocks. The axial chirality not only imparts excellent stereotopic bias but also provides unique reactivities that are not known for non-atropisomeric systems. Further research along this line in the Sivagroup at North Dakota State University is ongoing to unravel the richness and scope of this methodology.